

**Some parts of this thesis may have been removed for copyright restrictions.**

If you have discovered material in AURA which is unlawful e.g. breaches copyright, (either yours or that of a third party) or any other law, including but not limited to those relating to patent, trademark, confidentiality, data protection, obscenity, defamation, libel, then please read our [Takedown Policy](#) and [contact the service](#) immediately

AN INVESTIGATION INTO THE PLASTIC AND ELASTIC  
BEHAVIOUR OF REINFORCED CONCRETE SLAB ELEMENTS

THESIS SUBMITTED FOR THE DEGREE OF

DOCTOR OF PHILOSOPHY

BY

ROGER JOHN DOWNHAM

DEPARTMENT OF CIVIL ENGINEERING

THE UNIVERSITY OF ASTON IN BIRMINGHAM

SEPTEMBER 1968.

## SUMMARY

Since Yield Line theory was developed its use as a method of solution of load-carrying capacity problems in reinforced concrete slab structures has become more common and it is now included in many Codes of Practice. It has been pointed out that, with certain minor modifications, Yield Line Theory provides an upper bound solution to the real collapse load and is within the terms of reference of Limit Analysis which is based on the theory of perfectly plastic solids. Before either approach is accepted it is imperative that the continuum can be shown to behave in the way predicted. Although theoretical considerations provide important indications of behaviour it is experimental work that must be the ultimate test. Tests on whole slab structures have shown the originally supposed yield conditions to be approximately true but conservative. Membrane action, which is not encompassed by Limit Analysis, is known to have a considerable masking effect on a slab's behaviour in pure bending. Recently work has been carried out to determine the condition of yield in reinforced concrete slab elements not subjected to membrane and shear effects. The maximum variation in moment capacity of 15% or so predicted by subsequent yield conditions is easily influenced by difficulties arising from specimen construction and testing arrangements. This thesis describes the attempt to increase present knowledge by the analytical and experimental study of the behaviour in the elastic and plastic

range of slab elements subjected to uniaxial moment and particularly to combined torsional and bending moments. Special attention has been paid to the effect of this applied moment combination and to the behaviour of the basically discontinuous material prior and subsequent to the yielding of reinforcement, leading to the flow law, for which data is still sparse.

## ACKNOWLEDGEMENTS

The author wishes to express his thanks particularly to Professor M. Holmes, B.Sc., Ph.D., F.I.C.E., A.M.I.Struct.E., the Head of the Department of Civil Engineering at the University of Aston in Birmingham, for his continual help, encouragement and advice throughout this project and to Professor R. H. Evans, C.B.E., D.Sc., D.ésSc., Ph.D., F.I.C.E., M.I.Mech.E., M.I.Struct.E., the Head of the Civil Engineering Department of Leeds University.

Special thanks are due to Mr. W. Parsons, the Chief Technician in the Civil Engineering Department at the University of Aston and to his assistants, particularly Mr. J. Hollins, for their willing help during the experimental work. Thanks are also given to the clerical staff for their help in typing and particularly to Mrs. C. Taylor who typed the majority of this thesis.

## CONTENTS

	<u>Page</u>
Summary	
Acknowledgements	
Contents	iv
List of Plates	ix
Notation	xii
CHAPTER 1	
INTRODUCTION	1
1.1	
Object	1
1.2	
Outline of Experimental Investigation	2
1.3	
Outline of analytical study	3
CHAPTER 2	
THEORIES OF PLASTICITY FOR IDEALIZED SOLIDS	
AND REINFORCED CONCRETE	4
2.1	
Introduction	4
2.2	
Mathematical theory of perfectly plastic solids	5
2.3	
Limit analysis	18
2.4	
Plasticity in beams and plates	21
2.5	
The solution of plastic plate problems	23
2.6	
The inelastic behaviour of reinforced concrete	
slabs under uniaxial moment	26
2.7	
Yield line theory	32
2.8	
Yield conditions, flow laws and assumptions	
made for reinforced concrete slabs	34

	Page
2.8.1 Theoretically based yield criteria and flow laws	35
2.8.2 Experimentally based yield conditions and flow laws	45
2.9 Summary	70
CHAPTER 3 QUALITATIVE THEORETICAL ANALYSIS	74
3.1 Introduction	74
3.2 The general model of reinforced concrete slabs	74
3.3 Behaviour of the composite to failure	76
3.3.1 Zero load to the load at which cracking occurs	81
3.3.2 Cracking load to the load at which the first layer bars yield	82
3.3.3 Load at yield of first set of bars to load at yield of second set of bars	85
3.3.4 Load at second layer yield to failure	86
3.4 Conclusions	86
CHAPTER 4 DESCRIPTION OF EXPERIMENTAL METHODS	89
4.1 Introductory remarks	89
4.2 Materials in both test series	91
4.2.1 Cement	91
4.2.2 Aggregates	91

4.2.3	Concrete mixes	91
4.2.4	Concrete control specimens	91
4.2.5	Reinforcement	93
4.3	Experimental methods used in Plant test series	94
4.3.1	Description of specimens	94
4.3.2	Test set-up	97
4.3.3	Instrumentation	100
4.4	Experimental methods used in General moment tests	105
4.4.1	Description of specimens	106
4.4.2	Test set-up	108
4.4.3	Instrumentation	113
4.5	Summary	116
CHAPTER 5	TEST PROCEDURE AND RESULTS FROM INDIVIDUAL TESTS	117
5.1	Introductory remarks	117
5.2	Plank test series	118
5.2.1	Description of general test procedure	118
5.2.2	Description of individual plank tests and results	119
5.3	General moment test series	134
5.3.1	Description of general test procedure	134
5.3.2	General method of presentation of objective observations	134

	5.3.3	Presentation of steel strain observations	140
	5.3.4	Description of individual tests and presentation of objective observations	143
	5.4	Summary of results	162
CHAPTER 6		COMPARATIVE ANALYSIS OF RESULTS FROM THE PLANK TEST SERIES	165
	6.1	Introduction	165
	6.2	Standardization of section properties	166
	6.3	The effect of bar arrangement on the 'effective' width of the slab	168
	6.4	Comparison of results	172
	6.4.1	The effect of mesh orientation on the stiffness of the element in the span direction before yielding	173
	6.4.2	The effect of mesh orientation on the ultimate moment of the element	179
	6.5	Concluding remarks	184
CHAPTER 7		COMPARISON OF RESULTS FROM THE GENERAL MOMENT TEST SERIES	186
	7.1	Introduction	186
	7.2	The elastic behaviour and variations in stiffness	186
	7.2.1	'Isotropically' reinforced slabs	186
	7.2.2	'Non-isotropically' reinforced slabs	193

	7.3	The yield behaviour of reinforced concrete slab elements	196
CHAPTER 8		CONCLUSIONS	203
	8.1	General behaviour	203
	8.2	Elastic behaviour	204
	8.3	Post-yield behaviour	206
	8.4	Suggestions for future research	208
REFERENCES			209

LIST OF PLATESPlate

- 4.1 Plank Meshes before casting,  $\mu = 1$
- 4.2 Typical Plank test set up
- 4.3 Close up of steel strain gauges in position
- 4.4 Concrete strain gauges in position for Plank test
- 4.5 General moment mesh before casting,  $\mu = 1$ ,  $\beta = 0^\circ$
- 4.6 Typical General moment test set up,  $Ta = 3in.$
- 
- 5.1 Crack formation - P1
- 5.2 Side view of cracks at failure - P1
- 5.3 Crack formation - P2
- 5.4 Crack formation - smaller cracks marked - P2
- 5.5 Crack formation - P3
- 5.6 Crack formation - P4
- 5.7 Crack formation - P5
- 5.8 Crack formation - P6
- 5.9 Crack formation - P7
- 5.10 Crack formation - P8
- 5.11 Crack formation - P9
- 5.12 Shear effect - P9
- 5.13 Crack formation - P10

5.14	Crack formation - P11
5.15	Crack formation - P12
5.16	Crack formation - P13
5.17	Crack formation - P14
5.18	Crack formation - P15
5.19	Shear effect - P16
5.20	Crack formation - P16
5.21	Crack formation - P17
5.22	Crack formation - TB1
5.23	Crack formation - TB2
5.24	Crack formation - TB3
5.25	Crack formation - TB28
5.26	Crack formation - TB4
5.27	Crack formation - TB5
5.28	Crack formation - TB6
5.29	Crack formation - TB29
5.30	Curvature at failure - TB7
5.31	Crack formation - TB7
5.32	Crack formation - TB8
5.33	Crack formation - TB9
5.34	Crack formation - TB30
5.35	Crack formation - TB31
5.36	Crack formation - TB10
5.37	Crack formation - TB11
5.38	Crack formation - TB12

5.39	Crack formation - TB13
5.40	Crack formation - TB14
5.41	Curvature at failure - TB14
5.42	Crack formation - TB25
5.43	Crack formation - TB16
5.44	Crack formation - TB16
5.45	Crack formation - TB17
5.46	Crack formation - TB18
5.47	Crack formation - TB19
5.48	Crack formation - TB26
5.49	Crack formation - TB20
5.50	Crack formation - TB21
5.51	Crack formation - TB22
5.52	Crack formation - smaller cracks marked TB22
5.53	Crack formation - TB23
5.54	Crack formation - smaller cracks marked TB23
5.55	Crack formation - TB24
5.56	Crack formation - TB27
5.57	Shear effect at edge - TB27

## NOTATION

$A_{st}$	area of steel in bar direction per unit width of slab
a-direction	Direction of main, lower layer of steel reinforcement
b-direction	Direction at upper layer of steel reinforcement, orthogonal to a-direction
b	Length of yield line on specimen
$b^1$	Effective length of yield line
$d_1$	Depth of main steel layer below compressive, upper, slab surface.
$d_n$	Depth of neutral plane below upper concrete surface
E1	Principal compressive concrete strain on upper surface
E2	Minor principal concrete strain on upper surface
EA	Concrete strain on upper surface in a-direction
EB	Concrete strain on upper surface in b-direction
EAB	Shear strain on upper surface in a and b-directions.
exp	Suffix used to denote experimental observations
$K_s$	Youngs modulus for steel reinforcement
$E_x$	Secant elastic modulus for concrete
$f_b$	modulus of rupture
k	Constant used during tests to calculate ultimate moments in the bar directions from equ. (6.1)
K1	Principal curvature (sagging positive)

K <sub>2</sub>	Minor principal curvature
m	Calculated ultimate moment of resistance in bar direction used by Johansen
m <sub>a</sub>	Ultimate moment of resistance in a-direction
m <sub>b</sub>	Ultimate moment of resistance in b-direction
m <sub>n</sub>	Ultimate moment of resistance normal to crack direction at failure
m <sub>nt</sub>	Twisting moment on crack at failure associated with m <sub>n</sub>
m <sub>t</sub>	Tangential moment at failure in t-direction
m <sub>nj</sub>	Ultimate normal moment on yield line predicted by Johansens yield criterion
M <sub>1</sub>	Principal applied moment
M <sub>2</sub>	Minor principal applied moment
M <sub>x</sub>	Applied moment in span or x-direction
M <sub>xy</sub>	Twisting moment applied in X and Y direction
n <sub>1</sub>	Number of bars in a-direction crossing yield line
n <sub>2</sub>	Number of bars in b-direction crossing yield line
P	Prefix used as reference for plank test specimens
S <sub>x</sub>	Stiffness measured in X-direction
s <sub>1</sub>	Spacing bars in a-direction
s <sub>2</sub>	Spacing of bars in b-direction
Ta	Torsional lever arm used to produce twisting moments M <sub>xy</sub>
TB	Prefix used as reference for general moment test specimens
u	Concrete compression strength

W	Load measured by proving ring.
X-direction	Span direction in both test series
Y-direction	Direction transverse to span
$\beta$	Angle between X-direction and a-direction
$\gamma$	Angle between X-direction and principal concrete strain direction measured clockwise positive from X-direction
$\eta$	Coefficient of mutual influence
$\theta$	Angle between X-direction and M1 direction, clockwise positive
$\mu$	Degree of orthotropy i.e. $\frac{m_b}{m_a}$ , $\mu < 1$
$\mu$ strains	Microstrains
$\nu$	Poissons ratio
$\psi$	Angle between X-direction and measured average normal to crack direction, clockwise positive
$\sigma_o$	Yield stress of reinforcement bars
$\omega$	Angle between X-direction and principal curvature K1 direction, clockwise positive
$\alpha$	Angle between a-direction and n-direction i.e. $(\beta - \psi)$

CHAPTER 1INTRODUCTION1.1      Object

In recent years renewed interest has been shown in the prediction of the ultimate strengths of reinforced concrete slab structures. The more recent studies have stemmed from the work of Johansen on Yield Line theory and the work of Drucker, Greenberg and Prager on Limit Analysis. Attempts have been made to justify the use of the yield condition employed in Yield Line theory and to encompass it within the stricter terms of reference of Limit Analysis. Most of the work carried out has been of a theoretical nature although a few attempts have been made to verify the yield criteria experimentally for uniaxial bending and pure torsion. In the majority of research carried out only the ultimate strength conditions have been considered.

The ultimate test of any theory must be an experimental study, hence the main object of this research was to increase the experimental data available in relation to the general behaviour of reinforced concrete slabs in pure bending. Tests were carried out on 48 slab elements subjected to uniaxial bending or combined bending and torsional moments. Attention has been paid, not only to the ultimate behaviour of such elements but to the elastic characteristics which

may affect the ultimate behaviour significantly. Knowledge of the elastic behaviour of such elements is imperative to the control of deformations and cracking, particularly in view of the new combined Codes of Practice based on Limit State design concepts. Information relating to the post-yield behaviour of such slabs is of course essential to the prediction of ultimate strengths and to the flow laws related to them.

### 1.2 Outline of Experimental investigation

Two types of test were carried out on reinforced concrete slab elements. The first type of test was one in which the element was set up as a plank and was subjected to uniaxial bending. This type of test has been carried out before but was included in this investigation so that direct comparisons could be made both with existing theories and with the results obtained from the second series of tests. Seventeen specimens were tested in this Plank test series with both the mesh orientation relative to the span and the degree of orthotropy as variables. The attempt to restrain principal strain directions to the span direction was on the whole successful.

The second series of tests was carried out on slab elements with variable mesh orientation and degree of orthotropy under varying conditions of combined bending and torsion. Thirty one specimens were tested in all, of which thirteen were 'isotropically' reinforced and eighteen were

were reinforced with a degree of orthotropy of 0.5.

The results in all load ranges have been presented in detail for all specimens in Chapter 5 in such a way that any information not directly presented may be calculated.

### 1.3 Outline of analytical study

As stated in section 1.1 the main object of the study was to obtain experimental data in both the elastic and plastic ranges of behaviour of a reinforced concrete slab element. The analytical study made here is therefore of a qualitative nature only. It is suggested that the material should be treated as a multiphase composite with varying elastic properties in both a continuous and discontinuous state. Models can be formed whose varying properties describe the behaviour of the element from no load to ultimate load. These suggestions are put forward in Chapter 3 and references to some of the possible modes of behaviour presented are made in the chapters relating to the experimental investigation.

CHAPTER 2THEORIES OF PLASTICITY FOR IDEALIZED SOLIDS AND REINFORCED CONCRETE.2.1      Introduction

Of the basic requirements of any theory concerning the plastic behaviour of materials the description of the limits within which plastic behaviour takes place and of the way the material behaves within these limits is among the most basic.

Perfectly plastic behaviour is described within the Mathematical Theory of Perfectly Plastic Solids, itself embraced by the General Mathematical Theory of Plasticity, which postulates the basic requirements referred to above in the yield criterion and flow law for such a perfectly plastic solid.

Although it has been shown that the inelastic behaviour of some metals including mild and annealed steel approximated closely to that required in a perfectly plastic solid, it has still to be demonstrated with any certainty that reinforced concrete structures obey the same basic relationships. Two dimensional frameworks composed of beams and columns appear to satisfy approximately the necessary requirements except that plastic strains have a fairly low upper limit at concrete compression failure unlike structures in steel in which the ductility of the material allows very large plastic straining before complete failure of the section.

However, since an inelastic theory for reinforced concrete

slabs was suggested in the form of Yield Line Theory much controversy has existed over the form of the yield criterion and the flow law, and although these relationships were basically intuitive at the outset many authors have attempted to justify the assumptions by showing that, at least in a modified form, they fit into the terms of reference of the theory of perfectly plastic solids.

It is the object of this chapter to review critically the suggestions put forward both in the development of the yield criterion and flow law for reinforced concrete slabs and in the attempted justification of the inclusion of the material and its related inelastic relationships into the theory of perfectly plastic solids and hence into the associated theory of Limit Analysis.

Firstly however, a brief introduction into the basic concepts of the theory of perfectly plastic solids and the theory of Limit Analysis will be given so that a direct comparison of basic assumptions can be made.

## 2.2. The Mathematical Theory of Perfectly Plastic Solids.

The genesis of the theory of perfectly plastic solids occurred around 1870 with the work of St.Venant. Since then research has been carried out by many investigators but generally the two theories of perfectly plastic solids are due to St. Venant, Lévy and Mises in which plastic strains are assumed to be so much larger than elastic strains that the latter may be neglected and Prandtl and Reuss in

which elastic and plastic strains are of the same order of magnitude. The idealized materials dealt with in the above theories are rigid-perfectly plastic and elastic - perfectly plastic respectively. The stress-strain characteristics in simple tension and compression of these idealized materials are illustrated in Fig 2.1. (a) (b) along with the characteristics of a rigid-strain hardening material and an elastic strain hardening material Fig 2.1 (c) (d) which are not dealt with in the theory of perfectly plastic solids but are encompassed by the General theory of Plasticity.

The necessity to base a mathematical theory on a material with highly idealized characteristics becomes evident when the stress-strain diagrams for the most highly idealized plastic solid, the rigid-perfectly plastic material (Fig 2.1. (a) ), and for the perfectly elastic body (Fig.2.1. (b), X Y O A C ) are compared. Analytically these diagrams can be described by the following relations:

- 1) Perfectly Elastic Solid obeying Hookes Law,

$$\sigma = E\epsilon \quad (2.1)$$

where E is a positive constant usually referred to as Young's Modulus or the Modulus of Elasticity

- 2) Rigid - Perfectly Plastic Solid 1

$$\dot{\epsilon} = 0, \text{ if } \sigma^2 < \sigma_0^2 \text{ or if } \sigma \geq \sigma_0^2 \text{ and } \dot{\sigma} < 0 \quad (2.2a)$$

$$\text{and } \text{sgn } \dot{\epsilon} = \text{sign } \dot{\sigma}, \text{ if } \sigma \geq \sigma_0^2 \text{ and } \dot{\sigma} = 0 \quad (2.2b)$$

It can be seen from equation 2.1 and equation 2.2 that whilst a one to one relationship governs the stress-strain characteristics for an elastic solid it is necessary to describe the behaviour of a

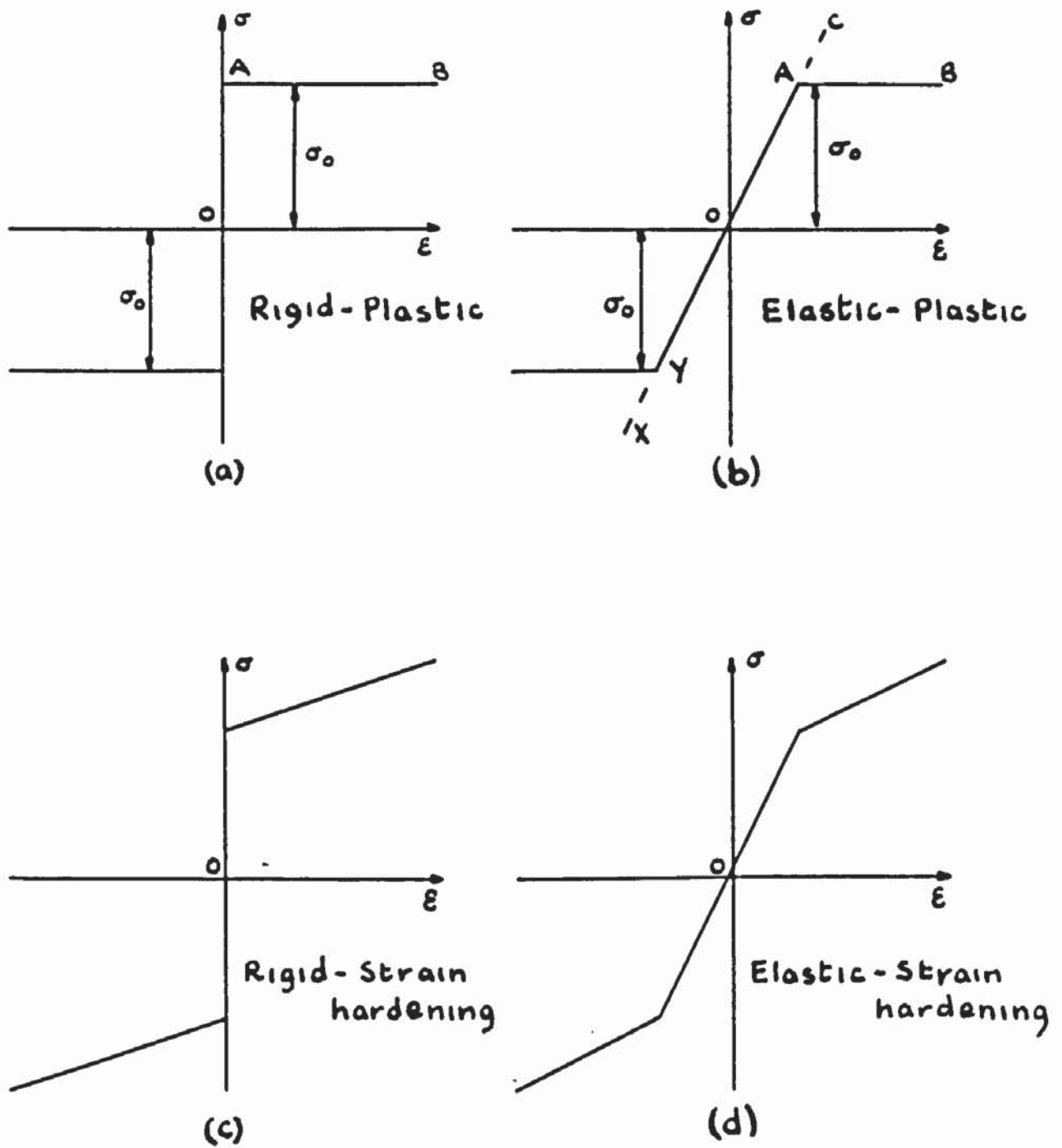


FIG 2.1

rigid-perfectly plastic solid in terms of the stress and strain rates  $\dot{\sigma}$  and  $\dot{\epsilon}$  as well as the actual stress  $\sigma$ . Equation 2.2a states that the plastic strain rate,  $\dot{\epsilon}$ , is zero whenever the stress,  $\sigma$ , is below the yield stress,  $\sigma_0$ , or is at the yield stress but about to approach zero. Equation 2.2b, in which 'sgn' denotes the signum function for which  $\text{sgn } n = 1$  for  $n > 0$ ;  $\text{sgn } n = -1$  for  $n < 0$  and  $\text{sgn } n = 0$  for  $n = 0$ , states that plastic elongation or contraction is possible so long as the stress remains at the yield stress either in tension or compression.

Thus one definition of a perfectly plastic solid at least with respect to simple tension and compression can be stated as:

A Perfectly Plastic Solid is a material in which strains are independent of time, which is capable of indefinite strains once the condition of yield is reached and which exhibits no strain hardening characteristics.

It is important to note that although the terms 'stress rate' and 'strain rate' are used these are not indicative of functions of time and therefore 'plastic flow' does not show viscosity effects which are time dependent. Both theories of St.Venant - Lévy - Mises and Prandtl - Reuss shows that straining is independent of time and thus neither theory reflects viscosity effects. [2]

In all deformable materials the three equations of equilibrium must at all times be obeyed. These equations are written in terms of the components of the stress tensor in the usual way and since slow plastic deformations are considered, and hence no components of inertia are significant, the equations of equilibrium can be used in place of

the more general equations of motions [3] The three equations of equilibrium

$$\frac{\partial \sigma_x}{\partial x} + \frac{\partial \bar{\tau}_{xy}}{\partial y} + \frac{\partial \bar{\tau}_{zx}}{\partial z} + X = 0$$

$$\frac{\partial \bar{\tau}_{xy}}{\partial x} + \frac{\partial \sigma_y}{\partial y} + \frac{\partial \bar{\tau}_{yz}}{\partial z} + Y = 0$$

$$\frac{\partial \bar{\tau}_{zx}}{\partial x} + \frac{\partial \bar{\tau}_{yz}}{\partial y} + \frac{\partial \sigma_z}{\partial z} + Z = 0$$

where  $\sigma_x$ ,  $\bar{\tau}_{xy}$ ,  $\bar{\tau}_{xz}$ ,  $\sigma_y$ ,  $\bar{\tau}_{yx}$ ,  $\bar{\tau}_{yz}$ ,  $\sigma_z$ ,  $\bar{\tau}_{zx}$ ,  $\bar{\tau}_{zy}$

are the nine components of the stress tensor for which the equalities

$$\bar{\tau}_{zy} = \bar{\tau}_{yz}, \quad \bar{\tau}_{xz} = \bar{\tau}_{zx}, \quad \bar{\tau}_{yx} = \bar{\tau}_{xy}$$

are due to symmetry and X, Y and Z are components of the forces

acting on the body. There are therefore six stress components and

three displacement components in only three equilibrium equations.

Six further equations are required to define the stresses and strains

completely. These extra equations are formed from the stress-strain

relationships at a generic point in the body considered. Thus for

an elastic body with a stress-strain relationship of the form of

equation 2.1 The extra six equations are readily obtained in terms

of the elastic constants G, the modulus of rigidity, and K, the bulk

modulus themselves both being dependent on E, the Young's modulus and  $\nu$

Poissons ratio. These elastic constants should be found experimentally

for any material exhibiting elastic characteristics.

To obtain the six extra equations required to define the stress state at a point in a perfectly plastic solid it is necessary

to know the stress-strain law governing the behaviour of such a solid, in the same way as the stress-strain law for an elastic solid was known. The information required to define the stress-strain law for a perfectly plastic solid must include:

- a) The stress-strain relationship in the elastic region.
- b) The condition or criterion indicating the start of plastic straining whilst loading and the end of plastic straining whilst unloading.
- c) The stress-strain relationship during plastic flow.

a) Elastic Stress-Strain Relationship

Hooke's law, in which stress is uniquely determined by strain or vice versa, adequately describes the relationship between stress and strain in the elastic range before previous yielding has occurred. A modified form of Hooke's law involving the stress rate and strain rate is used when, in an unloading cycle, plastic strains have already occurred. This relationship is only used in the Prandtl - Reuss equations governing an elastic perfectly plastic solid.

b) The Condition of Yield.

At first yield of a perfectly plastic solid, that is when no part of the solid has previously entered the plastic range, the strain is uniquely determined by the stress as the yield point lies on the intersection of elastic and plastic curves and the elastic stress-strain relationship is independent of the strain

history (implying that no permanent set effects are involved}. Thus for this first yielding the critical combination of stress and strain can be described in terms of stress components alone. This will take the form of a function:

$$f (\sigma_x, \sigma_y, \sigma_z, \bar{\tau}_{xy}, \bar{\tau}_{yz}, \bar{\tau}_{zx} )$$

As this function will contain some critical material property it is convenient to set this function equal to zero indicated that for negative values of the function yielding has yet to occur and for positive values to be unacceptable as no state of stress can exist which exceeds the yield function. Zero values of the yield function will then indicate that plastic straining is occurring at the stress point considered. Thus the yield condition is expressed as:

$$f (\sigma_x, \sigma_y, \sigma_z, \bar{\tau}_{xy}, \bar{\tau}_{yz}, \bar{\tau}_{zx} ) = 0 \quad (2.3)$$

So far in this chapter it has been implied but not stated that the perfectly plastic solid considered is an isotropic material. Previously, in referring to the elastic constants,  $G$ ,  $K$ ,  $E$  and  $\nu$  it was implied that their values were independent of direction in the material therefore defining the material as isotropic. In this section, for simplicity, only isotropic perfectly plastic materials will be discussed.

Equation 2.3, defining the yield condition at first yield, offers no information on the form of the yield condition for unloading or loading after plastic strains have previously existed

at the stress point considered. It is a supplementary condition to the definition of a perfectly plastic solid that the yield conditions for unloading or loading after previous plastic deformation are subject to the same restrictions concerning isotropy as the yield condition at first yielding and will therefore take the form of equation 2.3.

As the material is isotropic the yield condition must define the vanishing of an invariant of the stress tensor at a considered point and by choosing values of the invariant accordingly, negative values will indicate an elastic stress state and positive values on impossible stress state. The invariants of the stress tensor are usually expressed in terms of deviatoric stresses \* as it has been found that hydrostatic stress produces negligible plastic deformation when acting alone. Because the properties of the invariant must not change when the principal deviatoric stresses  $\sigma_1^1$ ,  $\sigma_2^1$ ,  $\sigma_3^1$  are interchanged in any way, the invariant of the principal deviatoric stresses must become a symmetric function of its components. Algebraically this symmetric function can be expressed in terms of three linear independent symmetric functions. Thus the well known functions chosen are:

$$\begin{aligned} J_1 &= \sigma_1^1 + \sigma_2^1 + \sigma_3^1 \\ J_2 &= \frac{1}{2} (\sigma_1^{12} + \sigma_2^{12} + \sigma_3^{12}) \\ J_3 &= 1/3 (\sigma_1^{13} + \sigma_2^{13} + \sigma_3^{13}) \end{aligned} \quad (2.4)$$

It can easily be shown that  $J_1$  reduces to zero and therefore

---

\* Deviatoric stress e.g.  $\sigma_n^1 = \sigma_n - 1/3 (\sigma_1 + \sigma_2 + \sigma_3)$

where 1, 2, 3 refer to principal stress directions.

the yield condition can be written in terms of  $J_2$  and  $J_3$ .

Many yield conditions have been devised to describe the yield limit of structural metals under the action of combined stresses. As Marin [4] has concluded in his paper correlating some sixteen yield or failure conditions with test results conducted independently by himself, Guest and Smith, a precise, correct failure theory or yield condition is probably a combination of a number of theories depending on the ratio of the principal stresses at failure. However, two well known and frequently applied yield conditions for mild steel will be briefly described here as a foundation for comparison with the yield conditions suggested for use with reinforced concrete slabs.

The yield condition formulated by Tresca (1868) which is in fact a special case of Mohr's General Shear Theory (1914), is, when the largest shear stress is known, one of the most simple yield criteria to use. It takes its simple form as:

$$\sigma_1 - \sigma_2 = \sigma_1^1 - \sigma_2^1 = 2K \quad (2.5)$$

where  $\sigma_1$  and  $\sigma_2$  are known to be the largest and smallest principal stresses respectively and  $K$  is the constant value of yield stress in simple shear and is equal to  $\sigma_0/2$ ,  $\sigma_0$  being the yield stress in simple tension. This criterion of yield may be stated as the 'yield condition of constant maximum shearing stress' and although it is used extensively in two dimensional problems including plate problems it can be seen to be non-symmetric as the labelling

of the principal uses affect the form of the function. Thus Ruess (1933) generalized the form of the function and in terms of the invariants of principal deviatoric stress the yield condition becomes:

$$4J_2^3 - 27J_3^2 - 36K^2J_2^2 + 96K^4J_2 - 64K^6 = 0 \quad (2.6)$$

It can be seen that this yield condition causes undue complexity in the solution of problems in the theory of plasticity and consequently Von Mises suggested a mathematically simpler yield condition which nowhere differed from that of Tresca by more than 15%. This yield condition which is also extensively used may be written:

$$J_2 - K^2 = 0 \quad (2.7)$$

where K retains the meaning given it in Tresca's yield condition, (equation 2.5). Equation 2.7 may be written in the more familiar form in terms of biaxial principal stresses:

$$\sigma_1^2 + \sigma_2^2 - \sigma_1 \sigma_2 - \sigma_0^2 = 0 \quad (2.8)$$

Although Von Mises only intended that the yield condition should be in a more simple mathematical form than Tresca's criterion of equation 2.6, attempts have been made to give it some physical significance, the result being that it is now often referred to as the 'yield condition of maximum shear-strain energy'.

It is frequently more convenient to express the yield function in terms of generalized stresses [1] which are variables not necessarily with the dimensions of stress but which specify the state of stress in the material. For example, in plate theory

$M_1$  and  $M_2$  the principal bending moments could be chosen as generalized stresses describing the stress state in a perfectly plastic plate. Other variables such as axial force can also be included and the yield function of equation 2.3 takes the form:

$$F (M_1, M_2, N_1, N_2) = 0$$

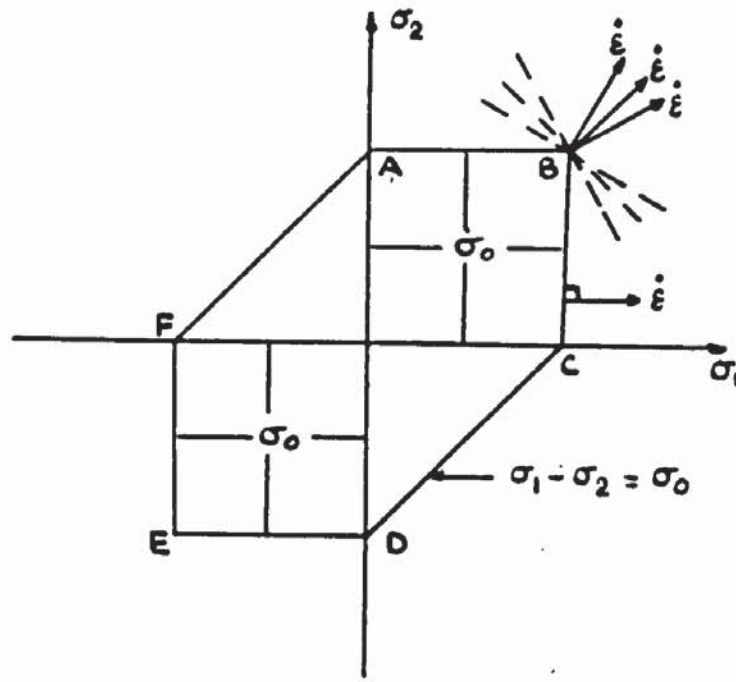
where  $N_1$  and  $N_2$  are the principal axial forces at the considered point.

More generally and using Pragers [1] notation:

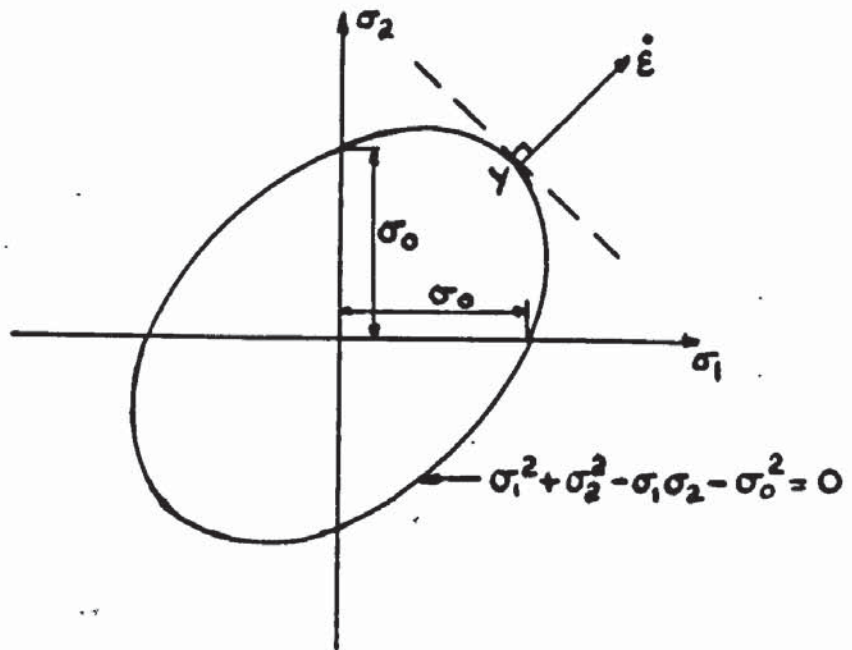
$$F (Q_1, Q_2, \dots, Q_n) = 0 \quad (2.9)$$

where  $Q_1, Q_2, \dots, Q_n$  are generalized stresses affecting the yield limit of the material.

Thus by translating these generalized stresses into a Cartesian coordinate system representing the stress point in  $n$  - dimensional generalized stress space the locus of the yield condition is a surface normally referred to as the yield locus. For example, the yield condition can be expressed graphically by a surface in three dimensional problems or by a bounded plane in two dimensional problems. This yield locus is often used in the literature to represent the yield condition especially in two-dimensional problems. The yield conditions of Tresca, (equation 2.5) and Von Mises, (equation 2.8) applied to biaxial problems are shown in Fig 2.2 in principal stress space. It should be noted that at any point on the Von Mises yield locus is a regular point [1] whereas the Tresca yield locus consists only of singular points of the first and second kind [1], that is, point



Tresca Yield Condition



Von Mises Yield Condition

FIG 2.2

Y on the Mises yield locus has only one tangential plane capable of passing through it whereas point B, on the Tresca yield locus, has an infinite number of tangential planes passing through it and is therefore designated a singular point of the first kind and any point on BC, for instance, has only one tangential plane passing through an infinite number of points on the yield locus and is designated a singular point of the second kind.

Before dealing with the stress-strain relation in the plastic range it should be noted that a further two restrictions are placed on the behaviour of a perfectly plastic solid. They are as stated by Prager <sup>[1]</sup>:

- 1) 'The stress increment does no work on the increment of plastic strain'. Thus the vectors representing the stress increments and the plastic strain increments are orthogonal. This is an important basic principle governing the interdependence of yield condition and stress-strain relationship for a perfectly plastic solid as will be described in Section 2.2(c)
- 2) 'If two states of stress, neither of which exceeds the yield limit, are linearly combined with positive weight  $\theta$  and  $1 - \theta$ , the resulting state of stress cannot exceed the yield limit'. This in effect restricts the shape of the yield locus to a convex form which can be made up of flat portions as in the Tresca yield condition but is then not strictly convex.

(c) Stress-Strain relations in the plastic region.

In early work by St. Venant, Mises, Lévy and others the yield condition and stress-strain relation in the plastic region, referred to subsequently as the flow law, were considered as separate parts of the total stress-strain law governing plastic behaviour. St. Venant and Lévy used an assumed flow law analogous to the stress-strain relationship in an elastic body in combination with the Tresca yield condition whilst Von Mises combined his own suggested yield condition, (equation 2.7), with the same flow law. The strain rate was considered proportional to the deviatoric stress associated with it. Prager and Hodge [2] show that with the extra condition of incompressibility used in the theory of plasticity to obtain one of the six, unknown, independent equations required in the solution of the equations of equilibrium, the flow law used by Von Mises in conjunction with his yield condition furnished a unique deviatoric stress when the strain rate is given. After further investigations, Von Mises (1928) postulated the Theory of Plastic Potential which made the flow law dependent on the yield condition. By use of the 'Principle of Maximum Specific Power of Dissipation', Mises concluded that for a perfectly plastic solid subject to all the previously mentioned restrictions and having a regular yield locus (i.e. each point on the yield locus is a regular point) there was an associated flow law of the form:

$$dq_1 = \lambda \frac{dF}{dQ_1}, \dots, dq_n = \lambda \frac{dF}{dQ_n} \quad (2.10)$$

where  $\lambda$  is a positive scalar factor,  $dq_1 \dots dq_n$  represent the generalized plastic strain increments\* associated with the generalized stresses  $Q_1 \dots Q_n$  and  $F$  is the yield function in terms of the generalized stresses. This follows from the basic assumption concerning orthogonality of stress and strain increment vectors. The stress increment vector will be tangential to the yield condition for any point on the yield locus and hence the strain increment vector associated with it will be normal to the yield locus at the considered stress point. Because mechanical energy is dissipated during plastic flow the scalar factor  $\lambda$  must be positive, this condition in turn defining the direction of the strain increment vector along the external normal to the yield locus.

Koiter (1953) removed the restriction imposed in Mises' work with regular yield loci only, by generalizing the theory of plastic potential and considering several yield functions thus allowing yield loci containing singular points to be covered. The concept of Plastic Potential is an important one in the theory

---

\* Considering for simplicity a rigid-perfectly plastic solid only, the generalized strains  $q_1 \dots q_n$  associated with the generalized stresses are defined by the work equation as  $dw = Q_1 dq_1 + \dots + Q_n dq_n$  where  $dw$  is the work done by the stresses on infinitesimal strain increments.

of perfectly plastic solids and physically states that plastic flow will take place in the direction of the external normal at the stress point considered on the yield locus. Graphically this is represented on the yield loci in Fig 2.2. For a stress state represented by point Y on the Mises yield locus the direction of plastic flow is uniquely determined as it is for a stress state represented by point X on the Tresca yield locus. However for a stress state represented by point B on the Tresca yield locus plastic flow may take place in an infinite number of directions within the limits of the right angle formed by AB and CB produced. As Prager<sup>[1]</sup> shows in an example dealing with biaxial stresses in a plate, although both the state of stress and the specific power of dissipation are uniquely determined by the plastic flow directions and plastic strain rates respectively for a material obeying the Mises yield condition and associated flow rule, only the specific power of dissipation is uniquely determined by the plastic strain rates for a material obeying the Tresca yield condition and the flow law associated with it through the generalized theory of plastic potential.

### 2.3 Limit Analysis

Limit Analysis deals with the determination of the load carrying capacity of rigid-perfectly plastic solids obeying all the rules mentioned in Section 2.2 including the observance of the concept of Plastic Potential sometimes referred to as the normality law.

As Limit Analysis has been used extensively in the solution of many problems concerning the load carrying capacity of structures including reinforced concrete slabs, it is thought important that the basic assumptions used in this analysis should be clearly understood, in the same way as the assumptions and restrictions of the theory of perfectly plastic solids described in the previous Section 2.2. For if reinforced concrete slab elements do not closely obey the principles of the theory of perfectly plastic solids or the principles of Limit Analysis then another method of solution more in keeping with its properties may have to be devised.

Drucker, Greenberg and Prager (1951) first put forward the principles of Limit Analysis and design, concerning the solution of load-carrying capacity problems in one, two or three dimensions. Prager [1] has explained the concepts of Limit Analysis more fully and demonstrated its method of application in different problems ranging from simple beams to cylindrical shells when used as a method of the theory of plasticity. Other applications including problems in Soil Mechanics are shown to be encompassed by the theory of Limit Analysis.

A brief list of definitions and laws used in Limit Analysis follows. A much more detailed description of the general theory can be found in relevant literature, much of which is due to Prager [1, 2] and references given therein. There are two fundamental theorems of Limit Analysis:

1) First theorem of Limit Analysis

In a rigid - perfectly plastic continuum, plastic flow cannot occur under loads for which a stable, statically admissible stress field can be found.

2) Second theorem of Limit Analysis

In a rigid - perfectly plastic continuum, plastic flow must occur under loads for which an unstable, kinematically admissible velocity field can be found.

Where;

a) A stress field is defined by making local stresses a function of position throughout the continuum. The stress field is statically admissible for given loads if it is in equilibrium with these loads and is stable if the stresses within it nowhere attain or exceed the yield limit.

b) A velocity field is defined by expressing the strain rate field in terms of velocities (i.e. rates of displacements) and their derivatives where the strain rate field is, as in the case of the stress field, defined by making the local quantities of strain rate functions of position throughout the continuum. The velocity field is said to be kinematically admissible if it satisfies the kinematical constraints to which the continuum is known to be subjected, (e.g. a beam with a built-in end has zero slope and deflexion at the built-in end as kinematical constraints) and is unstable for given loads if the strain rates associated with the loads produce a smaller power of dissipation for the whole

continuum than the power of dissipation of the loads.

The first theorem provides a lower bound on the true collapse load by employing statical considerations whilst the second theorem provides an upper bound on the true collapse load by employing kinematical considerations and by employing the principle of virtual velocities or virtual work.

The other theorem associated with Limit Analysis is the Theorem of Uniqueness and, briefly, states that an exact solution to the collapse load is obtained when the lower bound on the collapse load obtained from a stable, statically admissible stress-field coincides with the upper bound on the collapse load obtained from an unstable, kinematically admissible velocity field. A complete solution is obtained when a stable, statically admissible stress field is found for which a compatible unstable, kinematically admissible velocity field can be indicated.

#### 2.4 Plasticity in Beams and Plates

In traditional beam and plate theory in an elastic analysis the extension of the centre line is assumed to be zero and the angle between the centre line and cross section is assumed constant, or no membrane strains are considered and plane sections remain plane. In plastic theory applied to beam and plate problems it is likewise normal to assume that the rate of extension of the centre line and the rate of change of the angle between centre line and cross section is zero. Thus the only non-zero generalized strain rate is the curvature rate  $\dot{K}$  and the generalized stress

describing the state of stress at a cross-section associated with the non-zero generalized strain rate  $\dot{K}$  is the bending moment  $M$ . Thus the specific power of dissipation at a cross-section is given by the product  $M\dot{K}$  and for the continuum is the integral of the function described by  $M\dot{K}$  throughout the continuum with respect to position given by  $\int M \dot{K} dv$  where  $dv$  has the influence of length, area or volume depending on the type of structure under consideration. If  $P_k$  describes the generalized loads on the structure and  $\dot{p}_k$  describes the generalized velocities associated with these loads, then the power of these loads can be written as  $D = \sum_{k=1}^{\mu} P_k \dot{p}_k$  and by the principle of virtual velocities the fictitious external and internal power dissipation are equal, hence

$$\sum_{k=1}^{\mu} P_k \dot{p}_k = \int M \dot{K} dv$$

It is this equation of fictitious external and internal power dissipations that is commonly used to find the upper bound solution in Limit Analysis.

Proofs of the theorems of Limit Analysis are usually given when stress rates and strain rates are continuous functions of position throughout the continuum [1]. Discontinuous fields can however be accommodated [5] as can elastic - perfectly plastic materials, if, as in papers by Drucker, Greenberg and Prager (1951 - 1955) on the load - carrying capacity of an elastic - perfectly plastic structure, the changes in geometry due to elastic

deformations are regarded as insignificant.

The major assumptions made in Limit Analysis have therefore already been embraced by the idealizations and restrictions applied to perfectly plastic solids in Section 2.2. The assumptions commonly made in thin plate theory are also used in Limit Analysis and if these are good approximations in the 'plastic' range as well as the 'elastic' range at a reinforced concrete slab element then only the conditions for a perfectly plastic solid and considerations of geometry changes due to elastic deformations have to be satisfied.

#### 2.5 The solution of plastic plate problems

Complete solutions have been obtained by several investigators [1] for rotationally symmetrical loading and support conditions in plastic plate problems by integration of the governing equilibrium equation between certain points on the yield locus usually corresponding to the centre and the edge of the plate. However, in general, complete solutions are very difficult to obtain. Even some complete solutions have not been evaluated analytically. Numerical methods, such as the method of isoclines [6] or step by step iteration have been resorted to in cases where the solution of non-linear equations was required. It has been pointed out by Prager and Hopkins (1953) that the governing equations of equilibrium are elliptic and part elliptic - part parabolic for the Von Mises and Tresca yield conditions respectively. The solution of load - carrying capacity problems involving elliptical functions results in analysis of a first order, non-linear,

ordinary differential equation which normally can only be solved by numerical methods. [6] Thus a plate consisting of material obeying a yield condition with a non-polygonal yield locus, such as Van Mises, will be more difficult to deal with than one obeying a yield condition with a polygonal yield locus, particularly one in which the governing equations are all parabolic. [6] The Tresca yield condition provides this all-parabolic equation in the first and third quadrants of principal moment space in the yield diagram (Fig.2.2, ABC, DEF) where moments are of the same sign. However it is only in relatively simple support cases for which the whole plate will yield under moments of the same sign and hence points on the plate will be found where moments correspond to points in the second and fourth quadrants of the yield diagram (Fig 2.2 AF, CD) which are governed by elliptical equilibrium equations. Because of the difficulty presented by the solution of problems involving non-linear yield conditions it has become common to use the Tresca yield condition more frequently recently although the Von Mises yield condition has proved to be closest to the real yield criterion for ductile materials obtained from test results. Hodge [7] has pointed out the advantages of approximating a non-linear yield condition to a piecewise linear function and appropriately altered flow law [1]. Further reference to this technique is made in the following section 2.8.1c.

In cases where a complete solution cannot be found because a compatible kinematically admissible velocity field cannot be found

to coincide with a stable, statically admissible stress field, bounds on the correct solution must be obtained by use of the theorems of Limit Analysis. This method is used in most cases of unsymmetrical plates and exact but not necessarily complete solutions may be found when the upper and lower bounds to the collapse load coincide.

Because of the complexities involved with non-linear yield loci it is apparent that the collapse load of a plastically deforming plate may be considerably influenced by the yield condition and associated flow law used. Hopkins [8] has indicated the dependence of the complete solution of rotationally symmetrical plastic plate problems on the yield condition by comparing the solutions obtained when the Tresca, Von Mises and Johansen (Section 2.8.10) yield conditions are used. He points out that the solution of comparatively few classes of problems are independent of the shape of the yield locus in generalized principal stress space (plane strain is one such example). Although marked changes occur in the form of the governing equations, by the substitution of different yield conditions only relatively minor changes may occur in the macroscopic numerical features of the solutions whereas much larger errors than the  $\pm 8\%$  difference in collapse loads, as a result of the substitution of Tresca's yield condition for that of Von Mises mentioned by Hill [9], may occur in the microscopic features of the solution.

Hence, if the real yield condition obeyed by reinforced concrete slabs is found to approximate closely to the conditions

imposed on it by the Theory of Perfectly Plastic Solids and Limit Analysis, its form may appreciably affect the load-carrying capacity solutions predicted by other idealized yield conditions.

## 2.6 The inelastic behaviour of reinforced concrete slabs under uniaxial moment

Unlike the stress-strain diagram for a perfectly plastic solid as described in Section 2.2 (Fig 2.1) the composite of steel and concrete in a reinforced concrete structure provides far more complex characteristics. A perfectly plastic beam or plate, under pure uniaxial bending, has a stress distribution at a yielding cross-section which is asymmetrical as described graphically in Fig 2.3(a). If bending is positive (sagging) then the upper half of the beam or plate will be yielding in compression at the same time as the bottom half is yielding in tension. Every fibre across the section has reached the yield stress  $\sigma_0$  in tension or compression before plastic flow can take place. In a reinforced concrete beam or plate subjected to the same bending action as before, the stress distribution is far more complex and far from asymmetrical. The stress distribution at a cross-section is shown in Fig 2.3(b), (c), (d), (e) for a plate or slab with reinforcement near the tension face only. Fig 2.3 (b) describes the stress distribution on the cross section when a very small moment is applied. The concrete is still elastic in both the compression and tension zones as is the reinforcement. The neutral axis will be low and below mid-depth, (i.e. providing no reinforcement is present in the compression zone) its position

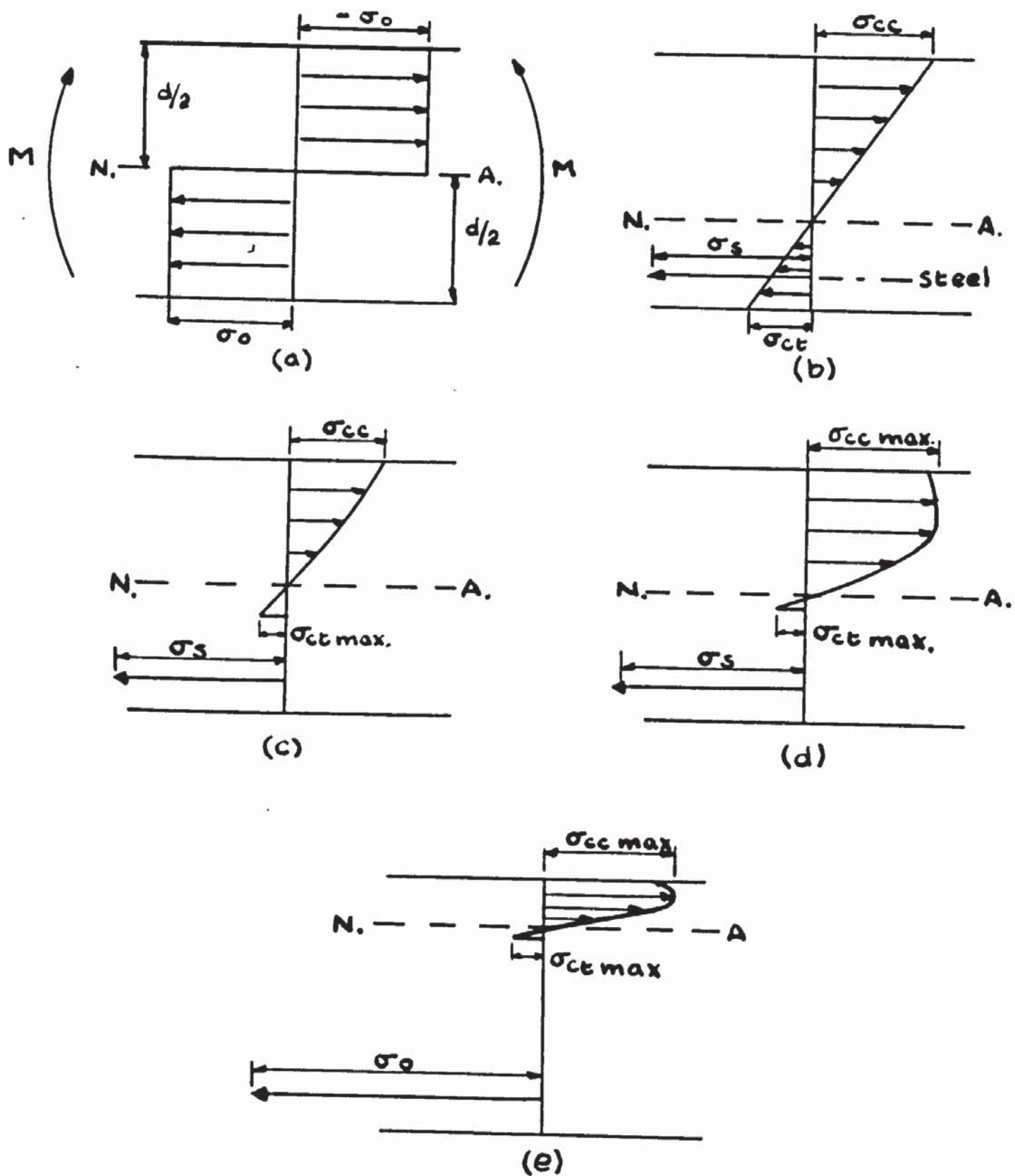


**FIG 2.3**

depending on the properties of the concrete and the properties and amount of reinforcement. As the moment is increased the stresses become larger in proportion to the strains, until the ultimate tensile strength of the concrete is reached at the bottom face. A crack begins to form and the stresses in the tensile concrete are gradually distributed onto the steel until at a higher moment the stress distribution takes the form of Fig 2.3 (c) where stresses in the concrete and steel can still be said to be elastic. As the moment is increased still further failure of the section will take place when the extreme fibres on the concrete compression face have reached their crushing strain. The steel stress may however be elastic or plastic by this time. Fig 2.3 (d) indicates the stress distribution on the cross section when the reinforcement stress is still elastic and the extreme concrete compression fibre is crushing. This type of cross section in which the compression concrete fails before the steel yields is known as an overreinforced section. Fig 2.3 (e) indicates the stress distribution on the cross section when the reinforcement stress has reached the yield stress in tension,  $\sigma_0$ . The steel stress will remain at this constant value of  $\sigma_0$  as the curvature is increased with a corresponding but small increase in moment due to the rising neutral axis, and hence increasing lever arm between tensile and compressive forces, upto a point at which the strain in the extreme concrete fibre has reached the crushing strain. This type of section is known as an underreinforced section.

Many design codes introduce the concept of a balanced section, at which the extreme concrete compression fibre crushes simultaneously with the reinforcement stress reaching the yield stress. Fig 2.4 (a) represents the moment-curvature characteristics of an underreinforced section. OA will be linear and represents the pre-cracking behaviour of the section where all concrete and steel stresses are elastic. At point A cracking occurs. The exact shape of the curve around point A will be non-continuous due to the sudden shedding of stress from the tensile concrete to the reinforcement. As the tensile concrete plays an increasingly less significant role in the resistance of the tensile forces the section AB of the curve is followed and represents the post-cracking behaviour of the section. The steel is still elastic and the concrete approximates closely to the elastic condition. At point B the reinforcement reaches its yield stress,  $\sigma_0$ , and an increase in moment capacity with increasing curvature is due to the rising neutral axis, as described previously. At point C the extreme concrete fibre crushes and the moment begins to drop as curvature is further increased. This falling curve develops as crushing progresses in the concrete fibres down to the neutral axis. The moment value at B is known as the yield moment of the section, the moment value at C as the ultimate moment. Usually the rise in moment between B and C is small compared to the rise in moment from O to B and thus the moment curvature relationship is often idealized into a bilinear or

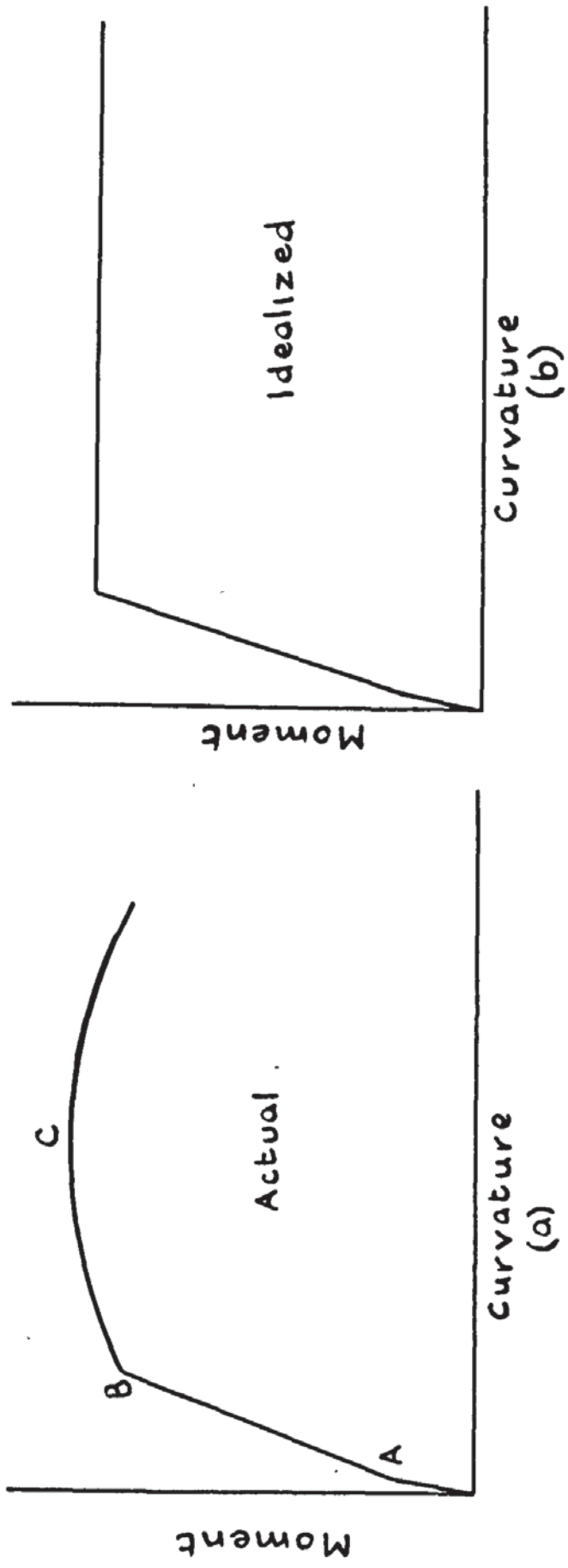


FIG 2.4

more accurately a tri-linear diagram Fig 2.4 (b). Although this moment -curvature diagram for uniaxial pure bending is a good approximation to the corresponding diagram for a perfectly plastic solid it must be remembered that assumptions have been made concerning the strain distribution across the section and the stress distribution in the compression concrete. The assumptions made in almost all theories are:

- 1) The strain distribution is linear i.e. strain proportional to distance from the neutral axis.
- 2) No slip or local band failure occurs between the reinforcement and the concrete.
- 3) The concrete carries no tensile stresses and hence cracking takes place up to the level of the neutral axis.

The concrete compression stress distribution curve varies in different theories, but for an under reinforced failure the compression zone is small and the shape of the distribution curve makes little difference to the ultimate load. The major points of the various theories concerning the failure of reinforced concrete beams have been reviewed clearly in the University of Illinois Engineering Experiment Station Bulletin 399 (1951) and selected theories have been examined by Evans (1943). The stress distribution in the compression concrete described previously in Fig 2.3 (d), (e) is often used and takes the form of the stress-strain curve obtained in pure compression tests on concrete. [24]

The normal procedure used in the ultimate load design of reinforced concrete beams or slabs under uniaxial moment is to equate the force in the yielding steel with the force in the compressive concrete at failure, and assuming the shape of the concrete compression curve, the ultimate moment is calculated. Fig 2.5 shows the assumed strain and stress distribution at failure. The depth to the centroid of the reinforcement from the upper surface is  $d_1$ , the depth to the neutral axis  $d_n$ , the area of steel  $A_{st}$ , the width of section  $b$ , and the crushing strength of the concrete  $u$ , The coefficient  $K_1$  defines the depth of the centroid of the compression curve as  $K_1 d_n$  below the upper surface and the coefficient  $K_2$  defines the average stress within the compression curve as  $K_2 u$ . Thus as usual the ultimate moment is given by the equations of equilibrium:

$$\text{Equating longitudinal forces} \quad A_{st} \sigma_o = K_2 u b d_n \quad (2.11)$$

and the resisting moment provided by these forces

$$M_{ult} = A_{st} \sigma_o (d_1 - K_1 d_n) \quad (2.12)$$

where  $M_{ult}$  is the ultimate moment

and, thus, by substitution

$$M_{ult} = A_{st} \sigma_o \left( d_1 - \frac{K_1 A_{st} \sigma_o}{K_2 u b d_1} \right) \quad (2.13)$$

The British Codes of Practice give values of the coefficients  $K_1 = \frac{1}{2}$  and  $K_2 = \frac{4}{9}$  thus assuming a rectangular stress block.

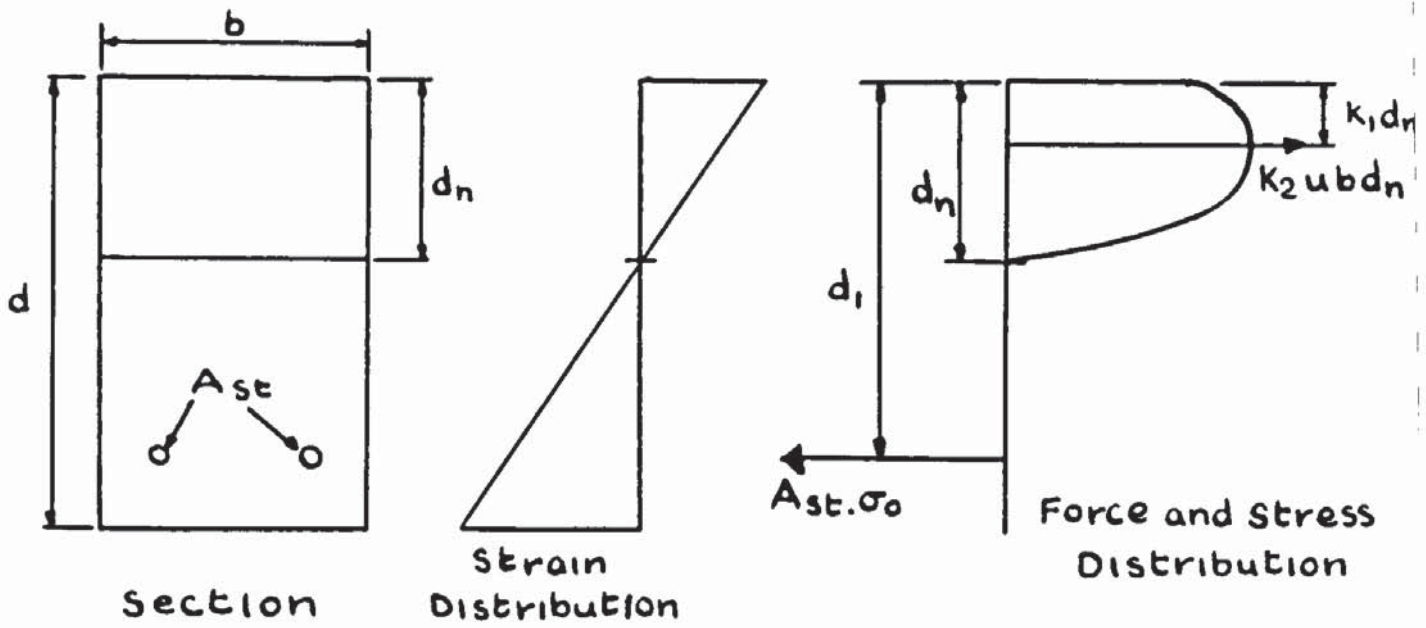


FIG 2.5

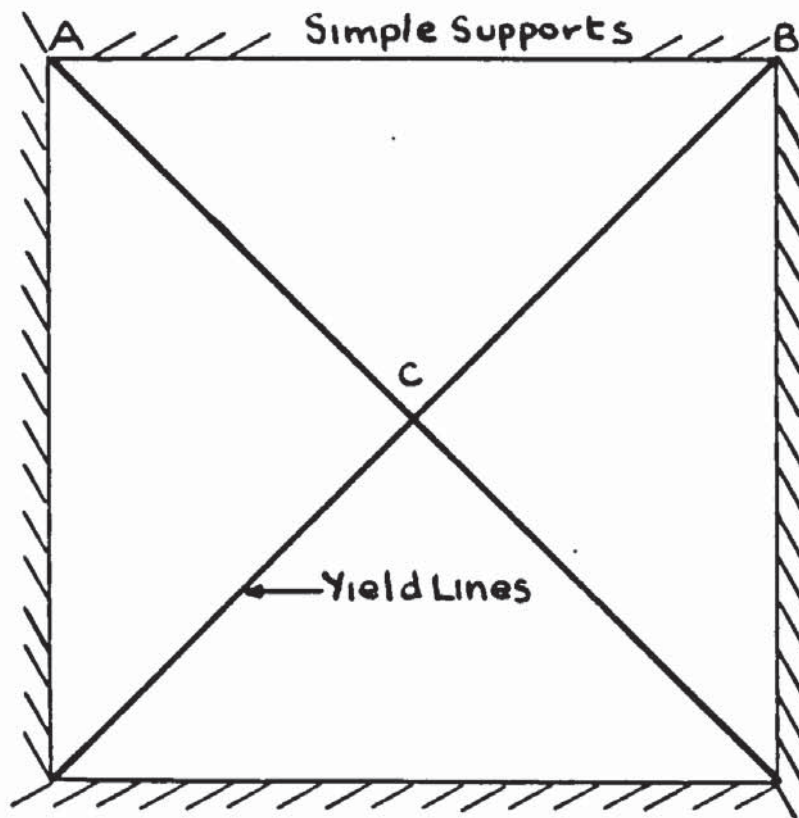


FIG 2.6

The advantage of ultimate load theory over elastic theory is that, unless the reinforcement can be arranged otherwise, a more economic design is possible particular for indeterminate structures. If a feasible and economic design is to be found the property of ductility of the structure is usually vital. Plastic sections in a framework must be capable of enough rotation to enable all other sections required to develop a failure mechanism to form. The same is true in the case of slabs where, as will be discussed later, 'yield lines' develop and must have the ductility required so that enough 'lines' can form for complete failure of the highly indeterminate slab. It is therefore necessary to ensure that the structure, be it beam or slab, is under reinforced if a safe and feasible ultimate load or inelastic theory is to be used. An over-reinforced element has far less ductility before concrete crushes and failure of the section can be said to have taken place.

So far only uniaxial bending has been considered when the reinforcement lay in the direction of the applied moment. It is when other loads are applied or non-symmetrical arrangements of reinforcement are used that ultimate load theory for slabs and even beams becomes less certain. Wood and Jones [10] in their chapter on assumptions and notation used in the ultimate load theory of slabs discuss briefly the combinations of stresses that can occur in a beam or slab. In the case of combined bending and torsion of beams, combined bending and axial loads and combined bending and out of plane shear complex interaction

curves exist between the two stressing components. Even these interaction relationships mentioned are not fully understood and yet all could be vitally important to the real failure criterion for a reinforced concrete slab. The overall interaction of these stresses in a reinforced concrete slab at failure is an extremely complex phenomenon which probably will never be understood completely. In this thesis axial loads and out of plane shear are assumed zero and the effects of combined bending and torsion are more carefully studied, along with the variation in direction of the reinforcement with respect to the applied moments.

## 2.7      Yield Line Theory

Yield line theory could be said to be a theory of plasticity or ultimate load theory applied to reinforced concrete slab structures. In Section 2.6 slabs or beams in uniaxial bending only were considered. Yield was assumed for reasons of symmetry to take place on a cross-section orthogonal to the direction of the applied bending moment. Generally of course slabs are two-way spanning structures and hence a more general moment distribution on an element in a reinforced concrete slab must be considered. The notations and systems usually adopted are used in this thesis and these can be found in books by Timoshenko [11] or Wood. [10, 12]

In 1921 Ingerslev [13] first developed a theory based on failure of a slab occurring when discrete lines of yielding formed in such a way that the slab acted as a 'mechanism' incapable of

withstanding an increase in load. Fig 2.6 shows a possible scheme that these yield or fracture lines could form to render the simply supported square slab a mechanism. Ingerslev assumed a constant normal moment to the yield line and zero twisting moment along the yield line.

Johansen<sup>[14]</sup> found that the normal moment on the yield line could not alone satisfy equilibrium of the elements of the slab bounded by yield lines. (e.g. ABC Fig 2.6). He introduced the concept of nodal or knot-force, to provide equilibrium. These concentrated forces acting at junctions of yield lines with edges or other yield lines were interpreted as the representation of the twisting moments and shear on a yield line. Thus two methods of analysis have developed from Johansens work. The first is an analysis by virtual work methods, the second is a so called 'equilibrium' method employing nodal forces. Work by Wood<sup>[10, 12]</sup> and Jones<sup>[10]</sup> has done much to clarify the methods, uses and objections to yield-line theory. Prager<sup>[1]</sup> has pointed out that Johansens 'failure mechanisms' constitute a kinematically admissible velocity field and thus the collapse load obtained is an upper bound in terms of Limit Analysis. Because the 'equilibrium' or 'nodal - force' theory only considers equilibrium across the yield line and not in the 'rigid' area of the slab the collapse load is also an upper bound solution. Johansens original intuitive yield criterion and flow law however are far from the form of those yield conditions used in Limit Analysis.

His yield criterion has been subtly altered to explain yield line theory in terms of Limit Analysis.

Although many problems, including some breakdown cases, have still to be solved in yield line theory in its own right, by far the most controversial and vital subject for argument has been the acceptance of a yield criterion and flow law for reinforced concrete slabs. A fair amount of confusion has developed in recent years because of a lack of understanding in detail of the implications of subtly differing yield criteria and a lack of information concerning the flow law. Wood [12, 16] has done much to clarify the situation but still no commonly acceptable yield criterion or flow law has been exhaustively established by experiment.

#### 2.8 Yield Conditions, flow laws and assumptions made for reinforced concrete slabs.

Most yield criteria have been based loosely on Johansens original intuitive relationships. However more recently varying yield criteria have been suggested particularly following work at the Building Research Station [12] where tests on one-way spanning slabs showed increases in load-carrying capacity of up to 16% when the reinforcement was rotated at an angle to the direction of the applied bending moment. Wood's [12] suggestions following tests of this kind also stimulated research into this field.

The development of yield criteria for reinforced concrete

slabs has roughly followed two paths. Firstly those criteria developed theoretically and preliminarily for the development of new or revised techniques in the solution of load-carrying capacity problems presenting particular difficulties within the original yield-line theory. [15] Some criteria have been developed theoretically in their own right and not for the purpose of justification of a new technique. [17, 18] Secondly, the criteria developed on both a theoretical and experimental basis. These are of the most significance, as, although they may not vary from the purely theoretical criteria, an attempt has been made at experimental justification which is the ultimate test of validity of any criterion and flow law. Some experimental work [19, 20, 21] has been carried out particularly on one-way spanning slabs that has not resulted in a new or revised criterion being produced, but in experimental justification of an existing criterion, within reasonable limits. More recent experimental work [22-29] has shown marked differences in conclusions and it will be shown that much can depend on even minor points in the test set up.

More detailed descriptions of each criterion and flow law developed and used will now be outlined.

### 2.8.1 Theoretically based yield criteria and flow laws

In the case of reinforced concrete slabs it is not general enough to consider only isotropic slabs. Slabs reinforced by a different amount in varying directions can be more economical

and are frequently used in practice. Orthotropic slabs such as these are allowed for in Johansens original yield criterion. In terms of the mathematical theory of plasticity therefore the yield condition is no longer described by the vanishing of an invariant as in Section 2.2 but is also a function of the angle at which the principal moments are inclined to the reinforcement.

a. Johansen's yield criterion [12, 14] and flow law.

This famous intuitive 'stepped' yield criterion is generally stated in the form

$$m_n = m \cos^2 \theta + \mu m \sin^2 \theta \quad (a)$$

$$m_t = \mu m \cos^2 \theta + m \sin^2 \theta \quad (b) \quad (2.14)$$

$$m_{nt} = m (1 - \mu) \sin \theta \cos \theta \quad (c)$$

$m_n$  is the normal bending moment on the yield line;  $m_t$ , the bending moment acting along or tangential to the yield line and  $m_{nt}$  is the twisting moment acting on the yield line.  $m$  is the ultimate moment due to the reinforcement in the X direction in Fig 2.7 if a uniaxial moment was to act in the X direction only.  $\mu m$  is the ultimate moment due to the reinforcement in the y direction in Fig 2.7 with uniaxial moment in y direction only.  $\mu$ , the coefficient of 'orthotropy' is usually given the condition

$$0 \leq \mu \leq 1$$

This criterion is obtained by considering local equilibrium on the yield line when all bars crossing it are yielding. The general moments  $m_n$ ,  $m_t$ ,  $m_{nt}$  are thus derived from the standard transformation of moment equations with the implicit

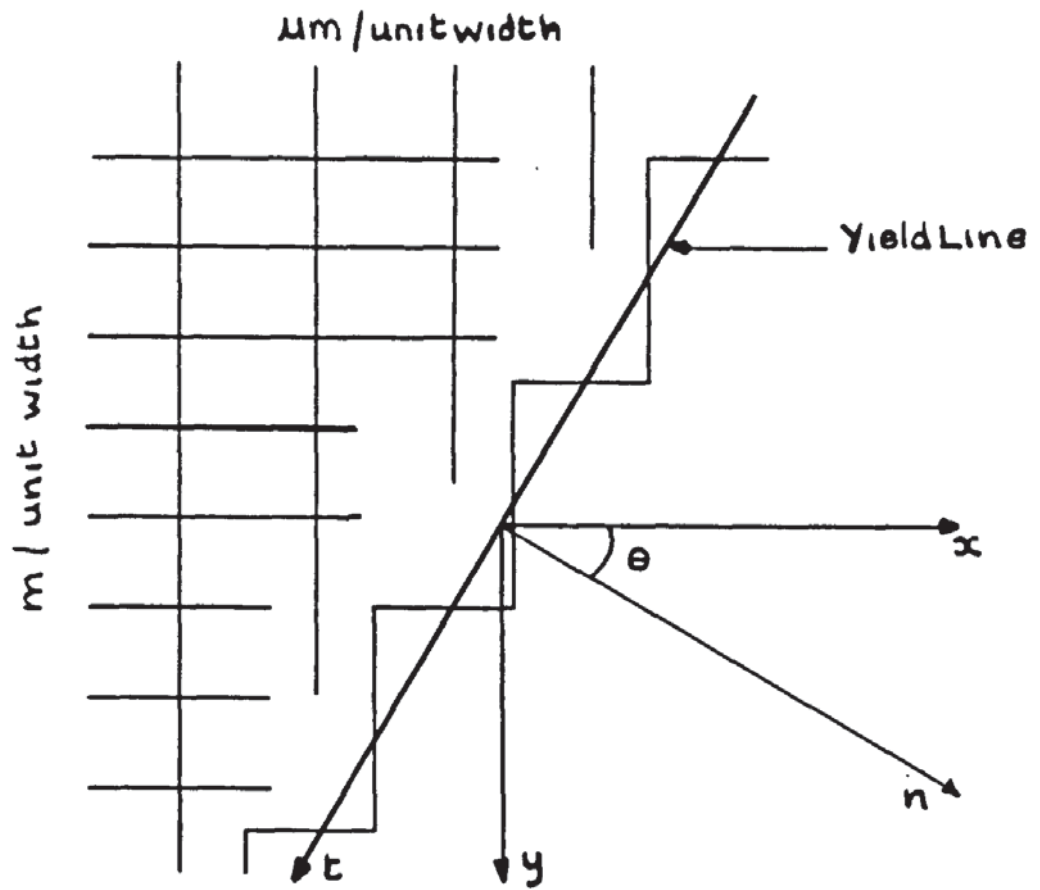


FIG 2.7 JOHANSENS 'STEPPED' MODEL

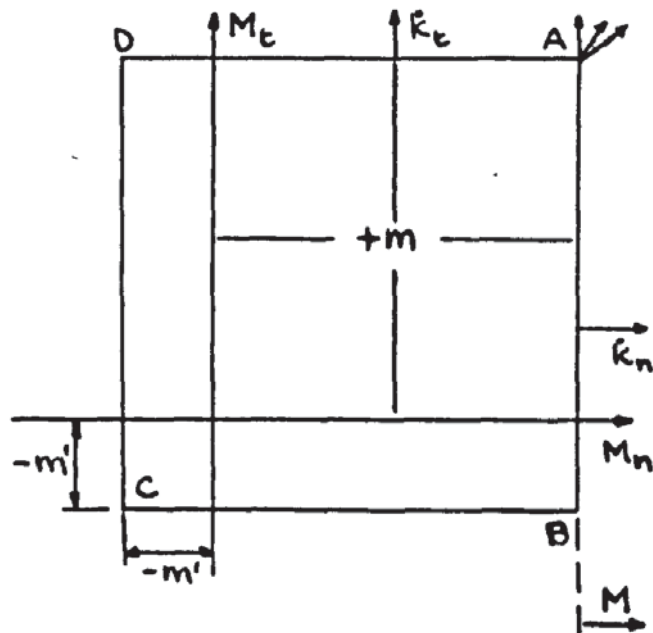


FIG 2.8 SQUARE Y.C.

condition that the principal moments during yielding are in the directions of the bars and are equal to the ultimate moments if uniaxial moment was applied in those directions. This condition is derived by imagining the yield line to be made up of an infinite number of steps running parallel to the bar directions. It has been pointed out that this 'stepped' yield line is kinematically inadmissible. The criterion is derived simply from resisting moments or section properties of the slab and takes no account of the combination of applied moments. All three equations in equation 2.14 are defined when yield takes place and hence severer restrictions are placed on mode of yield as Wood has shown. [10, 12 16] In addition to the yield criterion, Johansen allowed yield lines to form at any orientation to each other, be they positive yield lines or negative yield lines.

#### b. Square Yield Criterion

This criterion which is often accredited to Johansen has, in fact, basic differences with the original criterion of equation 2.14. The criterion was developed for use with Limit Analysis techniques and is usually represented graphically as in Fig 2.8 and only for isotropic slabs. Plastic potential or normality of strains as described in Section 2.2 is assumed to hold. This polyginal yield locus is drawn in principal moment space, following the convention used in the Tresca and Van Mises's yield loci. The square yield locus is obtained by first putting  $\mu = 1$  in Johansens yield criterion (equation 2.14)

thus

$$\begin{aligned} mn &= + m & (a) \\ mt &= + m & (b) \\ mnt &= 0 & (c) \end{aligned} \quad (2.15)$$

for negative yield lines

$$\begin{aligned} mn &= - m' & (a) \\ mt &= - m' & (b) \\ mnt &= 0 & (c) \end{aligned} \quad (2.15)$$

where  $- m'$  is negative ultimate moment in n direction.

However it can be seen that equation 2.15 denoted the state of stress at A on the square yield criterion and equation 2.16 the state of stress at C. Mixed positive and negative states of stress are not catered for. Thus the square yield criterion uses equation 2.15 (a) and (c) and equation 2.16 (a) and (c) only, discarding equation 2.15 (b) and equation 2.16 (b) so that the equilibrium equation can be satisfied as the stress state on a slab passing from A to B say. [16]

The flow law is now that of plastic potential theory and thus plastic curvatures can only take place in the direction of the external normal to the yield locus at the stress state considered for a stress state at B or D where positive and negative yield lines meet, plastic potential restricts these plastic curvature rates to a mutually orthogonal direction. Although these curvature rates need not be equal this condition insists that positive and negative yield lines meet at right

angles. Johansen does not state this restriction and tests tend to show that it is an incorrect assumption.

In Mansfield's [3] work on the solution of load-carrying capacity problems for plates obeying the square yield criterion by the utilisation of the calculus of variation (later shown to be the mathematical equivalent in the virtual work method to the steps taken in determining the nodal forces in the 'equilibrium' method [10, 15, 16]) the condition of orthogonality of positive and negative yield lines was disregarded.

#### c. Normal moment and Tangent-Line Yield Criteria

The use of the square yield criterion with its insistence on orthogonality of positive and negative yield lines which are also restricted to being principal moments invalidates many often considered yield mechanisms. [16] Work carried out using nodal force techniques was unduly restricted by the square yield criterion where  $M_n$  and  $M_t$  are principal moments. Kemp and Morley [15] utilised the fact that only the normal moment  $M_n$  on a yield line appeared in the virtual work equations and thus Johansen's equations defining  $M_t$  the tangential moment and  $M_{nt}$ , the twisting moment on the yield line in equations 2.14, 2.15 and 2.16 were disregarded, retaining only the equation defining the normal moment  $M_n$ . Thus the principal moment in an isotropic slab no longer necessarily acts normally to the yield line and the square yield criterion may be violated. Thus this criterion, devised to allow a greater flexibility in the use of upper-bound

stress fields is based entirely on the fact that the energy dissipation on a yield line  $M \overset{\circ}{K}_n$  would not change if the normal moment, although not necessarily a principal moment, were somewhere on the tangent line to AB say in Fig 2.8. This tangent-line criterion as described by Wood [15, 16] has led to certain controversy when applied to a fictitious upper-bound stress field obeying Von Mises' yield condition. Wood [15, 16] insisting that the yield criterion for a material is known 'a priori' shows that, by assuming a yielding conical portion surrounding a yielding spherical central portion of the circular simply supported plate, no load can be supported by the plate. Save [18] refutes Wood's conclusion and states that the moment - states in the conical and spherical portions of the plates may lay anywhere on the tangents to the Von Mises yield locus at the actual moment coordinates describing these regions (Fig 2.9) Save then arrives at a complete solution

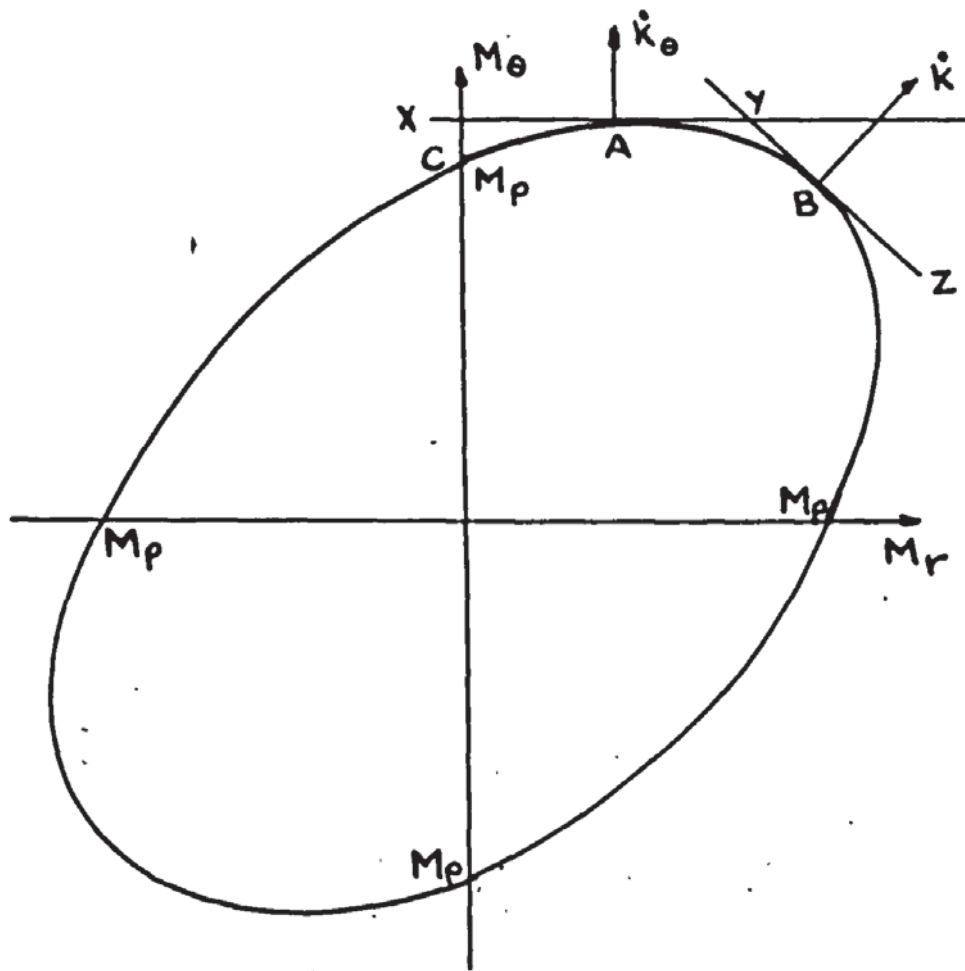
$$P = 6.67 \pi M_p$$

where  $P$  is total collapse load uniformly distributed over the plate and  $M_p$  the plastic moment in uniaxial bending. This exceeds the exact solution of  $P = 6.52 \pi M_p$  given by Hopkins and Wang [6] and is as Save admits the solution to a plate obeying a piece-wise linear yield condition and is therefore an approximation to the real yield condition of Von Mises. As described in Section 2.2 the solution of problems in which the material obeys a polyginal yield locus are more easily soluble

than those in which the yield locus is non-polyginal. However to say that Wood's approach and conclusion is incorrect because an approximation to the yield condition has resulted in a complete solution being obtained is wrong. The definition of an upper-bound field of generalized stress given by Morley [15] states that it must satisfy equilibrium and furnish a rate of work equal to the specific dissipation. Wood in effect has shown that the assumed upper bound stress field does not satisfy equilibrium conditions. This is not at all surprising when it is considered that the conical yielding portion is assumed to be in plastic regime A in Fig 2.9 throughout and yet at the edge of the simply supported plate  $M_r = 0$  and must be in regime C a condition used by Prager and Wang [6] to obtain the real complete solution.

Thus the assumed spherical - conical upper bound stress field is not a valid stress field for a material obeying the Von Mises yield locus as the plastic regime in the 'conical' portion varies from c at the edge to B in the central portion and does not remain as a plastic regime A throughout. The polyginal approximation XAYBZ (Fig 2.9) allows the assumed upper bound stress field to be valid as yield takes place in the same direction throughout the conical portion.

The use of criteria which depend on energy dissipation considerations only, may be used in nodal - force theory in the 'equilibrium' method or in the virtual work method used with



A - Peripheral Conical régime  
 B - Central Spherical régime

FIG. 2.9

fictitious upper-bound stress fields even though they do not seem to satisfy the basic requirements of a yield criterion. When, however, an approach is taken through the use of Limit Analysis it is necessary to find a lower bound solution to the collapse load. Energy dissipation is no longer a criterion of solution. Equilibrium conditions now govern the moments, which must nowhere exceed the yield condition.

d. Kemp's yield condition and flow law [17]

In 1962 Kemp [31] reduced the discrepancy between upper and lower bound solutions to the collapse of an orthotropically reinforced, simply supported, rectangular slab to a maximum value of 1½%. Previously, discrepancies between the bounds had been about 10%, using the assumed lower bound stress field suggested by Sawzuk [32] in 1957. By considering more carefully the stress-state in the corners of the slab, which has been shown to be critical by Wood [12], Kemp was able to adjust the assumed moment-field and hence reduce the discrepancy between the bounds, by comparing the normal moment of the assumed moment-field with Johansen's yield criterion in all directions. (equation 2.14)

Kemp begins by assuming the same physical property criterion as is used in the square yield criterion. That is by discarding the equation defining  $M_t$ , the tangential moment in equation 2.14. In the orthotropic slabs considered however this leads to

$$\begin{aligned}
 m_n &= m \cos^2 \theta + \mu m \sin^2 \theta \\
 m_{nt} &= m (1 - \mu) \sin \theta \cos \theta
 \end{aligned}
 \tag{2.17}$$

unlike the square yield criterion for isotropic slabs where the  $\mu$  is put equal to 1 in equation 2.17.

Then by using the general moment transformation equations in terms of principal applied moments  $M_1$  and  $M_2$ , the applied moment in the direction  $\psi$  from the maximum principal moment direction is given by

$$\begin{aligned}
 m_n &= M_1 \cos^2 \psi + M_2 \sin^2 \psi \\
 m_{nt} &= (M_1 - M_2) \sin \psi \cos \psi
 \end{aligned}
 \tag{2.18}$$

By equating applied moments to resisting moments, the condition for yield is obtained

$$\begin{aligned}
 m_n &= M_n \\
 m_{nt} &= M_{nt}
 \end{aligned}
 \tag{2.19}$$

This leads to the yield condition

$$mM_1 (\sin^2 \phi + \mu \cos^2 \phi) + mM_2 (\cos^2 \phi + \mu \sin^2 \phi) - M_1 M_2 - \mu m^2 = 0 \tag{2.20}$$

where  $\phi = (\theta - \psi)$

and the angle  $\psi$  is found from

$$\tan 2\psi = \frac{m (1 - \mu) \sin^2 \phi}{(M_1 - M_2 - m (1 - \mu) \cos 2\phi)} \tag{2.21}$$

the curves of  $m_n$  and  $M_n$  are reproduced in Fig 2.10. The yield loci representing equation 2.20 and its negative moment counterpart are reproduced in Fig 2.11 and are composed of two hyperbolas. It should be noted that as both normal moments and twisting moments

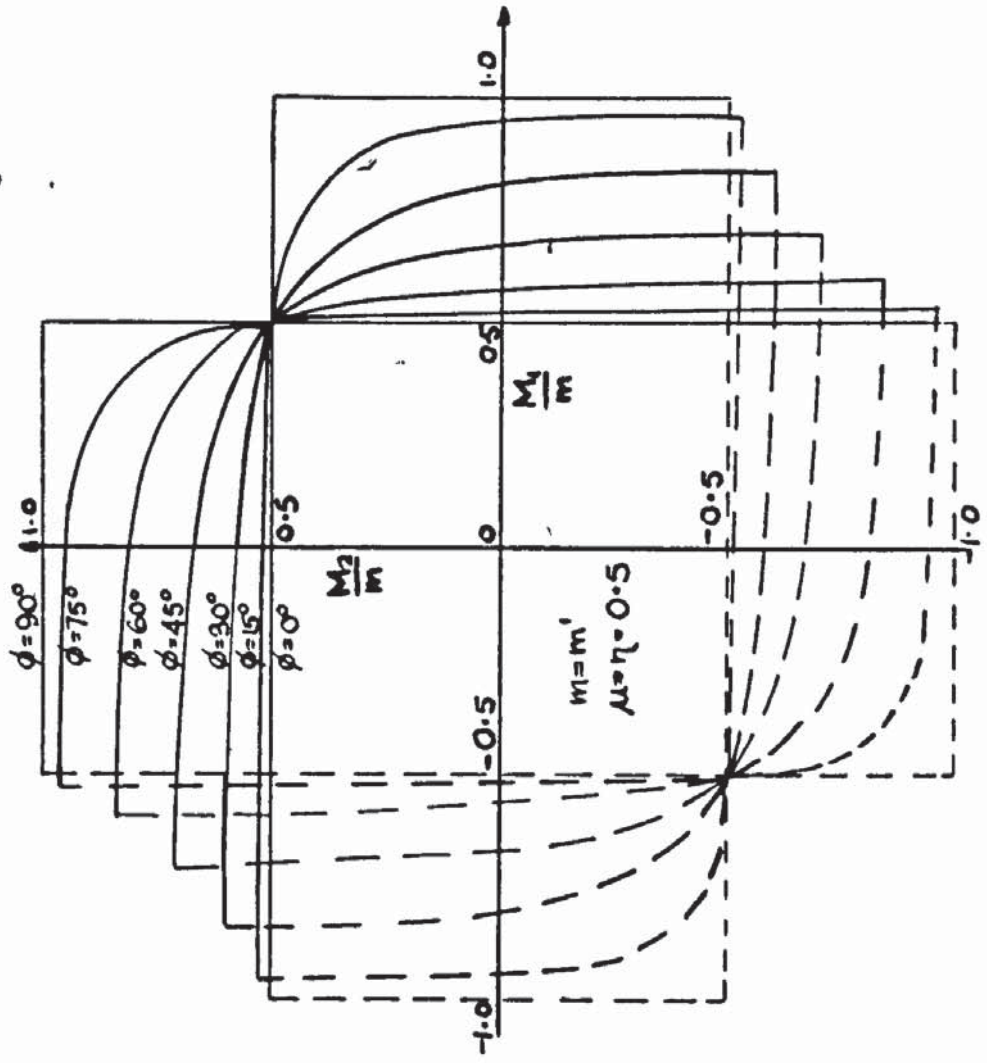


FIG 2.11 YIELD CONDITION-KEMP

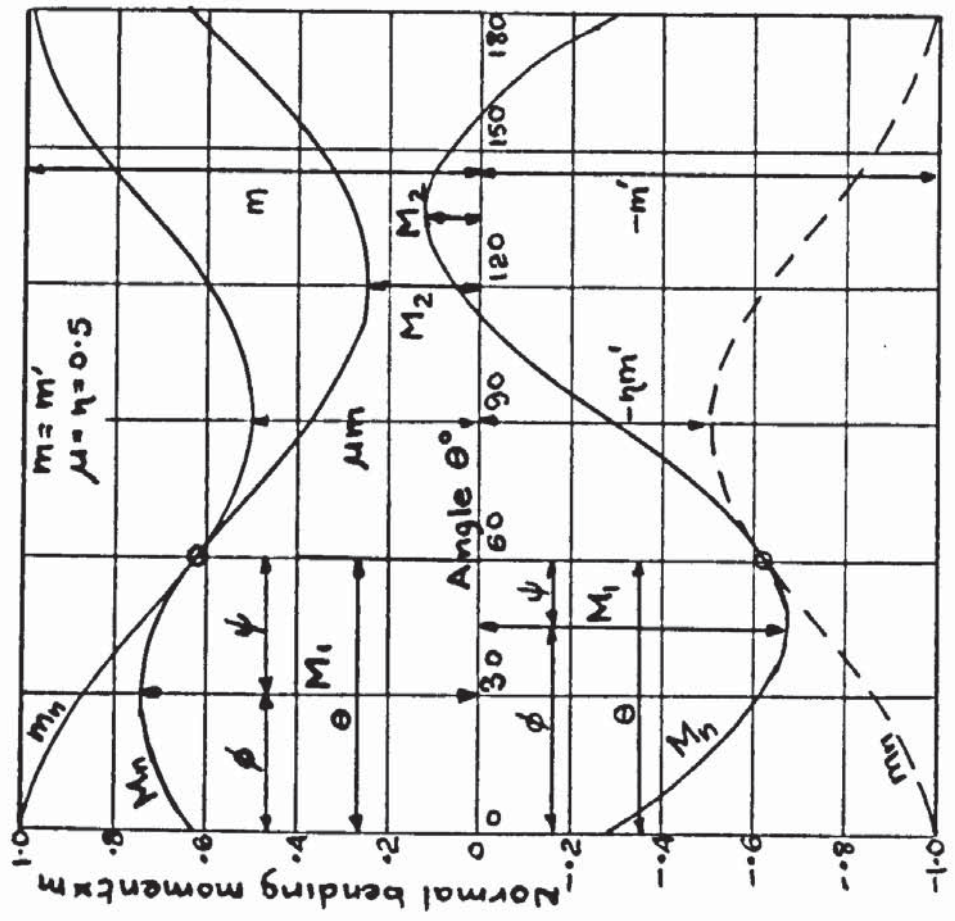


FIG 2.10 FAILURE IN SLAB - KEMP

are derived from general equilibrium consideration in the case of both resisting and applied moments, the value of  $\psi$  which fixes the yield line direction will be the same when considering equalities of normal or twisting moments. Kemp goes on to show that by expressing equation 2.20 in terms of the general moments  $M_x$ ,  $M_y$ , and  $M_{xy}$  the yield condition may be written independently of angle.

$$(m - M_n) (\mu m - M_y) - M_{xy}^2 = 0$$

for positive yield (2.21)

and  $(m' + M_x) (\beta m' + M_y) - M_{xy}^2 = 0$

for negative yield.

By comparing the flow rule given by equation 2.21 with the direction of flow predicted by the theory of plastic potential (Section 2.2) Kemp found that they were coincident and hence deduced that a material obeying the yield criterion of equation 2.17 suitably transposed to equation 2.20 obeyed the normality law and could thus be used in the Limit Analysis theory.

Although Save [18, 33], Nielsen [25] and Wolfensberger [4] have arrived independently at the same yield condition described in equation (2.21) albeit in slightly different form, the approach has slightly varied.

Save's [18, 33] approach has been to accept only the physical property criterion describing the normal moment  $m_n$  in equation 2.17. Then by using the moment transformation equations in terms of  $M_x$ ,  $M_y$ ,  $M_{xy}$  equating the applied moment to the resisting moment and making use of the fact that the

yield condition will have the form [33]

$$F ( M_x, M_y, M_{xy}, \theta ) = 0 \quad (a)$$

$$\frac{\partial F}{\partial \theta} = 0 \quad (b)$$

the same equation 2.21 is found to hold. The condition of equation 2.20 (b) is synonymous with Kemp's approach of equating twisting moments.

Massonett and Save's [33] formulation of the conditions needed to be satisfied (equation 2.22) to produce the yield surface do not depend on Johansen's physical yield criterion (equation 2.14) in any way, as the criterion is simply described as a function of  $\theta$  to be deduced experimentally. It was only later [18] that the normal - moment yield criterion, in the same form as Johansen's equation for normal plastic resisting moment, was substituted in equation 2.22 as the required function of  $\theta$ . Thus although the yield condition described by Kemp, Save etc has been an important advance it has not in any way changed or developed the physical plastic behaviour criterion and still uses, although in slightly modified form, Johansen's first assumed criterion given in equation 2.4

It is therefore necessary to review the experimental work carried out to investigate the real form of the physical, plastic or ultimate behaviour of reinforced concrete slabs.

#### 2.8.2. Experimentally based yield conditions and flow laws.

Wood, [12] Park [35], and others have shown the importance

of in - plane membrane forces in the collapse load of a real slab. However before membrane forces can be considered the yield criterion of reinforced concrete slabs in pure bending must be found and following Wood's [12] suggestion several investigators have attempted the testing of reinforced concrete slab elements rather than whole slab structures.

a. Tests by Johansen [14] Bach and Graf [36]

Johansen compared the collapse load predicted by his yield line theory and using his yield criterion with results of slab tests carried out by himself, Bach and Graf. He found that reasonably good agreement existed. However these experiments were not an explicit test of the yield criterion and it can only be concluded that the overall effects of his assumptions in the yield line theory are reasonably close to the real collapse load of a slab.

b. Tests by Kwiecinski [22]

It was implicit in Johansens derivation of the yield criterion given by equation 2.14 that the bars remained straight during yielding and hence the yield force in the bar acted in the original direction of the bars. After the tests reported by Wood [12] which gave moment capacities approximately 16% in excess of those predicted using Johansens yield criterion a suggestion [12] was made that the reinforcement may 'kink' across the crack so that it was normal to the yield line. This is usually represented as in Fig 2.12. Equilibrium at the yield

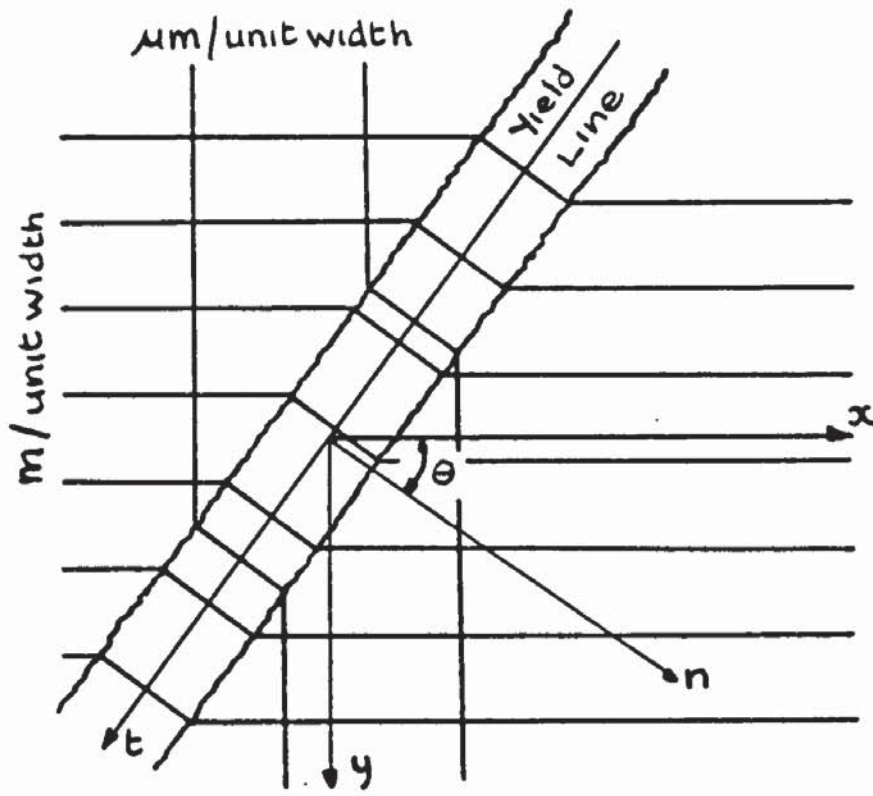


**FIG 2.12 FULL KINKING**

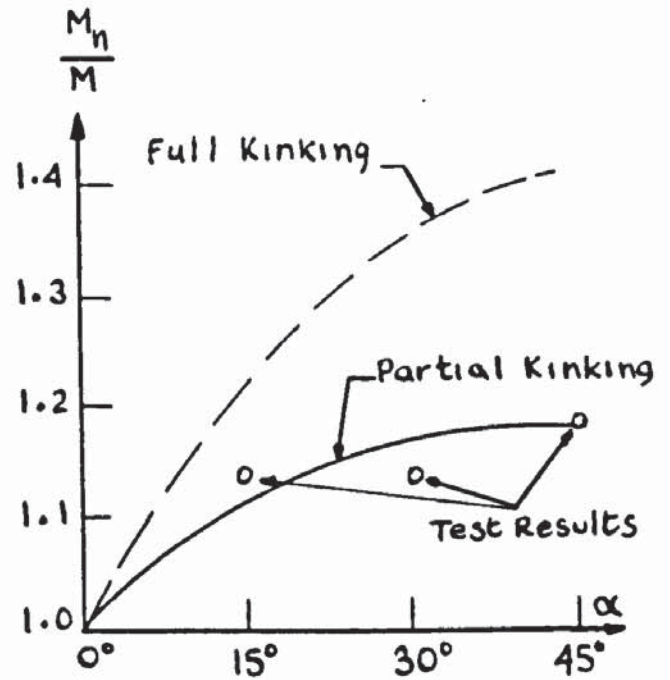
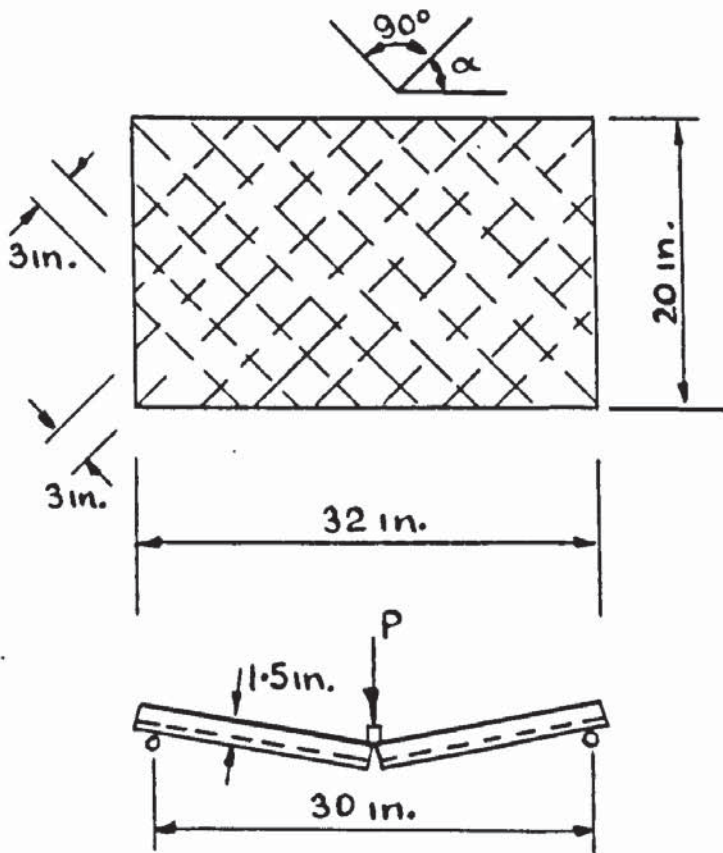


**FIG 2.13 KWIECINSKI PARTIAL KINKING**

line for this complete kinking will give a yield criterion.

$$\begin{aligned} m_n &= m \cos\theta + \mu m \sin\theta \\ m_{nt} &= 0 \end{aligned} \quad (2.23)$$

This twisting moment of resistance becomes zero because it is still assumed that the force in the tensile zone of the slab available to act along the yield line and hence form a couple with the force in the  $t$  direction in the concrete at the yield line resisting the applied twisting moment can only be the component of the axial forces in the bars in that direction.

This criterion predicts higher failure moments but it was realised that complete 'kinking' was too much of an idealization as crushing of the concrete at points such as P in Fig 2.12 would reduce the angle through which the bars actually kinked. Kwiecinski<sup>[22]</sup> developed a theory on the two basic assumptions.

- 1) Partial 'kinking' of the reinforcement across the crack.
- 2) No twisting moment on a yield line.

Along with these assumptions, the usual idealizations made in reinforced concrete bending theory including zero bending and shear stiffness of the reinforcement were implicitly accepted. Tests were carried out, on 16 approximately isotropic slabs in uniaxial bending set up as a one way spanning plank with a concentrated line load across the slab at mid span (Fig 2.13).

The slabs measured 32 in x 20 in x 1.1/2 in thick. Threaded mild steel wires of approximately 0.1 in diameter exhibiting a distinct plastic 'plateau' were spaced at 3 in centres in both orthogonal layers. The mesh so formed was rotated with respect to the longitudinal axis of the slab so that tests were carried out on slabs with  $\alpha = 0, 15^\circ, 30^\circ, 45^\circ$  where  $\alpha$  is the inclination of one set of bars with respect to the longitudinal axis.

Fig 2.13 also shows how the moment is enhanced by rotation of the mesh. A maximum value of 18.8% at  $\alpha = 45^\circ$  is obtained from this theory. The test results which look to be in fairly good agreement with the theoretical curve have been obtained only through modification of the actual results recorded. Because only about seven bars crossed the yield line and were provided with no extra anchorage at their ends bond failures were frequent. Kwiecinski considered a reduced width of slab, the reduction relying on an estimate of the number of bars actually involved in resisting the bending moment.

c. Tests by Hovbolt<sup>[19]</sup>, Silverj<sup>[20]</sup>, and Peter<sup>[21]</sup>

Tests carried out by these authors, although not necessarily directly concerned with the 'kinking' phenomena, provide useful information in this respect.

Chronologically, Hovbolt's test program was first. Carried out in 1942, its object was to examine the effectiveness

of reinforcement in skew bridge slabs. However the results obtained can be used as a measure of kinking. The test specimens were longer than those of Kwiecinski, measuring 63 in x 63 in x 5.17 m. The mode of testing however was similar, the slab being set up as one way spanning with loads applied at third points. Knife-edge supports allowed no lateral movement. The bars were hooked at the ends preventing the severe bond problems experience by Kwiecinski.

Instead of the enhancement of moment capacity expected if kinking were to exist a tendency for the moment capacity to decline when the direction of the reinforcement mesh deviated from the span-direction was observed.

As described for all the experimental work reviewed, the conditions imposed in the experimental test set up seems to be of considerable importance. The major factors affecting Houbolt's results are

- 1) No lateral movement of supports allowed.

Membrane forces may then be set up especially at large deflexions affecting the results.

- 2) Partial restrictions imposed on the twisting of the slab. Kinematically yield lines can only form perpendicular to the span if the slab remains seated uniformly on the supports. Hovbolt however reported cases in which the slab corners lifted from the support (See also Ch. 5.) indicating a

strong tendency that the twisting moments in the slab were trying to minimize the moment capacity for that particular arrangement of reinforcement.

The latter effect is one to which all slabs on unyielding supports and subjected to uniaxial moment may be subject.

Silverj [20] attempted a somewhat more sophisticated assembly for testing slabs under uniaxial bending. The size of his test slabs was 65 cm x 65 cm x 4.5 cm but the shape in plane varied slightly depending on the angle at which the unidirectional bars were placed as shown in Fig 2.14. The coefficient of orthotropy was thus zero and the test carried out by loading at the 24 points indicated in Fig 14 showed no tendency for the moment capacity to be enhanced. Fig 2.14 also shows the results obtained from the series of nineteen tests,  $j$  being the distance from the reinforcement to the centre of the compression block and  $n$ , the number of bars crossing the test area, these parameters being introduced in an attempt to standardize the results. The test rig is liable to the same condition 1) mentioned earlier but this time twisting movement was completely restricted by the support conditions. A further objection to the results is that the moment at which cracking occurred was of the same magnitude as the yield moment.

Peter's [21] tests were carried out on a plate subjected to torsion and not to bending. The bars were hooked and the

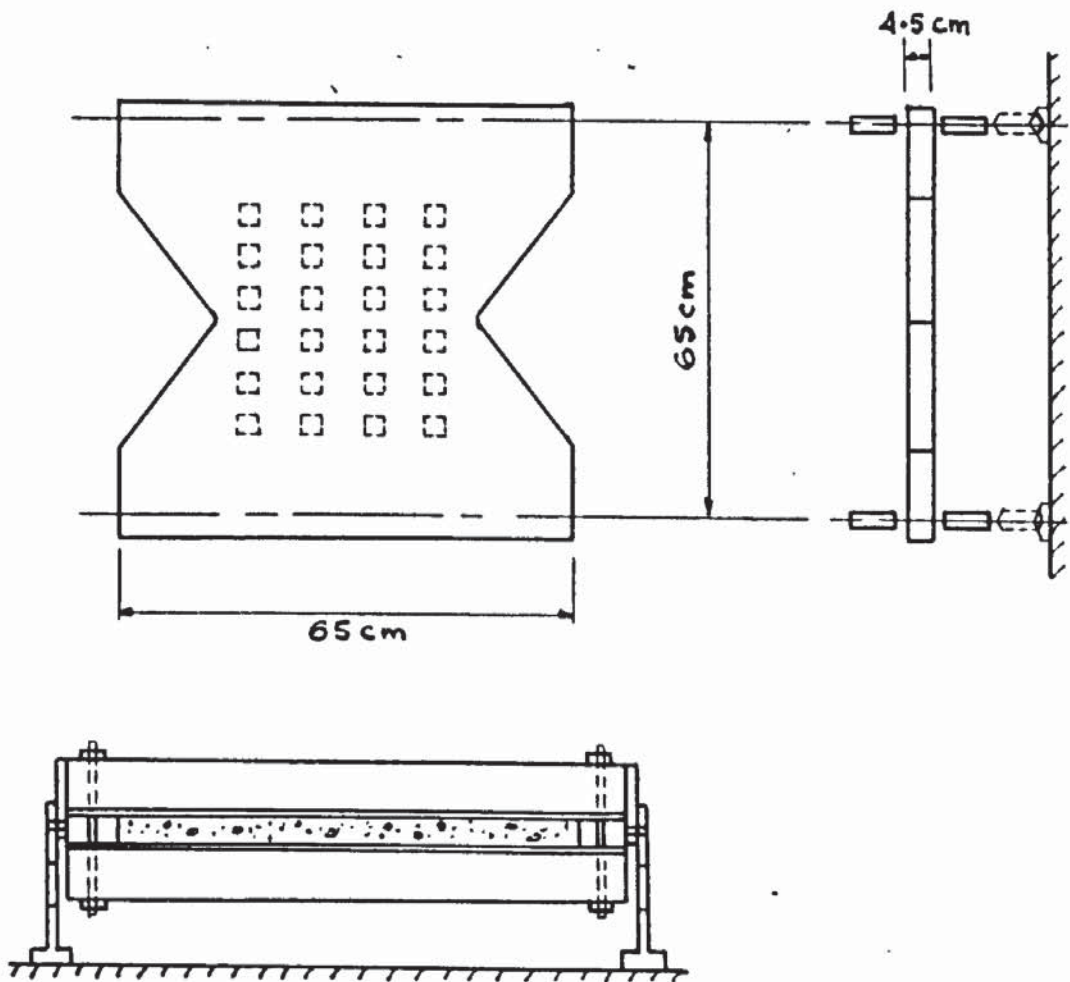


FIG 2.14 SILVERTJ TESTS

two layers were not necessarily orthogonal as was the case in Houbolt's earlier work. Peter concluded that 'kinking' was a local phenomena only related to the crack and reinforcement characteristics and his test results indicate as do those of Houbolt and Silverj that no significant change in ultimate load was effected.

The four following references deal with direct investigations into the yield criterion and flow law for reinforced concrete plates.

d. Tests by Baus and Tolaccia [23, 24]

Work carried out by Baus and Tolaccia under the direction of Professors Louis and Massonett at the University of Liege in 1963 was the first attempt to test an orthogonally reinforced concrete slab element subjected to biaxial and uniaxial moments for the express purpose of finding an experimental yield criterion for slabs in pure bending. The arrangements for testing are shown in Fig 2.15. The slabs measure 130 x 130 x 8 cm. Reinforcement is provided by 10 mm. bars with a good plastic 'plateau'. The moments were applied through the jack and lever arm system shown in Fig 2.15. Jacks marked A or B carrying the dead load of the system depending on whether a positive or negative moment is being applied. The moments applied will be principal moments  $M_1$  and  $M_2$ .

The conditions that the authors set out to meet are

- 1) The ability to introduce moments of the same

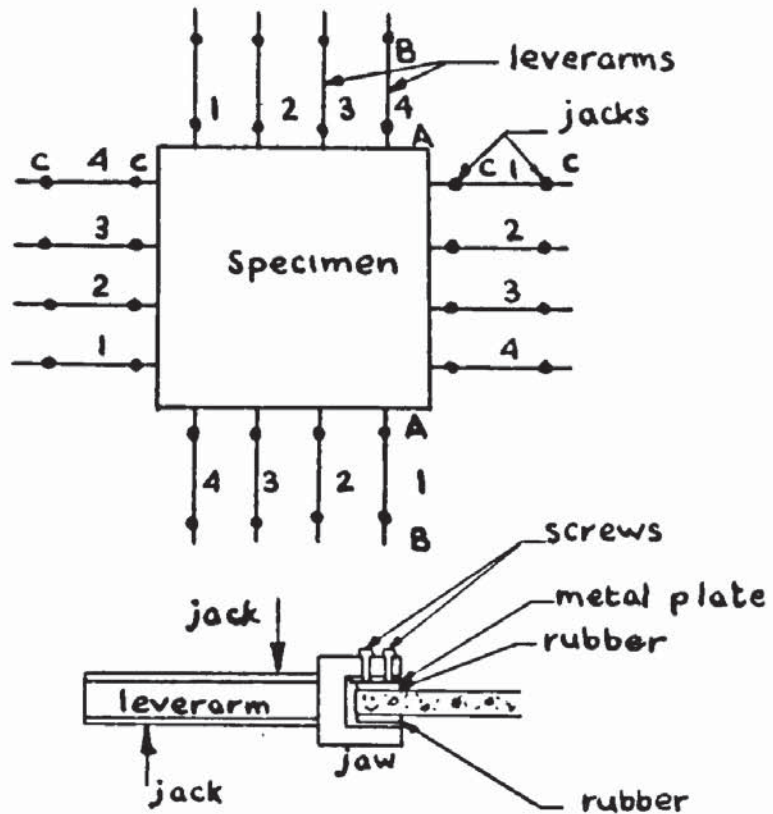


FIG 2.15 LOADING SYSTEM (LIÉGE)

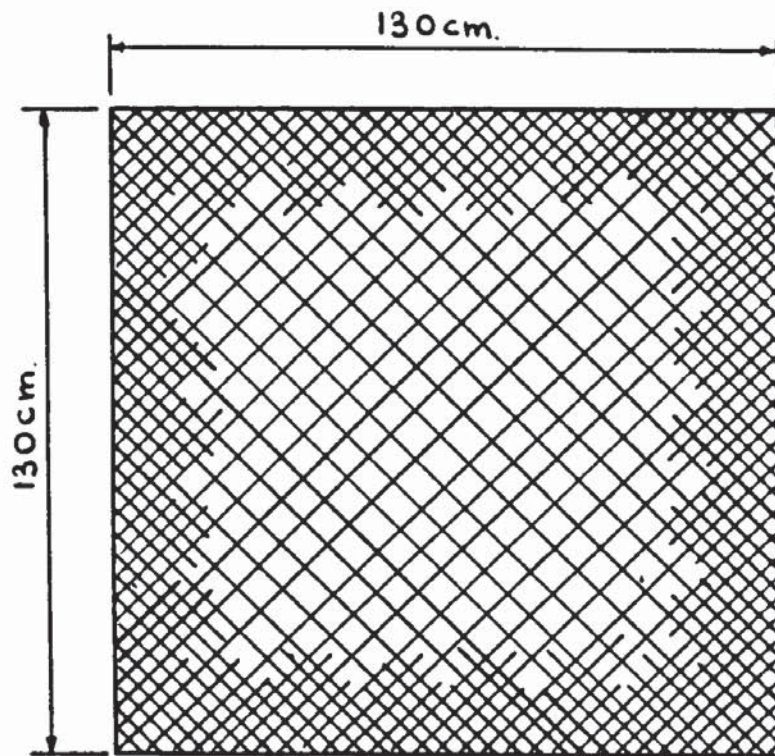


FIG 2.16 TYPICAL MESH (LIÉGE)

sign and of opposite sign in the two orthogonal directions.

2) The introduction of the moments had to interfere as little as possible with the free deformation of the edges of the slab.

3) The moments acting on the edges must be distributed as evenly as possible and their values must be known at any time.

4) There should be no shear force acting on the slab.

5) There should be no membrane forces acting in the slab.

It was considered that their test set up satisfied these conditions although it is not made clear how membrane forces were eliminated.

About 40 slabs were tested with the inclination of the orthogonal mesh at  $0^\circ$ ,  $22.5^\circ$ ,  $30^\circ$  and  $45^\circ$  to the sides of the slab. Some slabs were reinforced with a mesh adjacent to the upper surface as well as the usual mesh adjacent to the undersurface. The bars were spaced at 6 cm centres providing a near isotropically reinforced slab. The coefficient of orthotropy can be calculated to approximately  $\mu = 0.815$  using the yield moments in the reinforcement directions calculated by the authors. Fig 2.16 shows a typical reinforcement layout. The extra reinforcement around the periphery was spot welded to provide additional strength in the proximity of the

jaws, thus guarding against failures due to stress concentrations.

The principal moments in each test are in a different ratio and although it is not expressly stated, it is assumed that the moments are applied proportionally in that ratio from zero moment up to failure. This condition of proportional loading is of paramount importance in plastically yielding structures [1, 2].

The experimental yield criterion which is similar for varying angles is of the form shown in Fig 2.17.

It can be seen to vary considerably from the square yield criterion. It now represents a concave yield locus which is not permissible in the theory of perfectly plastic solids (Ref 1 and Section 2.2). The increase in moment capacity when  $M_1 = M_2$  or  $-M_2$  is of the order of 30% for slabs in which the mesh is parallel to the sides. This increase in moment capacity is explained in different ways depending on the angle at which the mesh is orientated. For example when the angle is zero the increase is explained for the 1st and 3rd quadrants of Fig 2.17. by stating that, because the concrete on the compression face is in biaxial compression an effect analagous to precompression of the specimen occurs. This being especially important when compressive strength and Poissans ratio are high. The increase in the 2nd and 4th quadrants is attributed to an increase in bond between reinforcement and concrete due to the transverse compressive forces acting. Cracking is thus hindered and assuming that cracking does not occur until the

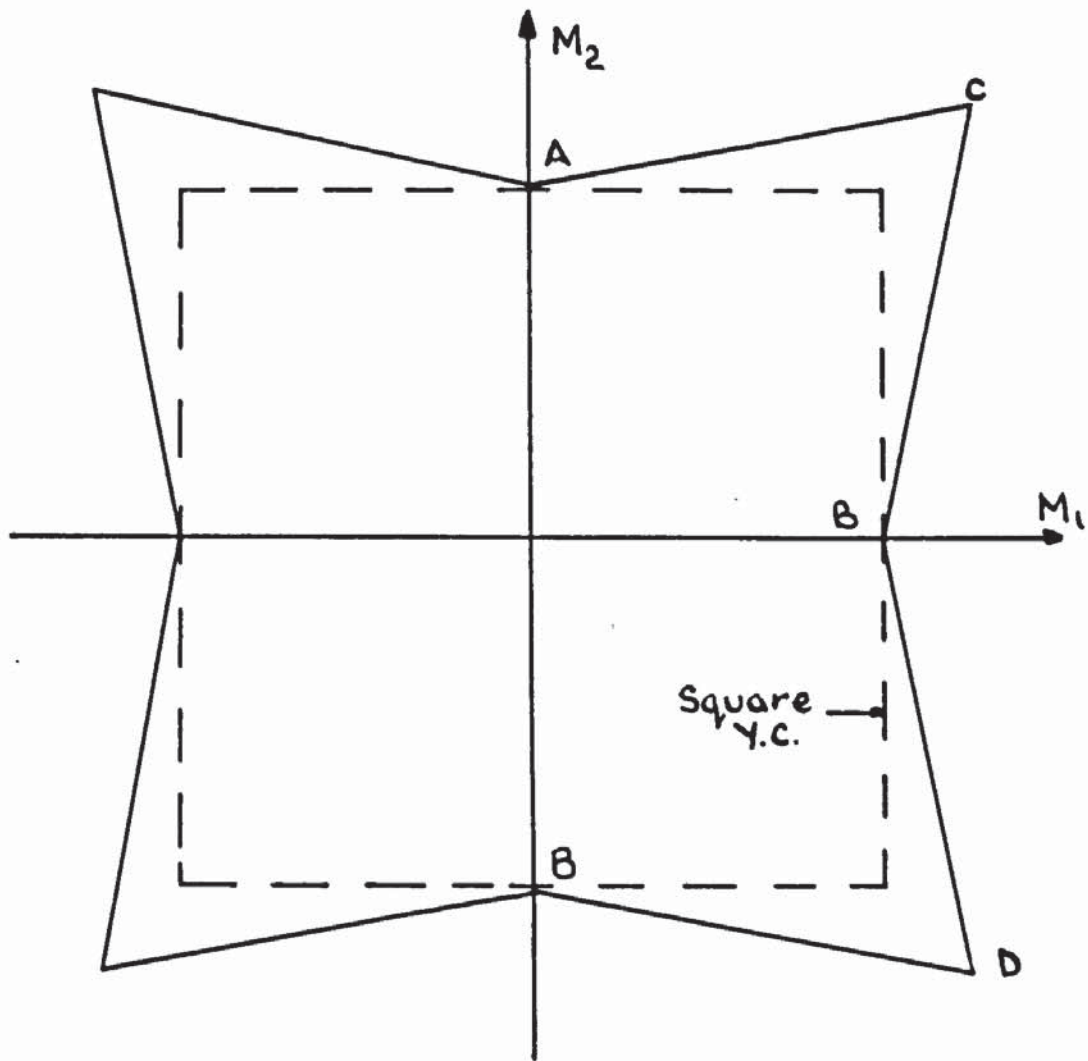


FIG 2-17 YIELD CRITERION (LIÉGE)

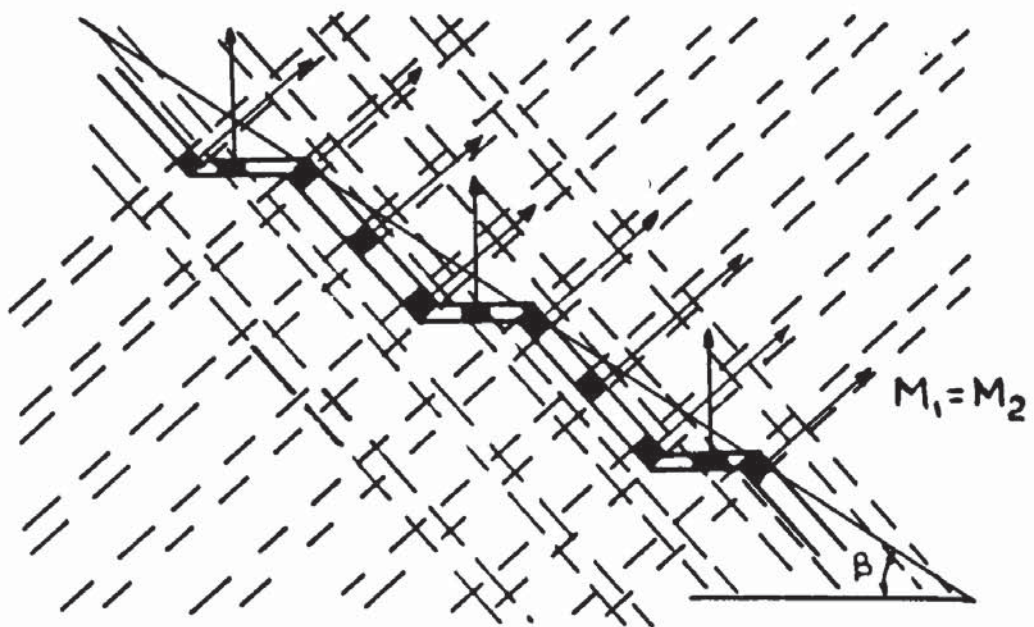


FIG 2-18 'STEPPED' YIELD LINE CONCEPT (LIÉGE)

reinforcement has yielded, the moment required to produce yielding is dependent on the tensile strength of the concrete.

When the mesh makes an angle with the sides the explanation of moment carrying enhancement follows different lines. The direction of the crack formed at yielding is made up of a general crack direction which in turn is formed by the addition of varying local crack directions. An example is shown in Fig 2.18. The bars are assumed to 'kink' across the crack in differing local directions. However many inconsistencies in approach to particular cases occur as pointed out by Lenschow and Sozen<sup>[29]</sup>. Little information is given concerning the directions of plastic flow in individual tests and no conclusions can be drawn as to whether plastic potential or another flow law is obeyed.

Careful consideration of the test specimen used indicates that the moments and stress conditions are not well controlled throughout the element<sup>[29]</sup>. In particular, the extra reinforcement provided around the edges, which amounts to a doubling of the strength in these areas and which, in addition, is spot welded, will tend to produce significant forces in the perpendicular direction to that in which the moment is acting. This confinement of the lighter reinforced area is enhanced by varying neutral axis positions between heavy and light reinforced areas and will have an overall tendency to produce membrane forces in the linear test area due to the

restraint on it from the heavier reinforced surrounding area.

The effect of such additional restraints for purely practical purposes is a critical factor affecting the results obtained. The same effect is a criticism of the following work.

e. Tests by Nielsen [26]

Slabs, 155 x 155 x 12 cm, reinforced top and bottom were tested in pure torsion in the manner shown in Fig 2.19. The upward and downward concentrated loads at the corners produce the torsional moment which is transmitted to the slab by four rigid steel channels cast into the edges. The reinforcement placed parallel to the sides at 10cm centres was welded to the channels. Eight slabs were tested, the coefficient of orthotropy varying from 0.24 to 1. In all tests failure took place due to yield lines forming at  $45^{\circ}$  to the sides.

Contrary to Johansens yield criterion which would predict a normal moment strength of  $\frac{m_x}{m} = \frac{m}{2} (1 + \mu)$  for  $\theta = 45^{\circ}$ , Nielsen, by assuming that the ratio between concrete compressive stresses in the reinforcement directions is  $\mu$ , the coefficient of orthotropy, and further that Mohr's circle for stresses holds, produces an equation for small percentages of steel of the form.

$$m_x = m \sqrt{\mu} \quad (2.24)$$

This equation does not vary significantly from Johansens prediction for  $\mu > 0.5$  and the results obtained

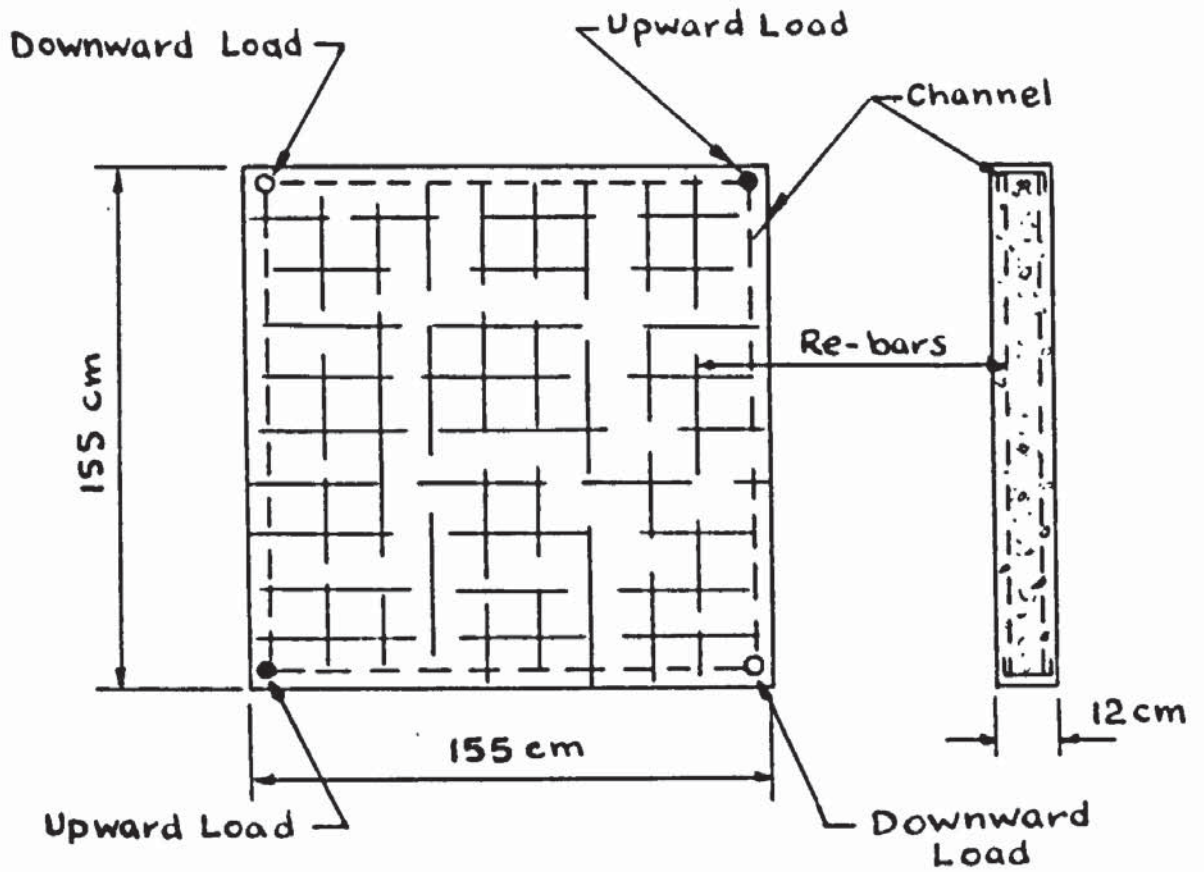


FIG 2.19 NIELSEN TESTS

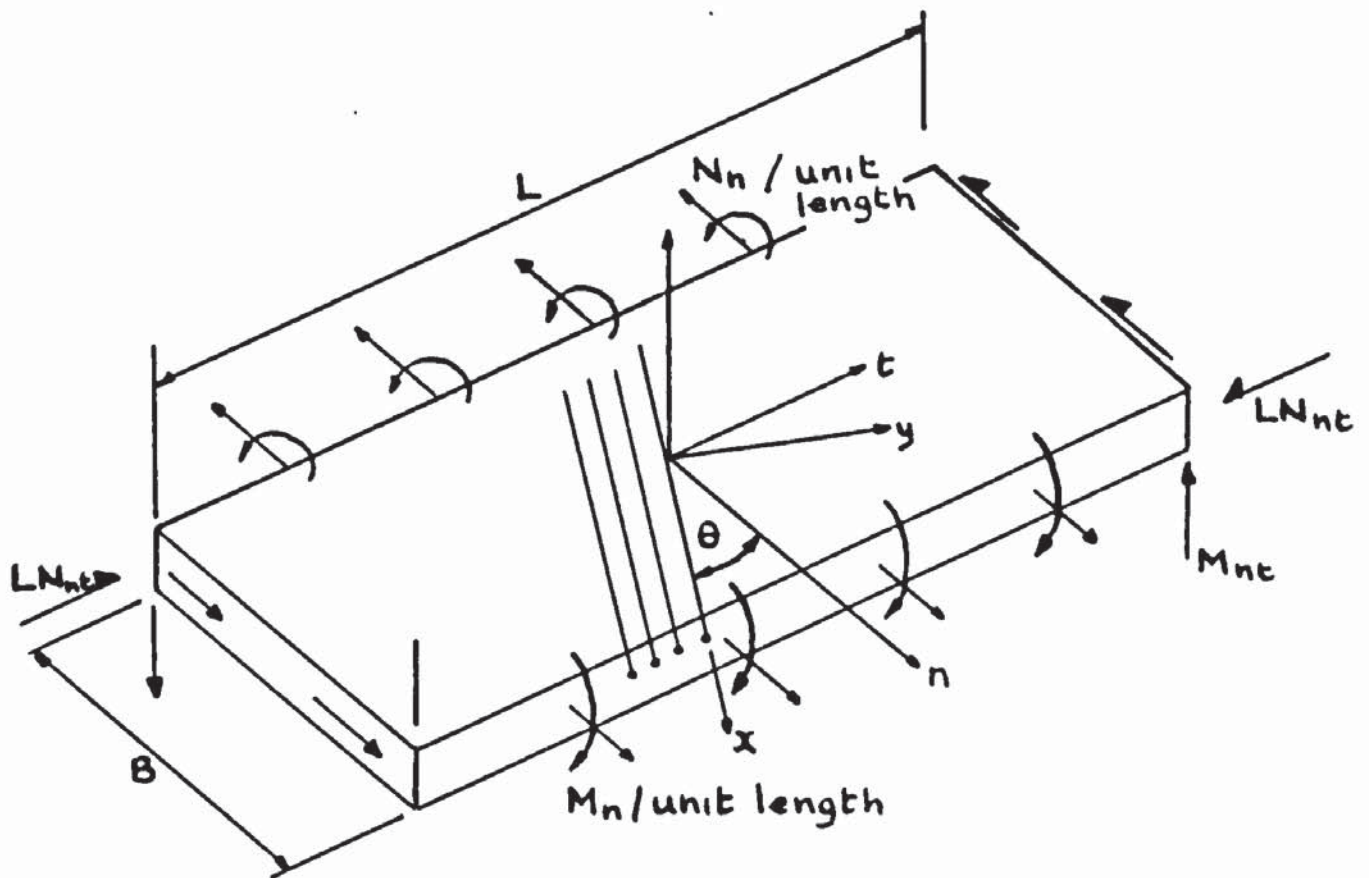


FIG 2.20 MORLEY TESTS

verify both equations in this case. The main objections to Nielsen's test set up are

- 1) The steel channels force the yield lines to form at an angle of  $45^{\circ}$  to the sides. Particularly in the case of non isotropic slabs a slab free from such restraints would not form yield lines at this angle under the moments applied in this case.
- 2) As the middle plane in a reinforced concrete slab which has cracked and is approaching yield will tend to expand, any restraint to this expansion will produce membrane forces in the plate. The rigid steel channels will tend to produce this restraining effect in a similar manner to the extra reinforcement in the case of slabs tested by Baus and Tolaccia [23].

f. Tests by Morley [27]

In 1965 Morley carried out tests on one - way spanning slabs to investigate the effect of the 'kinking' of reinforcement across yield lines and the effect of membrane forces on the moment capacity of the slab. The slabs measured 36 in long x 13.1/4 in wide x 1 in deep, and were reinforced with 3/32 in cold-drawn bright mild steel in one direction only. An essentially uniaxial strain condition was produced across the slab by applying in - plane shear forces and forces producing twisting moments on the slab as shown in Fig 2.20. The strains in the t - direction were small compared to strains

in the  $n$  direction because of the heavy clamps on the edges parallel to the  $t$  direction used to produce the moment  $M_n$  and force  $N_n$  in the slab. Shear strain  $\gamma_{nt}$  was eliminated by application of the shearing forces  $N_{nt}$  on the clamped edges, and thus the experiments simulated a yield line parallel to the  $t$  direction. Concrete strains were measured using 2in Demec gauges and Saunders Roe electrical resistance gauges. Fig 2.21 shows the test results plotted in relation to the theoretical curves for 'no-kinking' and 'complete kinking' for the series in which no membrane forces were acting and only the angle of the reinforcement  $\theta$  was varied. The experimental results associated with the shear stresses  $\tau_{nt}$  obtained from the forces  $N_{nt}$  acting along the slab edges were uncertain as the measurement of these forces was not accurate.

It was found that for slabs in which the reinforcement angle was less than  $30^\circ$ , results agreed with theoretical predictions in the elastic range but for angles greater than  $30^\circ$  more stress was apparently carried than 'no-kinking' theory allowed. However at yield, results for all slabs moved closer to the theoretical 'no-kinking' curve. From his results Morley concluded that at all stages after cracking the 'kinking' of steel across cracks was not significant. In tests in which membrane forces were applied the interaction curve was found to be similar to that given by Wood [12 p.228] and the directions

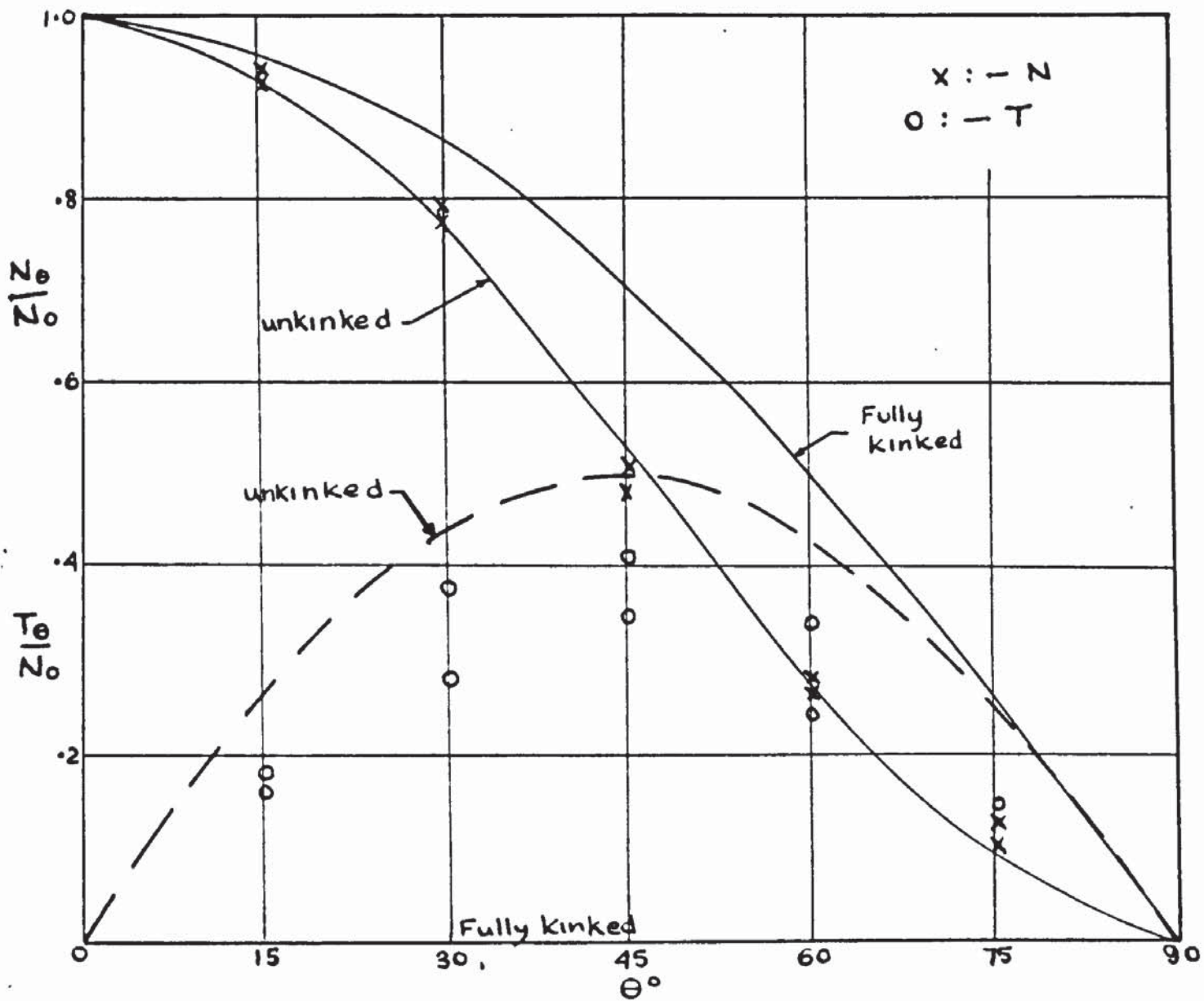


**FIG 2.21 STEEL FORCES AT ULTIMATE LOAD (MORLEY)**

of yielding was closely normal to the interaction curve, indicating that plastic potential theory was closely satisfied.

The other series of tests in which isotropically reinforced rhomboid slabs were tested under different ratios of principal moment was designed to produce results which could be compared with existing and developed yield criteria under biaxial moment. The test set up is shown schematically in Fig 2.22 13 slabs, 1.3/8 in. thick and reinforced with similar steel as had been used previously and slabs, 1.1/4 in. thick reinforced with Weldmesh were tested in this way. By varying the dimensions of the rhomboid it was possible to vary the ratio between the principal moments  $M_t$  and  $M_n$ . The ratio's chosen were 1.0, 0.6 and 0.2 for the normally reinforced slabs and 1.0 and 0.4 for the slabs reinforced with Weldmesh. Several slabs were tested in one-way bending under a uniformly distributed load so that a comparison of results gave some indication of the yield criterion for moments of the same sign. The reinforcement was inclined at  $0^\circ$ ,  $22.1/2^\circ$  and  $45^\circ$  to the n direction. Fig 2.23 shows the position of the test results in a principal - moment coordinate system. As for the 1.3/8 in. normally reinforced slabs the results indicate a square yield criterion for small negative ratios of  $M_t/M_n$  but with approximately a 5% decrease in yield moment for  $M_t = -M_n$  and a 10% increase in yield moment when  $M_t = M_n$ . Morley suggests that the increase in yield moment may be due

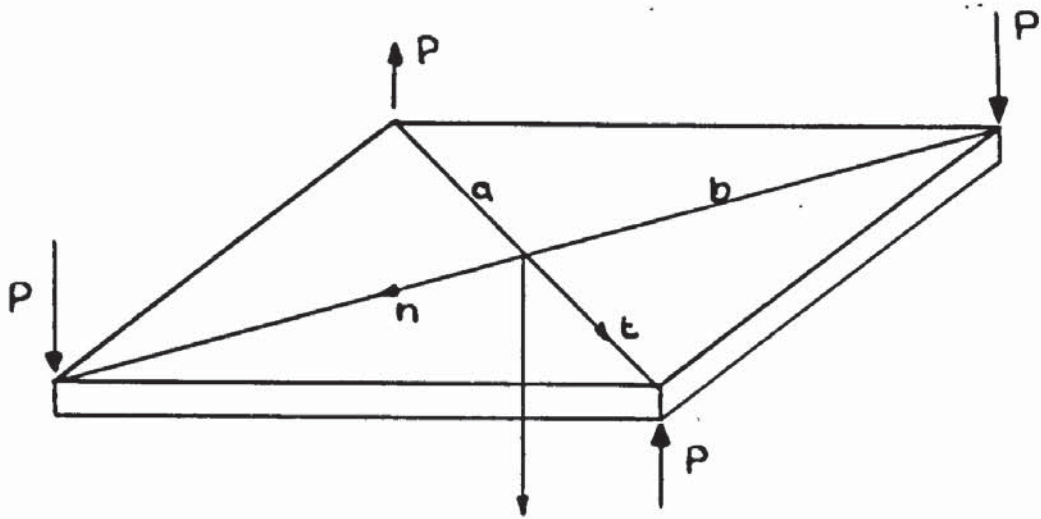


FIG 2.22 RHOMBOID SLABS (MORLEY)

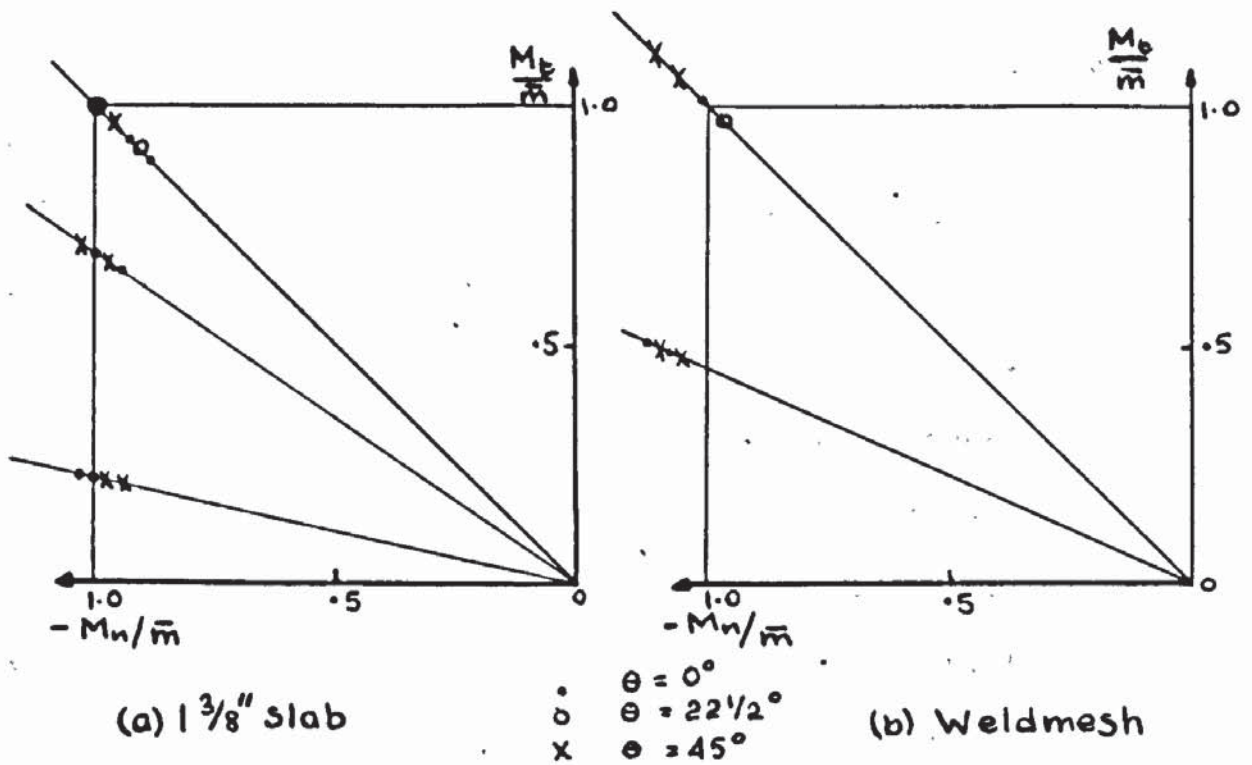


FIG 2.23 EXPERIMENTAL Y.C. (MORLEY)

to membrane forces occurring and that the decrease may be due to concrete failure properties under local stresses. No explanation was put forward to account for the increase in moment capacity for the Weldmesh reinforced slabs except the suggestion that the mesh was slightly displaced from its original position. A possible conclusion could be that, due to the very small diameter of the wires, some 'kinking' may occur thus enhancing the carrying capacity. It is interesting to note that Baus and Tolaccia [23] reported an increase in moment capacity of approximately 10% for  $M_t = -M_n$  whilst Morley's results indicate a 5% decrease.

Morley [27] concludes that although the yield criterion represented by the tests appears to be concave the predominately unidirectional curvature increments at failure indicate that if the plastic potential flow law is to be used a square yield criterion should be adopted.

Although the tests on one way slabs indicate that no 'kinking' of the reinforcement occurs the measurements of strain may well have been affected by the relatively narrow test specimen. As the long edges are heavily clamped it is not at all certain that stress concentrations set up by the application of moments through them had reduced to zero at the centre of the 13.1/4 in. wide slab. In the case of the rhomboid slabs the distinct differences in results obtained by other authors [23] suggests that the details in test set-up

producing externally or internally affected membrane forces, play a very significant role.

In Morley's theoretical work, bounds are obtained on the yield criterion for the reinforced concrete element by assuming the yield criterion of the constituent materials. The reinforcement mesh is replaced by a sheet of constant thickness, the properties of which are chosen to correspond to purely uniaxial stress in the original bar directions. Both the steel and the concrete are assumed elastic - plastic and hence the theory is only applied to slabs in which the ultimate properties are overwhelmingly determined by the steel. Nielsen<sup>[25]</sup> used a similar technique.

g. Tests by Lenschow and Sozen<sup>[29]</sup>

The experimental investigations carried out by Lenschow and Sozen at the University of Illinois in 1966 are among the best controlled of all tests to date. The first series was carried out on 'circular' test specimens. Three specimens of this type were tested under isostatic moment. Fig 23 shows a plan view of the 'circular' specimen. Moment was applied to the wings of the slab by steel hangers from the supporting frame acting through the circular holes onto channels bearing against the slab. Thus whilst the outer circle in Fig 2.24 was prevented from moving, the inner circle was forced up producing moments in the slab. The slabs were nominally, isotropically, reinforced with 1/4in. diameter bars placed in

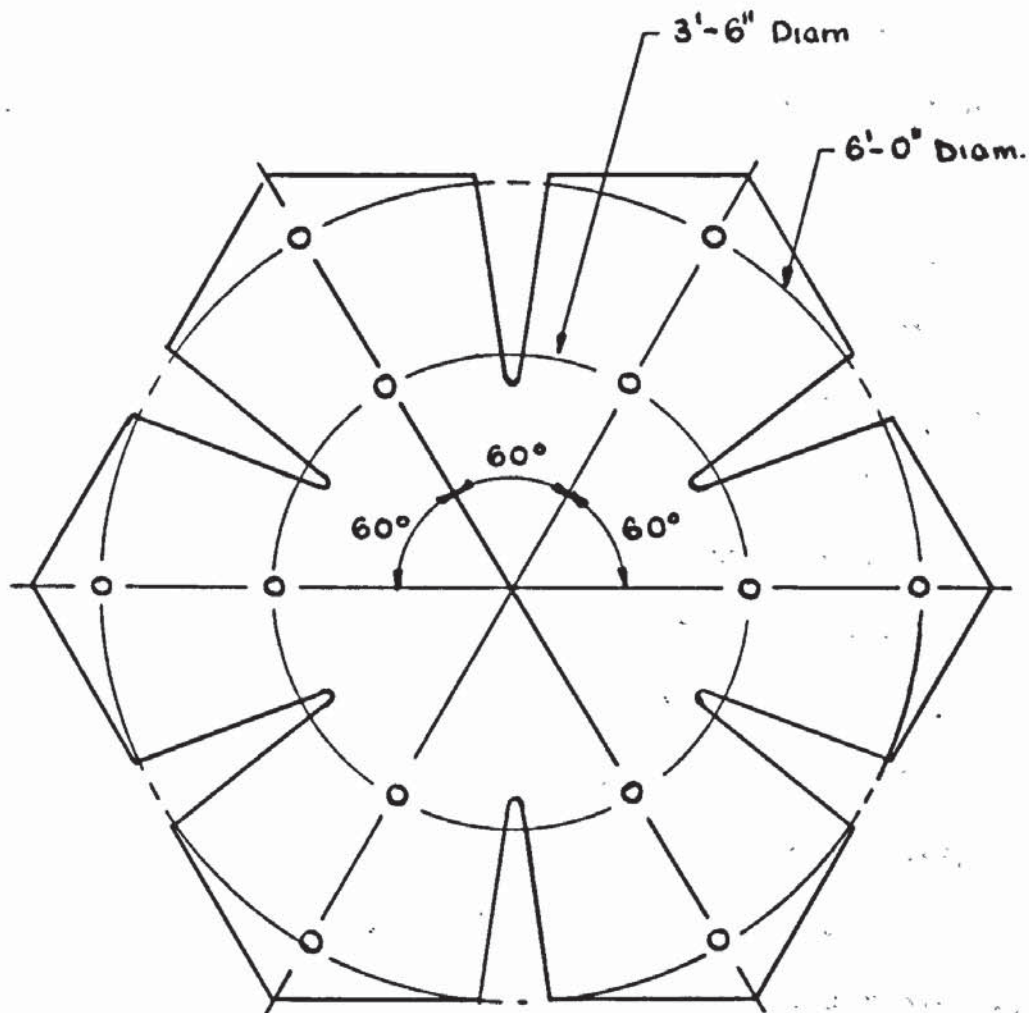
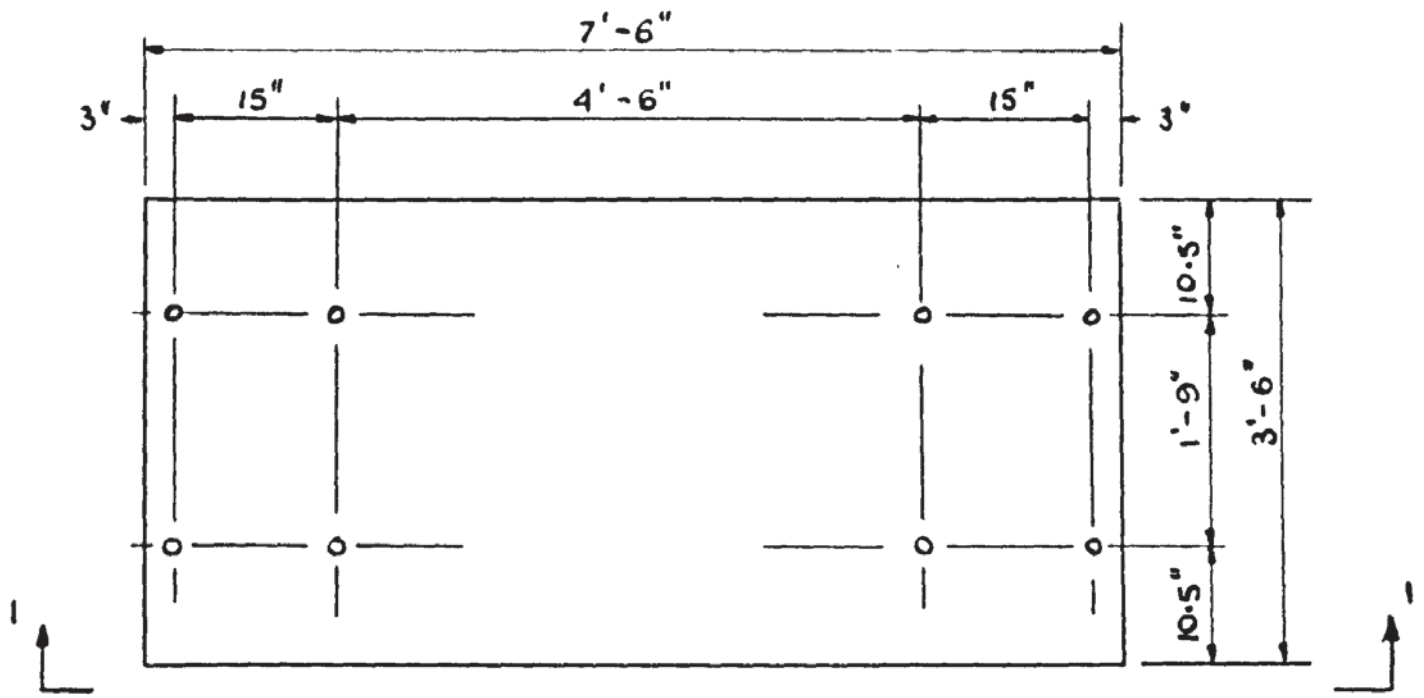


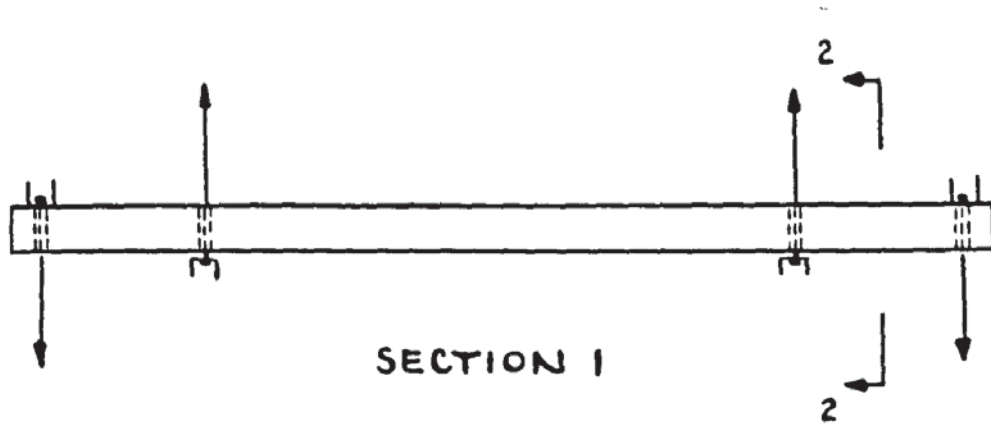
FIG 2.24 CIRCULAR SPECIMEN  
(LENSCHOW and SOZEN)

pairs at a spacing of 3 in. in the bottom layer and at a spacing of  $2\frac{3}{4}$  in. in the orthogonal upper layer. This smaller spacing in the upper layer compensated for the lower lever arm value produced as a consequence of placing that layer on top of the bottom one. The wings were provided with 50% more reinforcement to ensure failure in the test area.

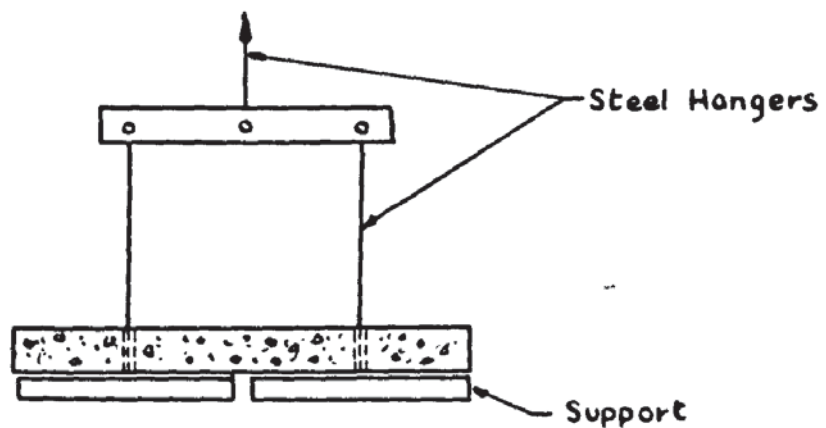
The larger test series was carried out on rectangular slabs 7ft 6in. long x 3ft 6in. wide x approx. 4.12 in. thick. The loading arrangements for these slabs is shown in Fig 2.25. The moments were produced in the same way as those in the previous series. The arrangements of the releases in the steel hanger system allowed fairly unrestricted deformation characteristics. Ten slabs were tested under uniaxial moment and nine slabs under pure torsion. Of the ten slabs tested under uniaxial moment nine were reinforced at one face only, the remaining one being reinforced at both faces as a 'standard' for the torsion tests. Six slabs were isotropically reinforced with the direction of reinforcement varying. The angles were  $0^\circ$ ,  $22\frac{1}{2}^\circ$ ,  $45^\circ$  and  $67\frac{1}{2}^\circ$ . Three slabs were non-isotropically reinforced. Of the nine torsional specimens, seven were isotropically reinforced and two non-isotropically reinforced. All bars were hooked at the ends to avoid bond failures. The test set-up was specifically designed to prevent restraints of any kind. Certain restraints on the curvature and strains in the transverse direction in the



PLAN



SECTION 1



SECTION 2

FIG2-25 RECTANGULAR SPECIMEN  
(LENSCHOW and SOZEN)

case of the slabs under uniaxial moment may have occurred. Strain measurements were taken both on the reinforcement and the concrete faces. Curvature was measured by the use of a grid of deflexion gauges and an attempt to measure it by the use of photogrammetry methods was made.

The test results were used to discover whether 'kinking' of the reinforcement was significant. The results, agreed with those of Morley<sup>[27]</sup> in as much as 'kinking' was found to be negligible. An analytical approach to this problem was also made assuming.

- 1) Stress-strain curve for concrete assumed linearly elastic.
- 2) Stress-strain curve for concrete assumed rigid-plastic.
- 3) Analysis of bar reorientation made independently of stress-strain characteristics by assuming a constant rate of transfer of force from the steel to the concrete over a feint length.

This analytical study, although conceding that a certain amount of 'kinking' must exist due to compatability across a crack, showed that the effect was insignificant in enhancing the moment capacity of a section. The authors pointed out that although the 'kinking' phenomom at a crack was usually represented by a diagram such as that in Fig 2.12 from Wood<sup>[12]</sup>, if the scale of the bar and crack at yield in a practical case was better represented as in Fig 2.26 it would seem almost

impossible for significant reorientation to exist. It is interesting to note that in further analytical work, amongst the additional premises to normal reinforced concrete theory is the assumption that the bars have zero bending and shear stiffness.

Further analytical studies show that by considering equilibrium and compatibility at a cracked section and by employing standard transformation equations, the flexibility of a reinforced concrete element is directly related to the direction of the reinforcement and the combination of applied moments for both isotropic and non-isotropic slabs. The flexibility of an element could increase more than threefold by rotating the reinforcement at an angle to the applied moments. An important corollary to this was the definition of over and under reinforced sections. Because of the higher concrete strains produced as a consequence of increased flexibility in some cases, a cross section may be under reinforced under one combination of applied loads and over reinforced under another, although it was admitted that the resisting moments would not transform according to equilibrium and hence Mohr's circle, due to neutral axis level differences, this was ignored as errors of between 5% and 10% only were obtained for a practical example and hence Mohr's circle transformation was used.

The development of the yield criterion was based on

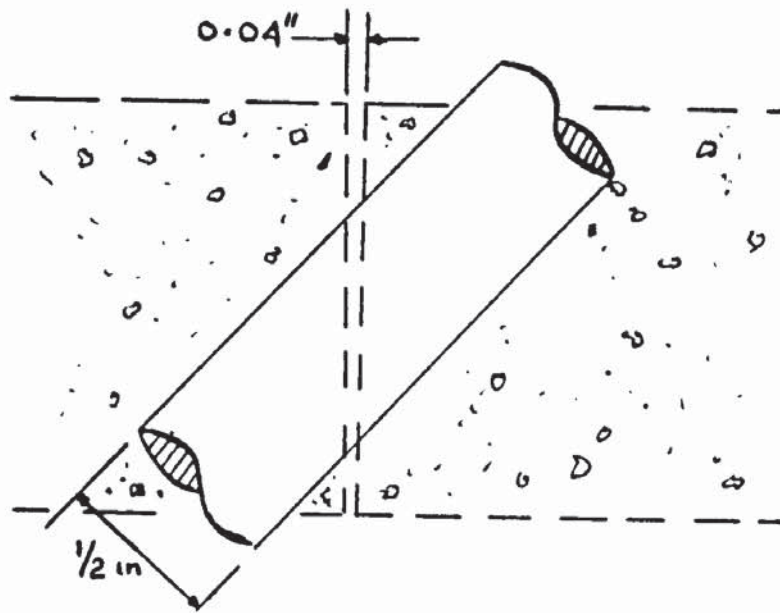


FIG 2.26

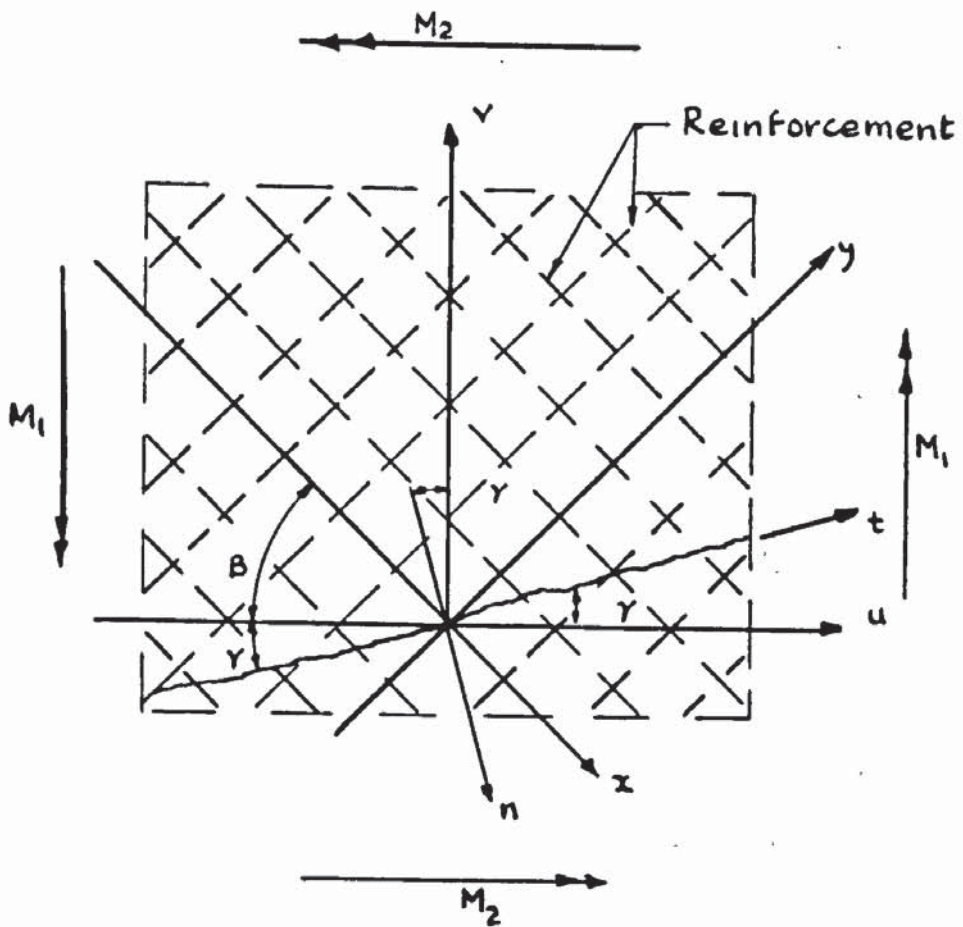


FIG 2.27 (LENSCHOW)

similar considerations to those used by Kemp [17] and Save [18, 33] and as the local equilibrium and compatibility at a crack was considered in the derivation of the equations a similar result in different notation and form was produced, as these were the same considerations that Johansen originally used. The results obtained were in good agreement with those predicted. A maximum difference of 11% occurring and being attributed to strain hardening effects. The predicted angle of yield were also approximately the same as those reported in the tests.

The yield criterion and flow law may be written in the notation of Lenschow and Sozen as described in Fig 2.27 as

$$M_2 = \omega M_1 = (M_y \cos^2 (\beta + \gamma) + M_x \sin^2 (\beta + \gamma) / \cos^2 \gamma \quad (2.25)$$

where  $\gamma$  is determined by

$$-\tan^2 \gamma - \omega c_1 \tan \gamma + \omega = 0$$

where

$$\omega c_1 = (\nu - \omega) \cotan^2 \beta + 1 - \nu \omega) / (1 - \nu) \cotan \beta)$$

where  $M_x$  and  $M_y$  are the ultimate moments calculated as for a beam in the x and y directions and  $M_y/M_x = \nu$  and  $M_2/M_1 = \omega$ .

h. Work by Prince [37]

The work carried out by Prince in 1967 under K.O.Kemp at the University of London was mainly of a theoretical nature. However, ultimate moments and directions of yield lines were reported for thirteen slabs tested under uniaxial moment by a system which allowed the yield lines or cracks to form in a

nearly unrestricted manner. Fig 2.28 shows diagrammatically the test set up utilised. Of the thirteen slabs three were orthotropically reinforced, the degree of orthotropy being approximately 0.5, the rest being isotropically reinforced. The results obtained did not generally verify his theoretical predictions and bond failures near the slab edges were said to account for this lack of agreement. Yield moments were calculated on the assumption that failure would occur at the cross-section with the least number of bars crossing it.

In all tests involving an inclined reinforcement mesh cast into a rectangular slab element the problem of inherently weaker cross-sections being present cannot easily be avoided. However to assume that failure will occur at the weaker cross-section is to presuppose the mode of failure of the specimen. The same problem occurs in the present work and a closer study of its effects will be made in later chapters.

The theoretical approach in Princes work was based in essence on a normal moment yield criterion. By working in terms of steel forces only and by taking account of the shear stresses and axial stresses developed in the reinforcement bars a yield criterion was evolved which predicted strengths between the unkinked and fully kinked yield criteria predictions.

Two cases were considered

- 1) No bending of reinforcement i.e. when the crack

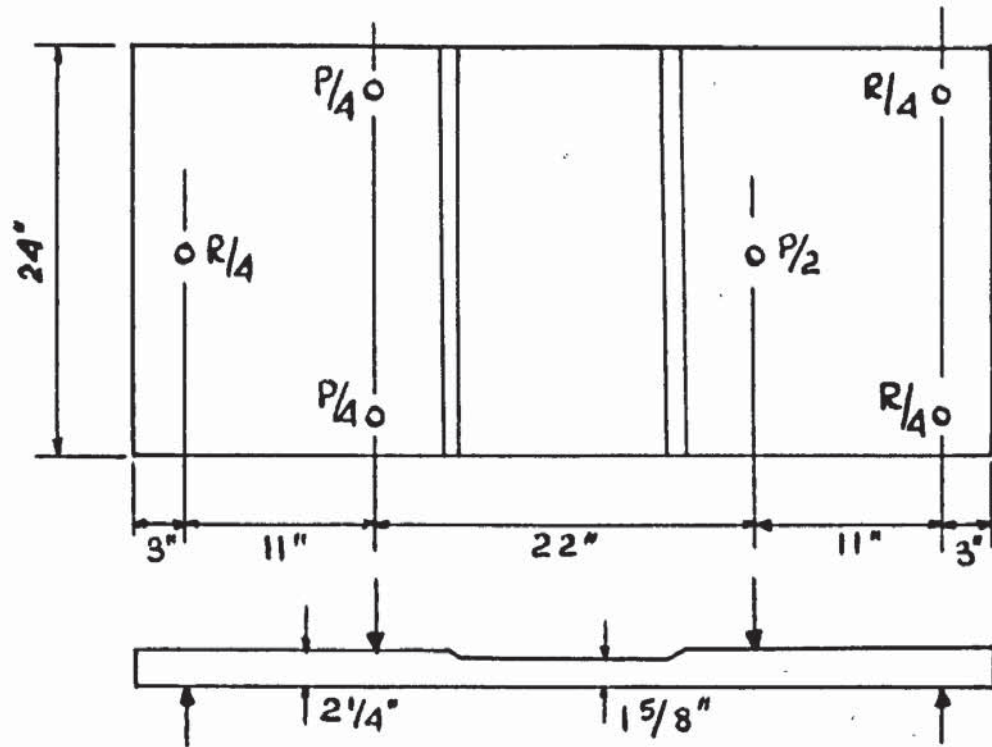


FIG 2.28 PRINCE TESTS

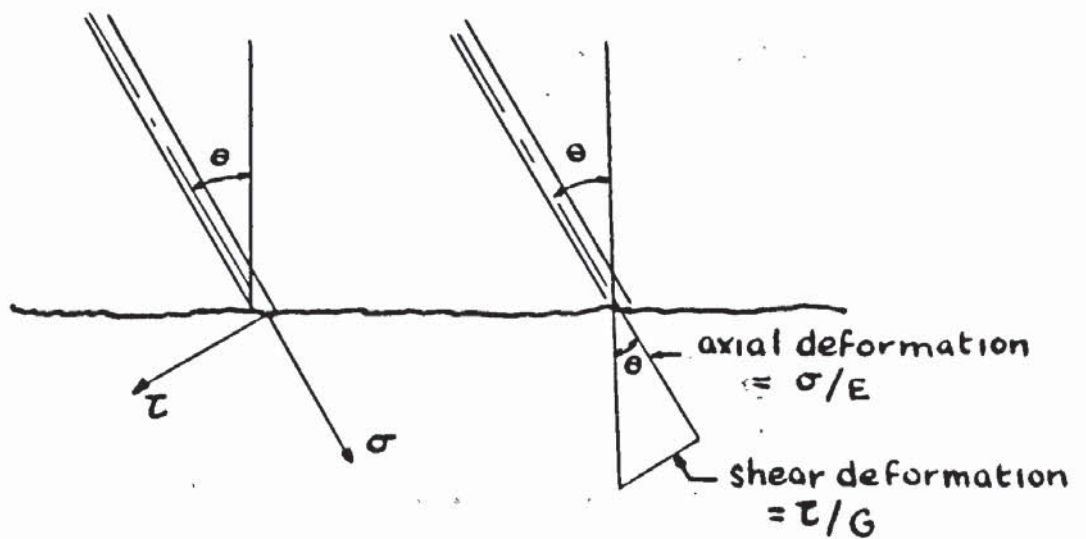


FIG 2.29 STRAIN COMPATABILITY

width is so small that bending deformation are negligible.

2) Bending of reinforcement across crack. i.e.

when crack widths are larger.

The 'no bending of reinforcement' concept although being dealt with first was shown to be a special case of the more general concept in which bending of reinforcement across the crack occurred. Fig 2.29. shows the basic model in which the normal force on the yield line was

$$N = \sigma A \cos^2 \theta + \bar{\tau} A \cos \theta \sin \theta$$

and the tangential force along the yield line was

$$T = \sigma A \cos \theta \sin \theta - \bar{\tau} A \cos^2 \theta$$

where  $A$  is the area of the bar,  $\sigma$  the axial stress and  $\bar{\tau}$  the tangential shear stress acting normal to the axis of the bar.

The first basic assumption made was that to relate the axial and shear stresses 'the principal elastic strain direction is normal to the yield line.' Thus it was implied that no shear strains can exist along the yield line or normal to it. This was named the 'strain compatibility condition and led to the expression

$$\bar{\tau} = \frac{G}{E} \sigma \tan \theta$$

where  $E$  is the Youngs Modulus and  $G$  the modulus of rigidity of the bar.

By application of the 'strain compatibility' concept to an isotropic reinforcement mesh and again assuming that at

and after yield principal strains occurred in a direction normal to the yield line which forms normally to the principal moment direction, equations were obtained for the normal and tangential forces on the yield line.

These were

$$N = A \sigma_n \left( \cos^2 \theta + \frac{G}{E} \sin^2 \theta \right) + A \sigma_y \left( \sin^2 \theta + \frac{G}{E} \cos^2 \theta \right)$$

and

$$T = A (\sigma_x - \sigma_y) \left( 1 - \frac{G}{E} \right) \sin \theta \cos \theta$$

where the bars running in the n direction make an angle of  $\theta$  to the normal to the yield line.

To express the two steel strains in terms of the yield stress three conditions were considered

- 1) Tangential force, T was equal to zero
- 2) The crack width remained constant for both sets of bars
- 3) Both sets of bars yielded and by using Von Mises yield criterion

$$\sigma_n = \sigma_y \left[ \frac{E^2 + 3G^2 \cos^2 \theta}{E^2 + 3G^2 \tan^2 \theta} \right]^{\frac{1}{2}}$$

Prince maintained that it was possible to ignore small tangential steel forces and that although the physical crack width must remain constant for each set of bars it was possible for the effective length of a bar unrestrained by concrete to vary as this was controlled by the amount of crushing taking place within the acute angle formed by the

yield line and the bar. Thus the third condition was utilised as large plastic deformations can only occur when both sets of bars are yielding.

Another assumption made was that the shear and axial stresses remain uniformly distributed over the bar cross-section after yield. Plastic deformations of the reinforcement were then calculated using the Von Mises yield condition and associated flow law, and because  $\frac{\tau_{n}}{\sigma_n} = 1/3 \tan \theta$ , an expression necessary for compatible deformations, did not differ from the elastic equations for mild steel by a great amount the elastic and plastic stress distributions were said to be the same. Thus the final expressions at yielding of the reinforcement were obtained for the ease of no kinking or bending of the bars

$$N = Afy \left[ \frac{E \cos^2 \theta + G \sin^2 \theta}{(E^2 + 3G^2 \tan^2 \theta)^{\frac{1}{2}}} + \frac{E \sin^2 \theta + G \cos^2 \theta}{(E^2 + 3G^2 \cos^2 \theta)^{\frac{1}{2}}} \right]$$

$$T = Afy [E - G] \sin \theta \cos \theta \left[ \frac{1}{(E^2 + 3G^2 \tan^2 \theta)^{\frac{1}{2}}} - \frac{1}{(E^2 + 3G^2 \cos^2 \theta)^{\frac{1}{2}}} \right]$$

These equations for isotropically reinforced slabs are illustrated in Fig 2.30.

By allowing for bending deformations across the crack a more general expression was derived for orthotropic reinforcement meshes. Again it was assumed that the principal strain direction lay normal to the crack or yield line but the error involved was reckoned small and the expressions for normal

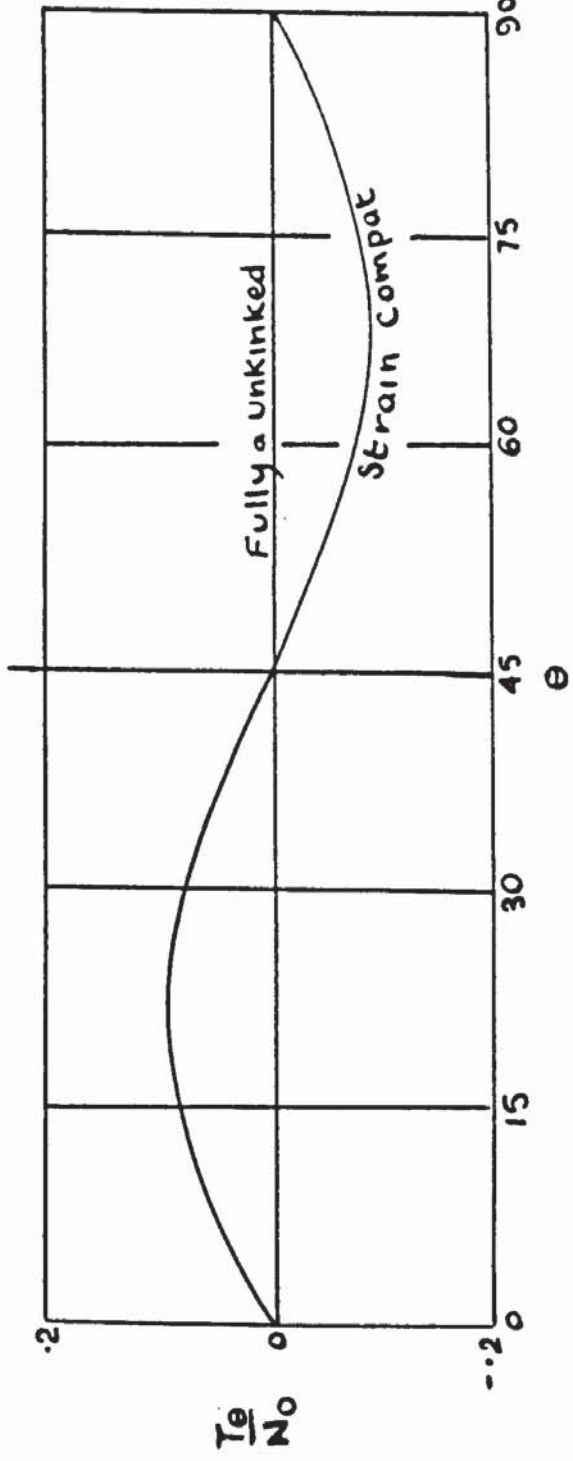
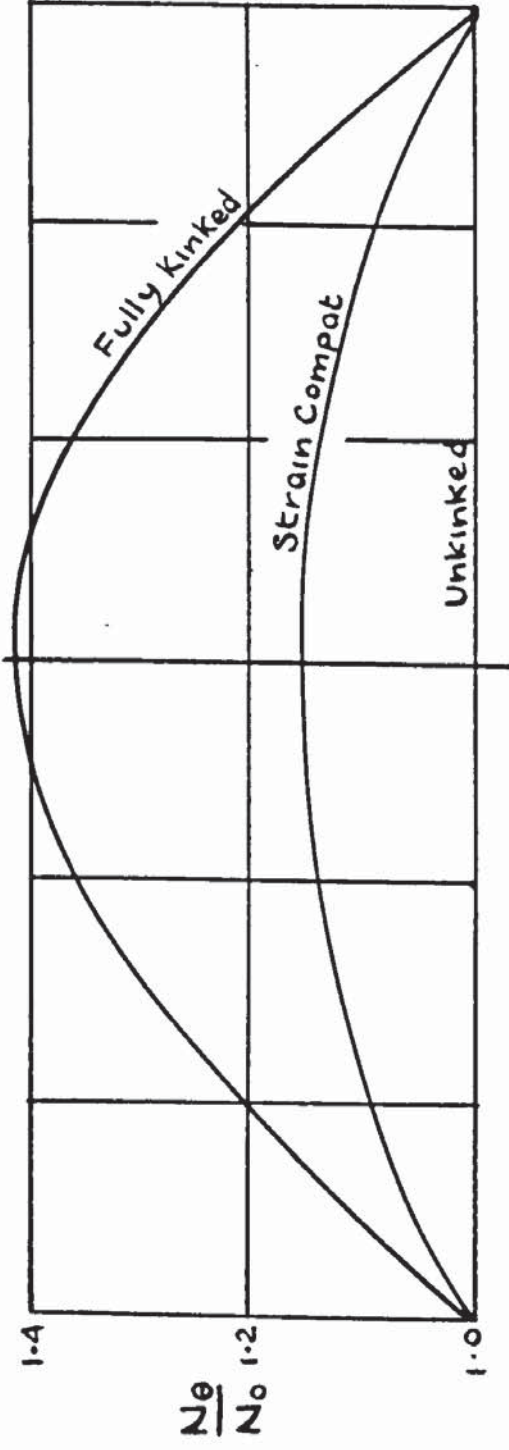


FIG 2.30 NO BENDING OF STEEL,  $\mu=1$  (PRINCE)

and tangential forces were evolved as

$$N = Af_y \left[ \frac{(\cos^2 \theta + K_1 \sin^2 \theta)}{(1 + 3K_1^2 \tan^2 \theta)^{\frac{1}{2}}} + \mu \frac{(\sin^2 \theta + K_2 \cos^2 \theta)}{(1 + 3K_2^2 \cos^2 \theta)^{\frac{1}{2}}} \right]$$

$$T = Af_y \sin \theta \cos \theta \left[ \frac{1 - k_1}{(1 + 3K_1^2 \tan^2 \theta)^{\frac{1}{2}}} + \mu \frac{1 - k_2}{(1 + 3K_2^2 \cos^2 \theta)^{\frac{1}{2}}} \right]$$

where  $K_1 = \frac{3G}{3E + Gk^2 \sec^2 \theta}$  and  $K_2 = \frac{3G}{3E + Gk^2 \operatorname{cosec}^2 \theta}$

where  $k = d/r$

$d$  being the crack width and  $r$  the radius of the bar.

Prince suggested a value of  $k = 2$  which implies that the crack width must be equal to the diameter of the bar. Fig 2.31 shows the above equations plotted for different values of  $\mu$  and  $\theta$  with  $k = 2$ .

The above yield criterion was treated in the same way as Kemp [17] (see 2.8.1(d)) treated Johansens normal moment expression to develop the yield condition in principal moment space.

The major assumptions made by Prince in his derivation of the yield condition were

- 1) Principal elastic strains take place at right angles to the crack whatever the applied moment distribution or reinforcement arrangement may be.
- 2) The elastic and plastic stress distribution on the bar were the same.
- 3) Both sets of bars must yield

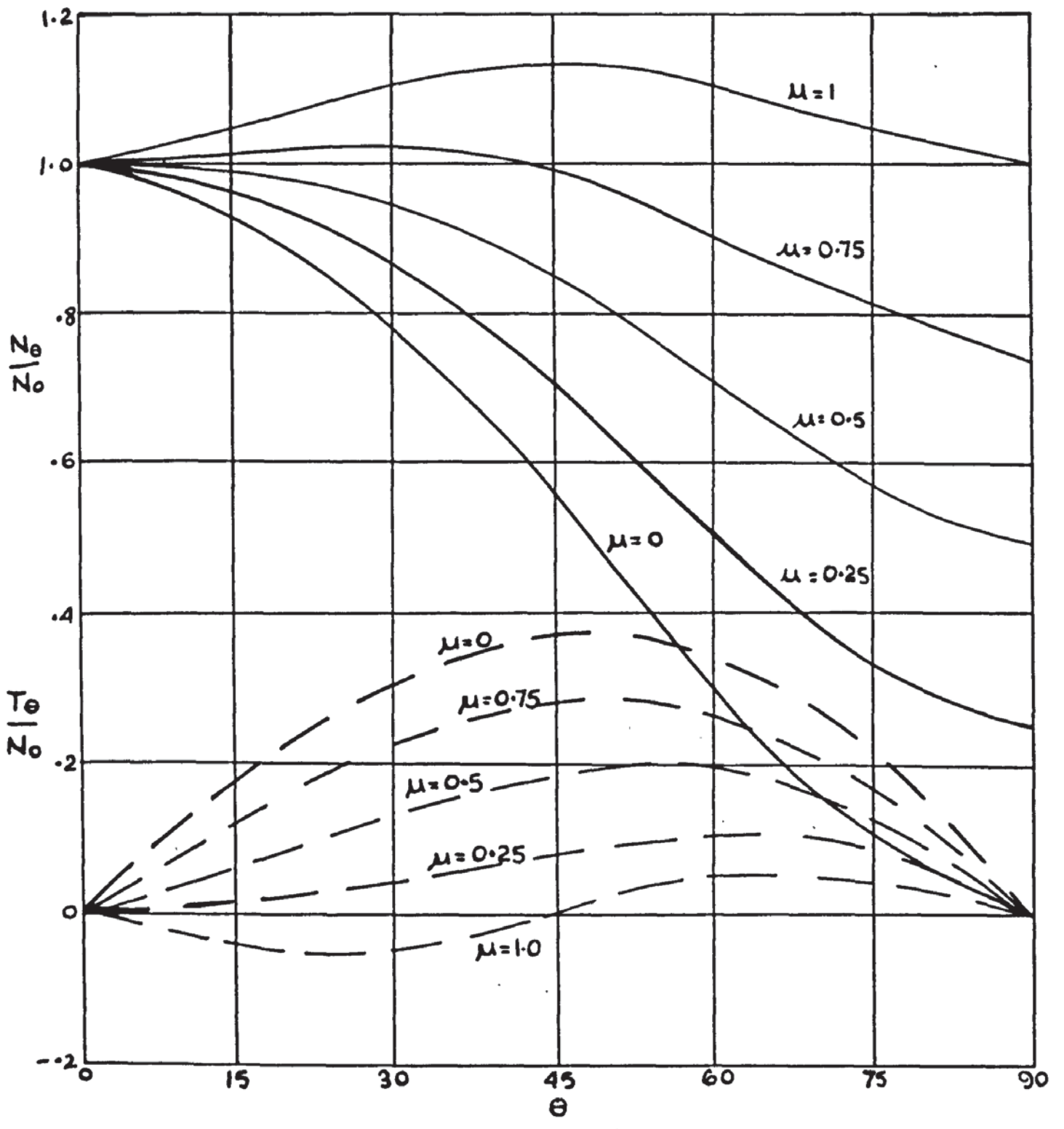


FIG 2-31 EQNS. DESCRIBING N and T, BENDING ALLOWED (PRINCE)

4) The ratio of crack width to bar diameter is 1 at failure.

and 5) The lever arm or neutral axis depth is the same in any direction.

The first assumption made will be dealt with in later chapters with reference to the tests carried out in this research work.

Lenschow and Sozen<sup>[29]</sup> have shown that assumptions (3) and (5) need not be true at failure and assumption (4) seems to be an excessive value of  $k$ . The fact that  $k$  can be varied according to results obtained makes verification of any theoretical analysis difficult.

### 2.9. Summary.

For problems involving the plastic behaviour of reinforced concrete slabs to be solved using Limit Analysis it is necessary for the slab to behave within the terms of reference of a rigid - perfectly plastic solid. The main, basic requirements of such a material are that:

- 1) Elastic deformations are small as compared to plastic deformations.
- 2) Strains should be independent of time, capable of indefinite strains once yield is reached and no strain hardening - characteristics are exhibited.
- 3) The yield conditions for unloading or loading after previous plastic straining takes the same form

as the yield condition at first yield.

4) The yield locus is convex.

5) The flow law obeys the theory of plastic potential.

As Prager and Hodge [2] have stated "Mathematical theory may give some indications as to the nature of the yield condition and stress-strain relation in the plastic range, but experiments will constitute the ultimate test for any such theory" and thus although yield conditions such as those developed by Johansen [14], Kemp [17], Prince [37] and others from purely theoretical considerations are of great significance, it must be experimental work that finally verifies their acceptance or modification, and consequently the inclusion or exclusion of reinforced concrete slabs as a continuum within the terms of reference of Limit Analysis. Tests by Nielsen [26], Morley [27] and Lenschow and Sozen [29] have shown that Johansen's original assumptions in terms of the normal moment on a yield line are close to those obtained from tests but more exact limitations on the flow law exist than those he suggested.

Alternatively tests by Kwiecinski [22] and Baus and Tolaccia [23, 24] have indicated that some amount of reorientation or 'kinking' of reinforcement exists on a yield line hence enhancing the moment capacity. The present situation would suggest that at least in practical cases 'kinking' of reinforcement on the yield line has an insignificant effect on the moment capacity.

Comparison of the tests carried out indicates that uncontrolled moment or stress states can easily occur inherently in the test specimens and loading arrangements. These restraints to the normal action of a freely deforming slab element seem to produce considerable nonuniformity of results and conclusions. Tests carried out on one way spanning slabs under uniaxial moment restrict twisting curvatures in the slab and also produce masking membrane action under certain conditions.

The problem in testing slab elements is to give the same freedom from restraints as a mathematically conceived theoretical slab element would have. If it is practically impossible to allow all degrees of freedom then at least a control over which restraints exist must be maintained. Lenschow and Sozen<sup>[29]</sup> have probably come the closest to these conditions upto the present but the number of slabs tested was fairly small and of those only uniaxial bending and pure torsion states were produced. Morley<sup>[27]</sup> tested only a small number of slabs with membrane forces acting and it seems that the present state of experimental investigation is not yet advanced enough to include variables over and above those involved in pure bending without confusion developing.

As has been stated previously tests have been carried out on either one way spanning slabs, slabs under uniaxial bending, slabs under pure torsion or slabs acted upon by applied principal moments<sup>[23, 25, 27]</sup>. As stated by Wood and Jones<sup>[10]</sup>

no tests have been carried out on slabs acting under conditions of combined bending and torsion. The main test series described in this thesis was designed to rectify this situation and relate it to the yield condition and flow law for reinforced concrete slabs.

CHAPTER 3QUALITATIVE THEORETICAL ANALYSIS.3.1 Introduction

The previous research work described in Chapter 2 has in the main part dealt only with the conditions at yield in a reinforced concrete slab. Little account has been taken of the behaviour of the slab throughout the history of loading to failure and consequently it has been inherently assumed that behaviour at yield is not a function of the behaviour in any other range.

The object of this chapter is to investigate theoretically the behaviour of a reinforced concrete slab element under combined applied moment conditions in a logical and qualitative manner and to show that the overall action of the element must depend on all phases of the loading cycle. Although in many respects the analysis is of an heuristic nature it will be shown in later chapters dealing with the analysis of experimental results that the suggestions put forward are endorsed by empirical data.

3.2 The general model of reinforced concrete slabs

Generally reinforced concrete can be described as a complex multiphase composite material. As concrete itself is a multiphase composite of coarse aggregate, fine aggregate and cement matrix it is not strictly sufficient

to idealize reinforced concrete into a two-phase system of reinforcement and concrete. However it is possible on a macroscopic engineering level to accept the properties of the complex multiphase reinforced concrete as being those of a statistically homogeneous, isotropic matrix in which homogeneous, isotropic cylindrical reinforcement inclusions are embedded.

Many fibre reinforced composites contain randomly aligned arrangements of reinforcing fibre. In a reinforced concrete structure the fibres are arranged in a non-random manner and therefore in the general case, the final reinforced concrete composite has non-homogeneous anisotropic properties although the separate components have at least pseudo-homogeneous, isotropic characteristics.

In most composite materials such as fibre-reinforced metals failure of the matrix or of the fibres constitutes the ultimate load condition. However in these materials it is usually assumed that the matrix has a lower breaking strength but higher breaking strain than the fibres [38,39] and either tensile failure of fibres, tensile failure of matrix or shear failure of matrix constitutes absolute failure of the composite. In reinforced concrete composites, particularly when subjected to tensile stresses the concrete matrix has a lower breaking strength and lower breaking strain than the reinforcing fibres. A fundamental difference also exists due to the fact that tensile failure of the concrete matrix

does not imply complete failure of the composite. In fact, in terms of reinforced concrete structures subjected to bending stresses complete failure is deemed to have occurred when the compression concrete fails or in the exceptional case when the reinforcing bars have snapped.

Thus, in the case of singularly reinforced concrete slabs, the complete system consists of an anisotropic composite of reinforcement bar and concrete matrix subjected principally to tensile stresses and an isotropic layer of concrete subjected principally to compressive stresses. In addition the depth of both layers changes as the load increases and the neutral axis rises. These two layers, are acted upon by equal and opposite forces so that equilibrium is maintained at all times. In addition to the condition of equilibrium the layers must also obey the laws of compatibility of deformations. Thus it is necessary for interaction between the layers to exist so that the deformations of the isotropic and anisotropic components are compatible when equal and opposite stress fields are applied to them.

### 3.3 Behaviour of the composite to failure

This section is divided into four subsections relating to different ranges throughout the history of loading. These are the load ranges from zero load to cracking load, from cracking load to the yield of the first set of bars, from yield of the first to yield of the second layer of bars and finally

from complete yield to failure.

Although these phases are treated separately some general patterns of behaviour are, essentially common to more than one range. Thus two important points are related to several load ranges.

They are:-

- a) The effect of the mesh orientation relative to the applied moments on the stiffness of the element in different directions.
- b) The way that twisting moments are resisted by the composite.

Lenschow and Sozen [29] have, by assuming that bars retain their original directions and are only subjected to axial forces concluded that the stiffness of an isotropic element varies by a factor of approximately two when the mesh is orientated through  $45^{\circ}$  to the principal moment direction. This however is said to be only true in a cracked section. In the uncracked state they assume that the orientation of the mesh has little effect on the stiffness of the element. The fact that the inclusion of reinforcement bars, particularly in the case of slabs in which  $\mu \neq 1$ , will form an anisotropic composite with the concrete matrix leading to different elastic properties in different directions in the uncracked state is not taken into account.

In the case of torsional moment resistance, Lenschow

and Sozen [29] have assumed that horizontal stresses in the concrete compression zone and equal and opposite forces in the tensile zone act as a resisting couple to the torsional moment on a crack or yield line. Because they have still retained the assumption that reinforcement bars are in pure axial tension it is stated that a torsional moment cannot exist on a crack or yield line in an isotropic slab as the components of force along the crack from each layer of bars will algebraically sum to zero. Because the shearing stiffness and bending stiffness of a reinforcement bar is not insignificant in relation to the enhancement of moment capacity of 15% which other authors have stated [22,37] it must be assumed that the bar is capable of withstanding shearing forces in both the cracked and uncracked ranges, a fact made use of by Prince [37]. Hence the resultant force acting on an uncracked section in the tensile zone will be made up of components from the concrete matrix, the axial force in the bars and the shear forces on the bars. Along a crack the component of force from the matrix is zero leaving only the contributions from the steel and the small tensile concrete zone adjacent to the neutral axis.

The component of the torsional resisting force in the tensile zone due to the shearing resistance of the reinforcement is often referred to in other contexts and is known to play a significant part in the resisting of applied forces. For

instance Gesund and Boston [41] as a conclusion to their work on longitudinally reinforced concrete beams subjected to combined torsion and bending state 'If there is no transverse reinforcement, the dowel action of the longitudinal reinforcement is of paramount importance in resisting the torsion'. The dowel action referred to is a common reference to the shearing resistance of reinforcing bars.

Further evidence of the anomalies that exist in relation to the shearing resistance or dowel action of intrusions in a matrix can be seen by comparing work done in the field of reinforced concrete with work done in relation to fibre reinforced metals.

It has always been the traditional approach in yield line theory to assume that the principal stress directions coincide with the bar directions in orthogonal meshes. This of course follows from the assumption that the reinforcing bar has no shearing stiffness and therefore cannot withstand shearing forces. Thus Johansen's yield criterion does not include a term describing the twisting resistance in the bar directions in the expression relating the plastic moments of resistance in the bar directions to the moment of resistance in any other direction as in equation (2.14). Only Prince [37] has not followed this assumption but replaces it with the assumption that the principal strain direction lies normal to a crack as described

in Chapter 2.

In contrast to the above approach, work carried out in the field of fibre reinforced metals in which tensile specimens with varying angles of unidirectional fibres embedded in a metal matrix suggests that the principal stress directions are not in the fibre directions. Jackson and Cratchley [38] assumed that the principal stress direction was in the direction of the tensile load as in a standard tensile test on a symmetrical isotropic material. This of course implied that shear stresses existed in the directions of the fibres. However they report that when self-aligning grips were used severe buckling of the specimen occurred and further tests were carried out with wedge grips running inside aligned guides. Thus it is apparent that although the principal strain directions coincided with the load direction there was no guarantee that the principal stress directions also corresponded with these directions as transverse shear stresses could have been set up in the specimen by the transverse reactions from the guides. Indeed in an anisotropic material the principal stress and principal strain directions will not coincide [42]. It is then unlikely that either assumption is correct for on the one hand the reinforcing bars do have shear stiffness and on the other the principal strain and stress directions do not coincide.

### 3.3.1 Zero load to the load at which cracking occurs

In the load range before cracking of the tensile concrete matrix the composite is a continuous system and the stress and strain state at all points in the element may be said to be a continuous function of position. As the load increases the stress or strain state in the composite approaches a critical value at which the concrete matrix fails. As mentioned before there is no reason for the principal stress and strain directions to coincide in the anisotropic composite and thus the type of failure criterion applied to the tensile concrete matrix is important. Research carried out on tensile concrete failures [40] suggests that the criterion of failure should be one of maximum tensile strain.

In a completely unrestrained slab element, analogous to the standard mathematical model of a plate, the stress system imposed on the anisotropically reinforced composite by the applied moments and twists will result in a strain distribution in the element obeying the compatibility of strains condition and of course the directionally varying elastic properties imposed by the positioning of the reinforcing mesh in the matrix. Any deformational restraints on the slab element can be taken into account so that it is possible for the direction of maximum tensile strain and thus the direction of cracking to be forecast.

Within the stress field covering the strain

distribution leading to failure an important factor will be the stress field due to the self-weight moment distribution of the slab element. Although it is normally assumed that the self-weight of the slab has no significant effect on the failure load because of the small percentage moment field that it creates the same assumption cannot be made at the low loads occurring at cracking. Thus the stress field due to the self-weight of the slab element superimposed onto the stress field due to the actual loading will be a significant factor in the distribution of strain in this load range and will consequently effect the direction of cracking.

### 3.3.2 Cracking load to the load at which the first layer of bars yield

Once cracking has taken place in the matrix the composite is no longer a continuous system and discontinuities in the stress and strain functions will exist at the matrix failure points. As many authors have pointed out with particular reference to beams the stress in the steel bars between cracks will be less than the stress in the bars at cracks due to the contribution of the still intact concrete matrix. Thus it would appear that the cracks or matrix failure lines become critical sections. However the behaviour of the intact matrix must not be ignored.

Once cracking has taken place a more complex distribution

of anisotropic properties exists. The uncracked bands of composite retain the same elastic properties that were present before cracking however these bands are separated effectively by thin lines of another composite in which the elastic properties of the matrix are all zero i.e. the bars in an air matrix. The cracked composite can therefore be represented by a model similar to Fig 3.1 in which areas marked A correspond to a concrete - reinforcement composite which retains the anisotropic elastic properties present before cracking and very narrow areas marked B (scale exaggerated) corresponding to an air - reinforcement composite with new anisotropic elastic properties.

Thus if the anisotropic elastic properties of a general composite including cylindrical inclusions were to be formulated taking into account the shearing stiffness of those intrusions the substitution of the appropriate elastic properties of both concrete and air (which would of course be zero) into the general expressions would yield the respective properties of the concrete - reinforcement and air - reinforcement composites. Thus the properties of zone A and B would be known in any direction and an analysis made of the whole system under stress.

Because of the varying properties of two composites A and B and because of the influence of the self-weight moment on the direction of the principal moment field the principal

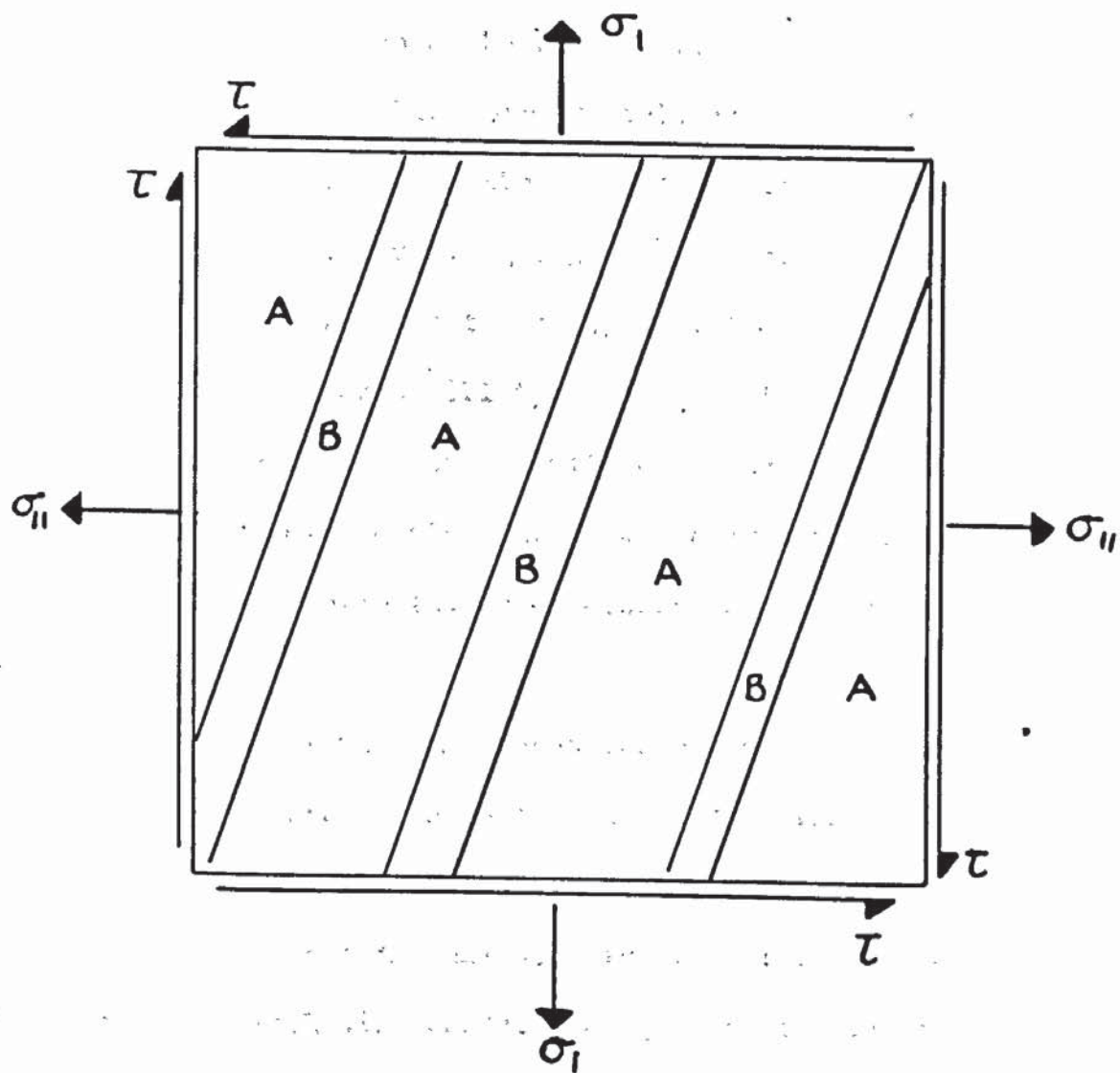


**FIG 3-1 BANDED COMPOSITE**

strain direction cannot be assumed to remain in the direction of the cracks. Hence shear strains will exist in both composites in the crack directions and a maximum tensile strain direction will exist at an angle to the crack directions.

Hence as the applied moment field is increased within this range maximum tensile strains are being set up in the concrete matrix at a varying angle to the crack direction. Once this strain has reached the critical value for a given direction new cracks will form at an angle to the original crack directions consequently changing the model of Fig 3.1 into a more complex form. Lenschow and Sozen [29] have reported this reorientation of cracks in their research work.

Many authors have mentioned the effect of local crushing of the concrete around the bars due to the resulting force along the crack. If such crushing should take place in any load range the anisotropic properties of the bars across the crack will change consequently causing a different mode of failure.

At some stage in the load range the combination of shear stress and axial stress on the bars in the cracked section will combine to cause yield of the steel. The criterion for yield of the steel bars will be that of Von Mises or Tresca as defined in Chapter 2 and thus the direction of plastic flow will not occur in the bar direction.

This critical state will generally occur in only one set of bars initially and thus the yield line will be in a state of elastically restrained plastic flow or an elasto-plastic state.

### 3.3.3 Load at yield of first set of bars to load at yield of second set of bars

This elasto-plastic range will continue until the stress in the second set of bars reaches the critical point dictated by the yield criterion for the steel. At this point plastic flow will occur in the second set of bars and the resultant direction of these plastic flows will become the principal strain direction.

It has been assumed in the theoretical models discussed that the cracks form straight lines across an element acted upon by uniformly distributed moments and that the crack width was a constant at any given load for both sets of bars. Although both assumptions seem fair in the elastic range once first yield has taken place a completely new material exists within the cracks (Zone B, Fig 3.1) Because of these new non-elastic properties cracking could form in the composite in a direction influenced by the first yielding causing new modes of failure to occur. Again it should be possible to reanalyse the problem from the moment at first yield using new properties for the composites.

#### 3.3.4 Load at second layer yield to failure

Once the second layer of bars has yielded the composite in the cracks has no elastic properties and yield should take place in the direction of resultant plastic flow. This direction can of course vary if the directions of the principal applied moments, under the influence of the selfweight moments, are still varying. The stress state in the reinforcement bars will alter and the stress point on the yield function move so that the normal to the curve corresponding to the principal plastic flow direction will change in orientation with respect to the principal moment directions (see Chapter 2). Plastic flow will continue until the stress state in the isotropic compression concrete reaches the critical value of strain resulting in crushing and consequent failure of the whole element.

#### 3.4      Conclusions

Because of the complete change in properties throughout the element at cracking an important factor influencing consequent behaviour of the composite is the orientation of the concrete matrix failure lines. Because of the change in properties described in 3.3.2 subsequent loading of the element will result in reorientation of the principal strain direction possibly leading to further cracking in a new direction at later load values. In addition the effect of the moment due to the self-weight of the slab will become less significant as loading is increased

resulting in a reorientation of the principal moment directions and subsequent redistribution of the stress field throughout the element.

The theoretical model of the slab element is therefore a continuously changing one at each critical stage. Once the properties of the element have changed due to concrete cracking or reinforcement yielding the model becomes increasingly more complex. Thus from the uncracked state in which the anisotropic elastic properties of the composite control the load-deformation characteristics of the element to the point at which failure of the compression concrete occurs the model passes through several stages of development but can, at least up to first yield, be represented by areas obeying strain compatibility conditions but having different anisotropic properties.

Furthermore, up to the present, work in relation to the failure theory of reinforced concrete slabs has assumed that only one yield criterion is obeyed irrespective of any other variables such as the angle between bar direction and principal moment direction. This contrasts directly with the approach taken by workers in the field of fibre reinforced metals [38, 39] where three types of failure criterion make up the overall expression depending on the orientation of the fibres relative to the principal stress direction. Although other failure criteria in reinforced concrete slabs will not be of the same form as those in fibre-

reinforced metals it must be kept in mind that the yield criterion may vary relative to some other variables.

The experimental work carried out and described in later chapters shows that the observations made here have a definite substance and that a more detailed theoretical model is required to describe the slabs behaviour thoroughly.

CHAPTER 4DESCRIPTION OF EXPERIMENTAL METHODS.4.1      Introductory Remarks

Two separate series of tests were carried out and are referred to as

- 1) Plank tests in which the slab elements were subjected to uniaxial moment.
- 2) General Moment tests, in which slab elements were tested under combined bending and torsional moments.

As this investigation was concerned only with the behaviour of reinforced concrete elements subjected to pure moments other generalized stresses had to be removed from the systems. In other words the slab elements had to be tested in such a way that

a) Transverse shear forces

and      b) Membrane forces

did not exist in the test area and did not therefore influence the behaviour of the slab element under load.

Sections 4.3.2 and 4.4.2 describe how releases were made in the loading system so that membrane forces were excluded and how loads were applied in such a way that transverse shear forces were zero in the critical areas.

The principal differences in the two test series

occur by virtue of the number of degrees of restraint against deflexion, curvature and strain existing in the testing arrangements used in either series. It will be seen that in the Plank test series principal curvatures are forced to occur at right angles to the span because of the rigid boundary conditions imposed on the element. (In fact this did not occur in all cases and will be described in detail in Chapter 6). In the General Moment series far greater freedom of deformation was allowed. The only restrictions being that curvatures in one direction were zero and deformations were made symmetrical about the centre line in the span direction. These restrictions are described in detail in 4.3.2 and 4.4.2 and are referred to elsewhere in the text.

The main variables controlled in both series of tests were

- a) the angle,  $\beta$ , between the reinforcement mesh and the span or X - direction.
- and b) the 'degree of orthotropy',  $\mu$  which here refers to the ratio of ultimate moments of resistance in the bar directions and will always lie within the range.

$$- 1 < \mu < 1$$

Other variables such as concrete strength and steel strength were held constant for the most part throughout both series of tests. These common and relatively constant material properties will be described first and will apply to

all test specimens. It should be noted that all test specimens were singularly reinforced and that reinforcement layers were always orthogonal.

#### 4.2      Materials in both test series

##### 4.2.1   Cement

Ordinary Portland Cement produced by the Blue Circle Group was used in all test specimens.

##### 4.2.2   Aggregates

Zone III sand and 3/8 in. crushed gravel supplied by the Midland Gravel Co.Ltd. from pits in the Birmingham area was used in all specimens. Sieve Analyses of both the sand and the crushed gravel are presented in Table 4.1 and 4.2 respectively.

##### 4.2.3.   Concrete Mixes

Trial mixes were used to produce a concrete mix with a seven day cube strength of about 6000 p.s.i. The dry weight proportions of cement, sand and crushed gravel and the water/cement ratio used in all specimens are 1 : 2 : 4 and 0.5 respectively. Fluctuations in properties (Tables 4.3 and 4.4) are believed to have been due to variations in the quality of cement supplied during the fifteen months in which testing was carried out.

##### 4.2.4   Concrete Control Specimens

With each mixing a set of concrete control specimens was cast. This set of control specimens consisted of

Sieve Size or No	%
Retained 3/16in.	4.61
Retained 7	7.39
Retained 14	6.08
Retained 25	8.92
Retained 52	44.8
Retained 100	22.8
Passing 100	5.75

TABLE 4.1  
Sieve analysis of Zone III sand

Sieve Size	%
Retained 3/8 in.	2.24
Retained 3/16 in.	81.89
Passing 3/16in.	15.92

TABLE 4.2  
Sieve analysis of 3/8in. crushed gravel

- a) Three 4in. cubes
- b) Three 20in. x 4in. x 4in. prisms
- c) One 12in. x 6in. cylinder.

In the case of plank tests, one set of control specimens was cast with every two test specimens as it was possible to cast both specimens from the same mix and also test them both on the same day. In the case of General Moment tests one set of control specimens was cast with each test specimen from the same mix.

Compressive strengths were determined by testing the 4in. cubes and averaging the three results. The Modulus of Rupture was obtained in a similar way by the standard flexure test on the prisms. The elastic modulus was taken as the tangent modulus at zero stress and strain as the stress-strain characteristics were linear up to considerable strain values. The value of this modulus was found by testing the cylinder which had been capped with a cement paste soon after casting. Strains were measured by two diametrically opposed Tinsley electrical resistance wire gauges, type 7A. Readings from these gauges being recorded on a Peekel B 103 U strain recorder. In all other respects the control tests were carried out in compliance with the instructions set out in B.S.1881 for the testing of concrete. Loading was applied by means of a 120 ton capacity Denison compression testing machine.

Table 4.3 and 4.4 lists the compressive strengths and

Plank No.	Nom $\mu$	$\beta$	Comp. Strength $u$ lb/in <sup>2</sup>	Mod. of Rup. $f_b$ lb/in <sup>2</sup>
P1	1.0	0°	9007	855
P2	1.0	30°	9007	855
P3	1.0	45°	7042	745
P4	0	0°	9431	755
P5	0	30°	6767	1075
P6	0	45°	7737	925
P7	0	60°	6767	1075
P8	0.25	0°	8736	1010
P9	0.25	30°	8601	870
P10	0.25	45°	8601	870
P11	0.25	60°	9431	755
P12	0.25	90°	8736	1010
P13	0.5	0°	7042	745
P14	0.5	30°	6897	745
P15	0.5	45°	6897	745
P16	0.5	60°	8167	890
P17	0.5	90°	8167	890

TABLE 4.3

Nominal  $\mu$  values,  $\beta$  values and Concrete Properties - Plank Test Series

No	Nom $\mu$	$\beta$	Ta in	Comp. Strength $u$ lb/in <sup>2</sup>	Mod. of Rup. $f_b$ lb/in <sup>2</sup>
TB1	1.0	0°	3.0	10864	1230
TB2	1.0	30°	3.0	5964	1065
TB3	1.0	45°	3.0	8134	1020
TB4	1.0	0°	11.25	8591	785
TB5	1.0	30°	11.25	7112	830
TB6	1.0	45°	11.25	7705	870
TB7	1.0	0°	17.5	8139	885
TB8	1.0	30°	17.5	6907	810
TB9	1.0	45°	17.5	6389	645
TB10	0.5	0°	3.0	6613	895
TB11	0.5	30°	3.0	6617	925
TB12	0.5	45°	3.0	7313	860
TB13	0.5	60°	3.0	6085	765
TB14	0.5	90°	3.0	6701	840
TB15	0.5	0°	11.25	7807	840
TB16	0.5	30°	11.25	6300	785
TB17	0.5	45°	11.25	6356	615
TB18	0.5	60°	11.25	6533	965
TB19	0.5	90°	11.25	6678	880
TB20	0.5	0°	17.5	7037	980
TB21	0.5	30°	17.5	6739	895
TB22	0.5	45°	17.5	7327	730
TB23	0.5	60°	17.5	7033	840
TB24	0.5	90°	17.5	6963	630
TB25	0.5	135°	3.0	4872	645
TB26	0.5	135°	11.25	4662	710
TB27	0.5	135°	17.5	5409	615
TB28	1.0	67.5°	3.0	4709	765
TB29	1.0	67.5°	11.25	3435	660
TB30	1.0	67.5°	17.5	2450	588
TB31	1.0	0°	17.5	5292	840

TABLE 4.4

Nominal  $\mu$  values,  $\beta$  values, Ta values and Concrete Properties  
General Moment Series

modulii of rupture obtained from the control tests associated with each test specimen, results for Plank test specimens being presented in Table 4.3 and results for General Moment test specimens being presented in Table 4.4 E- values were found to be almost constant in all tests at a value of  $4.2 \times 10^3$  lb/sq.m.

#### 4.2.5 Reinforcement

Two types of reinforcement were used. In most specimens the reinforcement mesh was made up of 3/8 in mild steel reinforcing rod supplied by G.K.N. Tensile test results on specimens supplied by the manufacturers indicated that elastic and plastic characteristics were favourable to the requirements of the investigation. A fairly sharp yield point and little strain hardening during yield were the principal properties influencing its choice. All the 3/8 in. mild steel rod was supplied in one delivery in twenty foot lengths cut from the same reel. Thirty six tensile tests were carried out on random samples of the steel in a Dennison Universal Testing machine. In twenty four of the tests strains were measured by means of a Lyndly dial strain gauge with 2in. gauge length. In the remaining twelve tests stress - strain plots were obtained using a Baldwin automatic strain recorder. The relative mechanical properties such as Youngs Modulus, yield stress and yield strain were found to be consistent enough to enable an averaging of results to be carried out. These are summarised in Table 4.5.

Youngs Modulus lb/in <sup>2</sup>	Yield Stress, $\sigma$ lb/in <sup>2</sup>	Yield Strain Microstrains
29.5x10 <sup>6</sup>	40550	1370

TABLE 4.5

Steel properties -  $\frac{3}{8}$ " diameter mild steel

Youngs Modulus lb/in <sup>2</sup>	Yield Stress, $\sigma$ lb/in <sup>2</sup>	Yield Strain Microstrains
39x10 <sup>6</sup>	51530	1325

TABLE 4.6

Steel properties - annealed  $\frac{1}{4}$ " diameter mild steel

In the case of slabs in the Plank Test series, P8 - P12, it was found that the use of 3/8in. mild steel in the upper layer would result in excessive spacings between bars occurring if the required 'degree of orthotropy' of 0.25 was to be achieved. A steel with a lower yield load was needed to limit the spacing in the upper layer. It was found that specimens of 1/4in mild steel supplied by G.K.N. had a yield strength close to that required to achieve a practical bar spacing. However this steel exhibited considerable strain hardening properties immediately after yield and it was decided that the annealing of a quantity of 1/4 in. mild steel bars would produce the necessary adjustment in properties. After annealing tests had been carried out in the Department of Metallurgy at the University of Aston it was found that annealing at 600°C for one hour with air cooling after heating produced the required properties. The British Heat Treatment (Deritend) Co of Birmingham carried out the annealing on the necessary quantity. The results of tension tests on this annealed 1/4 in. mild steel are presented in Table 4.6. Typical stress-strain curves for both the 3/8 in. mild steel and the 1/4 in. annealed steel are drawn in Fig 4.1.

#### 4.3. Experimental methods used in Plank test series

##### 4.3.1 Description of specimens

In all, seventeen specimens were tested in this series. Each slab bears a reference mark P. followed by the number of

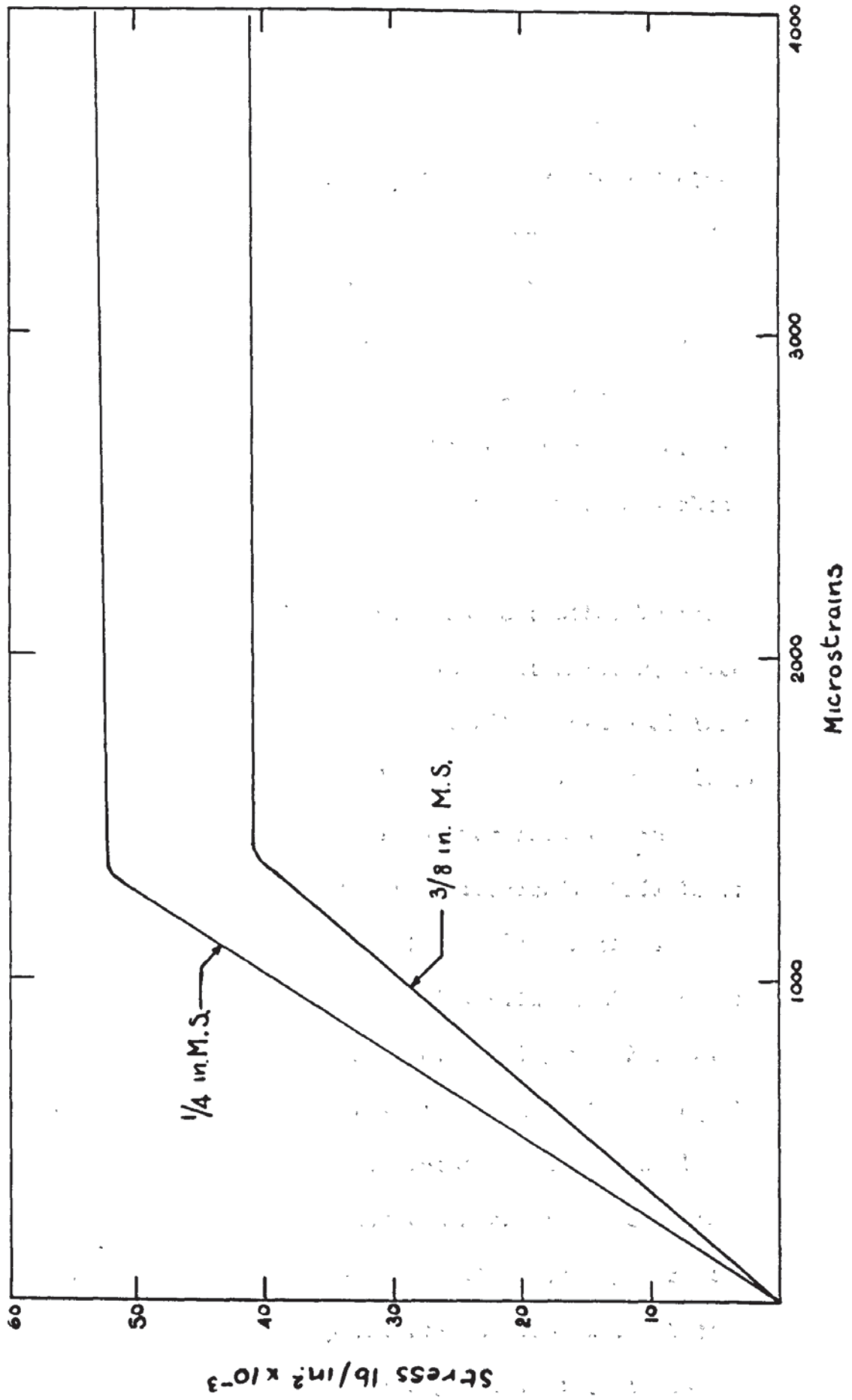


**FIG 4-1 REINFORCEMENT STRESS - STRAIN CURVES**

the specimen i.e. between one and seventeen. All slabs measured 38in x 30in. the uniaxial moment being applied across the shorter side. Thickness varied very slightly but averaged 3.003 in. which was very close to the nominal thickness of 3 in. Thicknesses were measured by means of a micrometer screw gauge set at the open end of a fork made up of light hollow section. The thickness is a critical factor in determining the ultimate moments of the slabs as listed in Table 6.1 for each plank specimen. The values used were the average of values obtained at twelve points in the test area.

The 'degree of orthotropy' was controlled by the spacing of the reinforcement bars. The bottom layer, which had a concrete cover to the bottom, tensile surface of 1/2in was made up of 3/8 in. mild steel bars at 3in. centres in all specimens. The top layer however had variable spacing according to the degree of orthotropy required. This layer also consisted of 3/8 in. mild steel bars in all slabs except P 8 - P12 where annealed 1/4 in. mild steel bars were used. In slabs P1 - P3 the top layer spacing was 2.5 in. These slabs had a nominal 'degree of orthotropy' of  $\mu$  equal to one and the bar spacing was calculated assuming a slab thickness of 3in a cover of 1/2in and a concrete strength of 6000 p.s.i. Because of the lower effective depth of the top layer of steel, which lay directly on top of the bottom layer and was in all specimens orthogonal to it, it was

necessary to reduce the spacing of the bars to compensate for the reduction in lever arm.

In all slabs whatever the nominal value of  $\mu$ , allowance was made for this reduced effective depth of the upper layer of reinforcement. Because slab thicknesses and concrete strengths varied however, the degree of orthotropy also varied from the nominal figure. Slabs P4 - P7 were reinforced only by the bottom layer thus having a value of  $\mu$  equal to zero. Slabs P8 - P12 had a top steel layer consisting of annealed 1/4 in. mild steel bars at a spacing of 5.25 in between centres giving a nominal  $\mu$  value of 0.25. Slabs P13 - P17 had a top layer spacing of 4.625 in. between centres of the 3/8 in. mild steel bars giving a nominal  $\mu$  value of 0.5. The nominal  $\mu$  values for each specimen are also indicated in Tabel 4.3 for reference. The actual values are presented later (see Chapter 6 Table 6.1)

Table 4.3 also shows the angle at which the reinforcement mesh was layed relative to the londitudinal axis of the slab element. These ahgles,  $\beta$  refer to the angle between the bottom layer of reinforcement and the X - direction (longditudinal) as shown in Fig 4.2. This figure shows a plan view from above the slab i.e. from compression to tension face, and shows how, during construction of the mesh bars always generated from the same corners A and B of the slab in every specimen. After setting these two reference bars, one in the

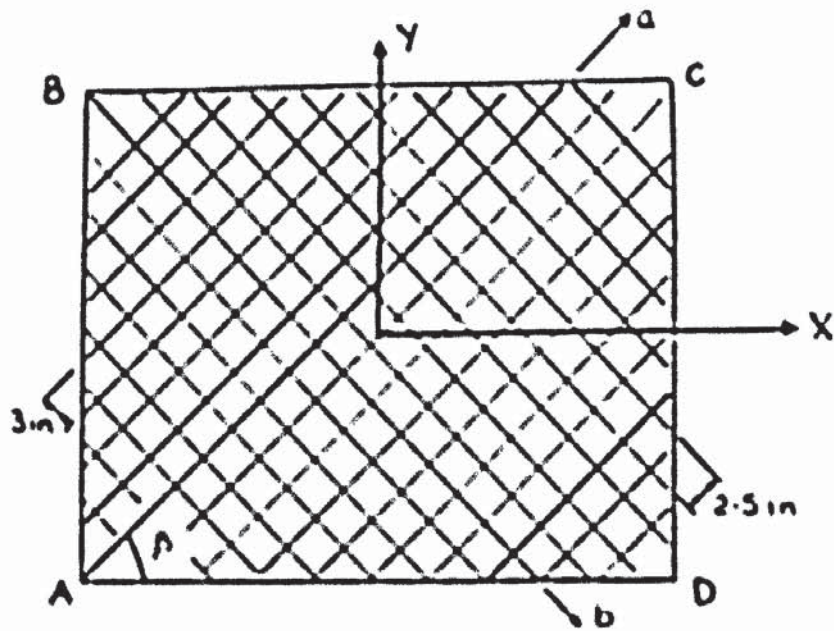


FIG. 4.2 PLAN OF TYPICAL MESH.  $\mu=1$

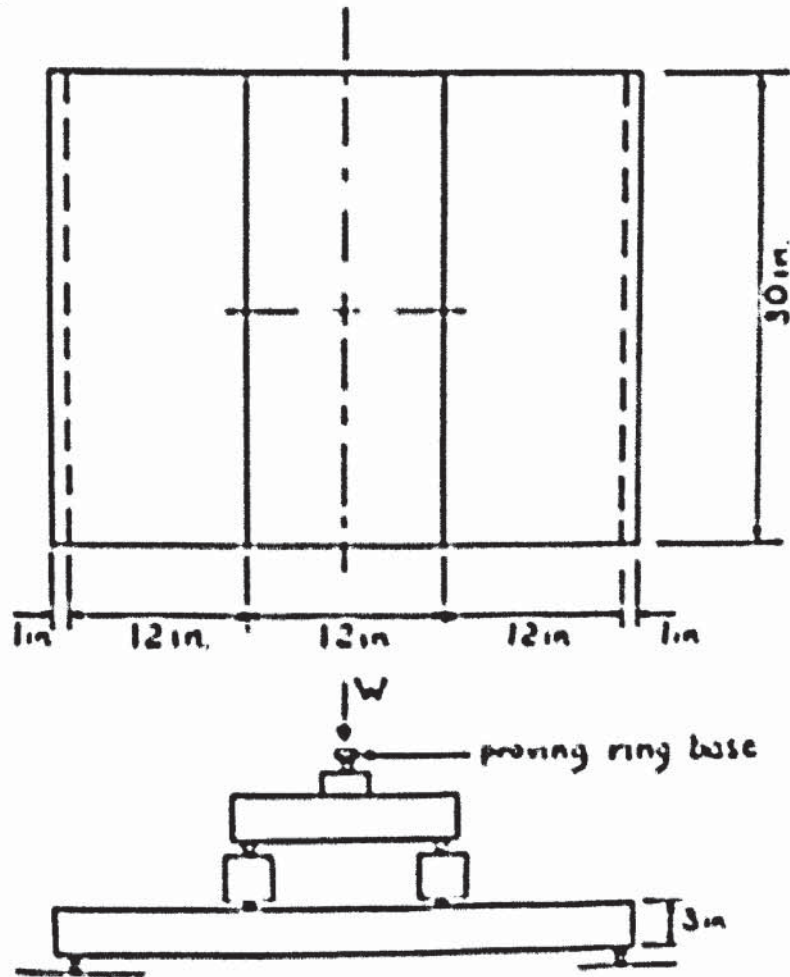


FIG. 4.3 TEST SET UP

top and one in the bottom layer, the rest of the mesh was made up by wiring together upper and lower layers at the given spacing with the aid of wooden spacing blocks. All bars were hooked at each end before wiring into the mesh. The hooks were formed in such a way as to give  $3/8$  in. cover to the top face and extended 5 in. into the compression face. Typical made up meshes ready for casting are shown in Plate 4.1.

Casting was carried out on a variable speed vibrating table after the concrete had been mixed in a mixer of the non-tilting drum type manufactured by Liner Concrete Machinery Co.Ltd. The  $1/2$  in. cover to the bottom steel was maintained by affixing  $1/2$  in mortar spacing blocks to the lower reinforcement layer. Curing of the slabs was carried out in a controlled humidity curing room, the specimens being stripped of their sides after two days. The plywood moulds were inspected frequently for wear and parts replaced if necessary. The base of the moulds consisted of  $1.1/2$  in. plywood and care was taken to support the underside adequately during casting and curing to avoid sagging and subsequent malformation of the specimens.

#### 4.3.2 Test set-up

Tests were carried out within a large permanent portal testing rig. The rig was constructed from I-sections in such a way that a 6 in. space existed between the two I-sections making up the base. The total width of the base was

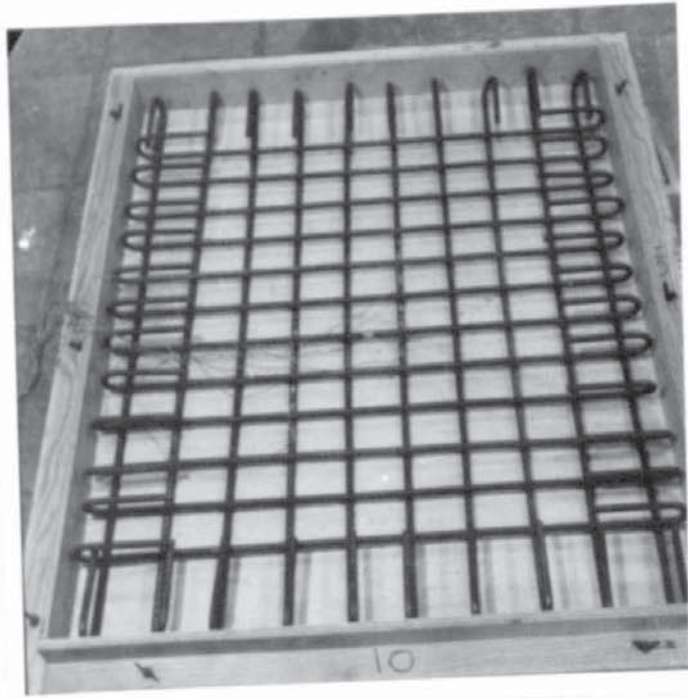


PLATE 4.1;  $\beta = 0^\circ$

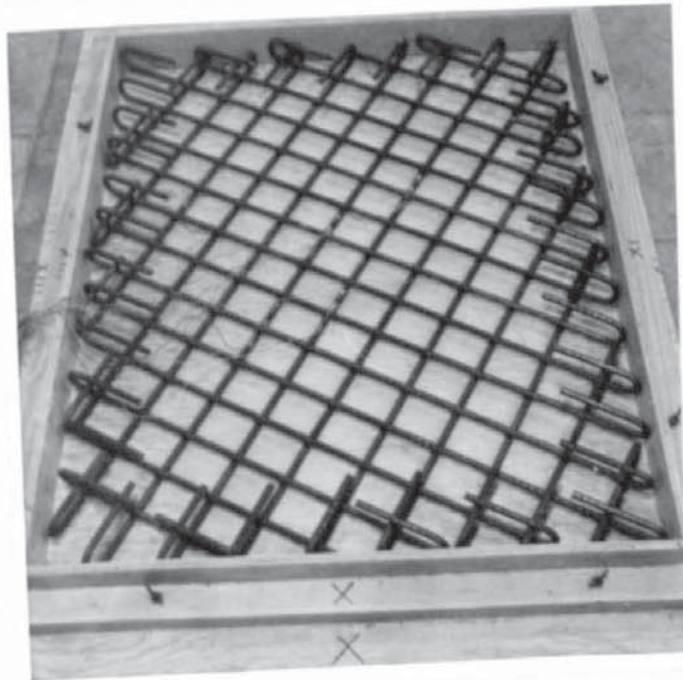


PLATE 4.1,  $\beta = 30^\circ$

2ft. and therefore it was necessary to support the shorter edges of the slab elements on suitably stiffened I-sections placed transversely to the length of the portal frame. These 6in x 6in I-sections were stiffened to give a solid base for the 1/2 in. diameter rollers which rested directly on the upper face of the transverse I-sections. One roller was fixed in position with wedges, the other allowed to roll, so preventing membrane forces from being present in the specimen. The rollers were 3lin. long thus allowing a little overlap at each side of the slab. Metal strips 3lin. x 1 in. x 1/2in. were fixed transversely to the under side of the specimen 1 in. in from either end of the slab. These strips rested on top of the rollers giving a total space of 36in. to the slab element. Loads were applied to the upper surface in the form of two line loads plastered transversely onto the upper surface 6 in. to either side of the slab centre line. The line loads were transmitted to the slab by two 3in. square rectangular hollow sections with a length of 3lin. A metal strip 3lin. x 1in. x 1/2 in. was welded onto one face at the hollow section and was plastered onto the slab surface thus giving an even distribution of load across the slab and over an area of 30in. x 1in. On top of each hollow section a 4in. x 4in. x 1/2in. was placed so that it lay centrally with respect to the longitudinal or span direction of the specimen and with respect to the hollow section itself. A 4in. x 1in.

diameter roller was placed in the centre of each of these plates which distributed load from the rollers to the rectangular hollow section without the upper face yielding locally under load. Again one roller was fixed and the other free to move. A rectangular hollow section 14in. x 3in. x 3in. was placed centrally and longitudinally on top of these rollers and a 4in. x 4in. x 2in. metal block with a ball recess in its upper face was placed centrally on to it. A 1 in. diameter hardened steel ball was placed into this recess and a 10 ton capacity proving ring with a similar ball recess in its base was placed on it vertically. A vertically aligned, centrally positioned, 10 ton capacity, long travel jack acted on the upper block of the proving ring and was operated by a hand pump system.

When each specimen was set up the jack, which had been initially checked for vertical alignment, was left in position and the slab centred around it. Any slight warp of the specimen which may have occurred during curing was taken up by careful levelling of the specimen whilst plastering the metal strips on to the base.

The test set up is shown in detail in Fig 4.3 and Plate 4.2. It can be seen that a maximum moment was produced by the loading system across the central 12in. of the slab. Consequently the transverse shear force was zero within this area.

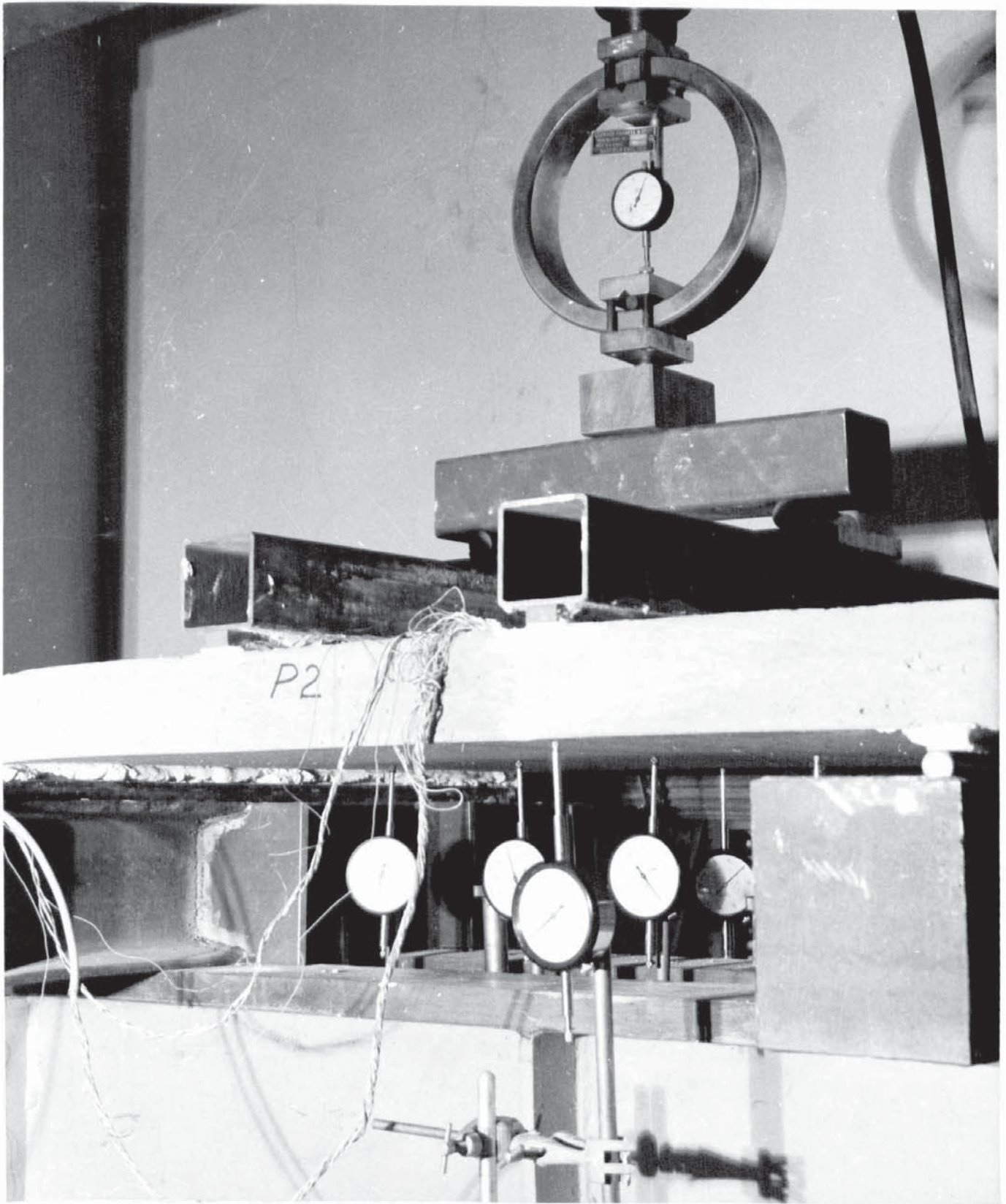


PLATE 4.2

### 4.3.3 Instrumentation

#### a) Steel Strains

Steel strains were measured by placing electrical resistance foil strain gauges on the reinforcing bars within the area under maximum moment which lay between the two line loads. Normally two bars in each layer were instrumented in this way with two gauges on each bar making a total of eight gauges in all. The gauges used were Budd Metal Film gauges, type c6 - 121 which had a nominal gauge length of 1/8in. Although Lenschow and Sozen [29] found that the c6 - 121 did not behave well at strains close to yield it was thought that this may have been due to the fact that Eastman 910 cement was used to adhere the gauges to the bars. The gauge manufacturers promised a strain of up to 4 or 5% for c6 - 121 gauges if surface preparation was correct and Budd G.A.2 strain gauge cement was used for bonding the gauge to the reinforcement. Consequently the manufacturers specifications were followed closely, special care being taken to sand the metal bright with wet and dry paper and to degrease and neutralize the surface with Trichlorethylene and 10% dilute Ammonia solution respectively. Initial difficulty was found in ensuring that the gauge, which was set in the direction of the reinforcement, followed the relatively high transverse curvature of the bar. After affixing the gauge with the aid of a cellotape strip wooden formers were screwed into place around

the gauge so that a uniform pressure was applied to it. Greased paper was inserted between the mould and the gauge to ensure that the two did not become bonded together. This method was found to be tedious however and equally satisfactory results were produced by applying a second cellotape strip around the bar and gauge in such a way that about 15 p.s.i. pressure was exerted on the gauge.

The gauges were positioned on the top side of the lower layer of bars and on the bottom side of the upper layer so that strains were measured at the same level below the upper concrete surface. The gauge positions for each individual test are described in Chapter 5. Plate 4.3 shows close up shots of gauges fixed to reinforcement in one of the specimens. After the gauges had been fixed to the bars the cement was cured under infra-red radiation for about 8 hours, after which time the cellotape strips were peeled off leaving the gauges exposed. Five electrical wires from a 25 - wire core manufactured by Radiospares Ltd was soldered to the exposed tabs of the gauges, the wires being led across the top of the reinforcement mesh to the side of the specimen. The gauges were then waterproofed using a mixture comprising of an epoxy resin (Shell Epikote 828) a plasticiser (Thiokol L.P. 33) and a hardener (Shell Epicure R.T.U) in the proportions of 5 : 2 : 1 by volume. This compound was cured for about 3 hours under infra-red lights. It was found that three applications

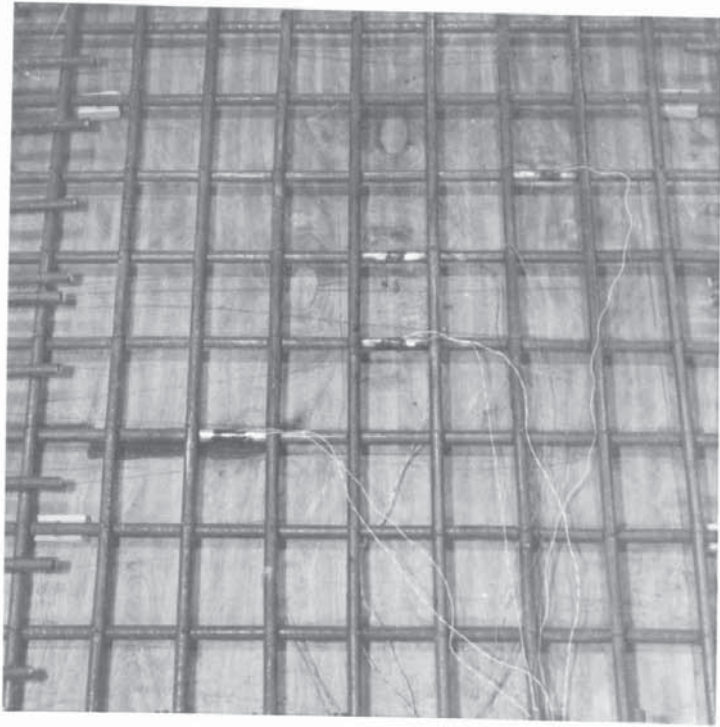


PLATE 4.3



PLATE 4.4

were required to give satisfactory results. On several specimens towards the end of the test series a synthetic rubber coating compound 'Gagekote #2' was substituted for the three part compound and although results were as satisfactory only one or two coats were needed of the two part compound and application was thus facilitated.

Gauge positions and respective coloured wires were noted before casting, so that connection to the strain recorder could be carried out easily. The same strain recorder was used to measure steel strains and concrete strains and will be described in the next section 4.3.3 (b).

b) Concrete Strains

Although, due to the restraints placed on curvature by the test setup, the principal directions should have been predetermined it was thought necessary to check this assumption by using strain gauge rosettes on the upper concrete compression surface. It was decided that in view of the large number of rosettes needed for all specimens in both test series, a 45<sup>o</sup> rosette would be made up using carefully aligned individual strain gauges. It had been found that good results can be obtained for concrete strains by using electrical resistance wire gauges manufactured by H. Tinsley and Co.Ltd. Type 6E with a nominal gauge length of 16 mm. and width of 2.5mm.

In all tests in this series the gauges were placed in the same position on the slab surface. Three 45<sup>o</sup> rosettes

were made up of nine gauges of the above type as shown in Fig 4.4 and plate 4.4. One rosette was placed at the centre of the slab the other two rosettes being placed anti-symmetrically about the centre in such a way that they lay 1.25 in along the longitudinal axis and 4.5 in transversely from it. In this way a check was introduced on the strain distribution within the nearly constant moment area between the line loads.

The rosette positions were sanded to remove any bad surface characteristics and carefully marked. F.88 dental cement manufactured by Tridox Products, Philadelphia, U.S.A. was used to fix the gauges to the concrete surface. This quick drying cement has been found to be particularly successful when used in conjunction with the Tinsley felt-backed wire gauges used throughout this investigation. The same type of wire used with the strain gauges on the reinforcement was soldered to the tabs of the strain gauges on the concrete compression surface.

All wires, from gauges on both steel and concrete, were led to an extension box type 48U designed to be used in conjunction with the Peekel B 103 U strain recorder which automatically converts resistance changes into microstrains. Although this model does not automatically scan the strain readings it does have the advantage that only one dummy gauge is needed to complete the Wheatstone circuit for every 24 active gauges employed. A dummy block was formed from a

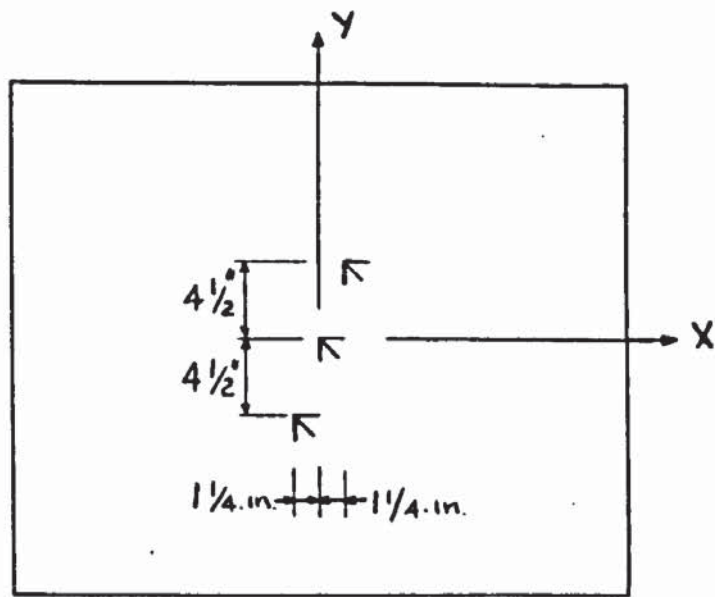


**FIG 4.4 CONCRETE GAUGE POSITIONS**

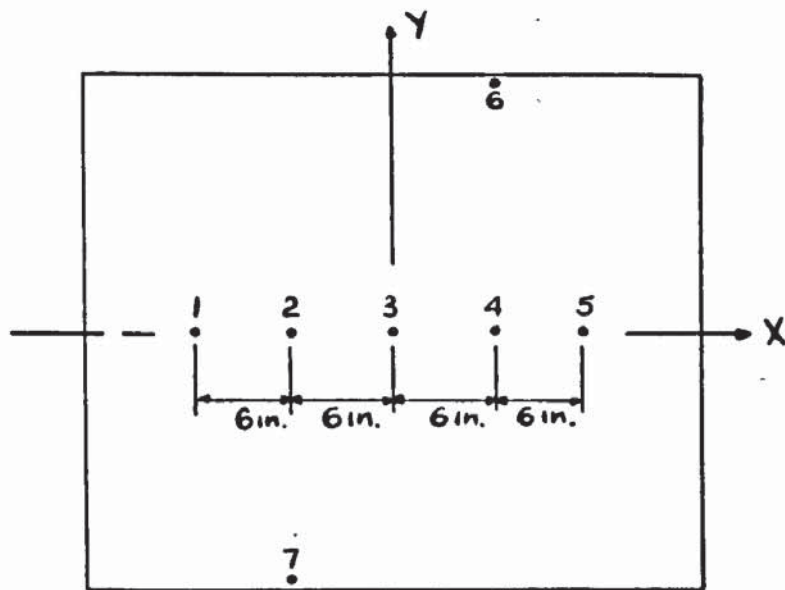


**FIG 4.5 DEFLEXION POINTS**

24in. x 4in. x 4in. prism cast from the first concrete mix and used subsequently throughout the test series. A short length of 3/8 in. reinforcement bar with a c6 - 121 gauge adequately waterproofed was cast into the prism and a Tinsley 6E gauge afixed to the concrete surface. These two gauges acted as the central dummy gauges for the two different sets of strain gauges, the dummy block being placed close to the specimens during test so that temperature compensation was adequate. The leads joining the dummy gauges to the extension box were of the same length as those connecting the active gauges to it so that no inaccuracies developed through electrical imbalance.

c) Mechanical dial gauges

Batty 2in. travel dial gauges were used to measure the deflexions of selected points on the bottom surface of the slab. The gauges were supported on adjustable stands set onto a solid, prepared base in between the I - sections making up the lower member of the permanent portal testing rig so that the gauges could be reset when deflexions exceeded 2in. Five dial gauges were set onto points on the longitudinal axis of the slab, so that the deflexions at the centre of the slab and at two points 6 in. and 12 in. either side of the centre could be measured. In addition the deflexions at the edges of the slab were measured by two gauges, one on either side of the slab and directly under each line load

i.e. 6in. from the centre. The gauge positions, which were the same for all slabs, are shown diagrammatically in Fig 4.5.

Curvatures in the X - direction or span direction were obtained from these deflexions at points, 2, 3 and 4. It was also possible to check the curvature at point 3 in the T direction as defined in Fig 4.5.

d) Load Measurement

Loads were measured by means of a ten ton capacity proving ring set up as described in section 4.3.2. The proving ring was calibrated in the Denison Universal testing machine before any tests were carried out and checks were carried out by recalibrating twice during the course of the test series. The proving ring factor was found to be the same in all calibration tests and was taken to be 0.0081 tons per division on the dial gauge in all subsequent calculations of load and moment.

4.4. Experimental methods used in General moment tests

Although basic size differences exist between slab elements in this series and slab elements in the previously described plank test series many of the methods, particularly instrumentational methods, are very similar and will not be described in the same detail as before. For completeness however the same format will be followed as that used in section 4.3 and reference will be made to that section when

appropriate.

#### 4.4.1. Description of specimens.

Thirty one specimens were tested in this series, one being a repeat test. The reference mark used in this series was T.B. followed by the number of the specimen i.e. between one and thirty one. All slabs measured 36in. x 36in. x 3in. nominally. The thicknesses were measured using the same micrometer - fork method employed in the plank series and described in 4.3.1. The average thickness was 2.97 in. and the actual average thicknesses of each specimen were used in the calculations of ultimate moment presented in Table 7.1. The values again used being the average of values at twelve points in the test area.

The 'degree of orthotropy'  $\mu$  was controlled in the same way as described in 5.3.1 although in this case only nominal values of 1.0 and 0.5 were considered. Consequently only 3/8 in. mild steel was used in the construction of the reinforcement mesh in all specimens. The orthogonal mesh was made up in the same way as before, hooks being the same size and for easy reference of bar position two orthogonal bars generated from corners A and B as indicated in Fig 4.6 and Plate 4.5 in all specimens, the mesh being built up from these reference bars. All slabs were singularly reinforced with reinforcement adjacent to the bottom face only, the concrete cover being 1/2in. as before. Due to the mode of application

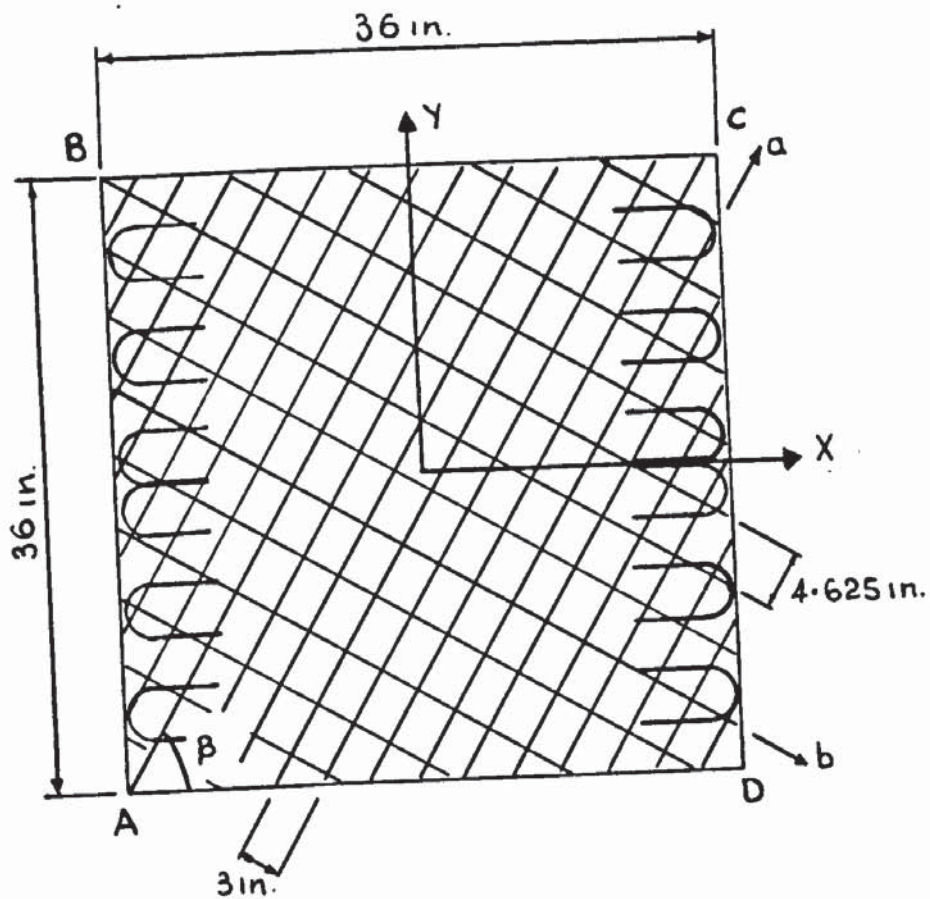


FIG.4.6 TYPICAL MESH,  $\mu = 0.5$ .

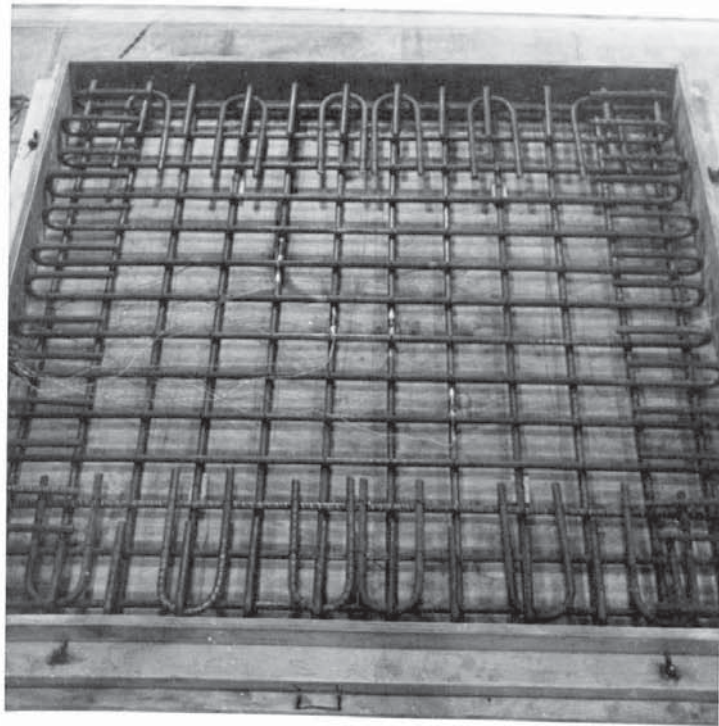


PLATE 4.5

of the bending and twisting moments to the edge of the slab as described in 4.4.2 it was necessary to provide extra reinforcement to the clamped edges of the slab. This consisted of 10 U-shaped reinforcement bars laid on top of the mesh so that the plane of the U lay in the plane of the mesh. These extra reinforcing pieces extended from the inside of the hooks 6in. into the slab and did not therefore fall within the central area of the slab defined by the outer dial gauge positions described in 4.4.3 (c). In addition to these extra reinforcement bars which were made up of 3/8in. reinforcing bars, 1/4 in. bars in stirrup shape were used along the clamped edges to prevent the corners breaking off, while load was applied. These extra reinforcing details are also shown in Fig 4.6.

The angle  $\beta$ , which the bottom layer of reinforcement made with the X-direction of span direction as defined in Fig 4.6 was varied as before and listed against each slab in Table 4.4. Again Fig 4.6 is a plan of the slab from above.

Casting was carried out in the same manner as that employed in the previous section 4.3.1, the 1/2in. cover being maintained by 1/2 in. mortar spacer blocks wired tightly to the bottom steel layer at appropriate points. Curing however could not be carried out in the constant humidity room as before, due to size restrictions, consequently the slabs were covered with a polythene covered wooden framework

immediately after casting. Wet hessian was layed over the slab surface after the initial set of the concrete was complete. The sides were stripped after two days, the sacking being soaked every day and the polythene covers being kept in position over the slabs to prevent excess evaporation. The moulds were of the same kind as those used in the plank test series except for the actual dimensions of the casting area. The mould was well supported during curing so that a plane surface developed. The upper surface was carefully trowelled after casting so that a smooth finish ensued.

As most specimens were tested after seven days the slab elements were allowed to dry and were set up on the day preceding the test.

#### 4.4.2. Test set up

The test rig employed in this series was to be as free from restraints as was practicable in applying a combined bending and torsional moment to the slab element, unlike the plank test series in which deformational or kinematic restraints were deliberately imposed in the form of rigid line loads and support conditions.

Complete freedom to deform whilst still applying moments would seem practically impossible or at best highly complex. It was decided therefore to contract certain deformations which in the mathematical model would have non-zero values. The system adopted prevented curvatures in the

Y - direction as defined in Fig 4.6 by clamping two opposite edges of the slab element into rigid channels. In this way the bending moment and twisting moment were introduced into the specimen. In all, a test rig was needed that would

- a) Exclude vertical shear forces from the system.
- b) Exclude membrane forces from the system.
- c) Enable different combinations of bending and twisting moments to be introduced proportionally into different specimens.
- d) Enable loading to be carried out easily and to allow curvatures to be measured readily by means of mechanical dial gauges.

The final test-rig satisfied these conditions and will be described in detail below.

Testing was to be carried out in a large permanent portal testing rig, in which the upper cross member was easily adjustable with respect to the lower cross member, forming the base. A support point was provided at one end by a ten ton capacity proving ring which slotted into a locating holder bolted onto a 16in. x 10in. x 2in. steel block; this in turn rested on two 1/2in diameter rollers which were placed transversely to the longitudinal I - sections making up the base of the portal rig and prevented membrane forces building up in the slab element. The other support point was made up of a 2in. diameter solid steel rod, 7in. long, one end of

which was recessed to hold a 1in. diameter steel ball the other being welded orthogonally onto a 16in. x 10in. x 2in. steel plate. This plate was placed, with its longest side at right angles to the portal base, onto two heavy blocks in such a way that when a 1in. diameter ball was placed into the recess in the top plate of the proving ring the two ball bearings were at the same height.

The ball bearings at the support points fitted into recesses in the underside of two similar stiffened plates 1/2in. thick which tapered from 36in. wide at one end to a 4in. radius arc at the other. The ball recess was situated at the centre of this 4in. radius circle, the distance from the other end of the plate to it measuring 16.3/4in. On top of and along the 36in. edge of the plate was welded a 4in. x 4in. x 1/4in. channel which acted as a location and clamp for the edge of the slab element. The bottom, open edge of the channel was welded flush with the edge of the 1/2in. plate and six holes were tapped in the upper leg of the channel at 6in. centres. The channel - plate system was stiffened by welding 6 1in. thick plates onto the channel and across the plate so that the stiffening plates were 8 in. deep at the front edge of the channel tapering to 1/4in. at the other edge.

Plaster of Paris was spread onto the inner walls of the channel so that when the specially reinforced slab edge

was located into it an even distribution of moment was ensured along its length. Care was taken to check that the centre of the slab and channel coincided. A 1/4in. x 3in. x 36in. plate was introduced between the top face of the slab and the channel and was screwed down onto the slab by hardened Allen screws acting through the six tapped holes in the channel. In this way the slab edge was effectively clamped against curvature along its length. Hooks at the ends of the channels were used to lift the slab and clamped plates onto the two support points. The system was then centred under a previously aligned twenty ton capacity long travel jack and was chocked from underneath to hold it steady.

Bending and twisting moments were applied to the slab element by a centrally positioned jack acting through a cross-beam onto metal blocks positioned on the top of the channels. The cross-beam was fixed rigidly to the base of the jack and could readily be orientated at any angle to the line between the support points i.e. the  $x$  - direction as defined in Fig 4.6. Thus by turning the cross-beam at an angle to the  $X$  - direction and loading through the metal blocks onto the channel varying twisting moments could be applied to the edges of the slab. The bending moment in the  $X$  - direction was constant across the slab and hence no vertical shear forces existed in this direction. By placing the metal blocks, which were recessed to receive a lin. ball between cross beam and

block, at 17.5in. and 11.25in. either side of the slab centre line defined as the Torsional leverarm,  $T_a$ ., nominal ratios of  $M_{xy}$  to  $M_x$  of 1.166 and 0.75 could be obtained as the distance between the support point and the centre of the block was always 15in. measured along the X axis. Because of lack of space a special system of loading was needed to produce a torsion arm of 3in. This was simply produced by placing a 2.1/2in. x 2in. x 14.1/4in. block onto two metal blocks 6in. either side of the centre line, the loading point being provided by a ball recess 3in. from the centre on the cross block. Thus another  $M_{xy}/M_x$  ratio of 0.2 was produced. A release was provided in the form of small rollers between the cross beam and channel so that the loading blocks did not tip as loading was applied. The test set up can be appreciated more readily by the diagrammatic representation in Fig 4.7 and in Plate 4.5.

It can be appreciated from Fig 4.7 and the preceding text that the point supports allow free rotation of the slab element. The balls between the cross beams and loading blocks also allow this rotational freedom without the blocks tilting and stability being lost. The system does not allow a uniaxial moment to be applied as this would be an inherently unstable position. Thus slabs were tested under three combinations of bending and torsional moment as described in Chapter 5. The fixity between cross beam and jack head was needed to prevent rotational instability of the whole slab system.

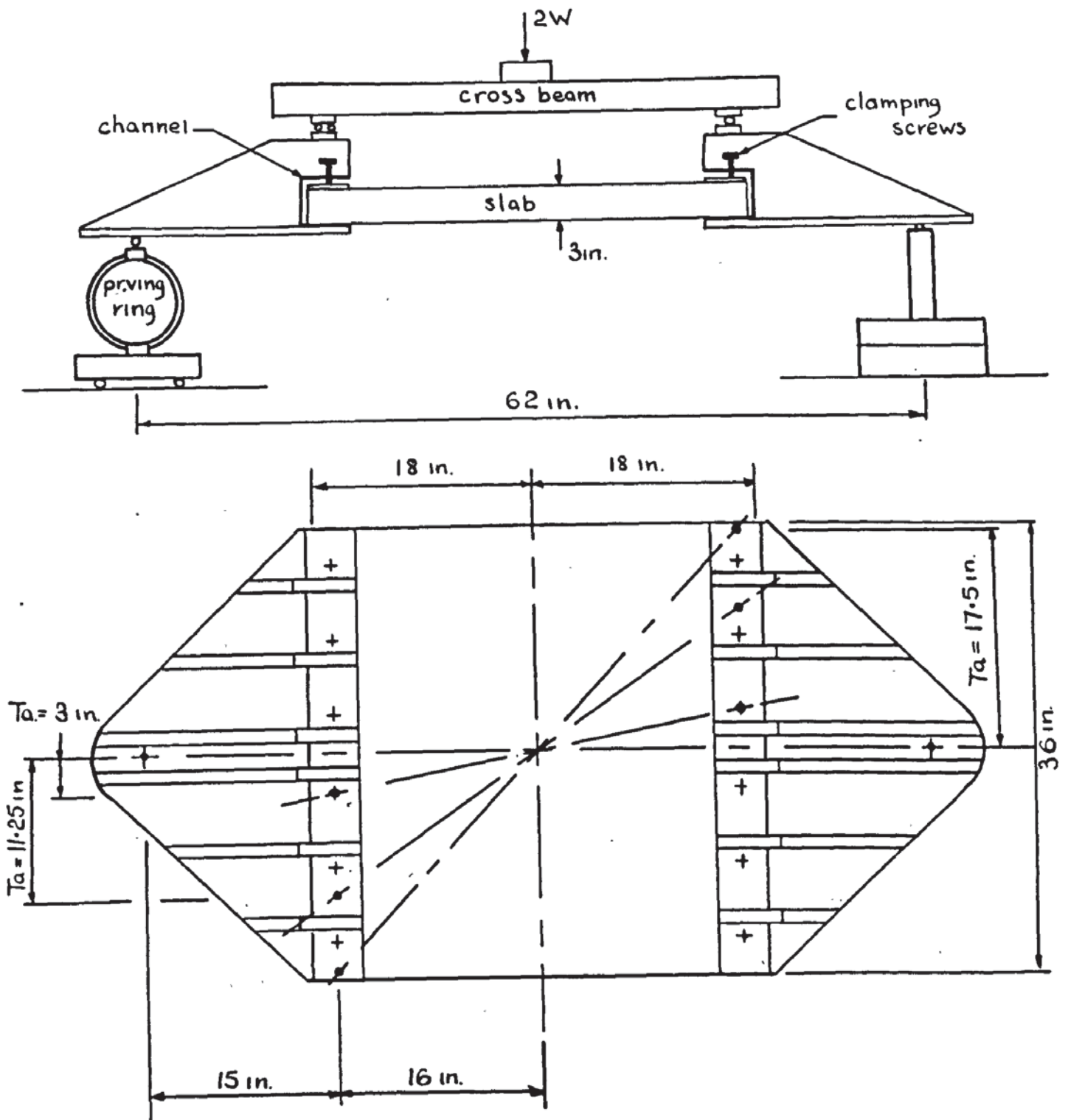


FIG.4-7 TEST SET UP

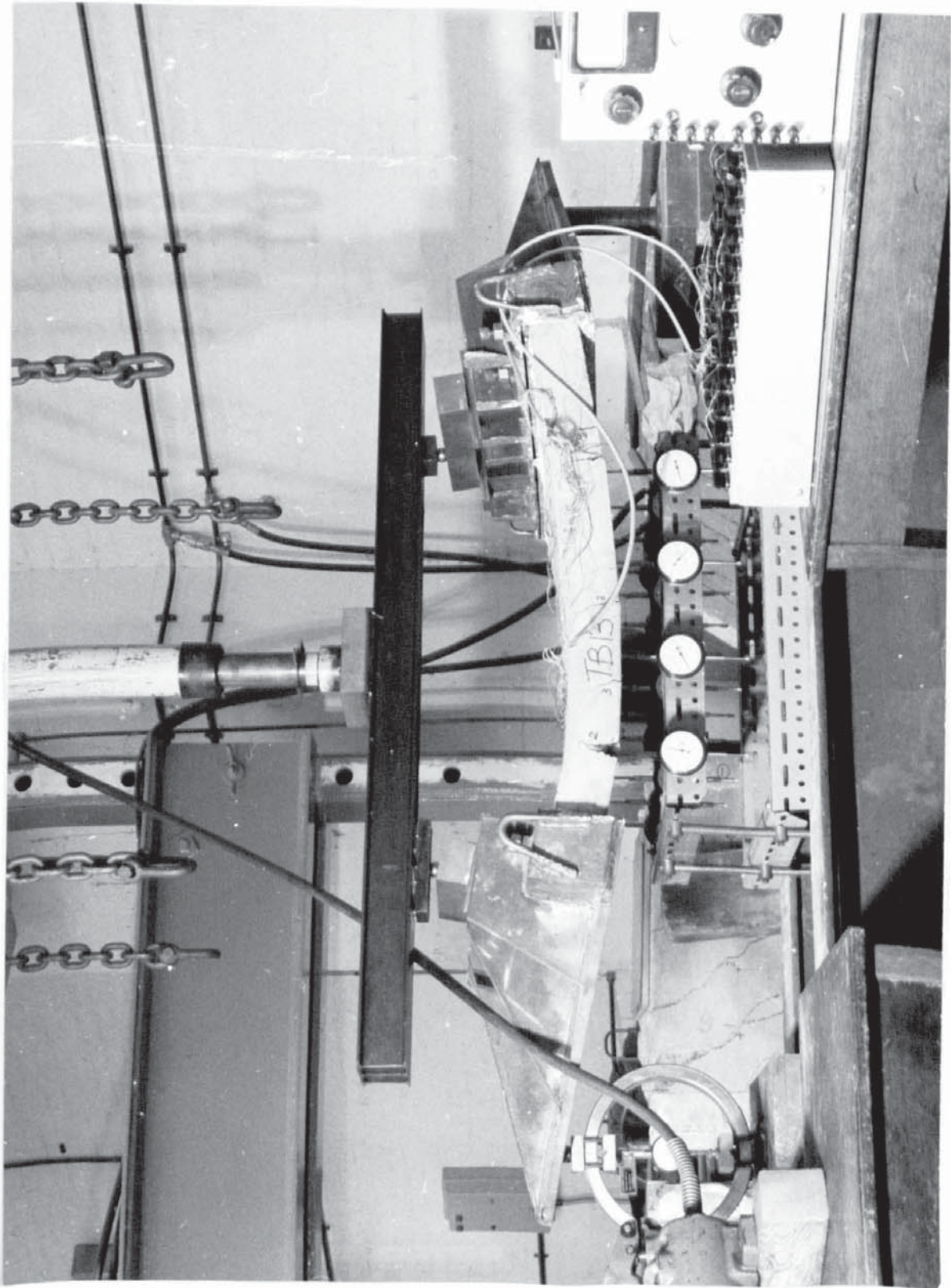


PLATE 4 • 6

Essentially then the test set up described allowed a bending moment,  $M_x$  to be applied in the X - direction and a twisting moment  $M_{xy}$  to be applied but no bending moment  $M_y$  in the Y direction i.e.  $M_y = 0$ . Also the curvature in the Y - direction was restrained by the clamping system and was equal to zero. In all other ways free deformation of the specimen was allowed under the loading system and the requirements mentioned earlier in this section were met.

#### 4.4.3 Instrumentation

##### a) Steel Strains

In all respects the method of application, the type of gauge and the strain measurement technique are identical to those described in 4.3.3. (a) for the plank test. The positions of all gauges in each individual test are described in Chapter 5. Gauges were however always placed on bars within the central 18in x 18in. area of the slab which can be described as the test area.

##### b) Concrete Strains

Four strain gauge rosettes were made up of Tinsley 6E electrical resistance wire gauges in the same way as that described in 4.3.3 (b) and affixed to the upper concrete surface. The rosette positions were disposed symmetrically about the centre of the slab at 6in. centres as shown in Fig 4.8. These positions were the same for all specimens tested. The strains were thus measured in the X, Y, and S

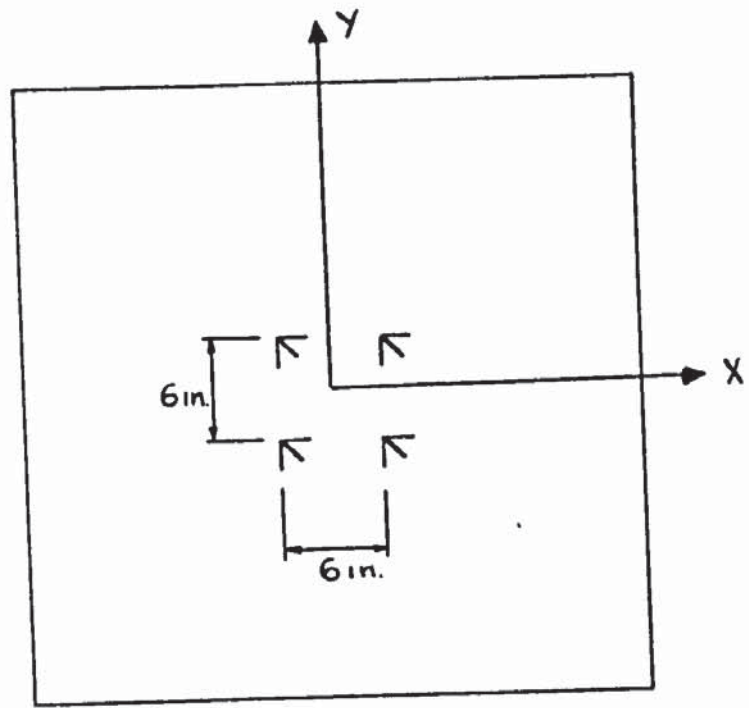


FIG. 4-8 CONCRETE GAUGE POSITIONS

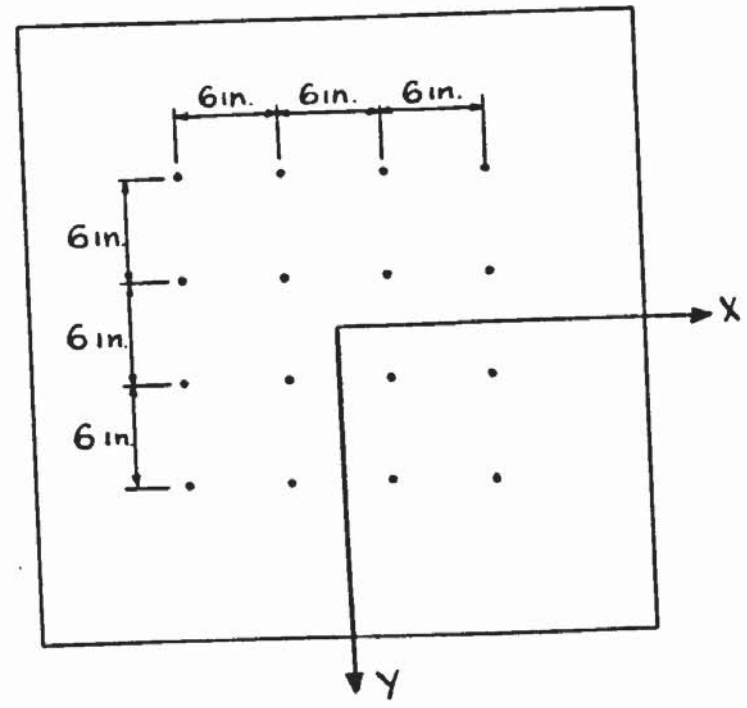


FIG. 4-9 DEFLEXION POINTS

directions as defined in Figs 4.6 - 4.8. All details of application, measurement etc. can be made with reference to 4.3.3.(b).

c) Mechanical dial gauges

Curvatures were measured indirectly by means of a grid of 16 - 2in. travel Mercer dial gauges. The deflexions of the bottom surface were measured by means of these gauges at the points indicated in Fig 4.9. which is a plan viewed from underneath the slab. The positions were symmetrically disposed around the centre of the slab in such a way that a grid of points at 6in. centres measured in the X and Y directions was formed. In this way the curvatures at the inner four dial gauge positions could be measured in three directions and hence the curvature in any direction could be deduced.

The dial gauges were set carefully into the required grid positions by fixing them by means of adjustable angles onto a framework made up of Handyangle. This framework consisted of two square Handyangle frames positioned one on top of the other, parallel to the initial plane of the slab. These two frames were joined by four 1/2in. bars at their corners in such a way that when the lower frame was positioned on the base of the portal rig and underneath the slab element the upper frame, carrying the gauges could be adjusted vertically by sliding it on the 1/2in. bars. The gauges were reset in this way when deflexions reached 2in. or a multiple

of 2in. The upper frame also carried two cross members parallel to the sides laying in the X - direction, to which were afixed the inner eight dial gauges.

Dial gauge positions were marked onto the underside of the slab element prior to setting up so that after the slab was in position it was simple to set the dial gauge grid underneath the slab and locate the deflexion points. The dial gauge grid was checked for accuracy several times during the test series.

d) Load measurement

Loads and hence moments were measured by means of the ten ton capacity proving ring acting as one support point as described in 4.4.2. This was the same proving ring as that used in the plank test series and hence had a factor of 0.0081 tons per division on the dial gauge obtained from the calibration tests described in 4.3.3.(d). In this case of course the load measured was in half that applied by the centrally acting jack as the system is statically determinant.

The jack was vertically aligned and left in position throughout the test series with checks being made on its verticality at frequent intervals. A two - speed hand operated hydraulic pump was used to apply load to the specimen through the jack.

4.5.      Summary

This chapter has described the experimental details of measurement and loading systems devised to obtain objective observations of the behaviour of reinforced concrete slab elements under pure moment. The two separate test series described impose certain restraints on the deformation of the element under load. The Plank test series, which is in effect a simple beam test imposes severe restrictions on the freedom of deformation of the slab element by virtue of the rigid line loading and support system. The General moment test series allows for greater freedom of deformation, only one restraint being made in the form of zero deformations in the Y direction. Thus the two test series are treated separately throughout this thesis although comparison can be made by allowing for the degrees of restraint.

The results obtained from the measurements obtained using the methods described in this chapter in each individual test along with a description of experimental test procedure are given in Chapter 5.

CHAPTER 5.TEST PROCEDURE AND RESULTS FROM INDIVIDUAL TESTS5.1      Introductory Remarks

The test procedures and objective results from both test series are presented in detail. First the test procedure and results from tests in the Plank test series are presented. For easy reference, graphs, tables and plates describing each specimen are presented after the description of individual specimens.

The test procedure and results from the General moment test series are then presented in the second half of this chapter. The graphs, tables and plates illustrating each specimen's behaviour in this series are presented at the end of the chapter.

The results described are those obtained directly from the tests. No comparison of data is made between specimens. These comparisons are described in the following chapters, 6 and 7.

A computer programme was written for the Elliott 805 computer at the University of Aston to convert the actual readings of load, strain and deflexion into moments, corrected strains (where the gauge factor differed from the gauge factor setting on the strain recorder) and curvatures. Curvatures were obtained from the deflexion readings by using the numerical

approximation used in Finite difference theory. Thus

$$\phi_b = \frac{w_a - 2w_b + w_c}{h^2}$$

where  $\phi_b$  is the curvature at point  $b$  in the direction  $abc$ ,  $w_a$ ,  $w_b$ ,  $w_c$  are the deflexions of points  $a$ ,  $b$ ,  $c$  respectively and  $h$  is the distance or grid size between adjacent points. It is understood that points  $a$ ,  $b$  and  $c$  lie on the same straight line. The programme also calculated principal concrete strains and directions, concrete strains in the bar directions, and principal curvatures and directions.

## 5.2. Plank Test series

### 5.2.1 Description of general test procedure

After the slab elements had been set up in the manner described in Chapter 4, zero moment values were recorded for all strains and deflexions and the proving ring dial gauge was zeroed. Load increments were applied through the jack by means of the hydraulic hand pump. In general about 15 load increments were carried out before crushing of the concrete on the compression face occurred and the ultimate moment was deemed to have been reached. At each load increment all observations were taken as quickly as possible to prevent creep effects influencing the results. After yielding of the reinforcement however loading was controlled by deflexion increments and care was taken to see that all gauges were holding steady values.

For this test series it was intended that the principal strain directions coincided with the X and Y directions or span direction. On the whole this is true (an error of around  $5^{\circ}$  occurring in some cases), and consequently it was decided to present plots of bending moment  $M_x$  against both average principal concrete strains. The values of  $\tan 2\gamma$ , which represents the angle between the X - direction and the maximum compressive principal strain direction, are tabulated. Plots of typical steel strains occurring in either direction are also presented against the span moment  $M_x$ , the remaining steel strains being tabulated. In the case of curvatures, the maximum curvature point has been represented in graphical form. The scales of all graphs have been standardised for comparison purposes except in particular cases described later.

Comparison can be made between graphs and tables and reference is made to individual specimens in the next section.

### 5.2.2 Description of individual plank tests and results

#### Specimen P1, $\mu = 1$ , $\beta = 0^{\circ}$

This was the first specimen tested and acted as a standard slab element as the reinforcement was placed parallel to the sides of the slab. The reinforcement bars in both top and bottom layers were laid symmetrically about the centre of the specimen at the spacings appropriate to a nominal value

of  $\mu = 1$  as described in Chapter 4. Consequently 10 bars lay parallel to the span direction and 12 bars lay transversely to it. Concrete strain gauges were placed as described in 4.3.3 (b) curvatures measured at points described in 4.3.3 (c) and steel strain gauges were placed at the points indicated in Fig 5.4

As this was the first test specimen, particularly small load increments were applied as indicated in Fig 5.1 - 5.4 and Table 5.1. The initial test up to 48.31 ton.in was carried out with the 4in. x lin. diameter rollers bearing directly onto the centre of the 3in. x 3in. hollow section line loads described in 4.3.2. At a moment of 48.31. ton.in the upper side of the hollow section began yielding locally under the rollers resulting in a premature discontinuation of loading. Thus the first test was carried out on an uncracked section and the second part of the test to failure was carried out on a cracked section. The consequence of this is most readily appreciated by reference to Fig 5.4 where steel strain plots after cracking show none of the discontinuities or slope changes associated with the first part of the test on an uncracked specimen. First cracking was noticed visually at about 31 ton.in. The steel strain plot in Fig 5.4 for gauge 5 which should be the most reliable measure of cracking, indicates cracking at around 25 ton.in by the change in its slope. This is not surprising as the sensitive strain gauge

should pick out cracking far more accurately than a visual inspection.

Fig 5.1, the curvature plot shows a change in slope at a moment of about 17.5 ton.in which corresponds with the change in slope of the transverse steel strain gauge 2 plotted in Fig 5.4 . The maximum value of curvature for the plotted curvature point 4 had a value of 11.5277 in  $\times 10^3$  at ultimate load.

The concrete strain plots are least affected by cracking as shown in Fig 5.2 and Fig 5.3. The maximum principal concrete strain at failure had a value of 3980 microstrains. It is interesting to note that a similar effect occurred for  $\epsilon_2$  strains as Lenschow and Sozen [29] noted for transverse concrete strains in their specimen B4 which was of a similar kind to P1. After increasing initially the minimum principal concrete strain maintained a nearly constant value up to yield of the steel where upon it began to increase as shown in Fig 5.3.

Table 5.1 give values of  $\tan 2\gamma$  at each load increment and shows that maximum discrepancies of about  $20^\circ$  occurred at very low loads of the order of 4% of the ultimate load. These errors which were probably due to initial settling of the test specimen rapidly reduced to about  $5^\circ$  over the greater part of the load range. It should also be noted that of the three rosettes used in calculating the average  $\epsilon_2$  values

plotted in Fig 5.3 one of the gauges indicated compressive strains in the transverse direction rather than the tensile strains expected and indicated in Fig 5.3 by virtue of any Poissons ratio effect present. EAB, the shear strain in the bar directions which should theoretically be zero because of symmetry has an increasingly significant value as the ultimate moment is approached. Plate 5.1 shows the crack formation on the tension surface at ultimate load. The cracks run generally at right angles to the span direction and are evenly spaced over the central area of the slab at a spacing of about 2.1/2in. The cracks in fact run along the transverse bars which were also spaced at 2.1/2in. centres. Plate 5.2 shows the cracks on the side face at failure and the effect of the main crack under the support on the curvature can be seen.

Specimen P2,  $\mu = 1$ ,  $\beta = 30^\circ$

On loading, first cracks were seen to appear at a moment of around 10 ton.in. This value is borne out by inspection of Fig 5.6 where the maximum principal concrete strain plot shows a definite change of slope at this moment value. Fig 5.5 - 5.7 show how, after initial yield the moment increases up to an ultimate value. Fig 5.5 showing the moment curvature characteristic at point 2 does not appear to have a definite change of slope at cracking and in fact follows a curved plot up to the yield point. The

maximum value of curvature at point 2 of  $15.4166 \text{ in}^{-1} \times 10^3$  shows a considerable increase over the curvature at failure of specimen P1. Fig 5.6 showing the maximum principal concrete strain plot indicates the increased concrete strain at yield of 1200 microstrain over the value of 900 microstrains in specimen P1. The maximum principal concrete strain at failure was 4481 microstrains. Fig 5.7 indicates the manner in which the transverse concrete strains appear to increase in tension before falling back to zero at yield and finally reaching a value of about 220 microstrains in tension. Typical steel strain characteristics presented in Fig 5.8 show the extra strain occurring in the main reinforcement bars during both elastic and plastic ranges. The fact that the cracks formed at an angle to the bar directions may explain the apparent absence of a definite slope change at cracking and it must be remembered that if a gauge lay between two cracks the strains would be considerably less than if the gauge were situated at a crack. This effect can mask yielding and cracking phenomena to varying extents.

Table 5.2 indicates the other observations. The error in principal strain direction is less in this case than in P1, the maximum error being around  $2.5^\circ$  during most of the test. In the bar directions the maximum shear strain EAB of 3813.7 microstrains contrasted with the tensile shear strains indicated in specimen P1.

Plate 5.3 shows the crack formation at ultimate load. Maximum curvature occurs around the yield line passing near point 2 and it was noticed in this test that failure occurred on one or two yield lines rather than on many as in specimen P1. This will be explained in more detail in Chapter 6. Plate 5.4 shows all the cracks formed before the main cracks became predominant. There is not the same order of uniformity as occurred in specimen P1 and spacing was generally between 3 and 3.1/2in.

Specimen P3,  $\mu = 1$ ,  $\beta = 45^\circ$

Although direct comparisons between specimens will be made in a later chapter (Chapter 6) it can readily be seen from Fig 5.9 and 5.10 that curvatures and maximum concrete strains at yield are again greater than those in P1 and P2 signifying a lower element stiffness and thus verifying, at least quantitatively Lenschow and Sozen's [29] hypothesis on the stiffness of elements with reinforcement meshes at varying angles to the principal moment direction. Cracking was noticed at a moment value of about 10 ton.in which is in agreement with the slope changes in Figs 5.9 - 5.12. Transverse concrete strains became compressive after cracking, changing to tensile after yield as shown in Fig 5.11. The steel strain plots in Fig 5.12 show that strains were closer in either direction than before although the existing discrepancy may be explained as due to the masking effects of

the gauge positions in relation to cracks. Table 5.3 shows that the error between assumed and actual principal strain directions is of the order of  $2^\circ$  until close to ultimate moment where it reaches  $5^\circ$ . The maximum principal concrete strain at failure was 3961 microstrains. Plate 5.5 shows that the cracks are more evenly spaced than those in P2 although it can be seen that one crack falls outside the central maximum moment area lying between point 1 and 2.

Specimen P4,  $\mu = 0$   $\beta = 0^\circ$

P4 was the first specimen with reinforcement in one direction only. Loading on this specimen was not carried out upto crushing of the concrete as the fixed roller was becoming loose. Cracking again appears to have occurred at a moment of 10 ton.in from Figs 5.13 and 5.14. although visual detection was not obtained until a moment value of about 17 ton.in, Fig 5.16 indicating the steel strain plot shows cracking to have occurred at a moment of 12.5.ton.in. Table 5.4 indicates that the principal strain direction was about  $5^\circ$  away from the span direction and Fig 5.15 shows that tensile strains occurred again in the transverse direction although the E2 plot shows a gradual increase in strain with load upto yield unlike Fig 5.3 for specimen P1. Plate 5.6 indicates the crack formation which does not run exactly parallel to the sides of the slab element and shows curvature to have been concentrated on two yield lines, both starting under a

load point.

Specimen P5,  $\mu = 0$ ,  $\beta = 30^\circ$

This was the first specimen in which the degree of orthotropy controlling the anisotropic behaviour of the element overcame the boundary conditions imposed on the slab. As well as the anisotropy of the element, the placing of bars at given positions in one direction results in a section at an angle to the transverse direction of the span in which fewer bars are required to resist the applied moment. The slab element therefore lifted at opposite corners so that a failure occurred at an angle to the sides of the element. Plate 5.7 shows how the main yield line crossed the constant moment area diagonally thus minimising the number of bars resisting the applied moment. Other cracks did form before the main crack developed at a moment of about 10.5 ton.in. Loading was discontinued when the twisting was noted as it was thought that the element may have been incorrectly set up. On checking it was found that this was not the case and the element was reloaded to failure. Figs 5.17 - 5.20 show this loading cycle. It should be noted however that the principal concrete strain directions were still only about  $2.1/2^\circ$  from the span direction as indicated in Table 5.5. The maximum principal concrete strain at failure was 4815 microstrains.

Specimen P6,  $\mu = 0$ ,  $\beta = 45^\circ$

Lifting from supports at opposite corners of the element

was again apparent but not so significant as in the previous case. Plate 5.8 shows the main crack running transverse to the span near the centre of the specimen but at an angle near the edges. In this way some bars did not resist the applied moment at failure. This could be described as a bond failure at the edges and the phenomenon will be discussed generally in Chapter 6 where allowance for such associated discrepancies will be made.

Fig 5.21 - 5.24 shows how a low ultimate moment was reached. Because of the localisation of curvature on one yield line the ductility of the element is not displayed in the Figures or tables. The crushing line in fact did not pass through the concrete gauges and consequently the concrete strains indicated in Fig 5.22 are very low at failure. The maximum being only 618 microstrains. Table 5.6 does show however that the principal strain and span direction nearly coincide.

Specimen P7,  $\mu = 0$ ,  $\beta = 60^\circ$

Failure was very similar to that in P5. The only yield line passing diagonally across the uniform moment area as shown in Plate 5.9. In this case however only one crack appeared, suddenly developing at a moment value of about 9 ton.in. with an associated drop in load as indicated by Fig 5.25 - 5.28. The scales have been changed in these figures so that a clearer plot of results ensued.

In Morley's [27] tests a similar phenomenon occurred when the unidirectional steel reinforcement made a high angle with the applied moment direction. In cases such as these the tensile concrete has a greater strength than the reinforcement and thus on cracking the load drops to the resisting capacity of the reinforcement. Again the localized curvature prevents good results being obtained for concrete strain or steel strain readings as Figs 5.26 - 5.28 indicate. Table 5.7 again shows however that the principal strain directions were close to the span direction throughout, the maximum principal concrete strain at failure being 1427 microstrains. *Mean of test*

Specimen P8,  $\mu = 0.25$ ,  $\beta = 0^\circ$

P8 was the first specimen tested, containing 1/4 in. diameter annealed steel as described in Chapter 4. Cracking was noticed to have occurred at a moment value of about 17 ton.in Fig 5.29, the moment - curvature plot indicates cracking at 15 ton.in as does the steel plot in Fig 5.32. The plot of principal concrete strains E2 in Fig 5.31 shows considerable scatter during the elastic range but does not appear to indicate a constant strain during this range as does Fig 5.3 for P1. Table 5.8 again shows  $\tan 2\gamma$  to be small. Plate 5.10 shows the crack formation at ultimate load. The spacing of cracks is not so even or close as that in P1 but follows approximately the transverse steel. The maximum principal concrete strain

was 2503 microstrains at failure.

Specimen P9,  $\mu = 0.25$ ,  $\beta = 30^\circ$

This element showed similarities to P6 where centrally the cracks ran transversely to the span direction but were inclined at the edges. Plate 5.11 illustrates the crack formation. The two other predominant cracks ran approximately parallel to the sides of the element but it can be seen that the major yield line between point 3 and 4 exhibits the tendency to be inclined at the edges. Plate 5.12 shows how one side of the crack was raised above the other side thus making the inclined portions of the crack kinematically admissible. Figs 5.33 - 5.35 describing the curvature and concrete strain plots show cracking to have occurred at the moment of about 10 ton.in which is the value at which visual detection was made. The curvature and principal concrete strain plots in Figs 5.33 and 5.34 show low curvature and strain at failure. The transverse concrete strains are definitely tensile throughout as illustrated in Fig 5.35. Steel strains plots in Fig 5.36 show the strains up to yield at the points plotted to be close. Table 5.9 shows  $\tan 2 \gamma$  to be small except at very low and very high moment values where the error is of the order of  $5^\circ$ .

Specimen P10,  $\mu = 0.25$ ,  $\beta = 45^\circ$

Again a tendency for the cracks to incline at the edges was noticed and is illustrated in Plate 5.13.

Although other cracks run parallel to the sides the main yield exhibits the same characteristics as the main crack in P9. Figs 5.37 and 5.38 again show low values of curvature and strain at the points measured when failure occurred. Fig 5.39 however indicates high tensile values of E2 at ultimate load. The steel strains plotted in Fig 5.40 exhibit similar characteristics in both layers but strains after yield are extremely low and it may be supposed that the gauges were not near the major crack area. Table 5.10 again indicates low values of  $\gamma'$ .

Specimen P11,  $\mu = 0.25$ ,  $\beta = 60^\circ$

The tendency for the yield lines to incline at an angle at the edges of the slab was not pronounced in this case although as Plate 5.14 illustrates one yield line predominated indicating a singular line of weakness. Fig 5.41 indicates the flexibility of this specimen, yielding commencing at a curvature of about  $3.5 \text{ in}^{-1} \times 10^3$ . The scales have been exaggerated in Figs 5.41 - 5.44 because of the relatively low failure moment. Fig 5.41 and 5.42 show that curvature and strain were not large at failure. The error occurring between principal strain and span directions was in this case larger than previously noticed, being of the order of  $5^\circ$  throughout as indicated in Table 5.11.

Specimen P12,  $\mu = 0.25$ ,  $\beta = 90^\circ$

Only one major yield line and crack formed in this

case between deflexion point 2 and 3 and coincided with a transverse reinforcement bar as shown in Plate 5.15. The ultimate moment, being about a quarter that for P8 had a value of about 18 Ton.in and consequently the scales of Fig 5.45 - 5.48 have been exaggerated for clarification. Cracking occurred at a value of about 7 ton.in as indicated in Figs 5.45, 5.46 and 5.48. Because of the highly localised curvature at the single yield line the principal concrete strain plot does not exhibit the usual increasing strains after yield as shown in Fig 5.45. The steel strain plots in Fig 5.48 show that the typical transverse steel strain had compressive characteristics throughout.

The error in angle  $\tan 2\gamma$  is quite large in this case as indicated in Table 5.12. It is difficult to explain this occurrence but as it occurred throughout the test it may be put down to incorrect levelling and loading of the specimen.

Specimen P13,  $\mu = 0.5$ ,  $\beta = 0^{\circ}$

Cracks were fairly straight in this specimen which was the first of the slabs tested with  $\mu = 0.5$ . Bad vibration of the concrete resulted in poor compaction around the bars and may have led to poor bond conditions. This may be seen in Plate 5.15. It can be seen that Fig 5.49 of the moment - curvature plot does not show up any cracking whereas the concrete and steel strain plots indicate cracking at about

10 ton.in in Figs 5.50 - 5.52 respectively. The maximum curvature and concrete strain values were  $11.14 \text{ in}^{-1} \times 10^3$  and 3133 microstrains respectively. The transverse concrete strains shown in Fig 5.51 were quite large and tensile whereas the transverse steel strains did not show great increases after yield as can be seen in Fig 5.51.  $\tan 2 \gamma$  values in Table 5.13 were of the order of  $5^\circ$ .

Specimen P14,  $\mu = 0.5$ ,  $\beta = 30^\circ$

Cracks were not very straight in this specimen. Plate 5.17 shows how one of the main cracks developed outside the central moment area near deflexion point 7 and extended into the test area on the other side of the slab. Cracking began again at a moment value of about 10 ton.in as the curvature, concrete and steel plots indicate in Figs 5.53 - 5.56 respectively. Steel strain plots shown in Fig 5.56 exhibit characteristics which could indicate a jump in steel strain at cracking. Whilst the main steel strains move along the dotted line the transverse steel strains become compressive upto yield. Concrete strains EB in the weaker steel direction were tensile throughout the test. Table 5.14 shows that  $\gamma$  was of the order of  $5^\circ$  for most of the test. The maximum concrete strain was 3065 microstrains at failure.

Specimen P15,  $\mu = 0.5$ ,  $\beta = 45^\circ$

Cracks again did not run transversely to the span

direction as shown in Plate 5.18. Plate 5.19 shows the influence of shear on the cracks near the supports. Cracking occurred at a lower moment value than previously noted as indicated in Figs 5.57 and 5.58. Fig 5.59 shows the large transverse concrete strains occurring at failure. The steel strain plots in Fig 5.60 indicate the close agreement between each steel layer strain up to yield and the high flexibility of the element. Table 5.15 shows  $\gamma$  to be less than  $2^\circ$  for most of the test. The maximum curvature and concrete strain values recorded were  $10.47 \text{ in}^{-1} \times 10^3$  and 3834 microstrains at failure.

Specimen P16,  $\mu = 0.5$ ,  $\beta = 60^\circ$

The cracks were fairly straight and transverse to the span direction as illustrated in Plate 5.20. Cracking again occurred at about 10 ton.in Curvature, concrete strain and steel strain plots are shown in Figs 5.61 - 5.64. Bad scatter occurred in E2 values in Fig 5.63 and Fig 5.64 shows the steel strains in the weaker reinforcement direction to be less than those in the main steel direction.  $\gamma$  values indicated in Table 5.16 show a small error in the elastic range increasing after yield. A maximum concrete strain of 2519 microstrains was recorded at failure.

Specimen P17,  $\mu = 0.5$ ,  $\beta = 90^\circ$

Cracks were straight, transverse and evenly distributed as shown in Plate 5.21. Scatter occurred in the pre-yield

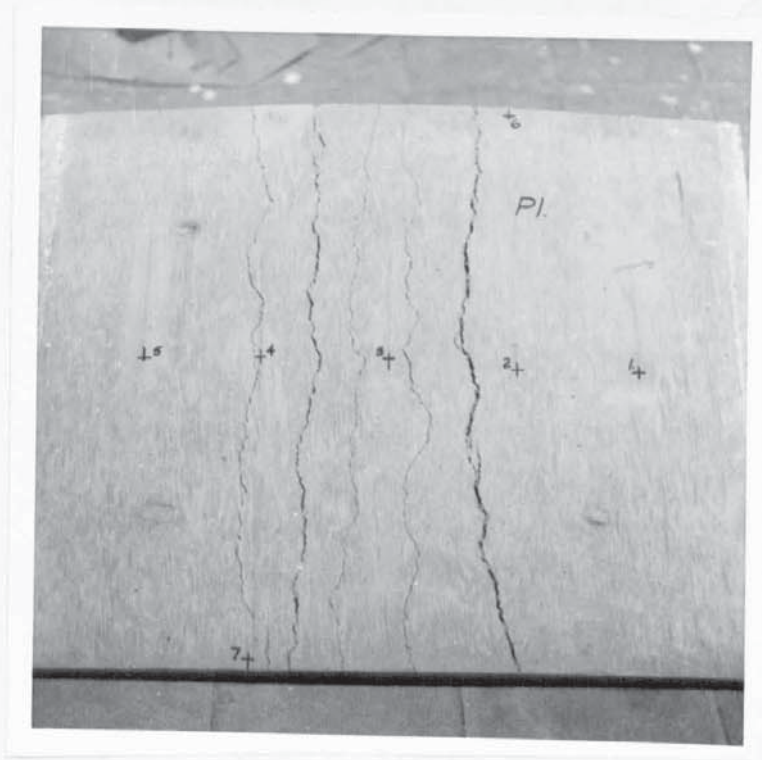


PLATE 5.1

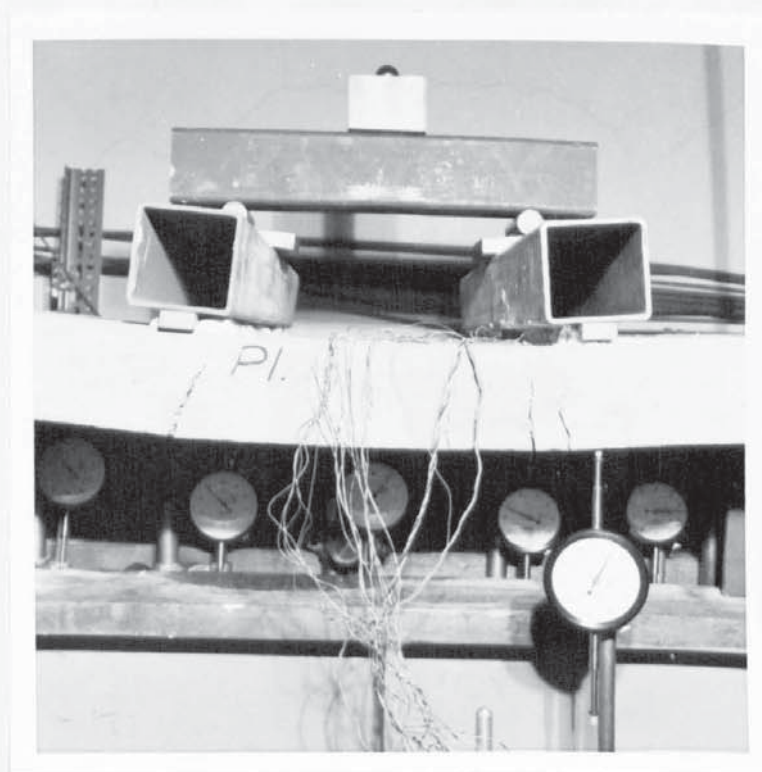


PLATE 5.2

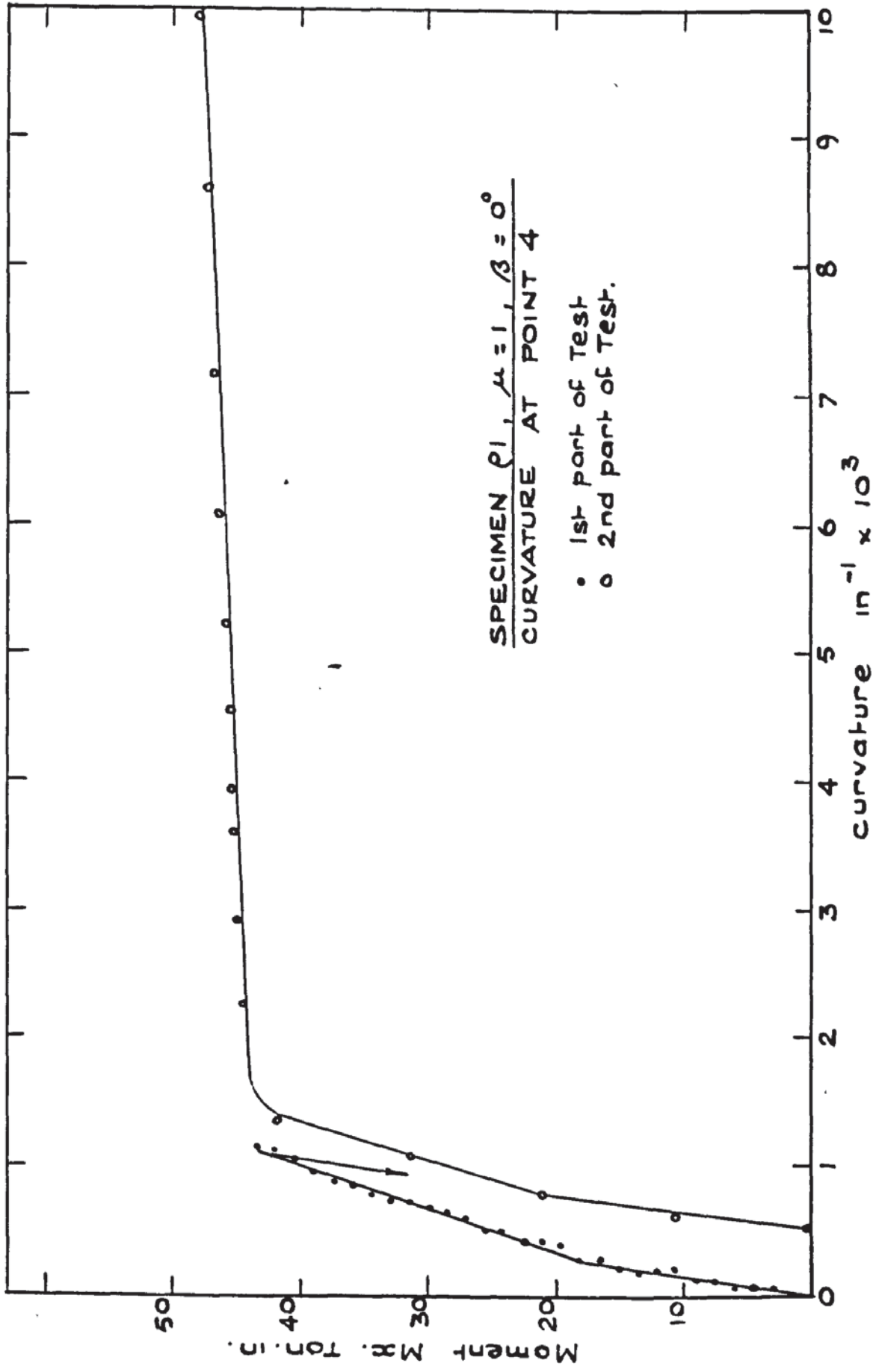


FIG. 5.1. MOVEMENT - CURVATURE PLOT - P.1.

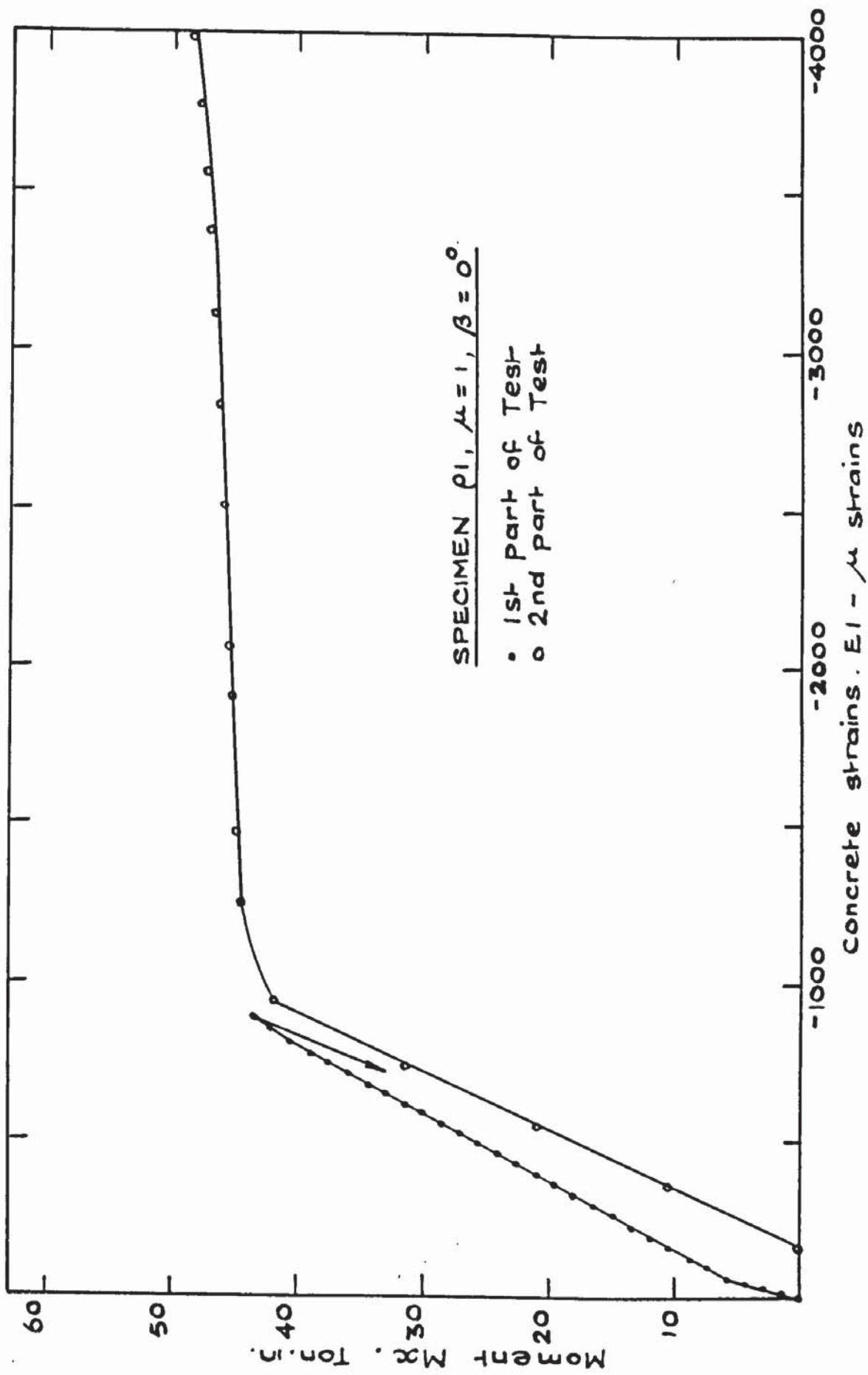


FIG. 5.2. AV. PRINCIPAL CONCRETE STRAIN EI PLOT - P1.

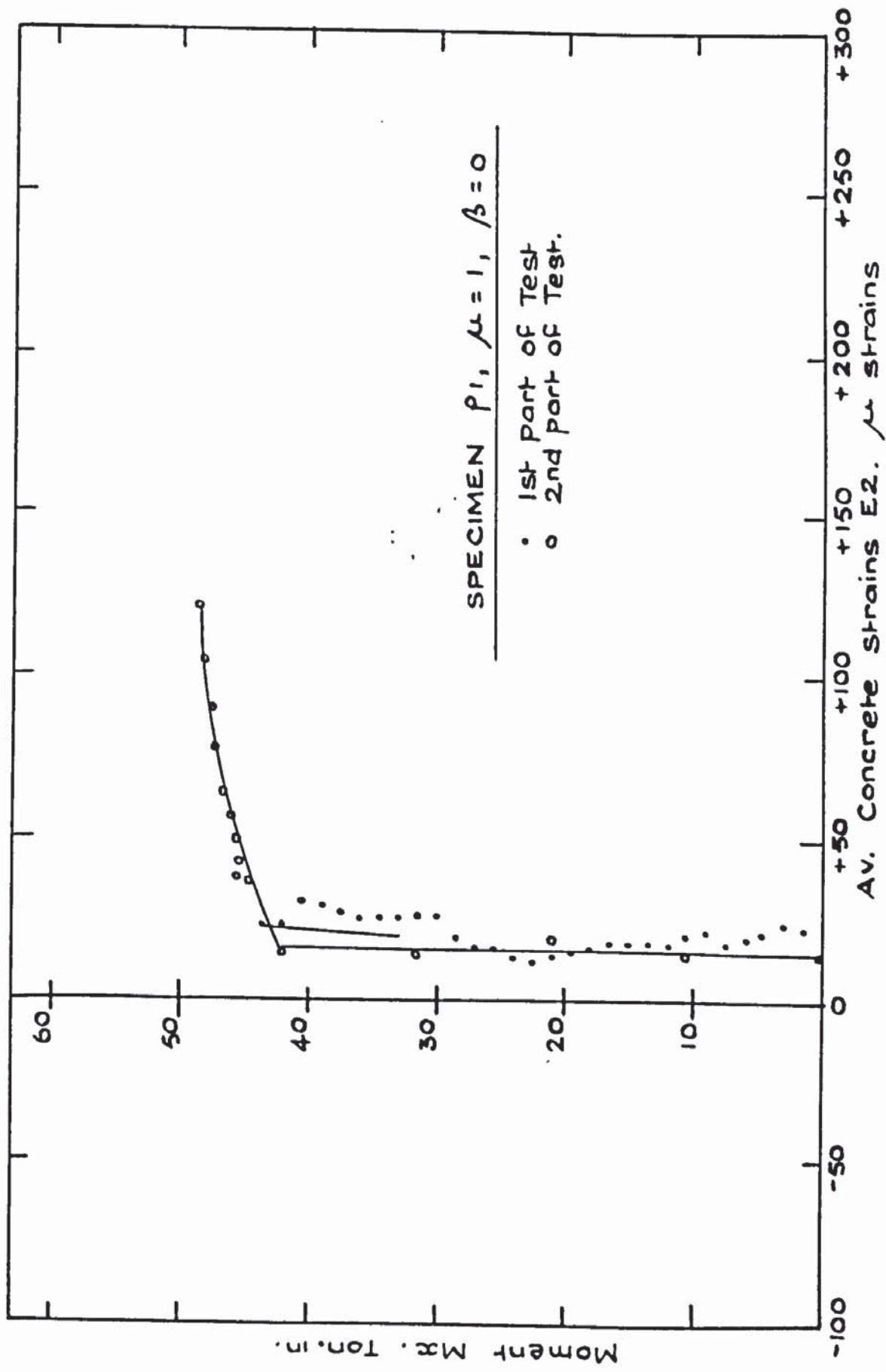


FIG. 5.3. AV. PRINCIPAL STRAIN PLOT E2 -  $\rho_1$ .

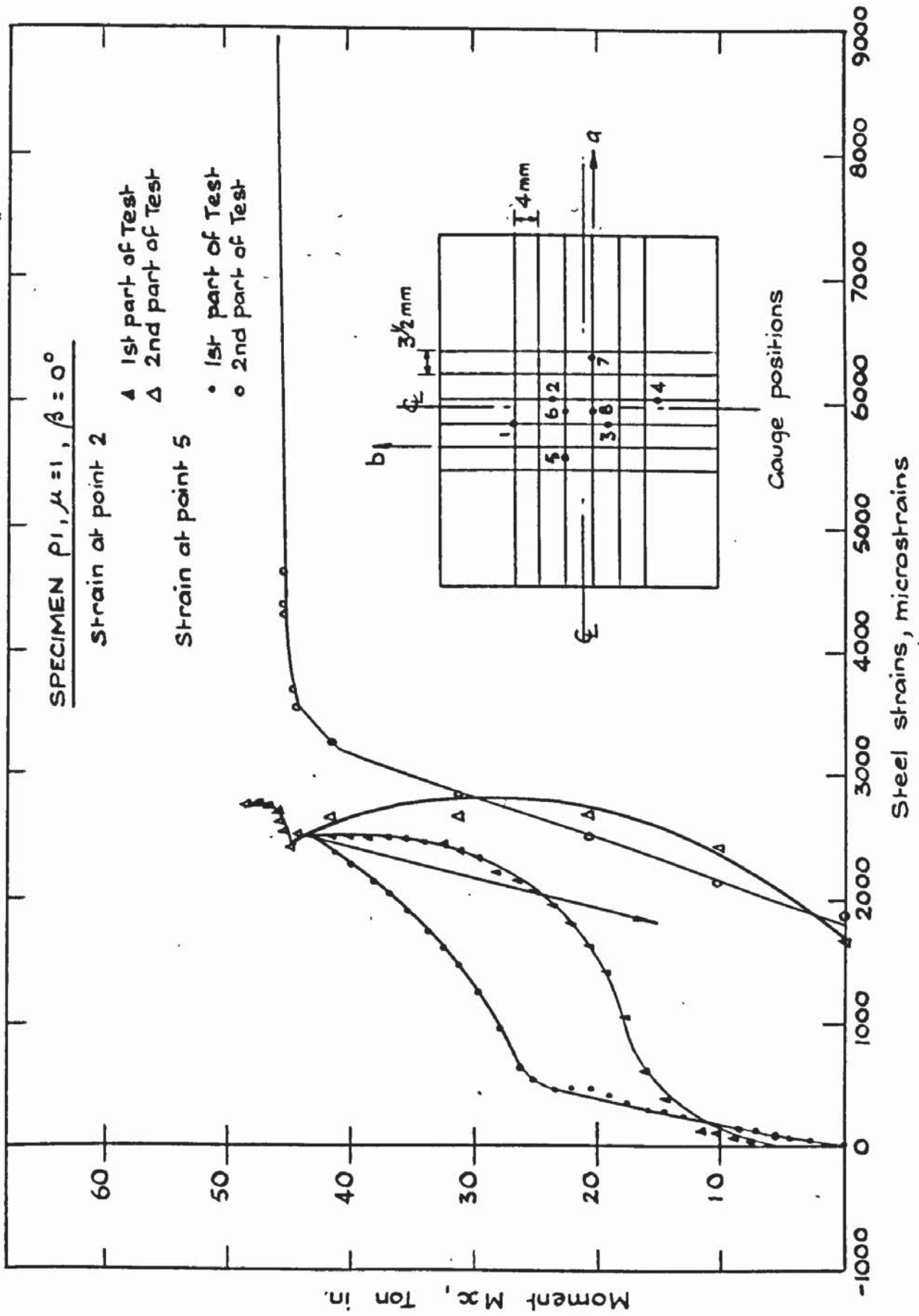


FIG. 5.4. TYPICAL STEEL STRAIN PLOT - P1

M <sub>x</sub> TON. IN	AVERAGE tan 2γ	STEEL STRAINS									
		1	2	3	4	5	6	7	8		
0.00	-	0.00	0.00	-	-	-	-	0.00	0.00	0.00	0.00
1.49	-1.000	-207.95	-29.71	-	-	-	-	-277.27	29.71	29.71	9.90
2.99	-.9205	-326.78	- 9.90	-	-	-	-	-297.07	39.61	39.61	29.71
4.48	-1.038	-346.59	9.90	-	-	-	-	-267.37	79.22	79.22	44.56
5.98	-.5482	-306.98	0.00	-	-	-	-	-267.37	79.22	79.22	69.32
7.47	-.4232	-316.88	39.61	-	-	-	-	-198.05	118.83	118.83	99.02
8.96	-.4622	-267.37	59.41	-	-	-	-	-158.44	138.63	138.63	123.78
10.46	-.4307	188.15	99.02	-	-	-	-	59.41	128.73	128.73	168.34
11.95	-.3551	297.07	118.83	-	-	-	-	99.02	158.44	158.44	207.95
13.45	-.3156	614.20	237.66	-	-	-	-	118.83	163.39	163.39	207.95
14.94	-.2797	1099.17	366.39	-	-	-	-	237.66	198.05	198.05	237.66
16.43	-.2728	1218.00	574.34	-	-	-	-	257.46	217.85	217.85	237.66
17.93	-.2160	1366.54	1019.95	-	-	-	-	316.88	257.46	257.46	277.27
19.42	-.2000	1584.39	1386.34	-	-	-	-	386.20	326.78	326.78	326.78
20.92	-.1545	1723.02	1594.29	-	-	-	-	465.41	465.41	465.41	386.20
22.41	-.1411	1812.15	1762.63	-	-	-	-	554.54	554.54	554.54	386.20
23.90	-.1099	1891.37	1901.27	-	-	-	-	604.05	604.05	604.05	406.00
25.40	-.0999	2039.90	2039.90	-	-	-	-	673.37	673.37	673.37	475.32
26.89	-.0947	2079.51	2119.12	-	-	-	-	772.39	772.39	772.39	544.63
28.39	-.0796	2158.73	2188.44	-	-	-	-	841.71	841.71	841.71	594.15
29.88	-.0593	2277.56	2307.27	-	-	-	-	930.83	930.83	930.83	653.56
31.37	-.0543	2366.68	2346.88	-	-	-	-	1029.85	1029.85	1029.85	693.17
32.87	-.0451	2391.44	2406.29	-	-	-	-	1128.88	1128.88	1128.88	742.68
34.36	-.0368	2436.00	2426.10	-	-	-	-	1218.00	1218.00	1218.00	792.20
35.86	-.0350	2485.51	2455.80	-	-	-	-	1277.41	1277.41	1277.41	821.90
37.35	-.0326	2515.22	2455.80	-	-	-	-	1386.34	1386.34	1386.34	911.02
38.84	-.0305	2535.02	2445.90	-	-	-	-	1425.95	1425.95	1425.95	930.83
				-	-	-	-	1485.37	1485.37	1485.37	1000.15

Table 5.1 continued

40.34	-	.0110	2564.73	2455.80	-	-	2237.95	1534.88	990.24	1059.56
41.83	-	.0044	2584.54	2445.90	-	-	2346.88	1599.24	1010.05	1138.78
43.33	-	.0073	2584.54	2445.90	-	-	2455.80	1683.41	1059.56	1227.90
0.00	-	.0815	2089.41	1356.63	-	-	1396.24	633.76	39.61	247.56
0.00	-	.0819	2336.98	1658.66	-	-	1861.66	861.51	247.56	485.22
10.46	-	.0848	2683.56	2396.39	-	-	2109.22	1208.10	425.80	693.17
20.92	-	.0641	2911.32	2663.76	-	-	2495.41	1574.49	663.46	980.34
31.37	-	.0092	2970.73	2624.15	-	-	2792.49	1822.05	871.41	1247.71
41.83	-	.0223	3049.95	2614.24	-	-	3228.20	2188.44	1089.27	1524.98
44.32	-	.0805	3069.76	2495.41	-	-	3485.66	2396.39	1277.41	1812.15
44.82	-	.1283	3158.88	2396.39	-	-	3624.29	2544.93	2525.12	1950.78
45.07	-	.1661	3515.37	2505.32	-	-	4258.05	3455.95	-	2247.85
45.32	-	.1744	3644.10	2594.44	-	-	4307.56	4198.63	-	2475.61
45.47	-	.1659	-	2594.44	-	-	4584.83	9575.66	-	-
45.82	-	.1697	-	2673.66	-	-	1.2x10 <sup>4</sup>	1.4x10 <sup>4</sup>	-	-
46.31	-	.1753	-	2742.98	-	-	-	1.5x10 <sup>4</sup>	-	-
46.81	-	.1816	-	2723.17	-	-	-	1.6x10 <sup>4</sup>	-	-
47.31	-	.1893	-	2742.98	-	-	-	1.7x10 <sup>4</sup>	-	-
47.81	-	.1832	-	2752.88	-	-	-	-	-	-
48.31	-	.1844	-	2742.98	-	-	-	-	-	-

Table 5.1 Principle Concrete Strain Directions & Steel Strains - P1

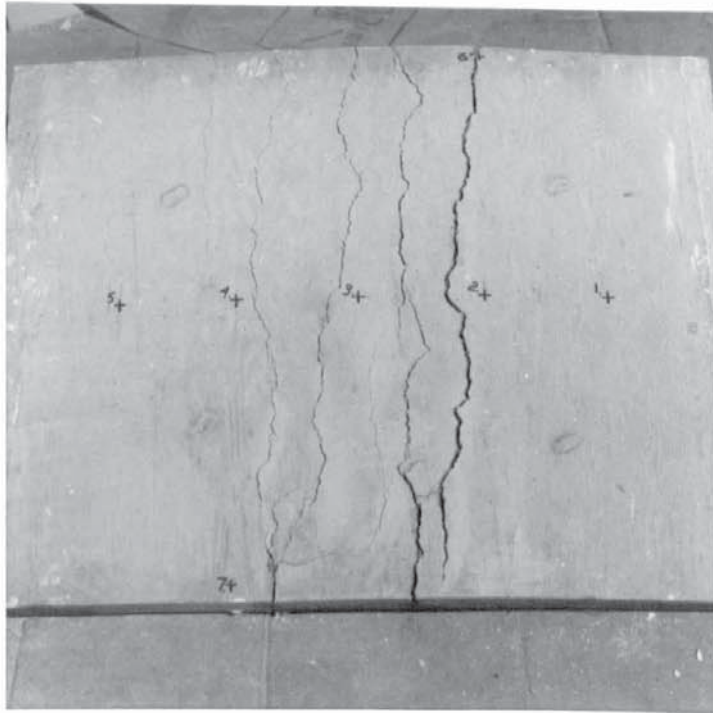


PLATE 5.3

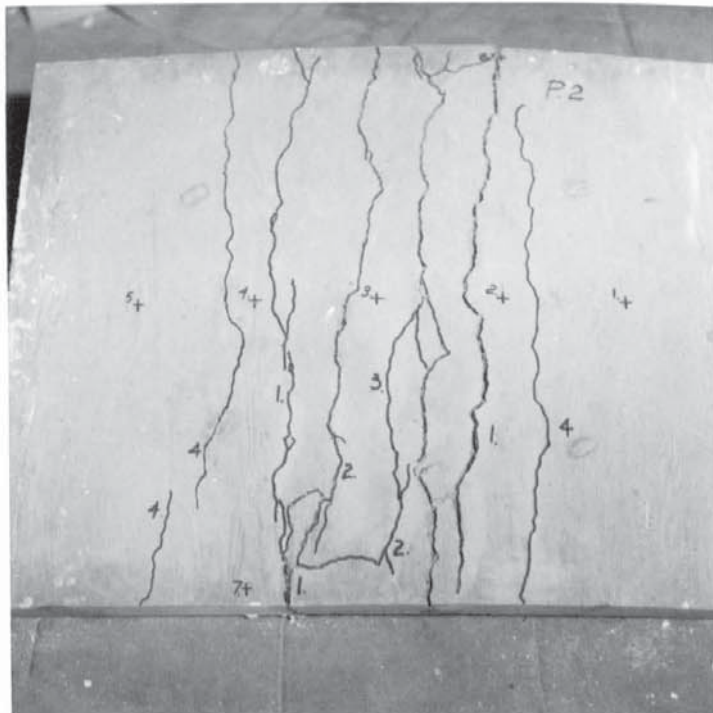


PLATE 5.4

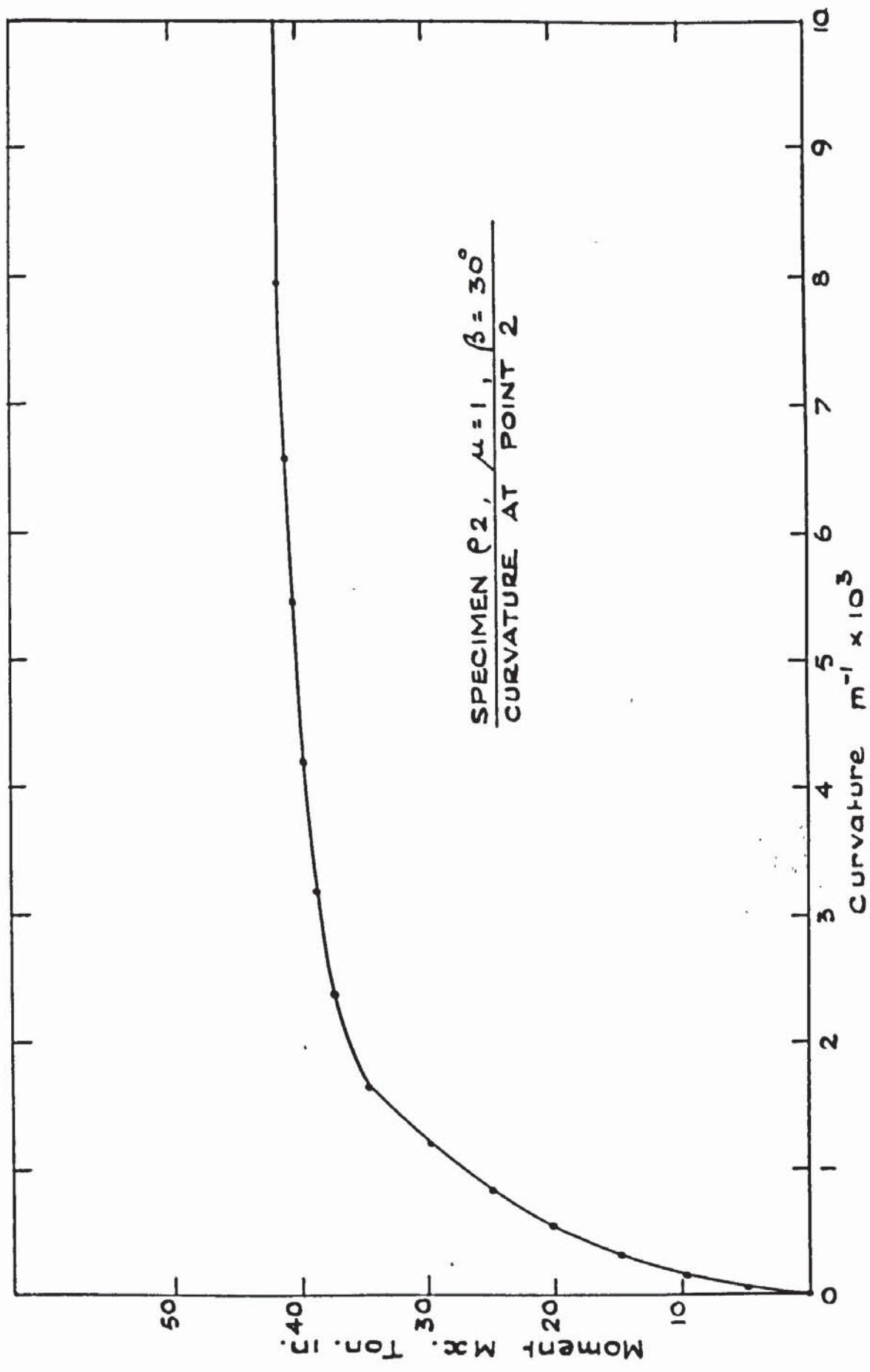


FIG. 5.5. MOMENT CURVATURE PLOT - P.2.

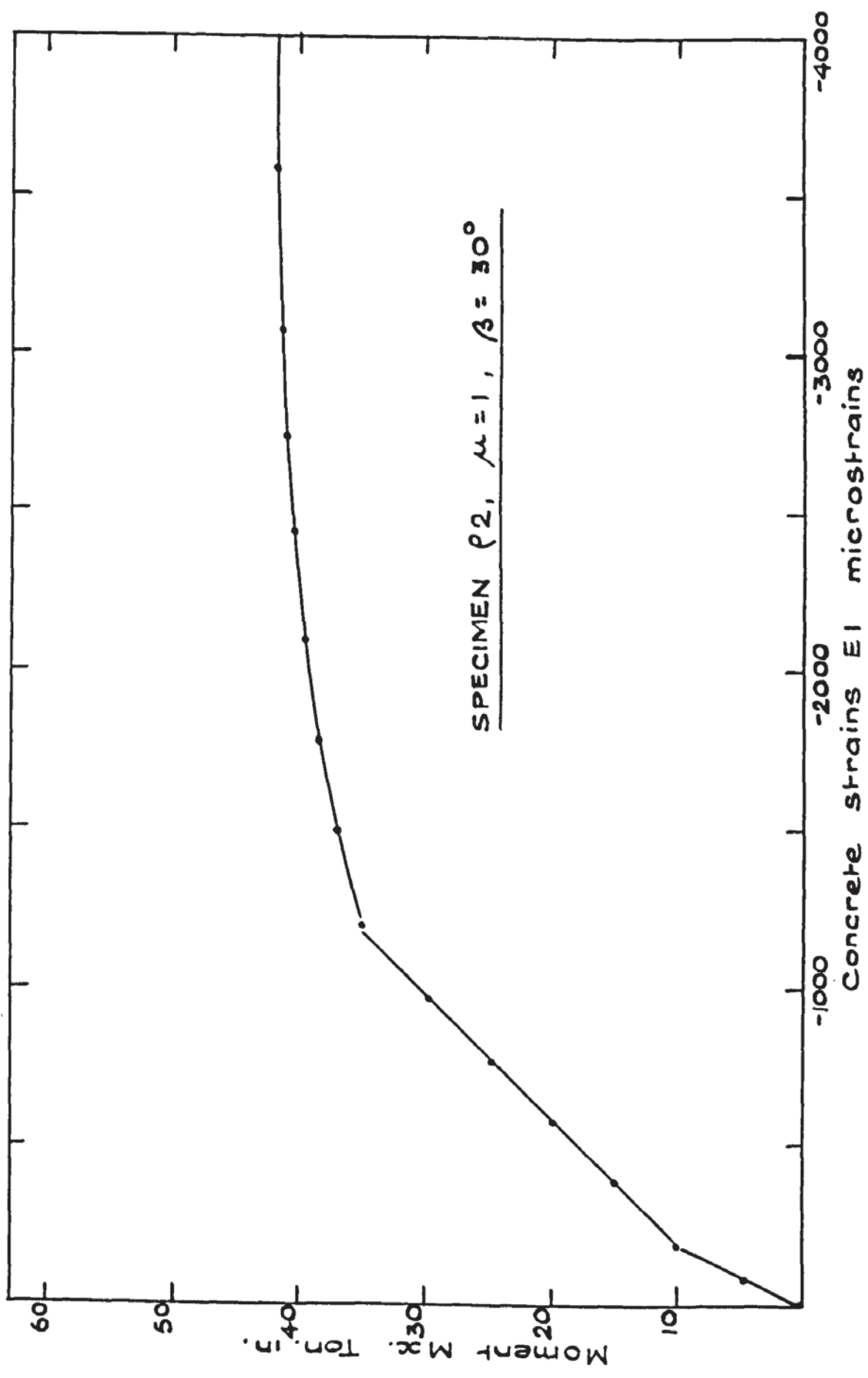


FIG. 5.6. AVERAGE PRINCIPAL CONCRETE STRAIN EI - P2

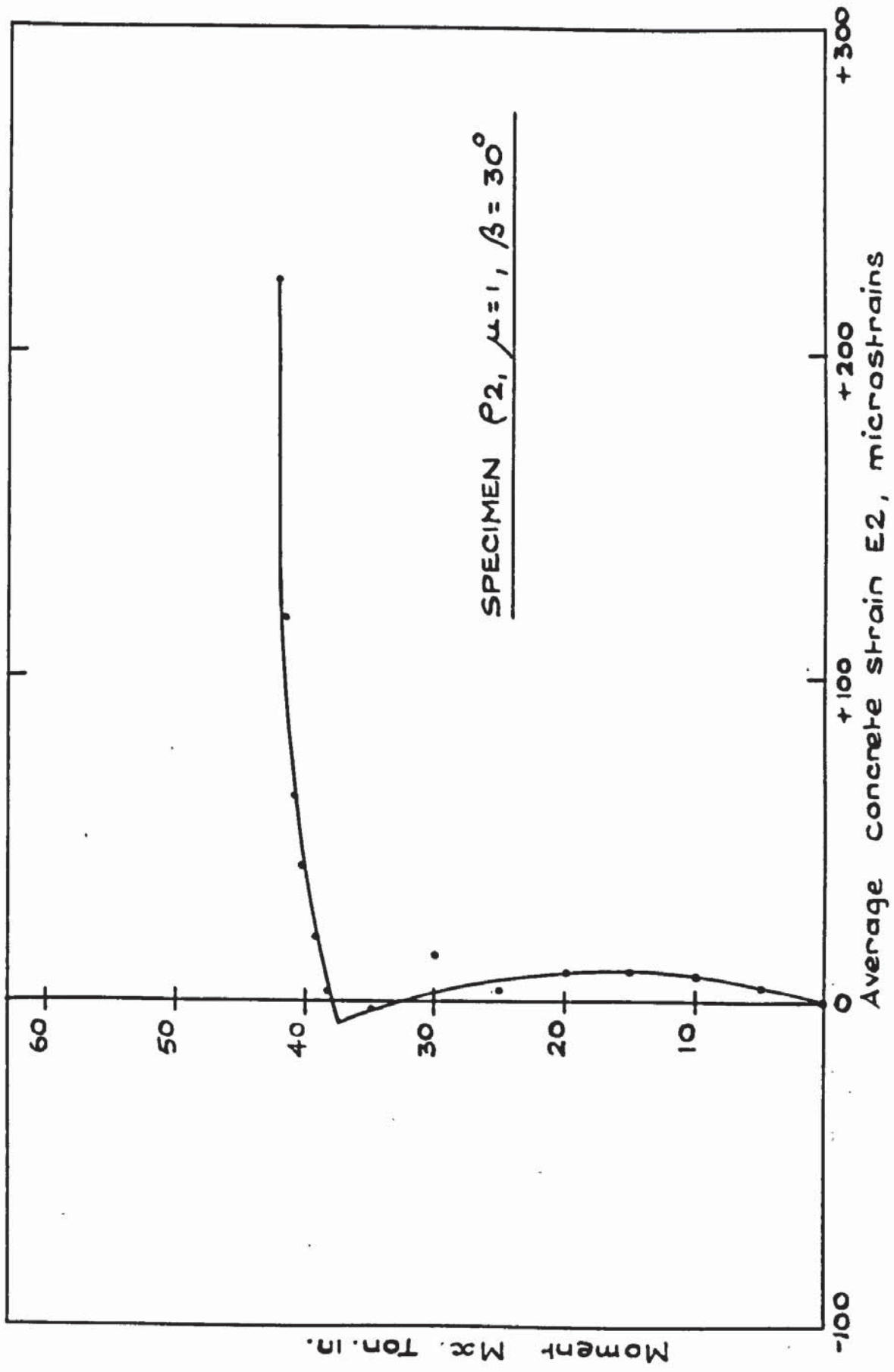


FIG. 5.7. AVERAGE PRINCIPAL CONCRETE STRAIN PLOT E2 - P2

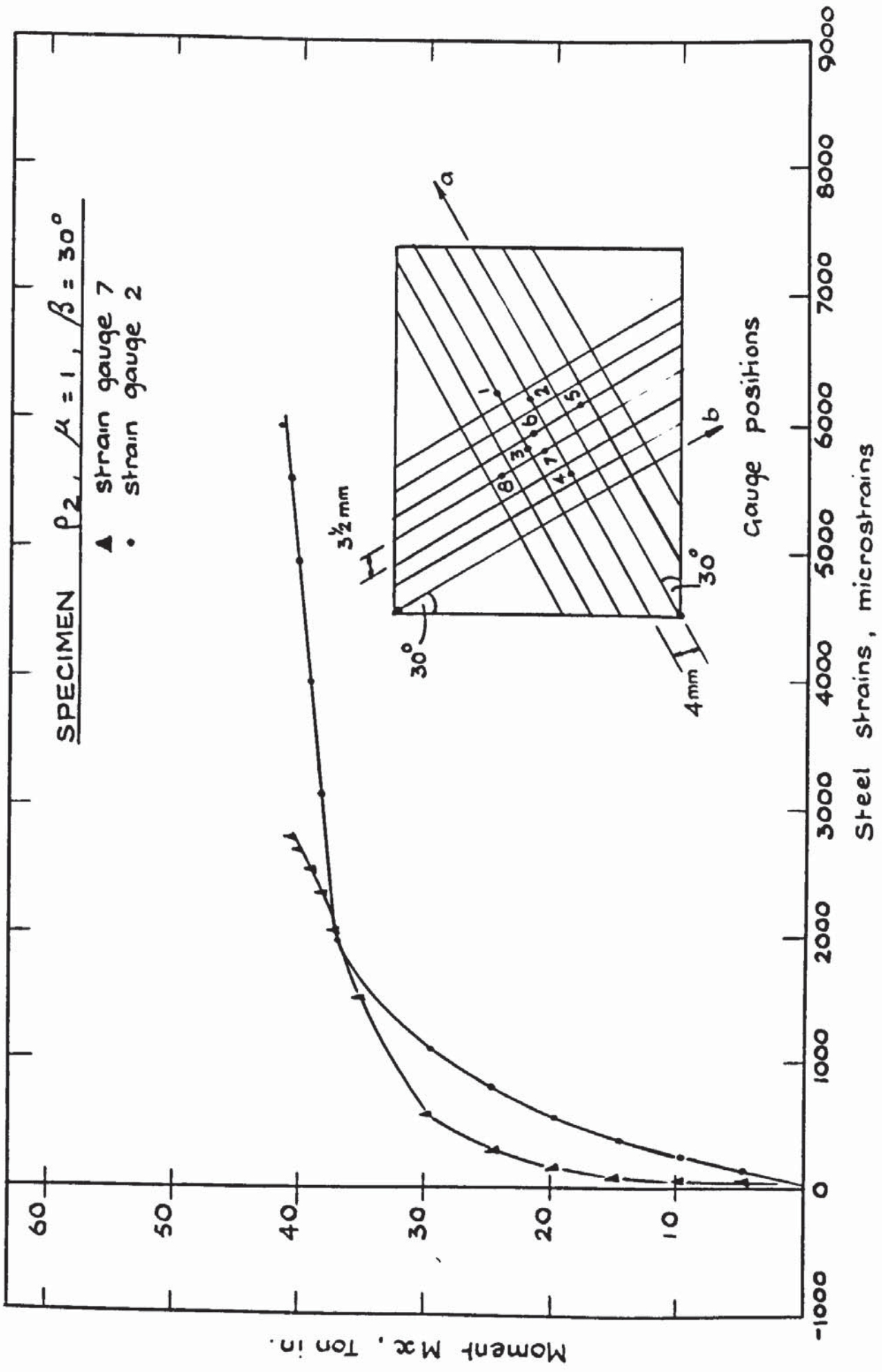


FIG. 5.8 TYPICAL STRAIN PLOT - P2

M <sub>x</sub> TON. IN	AVERAGE tan 2γ	STEEL STRAINS											
		1	2	3	4	5	6	7	8				
0.00	-	0.00	0.00	-	0.00	0.00	-	-	-	-	-	-	-
4.98	.2792	127.74	79.22	-	59.41	118.83	-	-	-	0.00	-	0.00	-
9.96	.2035	238.63	189.12	-	129.71	69.32	-	-	-	49.51	-	49.51	-
14.94	.1469	302.02	282.22	-	153.49	257.46	-	-	-	59.41	-	59.41	-
19.92	.1363	524.83	495.12	-	366.39	544.63	-	-	-	94.07	-	94.07	-
24.90	.1221	732.78	742.68	-	445.61	831.80	-	-	-	138.63	-	138.63	-
29.88	.1007	970.44	990.24	-	450.56	1089.27	-	-	-	227.76	-	227.76	-
34.86	.0918	1435.85	1455.66	-	534.73	1336.83	-	-	-	524.83	-	524.83	-
37.35	.0497	1911.17	1980.49	-	683.27	1524.98	-	-	-	1455.66	-	1455.66	-
38.35	.0522	3069.76	2376.59	-	841.71	1752.73	-	-	-	2000.29	-	2000.29	-
39.34	.0661	3931.27	2713.27	-	911.02	1940.88	-	-	-	2287.46	-	2287.46	-
40.34	.0827	4862.10	2970.73	-	960.54	2069.61	-	-	-	2495.41	-	2495.41	-
40.84	.0827	5525.56	1792.34	-	1230.71	2198.34	-	-	-	2624.15	-	2624.15	-
41.33	.0820	5911.76	-	-	1475.46	2267.66	-	-	-	2733.07	-	2733.07	-
41.83	.0919	-	-	-	1633.90	2327.07	-	-	-	-	-	-	-
41.83	.1035	-	-	-	-	2376.59	-	-	-	-	-	-	-

Table 5.2 Principle Concrete Strain Direction & Steel Strains P2

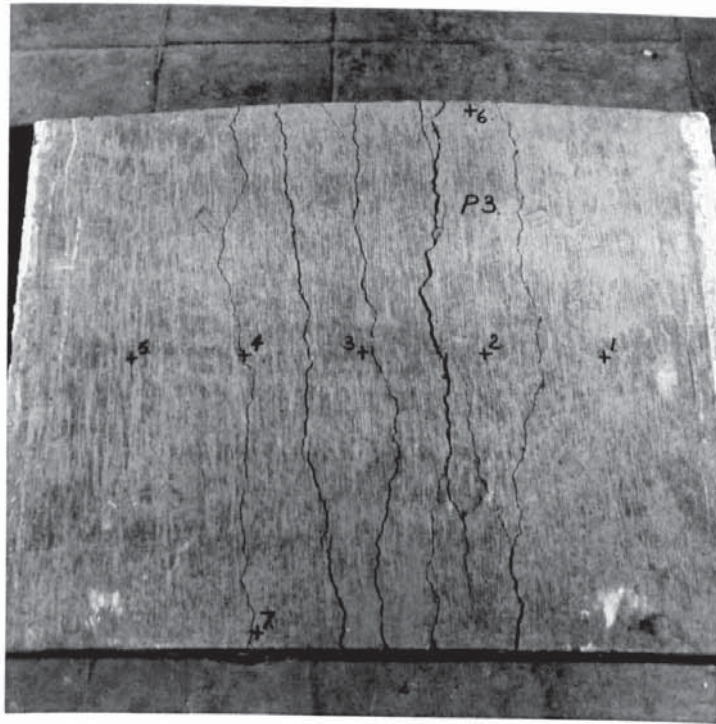


PLATE 5.5

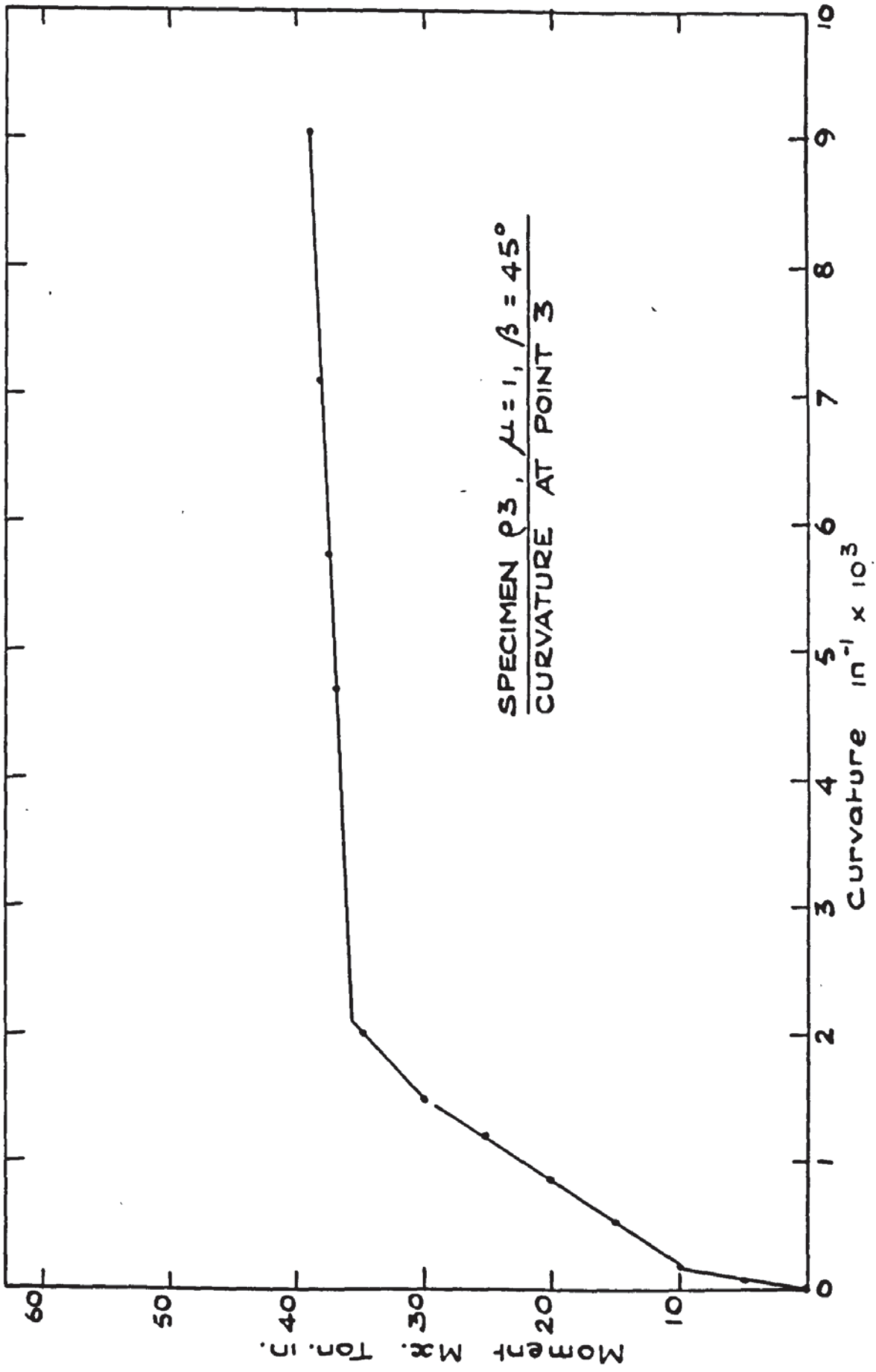


FIG. 5.9. MOMENT CURVATURE PLOT - P3.

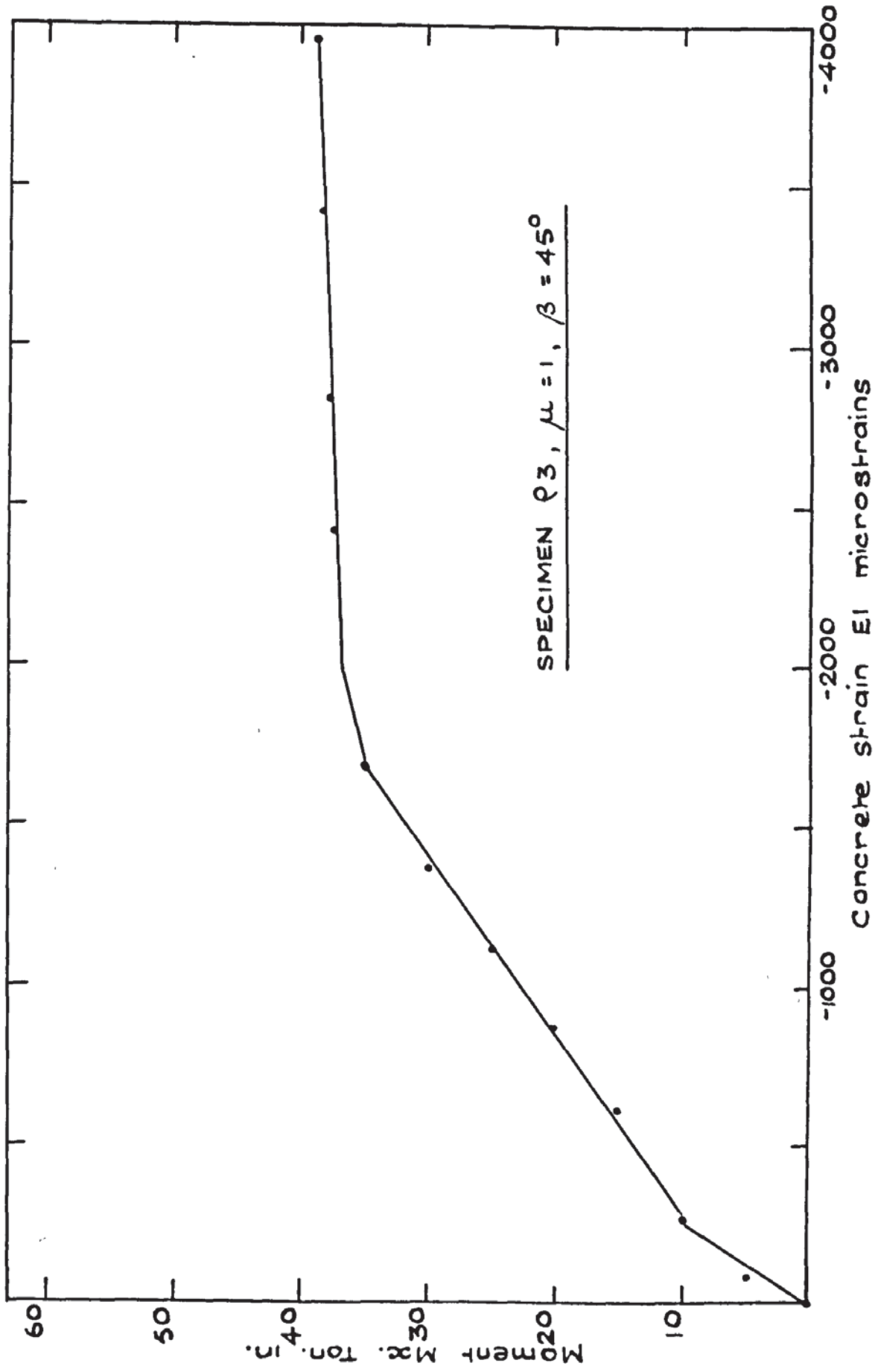


FIG. S.10. AVERAGE PRINCIPAL CONCRETE STRAIN PLOT EI - P.3.

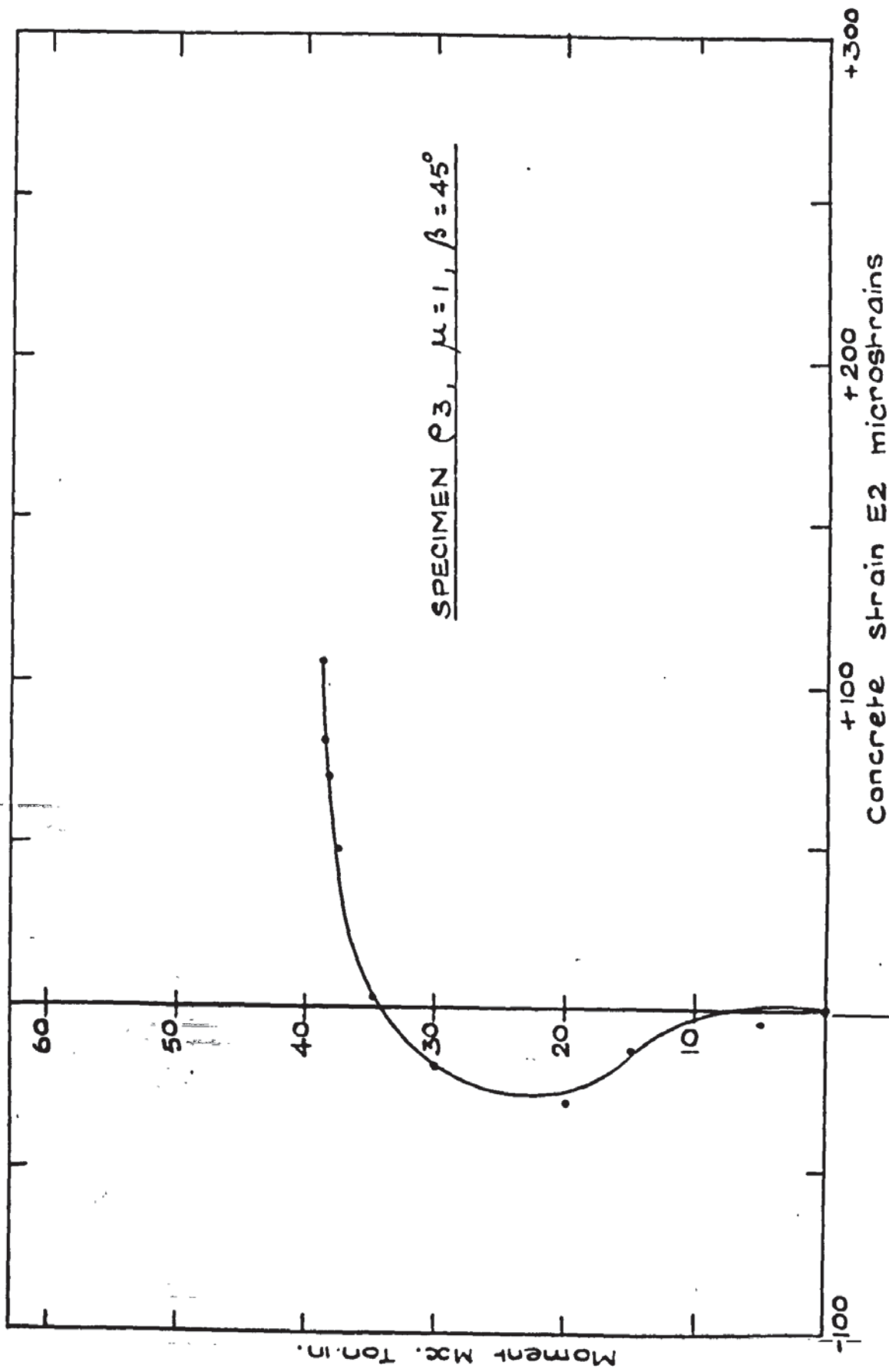


FIG. 5.11. AVERAGE PRINCIPAL CONCRETE STRAIN E2 - P.3.

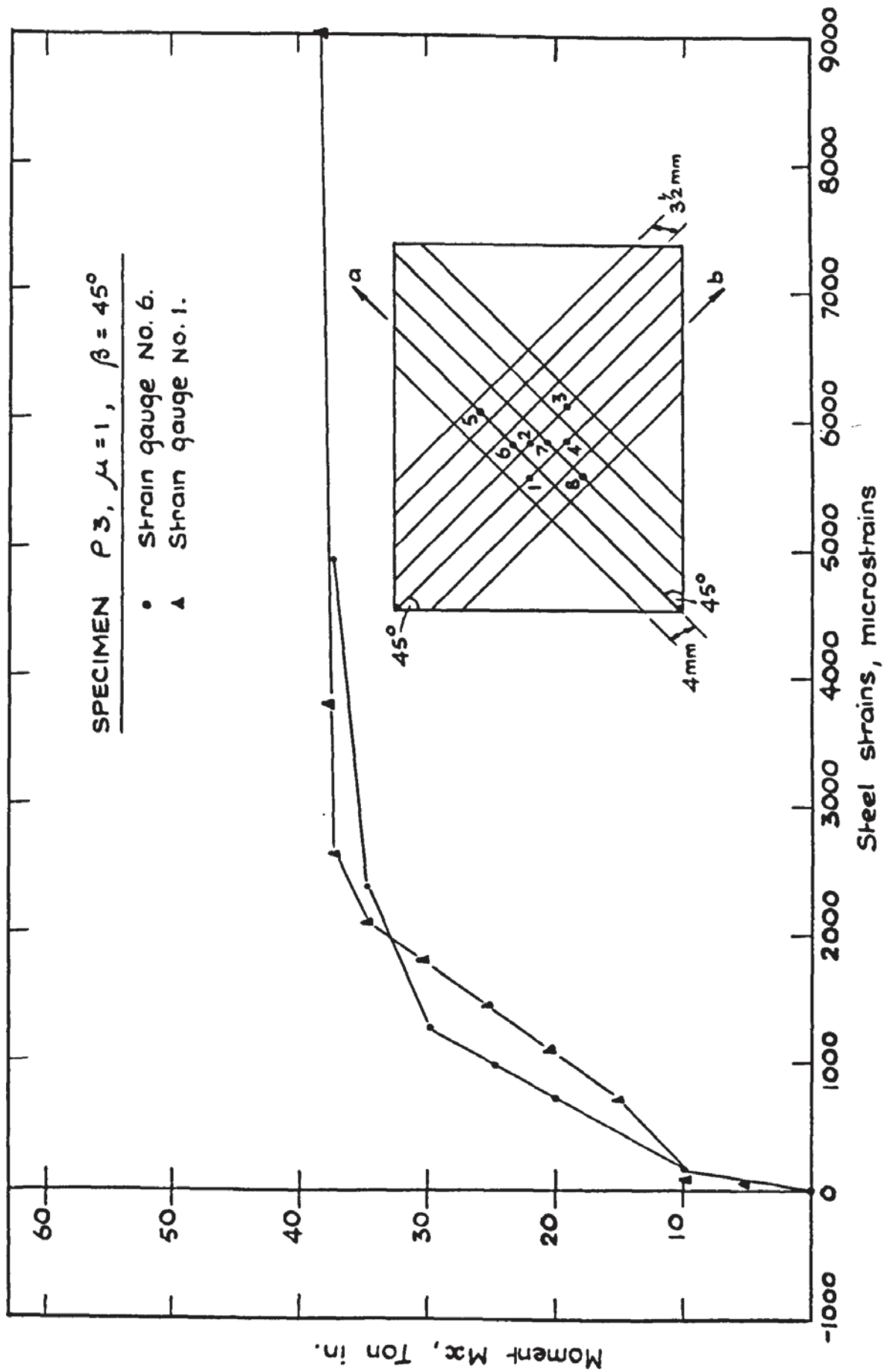


FIG. 5.12. TYPICAL STEEL STRAIN PLOT - P 3.

$M_x$	AVERAGE	STEEL STRAINS							
		1	2	3	4	5	6	7	8
TON.IN	$\tan 2\gamma$	MICROSTRAINS							
0.00	-	0.00	0.00	0.00	0.00	0.00	0.00	0.00	0.00
4.98	.2549	19.80	19.80	9.90	9.90	24.76	24.76	29.71	29.71
9.96	.0624	39.61	133.68	89.12	69.32	133.68	133.68	79.22	79.22
14.94	-.1095	673.37	445.61	376.29	356.49	440.66	440.66	207.95	207.95
19.92	.0029	1099.17	673.37	613.95	613.95	708.02	708.02	386.20	386.20
24.90	-.0081	1416.05	980.34	901.12	851.61	950.63	950.63	326.78	326.78
29.88	-.0193	1762.63	1277.41	1198.20	1109.07	1242.76	1242.76	485.22	485.22
34.86	-.0536	2039.90	1673.51	1683.41	1544.78	2336.98	2336.98	693.17	693.17
37.35	-.0967	2584.54	6099.90	2653.85	3317.32	4886.83	4886.83	930.83	930.83
37.85	-.1375	3743.12	9139.95	4832.39	4545.22	-	-	1604.20	1604.20
37.85	-.1667	9011.22	-	7634.78	7852.63	-	-	2475.61	2475.61
38.84	-.2027	-	-	-	-	-	-	-	-

Table 5.3 Principle Concrete Strain Direction & Steel Strains P3

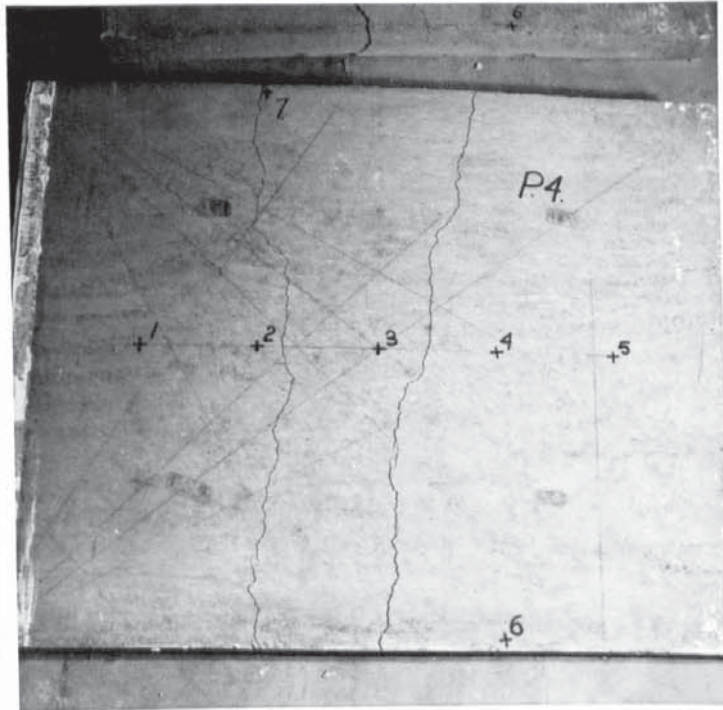


PLATE 5.6

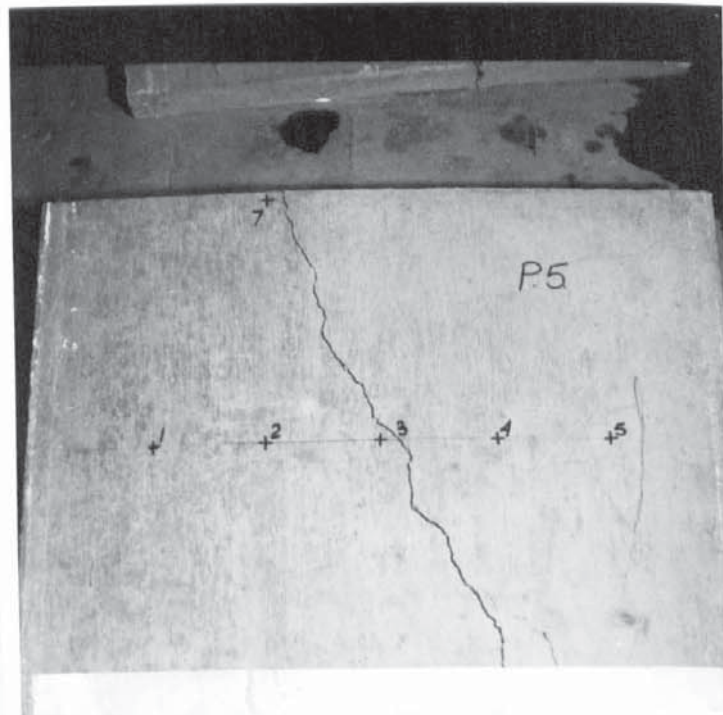


PLATE 5.7

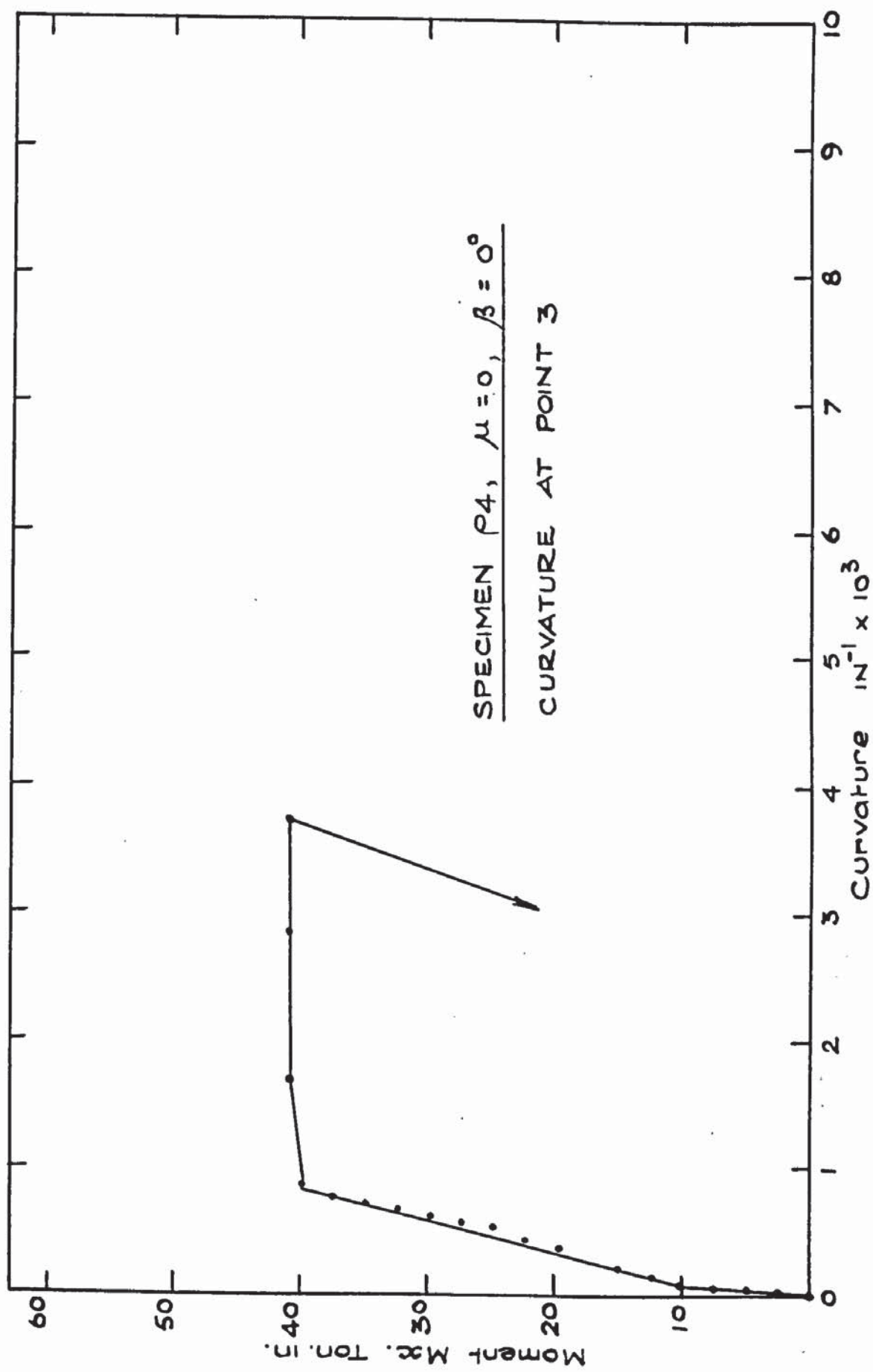


FIG. 5.13. MOMENT CURVATURE PLOT - P.4.

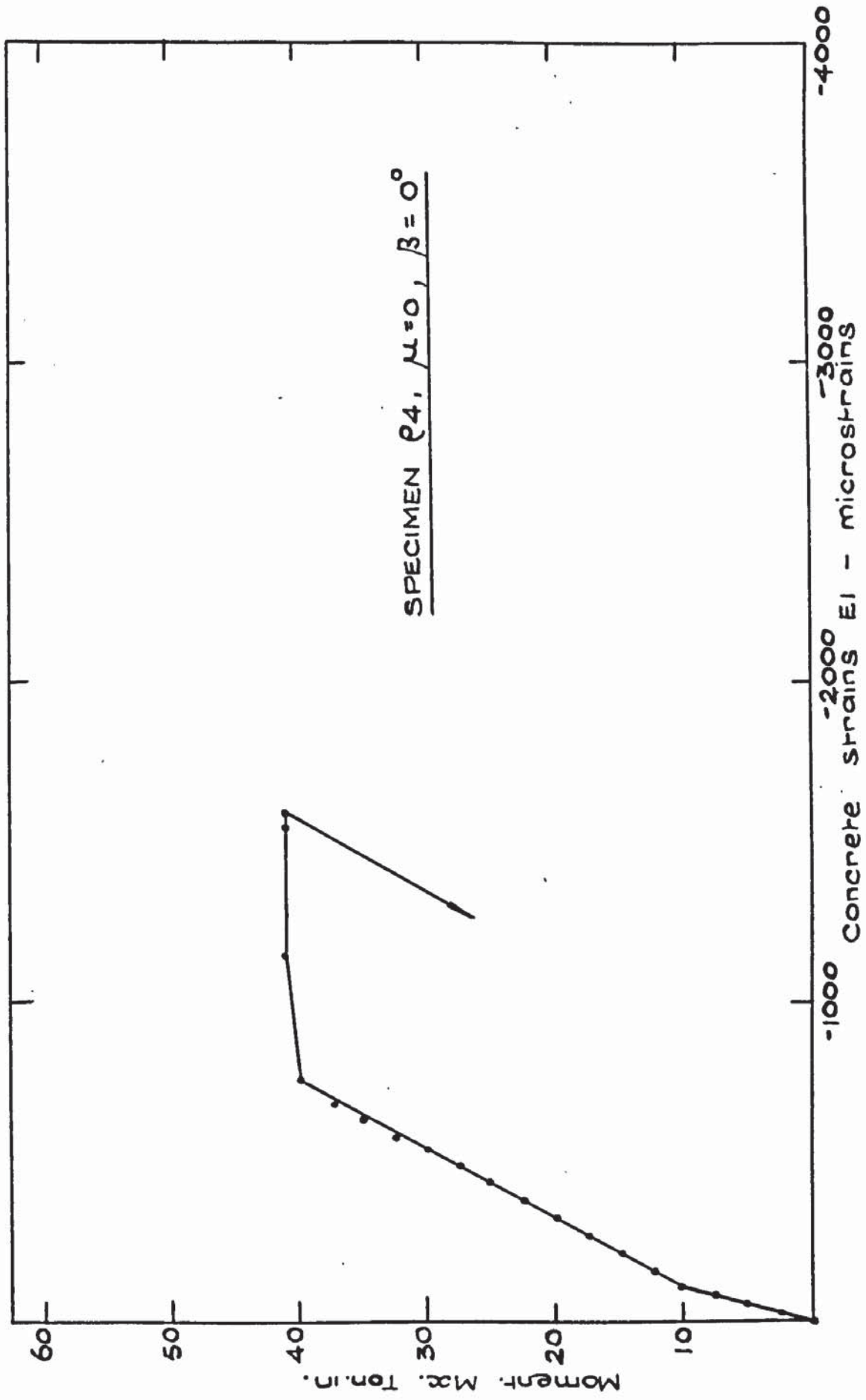


FIG. 5.14. AVERAGE PRINCIPAL CONCRETE STRAIN EI PLOT - P4.

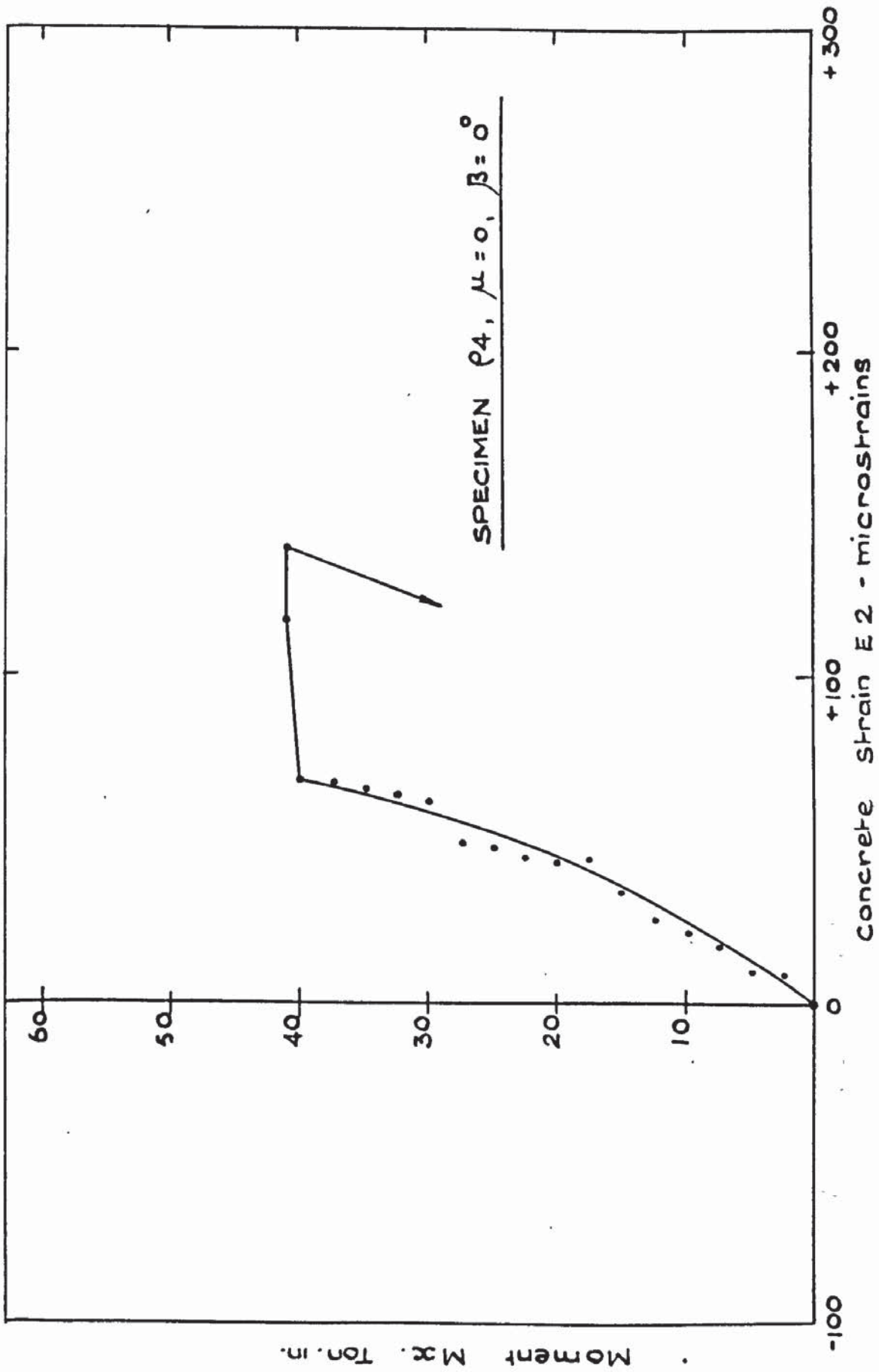


FIG. 5.15. AVERAGE PRINCIPAL CONCRETE STRAIN PLOT E2 - P4.

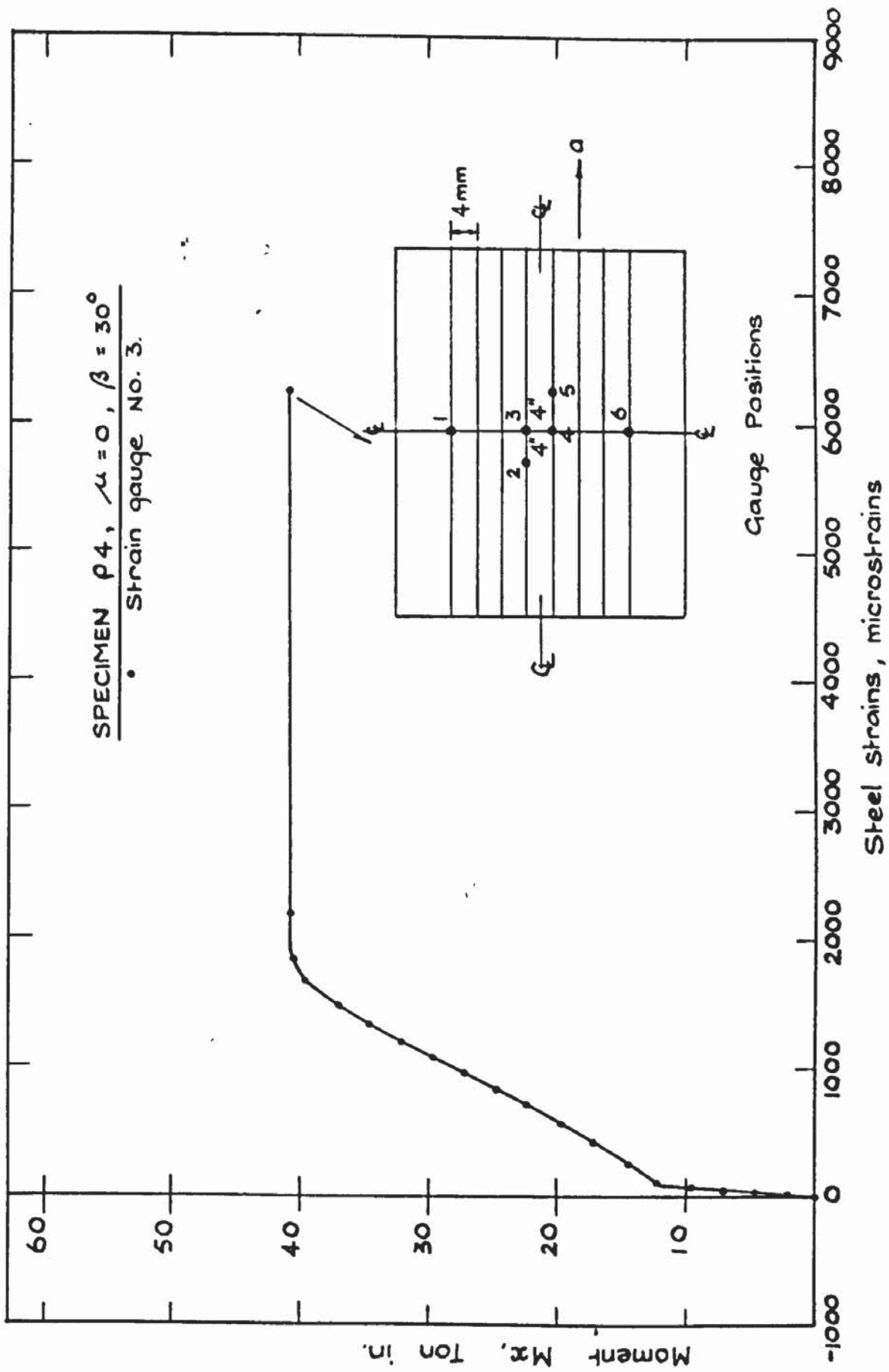


FIG. 5.16. TYPICAL STEEL STRAIN PLOT - P4.

M <sub>x</sub> TON.IN	AVERAGE tan 2γ	STEEL STRAINS							
		1	2	3	4	5	6	7	8
0.00	-	0.00	0.00	0.00	0.00	0.00	0.00	0.00	0.00
2.39	.5560	0.00	9.90	14.85	19.80	14.85	19.80	14.85	14.85
4.88	.5129	9.90	19.80	24.76	29.71	24.76	29.71	24.76	24.76
7.37	.5308	19.80	29.71	44.56	49.51	44.56	49.51	34.66	44.56
9.86	.4522	29.71	39.61	59.41	64.37	59.41	64.37	49.51	64.37
12.35	.3658	59.41	59.41	103.98	99.02	103.98	99.02	74.27	103.98
14.84	.3600	138.63	138.63	203.00	118.83	203.00	118.83	133.68	163.39
17.33	.3220	188.15	257.46	401.05	207.95	401.05	207.95	222.80	247.56
19.82	.2988	19.80	346.59	564.44	356.49	564.44	356.49	302.02	351.54
22.31	.2607	0.00	445.61	727.83	534.73	727.83	534.73	391.15	450.56
24.80	.2424	-59.41	544.63	846.66	663.46	846.66	663.46	509.98	559.49
27.29	.2144	54.46	653.56	846.66	802.10	846.66	802.10	668.41	658.51
29.78	.2140	128.73	742.68	1064.51	901.12	1064.51	901.12	787.24	747.63
32.27	.1999	356.49	841.71	1193.24	1010.05	1193.24	1010.05	906.07	846.66
34.76	.1919	485.22	930.83	1312.07	1114.02	1312.07	1114.02	1019.95	940.73
37.25	.1798	703.07	1019.95	1490.32	1208.10	1490.32	1208.10	1114.02	1034.80
39.74	.1751	747.63	1123.93	1658.66	1336.83	1658.66	1336.83	1208.10	1163.54
40.99	.1448	812.00	1346.73	1827.00	1643.80	1827.00	1643.80	1391.29	1317.02
40.99	.1163	-	-	2163.68	1752.73	2163.68	1752.73	1321.98	1341.78
40.99	.1054	-	-	6461.34	1851.76	6461.34	1851.76	-	1376.44

Table 5.4 Principle Concrete Strain Direction & Steel Strains P4

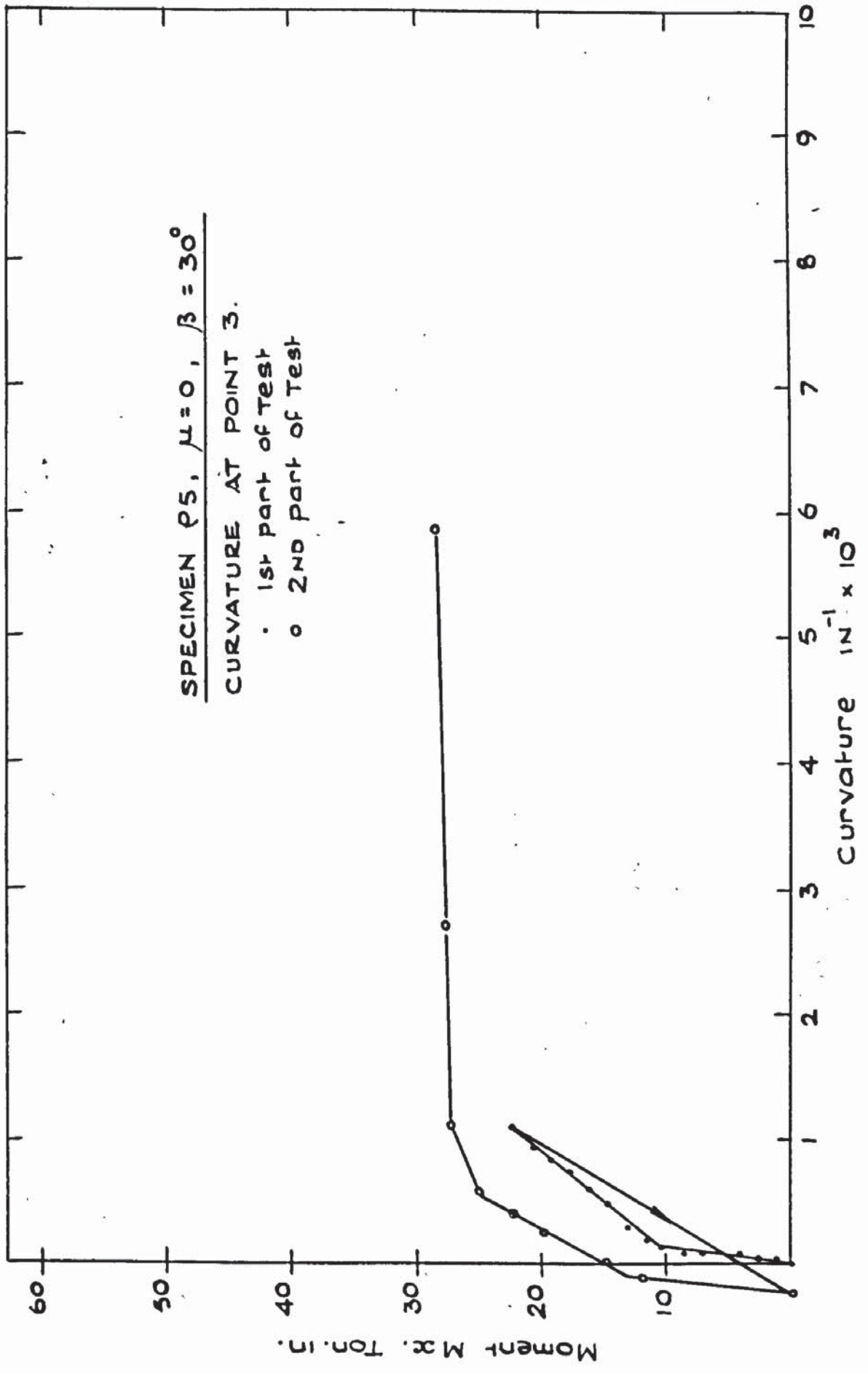


FIG. 5.17 MOMENT CURVATURE PLOT - P5.

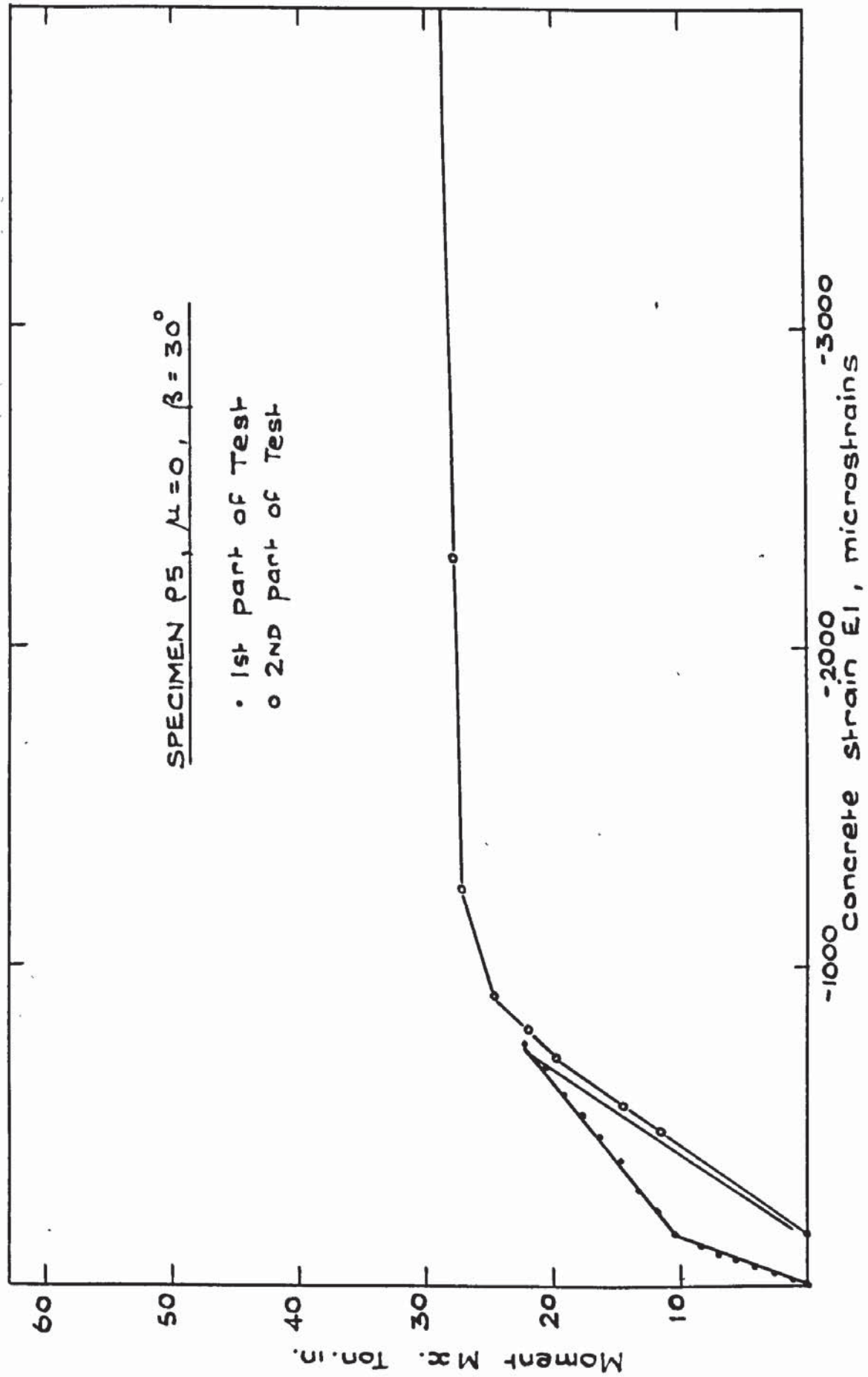


FIG. 5.18. AVERAGE PRINCIPAL CONCRETE STRAIN PLOT EI - P.5.

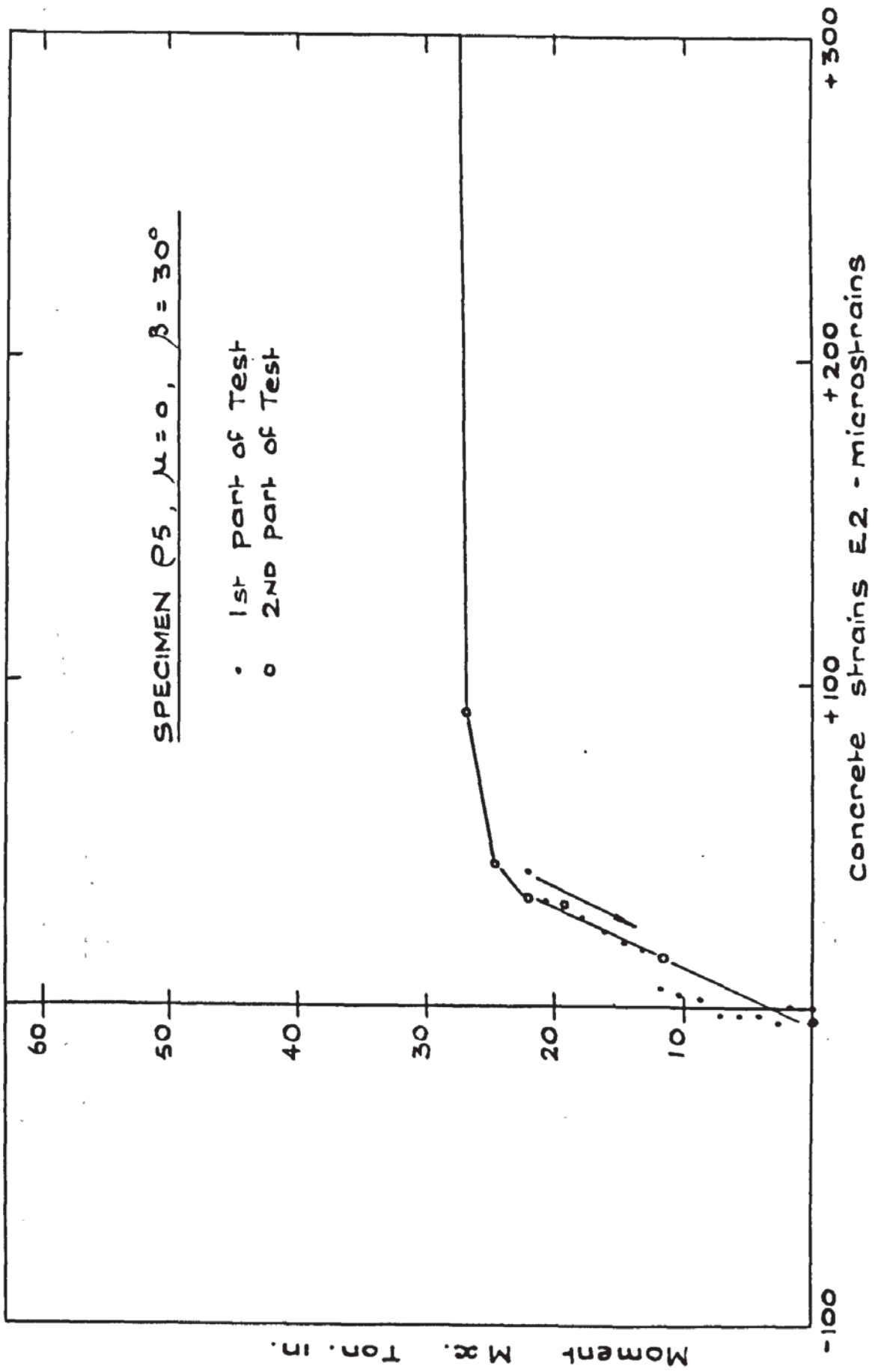


FIG. 5.19. AVERAGE PRINCIPAL CONCRETE STRAIN PLOT E2 - P5.

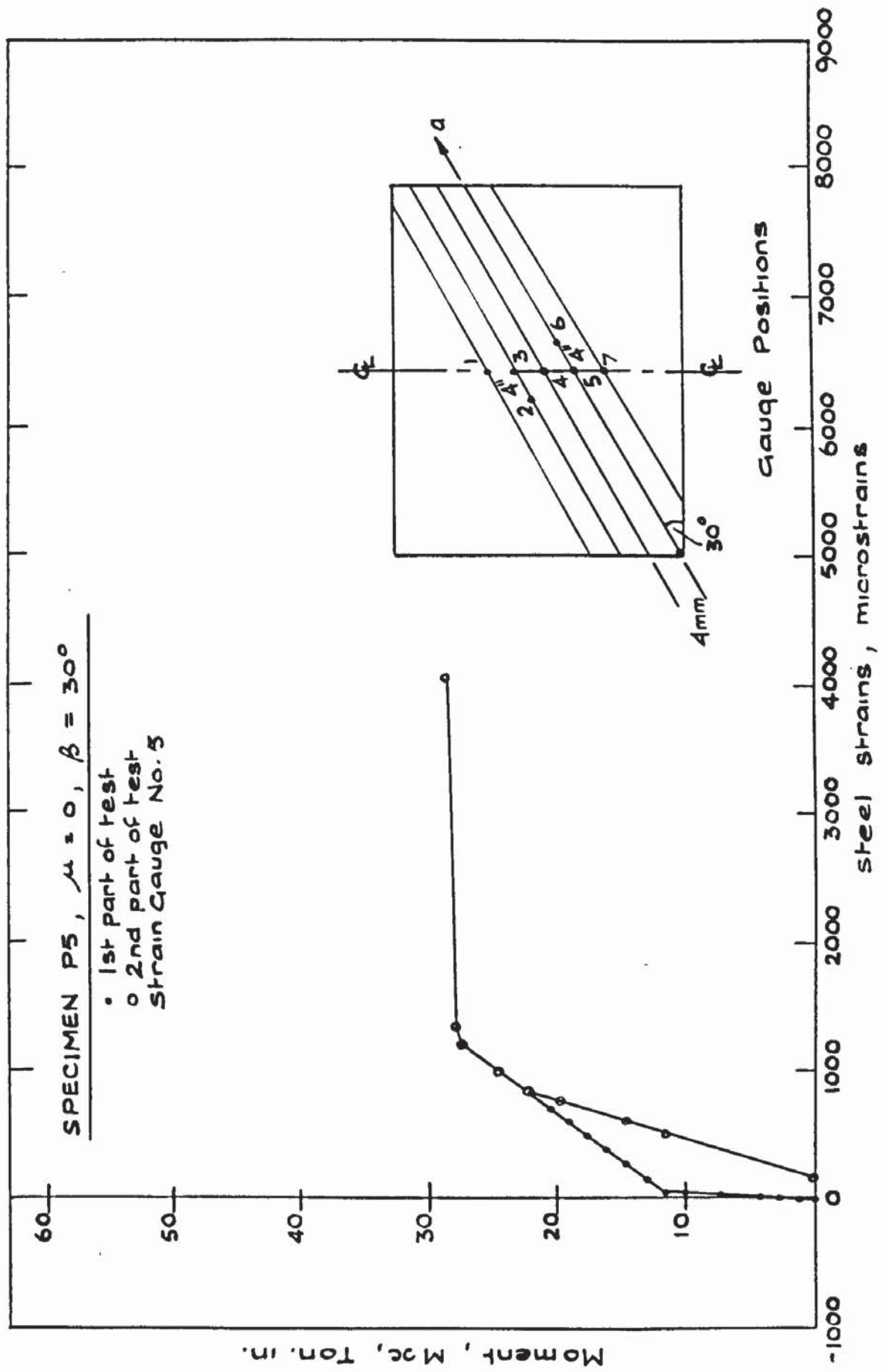


FIG. 5.20. TYPICAL STEEL STRAIN PLOT - P.5.

M <sub>x</sub> TON. IN	AVERAGE tan 2γ	STEEL STRAINS							
		1	2	3	4	5	6	7	8
0.00	-	0.00	0.00	0.00	0.00	0.00	0.00	0.00	0.00
1.20	.3333	-21.56	10.78	32.34	-107.80	0.00	5.39	75.46	0.00
2.69	.4444	-21.56	10.78	53.90	-129.37	10.78	5.39	75.46	
4.18	.1407	10.78	21.56	70.07	-215.61	21.56	16.17	97.02	
5.68	.0988	32.34	32.34	86.24	-237.17	21.56	26.95	129.37	
7.17	.1133	32.34	43.12	107.80	-312.63	32.34	32.34	150.93	
8.67	.0689	53.90	53.90	129.37	-334.20	43.12	37.73	204.83	
10.16	.1275	97.02	75.46	161.71	-420.44	53.90	70.07	-	
11.65	.1357	107.80	107.80	409.66	-442.00	86.24	113.20	-	
13.15	.1133	123.98	172.49	463.56	-463.56	172.49	177.88	-	
14.64	.1295	247.95	280.29	495.90	-377.32	301.85	307.24	-	
16.14	.1471	463.56	388.10	646.83	-301.85	420.44	425.83	-	
17.63	.1510	528.24	452.78	808.54	-237.17	506.88	501.29	-	
19.12	.1598	679.17	560.59	1007.98	-194.05	603.71	630.66	-	
20.62	.1243	808.54	668.39	1207.41	-113.20	733.07	803.15	-	
22.11	.1180	1218.20	786.98	1530.83	-32.34	851.66	997.20	-	
0.00	-.0076	2220.78	307.24	1099.61	-2161.49	183.27	226.39	-	
11.65	-.0076	2641.22	619.88	1536.22	-1956.66	506.68	668.39	-	
14.64	.1021	2716.68	722.29	1600.90	-1821.90	614.49	803.15	-	
19.62	.1021	3201.80	884.00	1768.00	-1627.85	797.76	1040.32	-	
22.11	.0982	3320.39	975.63	1940.49	-1476.93	894.78	1158.90	-	
24.60	.0854	3622.24	1121.17	2296.24	-1164.29	1013.37	1309.83	-	
27.09	.0070	3730.05	1304.44	2652.00	-927.12	1239.76	1547.00	-	
27.59	-.0909	3891.76	1347.56	3142.51	-571.37	1358.34	-	-	
28.59	.1579	4053.46	-	-	-409.66	-	-	-	

Table 5.5 Principle Concrete Strain Direction & Steel Strains P5

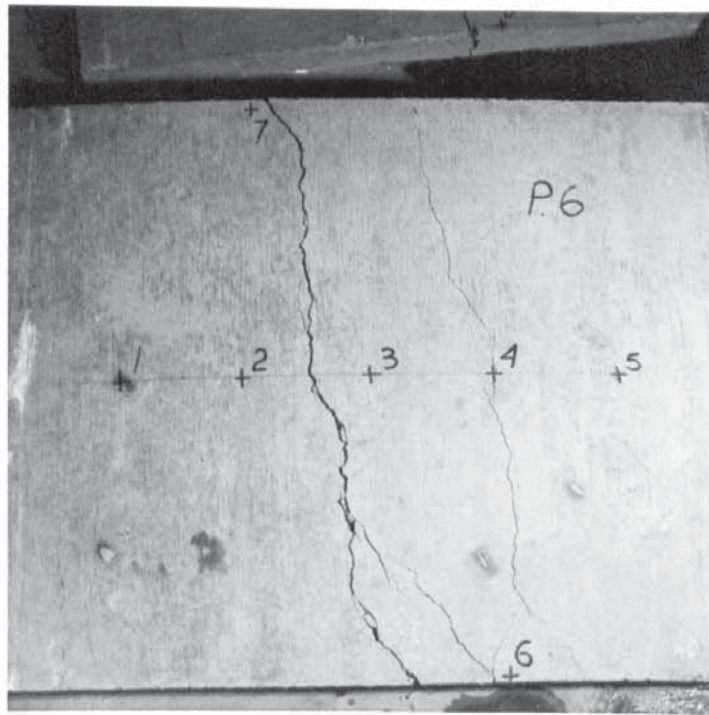


PLATE 5.8

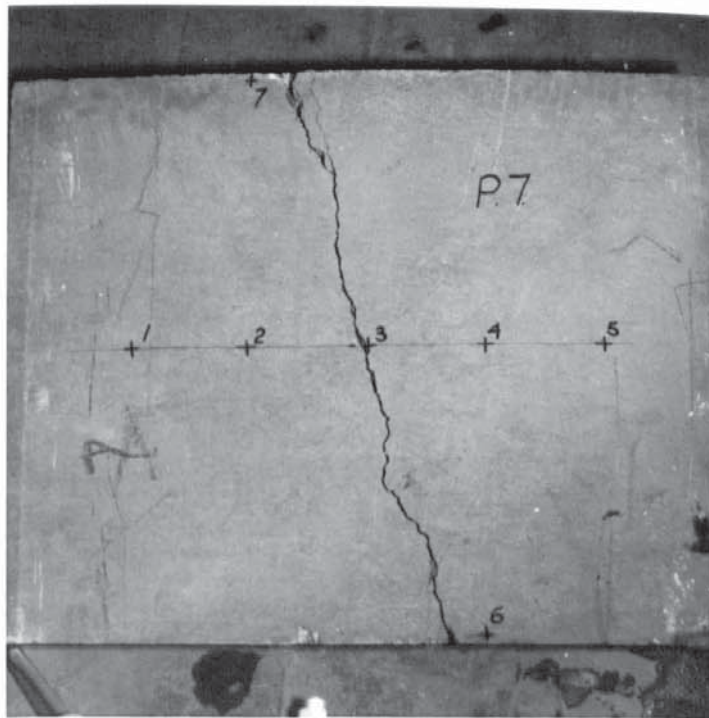


PLATE 5.9

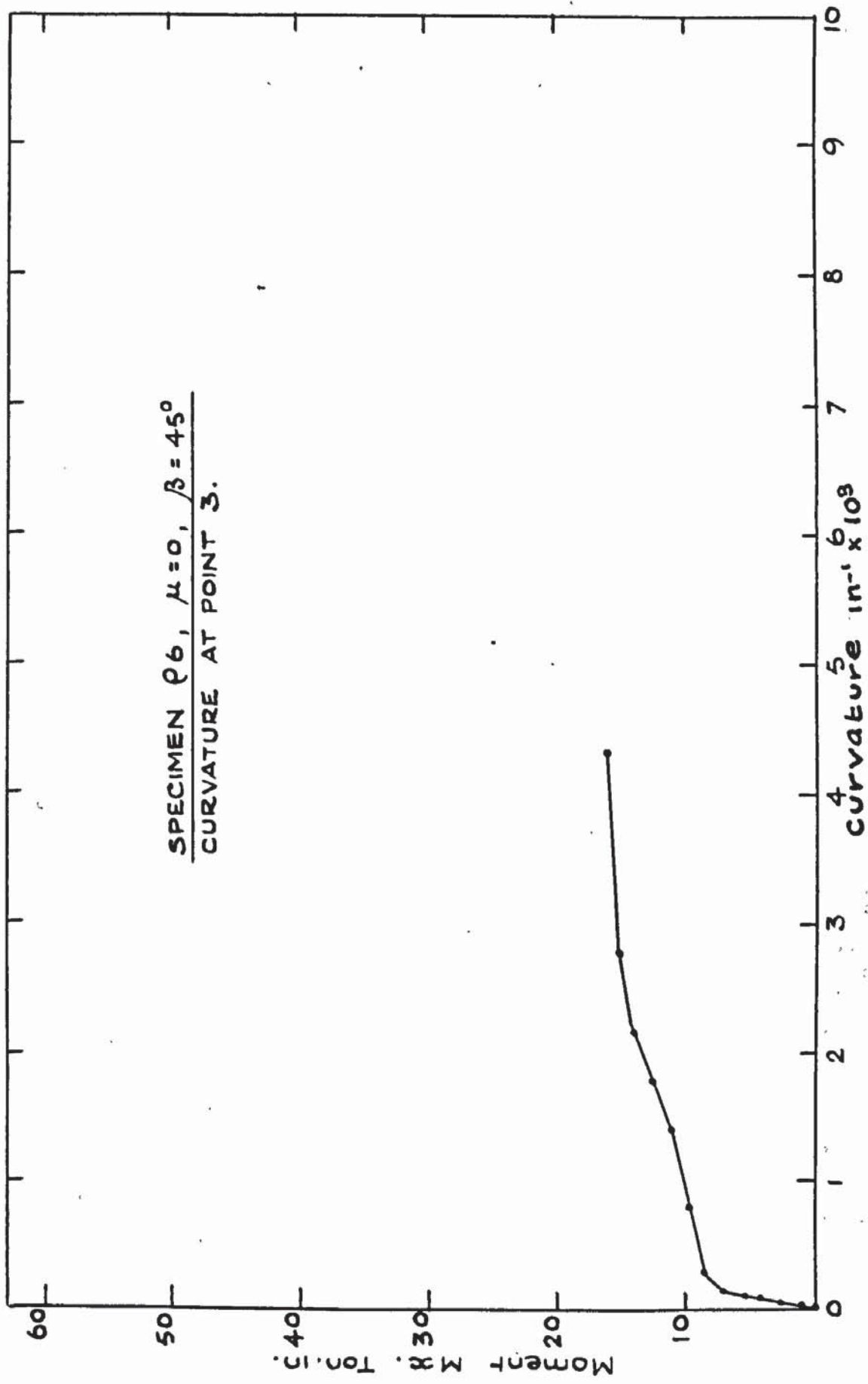


FIG. 5.21. MOMENT CURVATURE PLOT - P6.

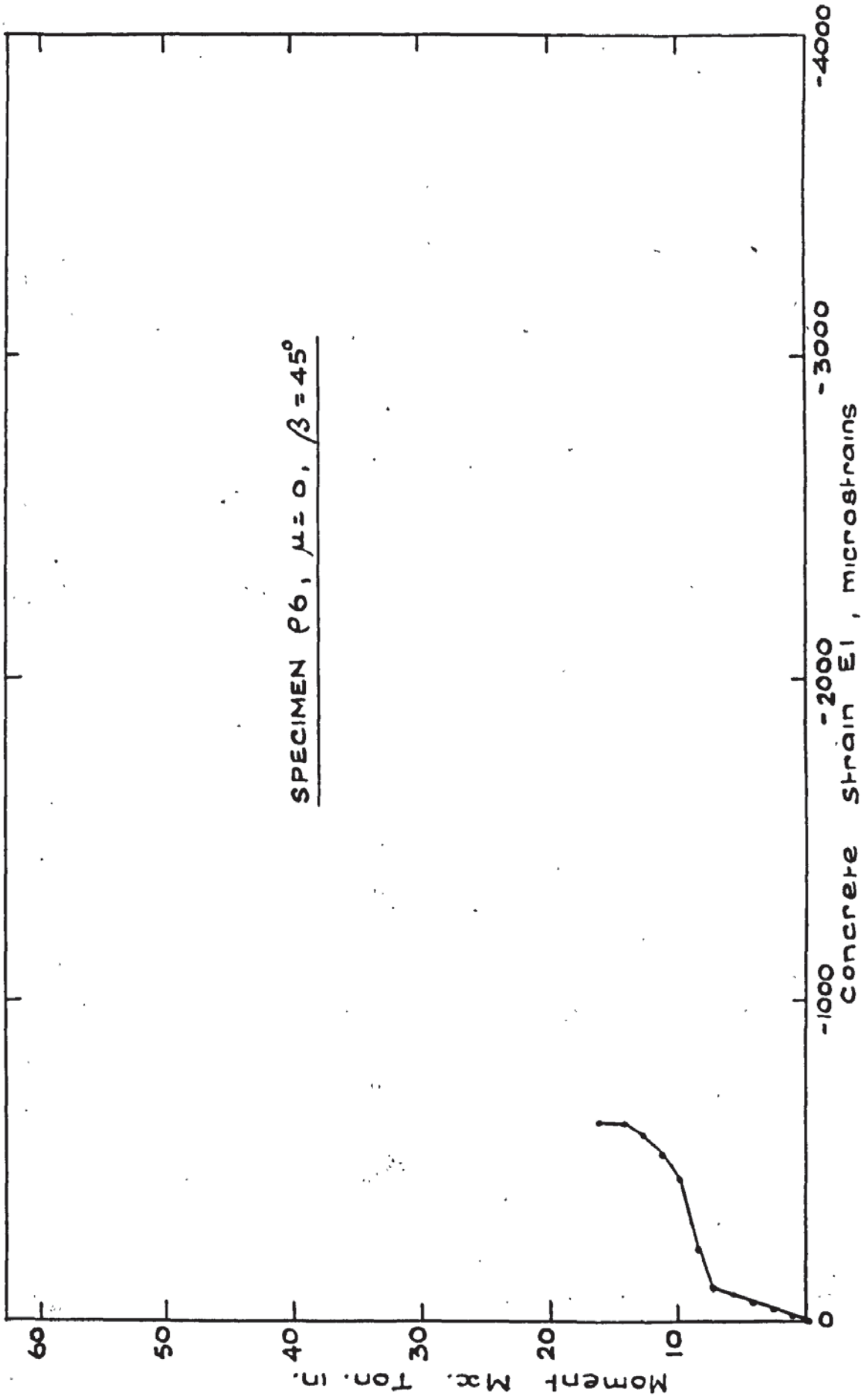


FIG. 5.22. AVERAGE PRINCIPAL CONCRETE STRAIN E1 - P.6.

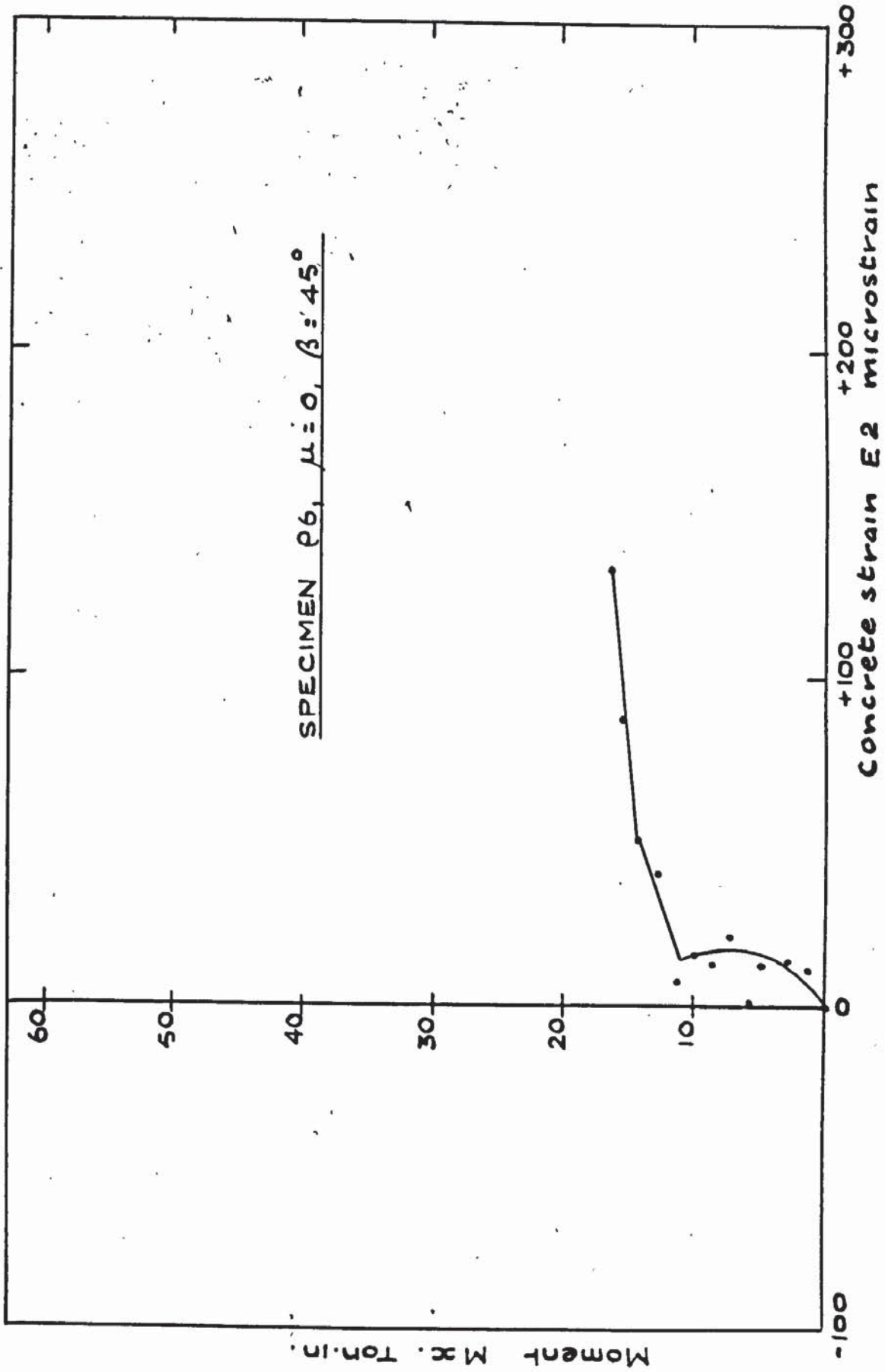


FIG. 5.23. AVERAGE PRINCIPAL CONCRETE STRAIN PLOT E2 - P6.

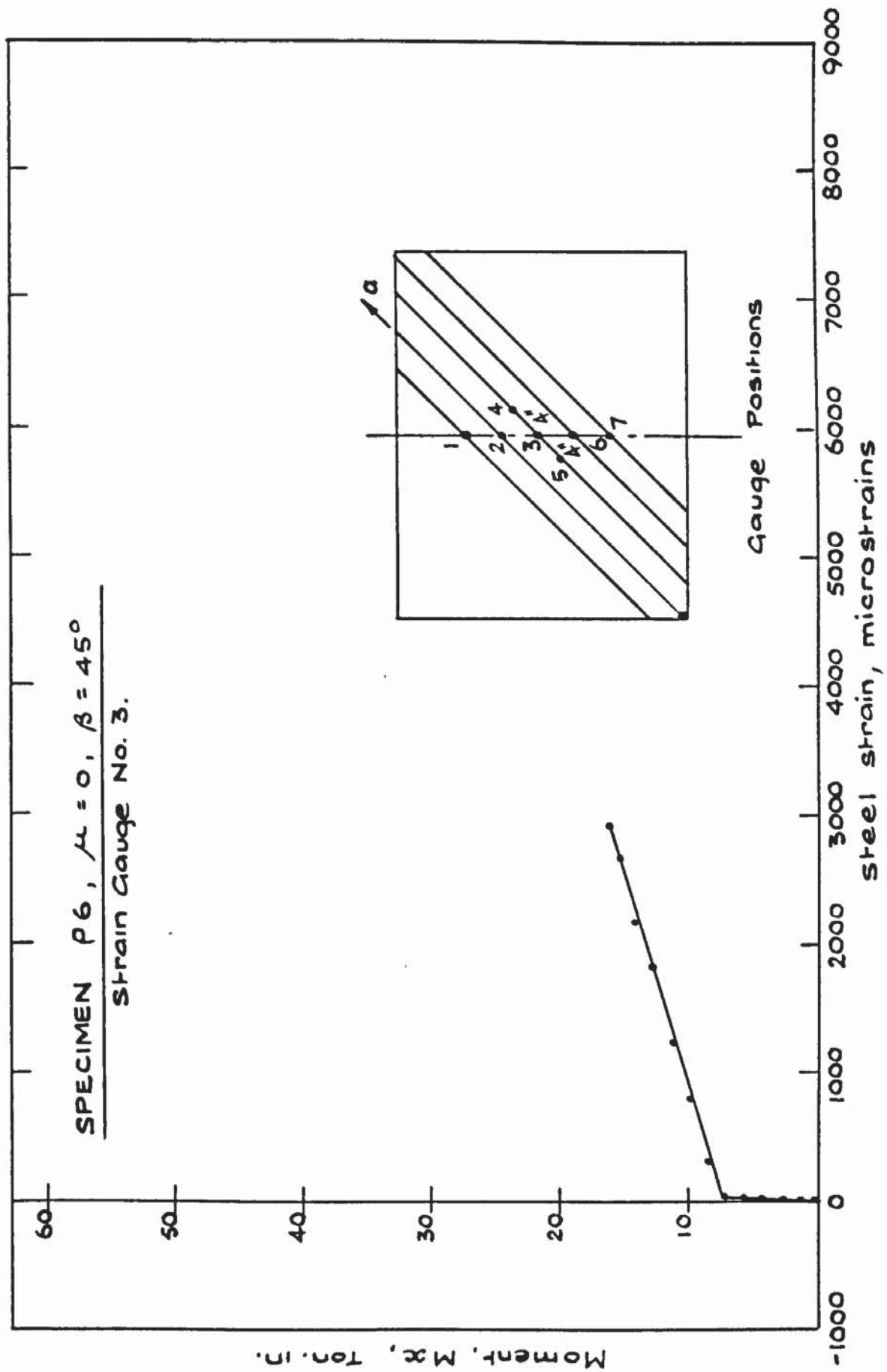


FIG. 5.24. TYPICAL STEEL STRAIN PLOT - P.6.

M <sub>x</sub>	AVERAGE	STEEL STRAINS										
		TON. IN	tan 2γ	1	2	3	4	5	6	7	8	
0.00	-	0.00	0.00	0.00	0.00	0.00	0.00	0.00	0.00	0.00	0.00	0.00
1.20	.6666	4.93	4.93	9.85	9.85	9.85	9.85	9.85	4.93	4.93	4.93	4.93
2.69	-.0666	9.85	4.93	9.85	9.85	9.85	9.85	14.78	14.78	14.78	4.93	4.93
4.18	.1750	9.85	14.78	14.78	14.78	14.78	14.78	19.71	14.78	14.78	9.85	9.85
4.68	.3653	19.71	14.78	14.78	14.78	14.78	14.78	19.71	19.71	19.71	14.78	14.78
7.17	.1884	39.41	24.63	39.41	29.56	29.56	29.56	29.56	24.63	24.63	24.63	24.63
8.67	.0477	187.22	83.76	275.05	64.05	64.05	64.05	98.54	300.54	300.54	280.83	280.83
9.91	-.0542	660.20	517.32	783.37	157.66	157.66	157.66	354.73	803.07	803.07	443.41	443.41
11.16	-.0370	837.56	607.46	1212.00	450.00	450.00	450.00	554.73	1473.12	1473.12	443.41	443.41
12.65	.0224	921.32	734.10	1803.22	610.93	610.93	610.93	778.44	1832.78	1832.78	492.68	492.68
14.14	.0202	1054.34	763.66	2148.10	817.85	817.85	817.85	1202.15	1995.37	1995.37	497.61	497.61
15.14	-.0563	1172.59	990.29	2650.63	990.29	990.29	990.29	-	2261.41	2261.41	448.34	448.34
16.14	-.0546	2532.39	-	2892.05	1236.63	1236.63	1236.63	-	2389.51	2389.51	596.15	596.15

Table 5.6 Principle Concrete Strain Direction & Steel Strains P6.

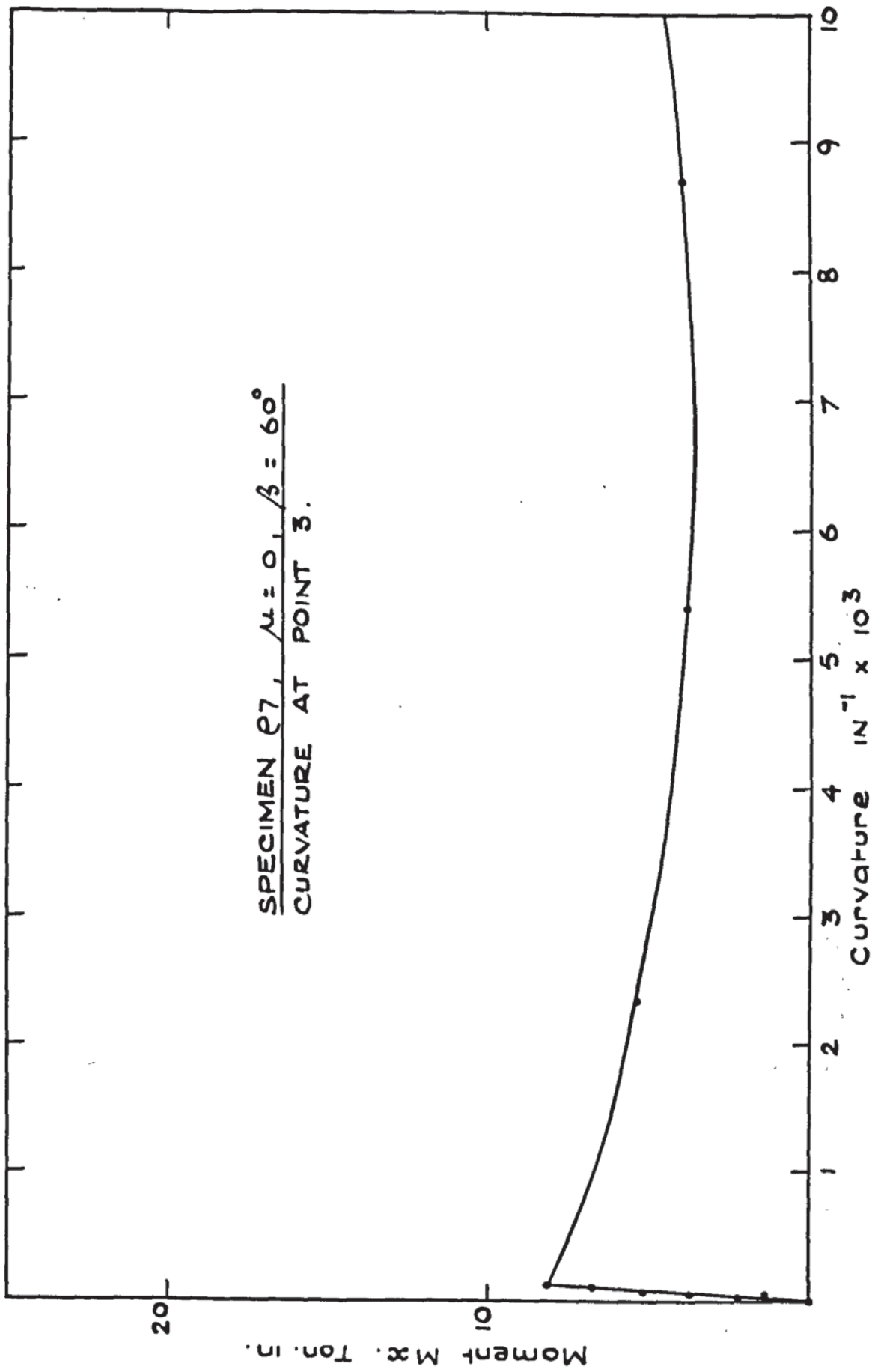


FIG. 5.25. MOMENT CURVATURE PLOT - P7.

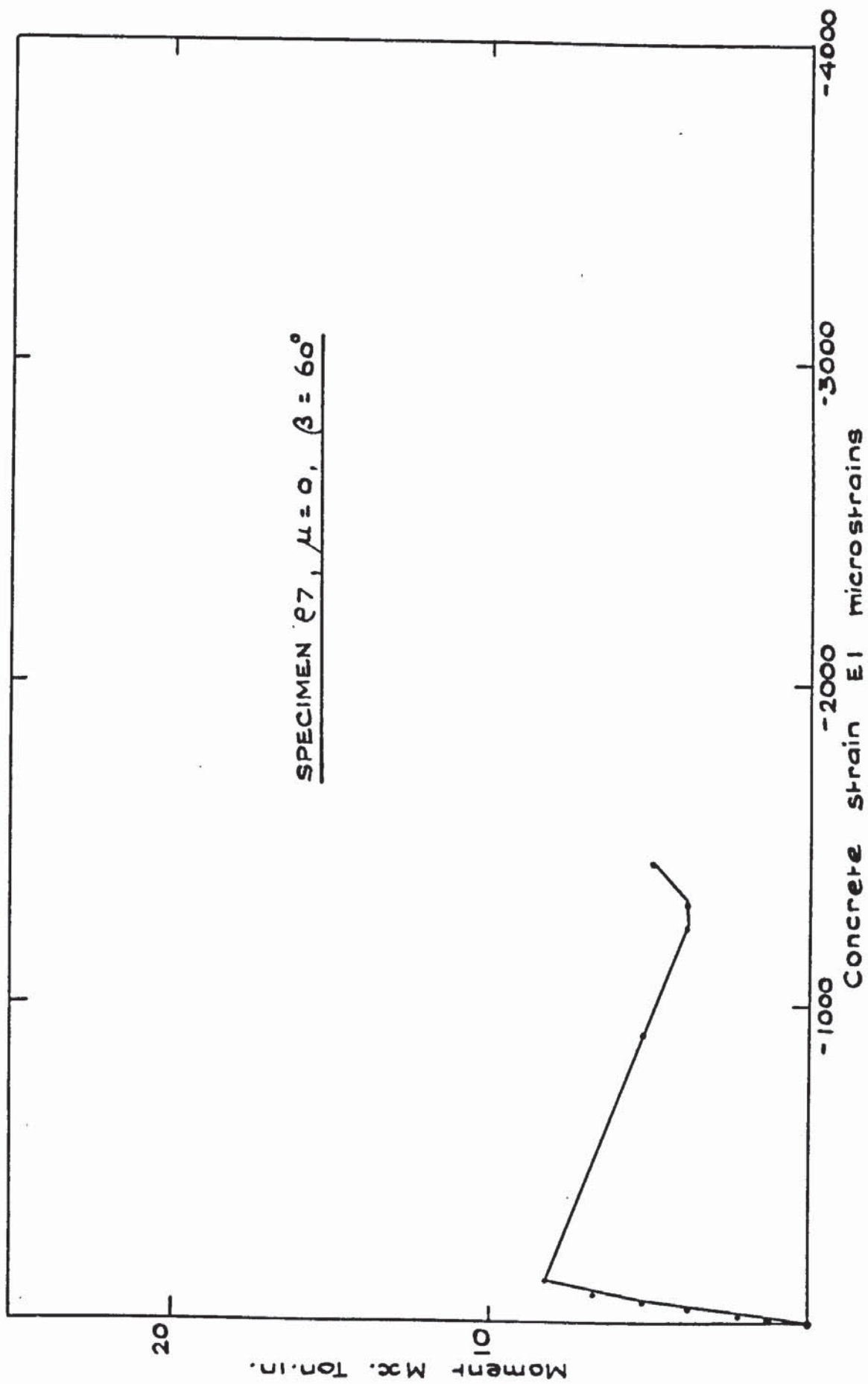


FIG. 5.26. AVERAGE PRINCIPAL CONCRETE STRAIN PLOT EI - P7

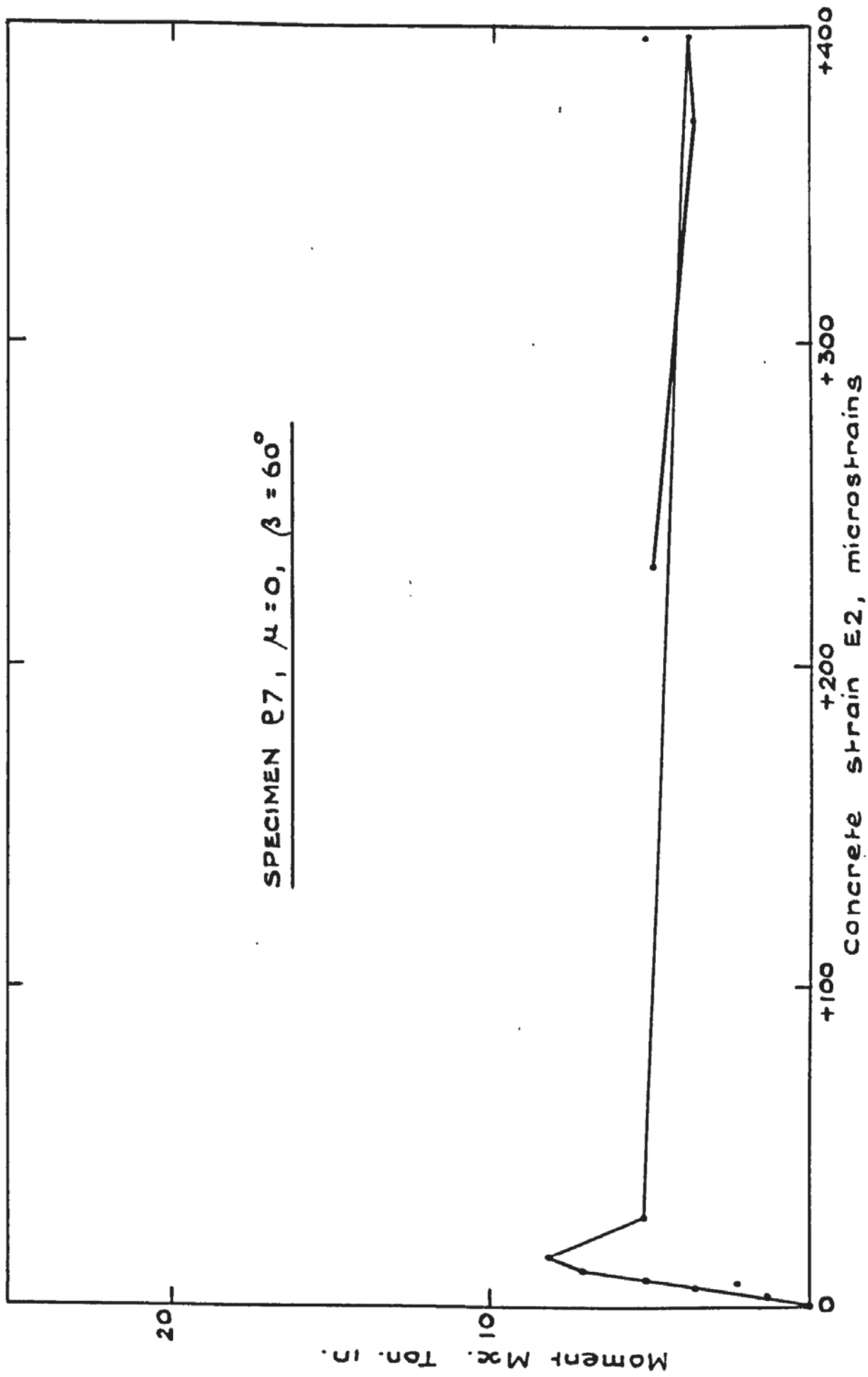


FIG. 5.27. AVERAGE PRINCIPAL CONCRETE STRAIN PLOT E2 - P7.

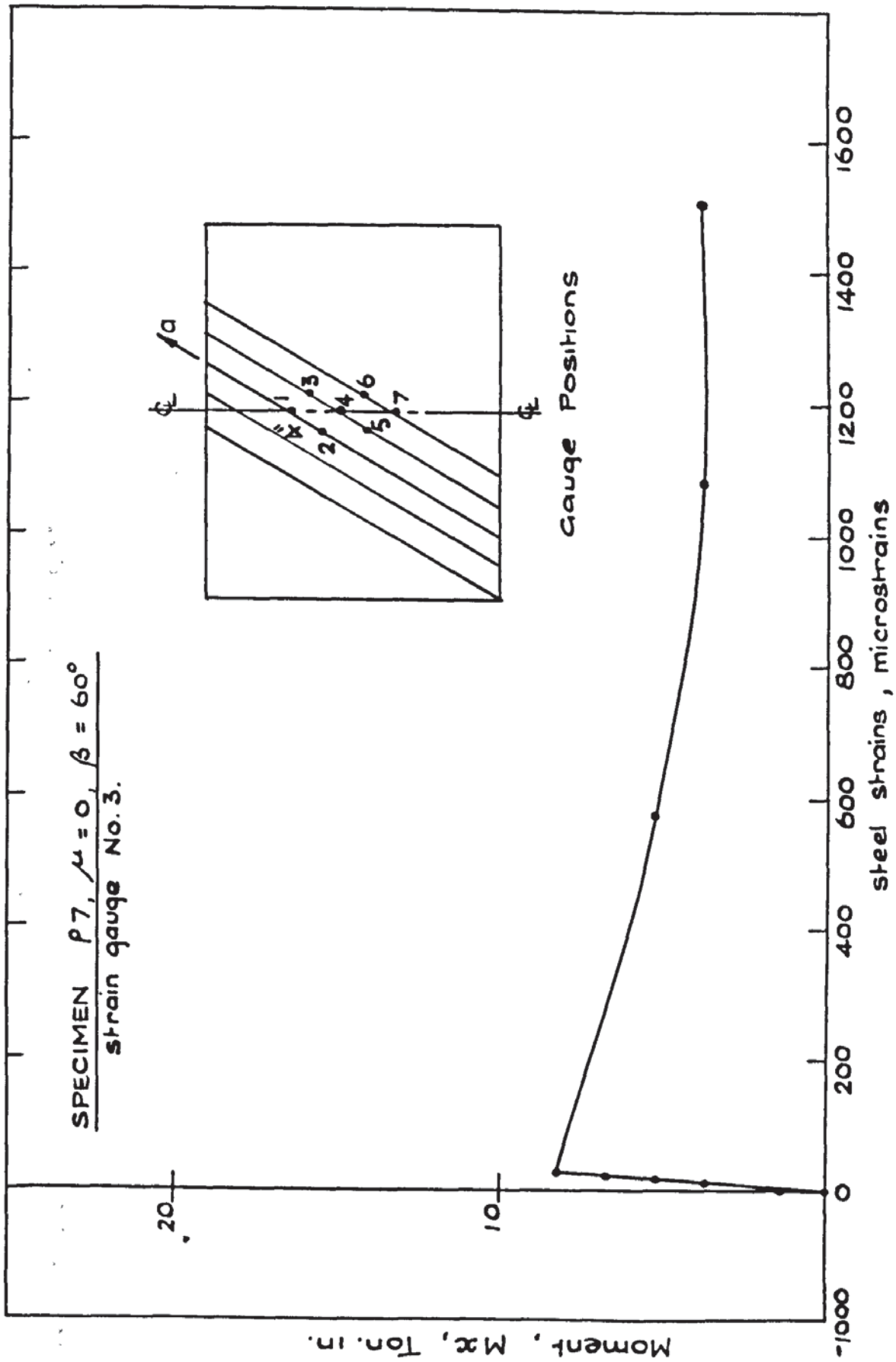


FIG. 5.28. TYPICAL STEEL STRAIN PLOT - P7.

M <sub>x</sub> TON. IN	AVERAGE tan 2γ	STEEL STRAINS MICROSTRAINS							
		1	2	3	4	5	6	7	8
0.00	-	0.00	0.00	0.00	0.00	0.00	0.00	0.00	0.00
1.29	-.3333	0.00	0.00	0.00	79.22	0.00	9.90	0.00	0.00
2.19	-	-9.90	0.00	4.95	108.93	0.00	49.51	0.00	-4.95
3.69	.0555	-9.90	-9.90	9.90	118.83	9.90	59.41	0.00	0.00
5.18	-.0615	-14.85	-9.90	14.85	118.83	9.90	89.12	-4.95	-4.95
6.67	-.0112	-19.80	-19.80	19.80	108.93	19.80	99.02	4.95	4.95
8.17	-.0979	-19.80	-19.80	29.71	227.76	39.61	138.63	-24.76	-24.76
5.18	-.1463	-39.61	-49.51	574.34	108.93	346.59	128.73	1549.73	1549.73
3.78	-.1957	-69.32	-49.51	1089.27	812.00	188.59	495.12	1995.34	1995.34
3.78	-.2893	-59.41	-	1455.66	-	-	-	2044.85	2044.85
4.93	.0438	-	-	-	-	-	-	2341.93	2341.93

Table 5.7 Principle Concrete Strain Direction & Steel Strains P7

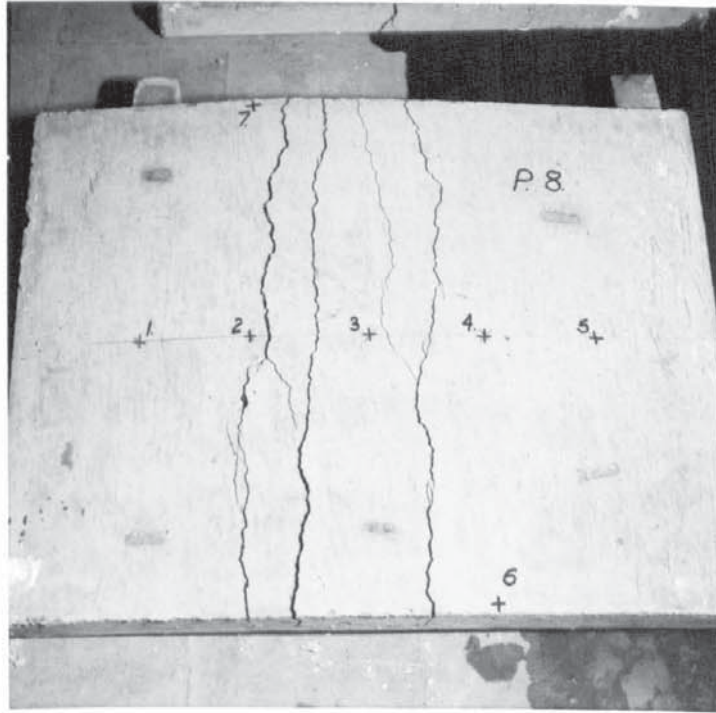


PLATE 5.10

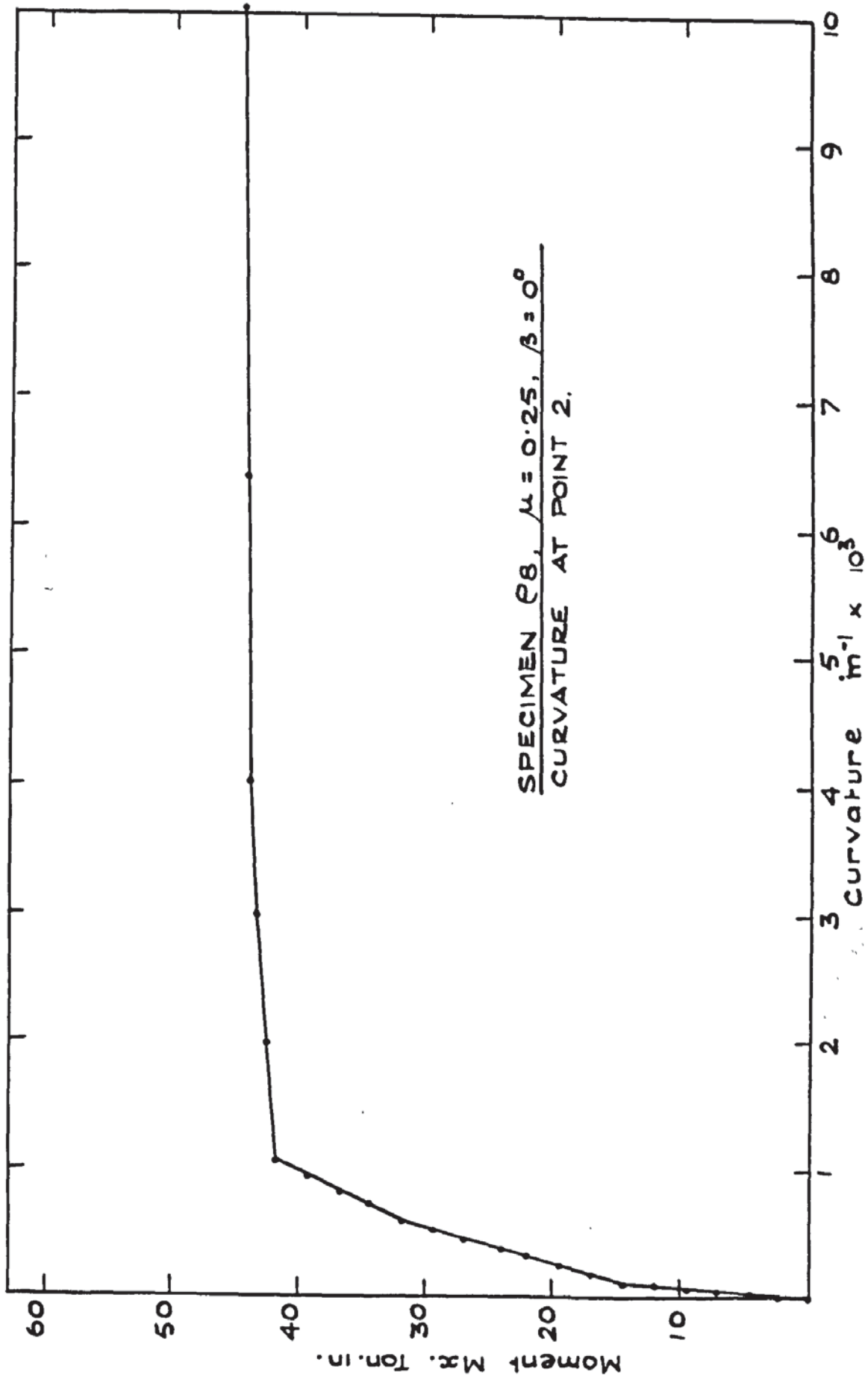


FIG. 5.29. MOMENT CURVATURE PLOT - P8

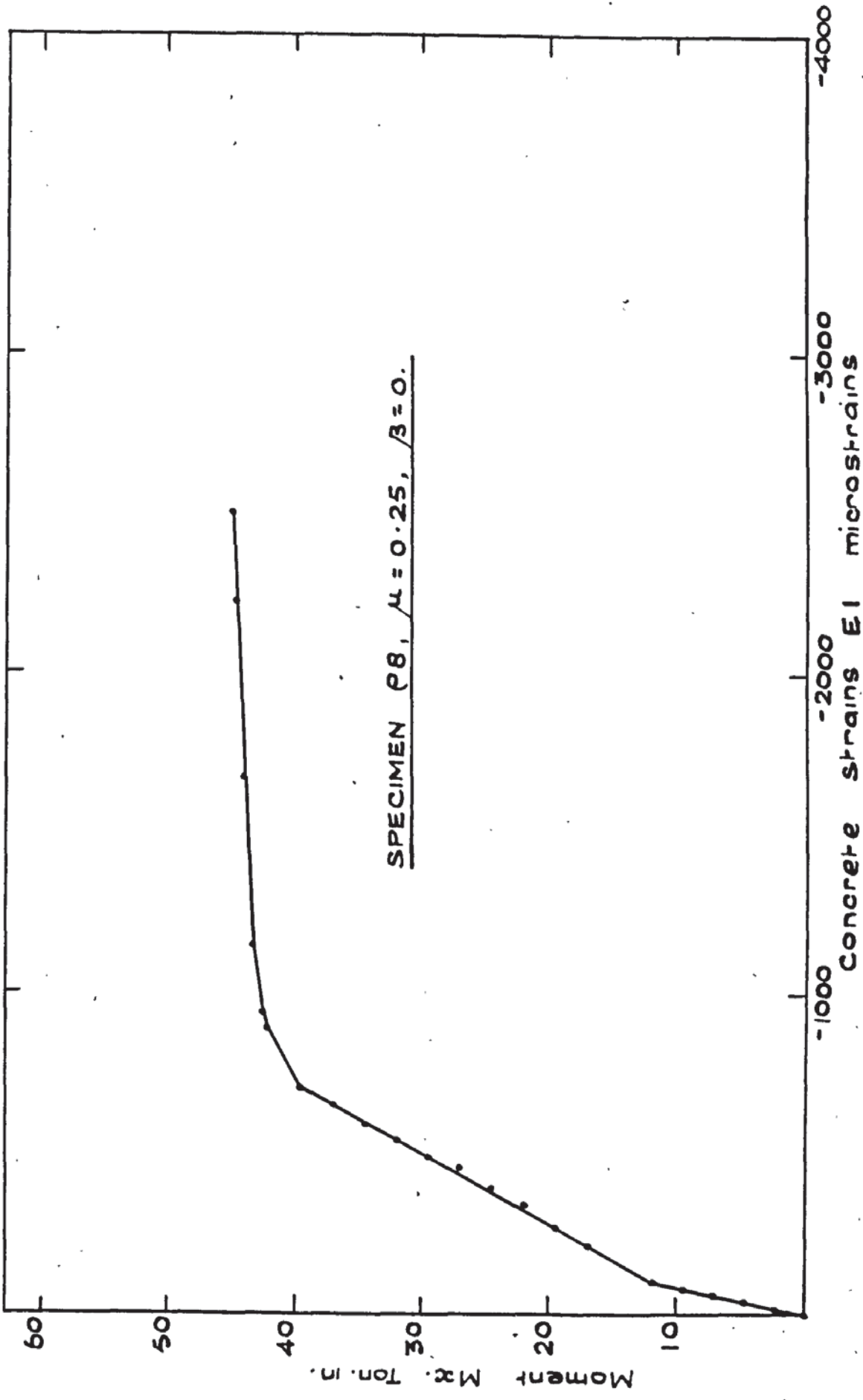


FIG. 5.30. AVERAGE PRINCIPAL CONCRETE STRAIN PLOT EI - P8

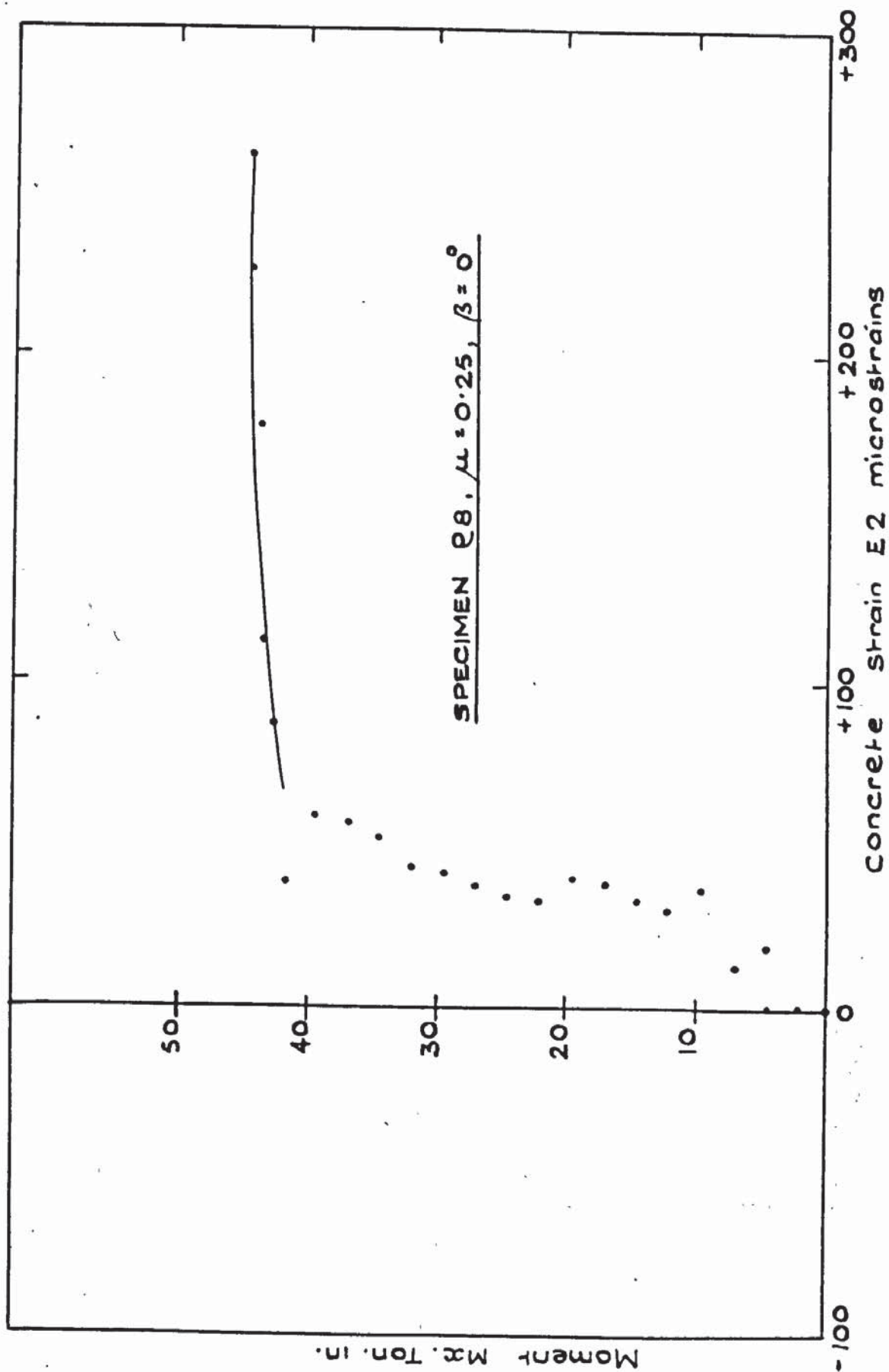


FIG. 5.31. AVERAGE PRINCIPAL CONCRETE STRAIN PLOT E2 - P8.

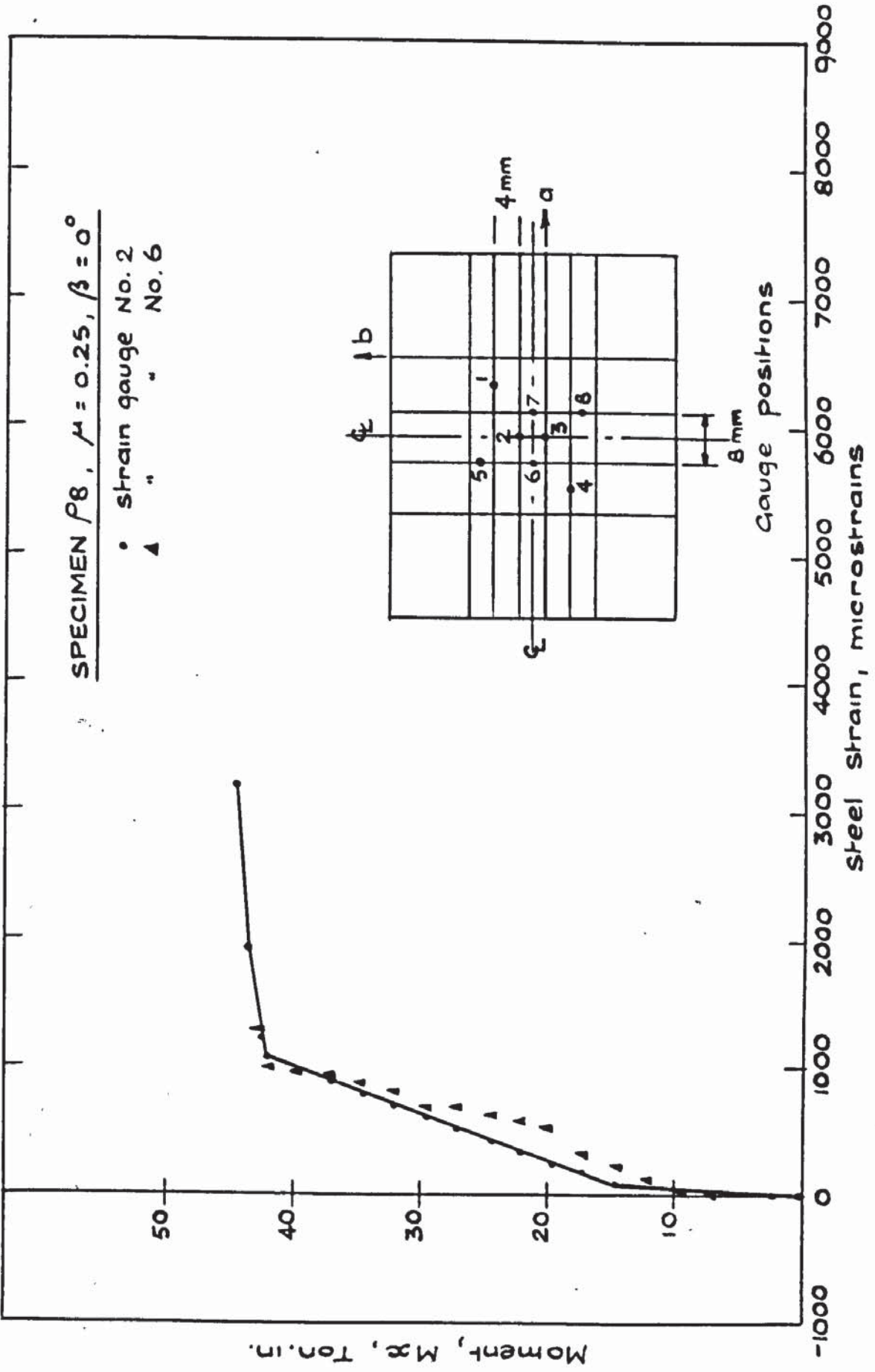


FIG. 5.32. TYPICAL STEEL STRAIN PLATE - P 8.

M <sub>x</sub> TON. IN.	AVERAGE tan 2γ	STEEL STRAINS MICROSTRAINS								
		1	2	3	4	5	6	7	8	
0.00	-	0.00	0.00	0.00	0.00	0.00	0.00	0.00	0.00	0.00
2.14	-.3333	9.90	0.00	9.90	9.90	9.90	9.90	4.95	29.71	9.90
4.63	-	19.80	14.85	29.71	19.80	9.90	9.90	9.90	34.66	9.90
7.12	.0714	34.66	29.71	49.51	29.71	9.90	9.90	9.90	49.51	14.85
9.61	-1.411	44.56	39.61	59.41	49.51	9.90	9.90	4.95	99.02	9.90
12.10	-.3915	59.41	59.41	118.83	74.27	19.80	19.80	89.12	237.66	19.80
14.59	-.2104	84.17	99.02	158.44	108.93	29.71	29.71	207.95	306.98	19.80
17.08	-.2506	99.02	168.34	277.27	148.54	34.66	34.66	376.29	420.85	29.71
19.57	.0266	200.00	242.61	366.39	99.02	39.61	39.61	514.93	420.85	59.41
22.06	-.0722	316.88	336.68	470.37	29.71	39.61	39.61	574.34	415.90	69.32
24.55	-.0401	376.29	415.90	554.54	-39.61	39.61	39.61	613.95	425.80	74.27
27.04	-.0296	450.56	519.88	678.32	-39.61	49.51	49.51	683.27	425.80	79.22
29.53	-.0460	529.78	604.05	772.39	0.00	49.51	49.51	683.27	415.90	89.12
32.02	-.0241	653.56	693.17	861.51	79.22	49.51	49.51	821.90	415.90	89.12
34.51	-.0281	767.44	772.39	950.63	99.02	54.46	54.46	866.46	415.90	99.02
37.00	-.0242	940.73	871.41	1059.56	193.10	59.41	59.41	911.02	425.80	108.93
39.49	-.0221	1064.51	960.54	1143.73	217.85	59.41	59.41	950.63	425.80	108.93
41.98	-.0004	1257.61	1089.27	1326.93	173.29	59.41	59.41	990.24	425.80	118.83
42.48	-.0820	1247.71	1227.90	1406.15	188.15	59.41	59.41	1277.41	396.10	118.83
43.48	-.0957	1297.22	1940.88	1475.46	2515.22	79.22	79.22	-	415.90	128.73
43.97	-.0910	1435.85	3188.59	-	-	79.22	79.22	-	485.22	94.07
44.22	-.0759	2148.83	3109.37	-	-	99.02	99.02	-	485.22	59.41
44.47	-.0707	-	3148.98	-	-	138.63	138.63	-	589.20	59.41

Table 5.8 Principle Concrete Strain Direction & Steel Strains P8

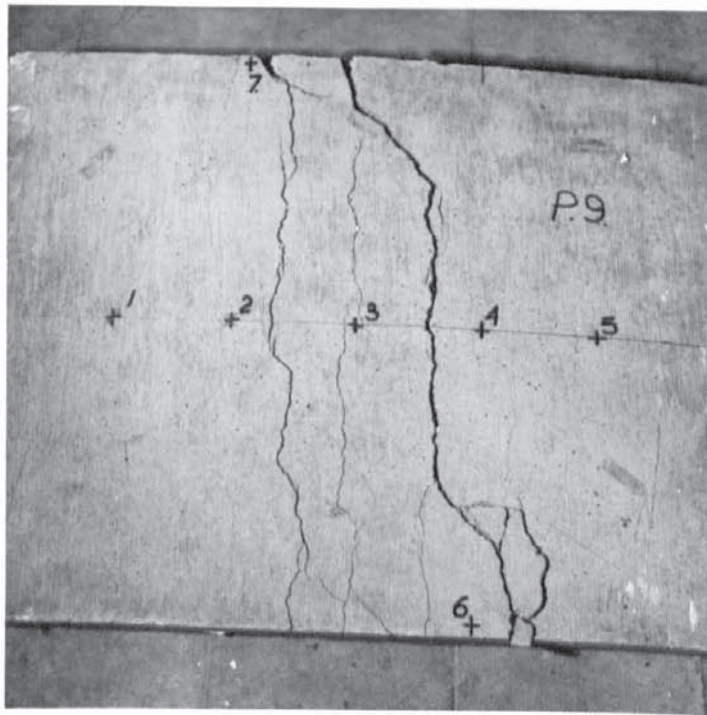


PLATE 5.11

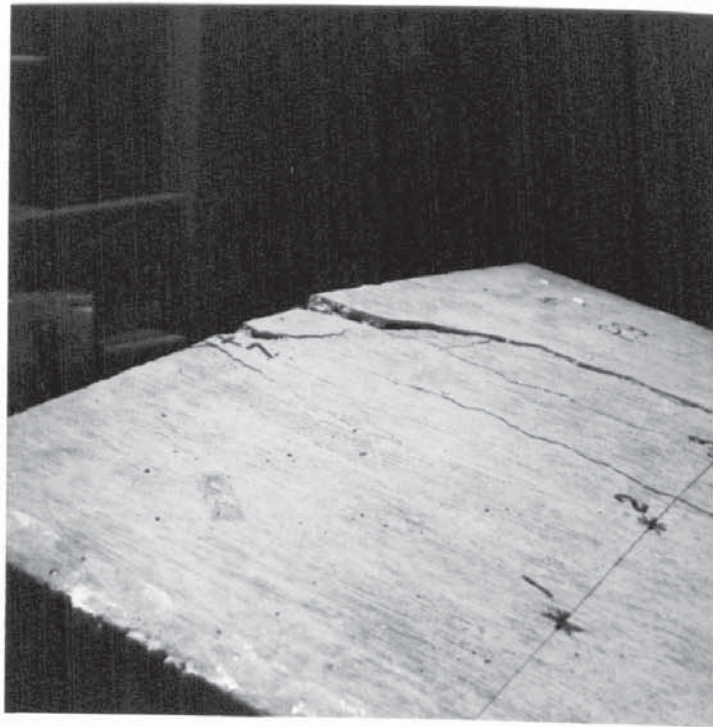


PLATE 5.12

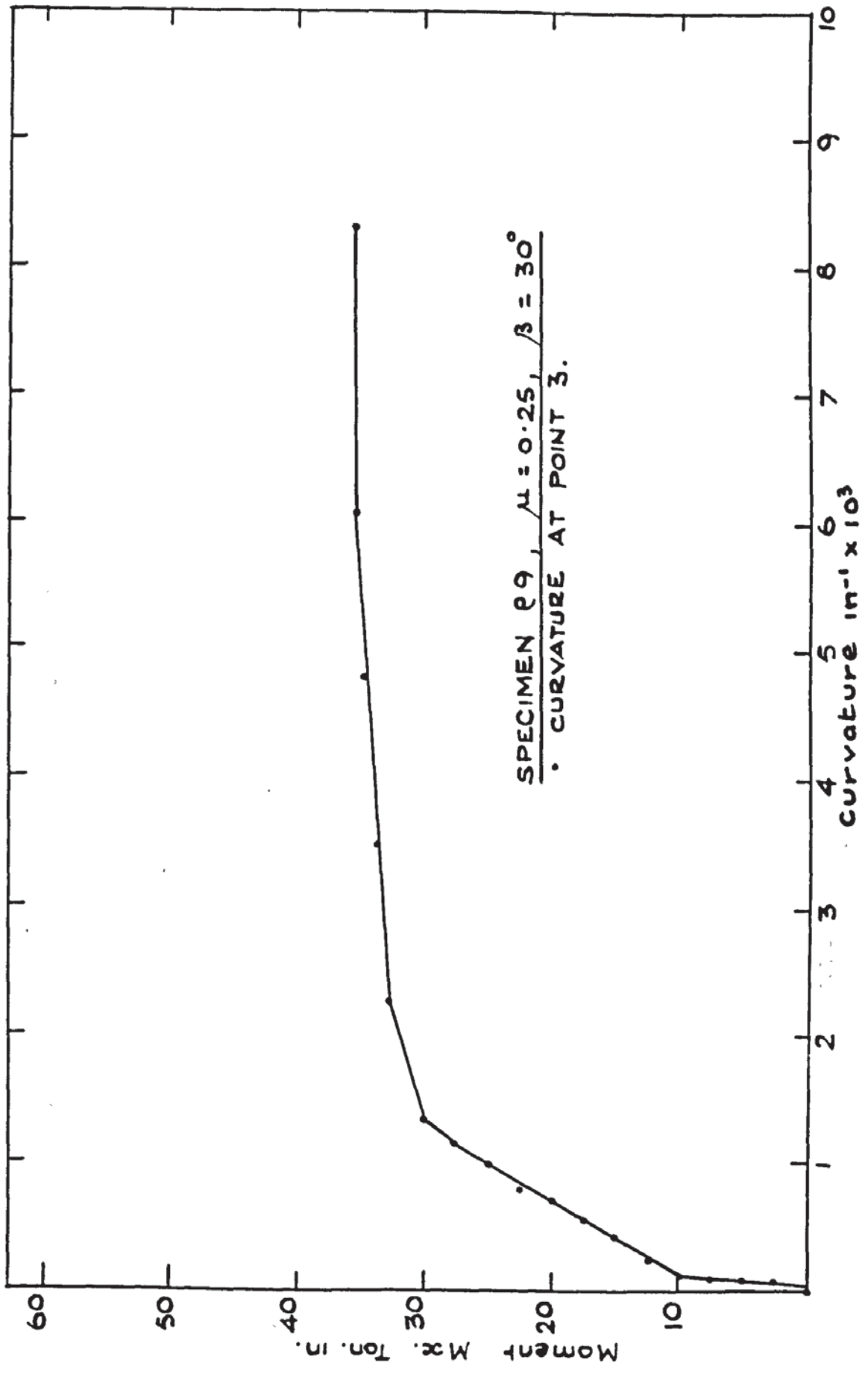


FIG. 5.33. MOMENT CURVATURE PLOT - P.9.

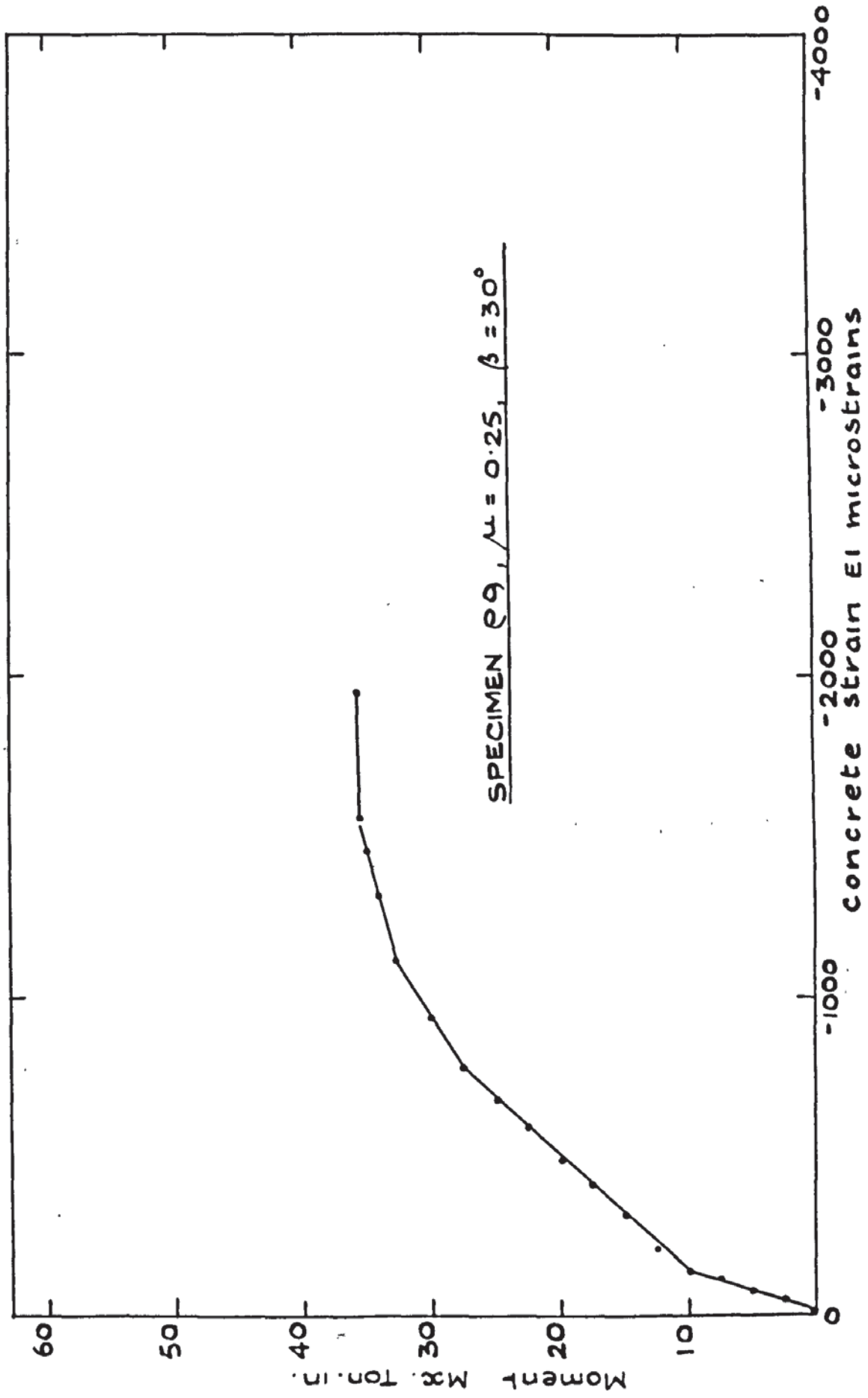


FIG. 5.34. AVERAGE PRINCIPAL CONCRETE STRAIN PLOT EI - P.9.

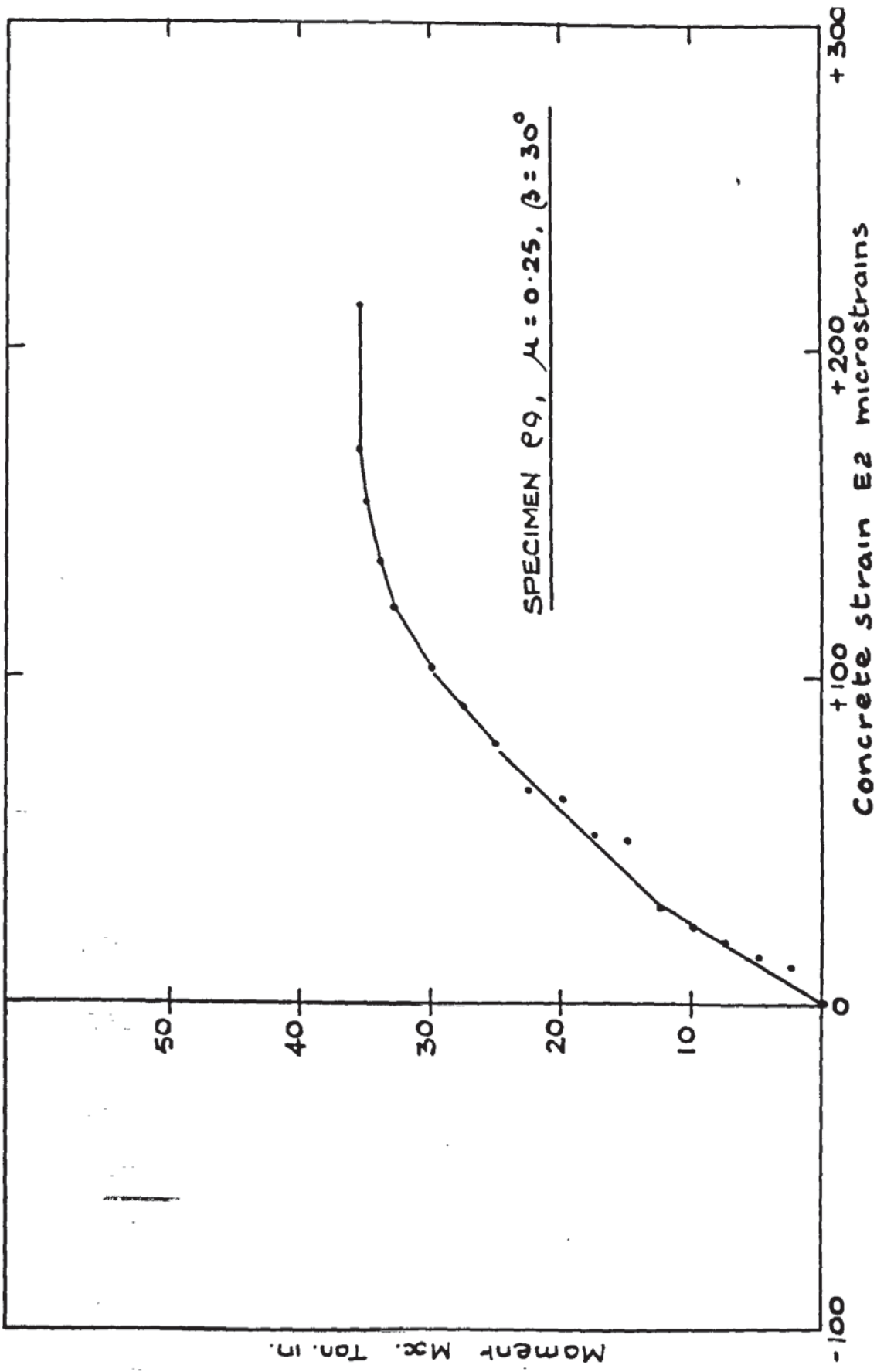


FIG. 5.35. AVERAGE PRINCIPAL CONCRETE STRAIN PLOT E2 - P.9.

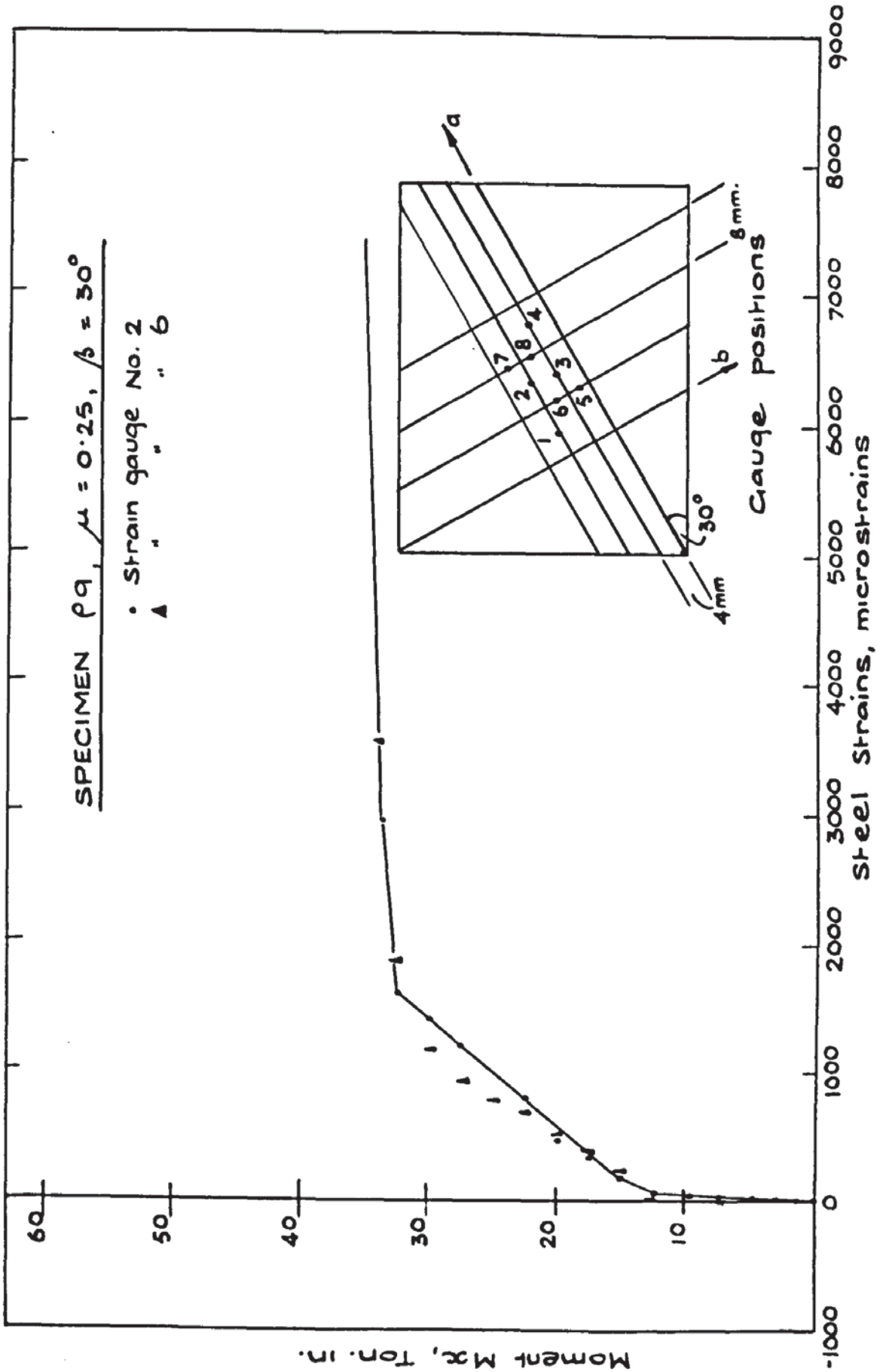


FIG. 5.36. TYPICAL STEEL STRAINS PLOT - P9.

M <sub>x</sub> TON·IN	AVERAGE tan 2γ	STEEL STRAINS								
		1	2	3	4	5	6	7	8	
0.00	-	0.00	0.00	0.00	0.00	0.00	0.00	0.00	0.00	0.00
2.49	.1110	9.23	13.84	4.61	0.00	0.00	0.00	0.00	0.00	4.61
4.98	.1877	18.45	23.07	18.45	18.45	13.84	9.23	13.84	9.23	9.23
7.47	.6070	27.68	32.00	32.30	27.68	18.45	13.84	18.45	18.45	18.45
9.96	-.0582	36.91	41.52	46.14	36.91	18.45	18.45	18.45	27.68	27.68
12.45	-.0750	55.36	100.00	73.82	92.27	36.91	36.91	36.91	64.59	55.36
14.94	-.1414	83.05	164.59	138.41	-138.41	83.05	83.05	212.23	147.64	110.73
17.43	-.1260	129.23	322.95	258.36	-147.64	129.18	129.18	378.32	184.55	156.86
19.92	-.0931	175.32	493.66	332.18	-83.05	184.55	184.55	525.95	262.98	221.45
22.41	-.0602	415.23	816.61	461.36	119.95	258.36	258.36	668.98	341.41	267.59
24.90	-.0309	479.82	964.25	553.64	203.00	341.41	341.41	775.09	396.77	341.41
27.39	.0016	572.09	1213.39	710.50	396.77	470.59	470.59	931.95	470.59	442.91
29.88	.0106	645.91	1416.39	839.68	701.27	636.68	636.68	1167.25	572.09	613.61
32.37	.0345	1328.73	1600.93	1033.45	2062.30	1051.91	1051.91	1822.39	770.48	830.45
33.86	.0598	2528.27	2948.11	1116.50	5905.45	1504.05	1504.05	3524.82	968.86	1190.32
34.86	.0855	-	6408.34	-	6680.55	1633.23	1633.23	-	1550.18	1421.00
35.36	.1438	-	7395.66	-	-	1679.36	1679.36	-	1743.95	-
35.41	.2612	-	-	-	-	-	-	-	-	-

Table 5.9 Principle Concrete Strain Direction & Steel Strains P9

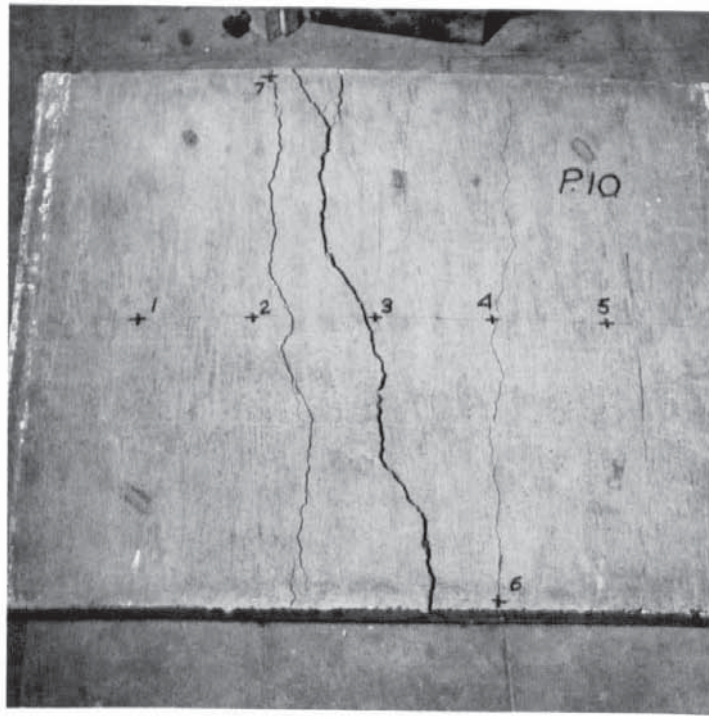


PLATE 5.13

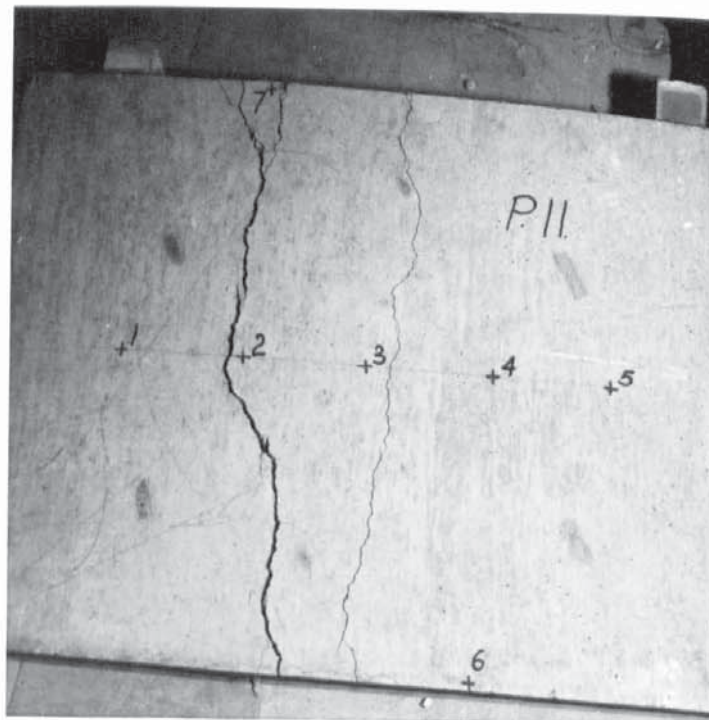


PLATE 5.14

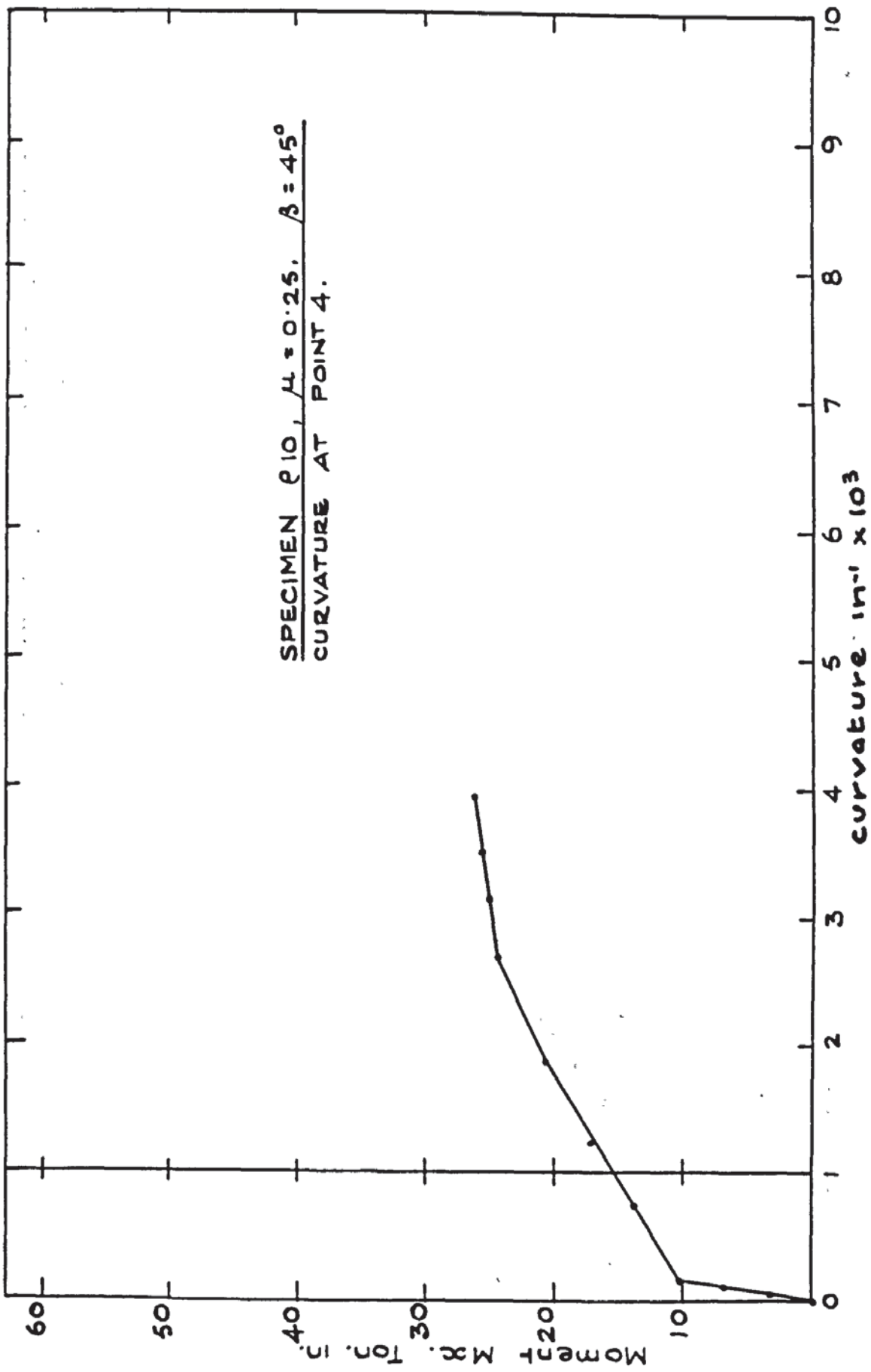


FIG. 5.37. MOMENT CURVATURE PLOT - P.10.

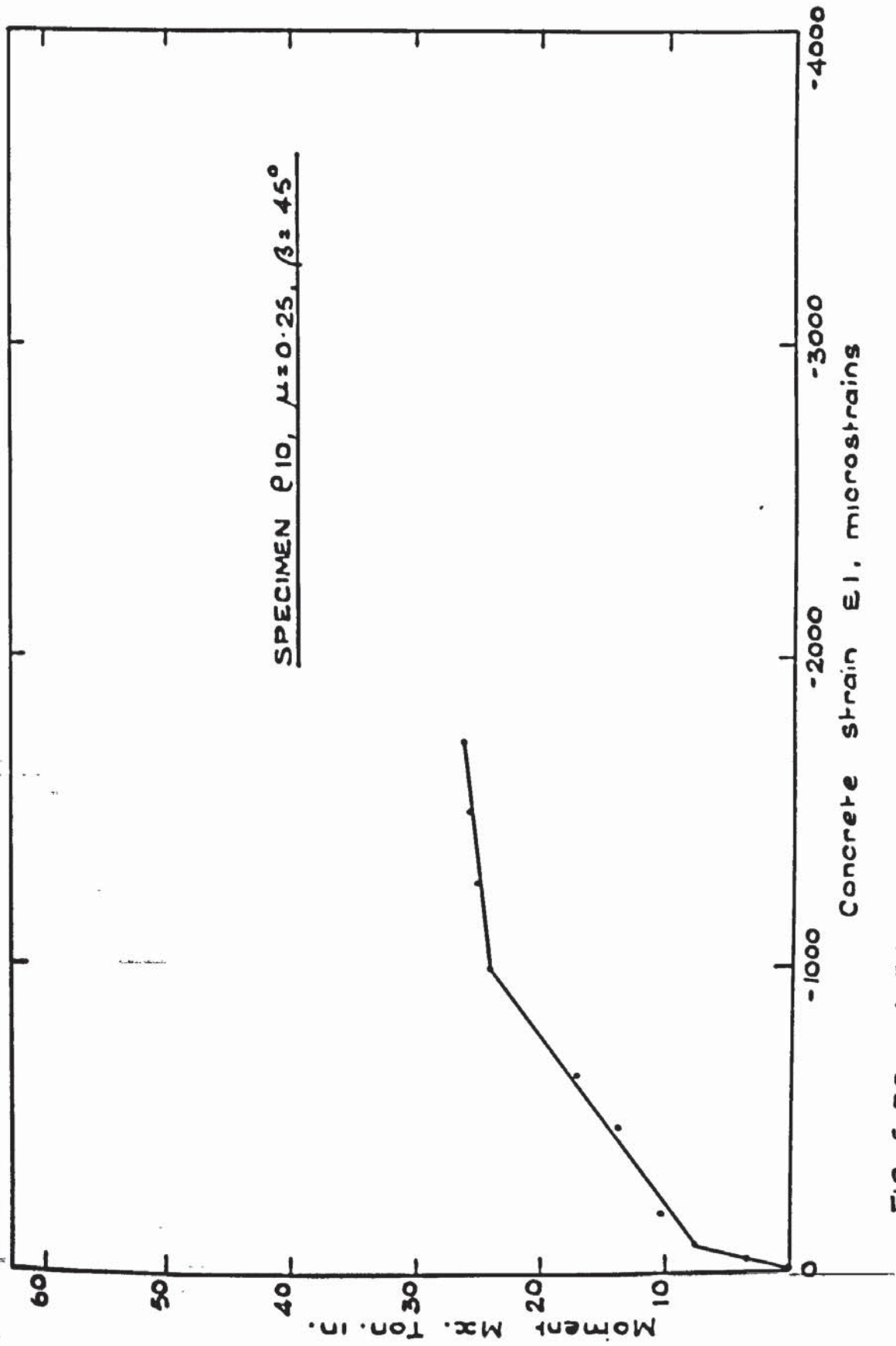


FIG. 5.38. AVERAGE PRINCIPAL CONCRETE STRAIN E1 - P.10.

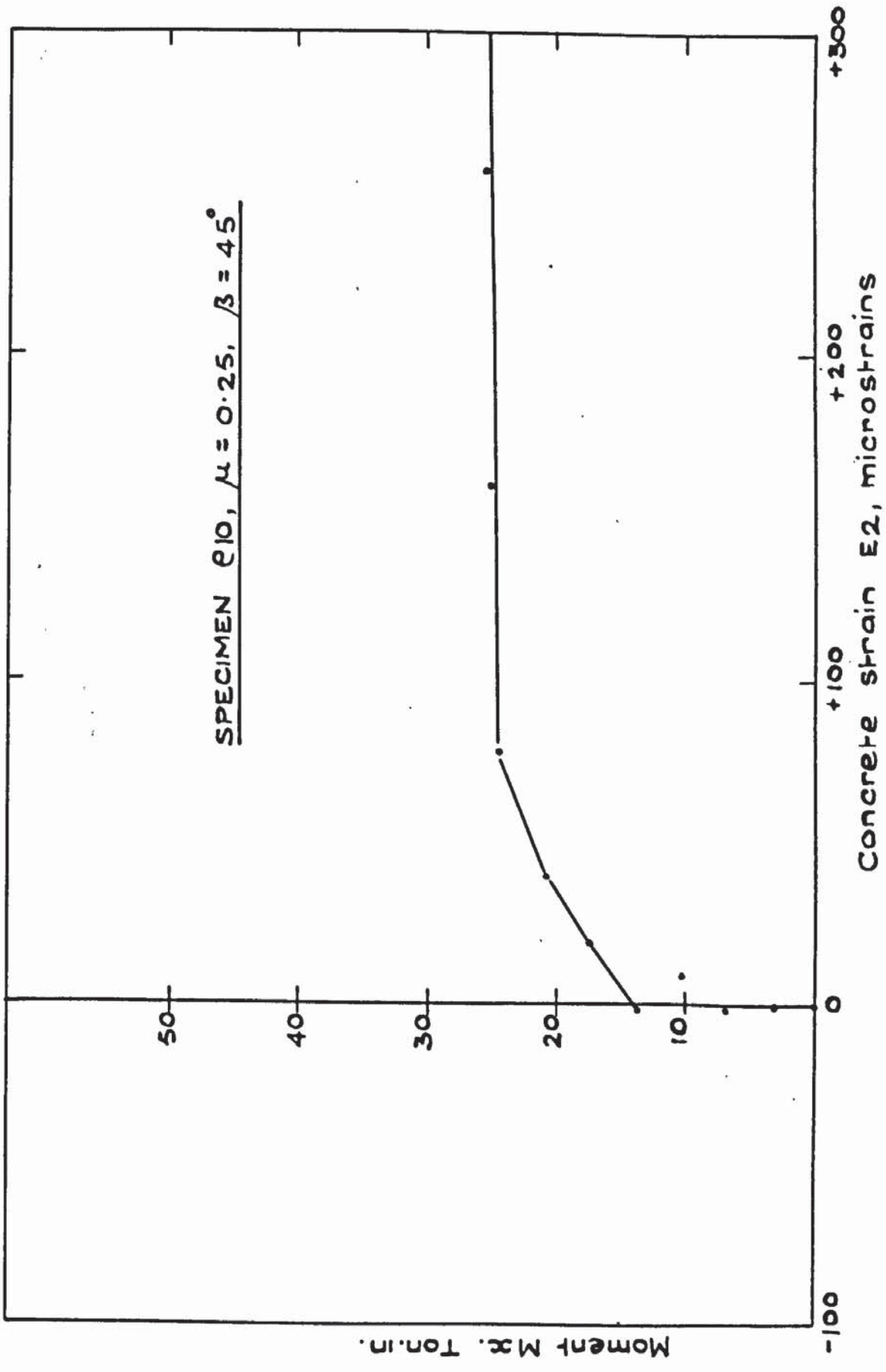


FIG. 5.39. AVERAGE PRINCIPAL CONCRETE STRAIN E2 - P.10.

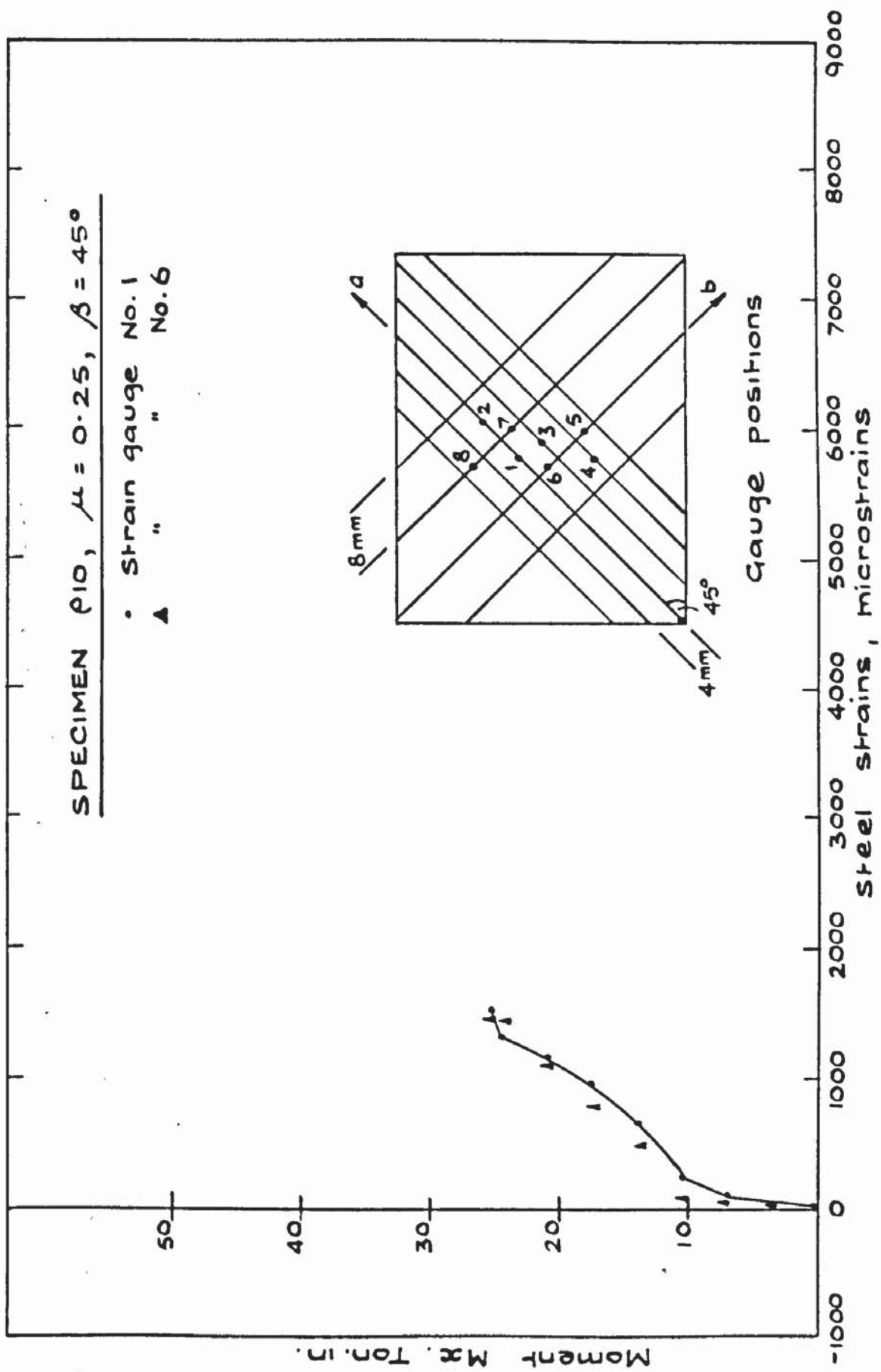


FIG. 5.40. TYPICAL STEEL STRAIN PLATE - P.10.

M<sub>x</sub> AVERAGE

STEEL STRAINS

TON.IN	tan 2γ	1	2	3	4	5	6	7	8
0.00	-	0.00	0.00	0.00	0.00	0.00	0.00	-	0.00
3.49	-.3030	55.36	-46.14	27.68	-27.68	41.52	18.45	-	9.23
6.97	-.1482	92.27	-27.68	41.52	0.00	46.14	36.91	-	18.45
10.46	-.0277	239.91	-193.77	96.91	-73.82	0.00	64.59	-	64.59
13.94	-.0635	655.14	-184.55	193.77	433.68	186.05	498.27	-	775.09
17.43	-.0519	968.86	1264.14	535.18	885.82	356.86	784.32	-	572.09
20.92	-.0661	1181.09	2657.45	775.09	1208.77	618.23	1116.50	-	-
24.40	.0106	1324.11	3367.95	1107.27	1651.68	-	1485.59	-	-
25.15	.2502	1522.50	3321.82	968.86	1882.36	-	1430.23	-	-
25.90	.2518	1522.50	2842.00	-	2205.32	-	1448.68	-	-
26.39	-.0025	-	-	-	-	-	-	-	-

Table 5.10 Principle Concrete Strain Direction & Steel Strains P10

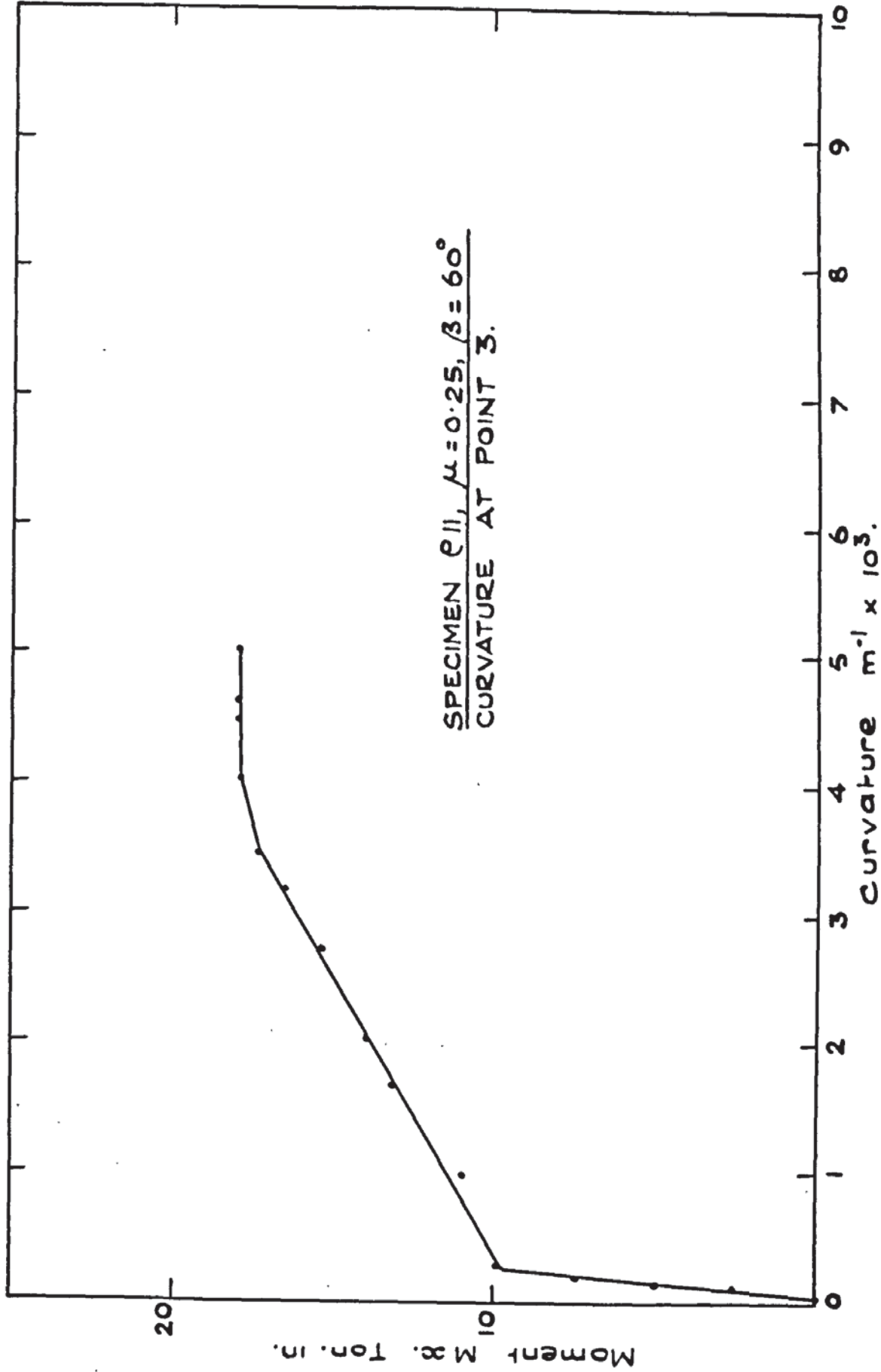


FIG. S.41. MOMENT CURVATURE PLOT - P.11.

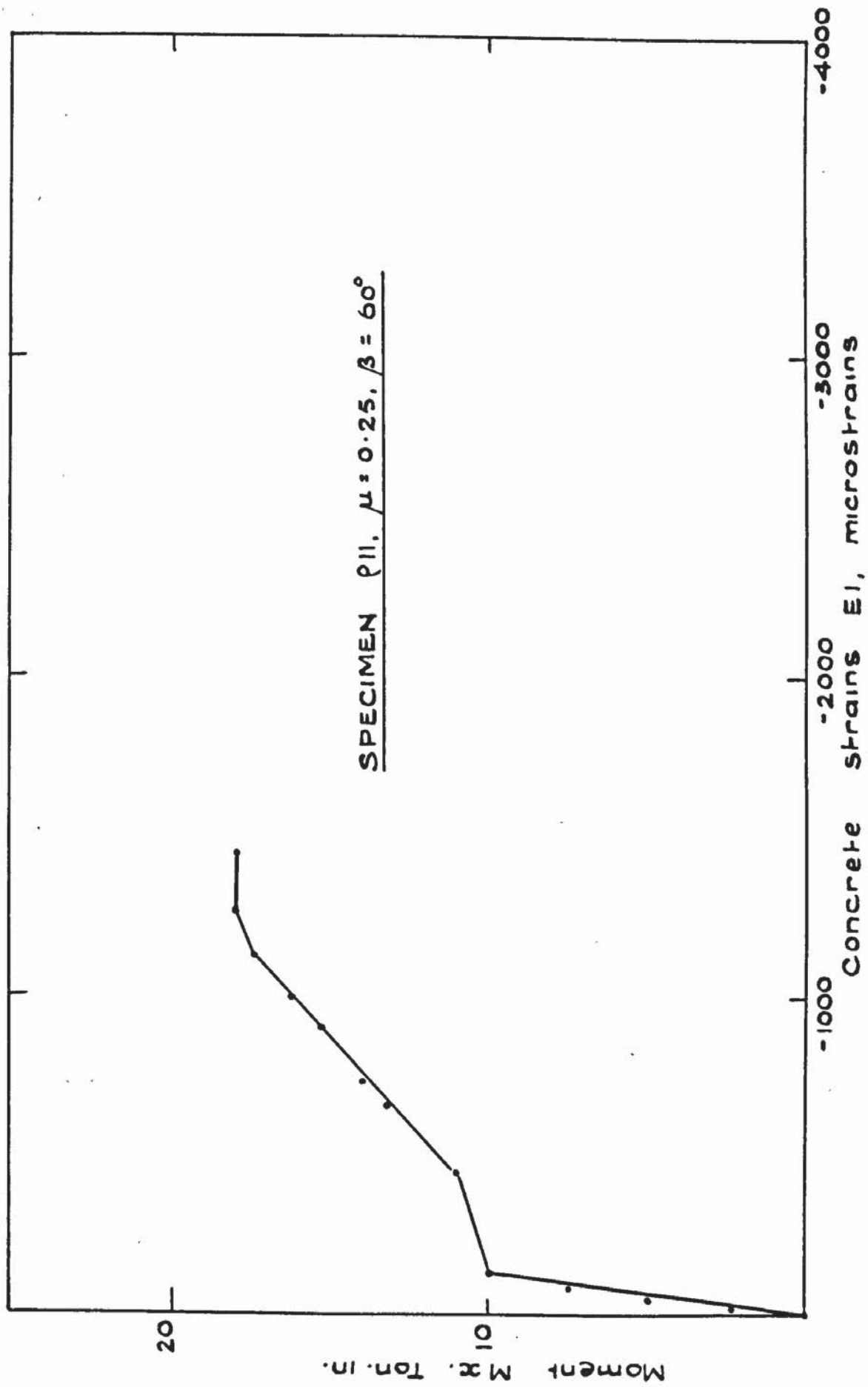


FIG. 5.42. AVERAGE PRINCIPAL CONCRETE STRAIN EI - P.11.

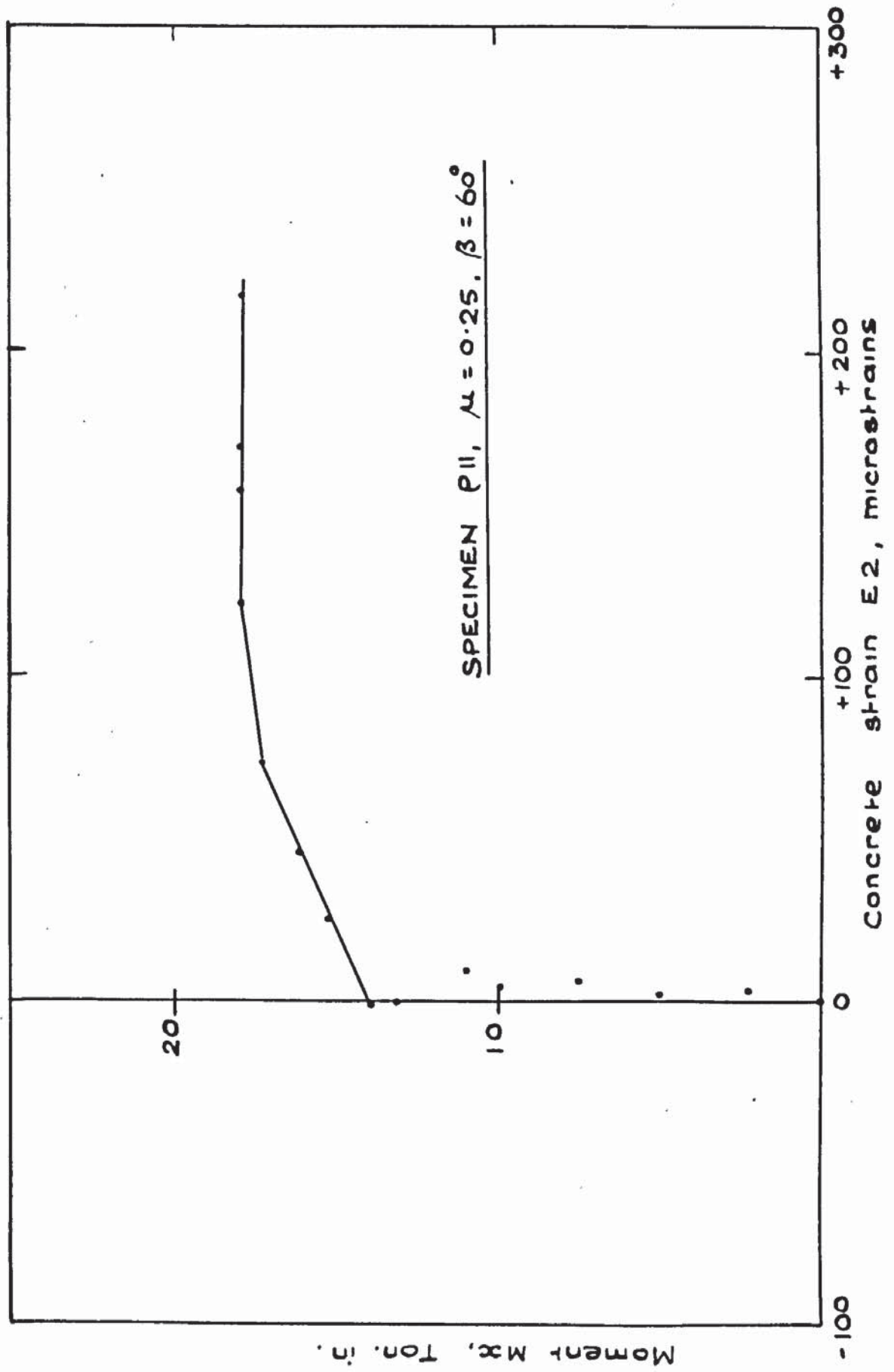


FIG. 5.43. AVERAGE PRINCIPAL CONCRETE STRAIN E2 - P.11.

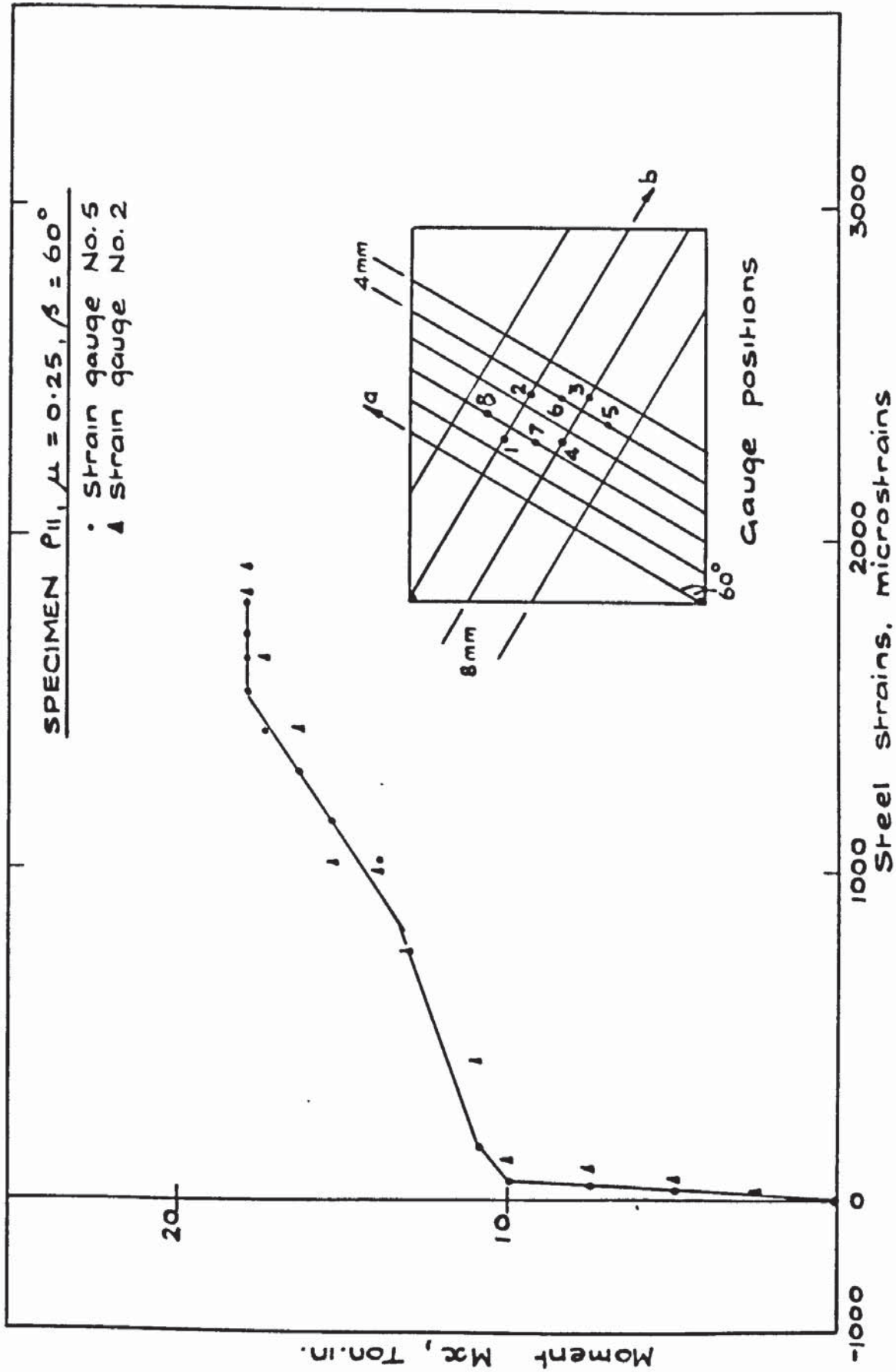


FIG. 5.44 TYPICAL STEEL STRAIN PLATE - P.II.

M <sub>x</sub>	AVERAGE	STEEL STRAINS							
		1	2	3	4	5	6	7	8
TON.IN	tan 2γ	MICROSTRAINS							
0.00	-	0.00	0.00	0.00	0.00	0.00	0.00	0.00	0.00
2.49	1.750	49.51	49.51	0.00	9.90	9.90	0.00	0.00	0.00
4.98	.3880	49.51	69.32	14.85	19.80	29.71	9.90	4.95	0.00
7.47	.5158	89.12	99.02	19.80	29.71	39.61	19.80	14.85	9.90
9.96	.3988	99.02	118.83	29.71	39.61	59.41	19.80	19.80	9.90
10.96	.2760	376.29	415.90	133.68	351.54	158.44	29.71	39.61	0.00
13.20	.1726	658.51	742.68	371.34	970.44	812.00	346.59	643.66	861.51
13.94	.1946	1039.76	990.24	371.34	1203.15	1024.90	663.46	1544.78	-
15.44	.2950	1218.00	1005.10	490.17	1505.17	1138.78	0.00	-	-
16.43	.2554	1445.76	1455.66	856.56	1703.22	1287.31	-89.12	-	-
17.43	.2288	1579.44	1643.80	1054.61	1782.44	1401.20	188.15	-	-
17.93	.3071	1713.12	1831.95	1143.73	1831.95	1534.88	430.76	-	-
17.93	.3244	1703.22	1901.27	1133.83	1831.95	1628.95	623.85	-	-
17.93	.3773	1762.63	-	-	1831.95	1703.22	653.56	-	-
17.93	.4292	1871.56	-	-	1831.95	1797.29	911.02	-	-
					1871.56	1797.29	995.20	-	-

Table 5.11 Principle Concrete Strain Direction & Steel Strains P11

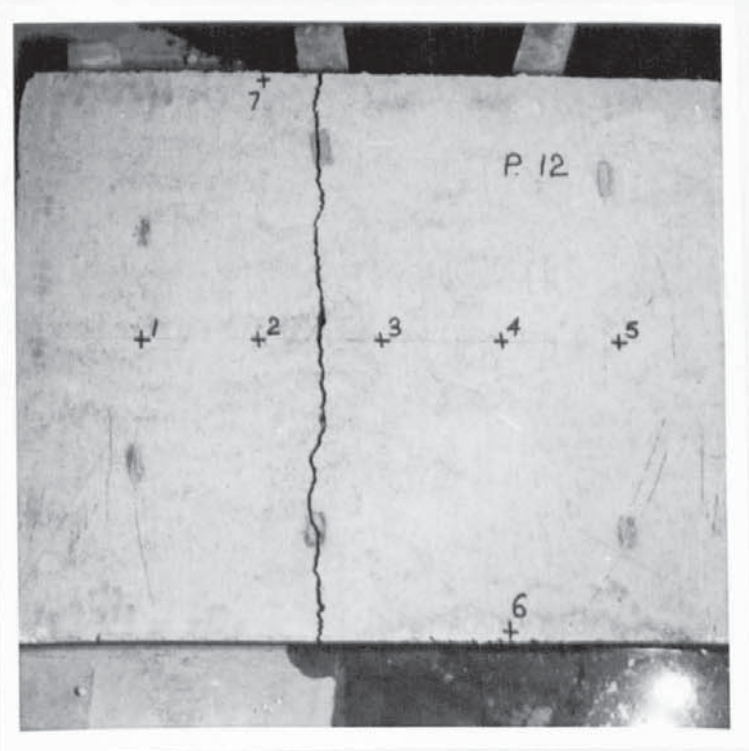


PLATE 5.15

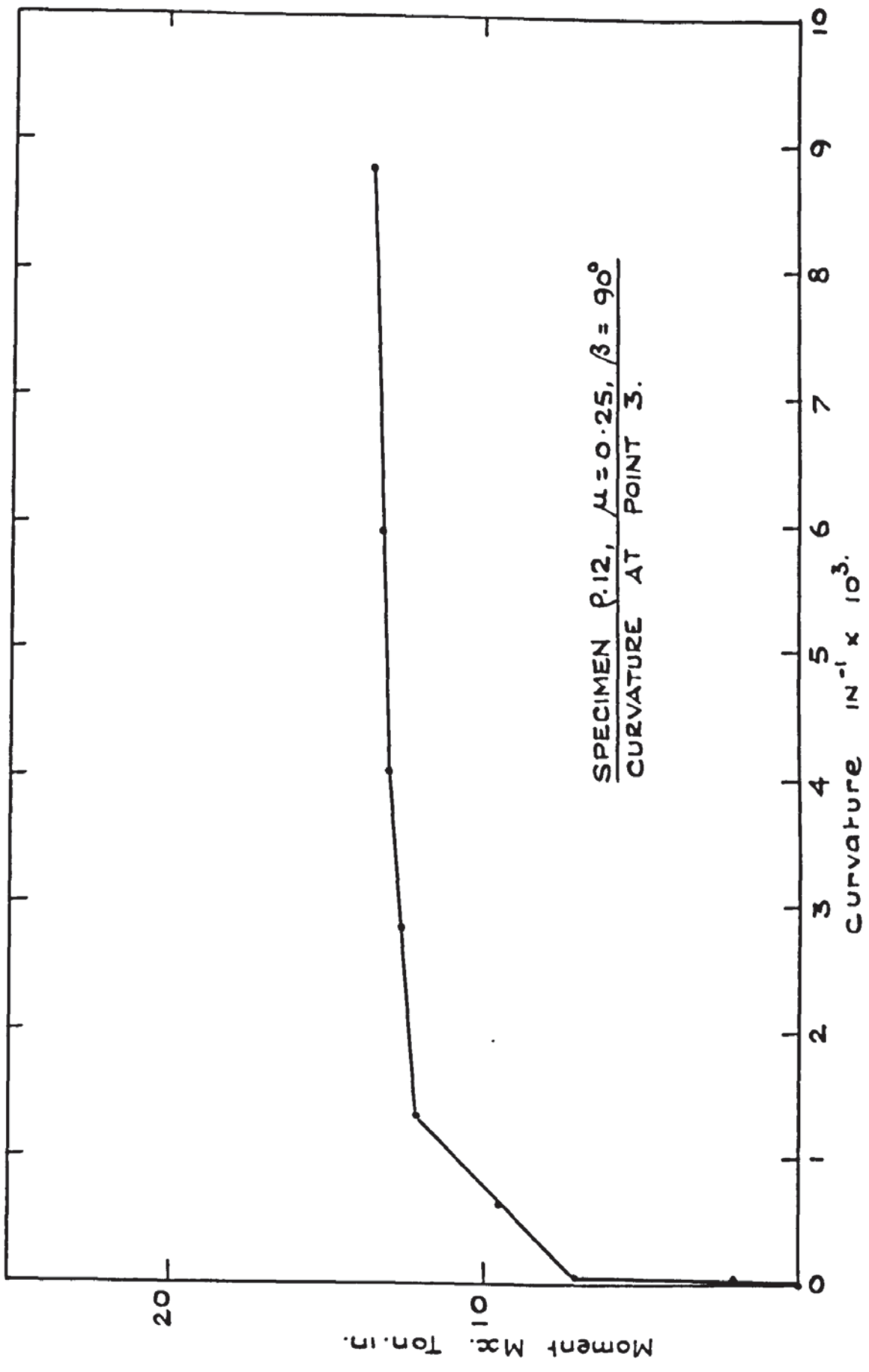


FIG. 5.45. MOMENT CURVATURE PLOT - P.12.

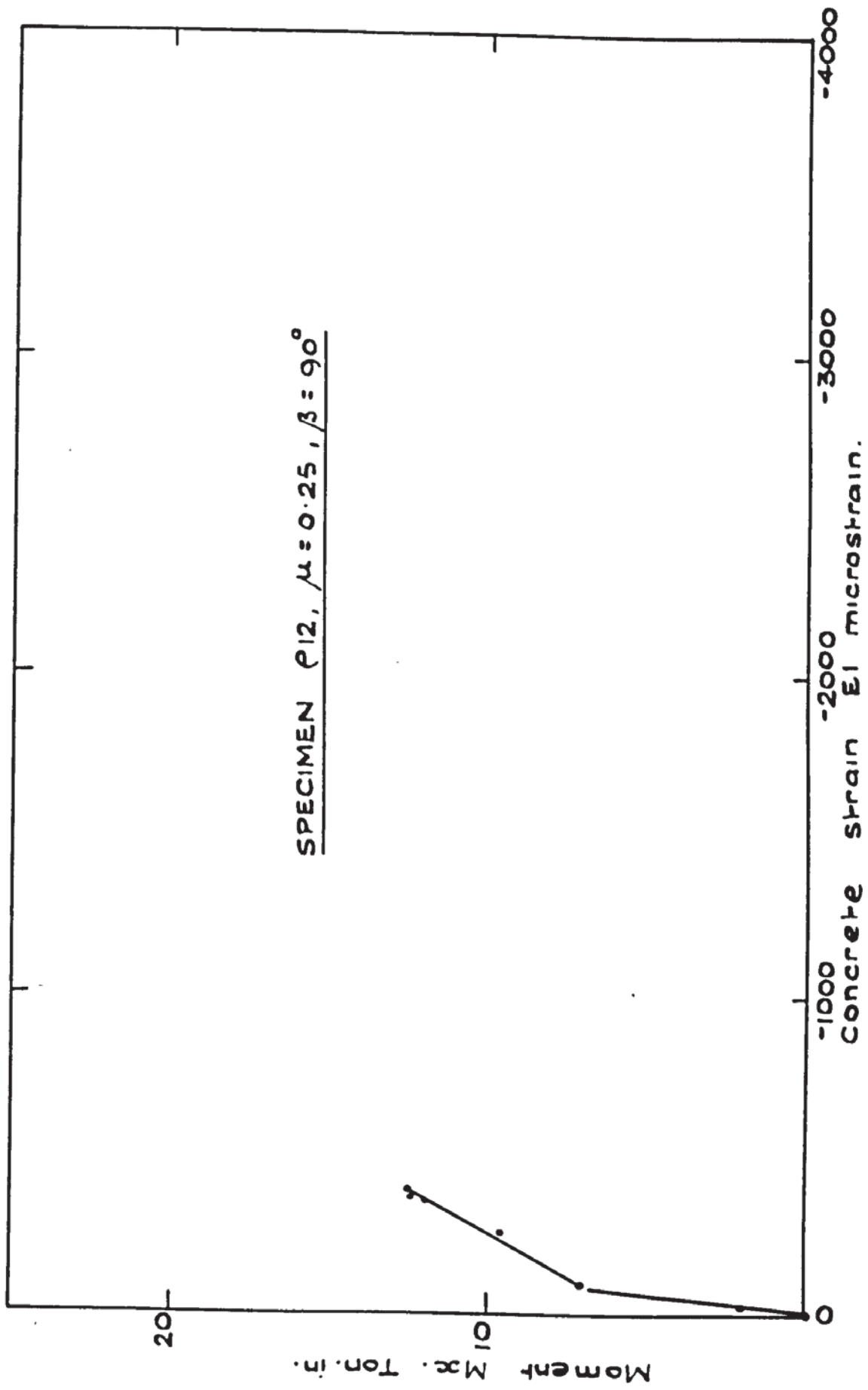


FIG. 5.46. AVERAGE PRINCIPAL CONCRETE STRAIN PLOT EI - P.12.

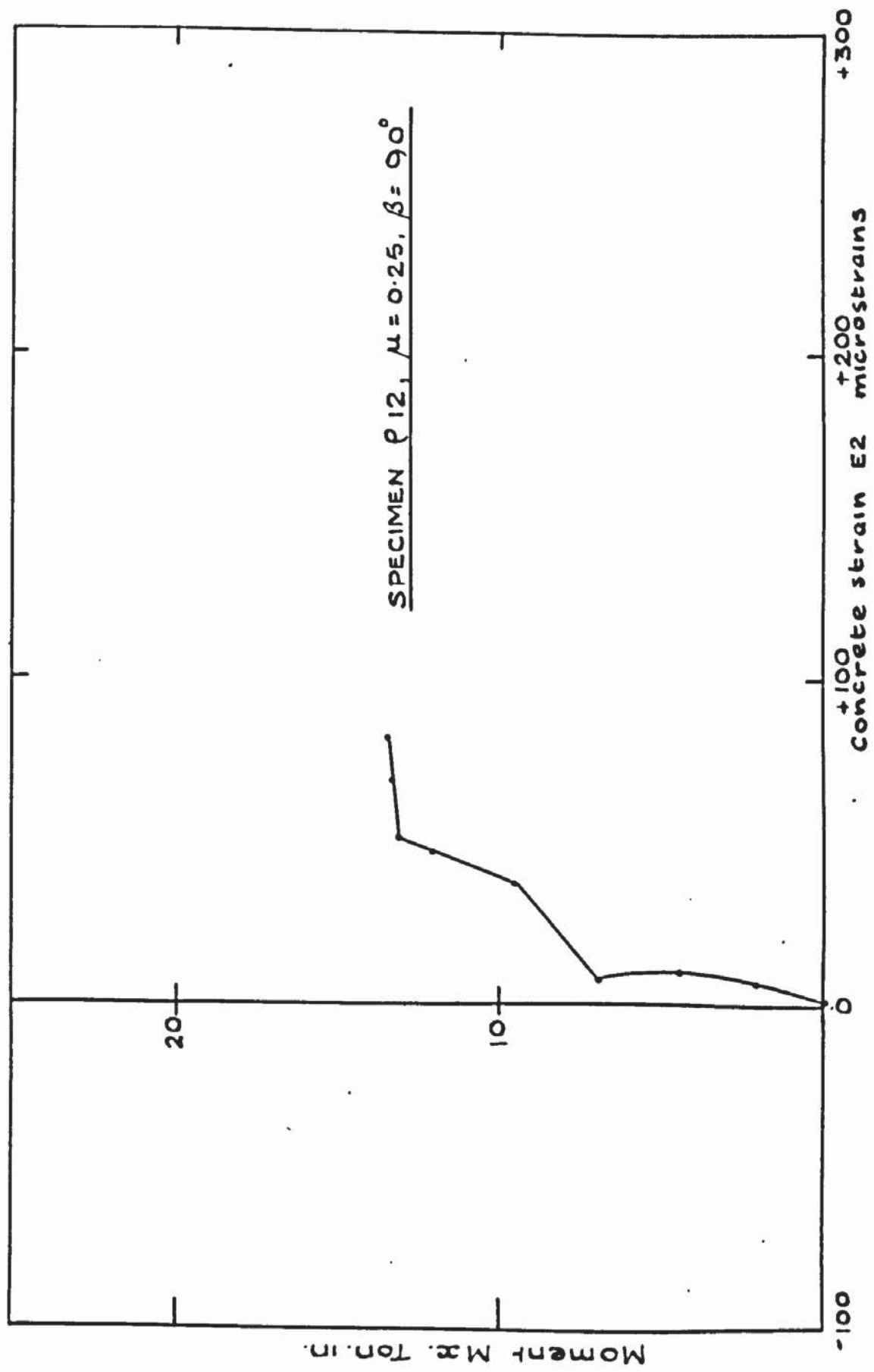


FIG. 5.47. AVERAGE PRINCIPAL CONCRETE STRAIN E2 - P.12.

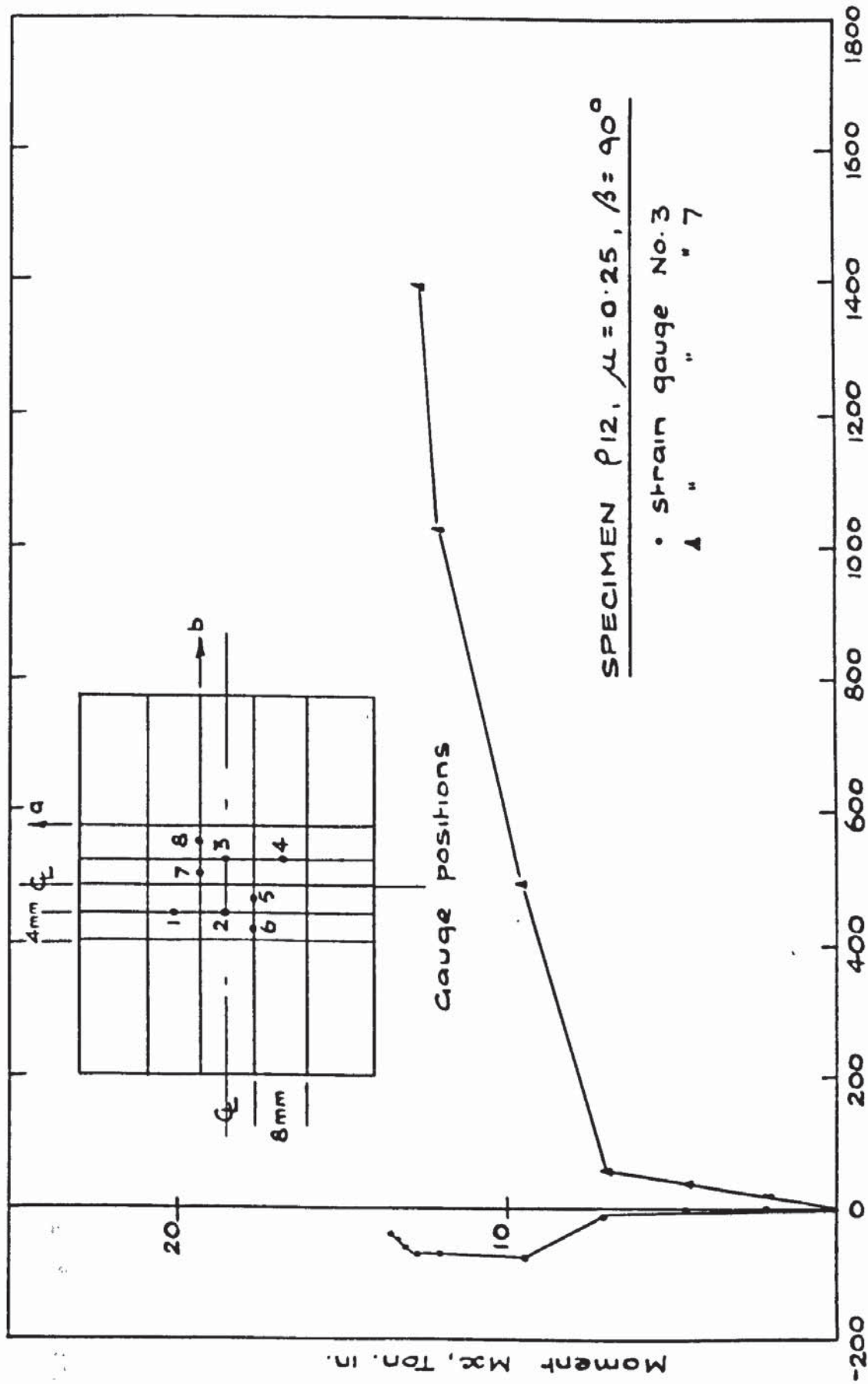


FIG. 5.48. TYPICAL STEEL STRAIN PLOT - P.12.

M <sub>x</sub> TON.IN	AVERAGE tan 2γ	STEEL STRAINS								
		1	2	3	4	5	6	7	8	
0.00	-	0.00	0.00	0.00	0.00	0.00	0.00	0.00	0.00	0.00
2.14	.9555	0.00	0.00	0.00	0.00	0.00	0.00	9.90	0.00	24.76
4.63	.9764	4.95	0.00	0.00	9.90	24.76	9.90	34.66	9.90	34.66
7.12	.7091	-29.71	9.90	-9.90	14.85	39.61	29.71	54.46	29.71	54.46
9.61	.8012	0.00	-64.37	-79.22	48.54	792.20	1099.17	490.17	1099.17	490.17
12.10	.8144	-326.78	-113.88	-69.32	69.32	1079.37	1663.61	1049.66	1663.61	1049.66
12.70	.7377	-920.93	29.71	-69.32	148.54	1485.37	1792.34	1396.24	1792.34	1396.24
13.10	.6266	-1024.90	49.51	-59.41	198.05	812.00	-	-	-	-
13.35	.4920	-	49.51	-44.56	198.05	257.46	-	-	-	-
13.45	.4478	-	44.56	-39.61	89.12	163.39	-	-	-	-

Table 5.12 Principle Concrete Strain Direction & Steel Strains P12

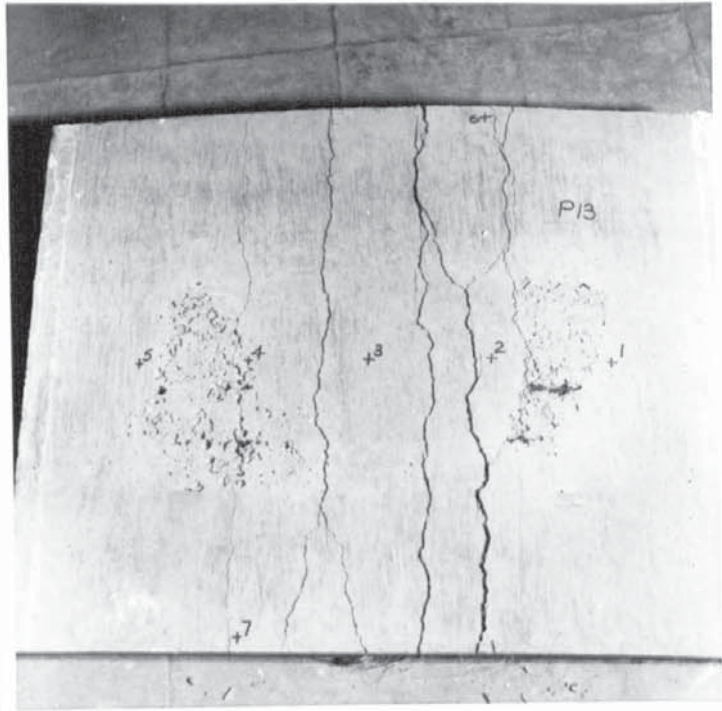


PLATE 5.16

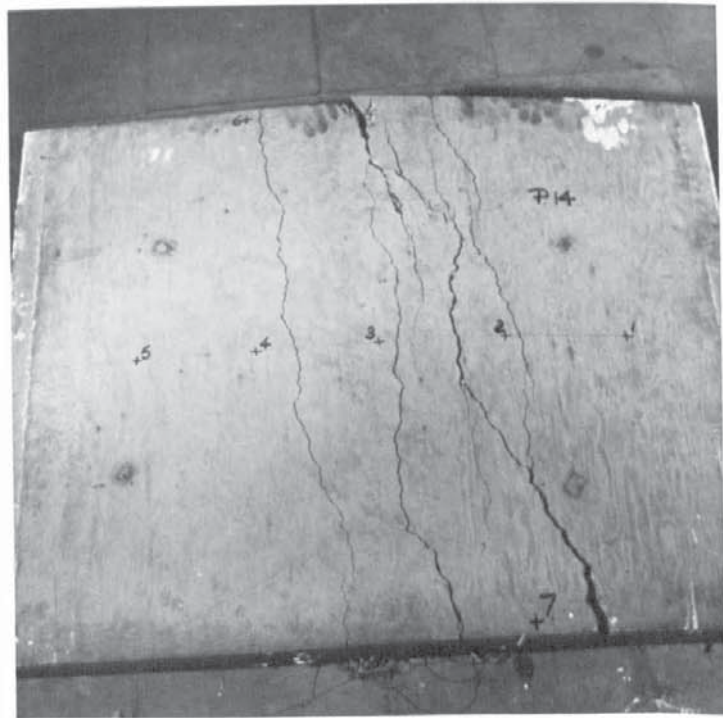


PLATE 5.17

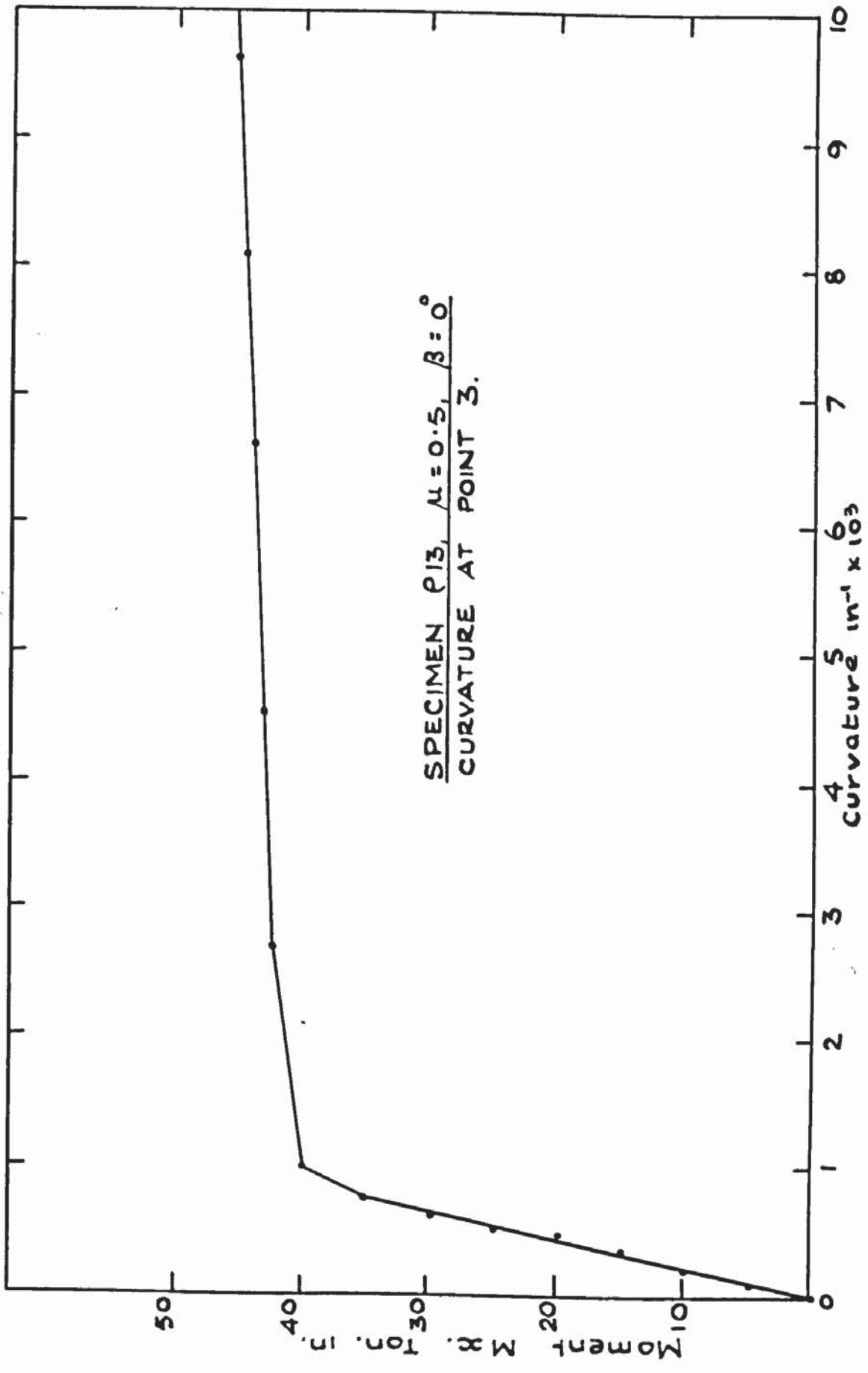


FIG. 5.49. MOMENT CURVATURE PLOT - P.13.

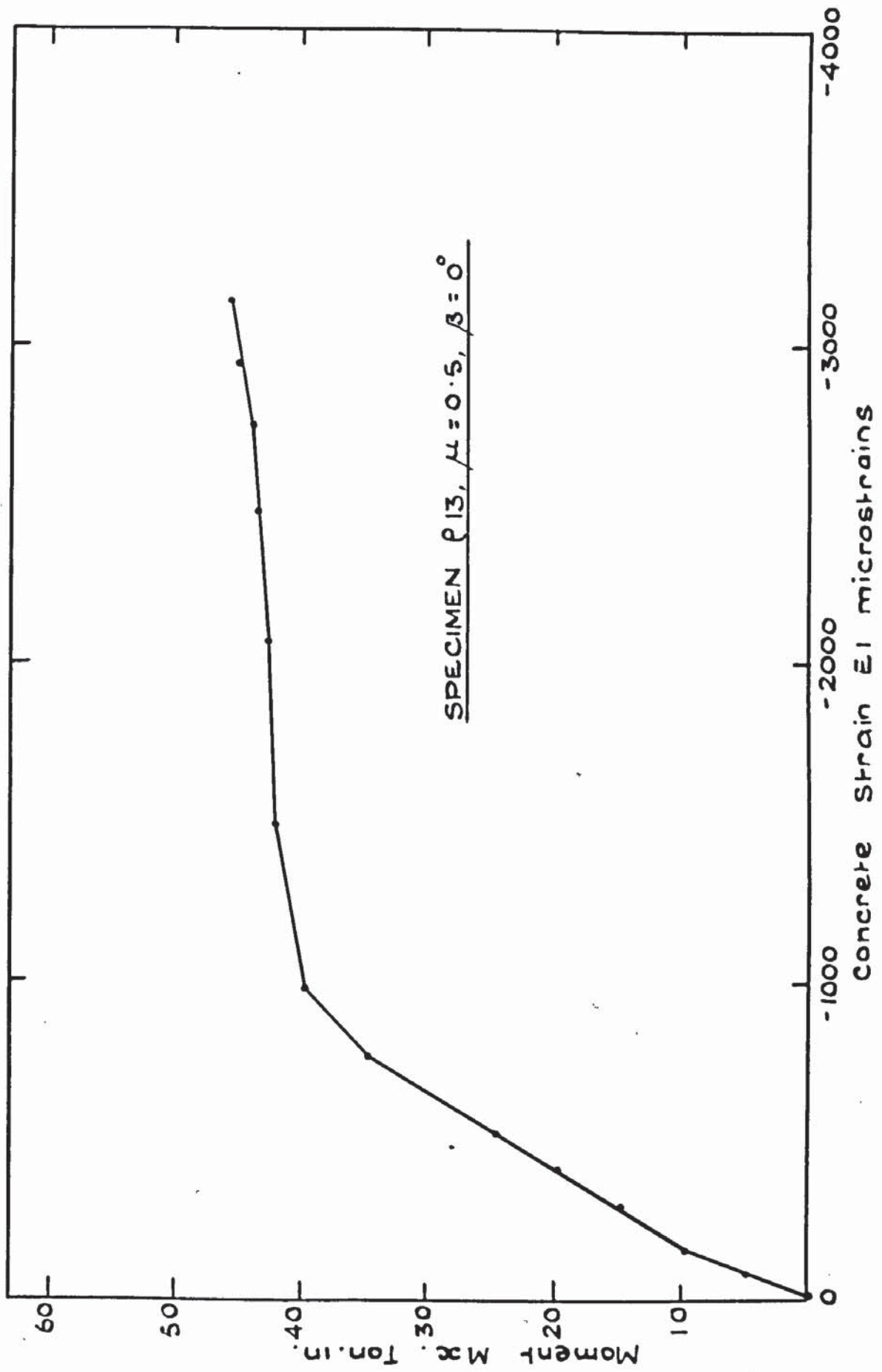


FIG. 5.50. AVERAGE PRINCIPAL CONCRETE STRAIN PLOT EI - P.13.

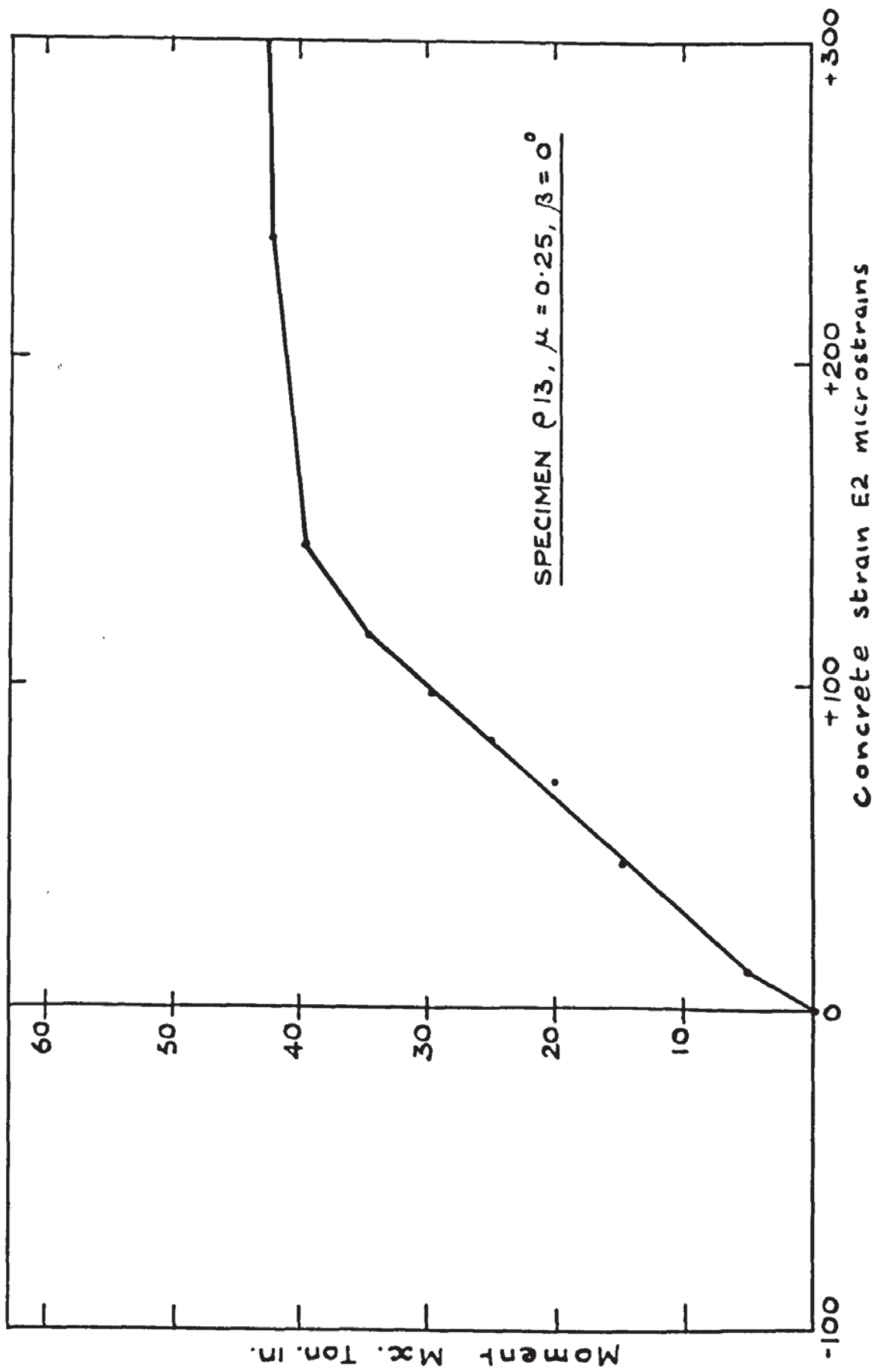


FIG. 5.51. AVERAGE PRINCIPAL CONCRETE STRAIN PLOT E2 - P.13.

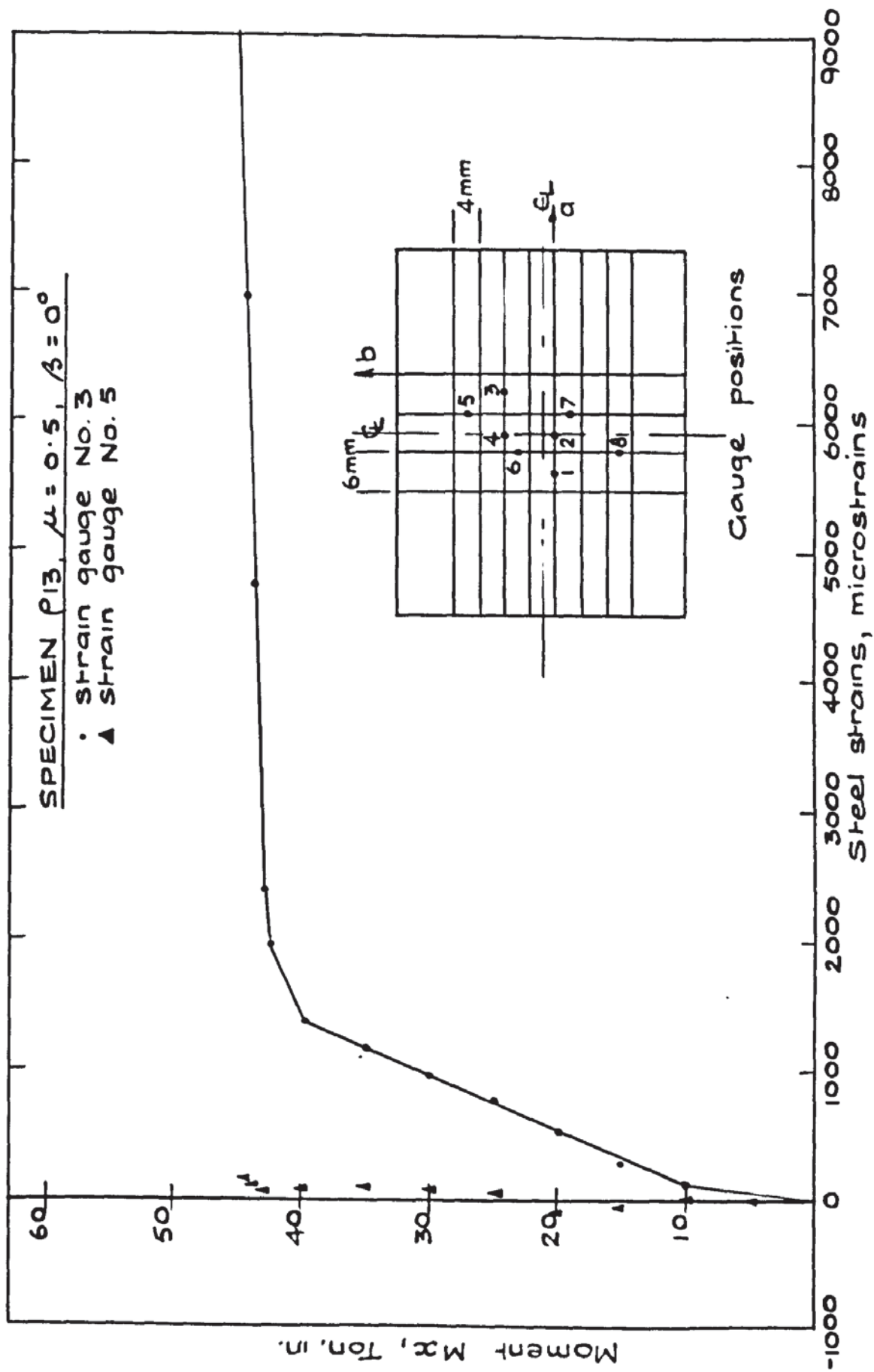


FIG. 5.52. TYPICAL STEEL STRAIN PLOT - P.13.

M <sub>x</sub> TON·IN	AVERAGE tan 2γ	STEEL STRAINS								
		1	2	3	4	5	6	7	8	
0.00	-	0.00	0.00	0.00	0.00	0.00	0.00	0.00	0.00	0.00
4.98	-.7172	14.85	29.71	39.61	19.80	4.95	0.00	0.00	0.00	14.85
9.96	-.4880	84.17	49.51	123.78	79.22	4.95	0.00	0.00	0.00	29.71
14.94	-.4299	282.22	267.37	267.37	198.05	-64.37	19.80	19.80	19.80	39.61
19.92	-.4098	445.61	693.17	505.02	381.24	-84.17	39.61	39.61	39.61	59.41
24.90	-.3498	688.22	1000.15	772.39	584.24	34.66	69.32	69.32	69.32	59.41
29.88	-.3032	836.76	1188.29	980.34	762.49	64.37	99.02	99.02	99.02	79.22
34.86	-.2874	1015.00	1376.44	1178.39	960.54	84.17	118.83	118.83	118.83	89.12
39.84	-.2517	1173.44	1554.68	1396.24	1208.10	74.27	148.54	148.54	148.54	89.12
42.33	-.2039	3777.78	2188.44	1930.98	1713.12	71.34	99.02	99.02	99.02	94.07
43.08	-.1597	8065.54	2436.00	2386.49	2010.20	54.46	19.80	19.80	19.80	89.12
43.82	-.1326	1.1x10 <sup>4</sup>	3198.49	4733.37	2624.15	103.98	-	-	108.93	-
44.32	-.1182	-	-	6971.32	4446.20	133.68	-	-	-	-
45.07	-.1014	-	-	9902.44	-	103.98	-	-	-	-
45.82	-.1024	-	-	1.1x10 <sup>4</sup>	-	108.93	-	-	-	-

Table 5.13 Principle Concrete Strain Direction & Steel Strains P13

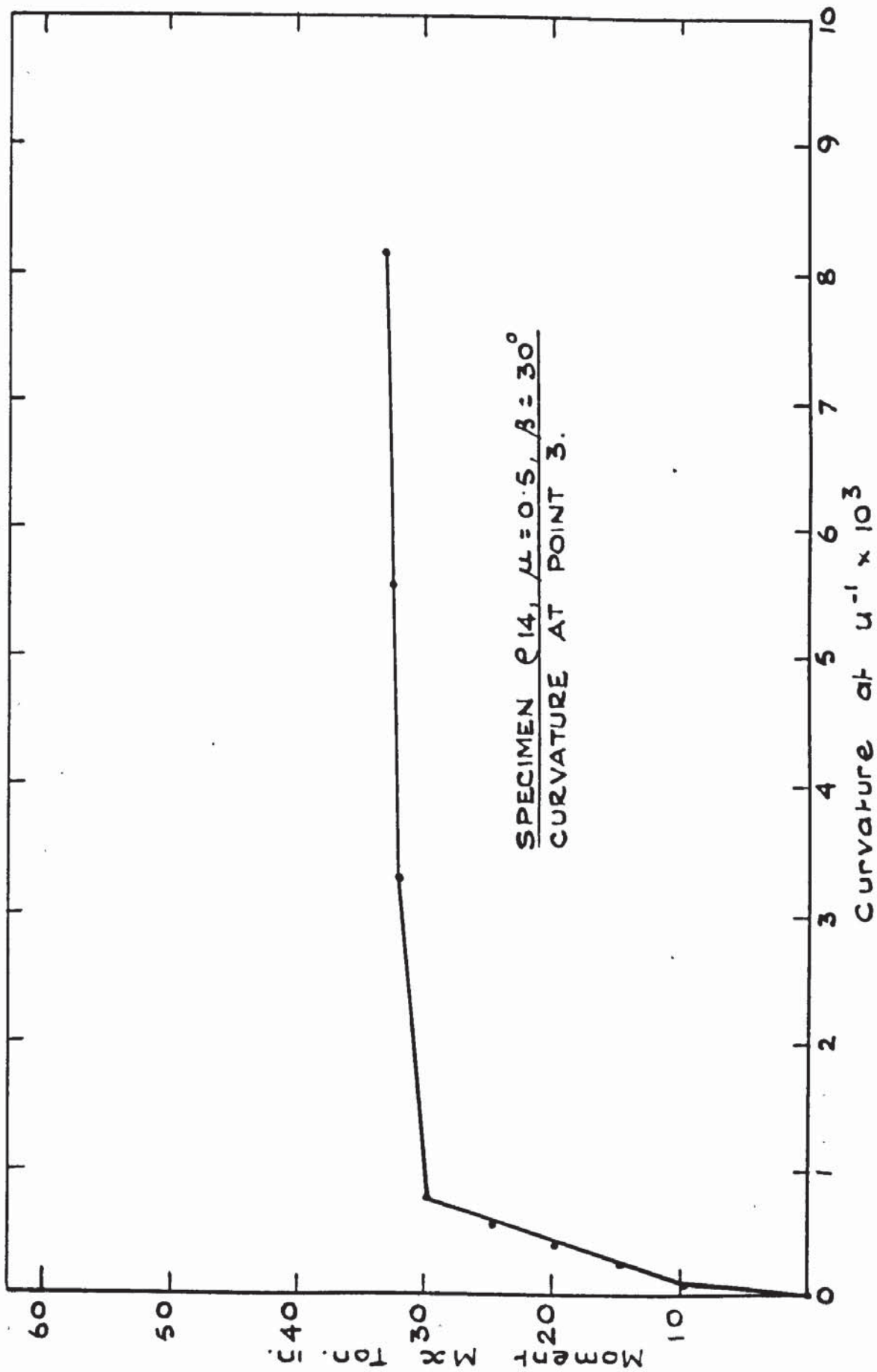


FIG. 5.53. MOMENT CURVATURE PLOT - P. 14.

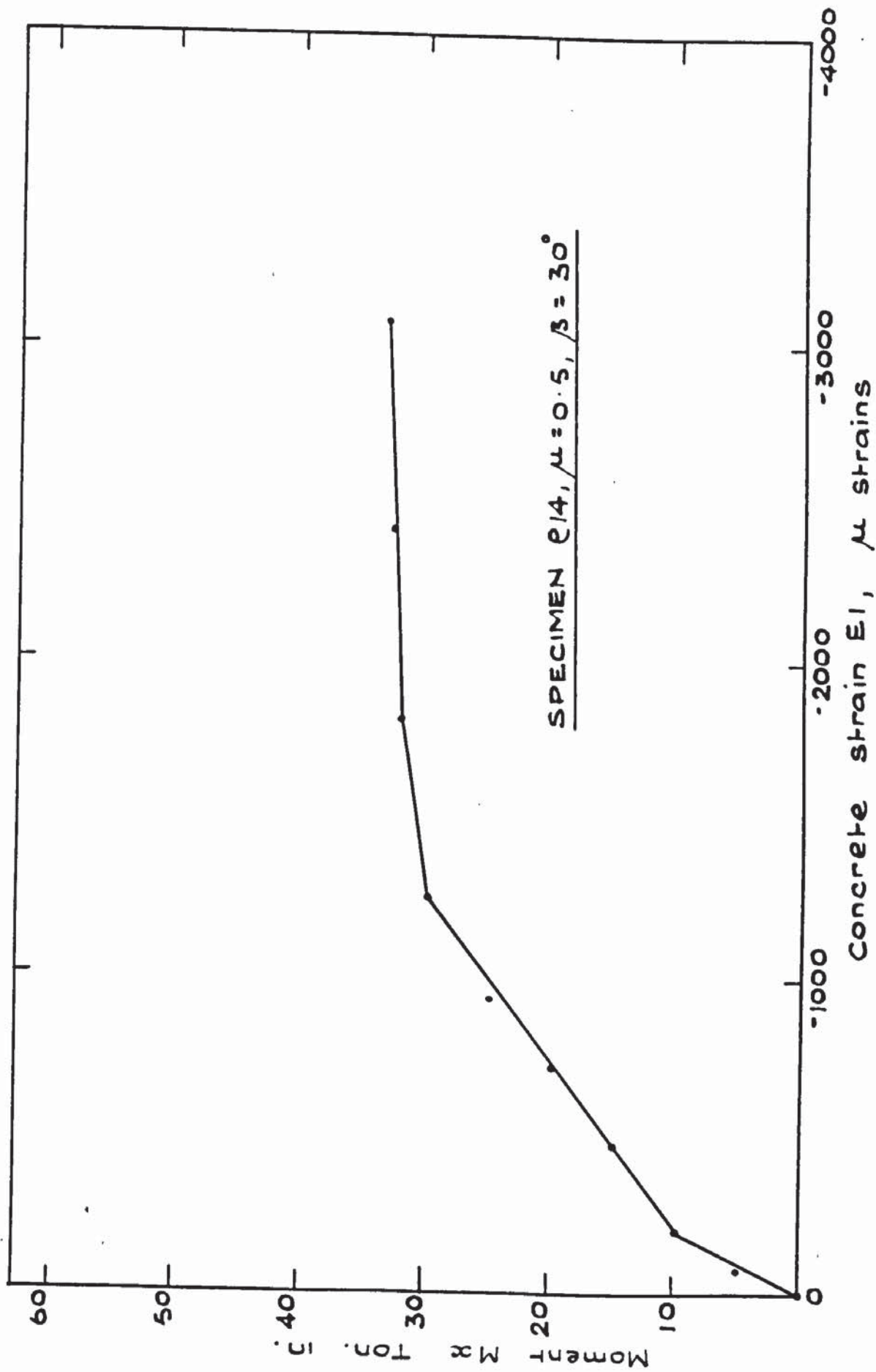


FIG. 5.54. AVERAGE PRINCIPAL CONCRETE STRAIN E1 - P.14.

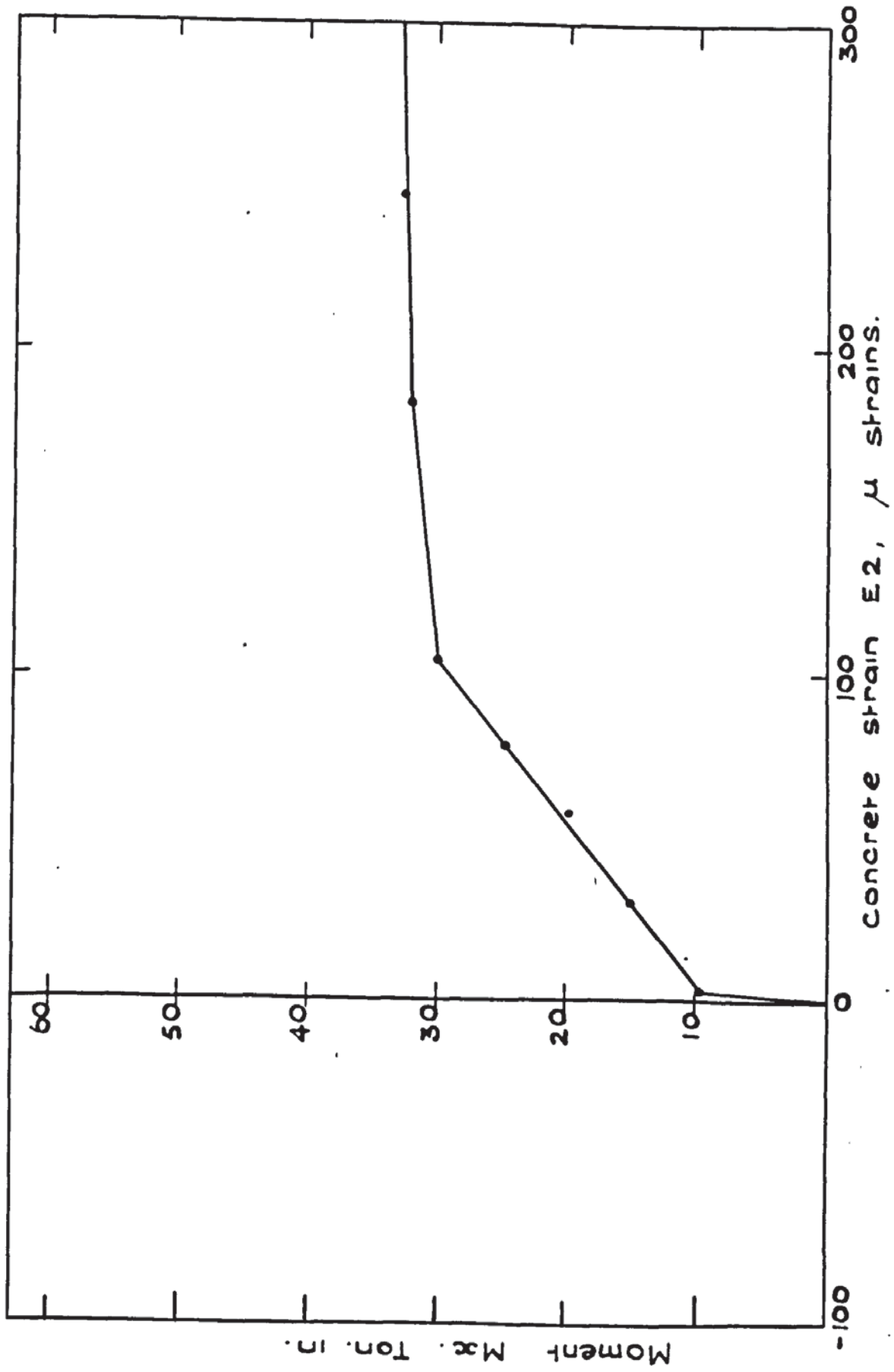


FIG. 5.55. AVERAGE PRINCIPAL CONCRETE STRAIN E2 - P.14.

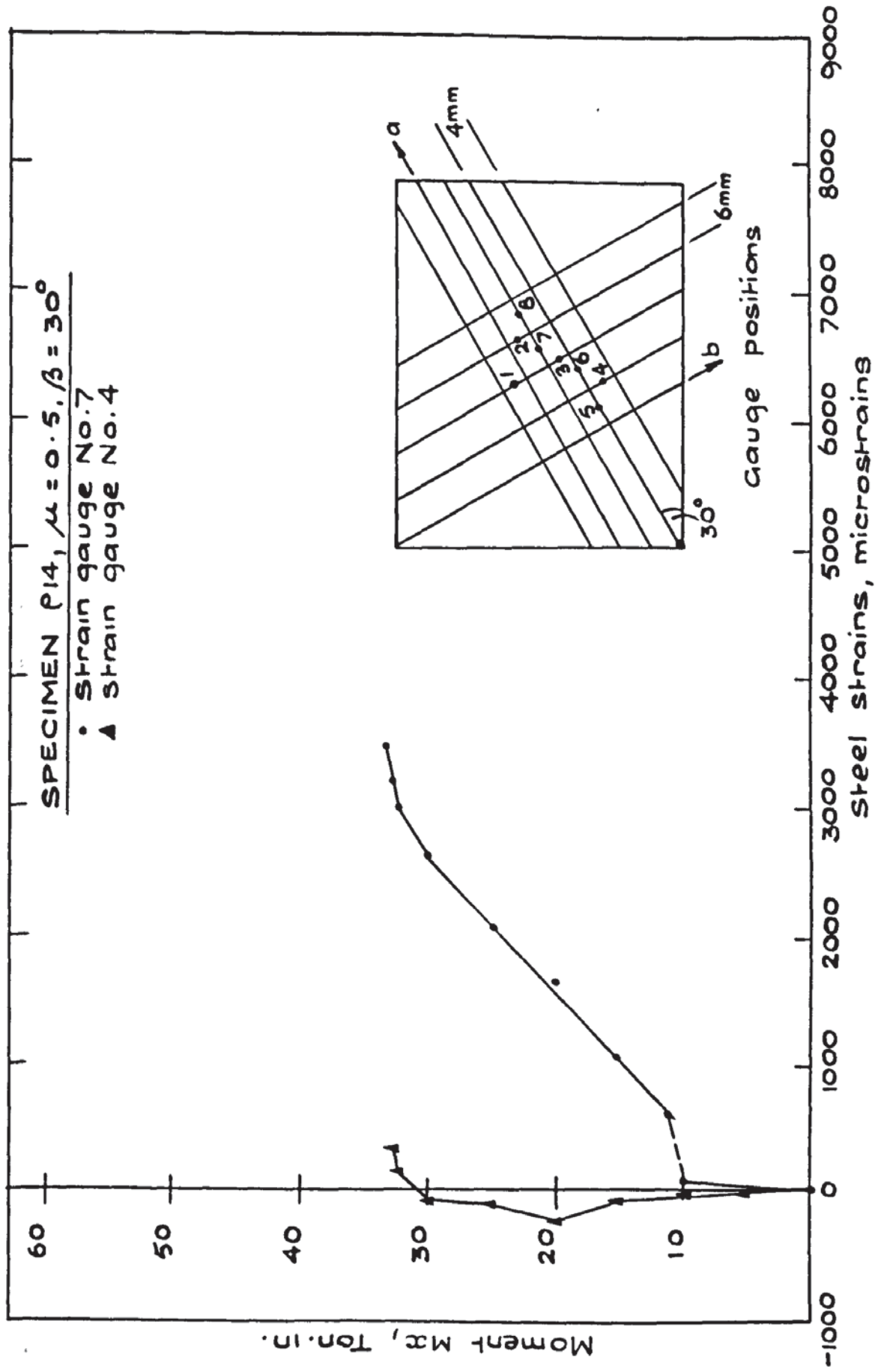


FIG. 5.56. TYPICAL STEEL STRAIN PLOT - P.14.

M <sub>x</sub>	AVERAGE tan 2 $\gamma$	STEEL STRAINS							
		1	2	3	4	5	6	7	8
TON. IN	$\tau$	MICROSTRAINS							
0.00	0.00	0.00	0.00	0.00	0.00	0.00	0.00	0.00	0.00
4.98	.2960	0.00	9.90	36.61	4.95	19.80	29.71	39.61	49.51
9.96	.1858	-9.90	0.00	118.83	0.00	69.32	89.12	108.93	49.51
14.94	.0883	-59.41	69.32	173.29	-69.32	613.95	831.80	1079.37	856.56
19.92	.1083	-198.05	148.54	59.41	-227.76	653.56	1366.54	1638.85	1416.05
25.10	.1119	425.80	237.66	-19.80	-99.02	643.66	2307.27	2020.10	1614.10
29.88	.0669	1218.00	207.95	178.24	-79.22	772.39	-	2544.93	2277.56
32.12	.0831	-1178.39	-435.71	-29.71	158.44	1287.32	-	2980.63	1752.73
32.87	.1016	-1010.05	-643.66	-168.34	336.68	-	-	3198.49	1812.15
33.12	.1113	-	-613.95	-69.32	-	-	-	3446.05	2604.34

Table 5.14 Principle Concrete Strain Direction & Steel Strains PL4.

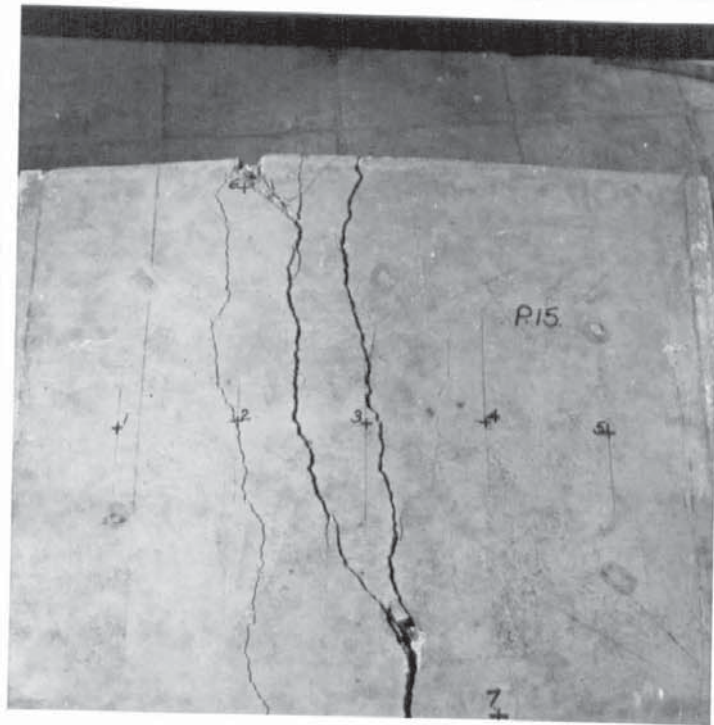


PLATE 5.18

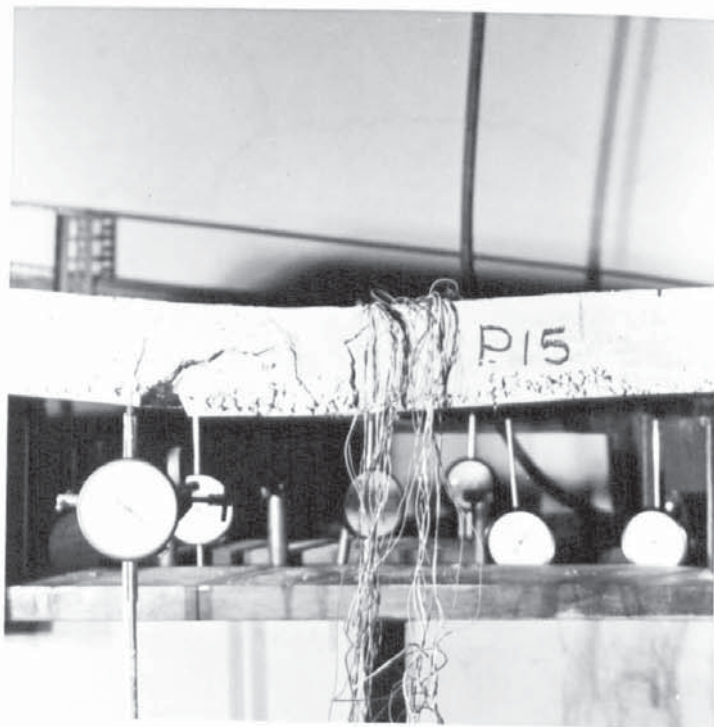


PLATE 5.19

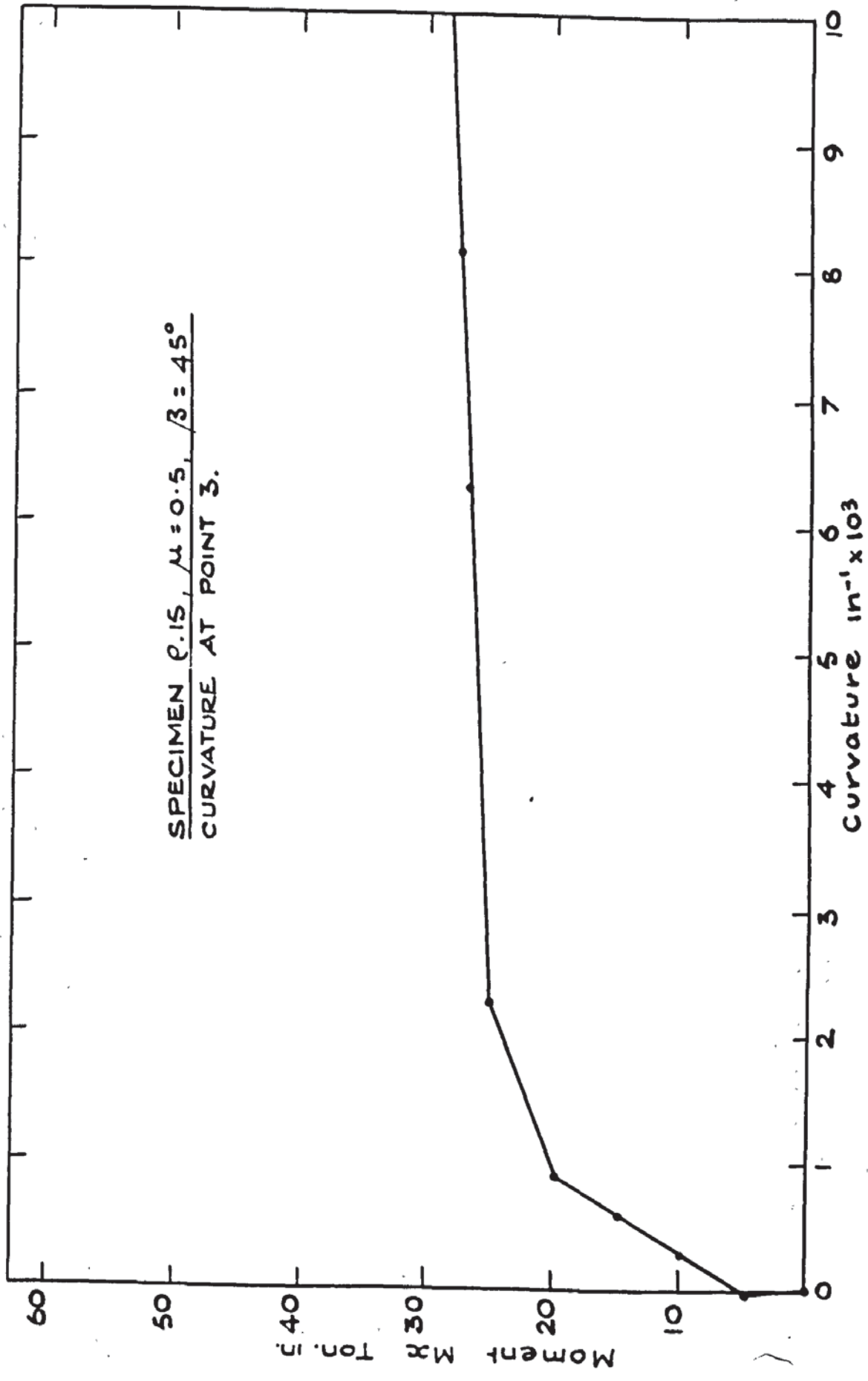
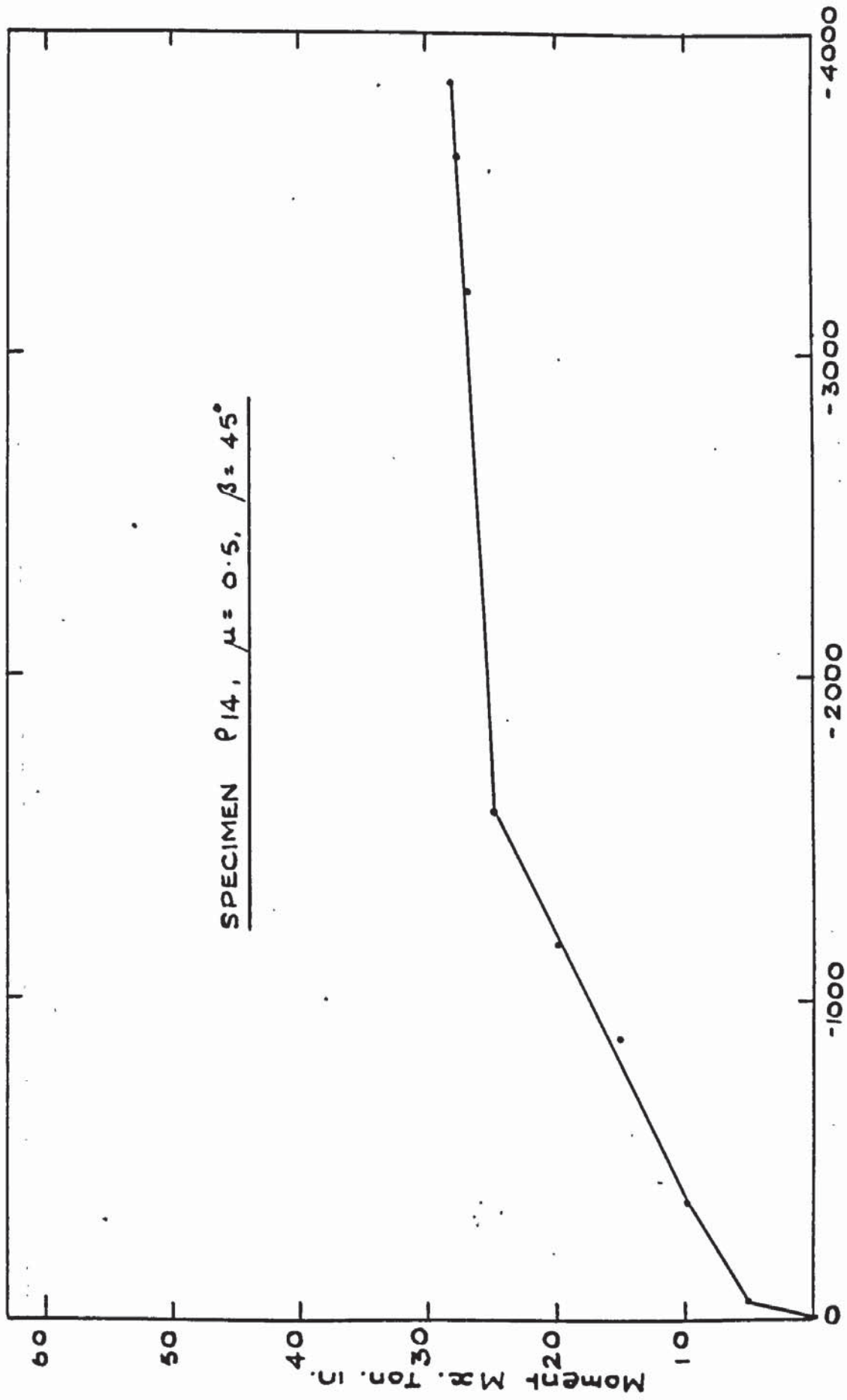


FIG. 5.57. MOMENT CURVATURE PLOT - P.15.



Concrete Strain  $\epsilon_1$ , microstrains

FIG. 5.58. AVERAGE PRINCIPAL CONCRETE STRAIN PLOT  $\epsilon_1 - P.14.$

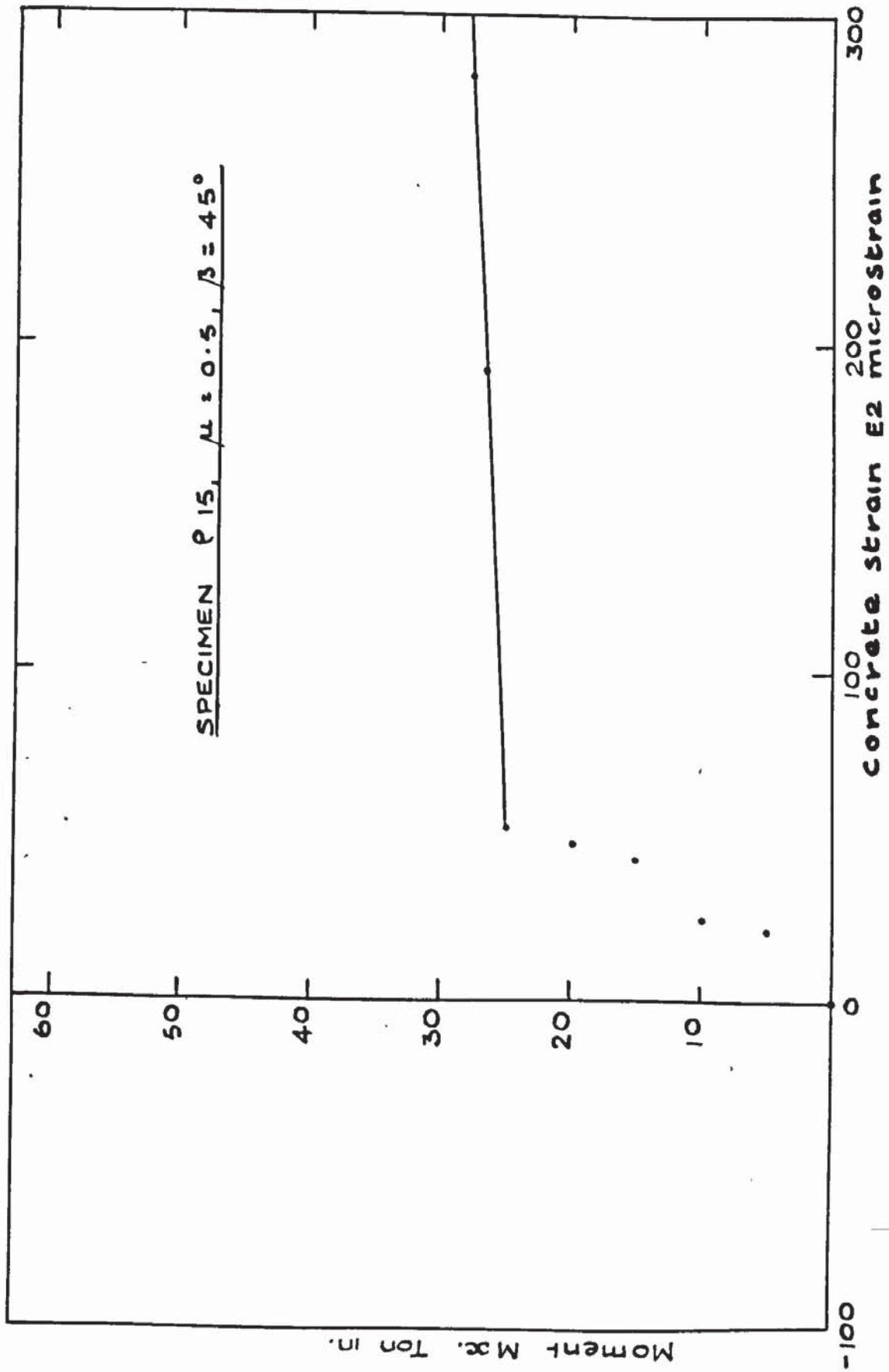


FIG. 5.59. AVERAGE PRINCIPAL CONCRETE STRAIN E2 - P.15.

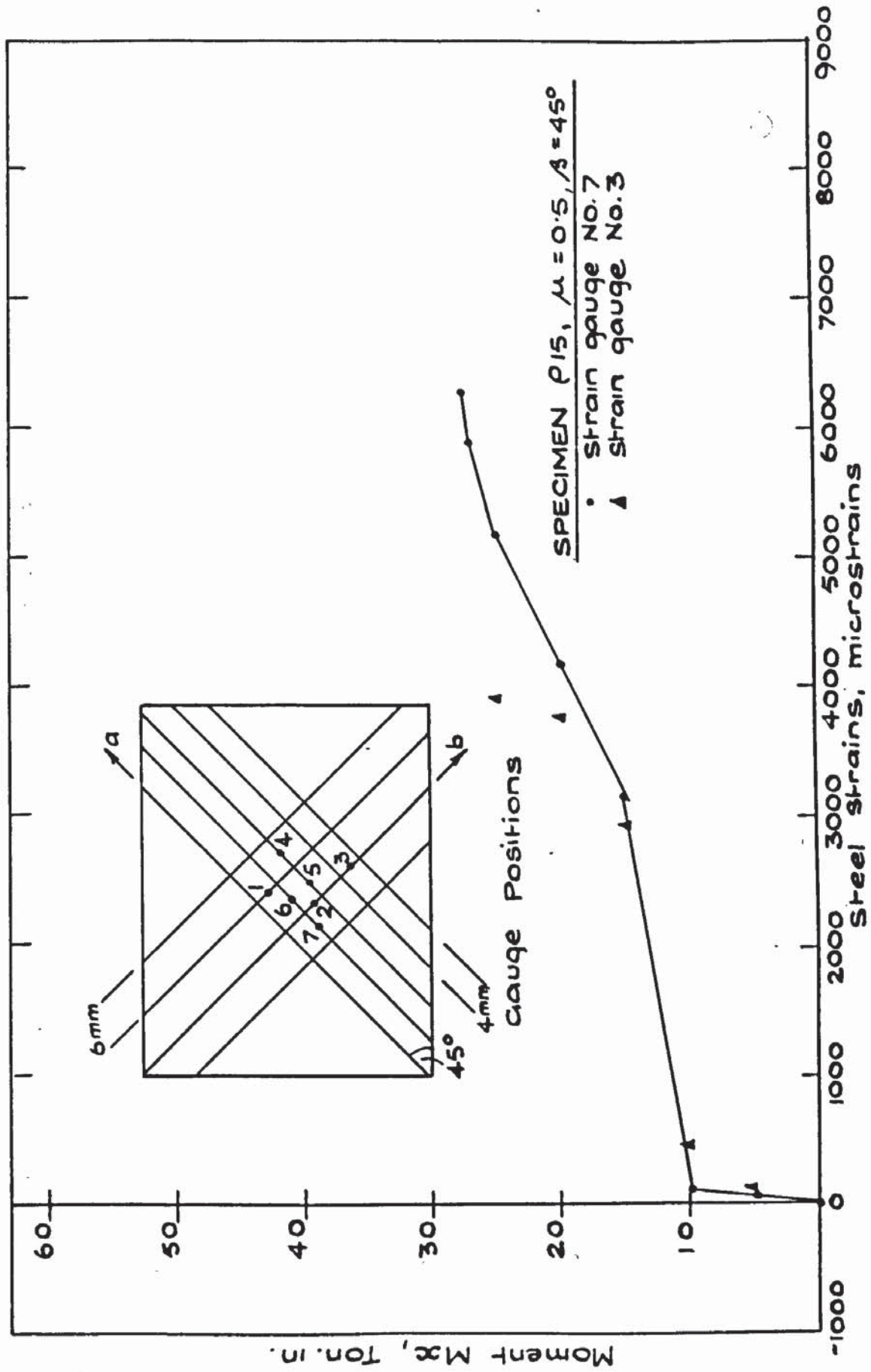


FIG. 5.60. TYPICAL STEEL STRAIN PLOT - P.15

M <sub>x</sub> TON.IN	AVERAGE tan 2γ	STEEL STRAINS									
		1	2	3	4	5	6	7	8		
0.00	-	0.00	0.00	0.00	0.00	0.00	0.00	0.00	0.00	0.00	-
4.98	-.2751	69.32	54.46	89.12	59.41	44.56	69.32	59.41	69.32	59.41	-
9.96	-.2723	663.46	386.20	455.51	108.93	-9.90	79.22	128.73	79.22	128.73	-
14.94	-.1462	2010.20	1109.07	2901.41	396.10	-9.90	99.02	3134.12	99.02	3134.12	-
19.92	-.0852	3109.37	1485.37	3743.12	732.78	69.32	178.24	4198.63	178.24	4198.63	-
24.90	-.0532	-	-	3891.66	1168.49	-19.80	158.44	5159.17	158.44	5159.17	-
26.89	-.0294	-	-	3852.05	1287.32	435.71	237.66	5891.95	237.66	5891.95	-
27.39	-.0446	-	-	-	1277.41	1534.88	-	6228.63	-	6228.63	-
28.14	-.1267	-	-	-	-	2574.63	-	-	-	-	-

Table 5.15 Principle Concrete Strain Direction & Steel Strains P15.

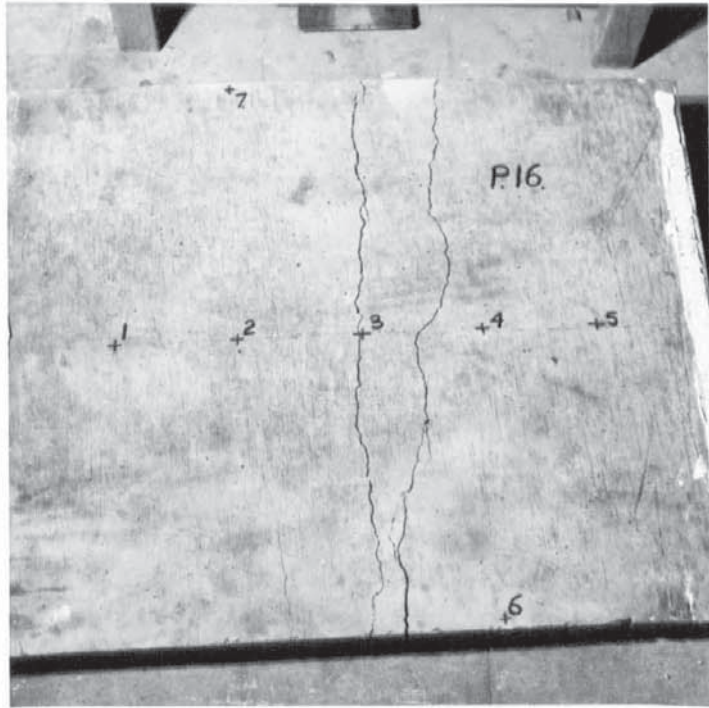


PLATE 5.20

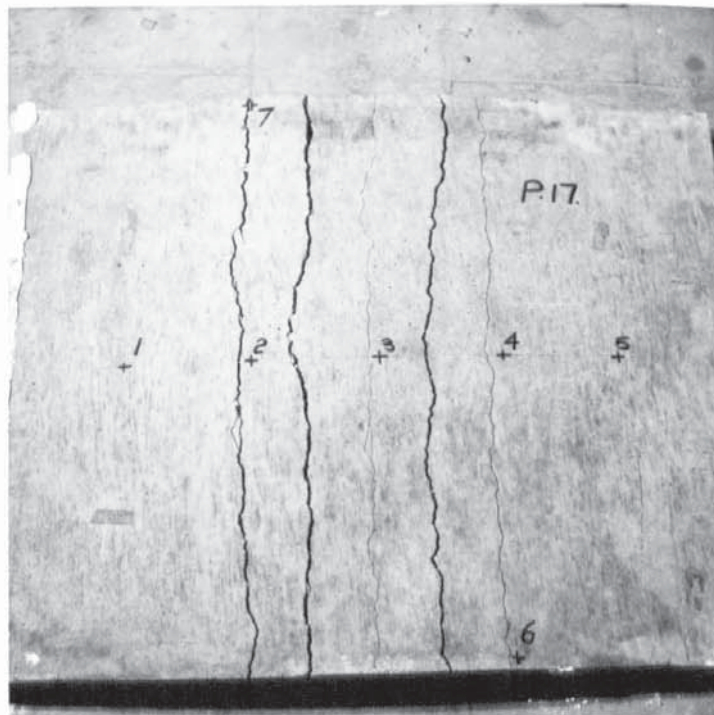


PLATE 5.21

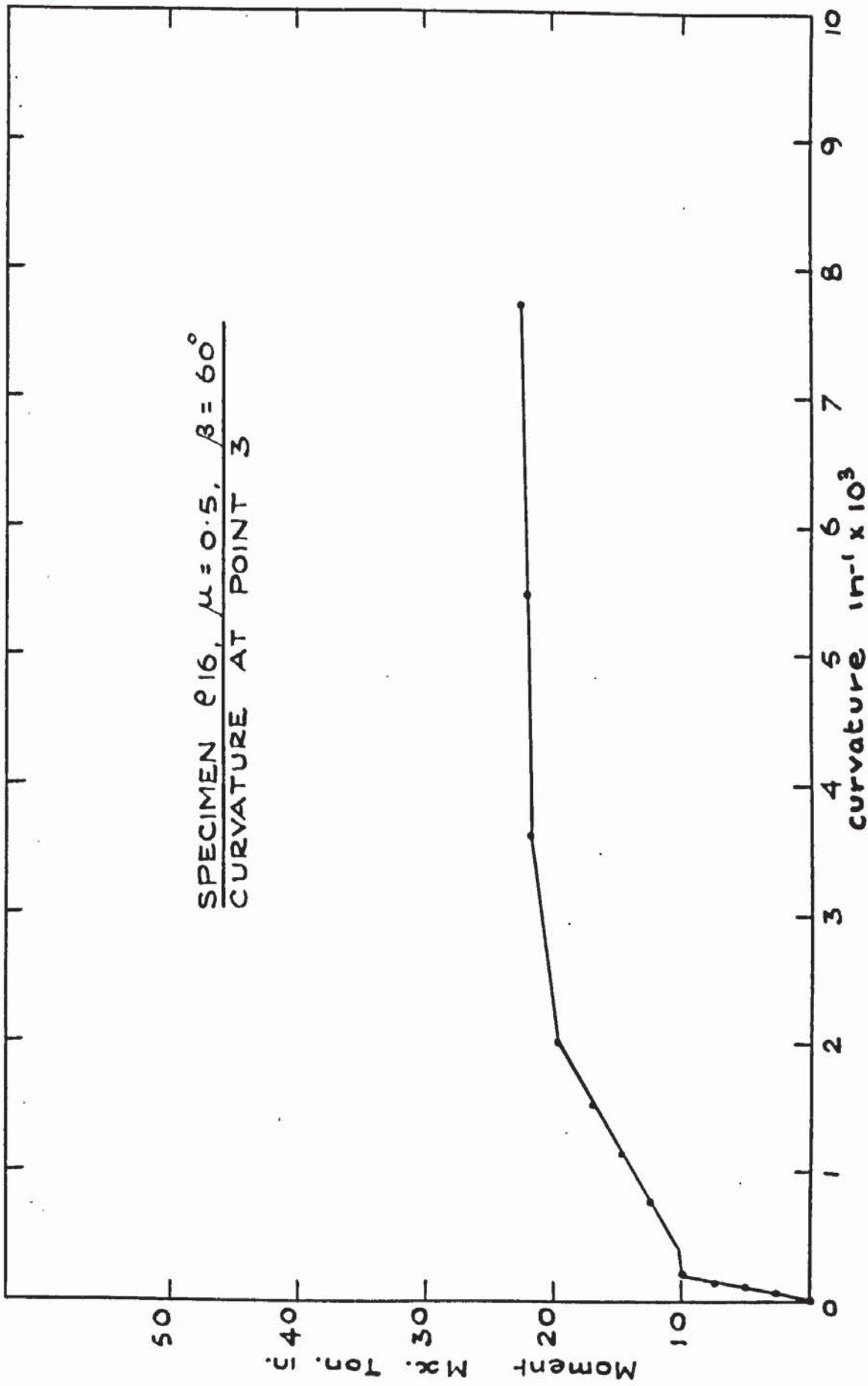


FIG. 5.61. MOMENT CURVATURE PLOT - P.16.

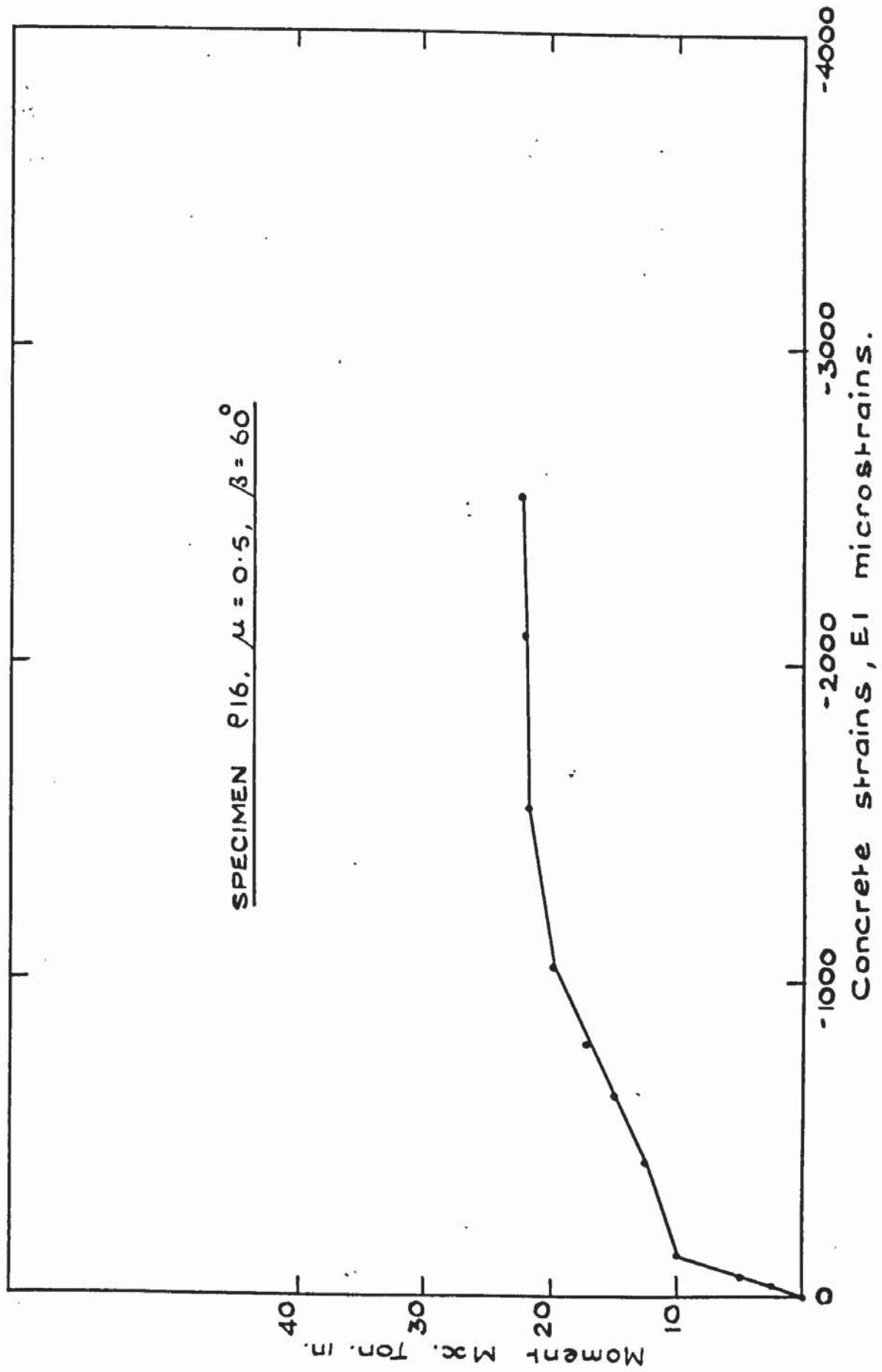


FIG. 5.62. AVERAGE PRINCIPAL CONCRETE STRAIN PLOT EI-P.16

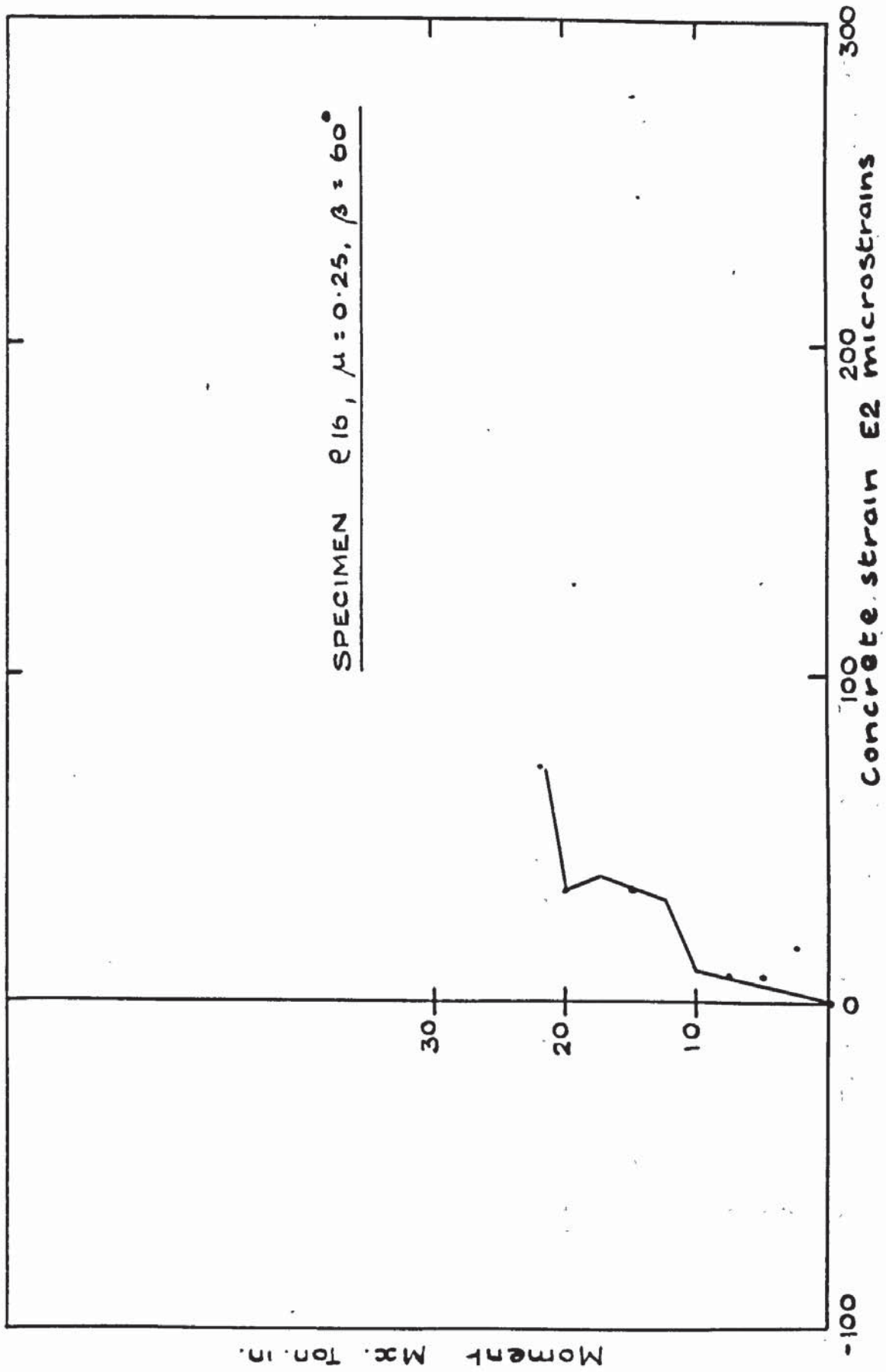


FIG. 5.63. AVERAGE PRINCIPAL CONCRETE STRAIN PLOT E2 - P.16.

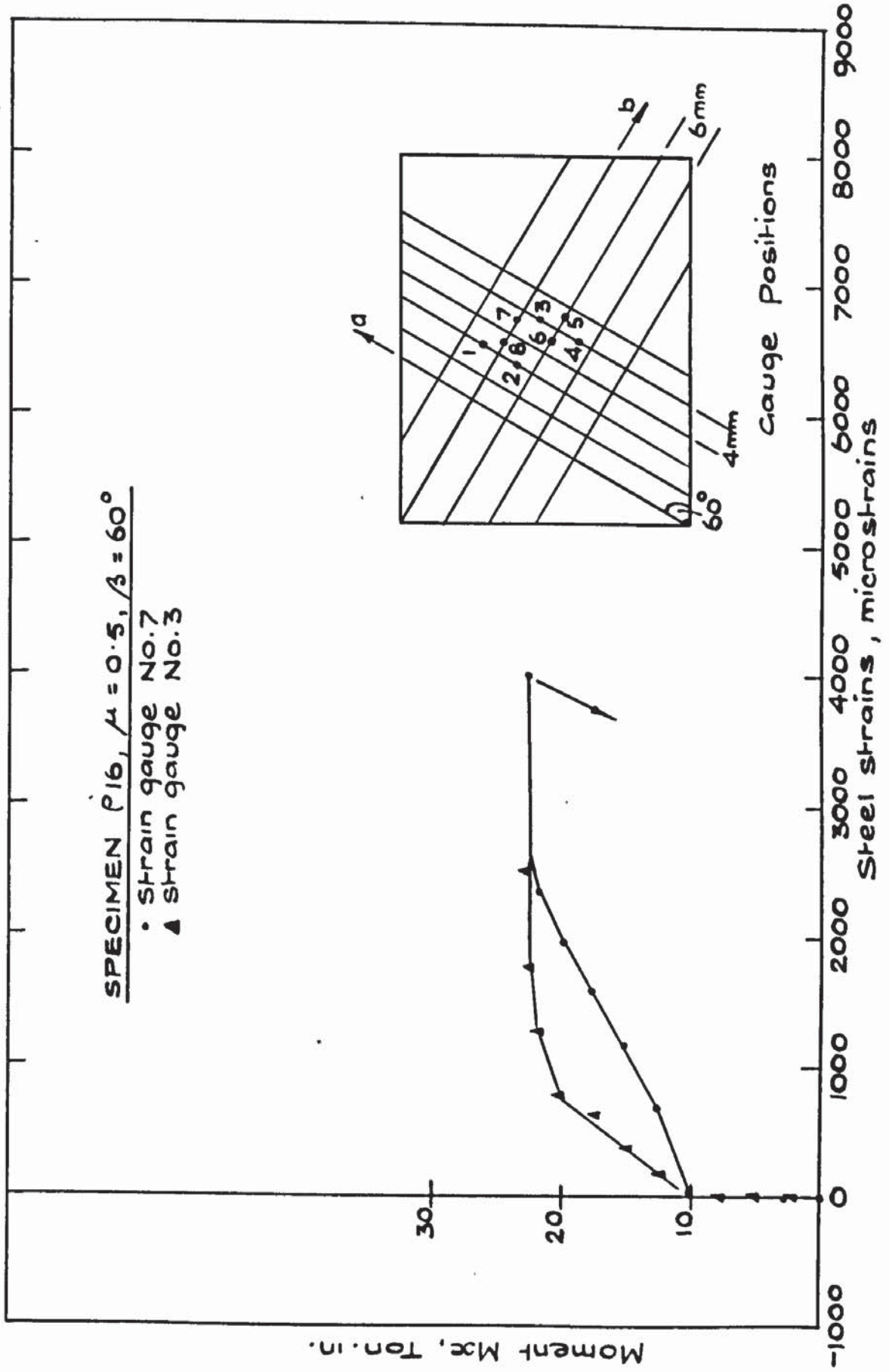


FIG. 5.64. TYPICAL STEEL STRAIN PLOT - P.16.

M <sub>X</sub> TON.IN	AVERAGE tan 2γ	STEEL STRAINS							
		1	2	3	4	5	6	7	8
0.00	-	0.00	0.00	0.00	0.00	0.00	0.00	0.00	0.00
2.24	-.2666	-59.41	-39.61	0.00	-19.80	0.00	0.00	-24.76	-9.90
4.73	-.2547	-29.71	-39.61	0.00	-19.80	0.00	4.95	-14.85	14.85
7.22	-.3000	-49.51	-39.61	0.00	-19.80	9.90	19.80	-4.95	34.66
9.71	-.2838	-29.71	-39.61	9.90	-9.90	19.80	34.80	-4.95	59.41
12.20	-.0626	-406.00	-19.80	158.44	89.12	465.41	683.27	648.61	1089.27
14.69	-.0540	2376.59	99.02	346.59	89.12	841.71	1153.63	1163.54	1396.24
17.18	-.0207	544.63	475.32	623.85	455.51	1218.00	1698.27	1599.24	2782.59
19.67	-.0271	703.07	663.46	752.59	584.24	2119.12	3351.98	1945.83	-
21.16	-.1625	1019.95	1168.49	1257.61	821.90	-	-	2341.93	-
21.91	-.2488	1029.85	1465.56	1742.83	-	-	-	2539.98	-
22.31	-.2734	1227.90	1950.78	2515.22	-	-	-	4025.34	-

Table 5.16 Principle Concrete Strain Direction & Steel Strains P16

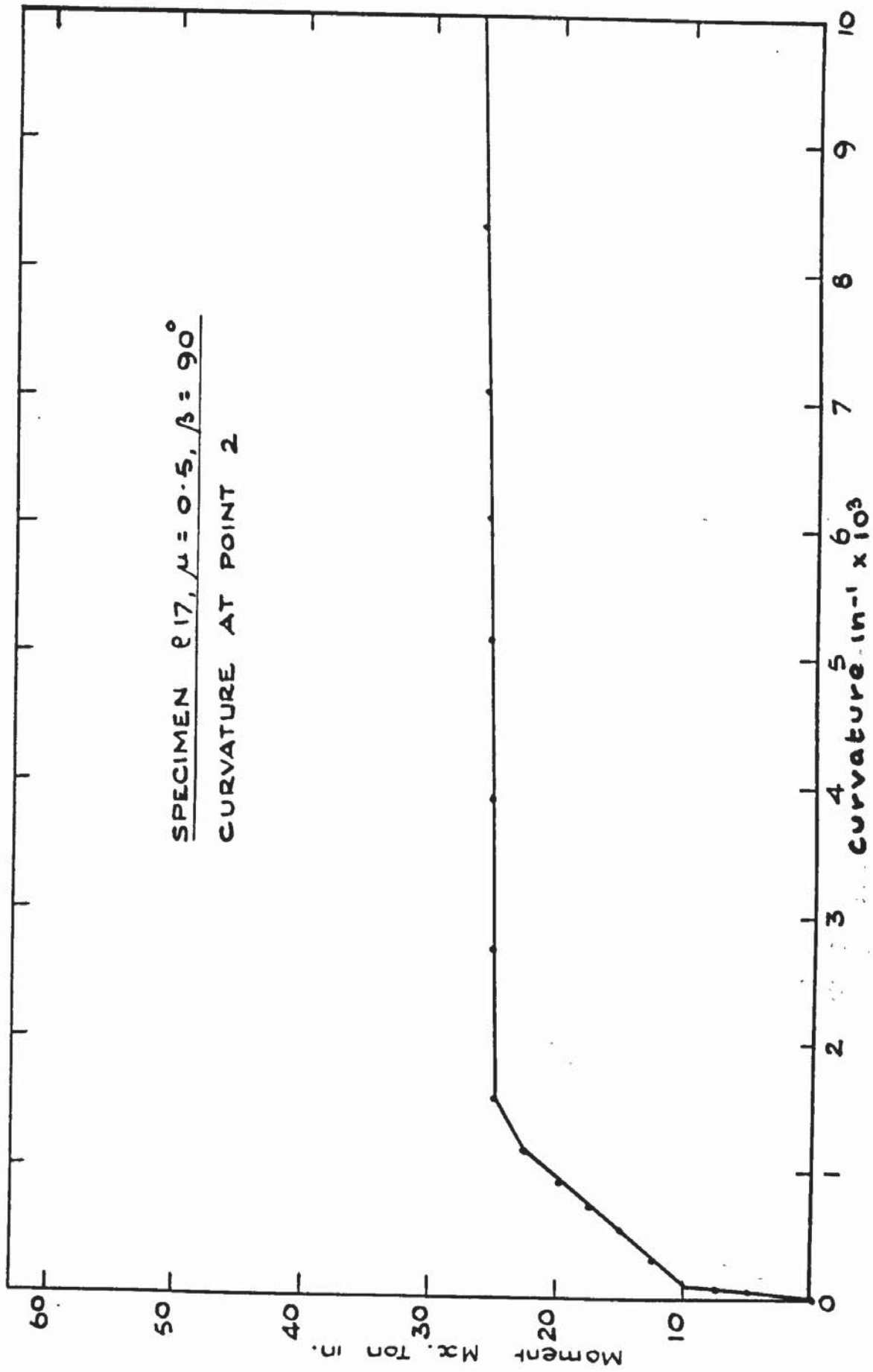


FIG. 5.65. MOMENT CURVATURE PLOT - P. 17.

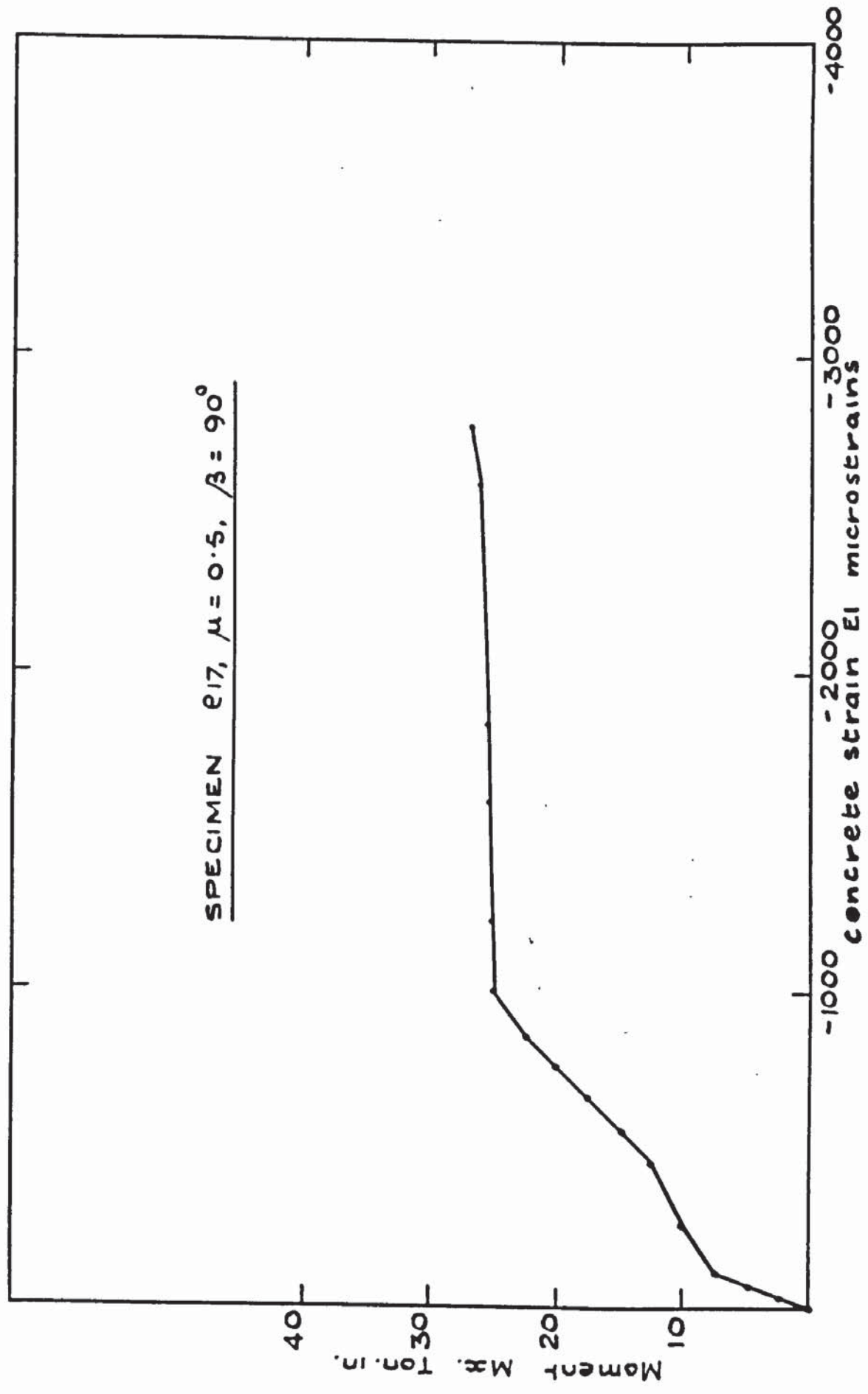


FIG. 5.66. AVERAGE PRINCIPAL CONCRETE STRAIN EI - P.17

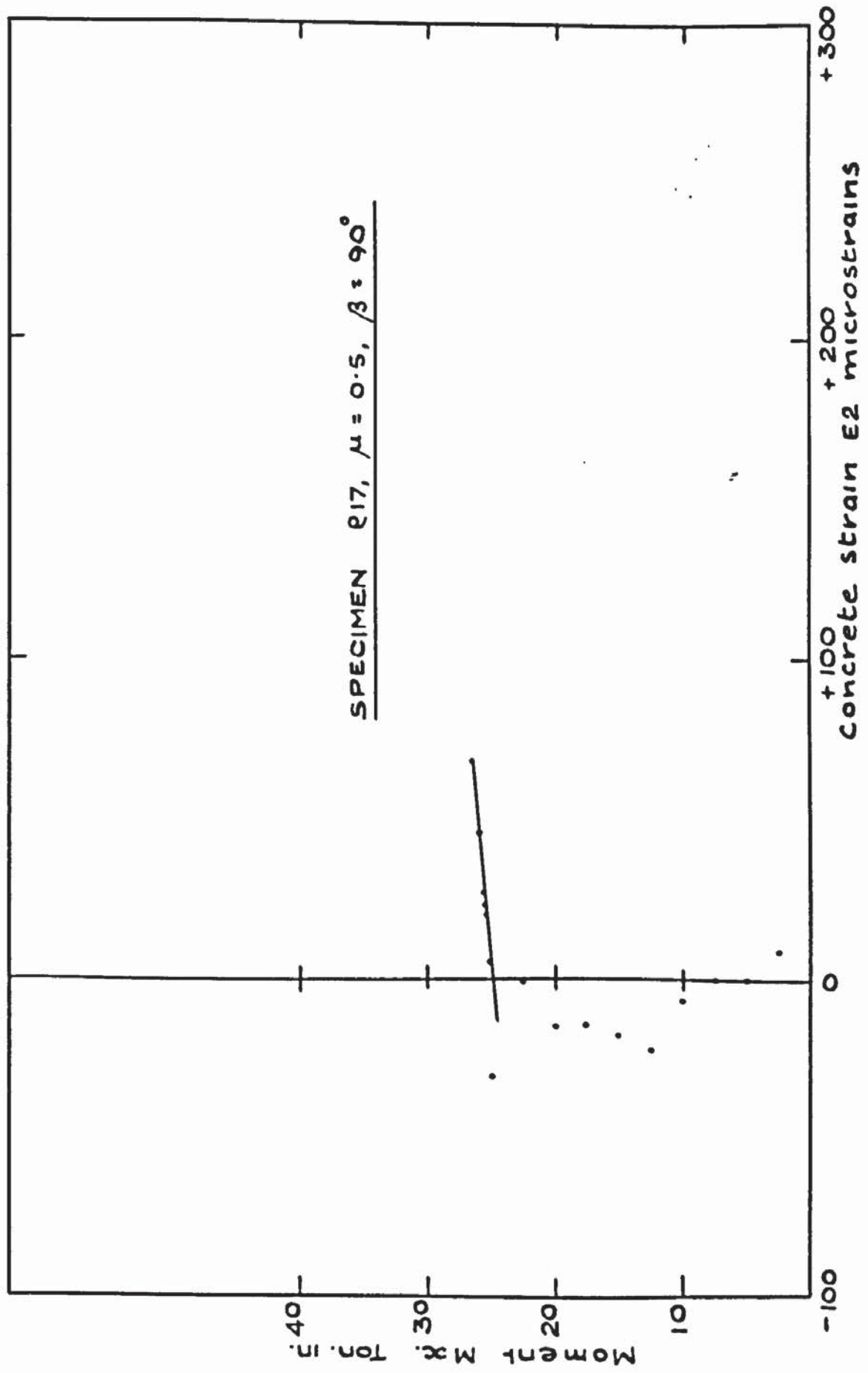


FIG. 5.67. AVERAGE PRINCIPAL CONCRETE STRAIN  $\epsilon_2$  - P.17

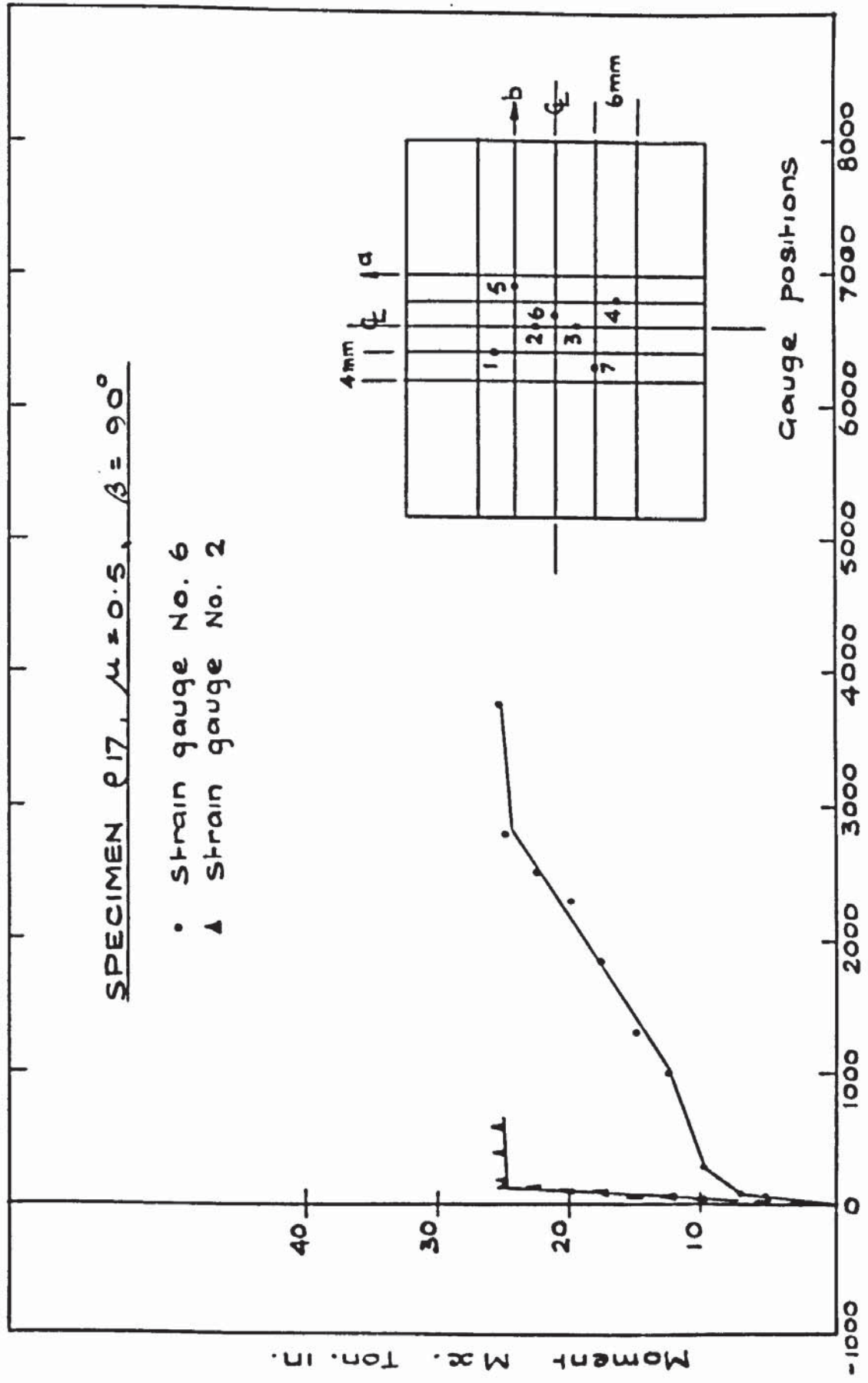


FIG. 5.68. TYPICAL STEEL STRAIN - P.17

M <sub>x</sub> TON.IN	AVERAGE tan 2γ	STEEL STRAINS										
		1	2	3	4	5	6	7	8			
0.00	-	0.00	0.00	0.00	0.00	0.00	0.00	0.00	0.00	0.00	-	
2.44	-.4166	9.90	49.51	19.80	29.71	19.80	29.71	19.80	29.71	29.71	9.90	-
4.93	-.6333	9.90	54.46	19.80	39.61	19.80	39.61	29.71	29.71	49.51	39.61	-
7.47	-.2639	0.00	59.41	19.80	29.71	19.80	29.71	39.61	39.61	69.32	44.56	-
9.91	-.3029	-19.80	39.61	138.63	39.61	138.63	39.61	59.41	59.41	267.37	138.63	-
12.40	-.1575	-29.71	49.51	227.76	406.00	227.76	406.00	297.07	297.07	990.24	435.71	-
14.89	-.1528	-39.61	39.61	217.85	237.66	217.85	237.66	480.27	480.27	1277.41	693.17	-
17.38	-.1173	-29.71	79.22	227.76	415.90	227.76	415.90	673.37	673.37	1812.15	891.22	-
19.87	-.1216	-39.61	99.02	267.37	445.61	267.37	445.61	841.71	841.71	2208.24	1128.88	-
22.36	-.0991	-39.61	128.73	297.07	455.51	297.07	455.51	1099.17	1099.17	2475.61	1356.63	-
24.85	-.0921	-49.51	128.73	306.98	460.46	306.98	460.46	1297.22	1297.22	2772.68	1611.02	-
24.90	-.0882	79.22	178.24	287.17	455.51	287.17	455.51	1376.44	1376.44	3733.22	1782.44	-
25.05	-.0913	99.02	376.29	415.90	465.41	415.90	465.41	1425.95	1425.95	-	-	-
25.35	-.0999	89.12	356.49	465.41	465.41	465.41	465.41	-	-	-	-	-
25.60	-.0894	89.12	346.59	475.32	485.22	475.32	485.22	-	-	-	-	-
25.85	-.0877	-	386.20	554.54	524.83	554.54	524.83	-	-	-	-	-
26.10	-.0876	-	366.39	623.85	534.73	623.85	534.73	-	-	-	-	-
26.84	-.0831	-	425.80	693.17	544.63	693.17	544.63	-	-	-	-	-

Table 5.17 Principle Concrete Strain Direction & Steel Strains P17

range in the E2 plot in Fig 5.67 but other values of curvature and strain in Figs 5.65 - 5.66 and 5.68 respectively give good plots. Cracking was again at a moment of 10 ton.in and Table 5.17 shows  $\gamma$  to be less than  $2.5^{\circ}$  for most of the test. Maximum curvature and concrete strain values were  $14.69 \text{ in}^{-1} \times 10^4$  and 2777 microstrains respectively.

### 5.3 General Moment test series

#### 5.3.1 Description of general test procedure

Once the test specimens in this series had been set up as described in 4.4.2 care was taken to level the element before the cross beam was jacked down onto the prepositioned loading blocks on the channels. Slight jack pressure was applied and the wooden packing pieces holding the element level were removed. Zero readings were then taken from all strain gauges, deflexion gauges and proving ring. As in the plank test series about fifteen load increments were applied before the ultimate moment was reached and deflexion increments controlled loading after yielding of the reinforcement occurred. When deflexions were excessive the dial gauges were reset by sliding the dial gauge grid down on the 1/2in. bars described in 4.4.3(c).

#### 5.3.2. General method of presentation of objective observations.

The presentation of results in this test series was more difficult to achieve than in the Plank test series. As

described in 4.4.2. the main controlled variables were  $\beta$ , the angle of the reinforcement mesh to the X and Y directions and the ratios between bending and twisting moments. As previously described in 5.1 a computer program was written to convert experimental readings into corrected observations. Thus steel strains in the bar directions, principal concrete strains and directions, concrete strains in the bar directions and principal curvatures and directions were all obtained. However, whereas in the plank test series the principal strain direction was constant throughout each test and moreover was forced to coincide with the span direction, in this test series there was no attempt made to force any principal generalized stress or strain direction to coincide with any other direction. Indeed, although at failure the principal moment direction could be said to be a function of the lever arms producing bending and torsional moments alone it would be very inaccurate to ignore the dead weight of the slab and clamp system at low loads near cracking. This point has been made previously in an analytical context in Chapter 3 and can now be referred to experimentally. The self weights of each slab were recorded before each test and an average weight over all the specimens was found to be 353.8 lbs. with a maximum variation from the mean of 2%. Using this data in conjunction with the weights of the steel clamp system it was estimated that a maximum moment of 0.18 kip in/in\*

\* Footnote: 1 Kip = 1000 lb abbreviated as k

acting over the centre of the 36in. slab element in the X - direction made up the dead weight moment of the system. Because of the symmetry of the system no dead weight torsional moment existed and because of the rigid clamps no dead weight bending moment in the Y direction existed. Thus this dead weight moment influenced only the bending moment in the X - direction and not the torsional moment.

Further assumptions must be made in order to calculate the magnitude and direction of the principal applied moments. Because of the restraint in the Y  $\pm$  direction due to the heavy clamps, moments,  $M_y$ , may have been introduced into the system by virtue of Poisson ratio and associated elastic constant effects. These effects are discussed more fully in section 7.2 and it is shown in this section that it is a good approximation to assume that  $M_y = 0$ . In addition to the conclusions reached in 7.2 it may be pointed out that Lenschow and Sozen<sup>[29]</sup> have assumed that Poisson ratio effects are insignificant in a cracked reinforced concrete slab.

Accordingly the bending moment  $M_x$  can be expressed in terms of W, the load in tons measured by the proving ring at one support point as

$$M_x = \left[ \frac{15 \times W \times 2.24}{36} + 0.18 \right] \text{ k.in/in (5.1)}$$

whereas the torsional moment  $M_{xy}$  can be expressed as

$$M_{xy} = \frac{W \times 2.24 \times Ta}{36} \quad \text{k.in/in} \quad (5.2)$$

where  $Ta = 3\text{in.}$   $11.25\text{in.}$  or  $17.5\text{in.}$  according to the lever arm set.

Thus the angle  $\theta$  between the X - direction and the principal moment direction is given by

$$\tan 2\theta = \frac{2M_{xy}}{M_x} \quad (5.3)$$

and by substituting equations (5.1) and (5.2) into equation (5.3) it can be seen that  $\tan 2\theta$  is a non linear function of  $W$ . Fig 5.69 illustrates how the direction of the principal moment  $\theta$  varies with the load for each of the three types of torsional moment lever arm used. The values of the principal applied moment  $M_1$  and  $M_2$  are also affected by the dead weight moment and they are expressed as

$$\frac{M_1}{M_2} = \frac{M_x}{2} \left[ 1 \pm \sqrt{1 + 4 \frac{M_{xy}^2}{M_x^2}} \right] \quad (5.4)$$

Fig 5.70 and 5.71 illustrate the variance of  $M_1$  and  $M_2$  with  $W$ , respectively. These graphs are used to convert the proving ring load reading  $W$ , directly to  $M_1$ ,  $M_2$  or  $\tan 2\theta$ .

Because of these directional variations between the variables the results have been presented graphically by plotting the load  $W$  in tons measured by the proving ring against the directions of principal moment, drawn as a continuous curve from equation (5.3), principal curvature and principal concrete strain relative to the X - direction in

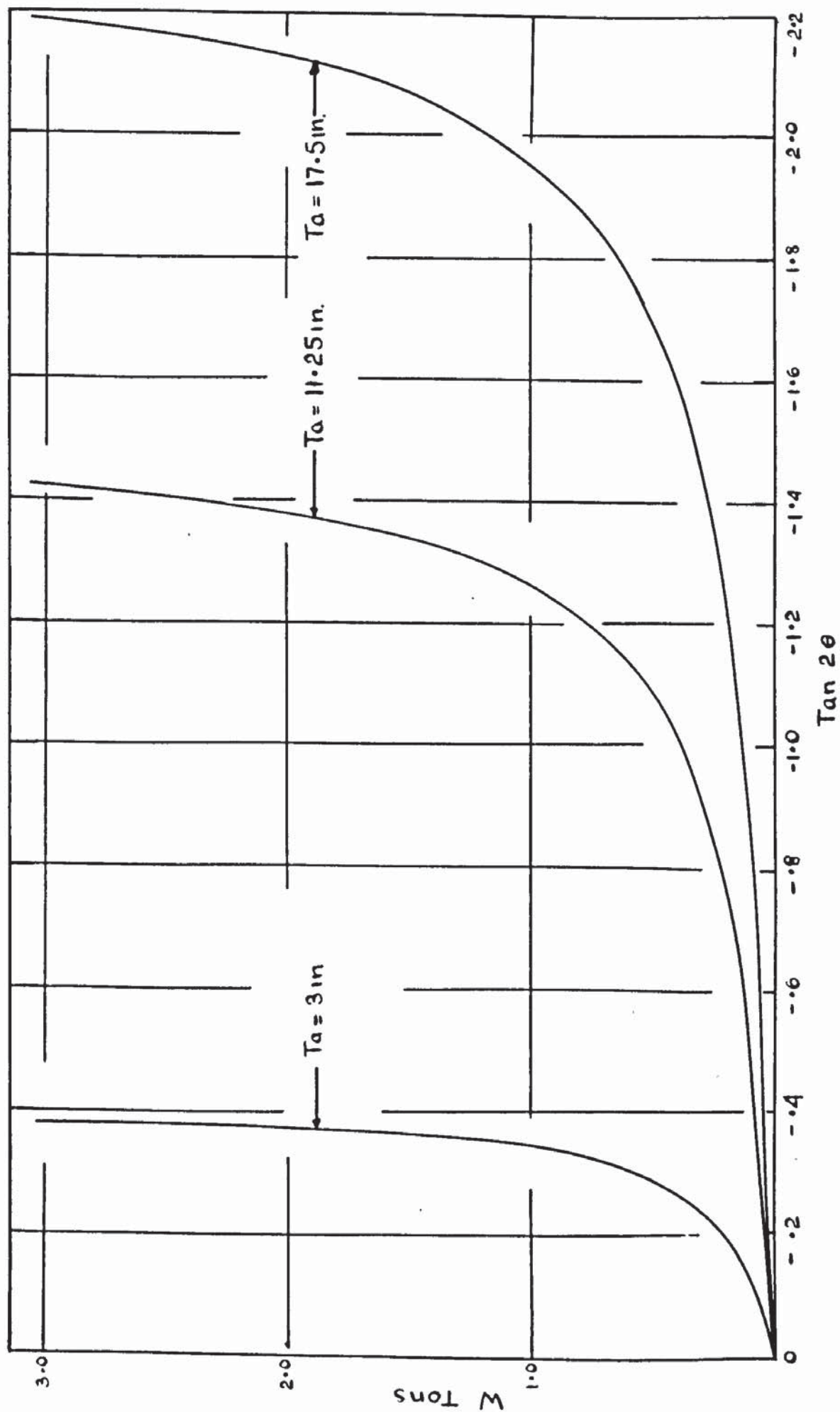


FIG 5.69 VARIATION OF  $\tan 2\theta$  WITH  $W$  - GENERAL MOMENTS.

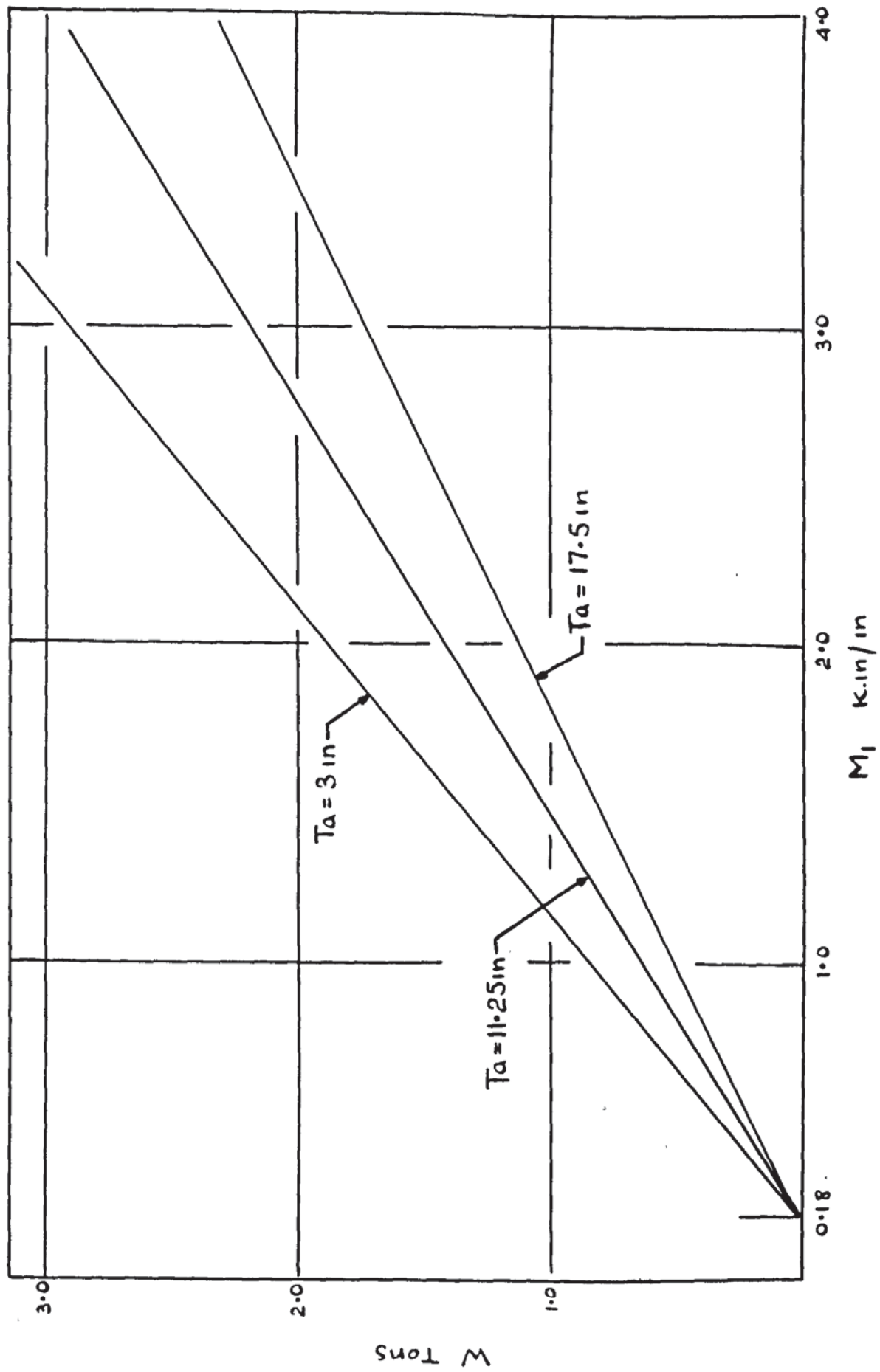


FIG5.70 VARIATION OF  $M_1$  WITH  $W$  - GENERAL MOMENTS.

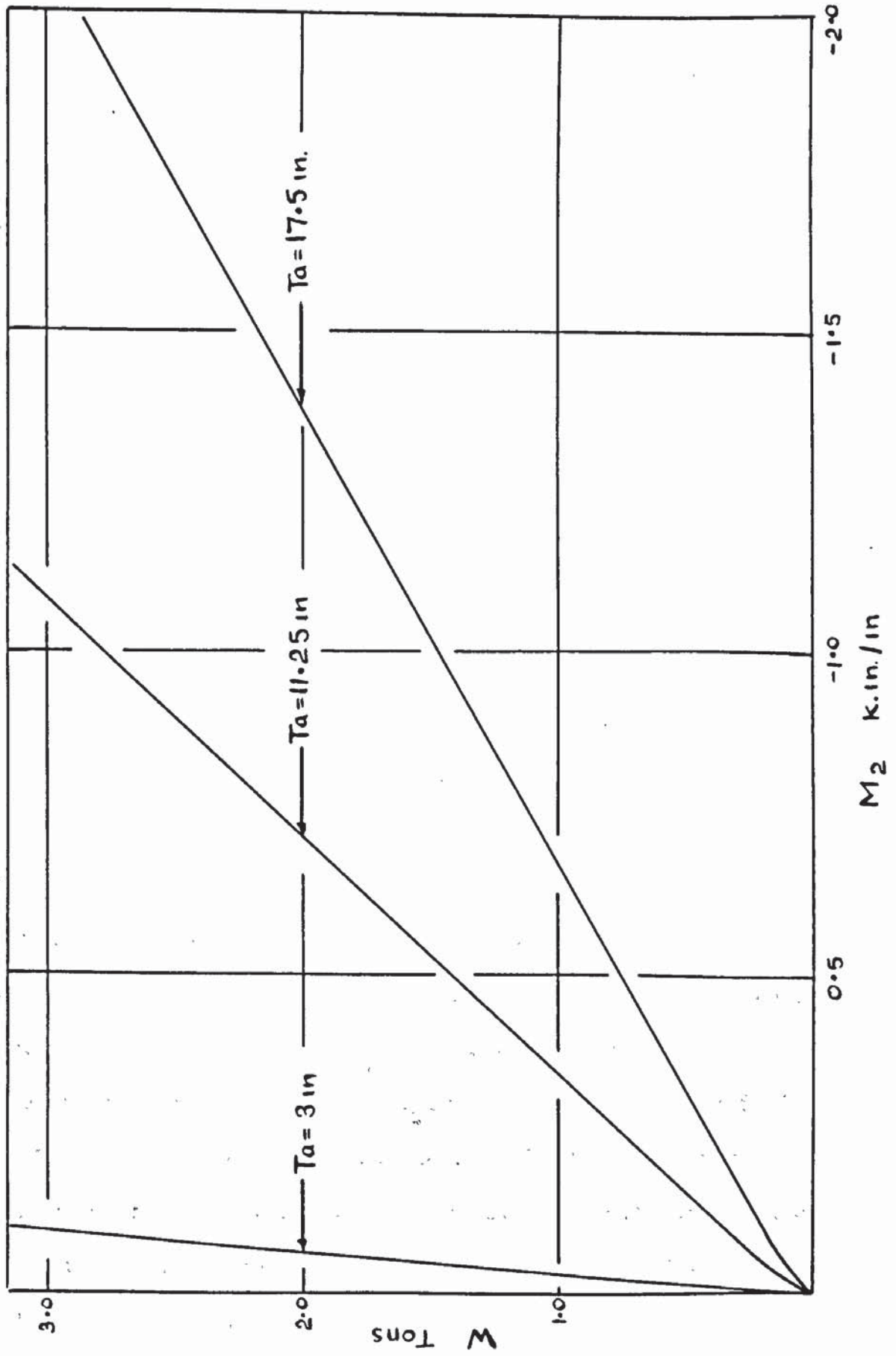


FIG 5.71 VARIATION OF  $M_2$  WITH  $W$  - GENERAL MOMENTS.

the form of  $\tan 2\theta$ ,  $\tan \omega$  and  $\tan 2\gamma$  respectively.  $\theta$  is the angle between the direction of maximum principal moment and the X - direction,  $\omega$  the angle between the maximum principal curvature direction and the X - direction and as in the plank test series,  $\gamma$  is the angle between the maximum compressive principal concrete strain direction and the X - direction. These angles are shown diagrammatically in Fig 5.72 and are measured clockwise positive from the principal direction to the X - direction as in the usual Mohr's circle notation. The average measured crack angle  $\psi$  defined in Fig 5.72 is also represented in the plots of principal directions.

The figures described above showing the variations of principal directions with load are presented individually for each specimen. However further graphical presentation of results has been carried out in a more directly comparative manner. Thus plots of load, W, against maximum principal curvature and maximum principal compressive concrete strain for several slab elements have been combined. The torsional lever arm,  $Ta$ ., producing the torsional moment  $M_{xy}$  has been used as a constant in each combined graph. Consequently Fig 5.91 and Fig 5.92 for instance show plots of load, W, against maximum principal curvature and maximum principal compressive concrete strain, respectively, for specimens TB1, TB2, TB3 and TB28 (which have a mesh angle  $\beta$  of  $0^\circ$ ,  $30^\circ$ ,  $45^\circ$  and  $67.5^\circ$  respectively) all of which have a degree of orthotropy,  $\mu = 1$  and are acted on by a torsional moment with a lever arm  $Ta$  of 3in. Similar graphs are presented



for the nominally isotropically reinforced elements acted upon by torsional moments with lever arm values of 11.25in and 17.5in. Results from specimen TB31, which was a repeat test of TB7, have been presented in the same figure as results from TB7.

For specimens with a nominal  $\mu$  value of 0.5 the principal curvature and principal concrete strain plots for each torsional lever arm value have been presented in four figures to avoid confusion. Six slab elements were tested under each of the three torsional lever arm values and thus for  $T_a = 3$ in, TB10, TB11 and TB12 have been represented together and TB13, TB14 and TB25 ( $\beta = 135^\circ$ ) have been represented together. The results from the other twelve specimens with  $\mu = 0.5$  have been presented in a similar manner.

The minimum principal curvature values and minimum (tensile) principal concrete strain values have been tabulated for each slab and presented with the figures as have the steel strains.

Plates illustrating the crack formation at failure and diagrams showing the positions of each steel strain gauge are presented for each specimen. The order of presentation is therefore arranged in section 5.3.4 so that the plates precede the individual graphs of load v.  $\tan 2\theta$  etc. associated with the combined graphs for any particular torsion arm value.

Tables of results for the relevant specimens follow each of the associated individual principal direction graphs and finally the combined figures showing principal curvature and principal concrete strains for those particular slab elements are presented.

From the figures and tables in this section it is possible to find the moment, curvature and concrete strains in any direction on the slab.

### 5.3.3 Presentation of steel strain observations

Steel strains have been presented in tabular form in section 5.3.4 for this series as a complete plot would be required for each slab element if an unconfused diagrammatic representation was to be made. The other figures describing curvatures and concrete strains indicate the general behaviour of the slabs sufficiently clearly so that steel strain plots have only been illustrated for typical examples of specimens. Fig 5.73 - Fig 5.82 show the strain gauge positions relative to the reinforcement mesh for all the various angles of mesh. The numbers of gauges in these figures correspond to the gauge numbers indicated in the tables showing steel strains and can be compared directly for any given mesh angle with varying bending and twisting moment ratios. As a typical example of steel strain comparison all specimens with mesh angle  $\beta = 0$  for both  $\mu = 1.0$  and  $0.5$  have been represented by one particular gauge in the lower (main steel) layer or

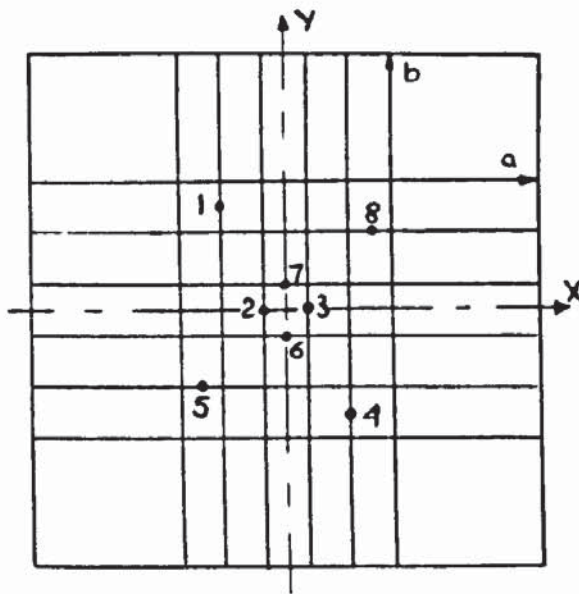


FIG 5.73  $\mu=1, \beta=0^\circ$

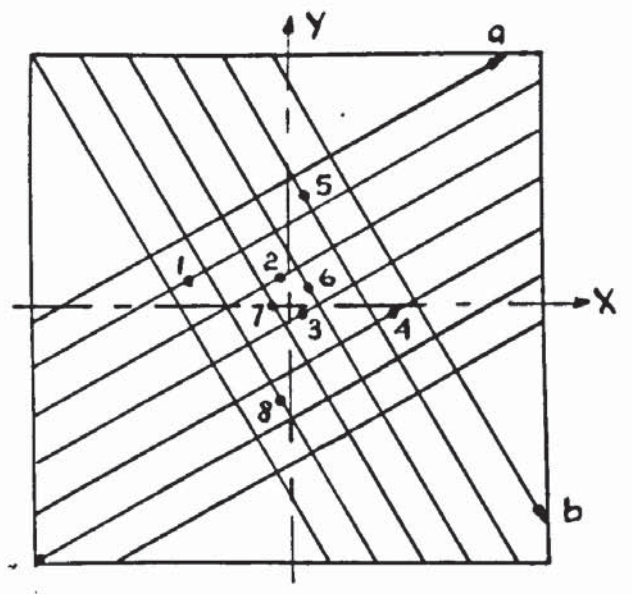


FIG 5.74  $\mu=1, \beta=30^\circ$

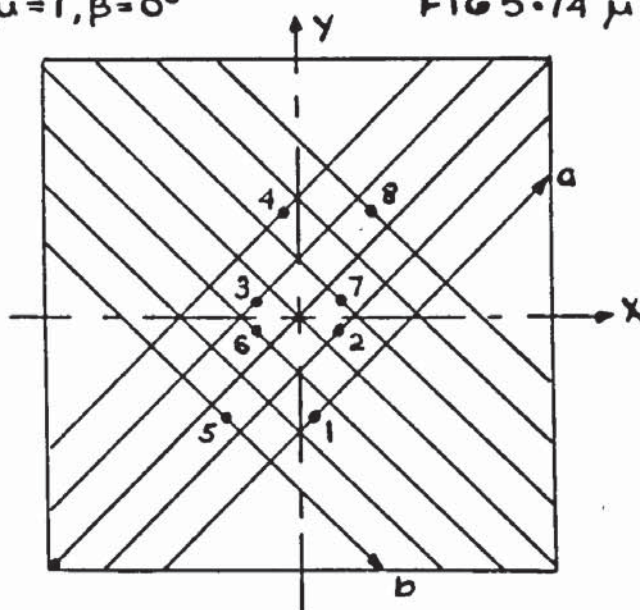


FIG 5.75  $\mu=1, \beta=45^\circ$

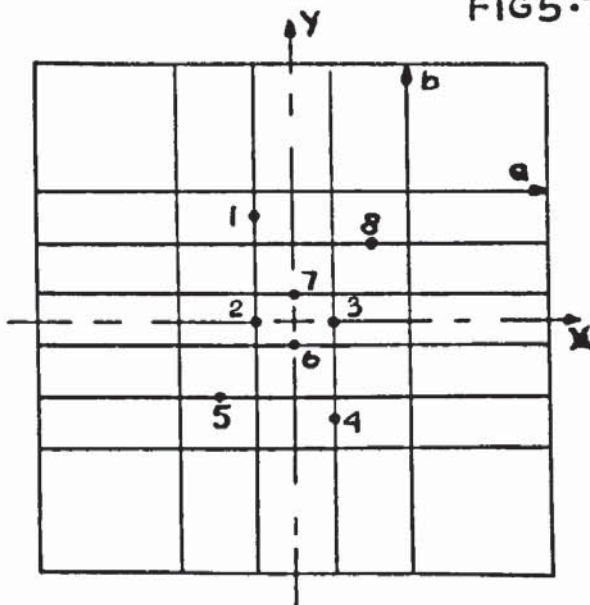


FIG 5.77  $\mu=0.5, \beta=0^\circ$

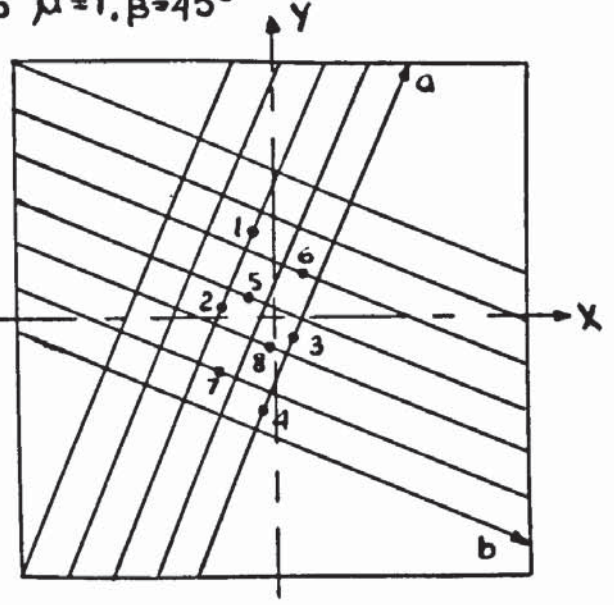


FIG 5.76  $\mu=1, \beta=67.5^\circ$

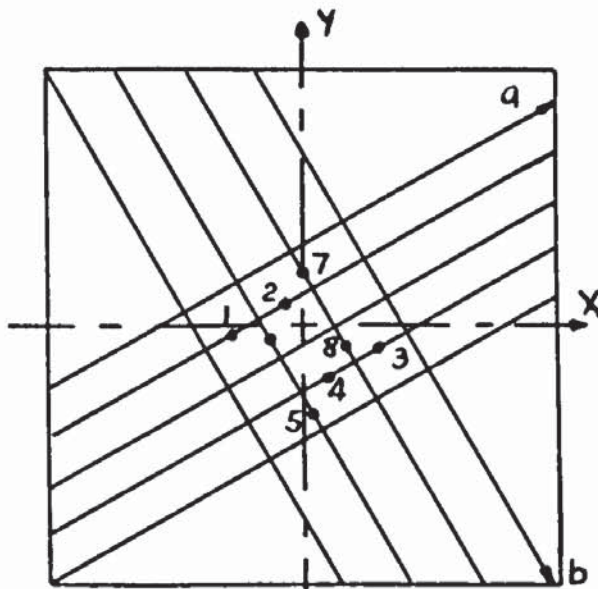


FIG 5.78  $\mu=0.5, \beta=30^\circ$

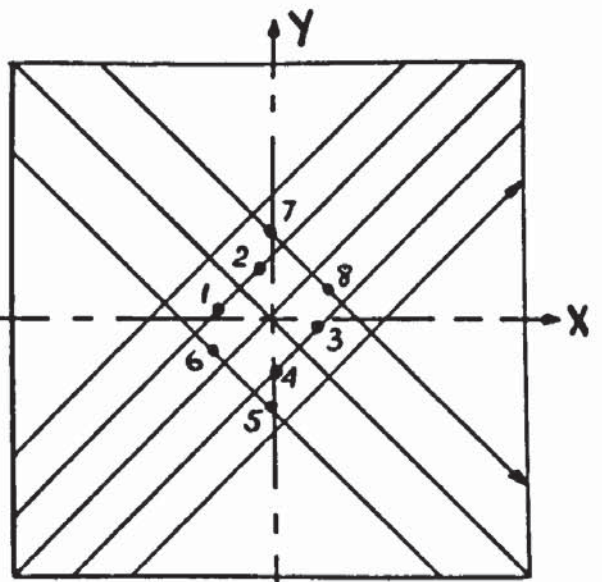


FIG 5.79  $\mu=0.5, \beta=45^\circ$

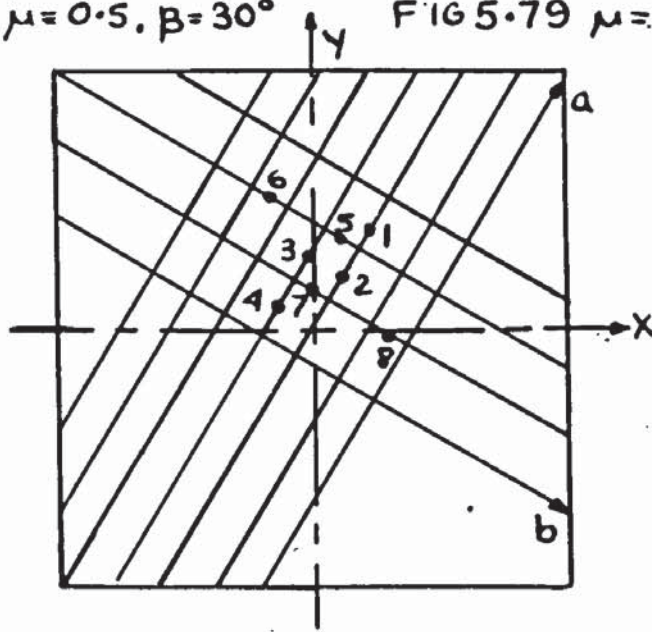


FIG 5.80  $\mu=0.5, \beta=60^\circ$

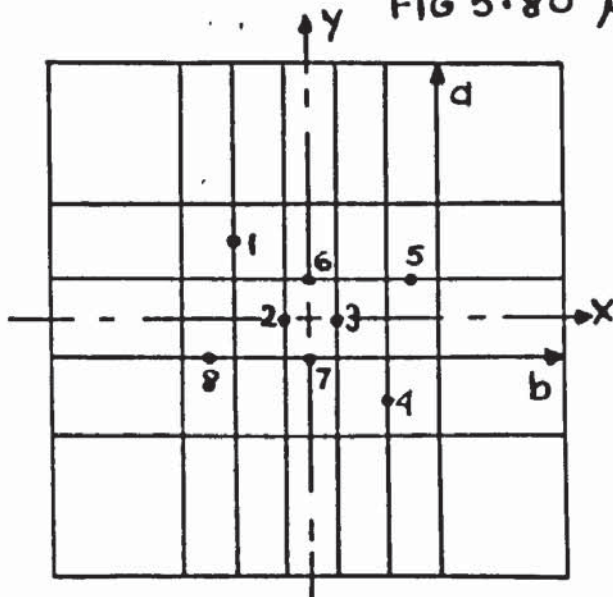


FIG 5.81  $\mu=0.5, \beta=90^\circ$

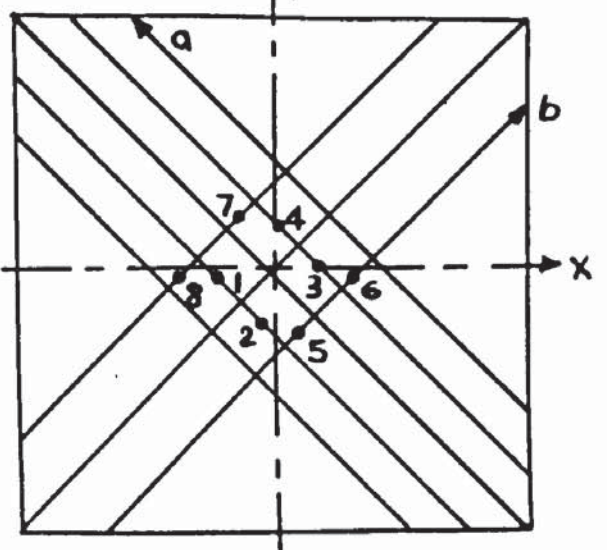


FIG 5.82  $\mu=0.5, \beta=135^\circ$

a - direction and one gauge in the upper layer or b - direction. Figs 5.83 - 5.86 show the plots of load  $W$  against the steel strain in both sets of bars for these slab elements with  $\beta = 0$ . Fig 5.83 shows the strains measured by gauge no. 7 which, as Fig 5.73 shows, was positioned near the centre of the element on the lower layer of reinforcement for the relevant isotropically reinforced slabs. In this case, in which the a - direction or lower bar layer direction coincides with the X - direction a direct comparison of the strains can be made for each torsional lever arm. The bending moment  $M_x$  acting in the bar direction is proportional to the load  $W$  as shown in equation (5.1) and thus the differences in the characteristics of the plots reflect the higher principal moment value for a given load  $W$  as indicated in Fig 5.70 for larger torsional lever arms.

The average yield strain of 1370 microstrains obtained from tensile tests on the steel as described in section 4.2.5 has been plotted on each graph and it can be seen that full plasticity of the element did not occur at this strain in the case of specimens TB4 and TB7 in which the yield lines are formed so that both sets of bars are playing a significant part in resisting applied moments. In the case of specimen TB1 however in which the angle of the yield line to the X - direction is close to  $90^\circ$  it can be seen from Fig 5.83 and Fig 5.84, which shows plots of b - direction or upper

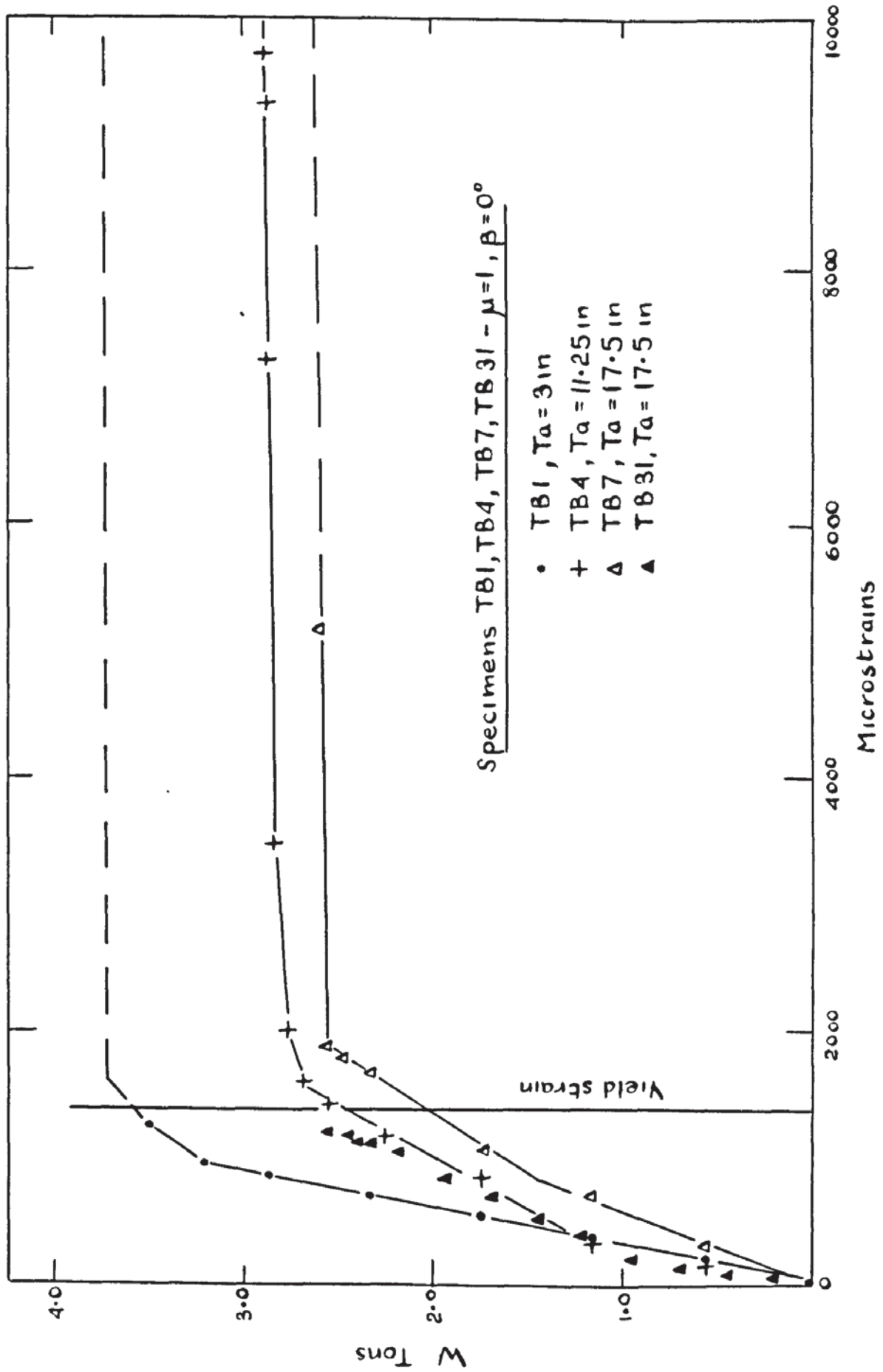


FIG 5-83 LOWER LAYER STEEL STRAINS - Gauge No 7,  $\mu=1, \beta=0^\circ$

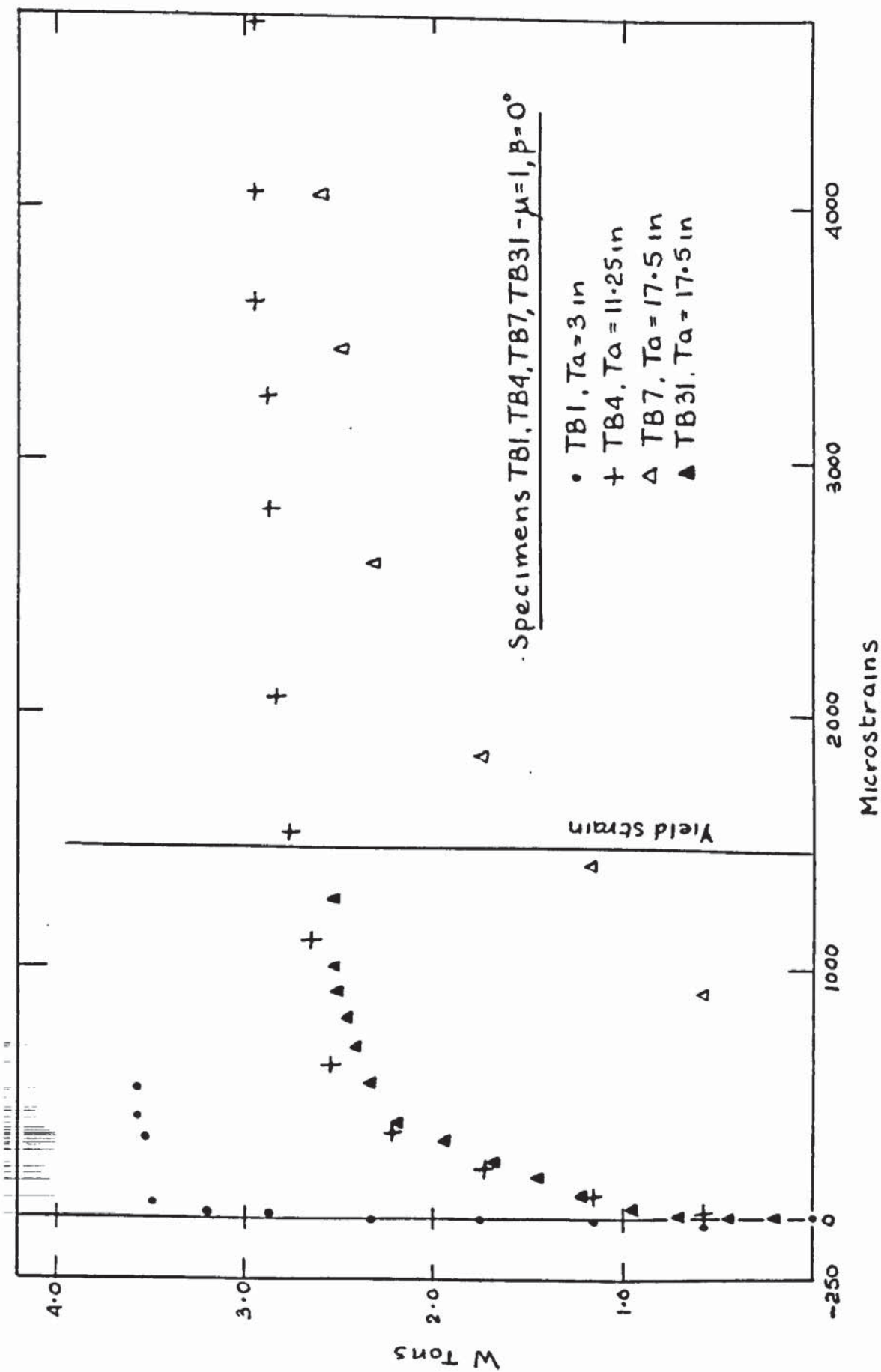


FIG 5.84 UPPER LAYER STEEL STRAINS - Gauge No. 3,  $\mu=1, \beta=0^\circ$

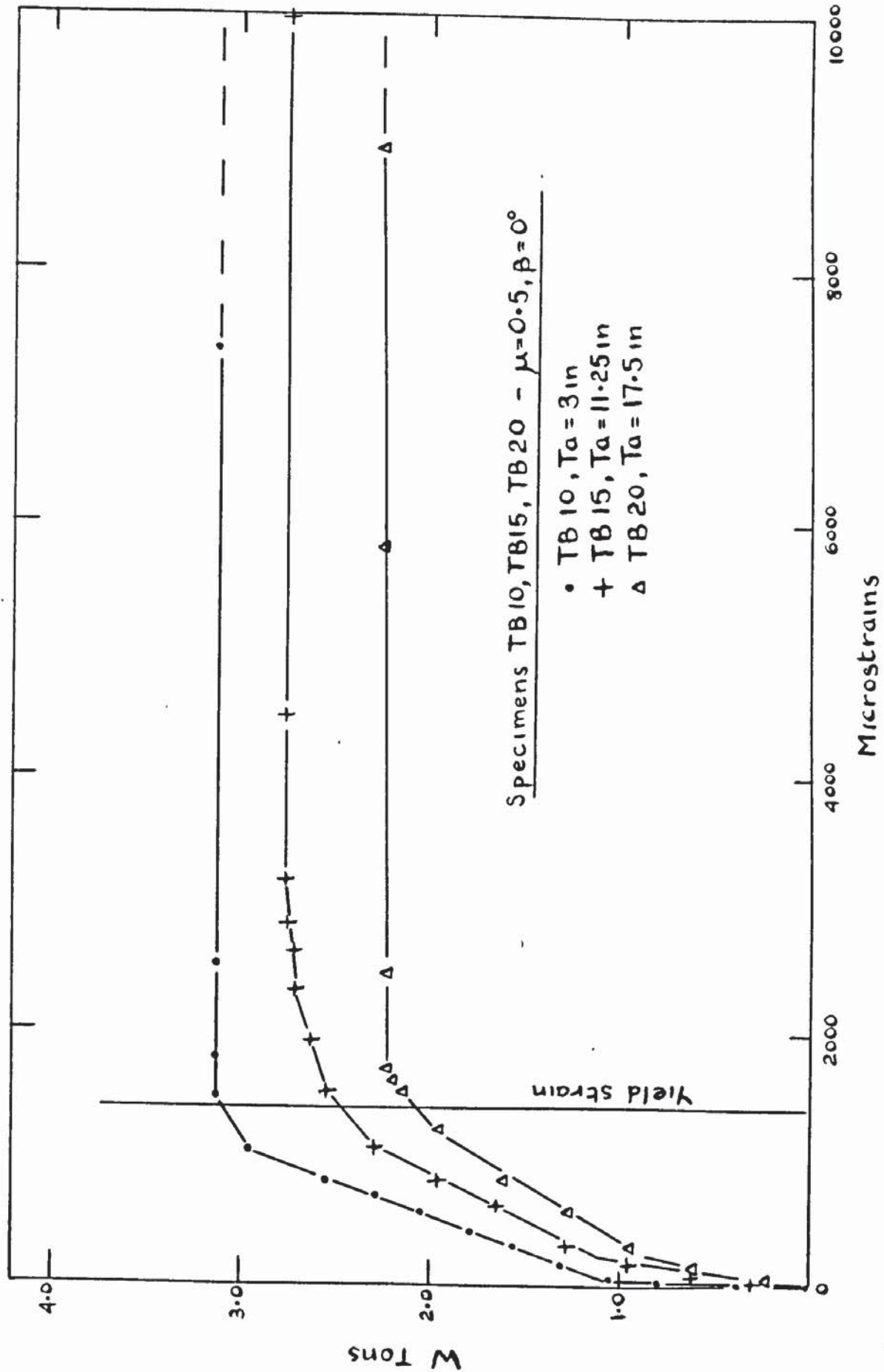


FIG 5.85 LOWER LAYER STEEL STRAINS - Gauge No 6,  $\mu=0.5, \beta=0^\circ$

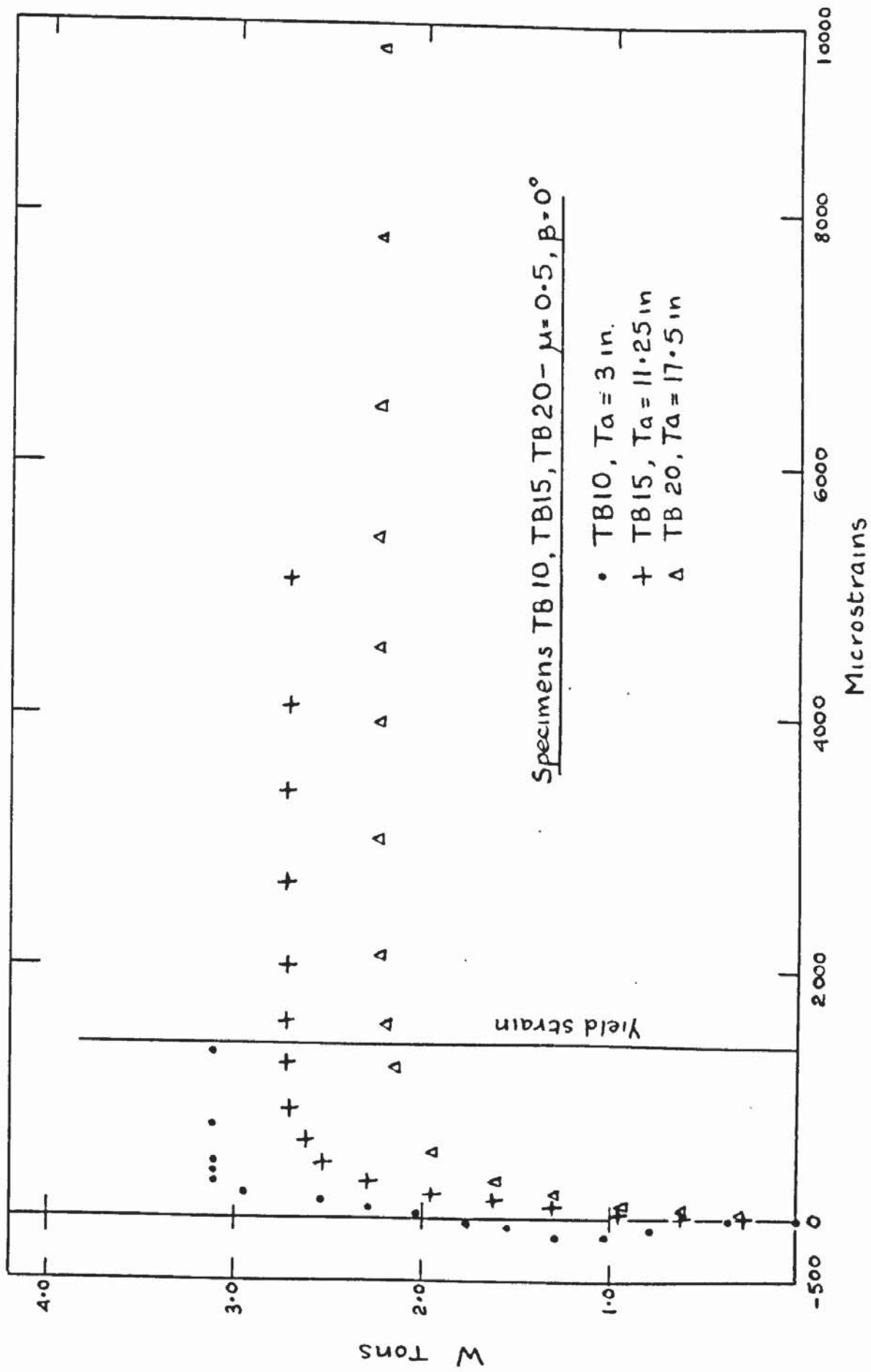


FIG 5-86 UPPER LAYER STEEL STRAINS - Gauge No. 3,  $\mu = 0.5, \beta = 0^\circ$

layer steel strains, that yield of the lower bars occurred at about 1370 microstrains and very little increase in load occurred after this point. The upper layer bars did not reach the yield strain as they were not acting across the yield line.

It must be remembered that these strain plots cannot be interpreted directly as stress-strain characteristics. Because the yield load is reached and therefore remains fairly constant it cannot be said that yield of any particular bar has occurred. The only measure of yield that can be applied is the exceeding of the average yield strain of any gauge point. Fig 5.85 and 5.86 show steel strain plots for the specimens with  $\mu = 0.5$  and  $\beta = 0$ . Similar behaviour is evident in this case. TB10 ( $T_a = 3\text{in}$ ) exhibits the same characteristics as TB1 with the b - direction steel not reaching the yield strain whereas the strain plot for TB15 ( $T_a = 11.25\text{in}$ ) in Fig 5.85 shows considerable evidence of restrained plastic flow after the yield strain was reached in the lower layer bar. The bars in this layer reached yield at a load, W of about 2.45 tons from Fig 5.85 whereas by inspection of Fig 5.86 it can be said that the strains in the transverse direction were still below the yield strain at this load. It can be seen that bars in this upper layer reached yield at about 2.74 tons whereupon unrestricted plastic flow occurred as indicated by both Fig 5.85 and 5.86.

A similar phenomenon can be seen to have occurred in the case of TB20 ( $T_a = 17.5\text{in}$ ) although the load differences between lower and upper layer yield were not so great.

Evidence of the difficulty resulting in the comparison of strains at a particular point due to the critical influence of the exact position of a crack or yield line relative to it occurs in Fig 5.83 and 5.84 where for the same gauge the plots of TB7 and TB31, which were duplicate tests, are significantly different.

Some gauges failed due to breakdown of insulation or excess strain and dashes in the relevant tables in section 5.3.4 signify the failure of a gauge.

#### 5.3.4 Description of Individual Tests and presentation of objective observations

##### a) Isotropically reinforced slab elements

TB1,  $\mu = 1$ ,  $\beta = 0^\circ$ ,  $T_a = 3\text{in}$ .

In this first test which was the nearest to a normal bending test on a slab with longitudinal reinforcement the first cracks appeared at a proving ring load of 1.16 tons and it can be seen from Fig 5.87 that at this load the principal concrete strain and principal curvature directions varied from the principal moment direction by approximately  $-3^\circ$  and  $+2^\circ$  respectively. As loading proceeded towards failure it can be seen that the principal concrete strain direction remained at a fairly constant value and at failure

was very close to the average measured crack angle  $\psi$ , varying from the principal moment direction by an angle of about  $-4^{\circ}$ . The principal curvature direction however is seen to exceed the principal moment direction by an angle of about  $2.5^{\circ}$  at failure. Although these values may be small they may be explained by the mode of failure of the specimen. Plate 5.22 shows the crack pattern at failure and it may be noticed that although the angles of the cracks to the Y - direction are of the order of  $8.5^{\circ}$  the main yield line is almost perpendicular to the X - direction and in fact ran along a reinforcing bar in the transverse direction. This yield line lay outside the central test area and may have been influenced by stress concentrations near the clamps. Thus the curvature measurements were taken within the central area where cracks averaged an angle of  $8.5^{\circ}$  to the Y -axis. The average angle of the crushing lines was however  $5.25^{\circ}$  which corresponds closely to the final value of  $5.6^{\circ}$  from Fig 5.87. The occurrence of cracks of obviously varying angles in which one only may lead to failure will be dealt with more fully in Chapter 7 where the strengths, stiffnesses and general slab behaviour are dealt with in a more comparative and analytical manner.

Figs 5.91 and 5.92 show the plots of maximum principal curvature and maximum principal concrete strain respectively. Loading was ceased at a curvature of around  $73\text{in}^{-1}\times 10^3$  which

corresponded to an average principal concrete strain of 2,500 microstrains. The values of curvature and concrete strain indicated in Fig 5.91 and 5.92 which correspond to specimens tested under a torsional lever arm of 3in. were smaller than expected and were due to the fact that in many cases in which  $Ta = 3in$ , although yield took place, a certain amount of rotational instability occurred because of the inherently unstable loading condition when the reactions and loading points lay very nearly in a straight line.

Table 5.18 shows the tensile principal concrete strains and curvatures and steel strains associated with the specimen.

TB2,  $\mu = 1$ ,  $\beta = 30^\circ$ ,  $Ta = 3in$

In the first slab with inclined reinforcement cracking again appeared to take place at a load of 1.16 tons. However Fig 5.91 and 5.92 indicate cracking, by the first slope change, at about 0.7 tons. Cracks were fairly evenly spaced at about 3in. centres. Fig 5.88 showing the plot of principal directions indicates that although the curvature and concrete strain trends appear to agree more closely than in TB1 the values of  $W$ , the principal curvature direction and  $\gamma$ , the principal strain direction exceed the value of  $\theta$ , the principal moment direction by a maximum of  $+ 4.6^\circ$  and  $+ 5.8^\circ$  respectively before yield. After yield the curvatures of  $W$  and  $\gamma$  approach closely the direction of the principal

moment. The measured angle,  $\psi$ , of the cracks however had a value of  $4.5^\circ$  less than the principal moment direction  $\theta$  which is of a similar order to that measured in TB1 and is also shown in Fig 5.88.

An important point noted in this and most other specimens was that almost all cracks began at a point where a bar met the free edge of the slab. Further reference to this behaviour is described in Chapters 6 and 7. Table 5.19 indicates the tensile principal concrete strains and curvatures and the steel strains recorded and Plate 5.23 illustrates the crack formation at failure.

TB3,  $\mu = 1$ ,  $\beta = 45^\circ$ ,  $T_a = 3\text{in.}$

In this test inaccuracies in test set up caused the loading to be discontinued at a proving ring reading of 2.24 tons as the tilting of the slab mentioned above became excessive.

The element was reset and the test carried out successfully to failure although of course the element had already cracked. Both sets of results are presented in Figs 5.89, 5.91 and 5.92. Fig 5.89 shows the plot of principal direction variation. For the first part of the test on an uncracked section the principal curvature directions appear to follow the curve describing the variation of the principal moment direction with load upto the cracking load of 0.75 tons obtained from Fig 5.91 and 5.92 as before. After this load the values of  $w$  have a slight trend away from the

principal moment curve but approximately at a constant difference of  $2.6^\circ$ . The principal concrete strain direction however does not appear to follow the principal moment curve but maintains a near constant value after cracking at a value of  $6.6^\circ$  less than  $\theta$ . Reloading in the second part of the test appears to have made the concrete strain directions and curvature directions coincide more closely although at yield the principal concrete strain direction approached closely the measured crack angle whereas the principal curvature direction approaches closely the principal moment direction. Fig 5.91 and 5.92 show that the slopes of the plots for TB2, TB3 and TB28 are very similar. Plate 5.24 shows the crack formation at failure and Table 5.20 the steel strains and tensile principal concrete strains and curvatures.

TB28,  $\mu = 1$ ,  $\beta = 67.5^\circ$ ,  $T_a = 3\text{in.}$

This slab element was tested after the main series to TB24 had been completed. It was included to ensure that assumptions made generally about symmetry in isotropic slabs were justified. Fig 5.90 shows clearly that the principal direction variations appear to be significantly different from the previous elements. The principal directions of all three variables are in close agreement up to a load of approximately 0.8 tons corresponding closely to the cracking load indicated in Figs 5.91 and 5.92. After this load the directions of both curvature and strain decrease significantly

in varying degrees. The principal curvature direction becomes positive just before yield but after yield again becomes positive and with the principal concrete strain direction converges on the measured average crack angle. This angle can be seen to vary from the principal moment direction by a value of  $-7^{\circ}$ . Plate 5.25 illustrates the crack formation and it was again noted that most cracks generated from a point at which one or more bars met the free edge. Table 5.21 indicates the tensile principal concrete strain and curvature and steel strain variation.

It is interesting to note that the measured average crack angle  $\psi$  was progressively smaller with increasing values of mesh angle  $\beta$ . Values of  $\tan 2\psi$  for TB1, TB2, TB3 and TB28 being 0.25, 0.21, 0.17 and 0.16 respectively.

TB4,  $\mu = 1$ ,  $\beta = 0^{\circ}$ ,  $T_a = 11.25\text{in.}$

This was the first slab tested under the intermediate torsion arm condition. Plate 5.26 shows the crack formation at failure. It can be seen that the cracks are very closely spaced and tend to cross into each other in places. (The cracks did not appear to all form at the same time, but over about four load increments) However, the general crack angle is indicated in Fig 5.93 as is the principal direction variation. Although in this case more scatter in results is evident the directions of both principal curvature and principal strain appear to have been close

to the principal moment direction just before yield. The principal curvature direction approached the measured crack direction closely at failure. The measured angle was approximately  $7.1^\circ$  less than the principal moment direction at failure. Fig 5.97 and 5.98, the principal curvature and strain plate respectively indicate the two-phase yielding of the reinforcement layers by the elasto-plastic characteristics just before full plasticity occurs. Table 5.22 again shows steel strains and tensile principal strains and curvatures.

TB5,  $\mu = 1$ ,  $\beta = 30^\circ$ ,  $T_a = 11.25\text{in}$

This was the first slab in which any bond effects were noticed. Failure was reached at a principal curvature of approximately  $9.5 \text{ in}^{-1} \times 10^3$  and was accompanied by a drop in the proving ring load value of 0.04 tons as indicated in Figs 5.97 and 5.98 and in Table 5.23 of steel strains and tensile principal concrete strains and curvatures. In this case it is evident from Figs 5.97 and 5.98 that the ultimate load had been reached before spalling of concrete at the slab edges caused a slight reduction in load carrying capacity. Cracking occurred between 0.5 and 0.75 tons and cracks were evenly spaced at about 3.5in. centres as indicated in Plate 5.27. Fig 5.94 shows the principal direction variations. The directions of principal curvature and principal strain appear to follow similar parallel curves gradually increasing up to failure at which both values closely approach the

measured crack angle which was at an angle of  $6.4^{\circ}$  less than the principal moment direction to the  $\bar{x}$  - direction.

$$\underline{\text{TB6, } \mu = 1, \beta = 45^{\circ}, T_a = 11.25\text{in}}$$

Fig 5.95 illustrating the principal direction variation shows the similarity to TB5. In this case the principal curvature direction plot particularly indicates a decreasing angle trend up to yield where the value of  $\tan 2 \omega$  coincides with the measured crack angle which can be seen to differ from the principal moment direction by an angle of  $-14.6^{\circ}$ . After yield however the directions of both principal curvature and strain increased towards the principal moment value at failure. It can be seen in Figs 5.97 and 5.98 that the load sustained by this element exceeded that of TB5 and Fig 5.98 particularly indicates the smaller slope of the characteristic in the post-cracking - pre-yield range. Plate 5.28 illustrates the way that the crack spacing was not so constant in this specimen.

$$\underline{\text{TB29, } \mu = 1, \beta = 67.5^{\circ}, T_a = 11.25\text{in}}$$

Unlike TB28 there was no tendency for the values of  $\tan 2 \gamma$  to reduce after cracking. Fig 5.96 illustrates the differences in principal strain and principal curvature values before cracking at about 0.75 tons. The principal curvature values followed the principal moment curve closely to cracking whereupon the direction reduced to a value close to the principal strain direction. The plots of both strain

and curvature agree closely up to failure, the directions remaining fairly constant. The value of  $\omega$  and  $\gamma$  indicate a difference of about  $2.5^\circ$  with the measured crack angle. Plate 5.29 illustrates the crack formation. In fact the predominant crack only cross the lower layer bars. Table 5.25 and Figs 5.97 and 5.98 show the fall off in load which could indicate a bond failure after considerable plastic yield.

TB7,  $\mu = 1$ ,  $\beta = 0^\circ$ ,  $T_a = 17.5\text{in.}$

TB7 showed high ductility up to failure, the principal curvature of ultimate moment being  $12.5 \text{ in}^{-1} \times 10^3$ . Plate 5.30 shows up this twist at failure. Plate 5.31 illustrates the fine spacing of cracks, no particular yield crack appearing to have dominated the failure mode. Fig 5.104 and 5.105 clearly indicates the range in which the main set of reinforcement bars in the a - direction had reached yield before the upper layer of bars. Fig 5.99 shows how the values of  $\tan 2\gamma$  and  $\tan 2\omega$  although not following the principal moment curve exactly increased up to a point which corresponds to first yield, whereupon the curvature direction plot decreases towards the measured crack angle whereas the strain direction plot increases and at failure exceeds the principal moment direction by  $2.6^\circ$ . Table 5.26 shows the variation of steel strains and tensile principal concrete strains and curvatures with load.

TB8,  $\mu = 1$ ,  $\beta = 30^\circ$ ,  $T_a = 17.5\text{in.}$

Again as Plate 5.32 illustrates the cracks were finely spaced, none predominating in the failure mode. Fig 5.100 shows the similarity in behaviour between this specimen and TB7 in relation to the principal direction characteristics. Fig 5.104 and Fig 5.105 clearly shows the elasto-plastic range between the yield of each sets of bars and the difference in slope of the curve to that of TB7. Table 5.27 again shows steel strains and tensile principal concrete strains and curvatures against load.

TB9,  $\mu = 1$ ,  $\beta = 45^\circ$ ,  $T_a = 17.5\text{in.}$

Fig 5.101 again shows the tendency for the curvature direction plot to approach the measured crack angle after yield although in this case it increased to that value after remaining fairly constant up to yield. The concrete strain direction plot also indicates a constant value after cracking and up to yield after which the direction again increased. The difference between the principal concrete strain direction and principal curvature direction before yield was  $8.6^\circ$ . Fig 5.104 and 5.105 show the increase in load capacity over TB8 and the slope difference. Plate 5.33 indicates the crack formation in which one yield line predominated after fairly evenly spaced cracks had previously developed.

TB30,  $\mu = 1$ ,  $\beta = 67.5^\circ$ ,  $T_a = 17.5$ in.

In this case the plots of  $\tan 2\gamma$  and  $\tan 2\omega$  agreed more closely as illustrated in Fig 5.102. After yield both curvature and strain direction increase away from the measured crack angle. Again as Plate 5.34 illustrates there was a tendency for one yield line to predominate after yield and the drop in load at high curvature may indicate a certain amount of bond failure well after yield as indicated in Fig 5.104 and 5.105 and Table 5.29.

TB31,  $\mu = 1$ ,  $\beta = 0^\circ$ ,  $T_a = 17.5^\circ$

This test was a repeat of TB7. Fig 5.104 and 5.105 show the close agreement between the two plots. Fig 5.103 again indicated the manner in which the principal concrete strain direction and principal curvature direction diverge after yield. The values of  $\tan 2\gamma$  and  $\tan 2\omega$  remained close to  $\tan 2\theta$  up to yield. Plate 5.35 indicates the crack formation at yield as as before the steel strain and tensile principal concrete strain and curvature values are presented in Table 5.30.

b) Non isotropically reinforced slab elements

TB10,  $\mu = 0.5$ ,  $\beta = 0^\circ$ ,  $T_a = 3$ in.

The first of the non isotropically reinforced slab elements was also the first specimen to show evidence of an increased crack angle over the principal moment direction at failure. Fig 5.106 shows the value of  $\tan 2\omega$  to have

coincided with the measured crack angle just before yield whilst the principal strain direction, which had lagged behind the principal curvature direction approached the measured crack angle after yield. The difference between measured crack angle  $\psi$  and  $\theta$ , the principal moment direction was only of the order of  $1.8^\circ$ . Plate 5.36 illustrates the crack formation and it was clear that unlike TB1 the yield line crossed both sets of bars. This behaviour is endorsed by the elasto-plastic range indicated in Fig 5.109 and 5.110.

TB11,  $\mu = 0.5$ ,  $\beta = 30^\circ$ ,  $Ta = 3in.$

Fig 5.107 shows a greater increase in measured crack angle over principal moment direction, although the values of  $\gamma$  remained fairly constant after yield whilst the principal curvature direction increased up to the measured value. The measured crack angle exceeded the principal moment value by  $8.5^\circ$ . Fig 5.109 and 5.110 illustrate the clear difference in slope of the curves between cracking and yielding Plate 5.37 shows the crack formation and indicates that one yield line predominated at failure.

TB12,  $\mu = 0.5$ ,  $\beta = 45^\circ$ ,  $Ta = 3in.$

Again the measured crack angle exceeded the principal moment direction by about  $9^\circ$  at failure as indicated in Fig 5.108 The values of  $\gamma$  and  $\omega$  appear to have been close to  $\theta$  up to

yield. Loading was dropped at a value of 1.86 tons, after yield, as the slab element was fouling one of the dial gauges. However on reloading the same yield value of 1.86 tons was attained. Fig 5.109 and 5.110 again shows clearly the progressive slope change between TB10, 11 and 12. Plate 5.38 shows the crack formation at failure.

TB13,  $\mu = 0.5$ ,  $\beta = 60^\circ$ ,  $T_a = 3\text{in.}$

This was the first specimen in which any evidence of the yield lines or cracks following the bar directions in a 'stepped' manner. Plate 5.39 illustrates this tendency occurring on one main yield line. Fig 5.111 indicates the difference in plots of principal directions as compared to those of TB. 10, 11, and 12. The general measured crack direction exceeded the principal moment direction by only  $1.8^\circ$  and it can be seen in Fig 5.111 that the principal directions of both strain and curvature reduced after cracking and upto yield whereupon the values increase up to the measured crack angle value as indicated in Figs 5.114 and 5.115. Cracking occurred at a value of 0.45 tons which was significantly lower than that indicated in Figs 5.109 and 5.110 of 0.75 tons.

TB14,  $\mu = 0.5$ ,  $\beta = 90^\circ$ ,  $T_a = 3\text{in.}$

In this specimen as indicated in Fig 5.112 the measured crack angle and plots of principal directions were less than the value of  $\theta$  at failure. The principal moment

direction,  $\theta$ , exceeds the measured crack angle by  $3^\circ$ . Plate 5.40 shows the crack formation at failure. Fig 5.114 and 5.115 show the high ductility of the specimen before failure. Crushing of the concrete took place at a principal curvature value of  $13.8 \text{ in}^{-1} \times 10^3$  and an idea of this curvature can be seen in the side view shown in Plate 5.41.

TB25,  $\mu = 0.5$ ,  $\beta = 135^\circ$ ,  $T_a = 3 \text{ in}$

The plots of principal directions in Fig 5.113A and 5.113B show the considerable difference in values of  $\theta$ , and  $\omega$ . The values of both principal strain and principal curvature directions reduce from positive to negative values of angle at failure. The measured crack angle was  $11.7^\circ$  less than the principal moment direction. Plate 5.41 illustrates the low angle of the crack formation. Fig 5.114 and 5.115 shows increased load capacity as compared to TB13 and TB14.

TB15,  $\mu = 0.5$ ,  $\beta = 0^\circ$ ,  $T_a = 11.25 \text{ in}$ .

Plate 5.43 illustrates the crack formation at failure. Cracks were evenly spaced at about 3in centres and yield involved both sets of bars as Fig 5.119 and 5.120 indicate by the progressive delineation of the elastic region before full plastic flow. From these figures first cracking took place at 0.6 tons. Fig 5.116 shows the variation of  $\gamma$ ,  $\omega$  and  $\theta$  with load  $W$ . The plots of principal strain and curvature directions run parallel to one another up to first yield where the directions increased resulting

in final curvature values  $2.8^{\circ}$  in excess of the principal moment direction at failure. The measured average crack angle however lay very close to the principal moment value at failure.

TB16,  $\mu = 0.5$ ,  $\beta = 30^{\circ}$ ,  $T_a = 11.25\text{in}$

Again values of  $\gamma$  and  $\omega$  gave a plot which leaves the principal curve and shows considerable increase after yield, approaching the measured crack angle closely at failure. Fig 5.117 illustrates these trends. It is interesting to note the differences in characteristic between Fig 5.119 and Fig 5.120 when the plots of TB16 and TB17 are compared. The slopes during the cracked elastic range are reversed in Fig 5.120. Plate 5.44 shows the crack formation at failure and the spalling of concrete near one edge of the slab. This spalling probably caused a certain amount of bond failure and this effect is endorsed by the load drop at failure indicated in Fig 5.120.

TB17,  $\mu = 0.5$ ,  $\beta = 45^{\circ}$ ,  $T_a = 11.25\text{in}$

As in TB13 there was definite evidence of 'stepping' in the main yield line, the crack following the lower bars at certain points in the element. Plate 5.45 illustrates this phenomenon and also shows the other smaller cracks adjacent to the main yield line. Fig 5.118 shows the difference in principal curvature direction as compared to the principal strain direction. The curvature values reduce after cracking and up to yield whereupon they increase

towards the measured crack angle. The differences between Fig 5.119 and Fig 5.120 may be due to the stepping of the yield lines.

TB18,  $\mu = 0.5$ ,  $\beta = 60^\circ$ ,  $T_a = 11.25$  in.

Again evidence of the yield lines having followed the bars was noticed as illustrated in Plate 5.46. The yield load was low as compared to other specimens described previously. Fig 5.121 shows the similarity between the characteristics of this specimen and TB17 although the final direction of curvature, strain and measured angle were considerably less than the principal moment direction. Fig 5.124 and 5.125 show the low slope of the plot during the cracked - elastic range.

TB19,  $\mu = 0.5$ ,  $\beta = 90^\circ$ ,  $T_a = 11.25$  in

Plate 5.47 illustrates the manner in which the yield lines tended to follow the line of two transverse bars just outside of the central gauged area. However the plate also shows the other cracks generating from the two mentioned above and traversing the specimen at an angle. Fig 5.122 shows the plots of principal directions and the measured crack angle which was  $10.1^\circ$  less than the principal moment direction. Figs 5.124 and 5.125 show the principal curvature and principal strain plots.

TB26,  $\mu = 0.5$ ,  $\beta = 135^\circ$ ,  $T_a = 11.25$  in

As the plot of principal directions in Fig 5.123 and

Plate 5.48 illustrate the principal directions and cracks were at a low angle. The measured crack angle was  $21.7^{\circ}$  less than the principal moment direction. The high curvatures at failure indicated in Fig 5.124 caused excessive cracking and consequent spalling at the edges. This resulted as before in a load drop at failure but the ultimate moment appears to have already been reached. Because of the manner in which bars in both layers met at the edge a shear crack formed causing the spalling mentioned, but not significantly affecting the ultimate moment.

TB20,  $\mu = 0.5$ ,  $\beta = 0^{\circ}$ ,  $T_a = 3\text{in}$

Plate 5.49 shows the finely spaced, evenly sloped crack formation. Fig 5.126 illustrates the manner in which the principal curvature values followed closely the principal moment curve, whereas the principal strain direction remained at a smaller angle from cracking. Both curvature and strain directions reduced after yield. The measured crack angle was close to the principal moment value at failure. Again the gradual flattening of the curve in Fig 5.129 and 5.130 indicates the two stage yielding of the two bar layers. The high curvature at failure of  $16 \text{ in}^{-1} \times 10^3$  indicates the high ductility of this specimen.

TB21,  $\mu = 0.5$ ,  $\beta = 30^{\circ}$ ,  $T_a = 17.5\text{in}$

There was definite evidence in this specimen that the crack direction changed at different stages of the test.

Plate 5.50 shows the main yield line crossing smaller cracks at an angle and a tendency to follow the bar directions in a 'stepped' manner. Fig 5.127 shows clearly the change in direction of both principal strain and principal curvature. Both measured crack angles (i.e. the smaller crack direction and the main crack direction) are indicated in Fig 5.127. The plots of  $\tan 2\gamma$  and  $\tan 2\omega$  remain fairly constant after cracking at a value close to the measured crack angle of the first formed smaller cracks. At about first yield the values of both  $\gamma$  and  $\omega$  began to increase until at yield of the second reinforcement layer they increased considerably towards the main crack direction which lay close to the principal moment direction at failure. Fig 5.129 indicates the high concentrated curvature at failure of  $12.00 \text{ in}^{-1} \times 10^3$ .

TB22,  $\mu = 0.5$ ,  $\beta = 45^\circ$ ,  $T_a = 17.5 \text{ in}$

Again as Plate 5.51 illustrates that the mode of failure in this specimen was very similar to that of TB21. The principal curvature and strain directions approached the original crack direction before yield, as shown in Fig 5.128, before the values increased up to the general crack direction of the main yield line. Plate 5.52 shows the original cracks marked in for clarity. The main yield line causing failure was again 'stepped' following the lower layer of steel as it crossed the element. It should be noted that as in the previous case rapid changes of

principal direction did not occur until yield. Fig 5.129 and 5.130 show the differences in ultimate load and slope between the three slabs TB20, 21 and 22.

$$\underline{\text{TB23, } \mu = 0.5, \beta = 60^{\circ}, \text{Ta} = 17.5^{\circ}}$$

Plate 5.53 shows that again there was significant stepping across the slab element. There was however only one main yield line at failure although other cracks had formed previously. These are marked in Plate 5.54. Fig 5.134 and Fig 5.135 indicate that first cracking took place at the low load of 0.2 tons. which corresponds closely with the point on the principal moment curve in Fig 5.131 at which the principal strain and principal curvature directions remain constant up to and after yield corresponding with the measured crack angle. This angle was  $10^{\circ}$  less than the angle of the principal moment at failure. The lack of an elasto-plastic range in Fig 5.134 and 5.135 suggests that only one or less bars in the lower bar layer took part in the failure mechanism.

$$\underline{\text{TB24, } \mu = 0.5, \beta = 90^{\circ}, \text{Ta} = 17.5\text{in}}$$

This specimen showed similarities to the behaviour of TB19 which had  $\beta = 90^{\circ}$ ,  $\text{Ta} = 11.25\text{in}$  as illustrated in Plate 5.55. Comparison of Fig 5.122 relating to TB19 and Fig 5.132 shows the similarity between the principal direction variations in the two specimens. The measured crack angle was  $9.5^{\circ}$  less than the principal moment direction at failure.

TB27,  $\mu = 0.5$ ,  $\beta = 135^\circ$ ,  $T_a = 17.5\text{in}$

Plate 5.55 shows the crack formation at failure.

As in TB26 shear affected the failure mode due to the way the bars in upper and lower layers did not meet at the slab edge. This is shown by the surface discontinuity in Plate 5.57. The crack formed in this gap between the bars and because of the lack of reinforcement at this point shear cracks developed causing spalling and consequent bond failure which is reflected in the load drop off illustrated in Figs 5.134 and 5.135. Fig 5.133 illustrates the manner in which the principal directions reduced after cracking up to the measured crack angle which was  $17.3^\circ$  less than the principal moment direction.

#### 5.4 Summary of results

As explained in the introduction the object of this chapter was to present the objective results only for each specimen tested.

In the plank test series the attempt to restrict principal strains and curvatures to the span direction was on the whole successful. Although the planks in which the reinforcement was only placed in one direction so that  $\mu = 0$  did show evidence of twisting as described in section 5.2.2 the values of principal concrete strain directions did not exceed a  $5^\circ$  variation from the span direction throughout the series.

In the general moment test series the variations in

direction of principal moment, curvature and strain throughout each range were illustrated graphically for all specimens. Although results from the pre-cracking range were not sufficiently numerous it was noticed that due to the low values of strain and deflexion in this range subsequent direction transformations were not as accurate as those in the other ranges. More sensitive instrumentation would be required to investigate the behaviour in this range thoroughly and would not be suitable for the measurement of data close to yield and at failure. However in most cases it was noted that both curvature and strain directions coincided with the direction of the applied principal moment up to a value close to cracking whereupon there was significant variation. The incidence of cracks following bars, sometimes resulting in 'stepping' of cracks between bars, was noticed in elements in which the principal moment direction was close to the bar direction. In certain cases this 'stepping' phenomenon, also referred to by Baus and Tolaccia [23] occurred after cracks had already formed at another angle to the X - direction. The behaviour of the specimens was only influenced by shear effects on the free edges in two cases where, because of the location of adjacent bars at the edge an unreinforced area occurred between them. This effect however only appeared to influence load and curvature values well after yield.

The main influence on the ultimate moment and

general behaviour of the specimens in both series was the effect of non-uniform cross-sections caused by the placing of bars. Unless specimens were made extremely large with relation to the bar diameters and subsequent spacing or the bars were made extremely fine so that the effect of bar placing was insignificant allowances must be made as both Kwiecinski<sup>[22]</sup> and Lenschow and Sozen<sup>[29]</sup> have mentioned.

These allowances are made in the following chapters (6 and 7) where the objective results presented in this chapter area analysed more fully and comparisons made between each specimen and existing hypotheses.

## KEY TO PRINCIPAL DIRECTION GRAPHS

- + Principal concrete strain direction  $\gamma$
- . Principal curvature direction  $\omega$
- Average measured yield line orientation  $\psi$
- Principal Applied Moment direction  $\theta$ .

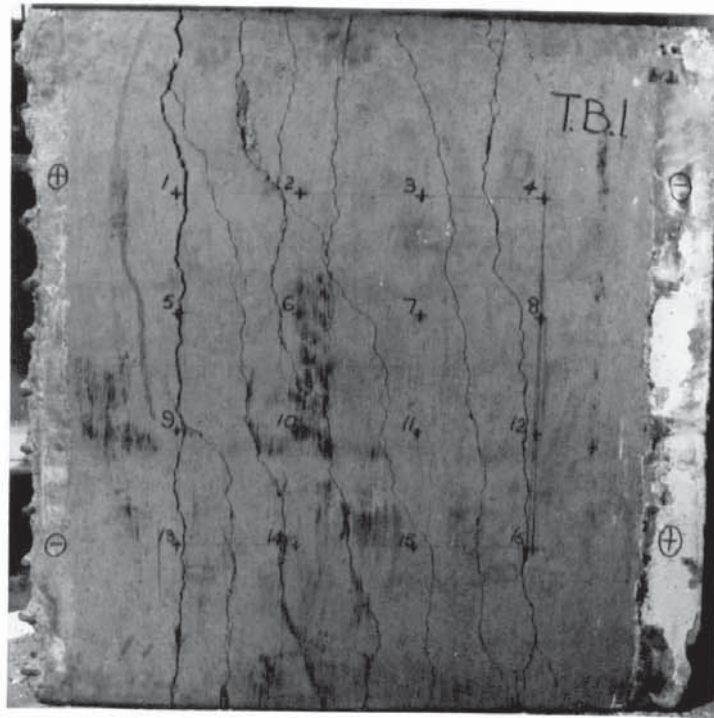


PLATE 5.22

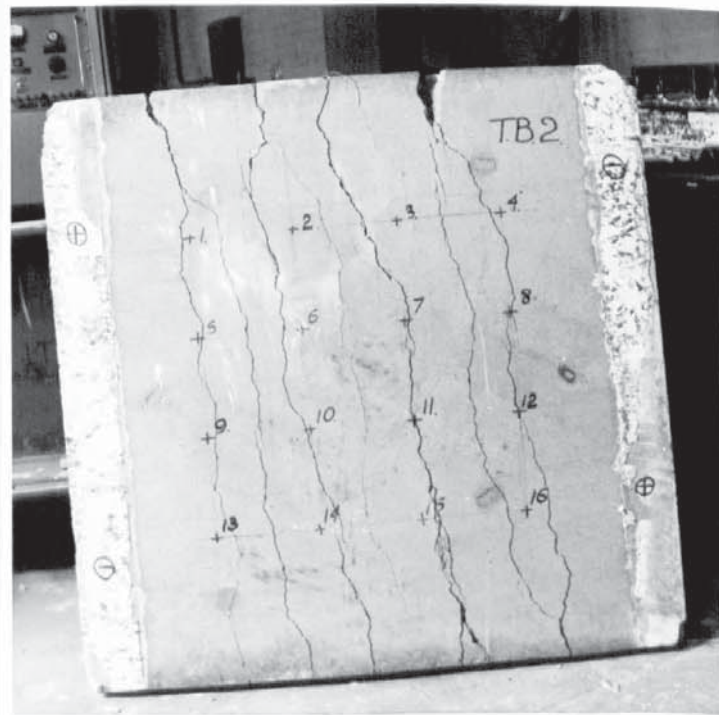


PLATE 5.23

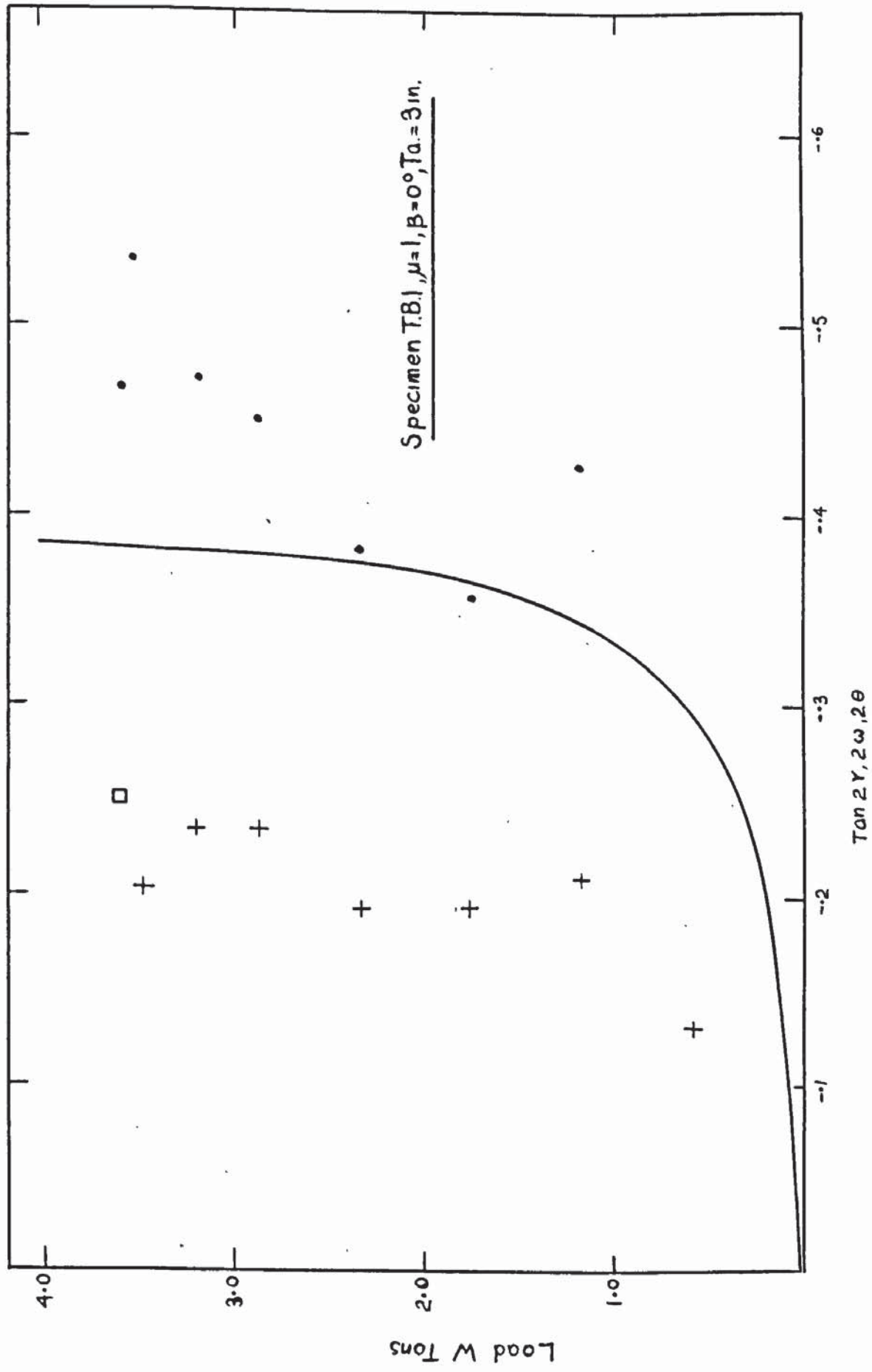


FIG. 5.87 PLOT OF PRINCIPAL DIRECTIONS - T.B.1

LOAD W TONS	MIN. PRINC. CONC. STRAIN E2	MIN. PRINC. CURVATURE K2 in <sup>-1</sup> x10 <sup>3</sup>	STEEL STRAINS MICROSTRAINS										
			1	2	3	4	5	6	7	8			
0.00	0.00	0.00	0.00	0.00	0.00	0.00	0.00	0.00	0.00	0.00	0.00	0.00	0.00
0.58	-9.38	0.0265	14.8	19.8	-29.7	-9.9	178.2	168.3	178.2	168.2	178.2	168.2	168.2
1.16	-30.66	0.0366	14.8	39.6	-19.8	0.0	336.6	336.6	346.5	336.6	346.5	336.6	336.6
1.74	-47.13	.0587	29.7	49.5	-9.9	99.0	514.9	514.9	514.9	514.9	514.9	505.0	505.0
2.32	-60.08	.0928	44.5	79.2	-9.9	29.7	633.7	683.2	693.1	683.2	693.1	633.7	633.7
2.87	-75.99	.0683	54.4	108.9	9.9	39.6	812.0	881.3	846.6	881.3	846.6	802.1	802.1
3.20	-87.39	.1043	74.2	148.5	9.9	49.5	940.7	1029.8	930.8	1029.8	930.8	930.8	930.8
3.49	-138.22	.1111	143.5	188.1	59.4	138.6	1386.3	1307.1	1208.1	1307.1	1208.1	1118.9	1118.9
3.53	-252.39	-.0075	351.5	574.3	306.9	336.6	-	1663.6	-	1663.6	-	2079.5	2079.5
3.57	-320.07	-.2273	430.7	762.4	396.1	445.6	-	2228.0	-	2228.0	-	-	-
3.57	-372.18	-.1422	480.2	-	505.0	-	-	2911.3	-	2911.3	-	-	-

Table 5.18 Minimum Principle Concrete Strains & Curvatures & Steel Strains TB.1

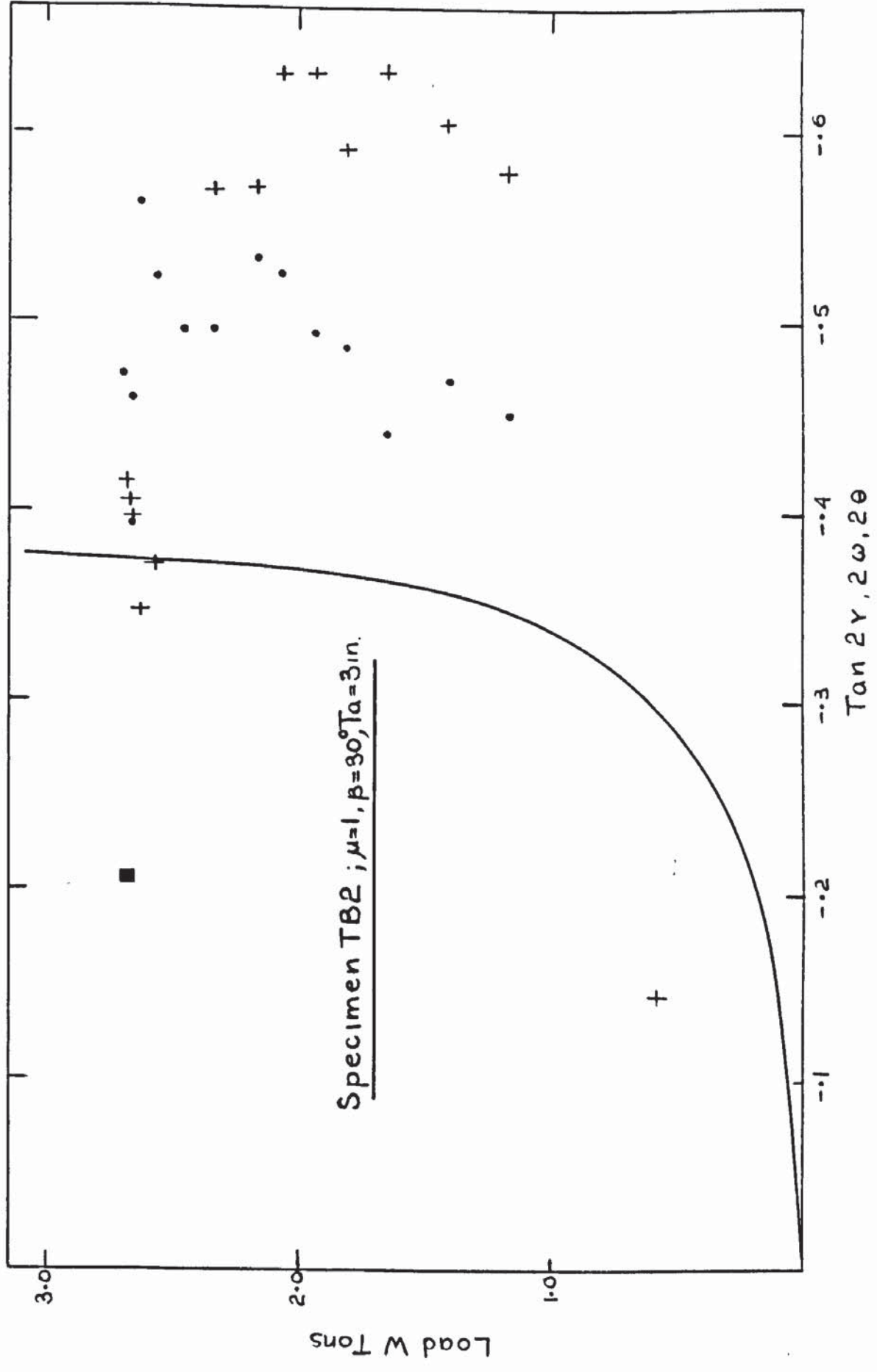


FIG 5-88 PLOT OF PRINCIPAL DIRECTIONS - T.B.2

LOAD W TONS	MIN. PRINC. CONC. STRAIN E2 μ STRAINS	MIN. PRINC. CURVATURE K2 in <sup>-1</sup> x10 <sup>3</sup>	STEEL STRAINS										
			1	2	3	4	5	6	7	8			
0.09	0.00	0.00	0.0	0.0	0.0	0.0	0.0	0.0	0.0	0.0	0.0	0.0	0.0
0.58	1.98	-.0467	-89.1	59.4	39.6	9.9	9.9	-108.9	148.5	19.0	19.0	19.0	-574.3
1.16	-18.16	-.0522	287.1	336.6	594.1	2000.2	2000.2	29.7	267.3	257.4	257.4	257.4	-396.1
1.41	-32.95	-.0089	722.8	465.4	1435.8	2703.3	2703.3	39.6	-	376.2	376.2	376.2	-287.1
1.66	-58.06	-.0126	881.3	574.3	1851.7	2980.6	2980.6	148.5	-	524.8	524.8	524.8	-158.4
1.80	-64.00	-.0309	1019.9	633.7	2198.3	3139.0	3139.0	247.5	-	584.2	584.2	584.2	-89.1
1.93	-88.39	-.0191	1109.0	703.0	2366.6	3238.1	3238.1	396.1	-	663.4	663.4	663.4	-9.9
2.06	-102.38	-.0200	1307.1	762.4	2584.5	3376.7	3376.7	485.2	-	722.8	722.8	722.8	69.3
2.17	-126.75	-.0270	1524.9	841.7	2733.0	3495.5	3495.5	623.8	-	821.9	821.9	821.9	138.6
2.33	-139.39	-.0513	1822.0	920.0	2960.8	3792.6	3792.6	752.5	-	940.7	940.7	940.7	227.7
2.45	105.08	-.0541	1901.2	940.7	3129.1	4089.7	4089.7	901.1	-	1069.4	1069.4	1069.4	336.6
2.56	100.15	-.1631	2168.6	1049.6	3257.9	4505.6	4505.6	950.6	-	1218.0	1218.0	1218.0	485.2
2.61	192.36	-.2514	2406.2	1277.4	3327.2	4832.3	4832.3	1089.2	-	1396.2	1396.2	1396.2	703.0
2.65	76.37	.0110	2901.3	1901.2	3465.8	-	-	1118.9	-	1524.9	1524.9	1524.9	891.2
2.66	53.10	.1320	3525.2	3030.1	3624.2	-	-	1178.3	-	1762.6	1762.6	1762.6	1099.1
2.67	30.72	.1537	3416.3	4337.2	3723.3	-	-	1208.1	-	1970.5	1970.5	1970.5	1188.2

Table 5.19 Minimum Principle Concrete Strains & Curvatures & Steel Strains TB.2

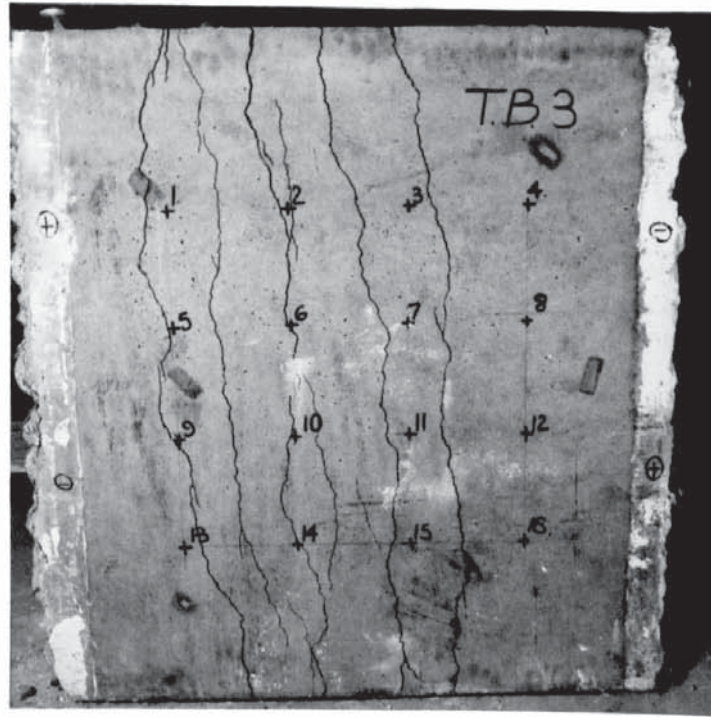


PLATE 5.24

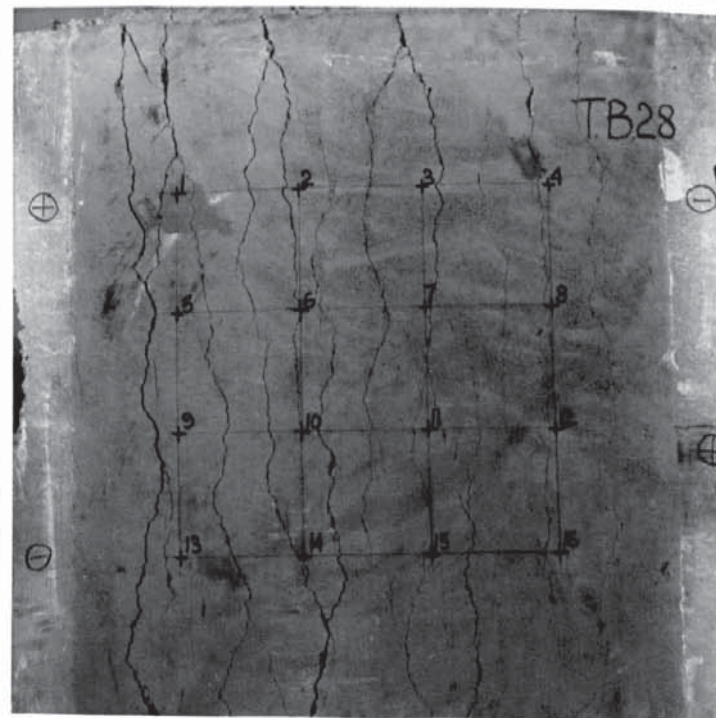


PLATE 5.25

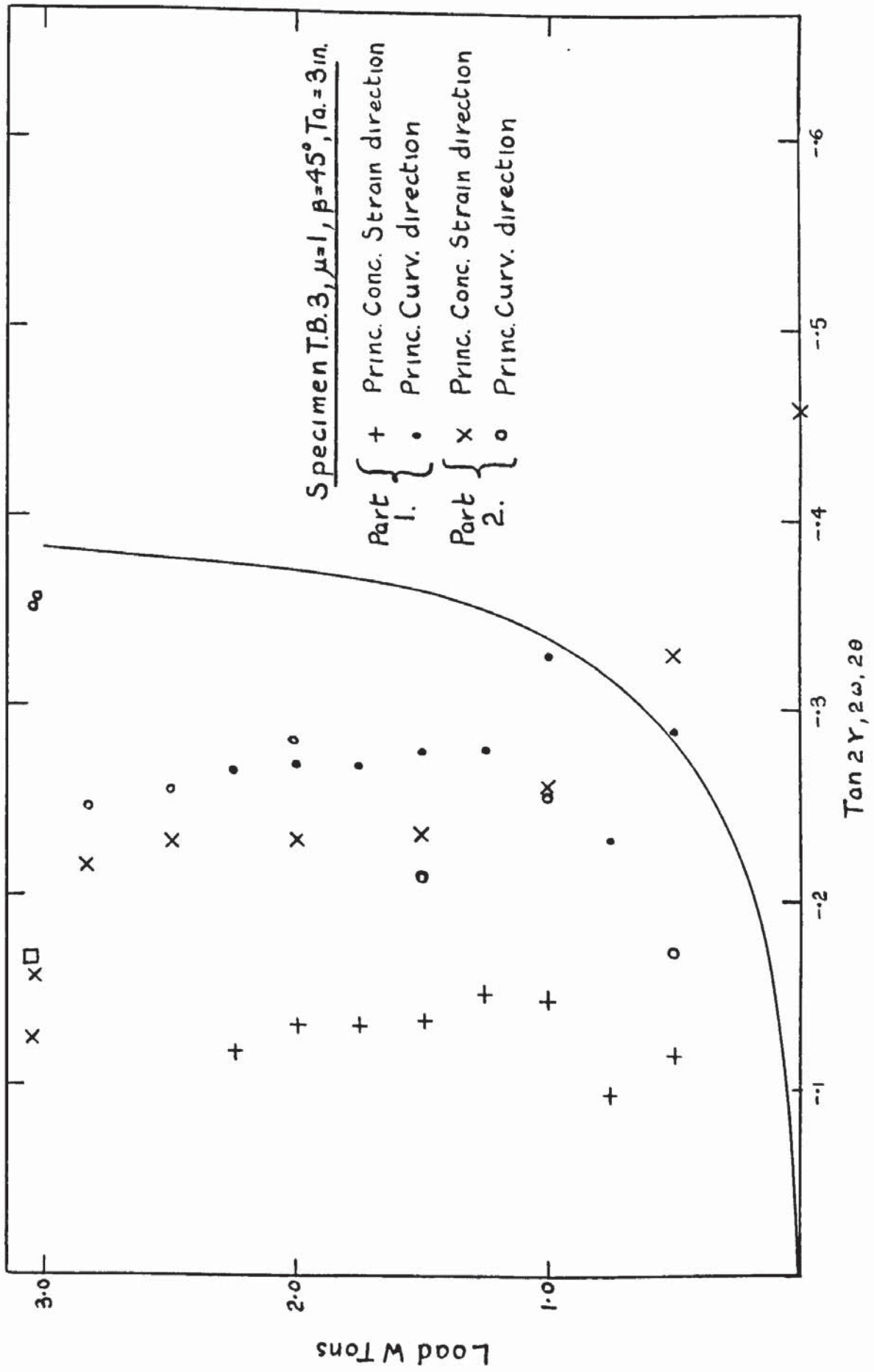


FIG. 5-89 PLOT OF PRINCIPAL DIRECTIONS - T.B.3

LOAD W TONS	MIN. PRINC. CONC. STRAIN E2 μ STRAINS	MIN. PRINC. CURVATURE K2 in <sup>-1</sup> x10 <sup>3</sup>	STEEL STRAINS																		
			1	2	3	4	5	6	7	8											
0.00	0.00	0.00	0.00	0.00	0.00	0.00	0.00	0.00	0.00	0.00	0.00	0.00	0.00	0.00	0.00	0.00	0.00	0.00	0.00		
0.25	5.32	.0137	19.80	14.85	29.71	69.32	69.32	0.00	0.00	0.00	9.90	9.90	14.85	14.85	14.85	14.85	14.85	14.85	14.85	9.90	
0.50	9.95	-.0019	39.61	29.71	44.56	69.32	69.32	19.80	19.80	19.80	24.76	24.76	29.71	29.71	29.71	29.71	29.71	29.71	29.71	29.71	29.71
0.75	9.93	-.0011	49.51	49.51	89.12	99.02	99.02	29.71	29.71	29.71	64.37	64.37	59.41	59.41	59.41	59.41	59.41	59.41	59.41	59.41	59.41
1.00	15.82	.0389	49.51	168.34	89.12	133.68	133.68	64.37	64.37	64.37	222.80	222.80	183.20	183.20	183.20	183.20	183.20	183.20	183.20	143.59	
1.25	10.78	.0214	99.02	326.78	306.98	316.88	316.88	118.83	118.83	118.83	460.46	460.46	297.07	297.07	297.07	297.07	297.07	297.07	297.07	326.78	
1.49	13.87	.0132	118.83	514.93	391.15	440.66	440.66	168.34	168.34	168.34	668.41	668.41	465.41	465.41	465.41	465.41	465.41	465.41	465.41	524.83	
1.74	14.89	.0422	247.56	653.56	475.32	564.44	564.44	198.05	198.05	198.05	826.85	826.85	584.24	584.24	584.24	584.24	584.24	584.24	584.24	727.83	
1.99	15.72	.0243	257.46	772.39	564.44	673.37	673.37	247.56	247.56	247.56	975.39	975.39	703.07	703.07	703.07	703.07	703.07	703.07	703.07	816.95	
2.24	-1.97	.0043	242.61	881.32	698.12	797.15	797.15	475.32	475.32	475.32	1114.02	1114.02	812.00	812.00	812.00	812.00	812.00	812.00	812.00	960.54	
0.00	0.00	0.00	0.00	0.00	0.00	0.00	0.00	0.00	0.00	0.00	0.00	0.00	0.00	0.00	0.00	0.00	0.00	0.00	0.00	0.00	
0.00	-4.24	0.00	599.10	475.32	415.90	445.61	445.61	613.95	613.95	613.95	628.80	628.80	415.90	415.90	415.90	415.90	415.90	415.90	415.90	574.34	
0.50	-4.44	.0056	688.22	544.63	475.32	514.93	514.93	693.17	693.17	693.17	747.63	747.63	480.27	480.27	480.27	480.27	480.27	480.27	480.27	683.27	
1.00	-4.65	.0101	792.20	693.17	594.15	633.76	633.76	871.41	871.41	871.41	960.54	960.54	638.71	638.71	638.71	638.71	638.71	638.71	638.71	881.32	
1.49	-5.14	-.0007	782.29	861.51	732.78	802.10	802.10	1069.46	1069.46	1069.46	1183.34	1183.34	802.10	802.10	802.10	802.10	802.10	802.10	802.10	1079.37	
1.99	-10.71	.0993	812.00	1000.15	851.61	930.83	930.83	1237.80	1237.80	1237.80	1381.39	1381.39	950.63	950.63	950.63	950.63	950.63	950.63	950.63	1237.80	
2.49	-18.84	.0151	1336.83	1168.49	1000.15	1109.07	1109.07	1445.76	1445.76	1445.76	1599.24	1599.24	1128.88	1128.88	1128.88	1128.88	1128.88	1128.88	1128.88	1445.76	
2.82	-17.83	-.0101	1460.61	1326.93	1158.59	1257.61	1257.61	1614.10	1614.10	1614.10	1688.37	1688.37	1297.22	1297.22	1297.22	1297.22	1297.22	1297.22	1297.22	1574.49	
3.03	-35.90	.4781	1534.88	1544.78	1782.44	1524.98	1524.98	1762.63	1762.63	1762.63	1817.10	1817.10	1406.15	1406.15	1406.15	1406.15	1406.15	1406.15	1406.15	1792.34	
3.05	-51.85	.5503	1594.29	1643.80	3455.95	1653.71	1653.71	1871.56	1871.56	1871.56	3233.15	3233.15	1425.95	1425.95	1425.95	1425.95	1425.95	1425.95	1425.95	2416.20	

Table 5.20 Minimum Principle Concrete Strains & Curvatures & Steel Strains TB.3

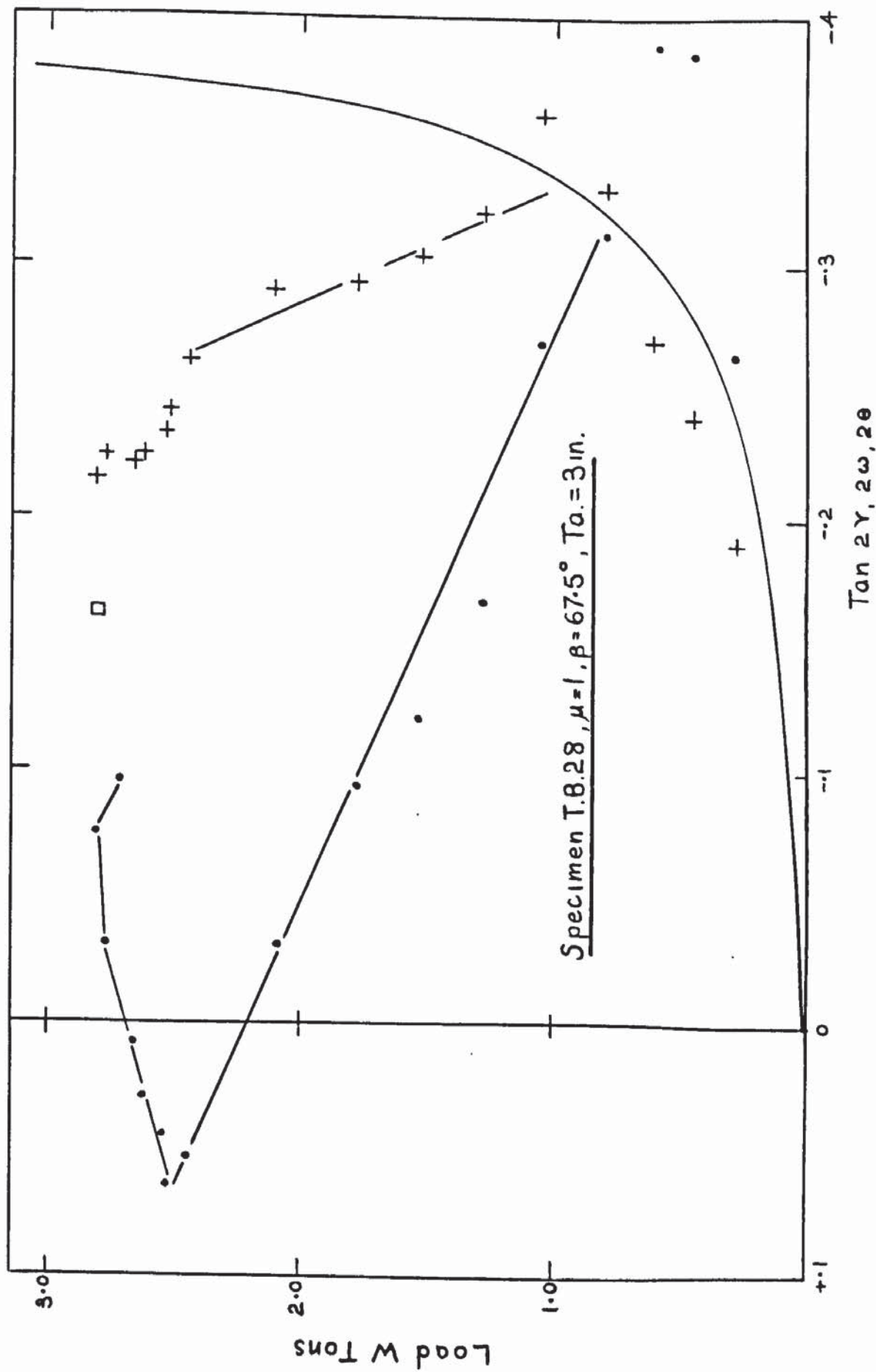


FIG.5-90 PLOT OF PRINCIPAL DIRECTIONS - T.B.28

LOAD W TONS	MIN. PRINC. CONC. STRAIN E2 μ STRAINS	MIN. PRINC. CURVATURE K2 in <sup>-1</sup> x10 <sup>3</sup>	STEEL STRAINS MICROSTRAINS																
			1	2	3	4	5	6	7	8									
0.00	0.00	0.00	0.0	0.0	0.0	0.0	0.0	0.0	0.0	0.0	0.0	0.0	0.0	0.0	0.0	0.0	0.0	0.0	0.0
0.12	.18	-.0106	4.70	4.7	0.0	9.4	9.4	9.4	9.4	9.4	9.4	9.4	9.4	9.4	9.4	9.4	9.4	9.4	9.4
0.28	-1.77	-.0141	9.4	9.4	9.4	14.0	14.0	28.1	28.1	28.1	28.1	28.1	28.1	28.1	28.1	28.1	28.1	28.1	28.1
0.45	-5.26	.0157	28.1	18.7	18.7	18.7	18.7	18.7	18.7	18.7	18.7	18.7	18.7	18.7	18.7	18.7	18.7	18.7	18.7
0.61	-3.04	.0025	32.8	37.5	46.9	32.8	32.8	32.8	32.8	32.8	32.8	32.8	32.8	32.8	32.8	32.8	32.8	32.8	32.8
0.78	-18.68	.0127	56.3	46.9	84.5	46.9	46.9	46.9	46.9	46.9	46.9	46.9	46.9	46.9	46.9	46.9	46.9	46.9	46.9
1.03	-30.48	.0006	65.7	75.1	103.3	56.3	56.3	56.3	56.3	56.3	56.3	56.3	56.3	56.3	56.3	56.3	56.3	56.3	56.3
1.28	-36.63	.0213	122.1	122.1	140.9	84.5	84.5	84.5	84.5	84.5	84.5	84.5	84.5	84.5	84.5	84.5	84.5	84.5	84.5
1.53	-44.94	.0187	178.5	159.7	169.1	122.1	122.1	122.1	122.1	122.1	122.1	122.1	122.1	122.1	122.1	122.1	122.1	122.1	122.1
1.78	-63.85	.0061	244.2	202.0	206.7	169.1	169.1	169.1	169.1	169.1	169.1	169.1	169.1	169.1	169.1	169.1	169.1	169.1	169.1
2.11	-93.55	-.0232	319.4	263.0	272.4	225.4	225.4	225.4	225.4	225.4	225.4	225.4	225.4	225.4	225.4	225.4	225.4	225.4	225.4
2.44	-136.59	.4458	422.7	357.0	375.8	310.0	310.0	310.0	310.0	310.0	310.0	310.0	310.0	310.0	310.0	310.0	310.0	310.0	310.0
2.52	-188.23	-.0828	610.7	507.3	535.5	422.7	422.7	422.7	422.7	422.7	422.7	422.7	422.7	422.7	422.7	422.7	422.7	422.7	422.7
2.54	-267.05	-.0637	798.6	591.9	714.0	601.3	601.3	601.3	601.3	601.3	601.3	601.3	601.3	601.3	601.3	601.3	601.3	601.3	601.3
2.62	-284.34	-.0447	873.7	638.8	817.4	704.6	704.6	704.6	704.6	704.6	704.6	704.6	704.6	704.6	704.6	704.6	704.6	704.6	704.6
2.66	-306.62	-.0606	920.7	652.9	883.1	798.6	798.6	798.6	798.6	798.6	798.6	798.6	798.6	798.6	798.6	798.6	798.6	798.6	798.6
2.77	-367.75	-.1440	1033.4	742.2	1024.0	958.3	958.3	958.3	958.3	958.3	958.3	958.3	958.3	958.3	958.3	958.3	958.3	958.3	958.3
2.81	-403.52	-.2102	948.9	798.6	1277.7	1338.8	1338.8	1338.8	1338.8	1338.8	1338.8	1338.8	1338.8	1338.8	1338.8	1338.8	1338.8	1338.8	1338.8
2.71	-323.86	-.2039	930.1	836.1	1493.8	2076.3	2076.3	2076.3	2076.3	2076.3	2076.3	2076.3	2076.3	2076.3	2076.3	2076.3	2076.3	2076.3	2076.3

Table 5.21 Minimum Principle Concrete Strains & Curvatures & Steel Strains TB.28

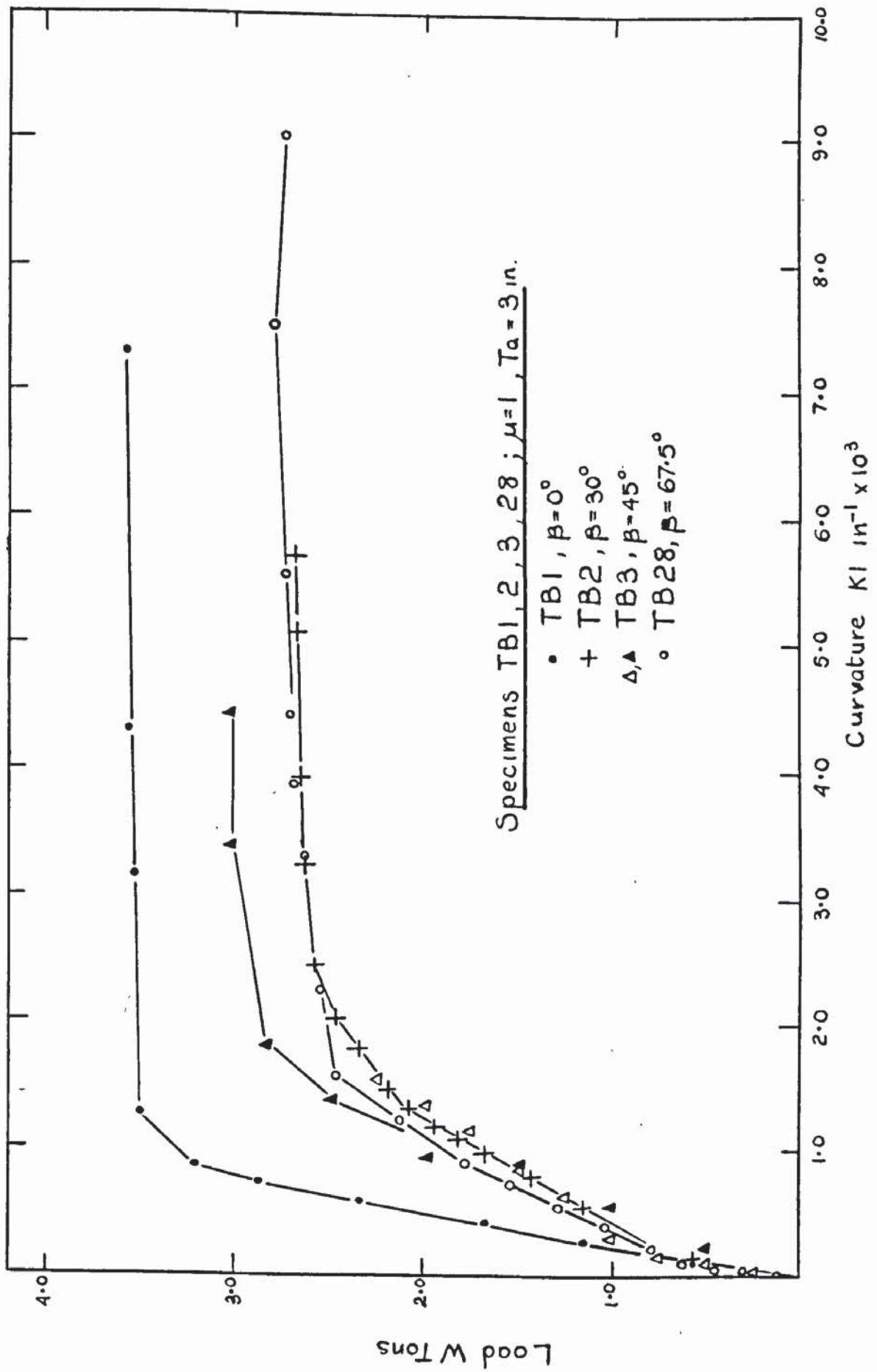


FIG. 5.91 PLOT OF MAXIMUM PRINCIPAL CURVATURES - T.B.1, T.B.2, T.B.3, T.B.28.

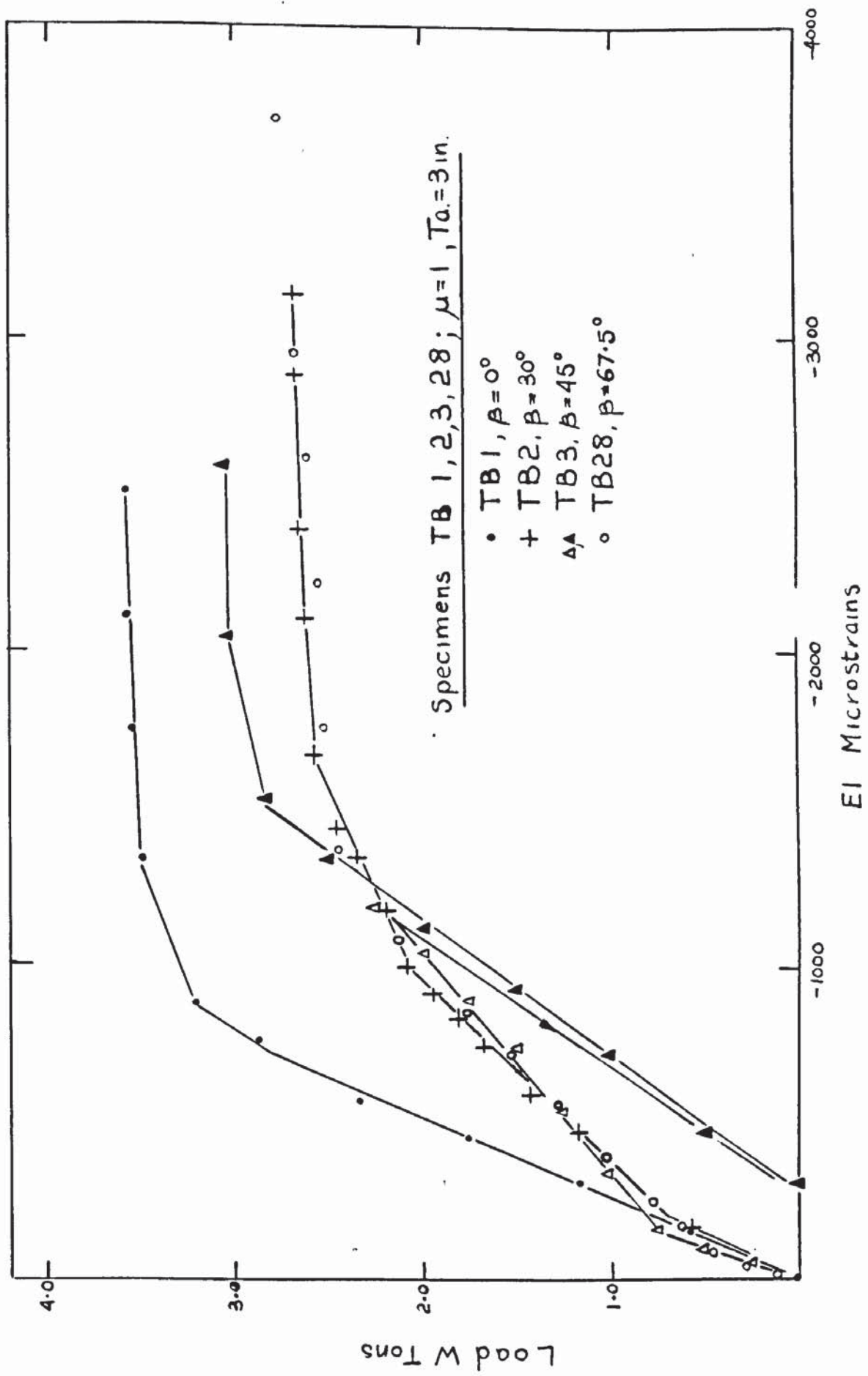


FIG 5.92 PLOT OF PRINCIPAL CONCRETE STRAINS, EI - TB1, TB2, TB3, TB28

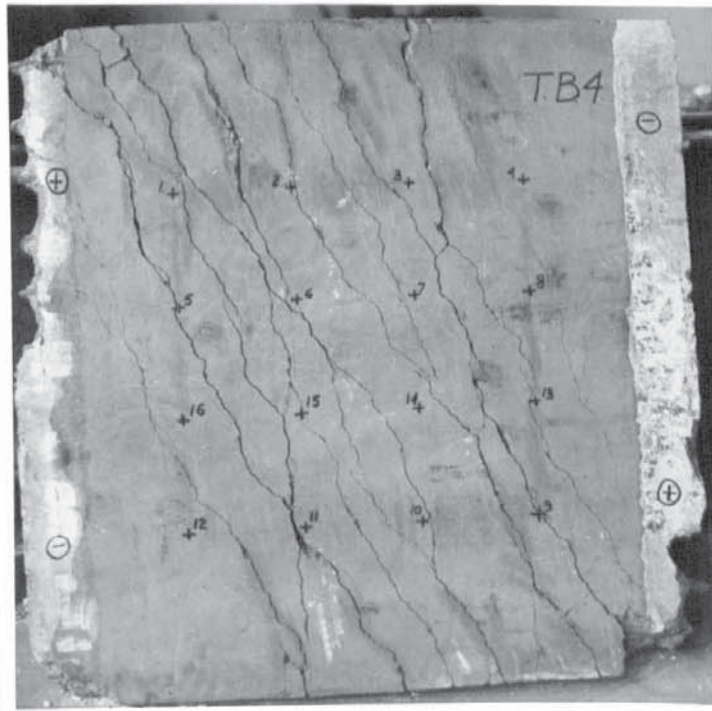


PLATE 5.26

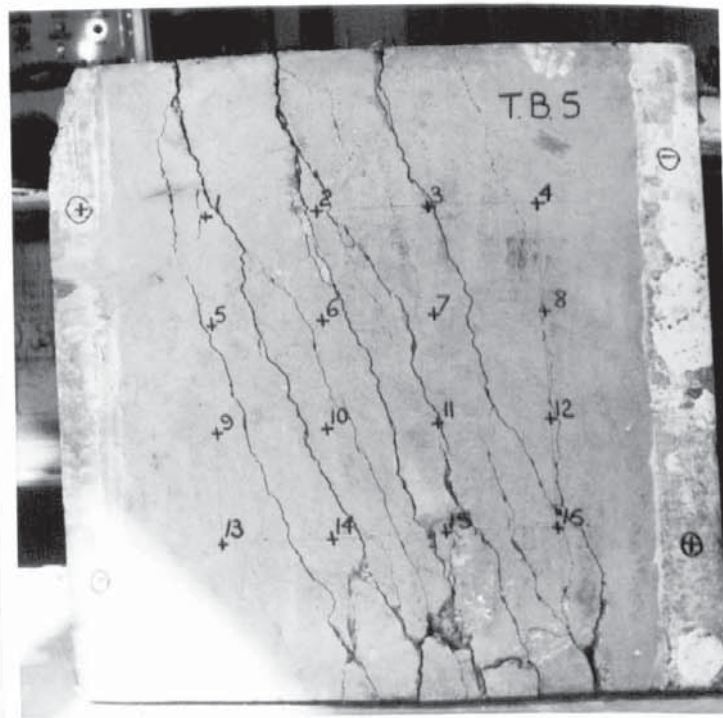


PLATE 5.27

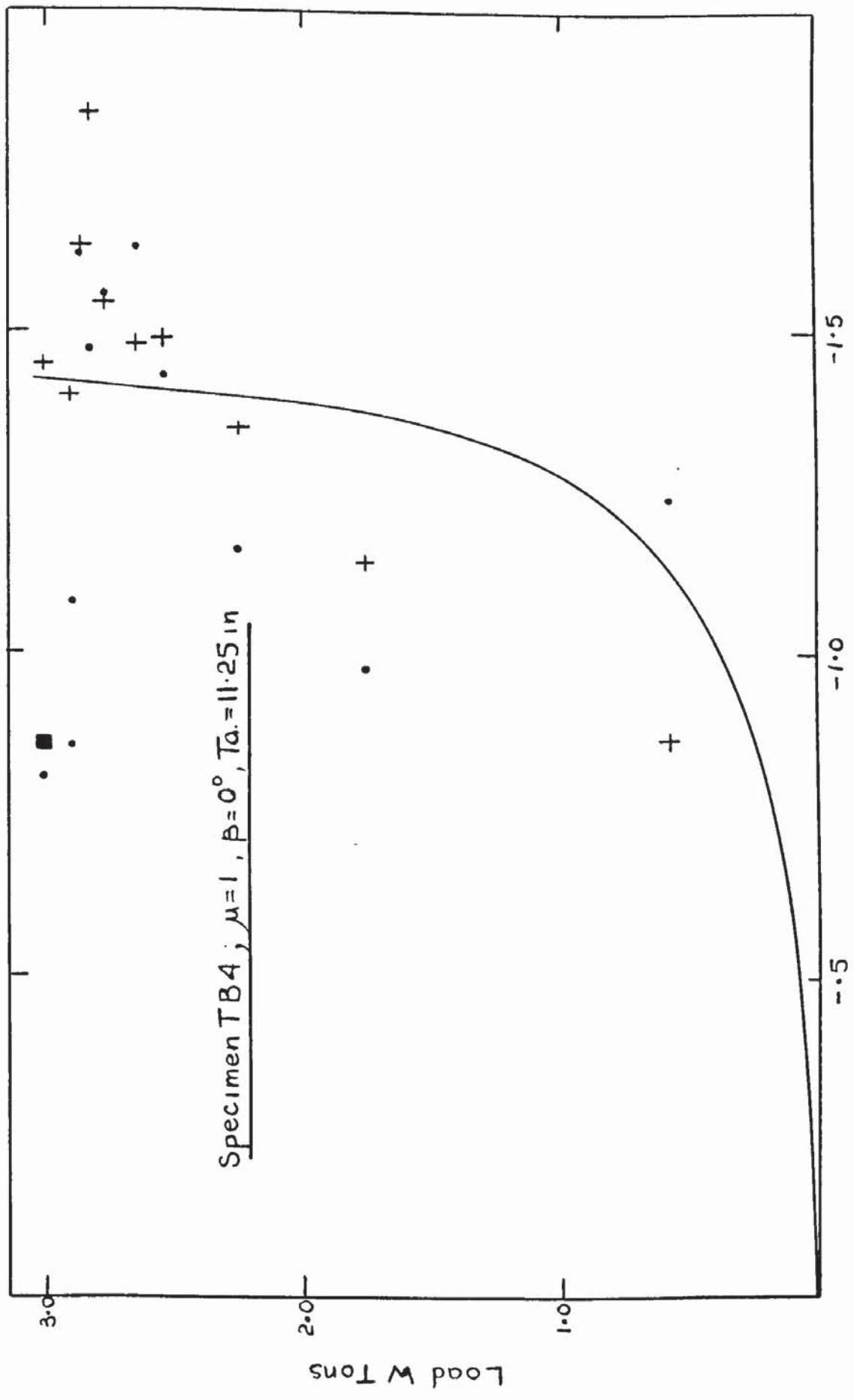


FIG 5.93 PLOT OF PRINCIPAL DIRECTIONS - TB4.

LOAD W TONS	MIN. PRINC. CONC. STRAIN E2 μ STRAINS	MIN. PRINC. CURVATURE K2 in <sup>-1</sup> x10 <sup>3</sup>	STEEL STRAINS MICROSTRAINS										
			1	2	3	4	5	6	7	8			
0.00	0.00	0.00	0.0	0.0	0.0	0.0	0.0	0.0	0.0	0.0	0.0	0.0	0.0
.58	-34.79	-.0070	24.7	9.9	64.3	39.6	64.3	64.3	69.32	128.73	59.4	59.4	59.4
1.15	-46.39	-.0040	59.4	39.6	222.8	0.0	222.8	222.8	237.6	311.9	198.0	198.0	198.0
1.73	-126.77	-.0297	148.5	158.4	1614.1	316.8	1614.1	1614.1	658.5	821.9	1039.7	1039.7	1039.7
2.25	-187.95	-.0238	257.4	356.4	1534.8	406.0	1534.8	1534.8	712.9	1153.6	1524.9	1524.9	1524.9
2.54	-281.49	.0533	366.3	-	4357.0	554.5	4357.0	4357.0	-	1406.1	3148.9	3148.9	3148.9
2.65	-348.51	.0889	544.6	-	5327.5	762.4	5327.5	5327.5	-	1584.3	3604.4	3604.4	3604.4
2.77	-382.97	.0796	802.1	-	7199.0	-	7199.0	7199.0	-	1970.5	4545.2	4545.2	4545.2
2.83	-381.04	.0589	1000.1	-	7921.9	-	7921.9	7921.9	-	3455.9	5070.0	5070.0	5070.0
2.86	-348.85	-.1288	960.5	-	2257.7	-	2257.7	2257.7	-	7278.2	-	-	-
2.87	-271.34	.4395	1079.3	-	6496.0	-	6496.0	6496.0	-	9308.2	-	-	-
2.94	-269.42	-.6638	-	-	6357.3	-	6357.3	6357.3	-	9714.2	-	-	-
2.95	-270.20	-	-	-	-	-	-	-	-	1.1x10 <sup>4</sup>	-	-	-
3.00	-364.36	-	-	-	-	-	-	-	-	-	-	-	-

Table 5.22 Minimum Principle Concrete Strains & Curvatures & Steel Strains TB.4

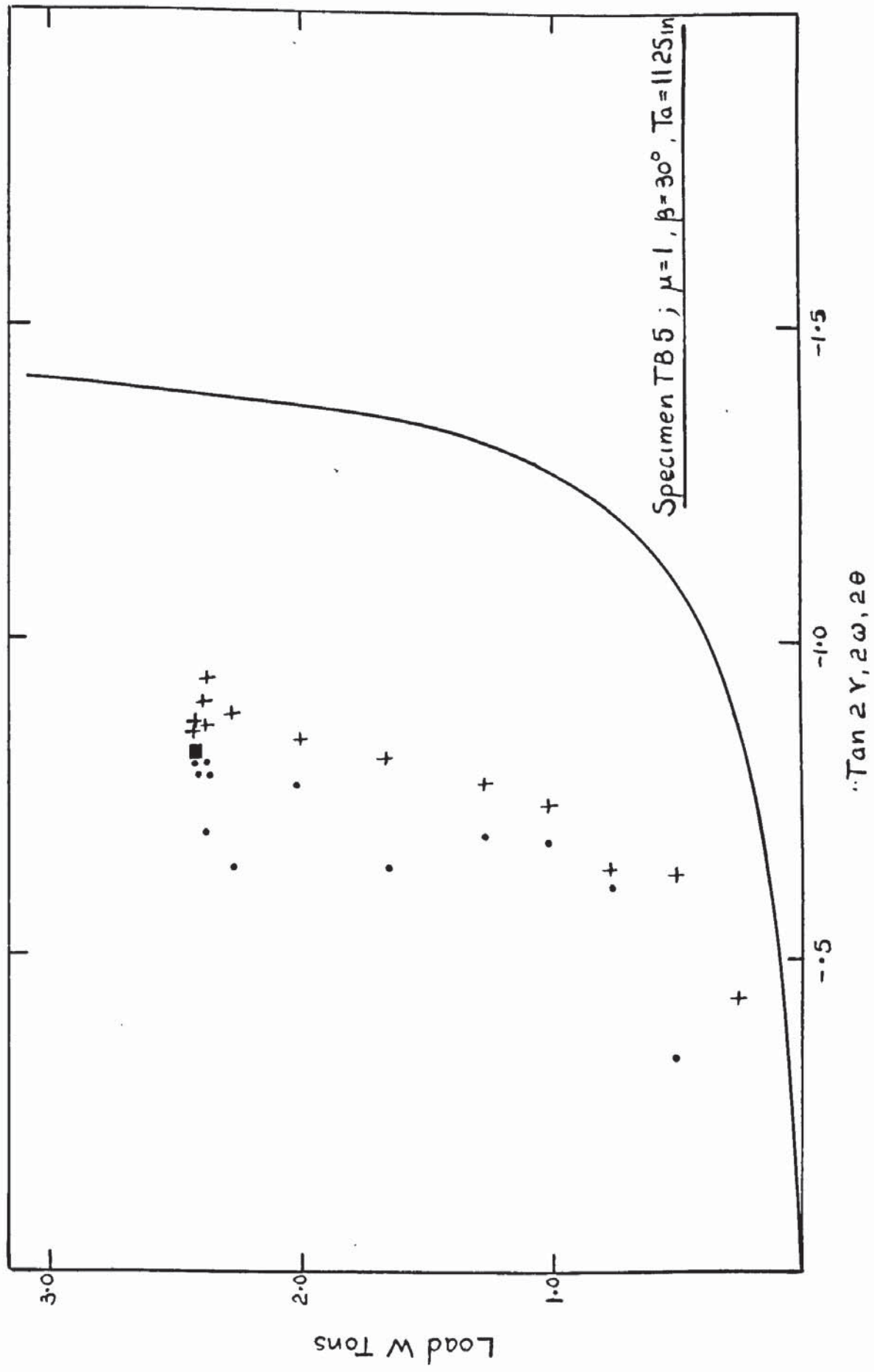


FIG 5.94 PLOT OF PRINCIPAL DIRECTIONS - TB5

LOAD W TONS	MIN. PRINC. CONC. STRAIN E2 $\mu$ STRAINS	MIN. PRINC. CURVATURE K2 in <sup>-1</sup> x10 <sup>3</sup>	STEEL STRAINS										
			1	2	3	4	5	6	7	8			
0.00	0.00	0.00	0.0	0.0	0.0	0.0	0.0	0.0	0.0	0.0	0.0	0.0	0.0
0.25	-1.57	0.00	39.61	207.95	39.6	39.6	39.6	128.7	-	128.7	32.6	32.6	148.5
0.50	-17.848	-.0006	49.51	227.76	49.5	49.5	59.4	148.5	-	148.5	44.5	44.5	158.4
0.75	-30.56	-.0144	49.51	564.44	49.5	49.5	49.5	158.4	-	158.4	113.8	113.8	148.5
1.00	-46.62	.0333	584.24	970.44	49.5	49.5	237.6	1386.3	-	1386.3	184.1	184.1	465.4
1.25	-71.73	-.0526	792.20	1643.80	89.1	89.1	465.4	2307.2	-	2307.2	227.7	227.7	772.3
1.66	-115.17	-.2562	782.29	1886.41	0.0	0.0	534.7	3188.5	-	3188.5	366.3	366.3	1138.7
1.99	-158.76	-.1598	950.63	2426.10	227.7	227.7	861.5	3743.1	-	3743.1	752.5	752.5	1208.1
2.26	-193.01	-.2449	831.80	2693.46	346.5	346.5	1079.3	4287.7	-	4287.7	891.2	891.2	1416.0
2.37	-228.35	-.2441	1564.59	3129.17	534.7	534.7	1267.5	4792.7	-	4792.7	1029.8	1029.8	1722.0
2.37	-262.54	-.2401	-	3881.76	643.6	643.6	1297.2	4961.1	-	4961.1	1039.7	1039.7	1960.6
2.40	-291.48	.2385	-	4614.54	752.5	752.5	1307.1	5139.3	-	5139.3	1079.3	1079.3	2277.5
2.41	-310.96	-.2878	-	5644.39	940.7	940.7	1326.9	5684.0	-	5684.0	1099.1	1099.1	2782.5
2.37	-445.73	-.4089	-	1.1x10 <sup>4</sup>	3876.8	3876.8	1356.6	-	-	-	1742.8	1742.8	7535.7

Table 5.23 Minimum Principle Concrete Strains & Curvatures & Steel Strains TB.5

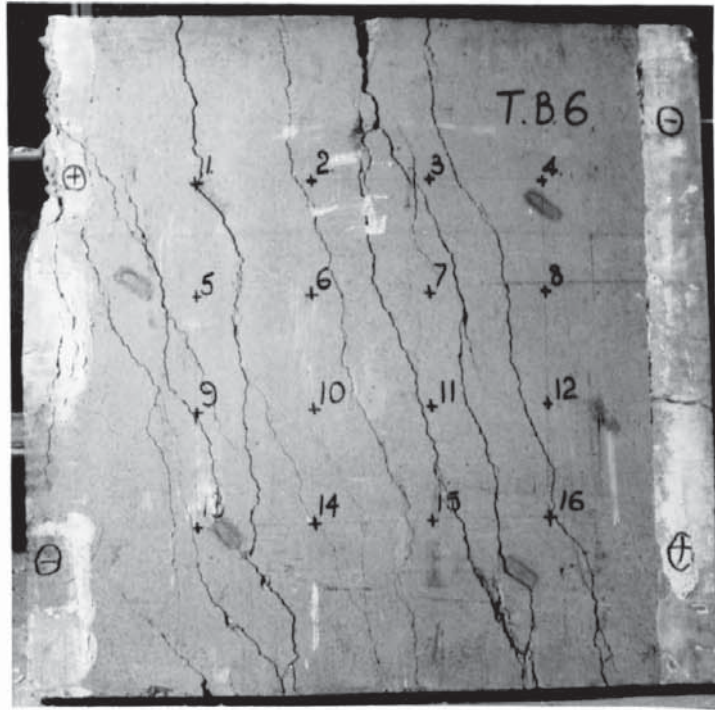


PLATE 5.28

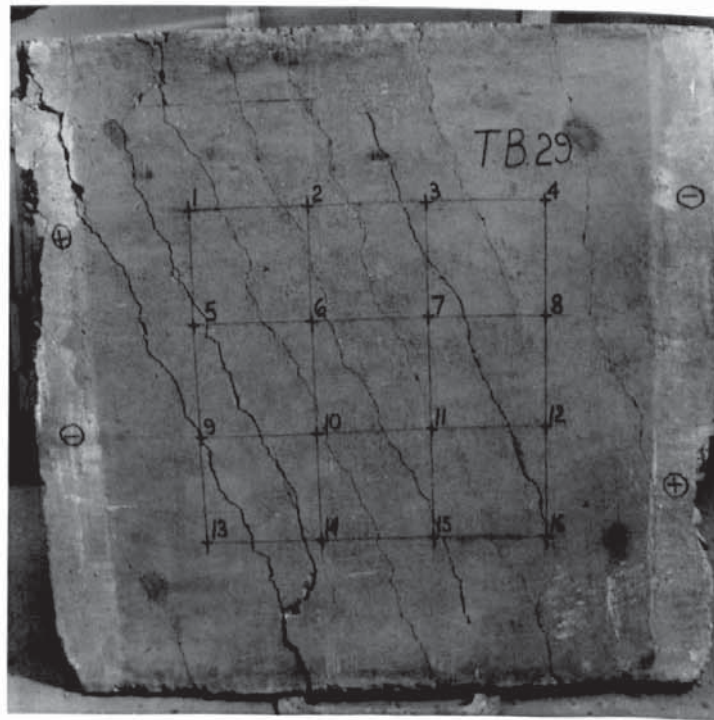


PLATE 5.29



LOAD W TONS	MIN. PRINC. CONC. STRAIN E2 μ STRAINS	MIN. PRINC. CURVATURE K2 in <sup>-1</sup> x10 <sup>3</sup>	STEEL STRAINS										
			1	2	3	4	5	6	7	8			
0.00	0.00	0.00	0.0	0.0	0.0	0.0	0.0	0.0	0.0	0.0	0.0	0.0	0.0
0.25	1.88	-0.0122	4.95	14.8	0.0	0.0	0.0	14.8	14.8	14.8	14.8	14.8	14.8
0.50	-5.80	-0.0220	9.90	29.7	9.9	9.9	9.9	24.7	24.7	24.7	24.7	24.7	24.7
0.75	-8.00	-0.0597	74.27	69.3	14.8	14.8	29.7	94.0	39.6	39.6	39.6	39.6	39.6
1.00	-11.17	-0.0349	148.54	168.3	74.2	74.2	99.0	262.4	-29.7	-29.7	-29.7	-29.7	-29.7
1.25	-14.33	-0.0440	257.46	316.8	138.6	138.6	178.2	490.1	-19.8	-19.8	-19.8	-19.8	-19.8
1.49	-27.38	-0.0420	356.49	435.7	217.8	217.8	257.4	663.4	108.9	108.9	108.9	108.9	108.9
1.74	-46.47	-0.0869	475.32	554.5	292.1	292.1	346.5	816.9	376.2	376.2	376.2	376.2	376.2
1.99	-69.59	-0.1066	574.34	668.4	371.3	371.3	435.7	1193.2	604.0	604.0	604.0	604.0	604.0
2.24	-90.08	-0.1325	703.07	821.9	485.2	485.2	554.5	1411.1	891.2	891.2	891.2	891.2	891.2
2.49	-131.39	-0.4494	950.63	1089.2	673.3	673.3	752.5	2084.4	1173.4	1173.4	1173.4	1173.4	1173.4
2.57	-166.89	-0.6843	1732.93	1376.4	782.2	782.2	851.6	2381.5	1297.2	1297.2	1297.2	1297.2	1297.2
2.59	-220.19	-0.9533	2346.88	1604.2	871.4	871.4	901.1	-	1455.6	1455.6	1455.6	1455.6	1455.6
2.59	-224.87	-1.0169	2663.76	1742.8	930.8	930.8	1010.0	-	1564.5	1564.5	1564.5	1564.5	1564.5
2.59	-241.81	-1.3650	2941.02	1871.5	1010.0	1010.0	1183.3	-	1713.1	1713.1	1713.1	1713.1	1713.1
2.59	-260.09	-1.1036	-	2178.5	1069.4	1069.4	1455.6	-	2039.9	2039.9	2039.9	2039.9	2039.9

Table 5.24 Minimum Principle Concrete Strains & Curvatures & Steel Strains TB.6

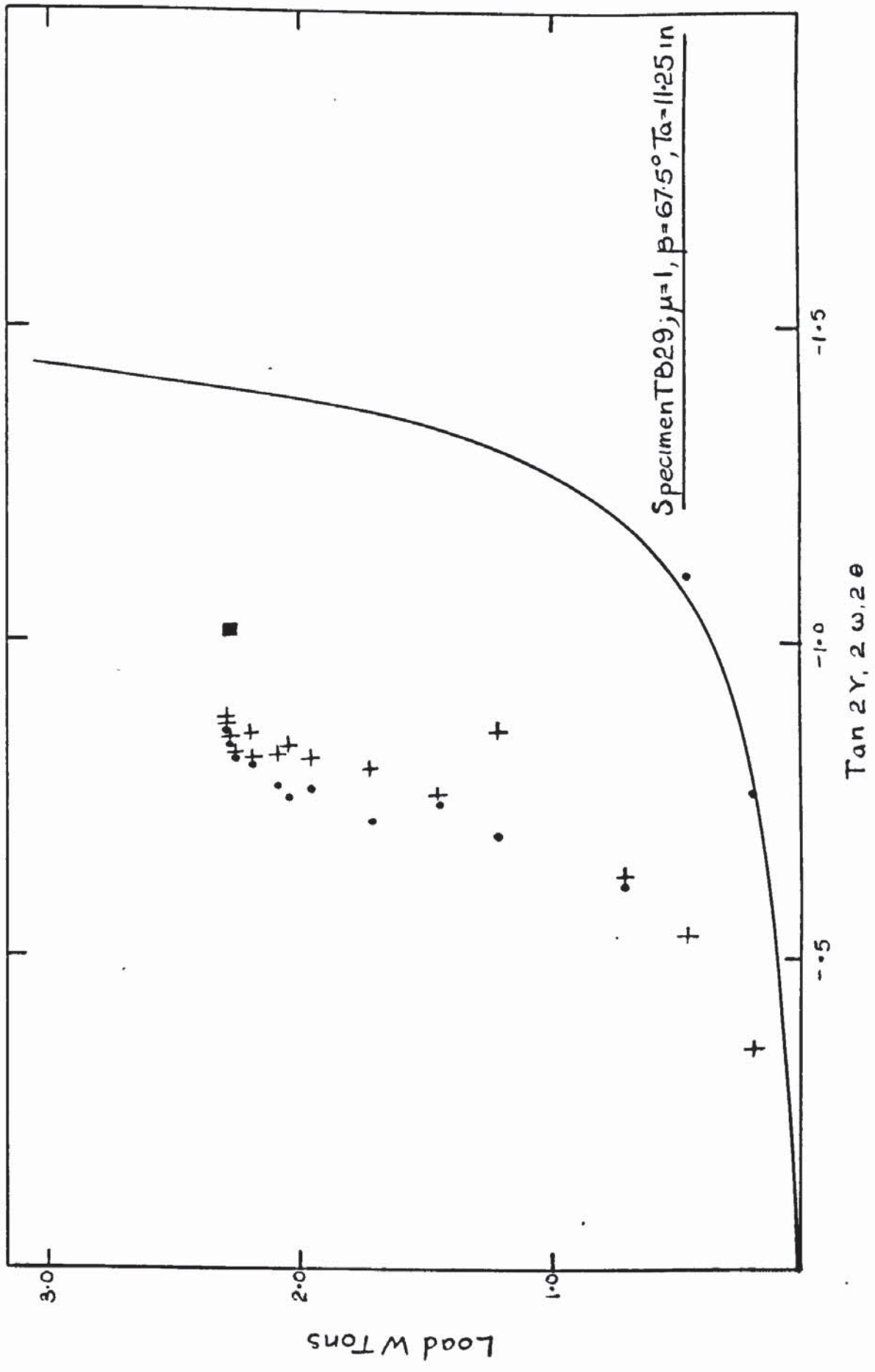


FIG 5.96 PLOT OF PRINCIPAL DIRECTIONS - TB 29

LOAD W TONS	MIN. PRINC. CONC. STRAIN E2 μ STRAINS	MIN. PRINC. CURVATURE K2 in <sup>-1</sup> x10 <sup>3</sup>	STEEL STRAINS MICROSTRAINS										
			1	2	3	4	5	6	7	8			
0.00	0.00	0.00	0.00	0.0	0.0	0.0	0.0	0.0	0.0	0.0	0.0	0.0	0.0
0.20	-5.34	-0.0058	-	-	0.0	0.0	0.0	9.4	18.79	56.3	-	-	-
0.45	-9.79	-0.0100	-	-	-9.4	0.0	0.0	46.9	65.7	84.5	-	-	-
0.70	-27.50	-0.0081	-	-	-9.4	9.4	9.4	155.0	164.4	173.8	-	-	-
0.95	-71.26	.0008	-	4.7	0.0	23.4	23.4	300.6	300.6	234.8	-	-	-
1.20	-76.35	-0.0183	-	0.0	9.4	46.9	46.9	460.3	450.9	394.6	-	-	-
1.44	-103.32	-0.0224	-	0.0	9.4	56.3	56.3	601.3	591.9	469.7	-	-	-
1.69	-134.03	-0.0309	-	-9.4	9.4	70.4	70.4	779.8	761.0	652.9	-	-	-
1.94	-238.13	-0.0920	4.70	-9.4	9.4	75.1	75.1	958.3	930.1	714.0	-	-	-
2.07	-225.85	-0.0773	9.40	-18.79	9.4	84.5	84.5	1042.8	1071.0	1038.1	-	-	-
2.17	-269.74	-0.1172	18.79	-9.4	9.4	93.9	93.9	1085.1	1155.6	1118.0	-	-	-
2.24	-311.35	-0.1019	28.19	0.0	0.0	112.7	112.7	1052.2	1183.8	1362.3	-	-	-
2.26	-428.39	-0.0784	65.77	28.1	18.7	103.3	103.3	1038.1	1174.4	1578.4	-	-	-
2.27	-529.63	-0.1143	84.56	46.9	28.1	145.6	145.6	1018.4	1141.5	2179.7	-	-	-
2.27	-677.20	-1.0015	112.74	70.4	46.9	164.4	164.4	1042.8	1165.0	2696.4	-	-	-
2.19	-772.55	-0.9472	117.44	75.1	84.5	239.5	239.5	995.9	1136.8	3861.4	-	-	-
2.03	-894.75	-0.8794	173.81	112.7	103.3	263.0	263.0	1183.8	1099.2	5261.4	-	-	-

Table 5.25 Minimum Principle Concrete Strains & Curvatures & Steel Strains TB.29

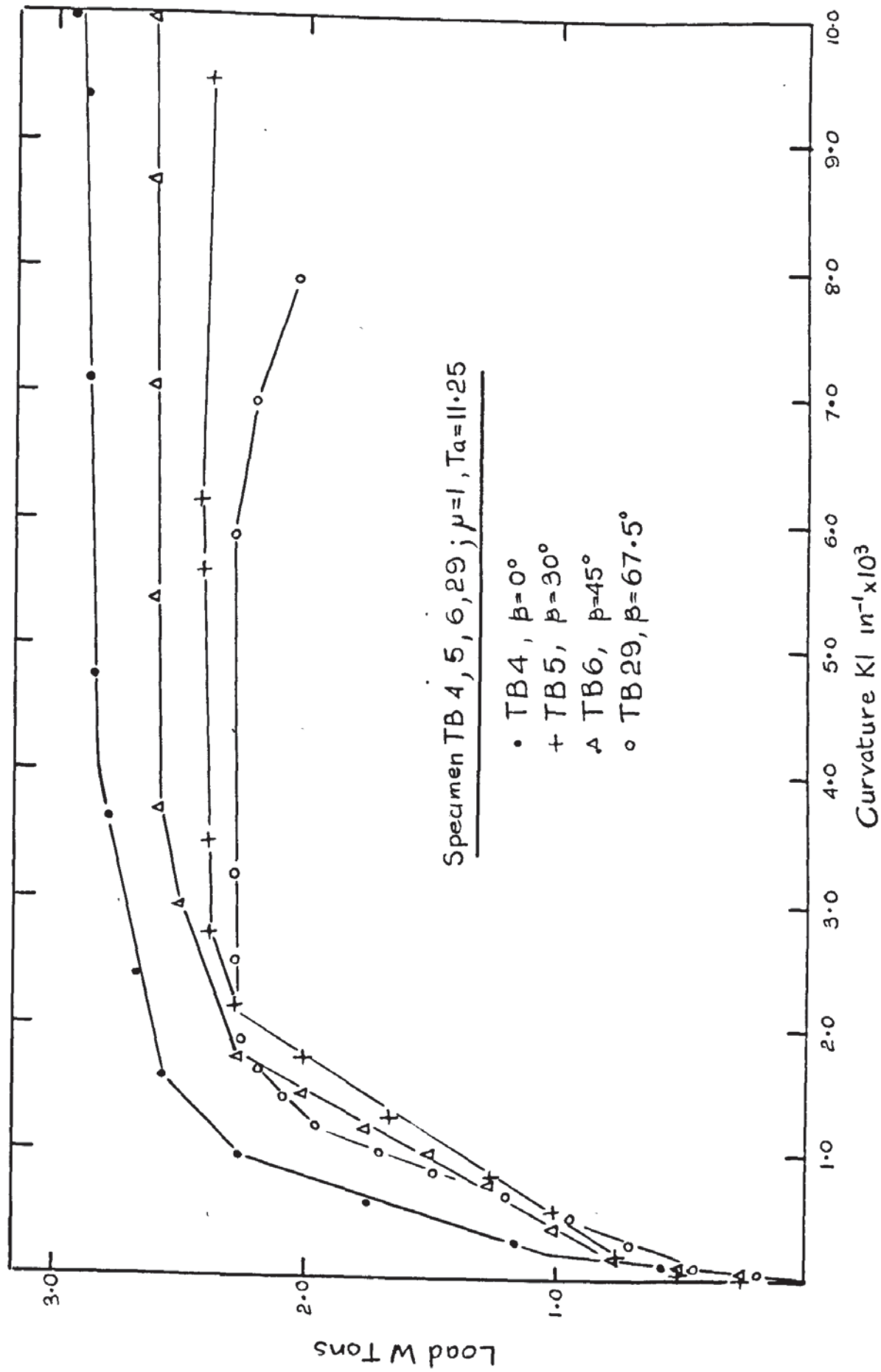


FIG 5.97 PLOT OF MAXIMUM PRINCIPAL CURVATURES - TB 4, TB 5, TB 6, TB 29

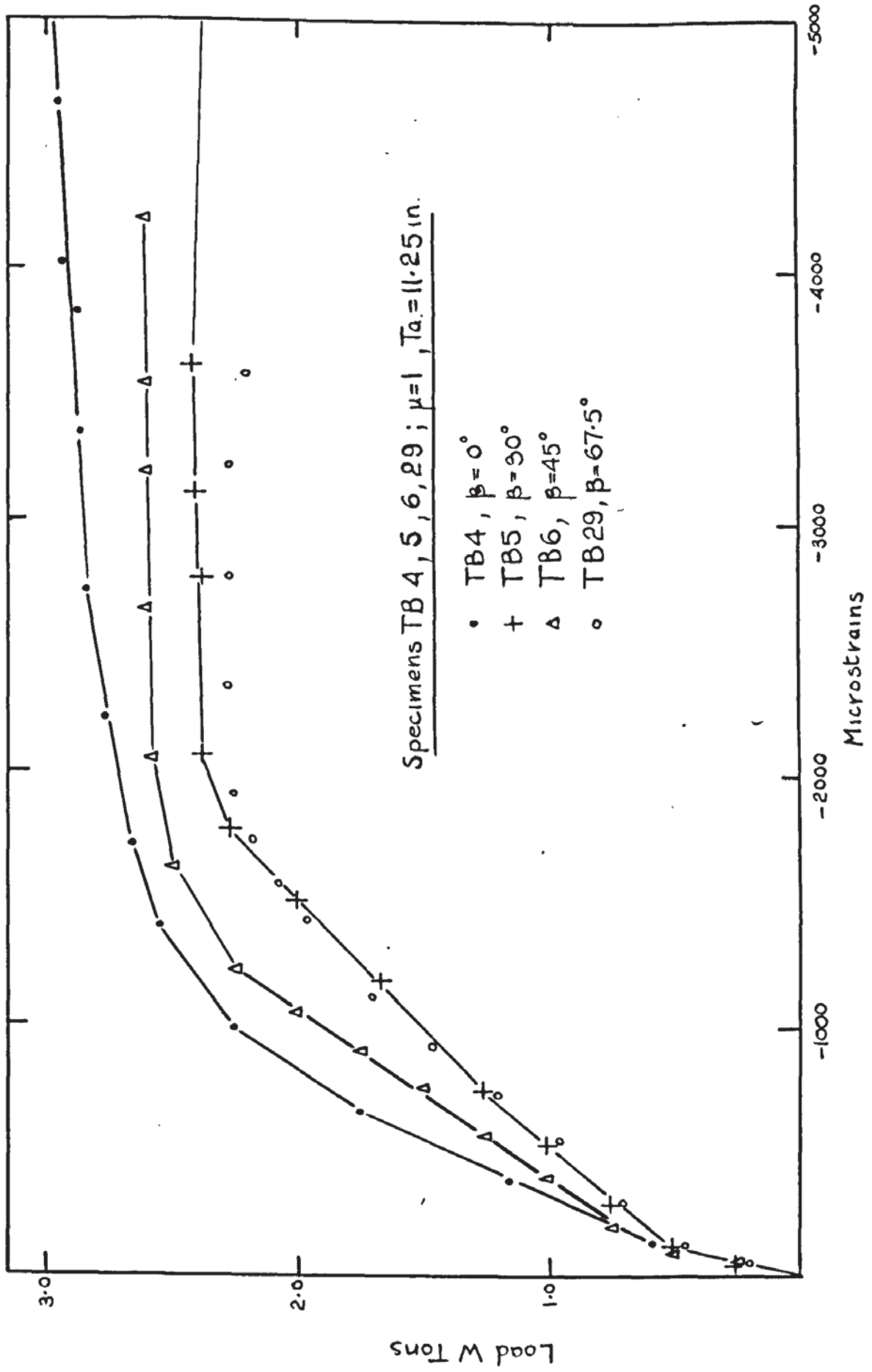


FIG 5.98 PLOT OF PRINCIPAL CONCRETE STRAINS EI - TB4, TB5, TB6, TB29

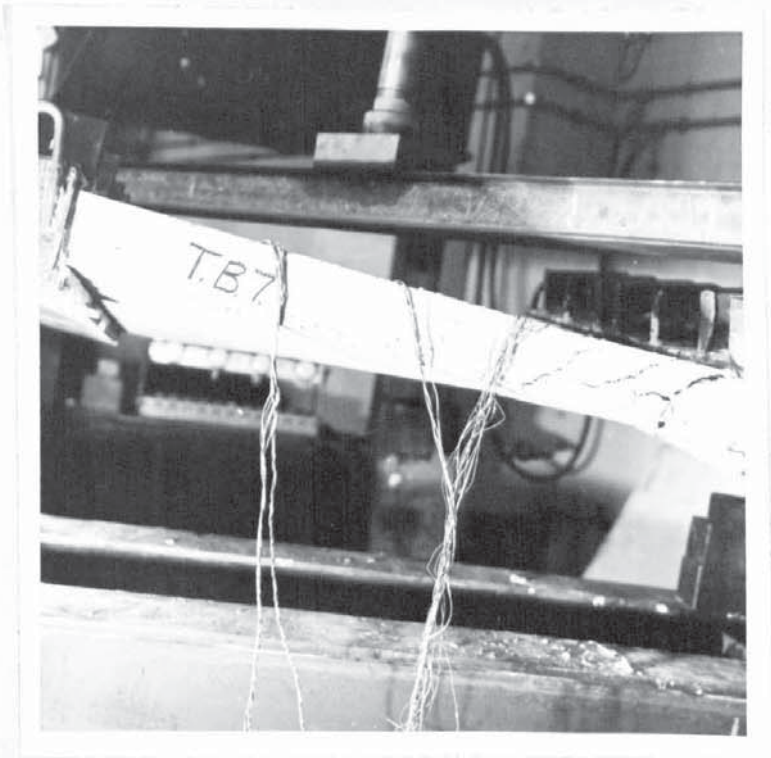


PLATE 5.30

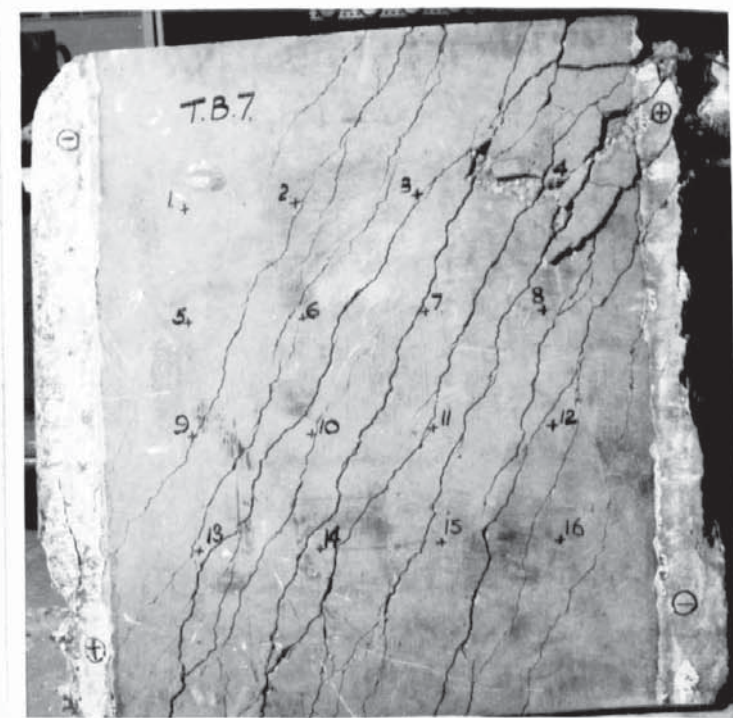


PLATE 5.31

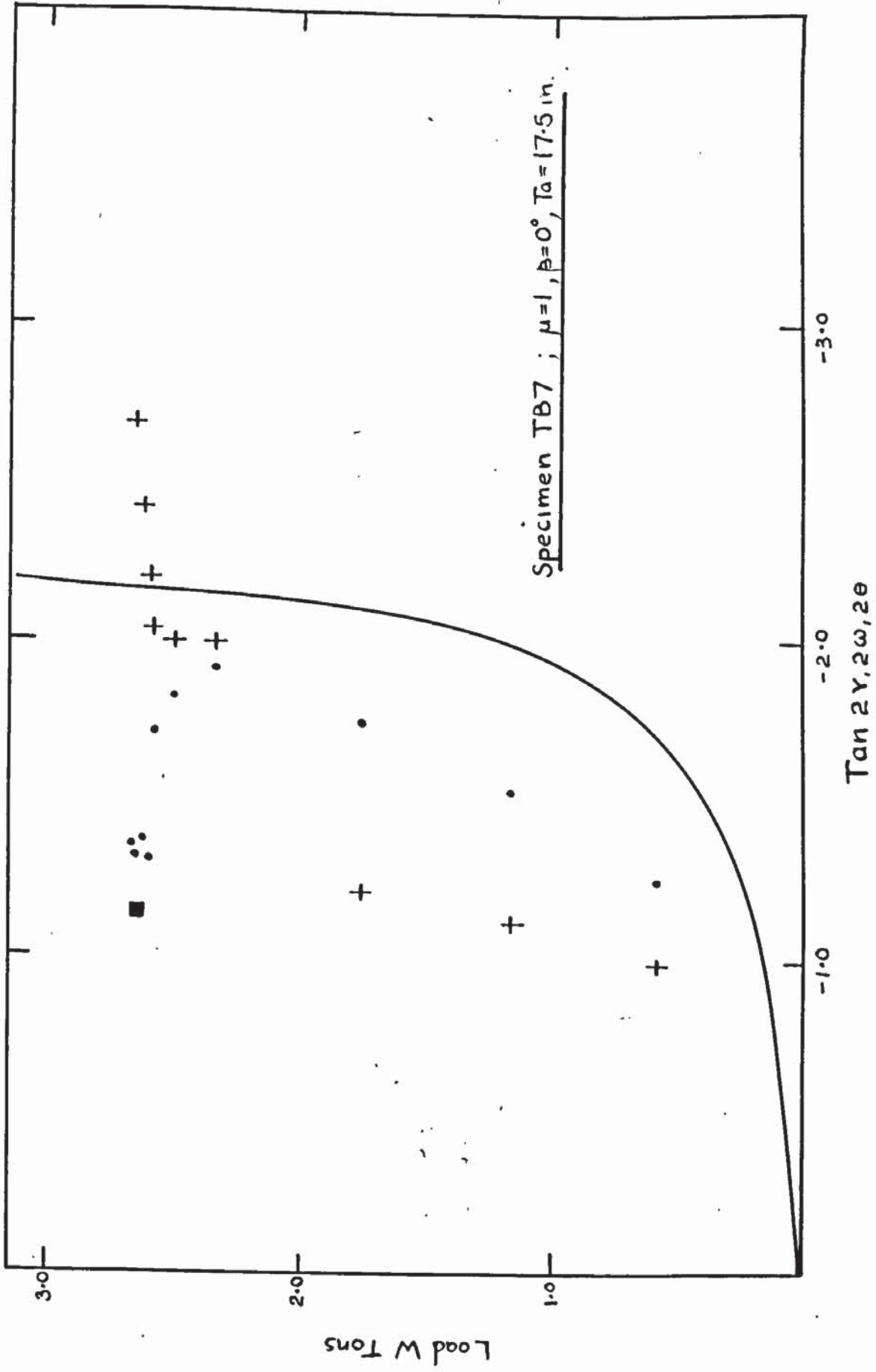


FIG 5-99 PLOT OF PRINCIPAL DIRECTIONS - TB7

LOAD W TONS	MIN. PRINC. CONC. STRAIN E2 μ STRAINS	MIN. PRINC. CURVATURE K2 in <sup>-1</sup> x10 <sup>3</sup>	STEEL STRAINS										
			1	2	3	4	5	6	7	8			
0.00	0.00	0.00	0.0	0.0	0.0	0.0	0.0	0.0	0.0	0.0	0.0	0.0	0.0
0.58	-31.50	-0.0625	0.0	9.9	881.3	316.8	316.8	183.2	306.9	277.2	376.2	376.2	376.2
1.16	-69.36	-0.1045	9.9	14.8	1376.4	673.37	673.37	782.2	475.3	683.2	633.7	633.7	633.7
1.74	-105.04	-0.1488	59.4	29.7	1812.1	1049.6	1049.6	1064.5	683.2	1029.8	772.3	772.3	772.3
2.32	-186.63	-0.2514	99.0	-148.5	2574.6	-	-	1074.4	1257.6	1653.7	1084.3	1084.3	1084.3
2.49	-206.39	-0.2843	108.9	-99.0	3416.3	-	-	1302.1	1574.4	1762.6	1326.9	1326.9	1326.9
2.57	-228.66	-0.3112	118.8	-99.0	4020.3	-	-	1371.4	1713.1	1841.8	1455.6	1455.6	1455.6
2.59	-248.78	-0.1043	118.8	-59.4	-	-	-	1341.7	-	5129.4	2366.6	2366.6	2366.6
2.61	-319.51	-1.2869	149.3	89.1	-	-	-	1034.8	-	-	-	-	-
2.63	-364.15	-1.4695	163.3	891.2	-	-	-	1074.4	-	-	-	-	-
2.65	-567.99	-1.5196	-	3277.7	-	-	-	1084	-	-	-	-	-

Table 5.26 Minimum Principle Concrete Strains & Curvatures & Steel Strains TB.7

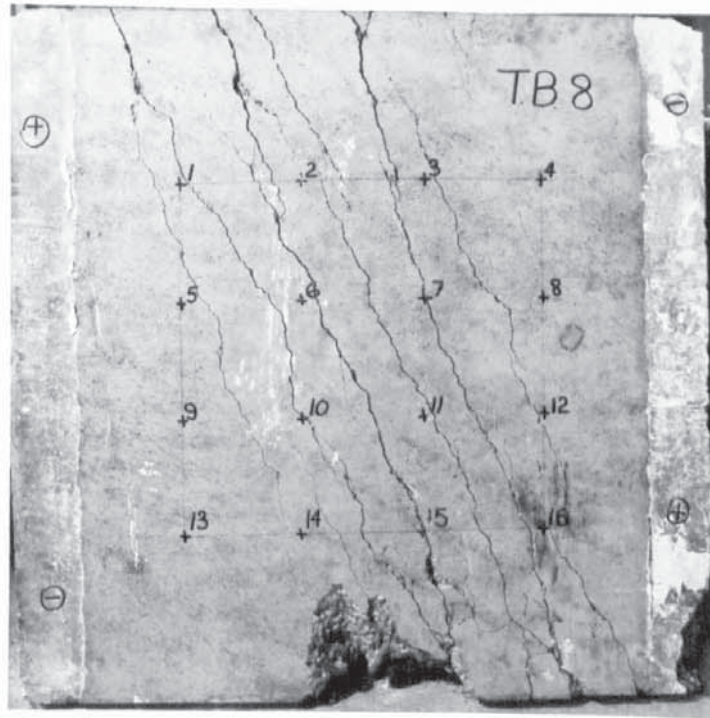


PLATE 5.32



PLATE 5.33

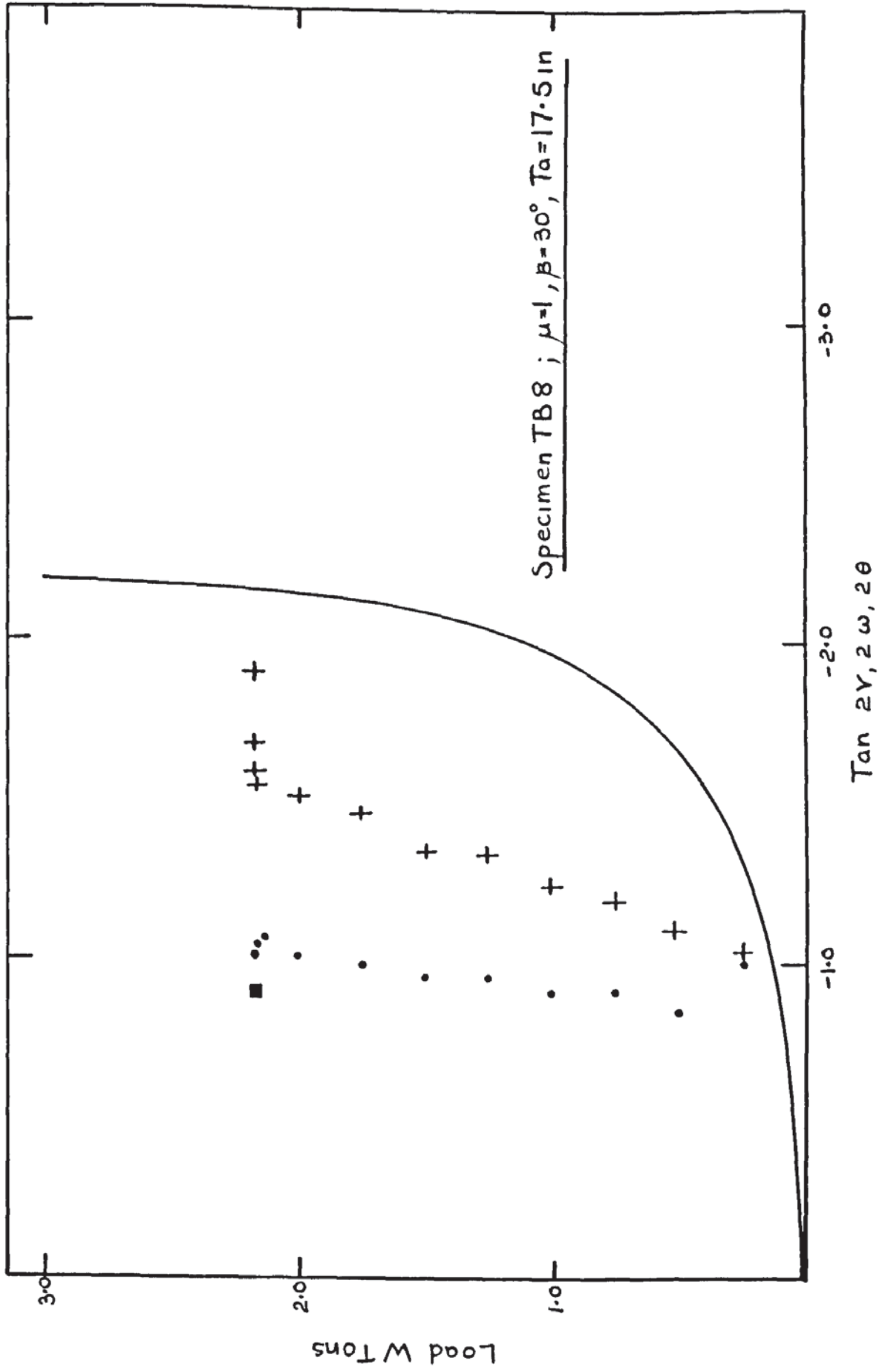


FIG 5-100 PLOT OF PRINCIPAL DIRECTIONS - TB 8

LOAD W TONS	MIN. PRINC. CONC. STRAIN E2 μ STRAINS	MIN. PRINC. CURVATURE K2 in <sup>-1</sup> x10 <sup>3</sup>	STEEL STRAINS MICROSTRAINS										
			1	2	3	4	5	6	7	8			
0.00	0.00	0.00	0.0	0.0	0.0	0.0	0.0	0.0	0.0	0.0	0.0	0.0	0.0
0.25	-14.95	-.0072	4.9	9.9	4.9	-	-	19.8	14.8	19.8	14.8	9.9	19.8
0.52	-20.29	-.0029	14.8	19.8	14.8	-	-	64.3	39.6	64.3	39.6	49.5	44.5
0.75	-30.13	-.0106	59.4	79.2	64.3	-	-	89.1	99.0	89.1	99.0	128.7	118.8
1.00	-61.85	-.0237	153.4	242.6	158.4	-	-	524.8	406.0	524.8	406.0	331.7	306.9
1.25	-112.09	-.0317	287.1	425.8	297.0	-	-	950.6	742.6	950.6	742.6	574.3	604.0
1.49	-140.66	.0708	331.7	554.5	386.2	-	-	1198.2	851.6	1198.2	851.6	732.7	782.2
1.74	-195.60	-.09.8	529.7	628.8	495.1	-	-	1515.0	1158.5	1515.0	1158.5	940.7	1000.1
1.99	-244.17	-.1243	628.8	613.9	712.9	-	-	1772.5	1604.2	1772.5	1604.2	1158.5	1227.9
2.13	-250.29	-.2019	826.8	604.0	1000.1	-	-	4436.2	4030.2	4436.2	4030.2	1257.6	1297.2
2.16	-176.12	-.2314	836.7	653.5	1059.5	-	-	8347.7	5060.1	8347.7	5060.1	1277.4	1297.2
2.17	-160.22	-.2662	886.2	663.4	1128.8	-	-	1.0x10 <sup>4</sup>	5703.8	1.0x10 <sup>4</sup>	5703.8	1287.3	1277.4
2.17	-202.20	-.3732	906.0	663.4	1208.1	-	-	1.3x10 <sup>4</sup>	-	1.3x10 <sup>4</sup>	-	1326.9	1287.3
2.17	-99.91	-.3975	930.8	653.5	1336.8	-	-	-	-	-	-	-	1267.5

Table 5.27 Minimum Principle Concrete Strains & Curvatures & Steel Strains TB.8

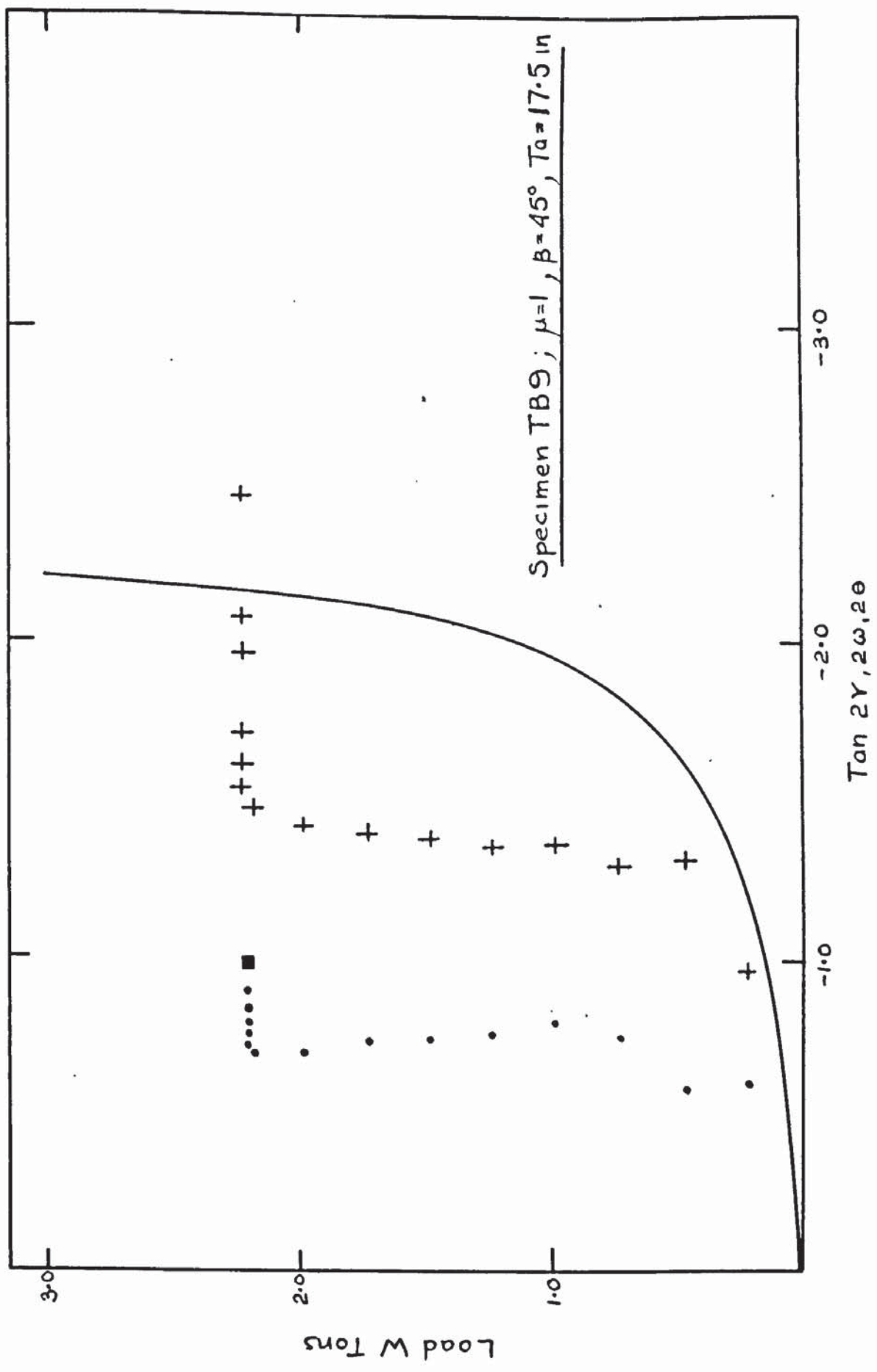


FIG 5.101 PLOT OF PRINCIPAL DIRECTIONS - TB 9

LOAD W TONS	MIN. PRINC. CONC. STRAIN E2 μ STRAINS	MIN. PRINC. CURVATURE K2 in <sup>-1</sup> x10 <sup>3</sup>	STEEL STRAINS MICROSTRAINS										
			1	2	3	4	5	6	7	8			
0.00	0.00	0.00	0.0	0.0	0.0	0.0	0.0	0.0	0.0	0.0	0.0	0.0	0.0
0.22	-20.18	-.0167	0.0	0.0	0.0	0.0	0.0	9.9	19.8	19.8	14.8	29.7	29.7
0.47	-36.41	-.0184	9.9	9.9	9.9	9.9	9.9	49.5	89.1	89.1	326.7	138.6	138.6
0.72	-58.31	-.0360	59.4	39.6	19.8	74.2	168.3	168.3	287.1	287.1	198.0	366.3	366.3
0.97	-98.72	-.0540	138.6	69.3	68.3	128.7	386.2	386.2	574.3	574.3	406.0	594.1	594.1
1.22	-135.32	-.0683	227.7	108.9	89.1	247.5	633.7	633.7	881.3	881.3	653.5	821.9	821.9
1.47	-190.88	-.1007	306.9	148.5	153.4	336.6	812.0	812.0	1168.4	1168.4	871.4	1049.6	1049.6
1.72	-403.55	-.1180	396.1	272.3	262.4	381.2	980.3	980.3	1445.7	1445.7	1099.1	1287.3	1287.3
1.97	-323.90	-.1841	480.2	361.4	316.8	430.7	1143.7	1143.7	1762.6	1762.6	1307.1	1569.5	1569.5
2.17	-398.97	-.2143	688.2	574.3	455.5	623.8	1381.3	1381.3	3683.7	3683.7	1356.6	-	-
2.22	-455.64	-.2845	762.4	693.1	396.1	762.4	1594.2	1594.2	9734.1	9734.1	1336.8	-	-
2.22	-481.63	-.2759	797.1	861.5	752.5	851.6	1782.4	1782.4	-	-	1341.7	-	-
2.22	-540.58	-.3136	871.4	1019.9	821.9	925.8	2148.8	2148.8	-	-	1351.6	-	-
2.22	-736.16	-.5094	930.8	1237.8	950.6	1010.0	3248.0	3248.0	-	-	1317.0	-	-
2.22	-890.11	-.8706	940.7	1312.0	960.5	1019.9	4357.0	4357.0	-	-	1297.2	-	-
2.22	-1572.97	-.8921	975.3	1425.9	920.9	1049.6	8753.7	8753.7	-	-	1247.7	-	-

Table 5.28 Minimum Principle Concrete Strains & Curvatures & Steel Strains TB.9

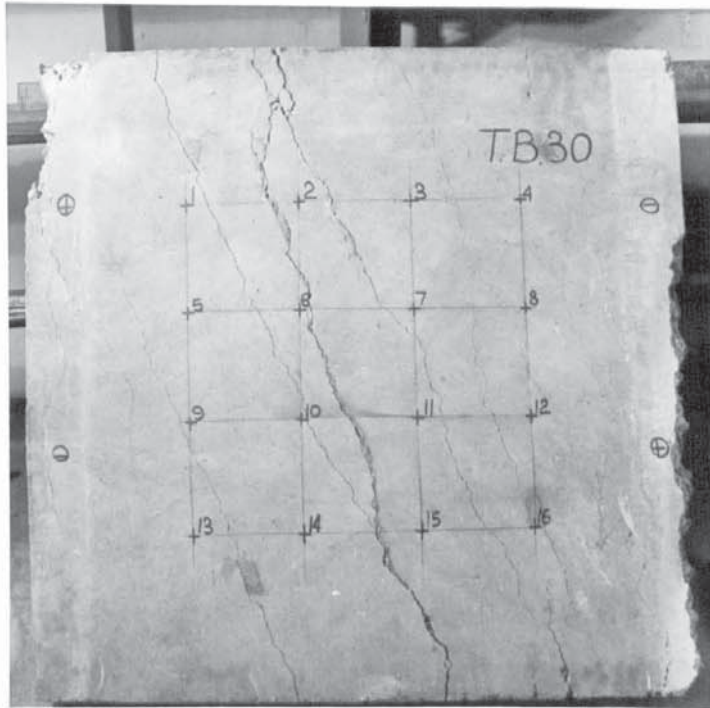


PLATE 5.34

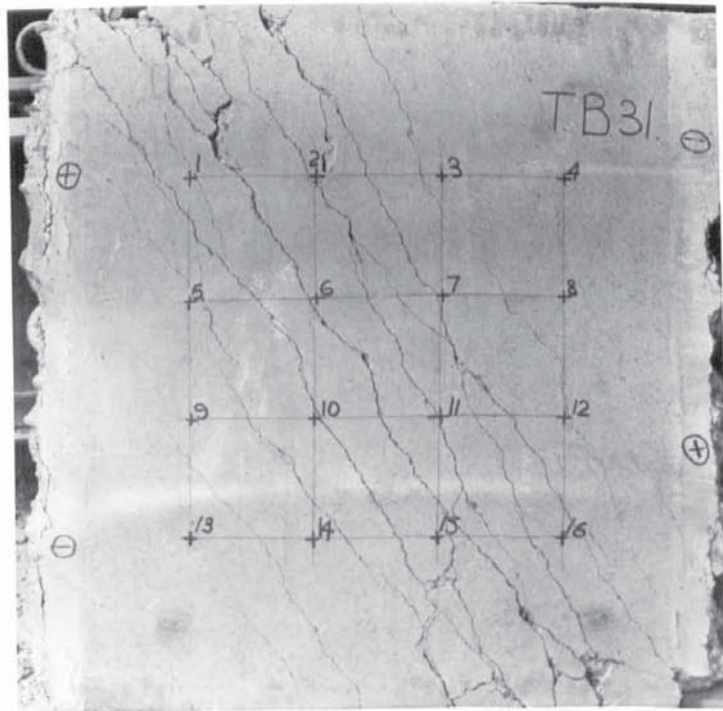


PLATE 5.35

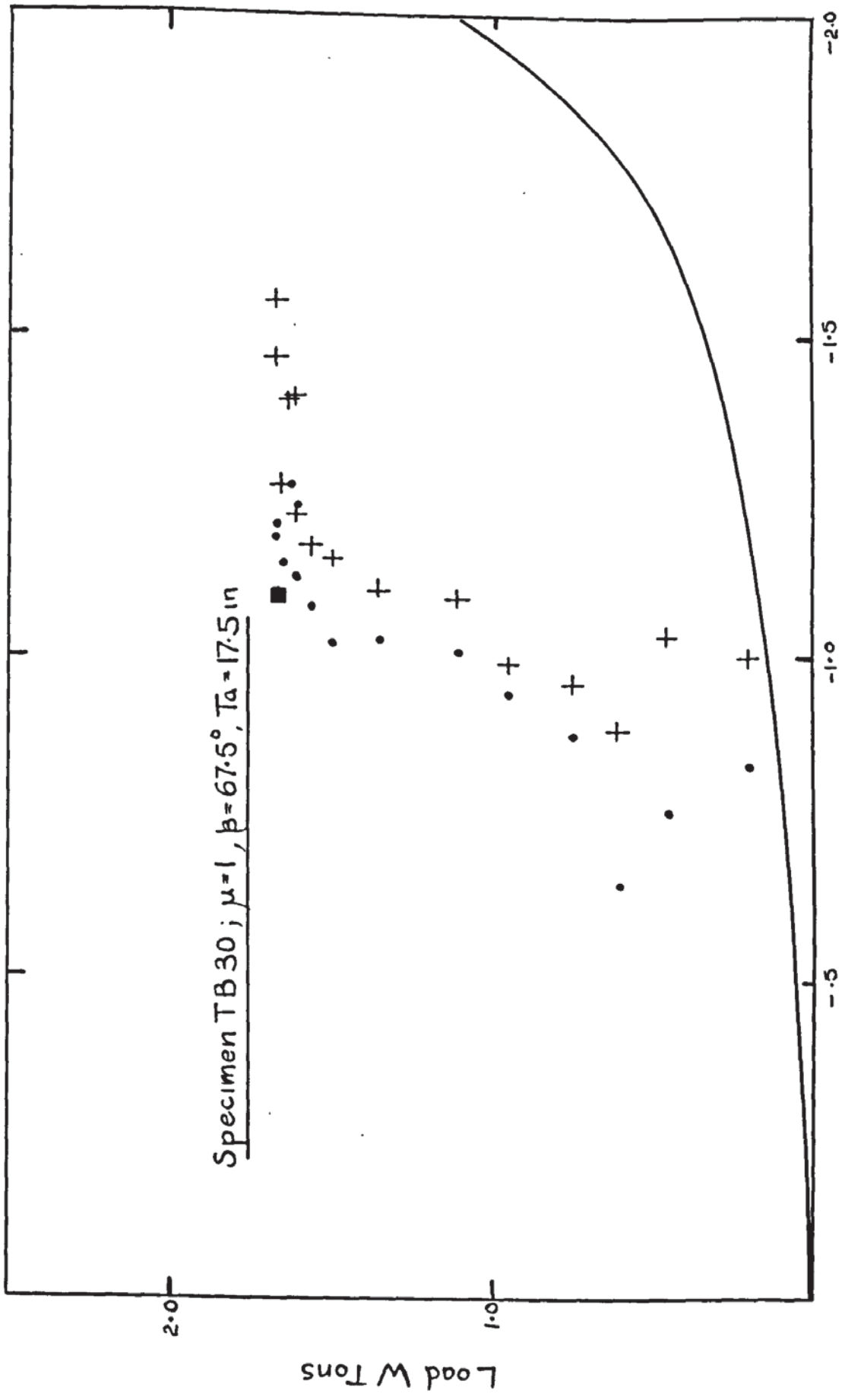


FIG 5-102 PLOT OF PRINCIPAL DIRECTIONS - TB30

LOAD W TONS	MIN. PRINC. CONC. STRAIN E2	MIN. PRINC. CURVATURE K2 in <sup>-1</sup> x10 <sup>3</sup>	STEEL STRAINS										
			1	2	3	4	5	6	7	8			
0.00	0.00	0.00	0.0	0.0	0.0	0.0	0.0	0.0	0.0	0.0	0.0	0.0	0.0
0.20	-19.41	-.0064	-4.70	0.0	0.0	-9.4	-9.4	37.58	28.19	28.19	28.19	28.19	32.8
0.45	-32.03	-.0025	0.0	0.0	0.0	-9.4	-9.4	216.0	253.6	253.6	159.7	159.7	169.1
0.61	-60.35	-.0322	9.4	-4.7	4.7	-9.4	-9.4	385.2	394.6	394.6	291.2	291.2	300.6
0.78	-97.05	-.0233	9.4	-14.0	4.7	-9.4	-9.4	535.5	526.1	526.1	413.4	413.4	441.5
0.95	-140.69	-.0303	18.7	-14.0	14.0	-4.7	-4.7	690.5	685.8	685.8	563.7	563.7	610.7
1.11	-225.38	-.0618	37.5	-4.7	37.5	18.7	18.7	859.6	845.5	845.5	732.8	732.8	779.8
1.36	-368.07	-.1263	37.5	-18.7	37.5	-4.7	-4.7	1127.4	1099.2	1099.2	1000.6	1000.6	1042.8
1.50	-554.66	-.2228	61.0	-9.4	65.7	18.7	18.7	1324.7	1352.9	1352.9	1202.6	1202.6	1240.1
1.57	-680.10	-.2899	103.3	28.1	93.9	46.9	46.9	1418.7	1597.2	1597.2	1315.3	1315.3	1371.7
1.62	-730.10	-.2991	140.9	70.4	122.1	93.9	93.9	1512.6	1930.7	1930.7	1371.7	1371.7	1446.8
1.67	-815.51	-.5408	178.5	140.9	150.3	159.7	159.7	1606.6	2245.4	2245.4	1409.3	1409.3	1475.0
1.68	-1119.64	-.7180	253.6	300.6	225.4	291.2	291.2	1672.3	3034.7	3034.7	1371.7	1371.7	1409.3
1.68	-1342.14	-.8760	310.0	413.4	319.4	375.8	375.8	1677.0	4063.4	4063.4	1352.9	1352.9	1381.1
1.65	-1616.69	-1.0383	385.2	493.2	422.7	479.1	479.1	1785.1	5298.9	5298.9	1399.9	1399.9	1296.5
1.64	-1605.72	-1.2287	474.4	554.3	497.9	526.1	526.1	1921.3	6435.8	6435.8	1071.0	1071.0	1305.9
1.39	-1498.52	-1.4016	535.5	657.5	535.5	507.3	507.3	4350.0	-	-	-	-	1056.9

Table 5.29 Minimum Principle Concrete Strains & Curvatures & Steel Strains TB.30



LOAD W TONS	MIN. PRINC. CONC. STRAIN E2 μ STRAINS	MIN. PRINC. CURVATURE K2 in <sup>-1</sup> dx10 <sup>3</sup>	STEEL STRAINS										
			1	2	3	4	5	6	7	8			
0.00	0.00	0.00	0.0	0.0	0.0	0.0	0.0	0.0	0.0	0.0	0.0	0.0	0.0
0.20	-11.66	-.0125	0.0	0.0	0.0	0.0	0.0	13.4	8.9	8.9	8.9	8.9	8.9
0.45	-27.50	-.0454	0.0	0.0	0.0	0.0	0.0	35.9	22.4	26.9	26.9	26.9	26.9
0.70	-44.64	-.0295	26.9	8.9	0.0	-8.9	94.2	76.3	89.7	89.7	89.7	89.7	89.7
0.95	-64.99	-.0604	98.7	44.8	86.9	0.0	184.0	188.5	170.5	170.5	170.5	170.5	170.5
1.20	-97.02	-.0451	175.0	116.7	80.8	17.9	354.6	377.0	323.2	323.2	323.2	323.2	323.2
1.44	-137.85	-.0788	260.3	215.4	143.6	62.8	552.1	556.6	484.8	484.8	484.8	484.8	484.8
1.69	-220.24	-.1420	332.1	287.2	215.4	112.2	695.7	700.2	646.4	646.4	646.4	646.4	646.4
1.94	-315.19	-.1703	404.0	377.0	287.2	161.6	834.9	834.9	799.0	799.0	799.0	799.0	799.0
2.19	-443.66	-.2278	493.7	484.8	395.0	242.4	969.6	960.6	1023.4	1023.4	1023.4	1023.4	1023.4
2.32	-562.58	-.2792	588.0	646.4	525.2	332.1	1027.9	1032.4	1077.3	1077.3	1077.3	1077.3	1077.3
2.40	-636.01	-.3232	700.2	754.1	664.3	430.9	1027.9	1104.2	1086.3	1086.3	1086.3	1086.3	1086.3
2.46	-710.07	-.3653	816.9	888.8	772.0	547.6	1072.8	1310.7	1122.2	1122.2	1122.2	1122.2	1122.2
2.50	-787.19	-.3991	906.7	960.6	888.8	668.8	1212.0	1728.2	1140.1	1140.1	1140.1	1140.1	1140.1
2.53	-822.25	-.4201	996.5	1158.1	996.5	790.0	1476.8	2657.4	1140.1	1140.1	1140.1	1140.1	1140.1
2.56	-885.72	-.4827	1122.2	2630.4	1256.8	1014.4	1988.5	6302.4	1104.2	1104.2	1104.2	1104.2	1104.2
2.56	-980.45	-.5247	1265.8	2980.6	-	1238.9	5005.1	1.0x10 <sup>4</sup>	-	-	-	-	-
2.56	-1198.48	-.6428	1212.0	3214.0	-	1678.8	-	1.2x10 <sup>4</sup>	-	-	-	-	-
2.56	-2101.63	-.9532	-	-	-	2630.4	-	-	-	-	-	-	-

Table 5.30 Minimum Principle Concrete Strains & Curvatures & Steel Strains TB.31

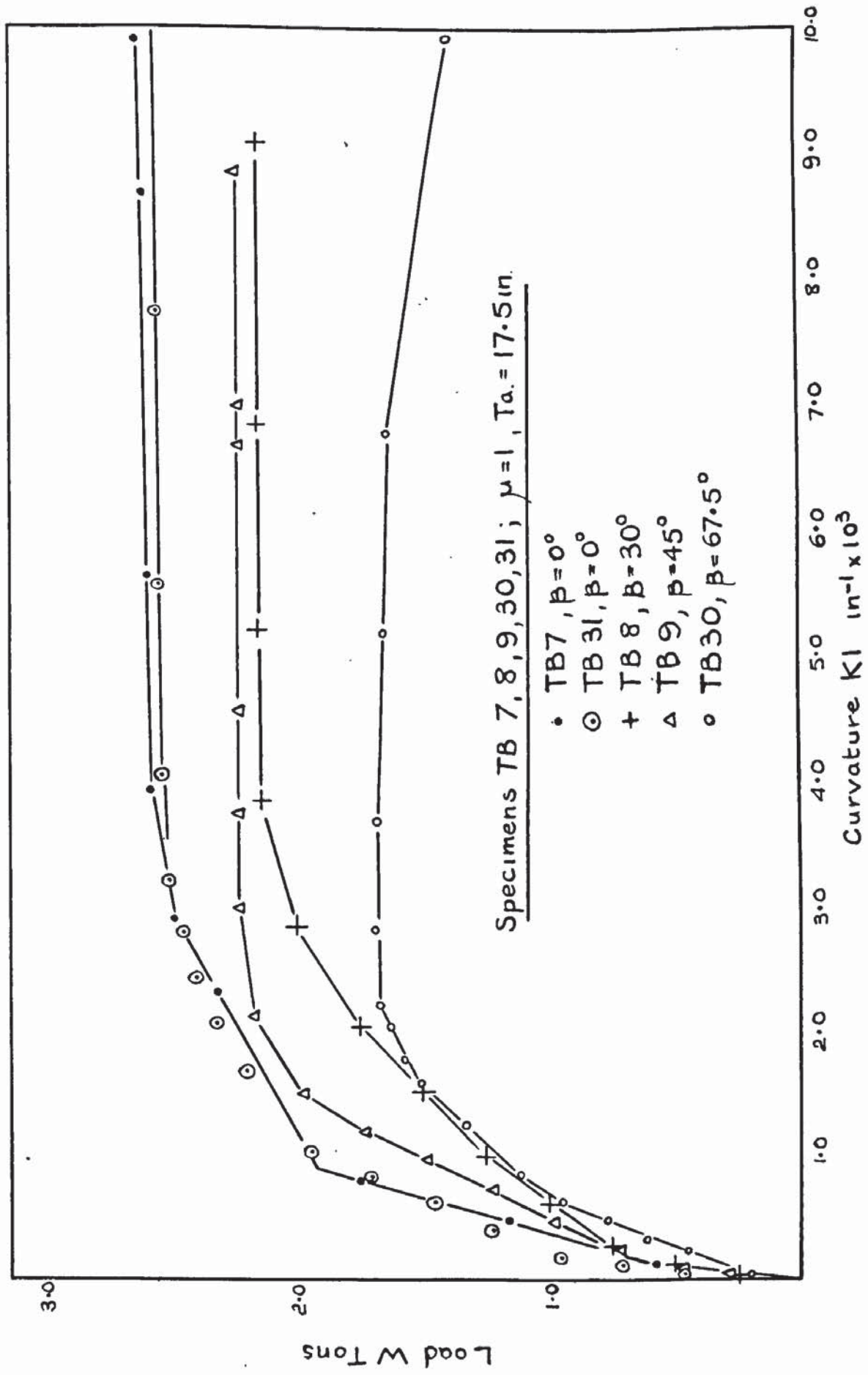


FIG5-104 PLOT OF MAXIMUM PRINCIPAL CURVATURES-TB7,TB8,TB9,TB30,TB31.

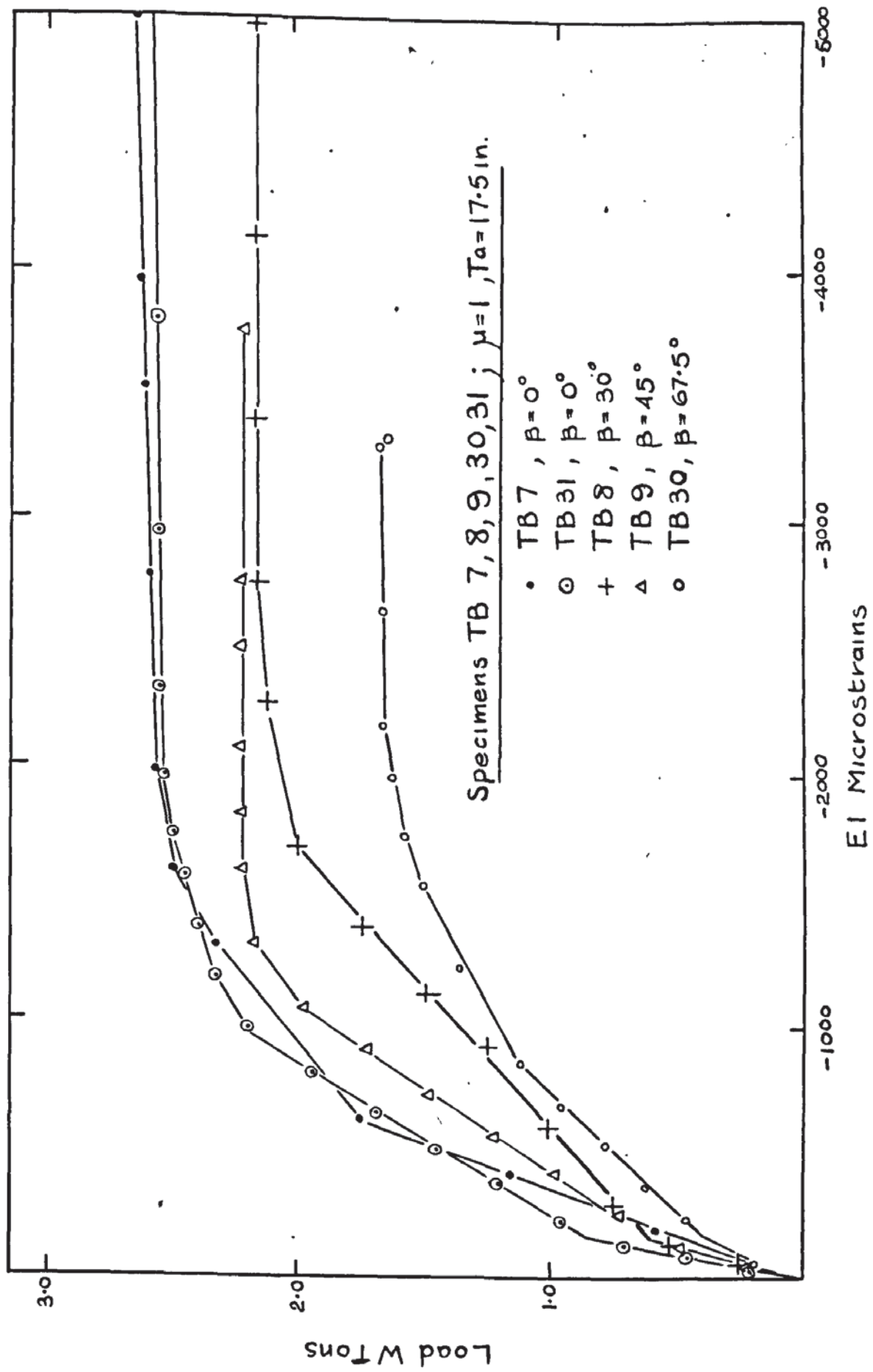


FIG 5-105 PLOT OF PRINCIPAL CONCRETE STRAINS EI - TB7, TB8, TB9, TB30, TB31.

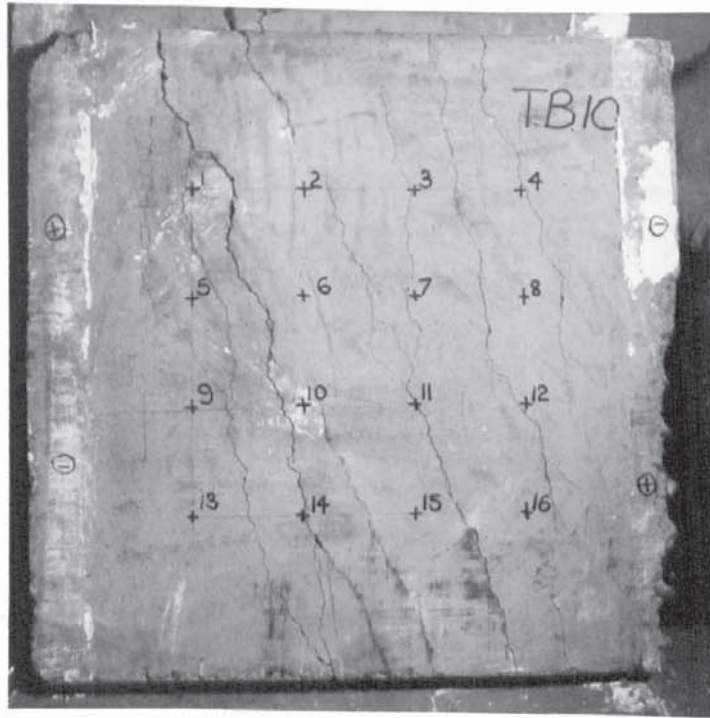


PLATE 5.36

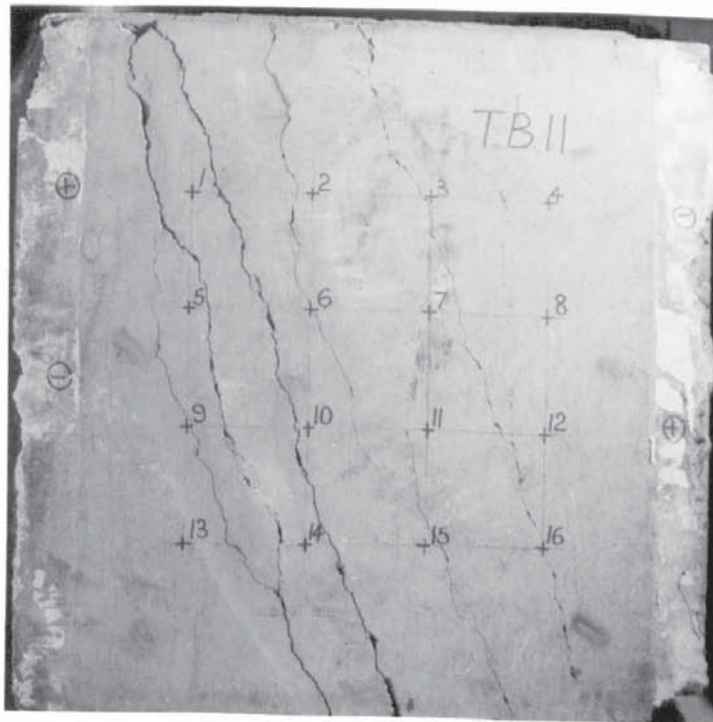


PLATE 5.37

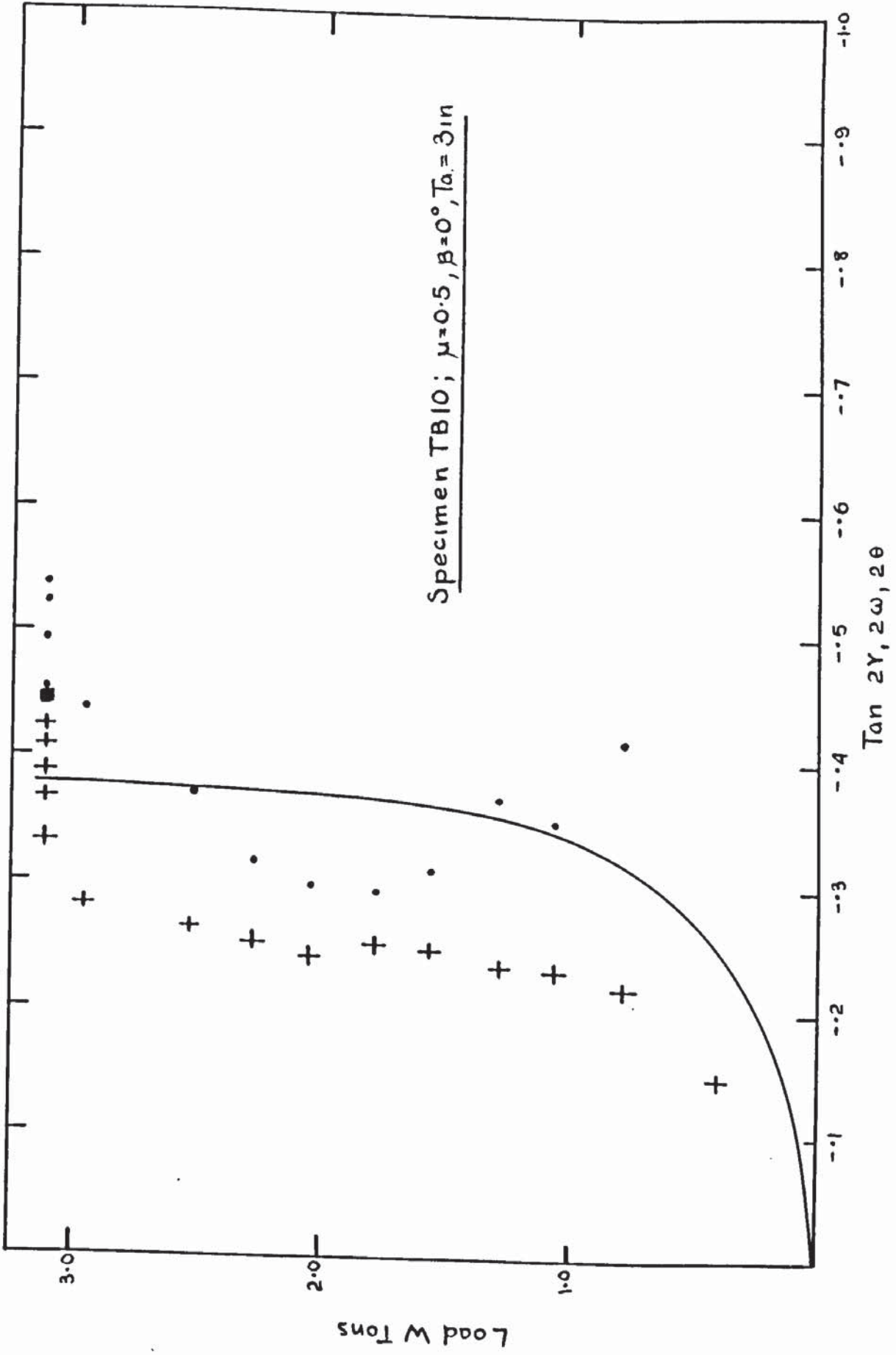


FIG 5.106 PLOT OF PRINCIPAL DIRECTIONS -TB10

LOAD W TONS	MIN. PRINC. CONC. STRAIN E2 μ STRAINS	MIN. PRINC. CURVATURE K2 in <sup>-1</sup> x 10 <sup>3</sup>	STEEL STRAINS MICROSTRAINS									
			1	2	3	4	5	6	7	8		
0.00	0.00	0.0	0.0	0.0	0.0	0.0	0.0	0.0	0.0	0.0	0.0	0.0
0.37	-11.83	.0060	19.8	-9.9	0.0	0.0	0.0	19.8	0.0	14.8	29.7	29.7
0.79	-12.86	.0230	40.0	9.9	-108.9	-108.9	-108.9	99.0	99.0	39.6	79.2	79.2
1.04	-17.98	.0228	59.4	0.0	-158.4	-158.4	-148.5	168.3	168.3	69.3	123.7	148.5
1.29	-22.82	.0012	84.1	9.9	-158.4	-158.4	-193.1	272.3	272.3	168.3	158.4	247.5
1.54	-26.83	.0263	128.7	9.9	-79.2	-79.2	-158.4	391.1	391.1	306.9	316.8	356.4
1.78	-29.10	.0110	138.6	19.8	-39.6	-39.6	-79.2	495.1	495.1	415.9	415.9	445.6
2.03	-34.19	.0014	178.2	19.8	19.8	19.8	9.9	613.9	613.9	553.5	519.8	534.7
2.28	-37.08	.0080	203.0	19.8	69.32	69.32	59.4	712.9	712.9	663.4	609.0	633.7
2.53	-40.63	-.0422	247.5	9.9	123.7	123.7	168.3	831.8	831.8	821.9	752.5	777.3
2.95	-61.79	.0093	267.3	29.7	178.2	178.2	188.1	1034.8	1034.8	1069.4	930	1049.6
3.11	-68.44	-.0508	316.8	89.1	287.1	287.1	415.9	1772.5	1772.5	1485.3	1336.8	1118.9
3.11	-75.75	-.0479	-	148.5	376.2	376.2	19.8	2079.5	2079.5	1782.4	1376.4	-
3.11	-87.98	-.1741	-	108.9	435.7	435.7	9.9	3139.0	3139.0	2539.9	1455.6	-
3.11	-147.68	-.0695	-	99.0	742.6	742.6	-	4822.4	4822.4	7362.4	1633.9	-
3.11	-209.70	-.2166	-	346.5	1307.1	1307.1	-	4990.8	4990.8	-	2317.1	-

Table 5.31 Minimum Principle Concrete Strains & Curvatures & Steel Strains TB.10



LOAD W TONS	MIN.PRINC. CONC. STRAIN E2 μ STRAINS	MIN.PRINC. CURVATURE K# in <sup>-1</sup> x10 <sup>3</sup>	STEEL STRAINS										
			1	2	3	4	5	6	7	8			
0.00	0.00	0.00	0.0	0.0	0.0	0.0	0.0	0.0	0.0	0.0	0.0	0.0	0.0
0.11	-1.36	.0040	9.4	4.7	0.0	4.7	4.7	-	4.7	0.0	0.0	0.0	9.4
0.27	1.77	-.0120	18.79	9.4	9.4	14.0	14.0	-	9.4	0.0	0.0	0.0	9.4
0.44	-3.41	-.0137	28.19	18.7	28.1	28.1	28.1	-	23.4	18.7	18.7	18.7	18.7
0.61	-4.57	-.0126	37.58	28.1	46.9	51.6	51.6	-	46.9	37.5	37.5	37.5	46.9
0.77	-11.42	-.0093	65.77	65.7	84.5	98.6	98.6	-	75.1	56.3	56.3	56.3	84.5
1.02	-25.29	-.0307	150.33	155.0	197.3	230.1	230.1	-	178.5	150.3	150.3	150.3	173.8
1.19	-26.57	-.0305	253.67	253.6	305.3	324.1	324.1	-	319.4	281.8	281.8	281.8	272.4
1.35	-27.04	-.0338	310.05	352.3	422.7	427.4	427.4	-	493.2	441.5	441.5	441.5	385.2
1.52	-28.05	-.0409	469.77	455.6	573.1	530.8	530.8	-	676.4	596.6	596.6	596.6	507.3
1.68	-43.86	-.0648	554.33	535.5	676.4	615.4	615.4	-	831.4	723.4	723.4	723.4	610.7
1.85	-52.34	-.0681	662.37	620.0	784.5	709.3	709.3	-	967.7	850.2	850.2	850.2	723.4
2.02	-71.07	-.0312	742.23	704.6	883.1	831.4	831.4	-	1136.8	986.5	986.5	986.5	845.5
2.27	-85.82	-.0989	995.91	854.9	1024.0	1033.4	1033.4	-	1963.6	1221.4	1221.4	1221.4	1089.8
2.35	-99.28	-.0889	1409.30	1014.7	1066.3	1103.9	1103.9	-	2734.0	1850.8	1850.8	1850.8	1310.6
2.37	-103.60	-.1399	3250.79	1052.2	1089.8	1141.5	1141.5	-	3344.7	2048.1	2048.1	2048.1	1381.1
2.39	-101.37	-.1402	-	1099.2	1118.0	1160.3	1160.3	-	4434.6	2259.5	2259.5	2259.5	1446.8
2.39	-107.74	-.1614	-	1973.0	1136.8	1150.9	1150.9	-	9968.4	3692.3	3692.3	3692.3	1550.2
2.39	-122.79	-.1743	-	3053.4	1155.6	1155.6	1155.6	-	-	6031.9	6031.9	6031.9	1601.9

Table 5.32 Minimum Principle Concrete Strains & Curvatures & Steel Strains TB.11

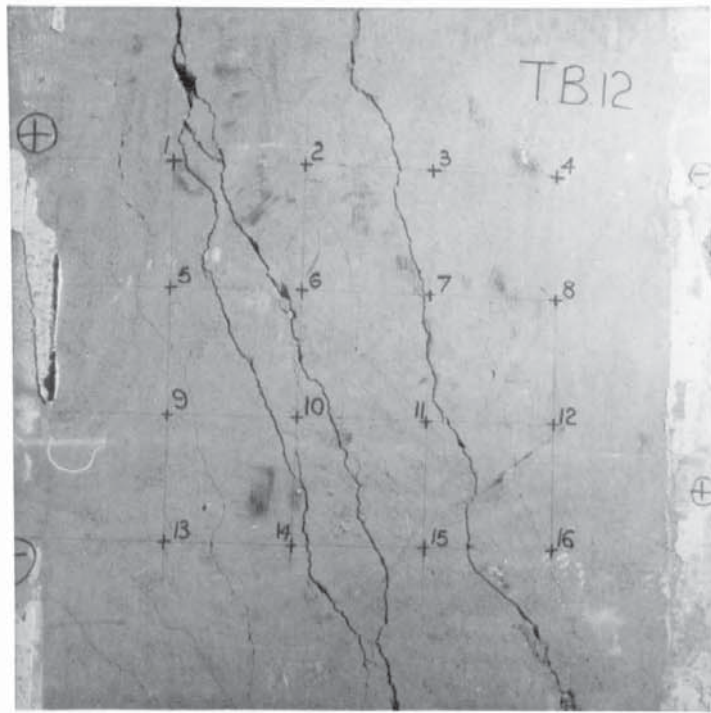


PLATE 5.38

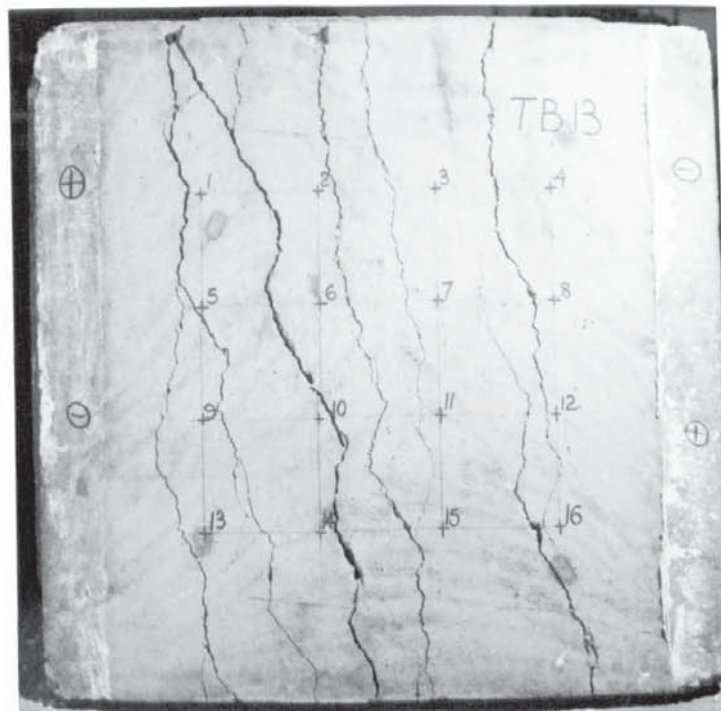


PLATE 5.39

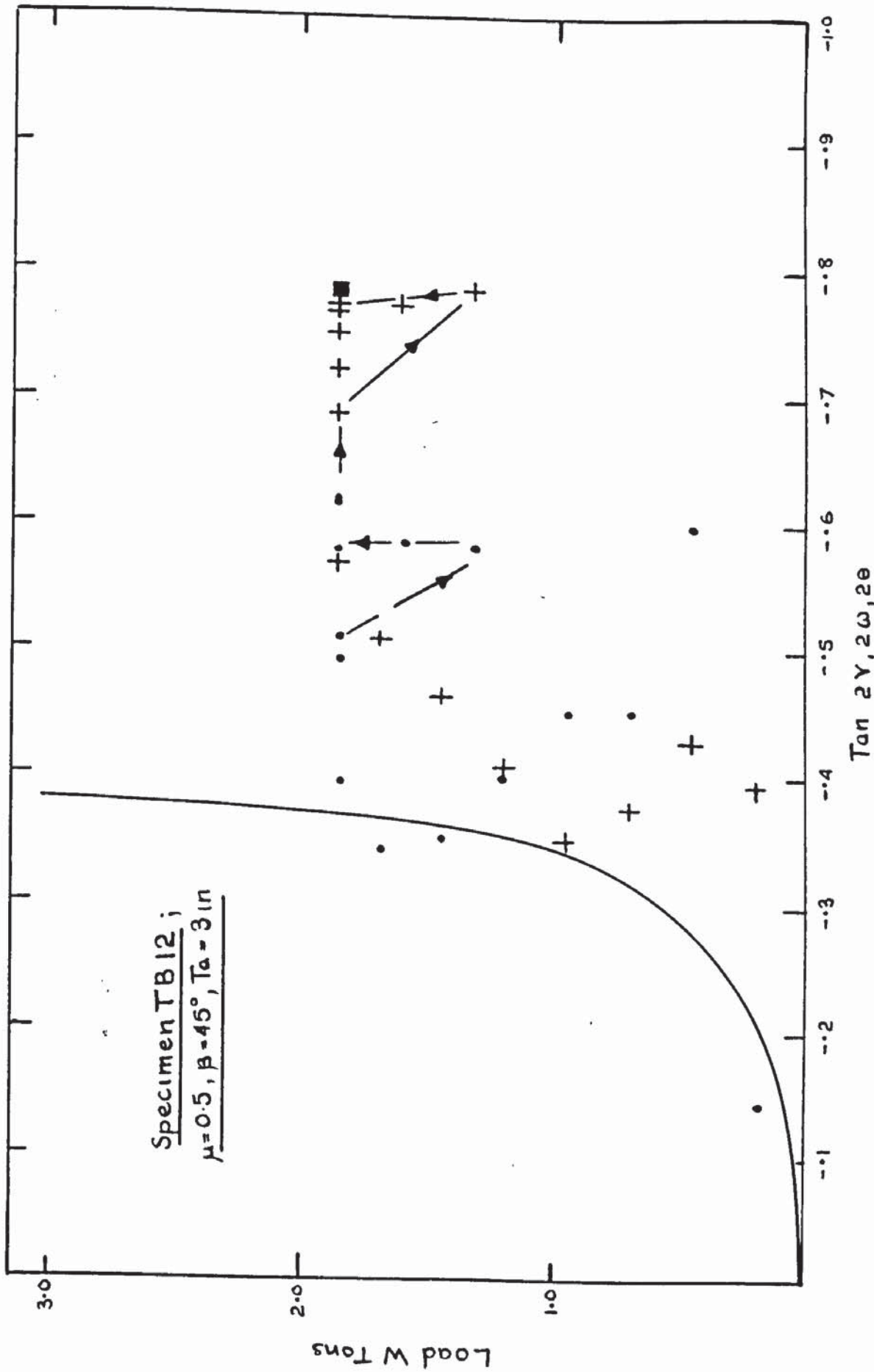
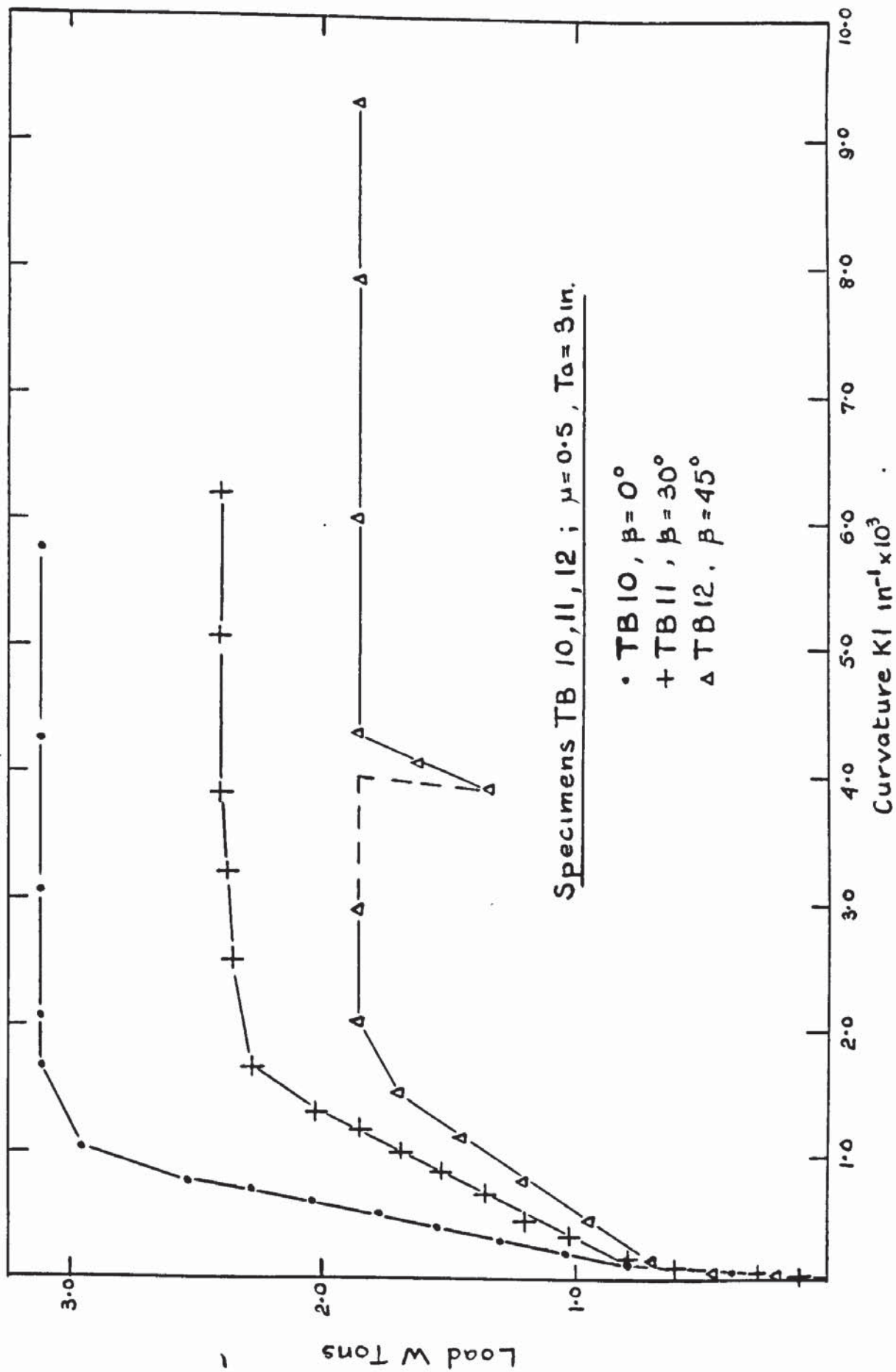


FIG 5-108 PLOT OF PRINCIPAL DIRECTIONS - TB12

LOAD W TONS	MIN.PRINC. CONC. STRAIN E2 μ STRAINS	MIN.PRINC CURVATURE K2 in <sup>-1</sup> x10 <sup>3</sup>	STEEL STRAINS MICROSTRAINS										
			1	2	3	4	5	6	7	8			
0.00	0.00	0.00	0.0	0.0	0.0	0.0	0.0	0.0	0.0	0.0	0.0	0.0	0.0
0.20	.38	.0102	14.0	9.4	9.4	4.7	18.7	9.4	14.0	14.0	18.7	14.0	23.4
0.45	.58	.0131	32.8	9.4	32.8	14.0	46.9	32.8	56.3	56.3	46.9	56.3	70.4
0.70	2.23	.0142	98.6	18.7	108.0	42.2	112.7	93.9	183.2	183.2	112.7	183.2	159.7
0.95	-9.09	.0189	248.9	150.3	286.5	183.2	300.6	385.2	521.4	521.4	300.6	521.4	380.5
1.20	-22.58	-.0178	408.7	319.4	465.0	361.7	591.9	648.2	887.8	887.8	591.9	887.8	657.6
1.44	-32.13	-.0282	530.8	469.7	624.7	512.0	854.9	958.3	1197.9	1197.9	854.9	1197.9	925.4
1.69	-52.30	-.0775	676.4	601.3	779.8	671.7	1127.4	1268.3	2489.7	2489.7	1127.4	2489.7	1188.5
1.86	-76.24	-.1066	854.9	728.1	916.0	831.4	1165.0	3316.5	-	-	1165.0	-	1470.3
1.86	-111.70	-.1123	1263.6	845.5	981.8	916.0	4763.4	4030.6	-	-	4763.4	-	1507.9
1.32	-151.48	-.1165	1273.0	248.9	897.2	869.0	-	5045.3	-	-	-	-	1329.4
1.61	-158.17	-.1426	1320.0	582.5	958.3	901.9	-	5158.0	-	-	-	-	1479.7
1.86	-172.48	-.1553	1399.9	652.9	1033.4	944.2	-	5270.7	-	-	-	-	1658.2
1.86	-253.82	-.3859	1432.7	-	1179.1	1150.9	-	5374.1	-	-	-	-	4542.6
1.86	-343.76	-.1864	1460.9	-	1150.9	1414.0	-	5411.7	-	-	-	-	-
1.86	-384.56	-.3439	1442.1	-	1179.1	1611.3	-	5533.8	-	-	-	-	-

Table 5.33 Minimum Principle Concrete Strains & Curvatures & Steel Strains TB.12



FIGS. 109 PLOT OF MAXIMUM PRINCIPAL CURVATURES - TB10, TB11, TB12.

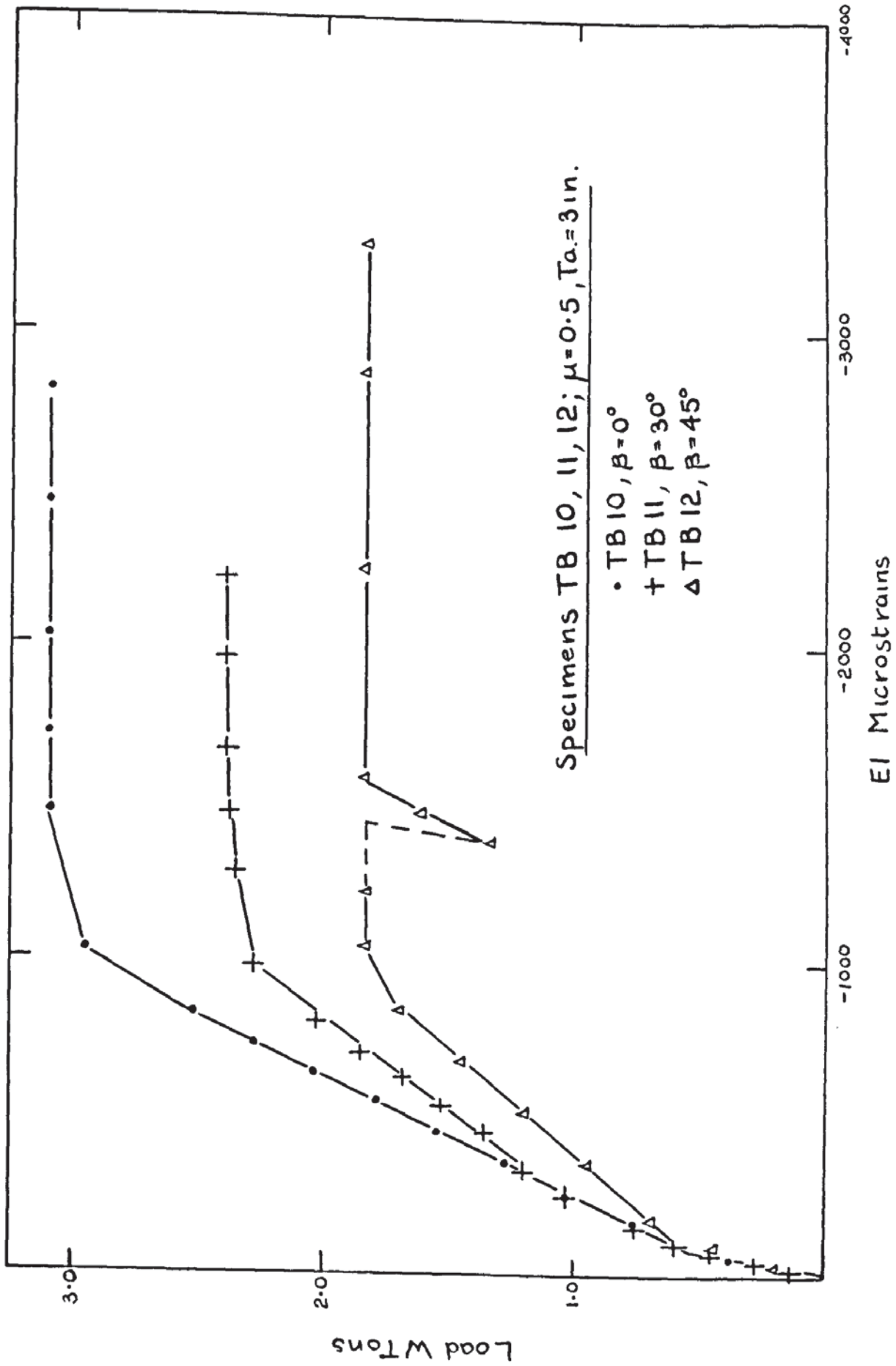


FIG 5-110 PLOT OF PRINCIPAL CONCRETE STRAINS EI - TB10, TB11, TB12.

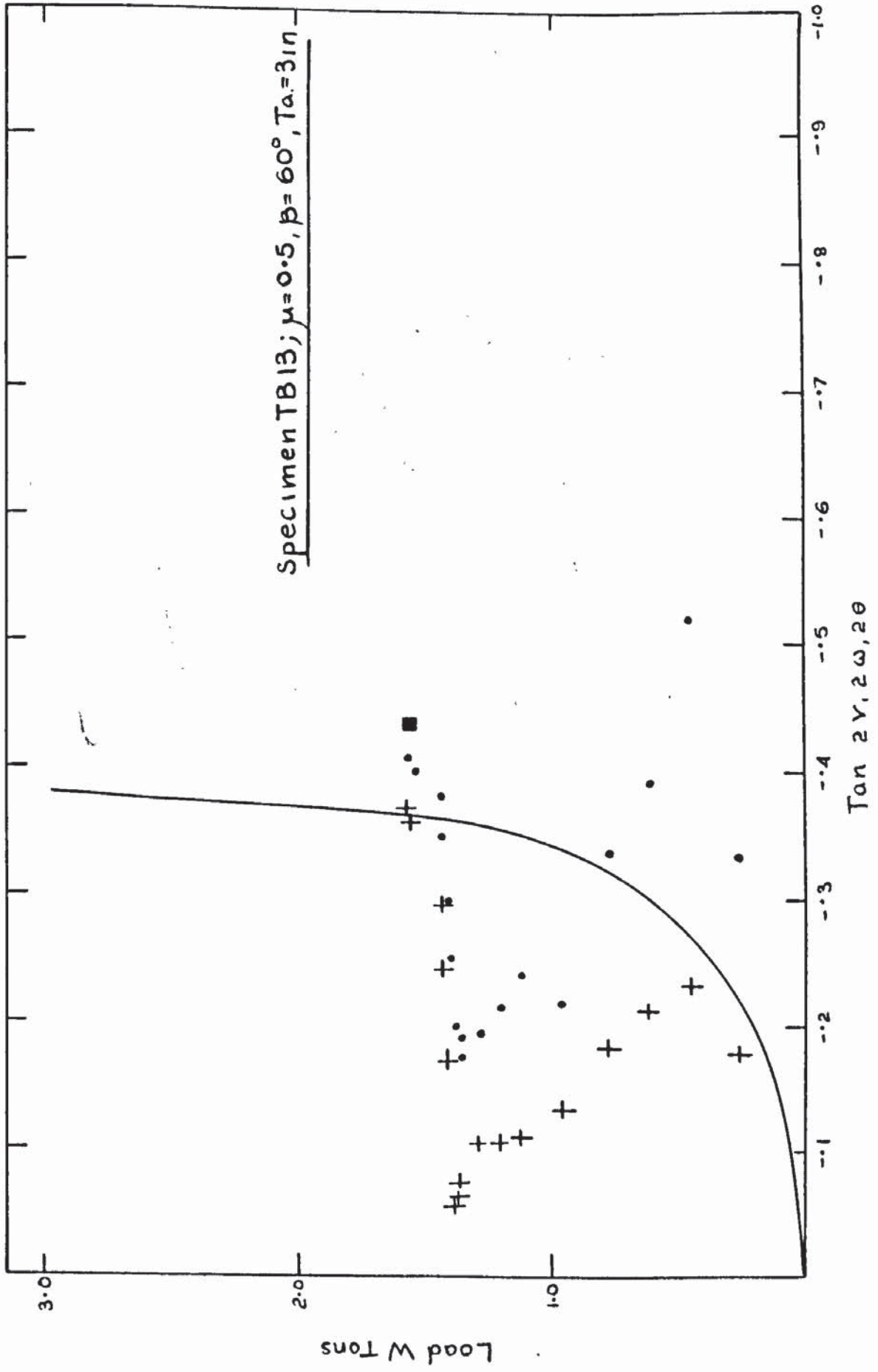


FIG 5.111 PLOT OF PRINCIPAL DIRECTIONS - TB13.

LOAD W TONS	MIN. PRINC. CONC. STRAIN E2 μ STRAINS	MIN. PRINC. CURVATURE K2 in <sup>-1</sup> x10 <sup>3</sup>	STEEL STRAINS										
			1	2	3	4	5	6	7	8			
0.00	0.00	0.00	0.0	0.0	0.0	0.0	0.0	0.0	0.0	0.0	0.0	0.0	0.0
0.12	-6.85	-0.0008	4.7	0.0	0.0	0.0	0.0	0.0	9.4	56.3	9.4	9.4	46.9
0.28	-17.68	-0.0049	4.7	4.7	4.7	4.7	4.7	4.7	28.1	98.6	28.1	28.1	89.2
0.45	-24.14	-0.0098	28.1	14.0	23.4	28.1	28.1	28.1	117.4	155.0	89.2	89.2	112.7
0.61	-37.20	-0.0056	37.5	42.2	46.9	61.0	61.0	291.2	291.2	291.2	239.5	239.5	197.3
0.78	-52.12	-0.0045	93.9	79.8	75.1	108.0	108.0	582.5	582.5	526.1	450.9	450.9	300.6
0.95	-76.64	-0.0531	150.3	117.4	131.5	155.0	155.0	836.1	836.1	723.4	676.4	676.4	723.4
1.11	-90.90	-0.0430	206.7	197.3	211.4	225.4	225.4	1118.0	1118.0	977.1	920.7	920.7	1399.9
1.20	-104.41	-0.0452	244.2	239.5	244.2	253.8	253.8	1268.3	1268.3	1085.1	1005.3	1005.3	1677.0
1.28	-116.44	-0.0476	286.5	291.2	281.8	291.2	291.2	1489.1	1489.1	1202.6	1052.2	1052.2	1893.1
1.36	-148.77	-0.0869	413.4	446.2	460.3	413.4	413.4	7065.3	7065.3	1268.3	1052.2	1052.2	2630.7
1.36	-155.44	-0.1108	544.9	624.7	681.1	595.6	595.6	-	-	1282.4	1094.5	1094.5	7178.0
1.37	-164.68	-0.1185	676.4	718.7	761.0	685.8	685.8	-	-	1287.1	1108.6	1108.6	-
1.39	-257.22	-0.1031	845.5	897.2	826.7	775.1	775.1	-	-	1376.4	1399.9	1399.9	-
1.40	-195.49	-0.0841	1024.0	1155.6	934.8	845.5	845.5	-	-	1005.3	2189.1	2189.1	-
1.42	-184.97	-0.0092	1531.4	-	995.9	920.7	920.7	-	-	244.2	3419.9	3419.9	-
1.42	-217.34	-0.0076	1756.9	-	1052.2	1005.3	1005.3	±	±	-	-	-	-
1.55	-267.19	-0.0278	2066.9	-	1085.1	1118.0	1118.0	-	-	-	-	-	-
1.57	-310.54	-0.0704	-	-	1099.2	1230.7	1230.7	-	-	-	-	-	-

Table 5.34 Minimum Principle Concrete Strains & Curvatures & Steel Strains TB.13

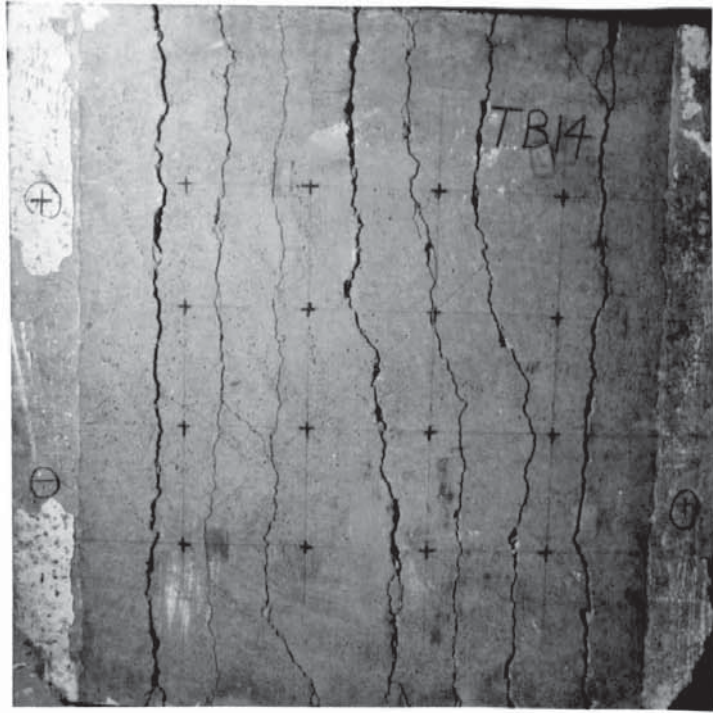


PLATE 5.40

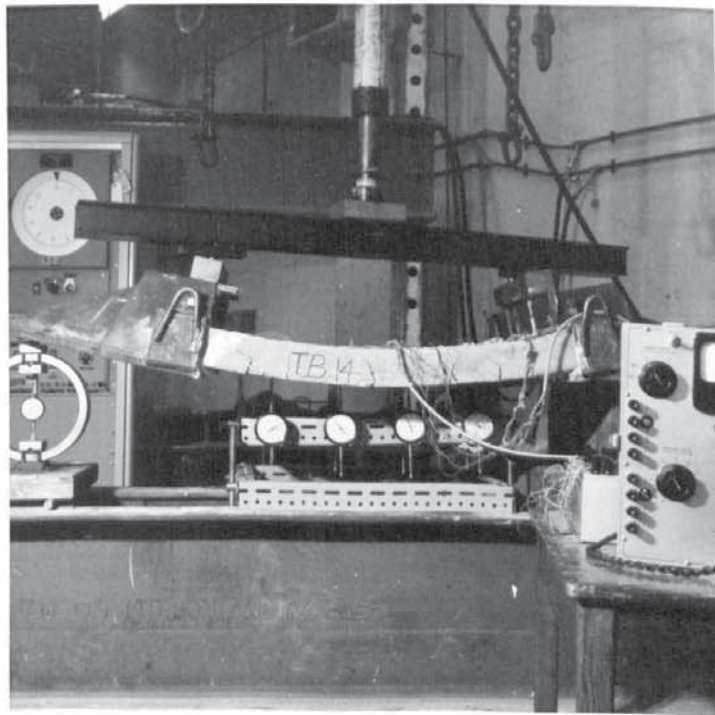


PLATE 5.41

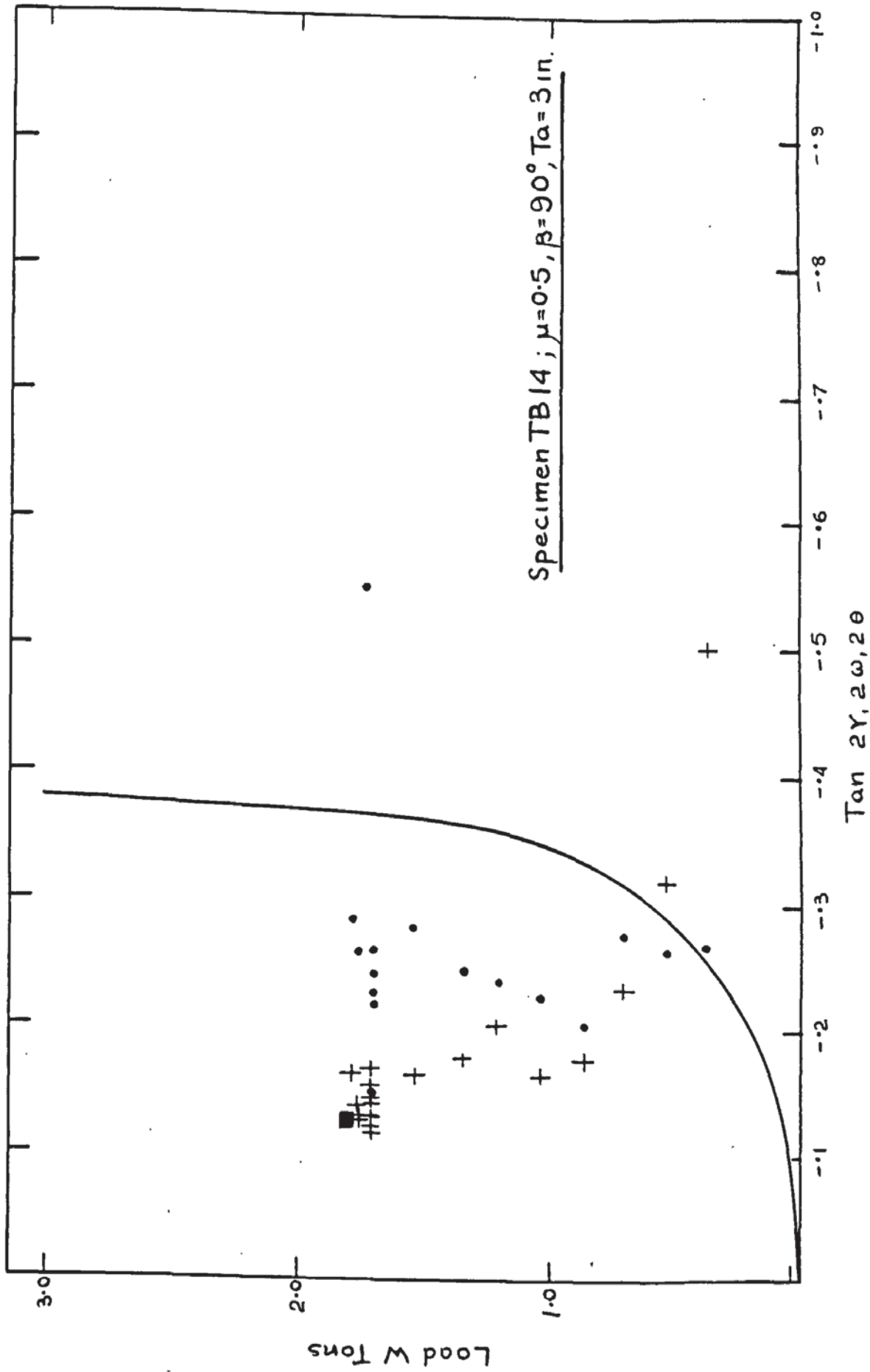


FIG 5-112 PLOT OF PRINCIPAL DIRECTIONS - TB14.

LOAD W TONS	MIN. PRINC. CONC. STRAIN E2 μ STRAINS	MIN. PRINC. CURVATURE K2 in <sup>-1</sup> x10 <sup>3</sup>	STEEL STRAINS MICROSTRAINS																
			1	2	3	4	5	6	7	8									
0.00	0.00	0.00	0.0	0.0	0.0	0.0	0.0	0.0	0.0	0.0	0.0	0.0	0.0	0.0	0.0	0.0	0.0	0.0	0.0
0.03	-1.67	-	4.93	0.0	0.0	0.0	9.5	0.0	0.0	0.0	0.0	0.0	0.0	0.0	0.0	0.0	0.0	0.0	4.9
0.20	23.22	-.0115	4.93	9.8	0.0	0.0	19.7	-	-	-	-	-	-	-	-	-	-	-	14.7
0.37	21.06	-.0188	-9.85	-9.8	-19.7	-19.7	-4.9	-	-	-	-	-	-	-	-	-	-	-	4.9
0.53	19.71	-.0096	9.85	0.0	-9.8	-9.8	0.0	-	-	-	-	-	-	-	-	-	-	-	34.4
0.70	11.40	-.0199	9.85	-	-9.8	-9.8	9.8	-	-	-	-	-	-	-	-	-	-	-	142.8
0.86	-24.87	-.0329	14.78	-	-9.8	-9.8	24.6	-	-	-	-	-	-	-	-	-	-	-	320.2
1.03	-42.19	-.0245	29.56	-	-9.8	-9.8	49.2	-	-	-	-	-	-	-	-	-	-	-	497.6
1.20	-58.78	-.0487	34.49	5.9	-9.8	-9.8	68.9	-	-	-	-	-	-	-	-	-	-	-	665.1
1.36	-79.74	-.0503	44.34	-	-9.8	-9.8	108.3	-	-	-	-	-	-	-	-	-	-	-	852.3
1.53	-92.85	-.0697	49.27	-	-9.8	-9.8	118.2	-	-	-	-	-	-	-	-	-	-	-	1049.4
1.69	-119.19	.1723	49.27	-	-19.7	-19.7	157.6	-	-	-	-	-	-	-	-	-	-	-	1379.5
1.69	-174.95	-	44.34	-4.9	-19.7	-19.7	177.3	-	-	-	-	-	-	-	-	-	-	-	1542.1
1.69	-234.01	-.0564	39.41	-19.7	-19.7	-19.7	266.0	-	-	-	-	-	-	-	-	-	-	-	1601.2
1.69	-308.16	-	14.78	-19.7	-19.7	-4.9	256.2	-	-	-	-	-	-	-	-	-	-	-	1655.4
1.69	-312.79	.0614	29.56	-9.8	-4.9	-4.9	246.3	-	-	-	-	-	-	-	-	-	-	-	1709.6
1.69	-329.17	-	34.49	-9.8	0.0	0.0	236.4	-	-	-	-	-	-	-	-	-	-	-	1886.9
1.69	-348.14	-.0394	39.41	0.0	9.8	9.8	216.7	-	-	-	-	-	-	-	-	-	-	-	-
1.73	-357.90	-	59.12	9.8	14.7	14.7	147.8	-	-	-	-	-	-	-	-	-	-	-	-
1.75	-389.68	.1093	59.12	0.0	4.9	4.9	128.1	-	-	-	-	-	-	-	-	-	-	-	-
1.76	-409.21	-	98.54	-19.71	4.9	4.9	73.9	-	-	-	-	-	-	-	-	-	-	-	-
1.78	-464.51	-.2287	305.46	-49.2	118.2	118.2	9.8	-	-	-	-	-	-	-	-	-	-	-	-
1.72	-452.92	-6266	359.66	-59.1	-	-	152.7	-	-	-	-	-	-	-	-	-	-	-	-

Table 5.35 Minimum Principle Concrete Strains & Curvatures & Steel Strains TB.14

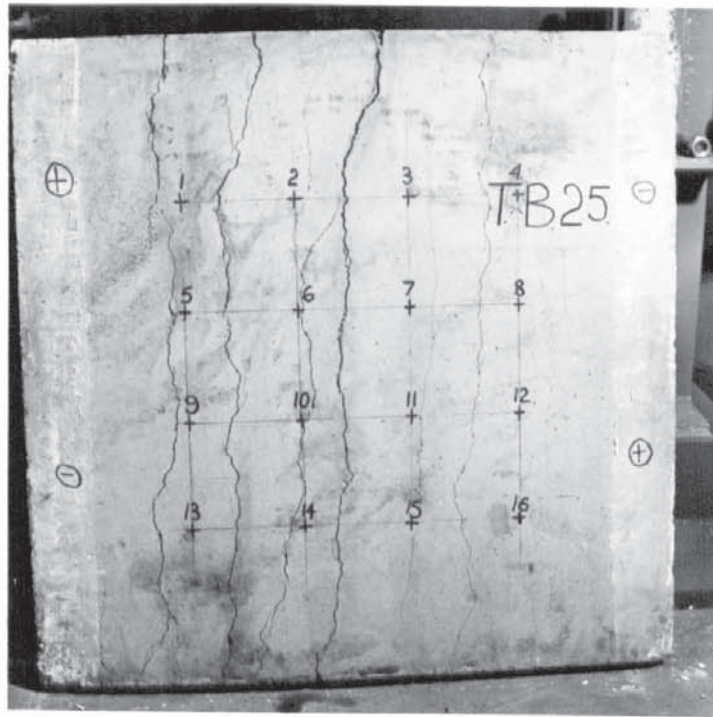


PLATE 5.42

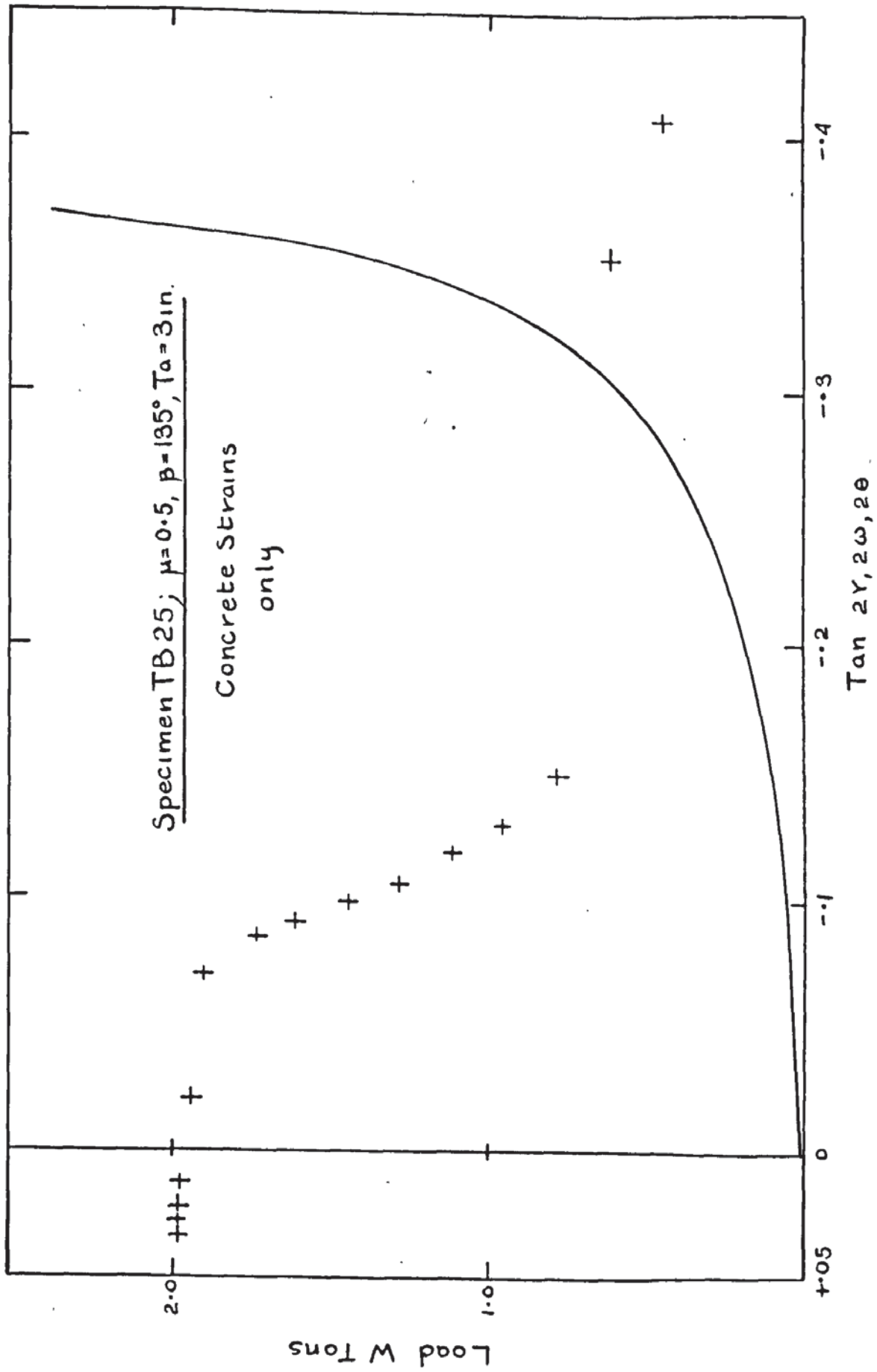
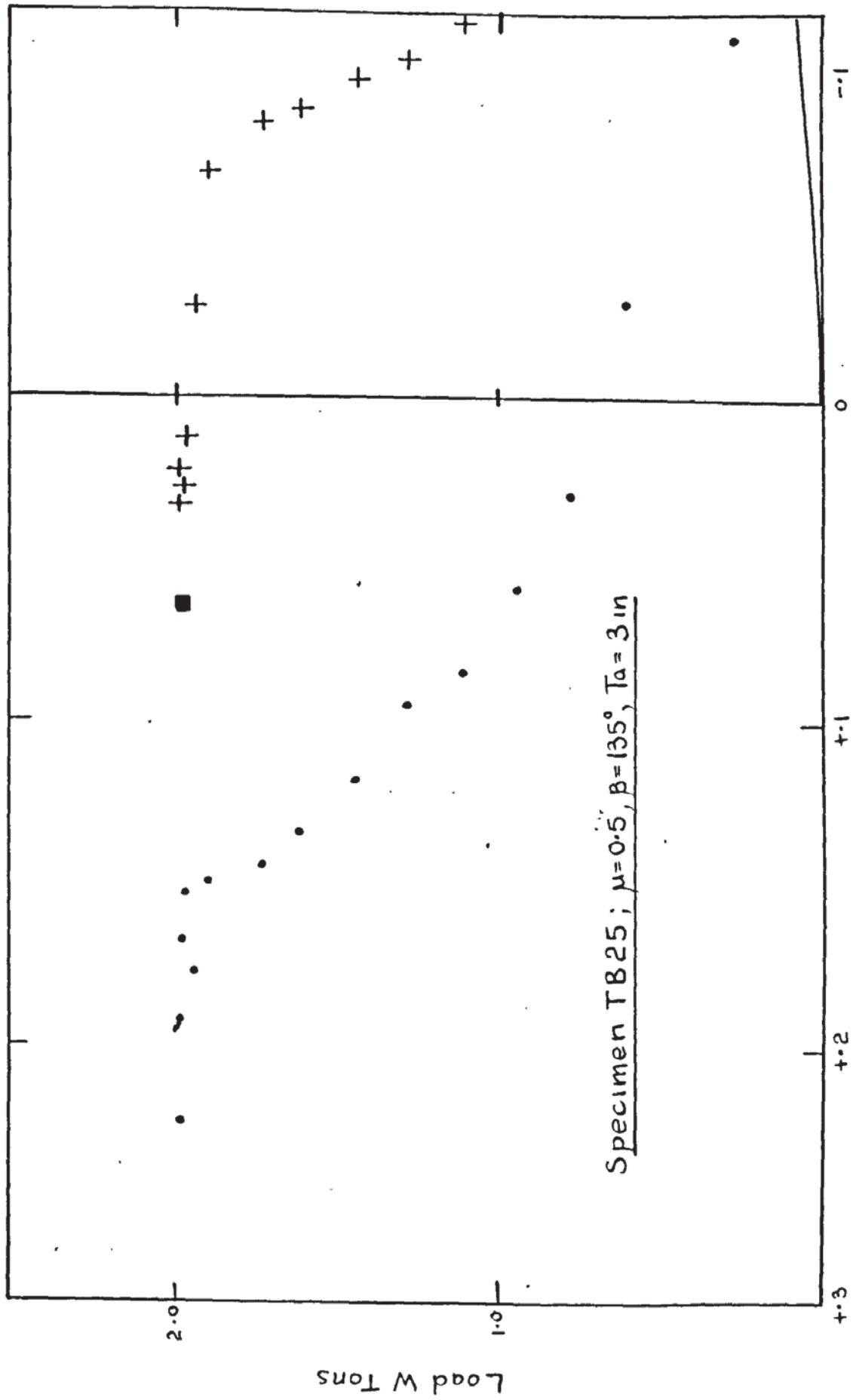


FIG 113A PLOT OF PRINCIPAL DIRECTIONS - TB 25.



Tan  $2\gamma, 2\omega, 2\theta$

FIG 5-1138 PLOT OF PRINCIPAL DIRECTIONS - TB25.

LOAD W TONS	MIN.PRINC. CONC. STRAIN E2 μ STRAINS	MIN.PRINC. CURVATURE K2 in <sup>-1</sup> x10 <sup>3</sup>	STEEL STRAINS MICROSTRAINS										
			1	2	3	4	5	6	7	8			
0.00	0.00	0.00	0.0	0.0	0.0	0.0	0.0	0.0	0.0	0.0	0.0	0.0	0.0
0.12	-91.36	-.0166	9.6	0.0	4.8	9.6	9.6	0.0	0.0	0.0	4.8	4.8	4.8
0.28	-88.29	-.0036	14.4	9.6	9.6	9.6	9.6	9.6	9.6	9.6	9.6	9.6	9.6
0.45	-88.69	.0224	24.0	19.2	19.2	28.8	28.8	19.2	19.2	24.0	19.2	19.2	14.4
0.61	-82.95	-.0104	67.3	28.8	38.4	57.7	57.7	48.1	48.1	67.3	48.1	48.1	33.6
0.78	-79.67	.0035	149.1	86.5	144.2	182.7	182.7	110.6	110.6	192.3	144.2	144.2	101.0
0.95	-93.30	-.0486	250.1	298.1	259.7	365.5	365.5	269.3	269.3	413.6	405.3	405.3	331.8
1.11	-103.04	-.0423	360.7	442.4	355.9	529.0	529.0	442.4	442.4	606.0	610.8	610.8	514.6
1.28	-119.97	-.0638	456.9	557.9	432.8	663.7	663.7	586.7	586.7	769.5	774.3	774.3	687.7
1.44	-131.07	-.1006	567.5	692.5	538.6	808.0	808.0	750.2	750.2	952.2	947.4	947.4	889.7
1.61	-145.96	-.1759	673.3	817.6	625.2	933.0	933.0	904.1	904.1	1115.8	1106.1	1106.1	1058.1
1.73	-162.95	-.1636	769.5	904.1	682.9	1048.4	1048.4	1019.6	1019.6	1240.8	1240.8	1240.8	1168.7
1.90	-181.18	-.1866	933.0	1029.2	788.7	1221.6	1221.6	1144.6	1144.6	1490.9	1433.2	1433.2	1269.7
1.94	-196.34	-.1983	961.9	1067.7	913.8	1462.1	1462.1	1154.2	1154.2	2510.5	1462.1	1462.1	1447.6
1.97	-167.49	-.3526	1866.1	1086.9	990.7	1539.0	1539.0	1125.4	1125.4	3549.4	1414.0	1414.0	3823.5
1.98	-187.70	-.3884	-	1077.3	1014.8	1625.6	1625.6	1106.1	1106.1	4299.7	1423.6	1423.6	-
1.98	-237.54	-.4824	-	1115.8	1101.3	1702.5	1702.5	1115.8	1115.8	-	1500.5	1500.5	-
1.98	-278.31	-.7418	-	1106.1	1385.1	1769.9	1769.9	1115.8	1115.8	-	3203.1	3203.1	-

Table 5.36 Minimum Principle Concrete Strains & Curvatures & Steel Strains TR25

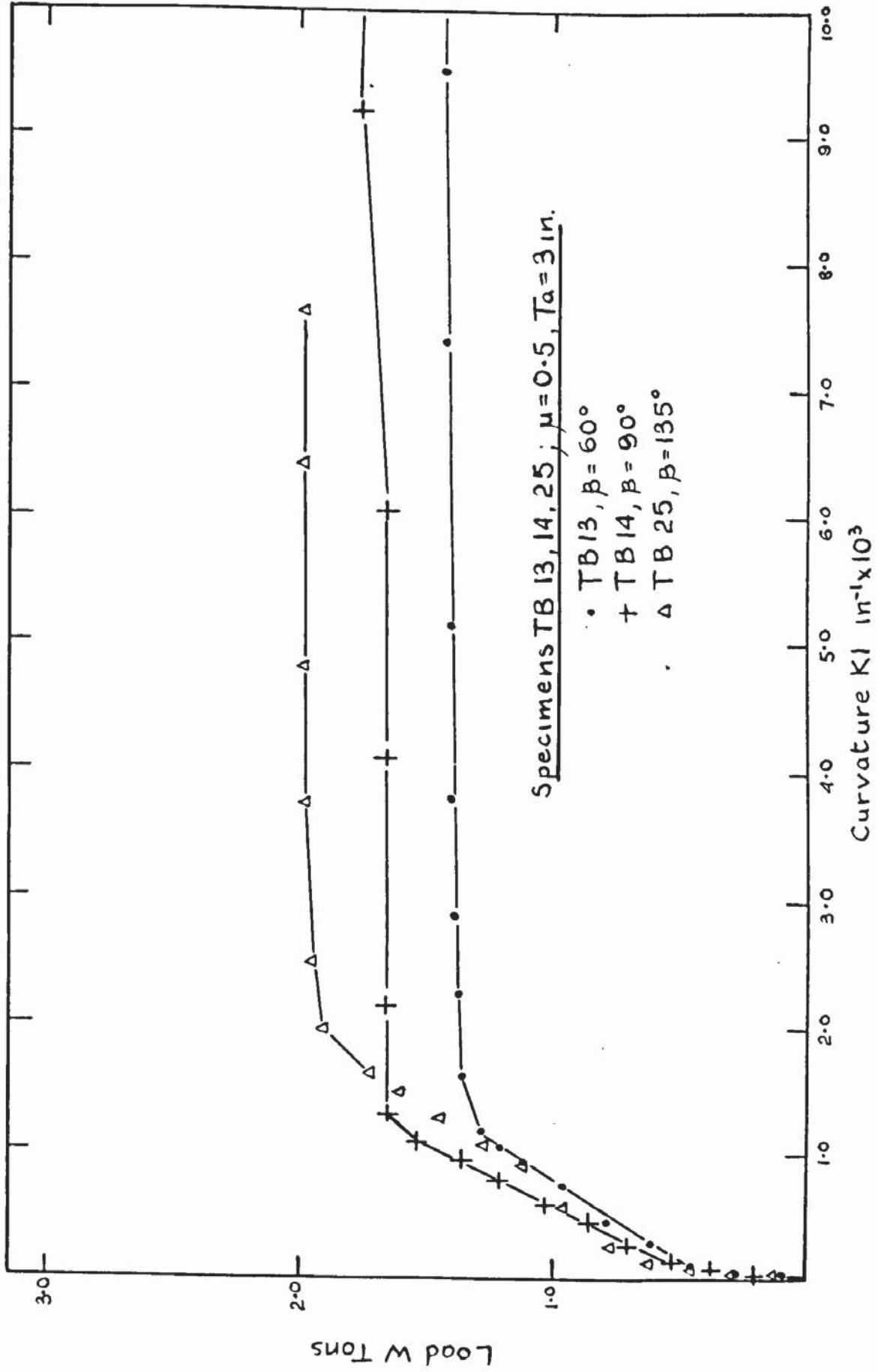


FIG 5-114 PLOT OF MAXIMUM PRINCIPAL CURVATURES- TB13, TB14, TB25

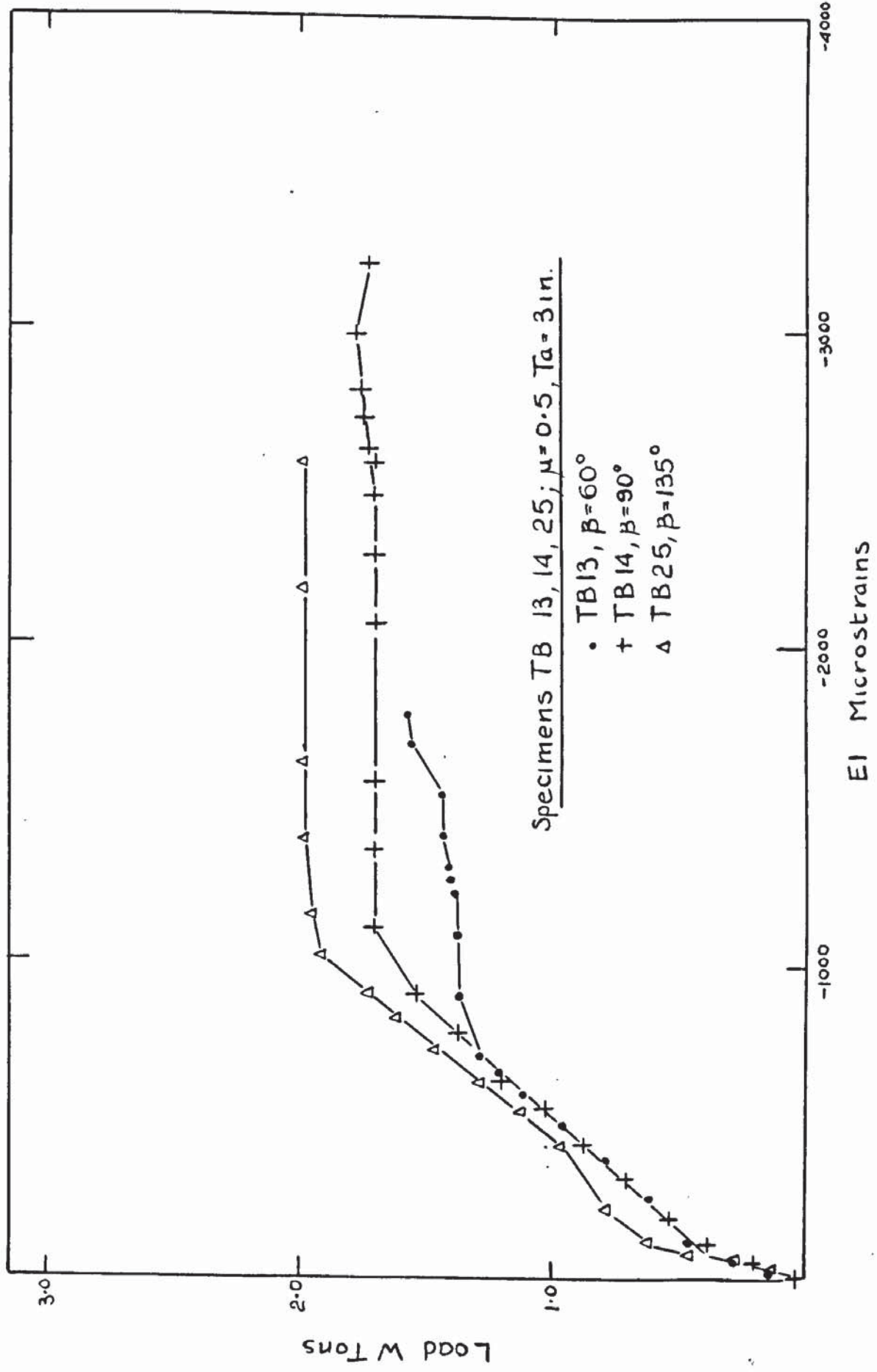


FIG 5-115 PLOT OF PRINCIPAL CONCRETE STRAINS EI-TB13, TB14, TB25.

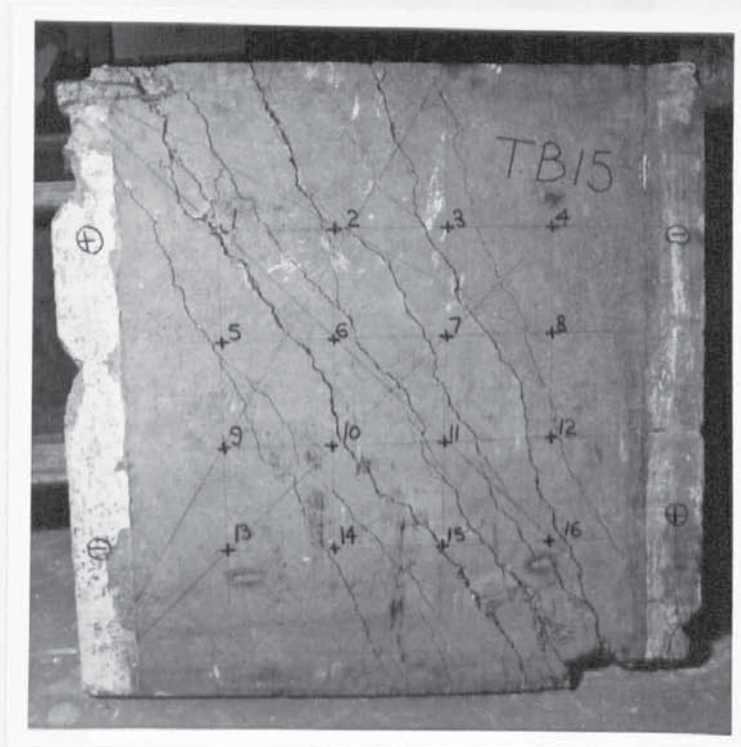


PLATE 5.43

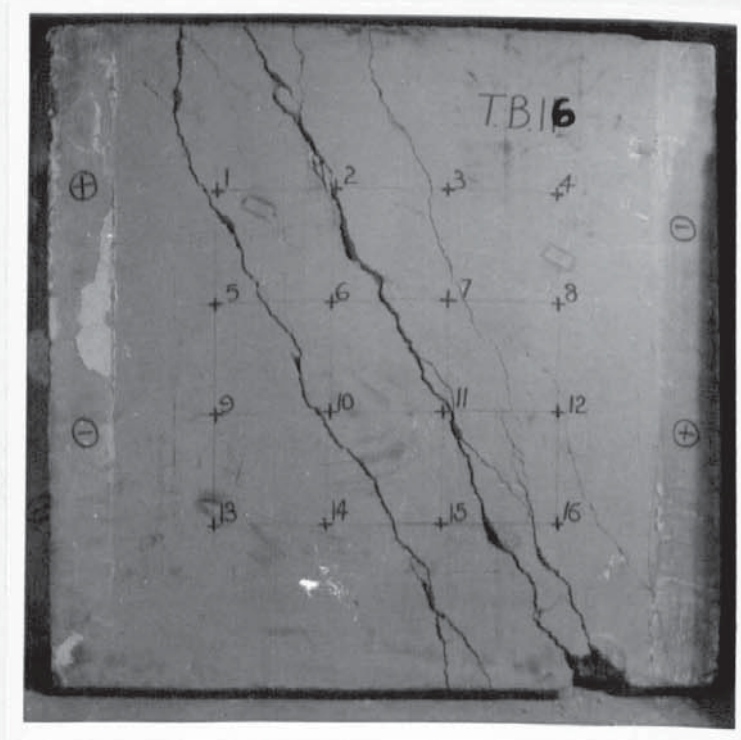
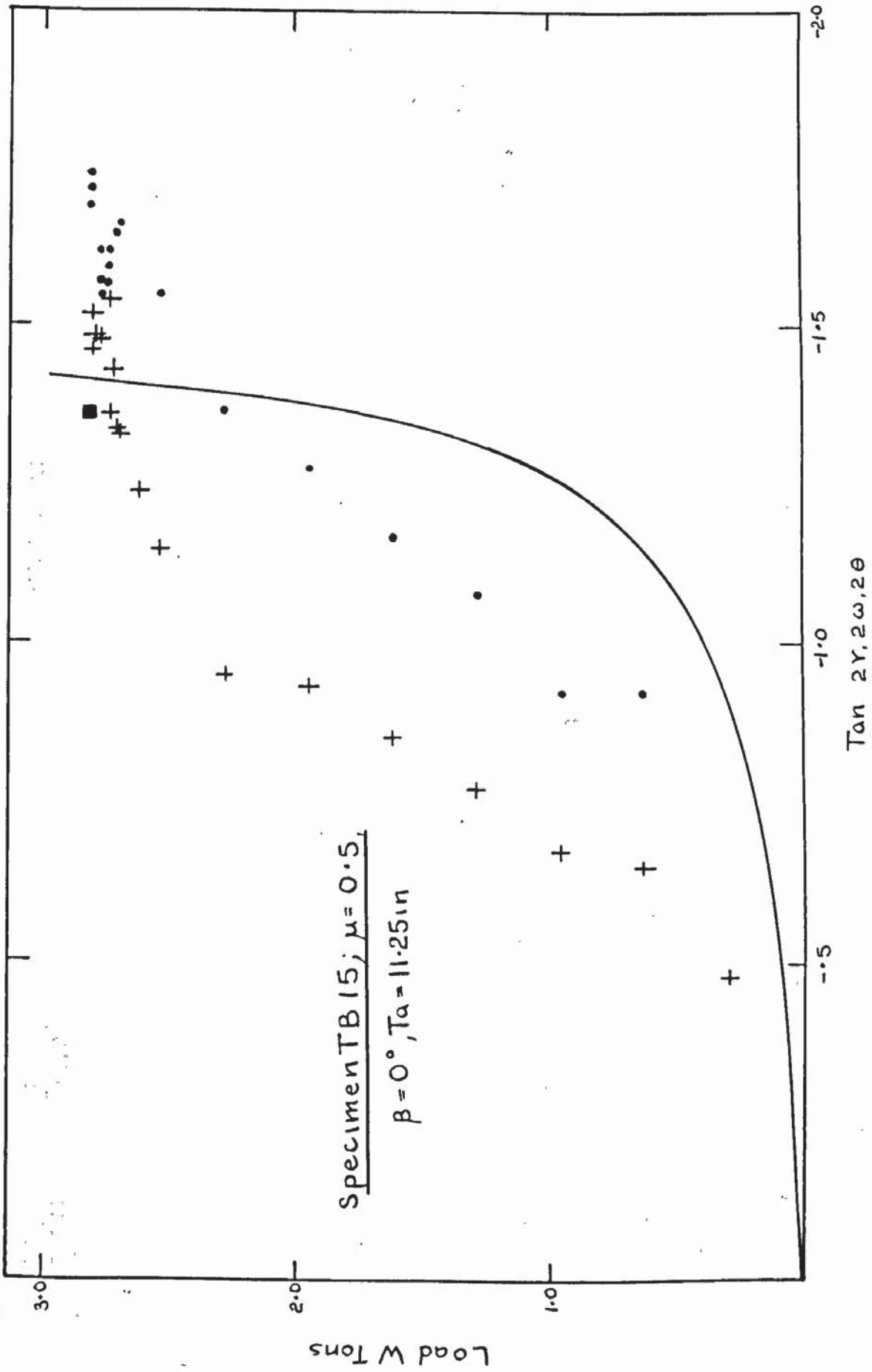


PLATE 5.44



FIGS. 116 PLOT OF PRINCIPAL DIRECTIONS - TB 15

LOAD W TONS	MIN.PRINC. CONC.STRAIN E2 μ S STRAINS	MIN.PRINC. CURVATURE K2 in <sup>-1</sup> x10 <sup>3</sup>	STEEL STRAINS										
			1	2	3	4	5	6	7	8			
0.00	0.00	0.00	0.0	0.0	0.0	0.0	0.0	0.0	0.0	0.0	0.0	0.0	0.0
0.29	-5.73	.0040	0.0	0.0	0.0	0.0	0.0	19.7	14.7	19.7	14.7	19.7	14.7
0.62	-16.02	-.0107	19.7	9.8	0.0	0.0	0.0	54.2	49.2	59.1	59.1	59.1	59.1
0.95	-24.31	-.0190	34.45	29.5	9.8	0.0	0.0	157.6	177.3	197.0	177.3	197.0	157.6
1.29	-43.16	-.0232	59.1	59.1	68.9	19.7	19.7	354.7	337.2	364.5	337.2	364.5	339.9
1.62	-62.97	-.0352	108.3	103.4	128.1	39.4	39.4	571.5	615.8	551.8	615.8	551.8	512.3
1.95	-90.33	-.0553	147.8	157.6	192.1	68.9	68.9	778.4	837.5	729.1	837.5	729.1	709.4
2.28	-113.03	-.0760	285.7	256.2	290.6	123.1	123.1	1005.0	1083.9	945.9	1083.9	945.9	975.5
2.53	-133.99	-.1040	404.0	472.9	423.7	192.1	192.1	1167.6	1537.1	1152.8	1537.1	1152.8	1478.0
2.61	-150.18	-.0760	561.6	748.8	601.0	295.6	295.6	1251.4	1921.4	1241.5	1921.4	1241.5	2059.4
2.70	-184.60	-.1815	739.0	965.6	867.1	522.2	522.2	1310.5	2305.7	1290.8	2305.7	1290.8	3645.8
2.71	-206.56	-.2219	916.3	1162.7	1216.9	689.7	689.7	1359.8	2630.9	1310.5	2630.9	1310.5	8257.3
2.74	-241.87	-.2765	1034.6	1280.9	1556.8	783.3	783.3	1389.3	2832.9	1330.2	2832.9	1330.2	-
2.74	-389.66	-.3043	1192.2	1379.5	1990.4	847.4	847.4	1448.4	3182.7	1428.7	3182.7	1428.7	-
2.74	-345.01	-.3839	1478.0	1532.2	2650.6	916.3	916.3	1753.9	4473.5	3074.3	4473.5	3074.3	-
2.78	-343.67	-.4550	1852.4	1734.2	3369.9	955.8	955.8	4197.6	1.1x10 <sup>4</sup>	-	-	-	-
2.78	-343.67	-.4817	2236.7	1852.4	4049.8	1000.0	1000.0	-	-	-	-	-	-
2.78	-118.75	-.5433	3054.6	1960.8	5054.9	1034.6	1034.6	-	-	-	-	-	-
2.82	-373.77	-.2338	-	2138.2	6966.5	1083.9	1083.9	-	-	-	-	-	-
2.82	-731.96	-.2075	-	2315.6	-	1113.4	1113.4	-	-	-	-	-	-
2.82	-905.88	-.1815	-	-	-	-	-	-	-	-	-	-	-

Table 5.37 Minimum Principle Concrete Strains & Curvatures & Steel Strains TB.15

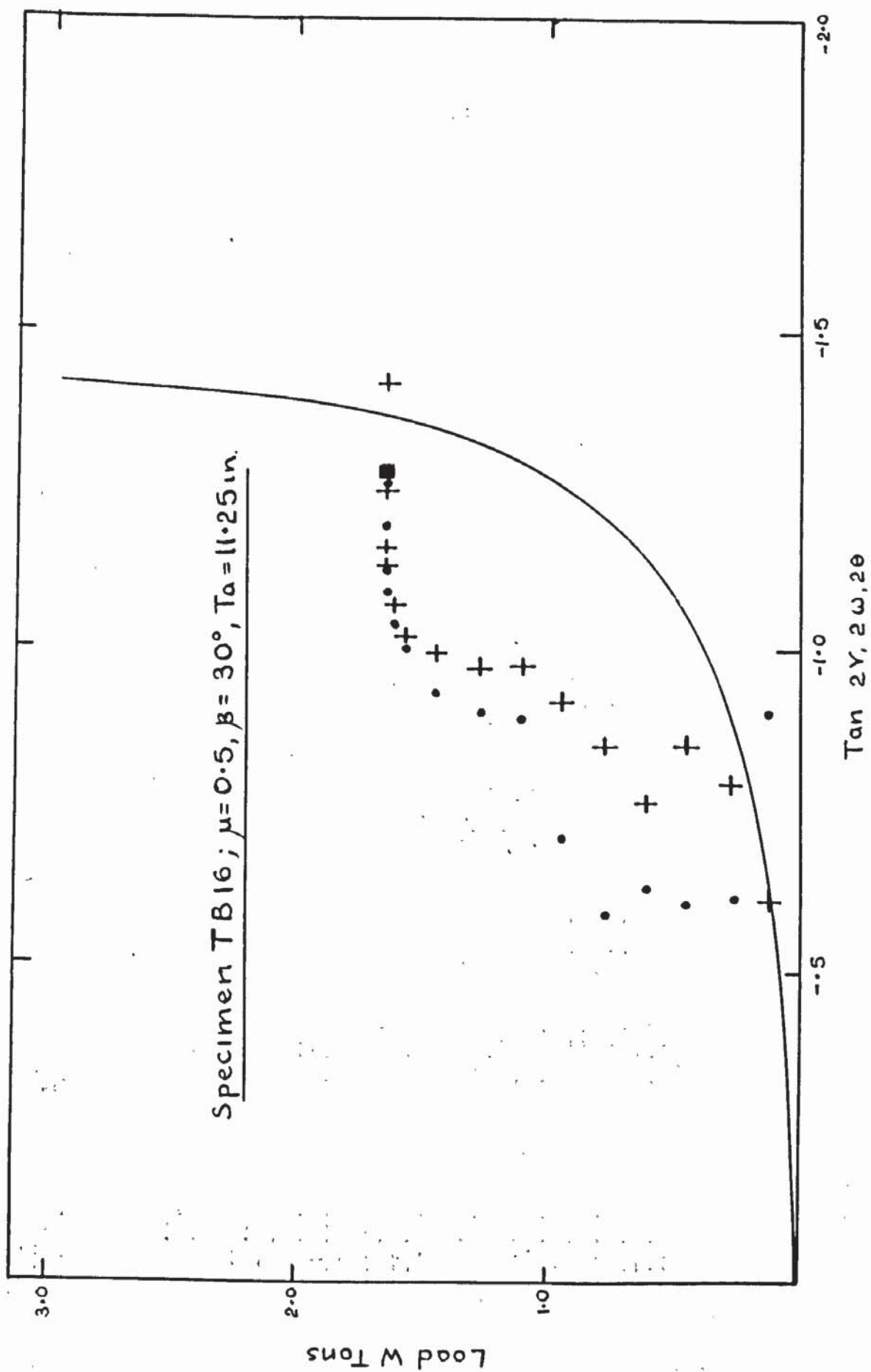


FIG 5-117 PLOT OF PRINCIPAL DIRECTIONS - TB16

LOAD W TONS	MIN.PRINC. CONC.STRAIN E2 μ STRAINS	MIN.PRINC. CURVATURE K2 in <sup>-1</sup> x10 <sup>3</sup>	STEEL STRAINS															
			1	2	3	4	5	6	7	8								
0.00	0.00	0.00	0.0	0.0	0.0	0.0	0.0	0.0	0.0	0.0	0.0	0.0	0.0	0.0	0.0	0.0	0.0	0.0
0.12	-3.39	.0094	0.0	0.0	18.7	0.0	0.0	0.0	0.0	0.0	0.0	0.0	0.0	0.0	0.0	0.0	0.0	0.0
0.28	-9.90	.0218	4.7	9.4	28.1	9.4	9.4	9.4	9.4	9.4	9.4	9.4	9.4	9.4	9.4	9.4	9.4	9.4
0.45	-15.0	.0323	32.8	56.3	65.7	56.3	56.3	37.5	37.5	37.5	56.3	56.3	37.5	37.5	56.3	56.3	56.3	56.3
0.61	-26.76	.0455	84.5	122.1	65.7	122.1	122.1	75.1	75.1	75.1	140.9	140.9	117.4	117.4	159.7	159.7	159.7	159.7
0.78	-45.10	.0530	202.0	216.0	281.8	263.0	263.0	197.3	197.3	197.3	347.6	347.6	300.6	300.6	366.4	366.4	366.4	366.4
0.95	-75.12	.0882	333.5	300.6	432.1	366.4	366.4	375.8	375.8	375.8	540.2	540.2	483.8	483.8	563.7	563.7	563.7	563.7
1.11	-102.33	.0944	427.4	394.6	582.5	488.5	488.5	591.9	591.9	591.9	751.6	751.6	685.8	685.8	761.0	761.0	761.0	761.0
1.28	-116.54	.1200	521.4	479.1	714.0	601.3	601.3	761.0	761.0	761.0	920.7	920.7	850.2	850.2	930.1	930.1	930.1	930.1
1.44	-126.89	.1322	629.4	573.1	854.9	742.2	742.2	977.1	977.1	977.1	1160.3	1160.3	1061.6	1061.6	1146.2	1146.2	1146.2	1146.2
1.57	-102.26	.2240	728.1	685.8	977.1	939.5	939.5	1061.6	1061.6	1061.6	1212.0	1212.0	1136.8	1136.8	1258.9	1258.9	1258.9	1258.9
1.61	-93.92	.2091	831.4	808.0	1056.9	1033.4	1033.4	1094.5	1094.5	1094.5	1249.5	1249.5	1155.6	1155.6	1287.1	1287.1	1287.1	1287.1
1.65	-105.18	.2413	925.4	869.0	1108.6	1080.4	1080.4	1136.8	1136.8	1136.8	1287.1	1287.1	1165.0	1165.0	1324.7	1324.7	1324.7	1324.7
1.65	-107.97	.3496	-	948.9	1165.0	1118.0	1118.0	1165.0	1165.0	1165.0	1324.7	1324.7	1183.8	1183.8	1371.7	1371.7	1371.7	1371.7
1.65	-113.68	.3943	-	-	1230.7	1193.2	1193.2	1818.0	1818.0	1818.0	1437.4	1437.4	1221.4	1221.4	9414.1	9414.1	9414.1	9414.1
1.65	-131.59	.5213	-	-	1334.1	1240.1	1240.1	-	-	-	-	-	1653.5	1653.5	-	-	-	-
1.57	-127.89	.8220	-	-	2245.4	-	-	-	-	-	-	-	-	-	-	-	-	-

Table 5.38 Minimum Principle Concrete Strains & Curvatures & Steel Strains TB.16

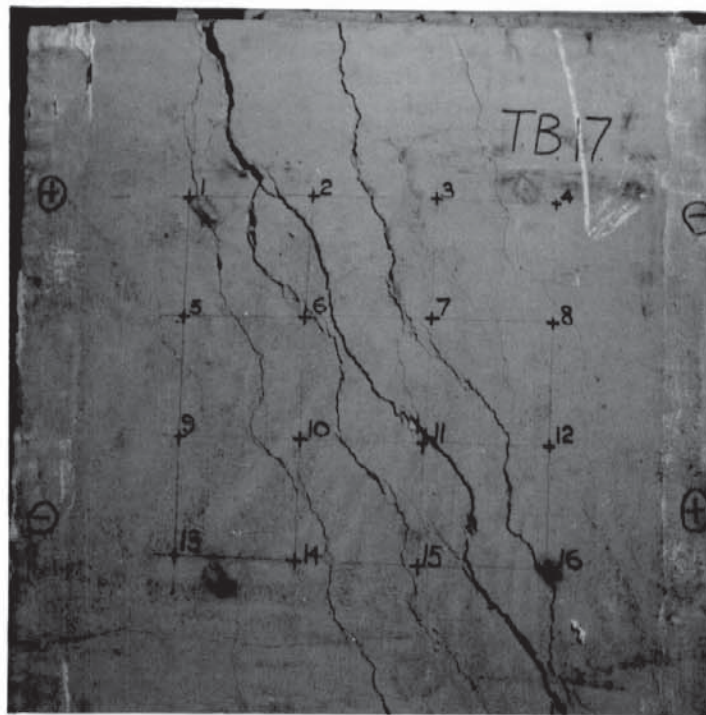


PLATE 5.45

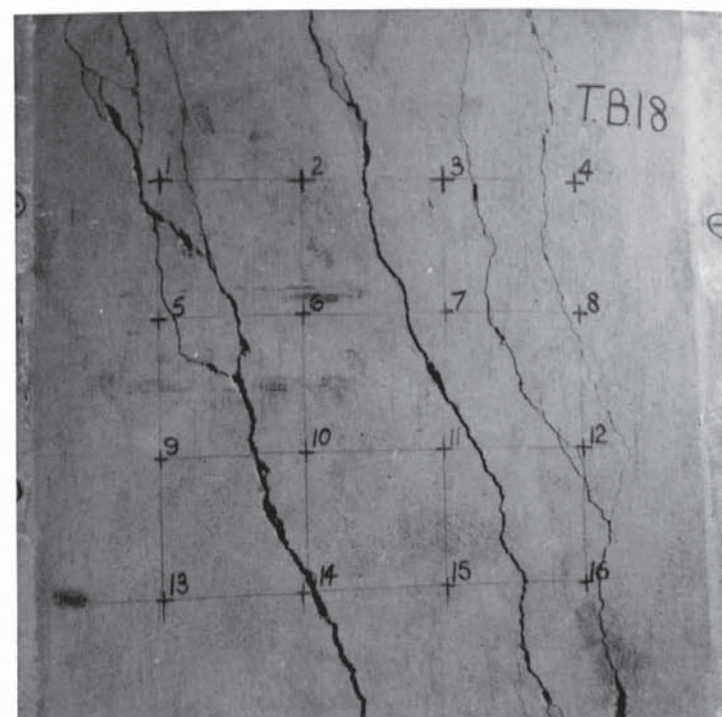
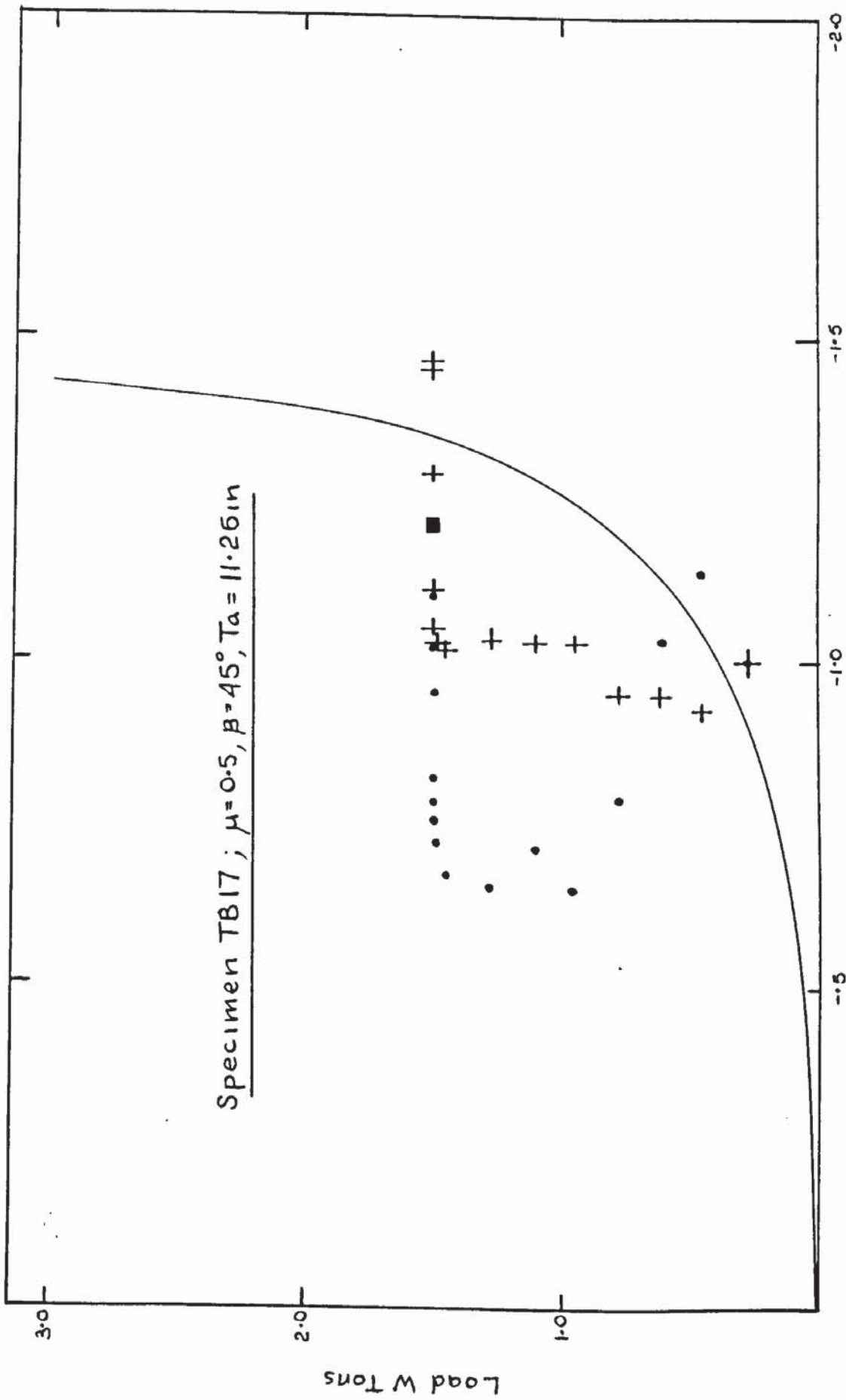


PLATE 5.46



Tan 2γ, 2ω, 2θ

FIG 5-118 PLOT OF PRINCIPAL DIRECTIONS-TB17

LOAD W TONS	MIN.PRINC. CONC.STRAIN E2 μ STRAINS	MIN.PRINC. CURVATURE K2 in <sup>-1</sup> x10 <sup>3</sup>	STEEL STRAINS																	
			1	2	3	4	5	6	7	8										
0.00	0.00	0.00	0.00	0.00	0.00	0.00	0.00	0.00	0.00	0.00	0.00	0.00	0.00	0.00	0.00	0.00	0.00	0.00	0.00	
0.11	-4.64	-.0002	0.00	0.00	0.00	0.00	0.00	0.00	0.00	0.00	0.00	0.00	0.00	0.00	4.7	4.7	4.7	4.7	4.7	0.0
0.27	-10.88	.0041	0.00	18.7	0.00	0.00	0.00	0.00	4.7	4.7	4.7	4.7	4.7	4.7	28.1	32.8	32.8	32.8	32.8	23.4
0.44	-17.94	-.0008	-4.7	37.5	4.7	4.7	-9.4	-9.4	18.7	18.7	18.7	18.7	18.7	18.7	61.0	70.4	70.4	70.4	70.4	65.7
0.61	-37.30	-.0409	4.7	65.7	37.5	37.5	9.4	9.4	75.1	75.1	75.1	75.1	75.1	75.1	126.8	140.9	140.9	140.9	140.9	159.7
0.77	-55.94	-.0448	46.9	131.5	103.3	103.3	112.7	112.7	338.2	338.2	338.2	338.2	338.2	338.2	239.5	324.1	324.1	324.1	324.1	357.0
0.94	-88.01	-.0244	150.3	206.7	197.3	197.3	192.6	192.6	723.4	723.4	723.4	723.4	723.4	723.4	502.6	559.0	559.0	559.0	559.0	620.0
1.10	-122.29	-.0825	253.6	277.1	314.7	314.7	267.7	267.7	1033.4	1033.4	1033.4	1033.4	1033.4	1033.4	746.9	793.9	793.9	793.9	793.9	854.9
1.27	-166.36	-.0991	366.4	357.0	450.9	450.9	357.0	357.0	1371.7	1371.7	1371.7	1371.7	1371.7	1371.7	995.9	977.1	977.1	977.1	977.1	1089.8
1.44	-217.40	-.1331	563.7	493.2	638.8	638.8	493.2	493.2	2132.7	2132.7	2132.7	2132.7	2132.7	2132.7	1338.8	1085.1	1085.1	1085.1	1085.1	1296.5
1.48	-256.24	-.1583	685.8	610.7	779.8	779.8	648.2	648.2	-	-	-	-	-	-	1916.6	1103.9	1103.9	1103.9	1103.9	1315.3
1.49	-298.45	-.2064	873.7	742.2	901.9	901.9	845.5	845.5	-	-	-	-	-	-	2748.1	1103.9	1103.9	1103.9	1103.9	1315.3
1.49	-324.17	-.4271	1014.7	850.2	939.5	939.5	1024.0	1024.0	-	-	-	-	-	-	2954.8	1103.9	1103.9	1103.9	1103.9	1315.3
1.49	-354.71	-.2757	1118.0	901.9	995.9	995.9	1446.8	1446.8	-	-	-	-	-	-	3293.0	1136.8	1136.8	1136.8	1136.8	1362.3
1.49	-402.85	-.0083	1155.6	892.5	1033.4	1033.4	1620.7	1620.7	-	-	-	-	-	-	4537.9	1193.2	1193.2	1193.2	1193.2	8563.8
1.49	-417.58	-.4149	-	920.7	1108.6	1108.6	1662.9	1662.9	-	-	-	-	-	-	-	4777.5	4777.5	4777.5	4777.5	-
1.49	-439.37	-.6514	-	1005.3	2593.1	2593.1	-	-	-	-	-	-	-	-	-	9954.3	9954.3	9954.3	9954.3	-
1.49	-488.30	-	-	-	1738.1	1738.1	-	-	-	-	-	-	-	-	-	-	-	-	-	-

Table 5.39 Minimum Principle Concrete Strains & Curvatures & Steel Strains TB.17

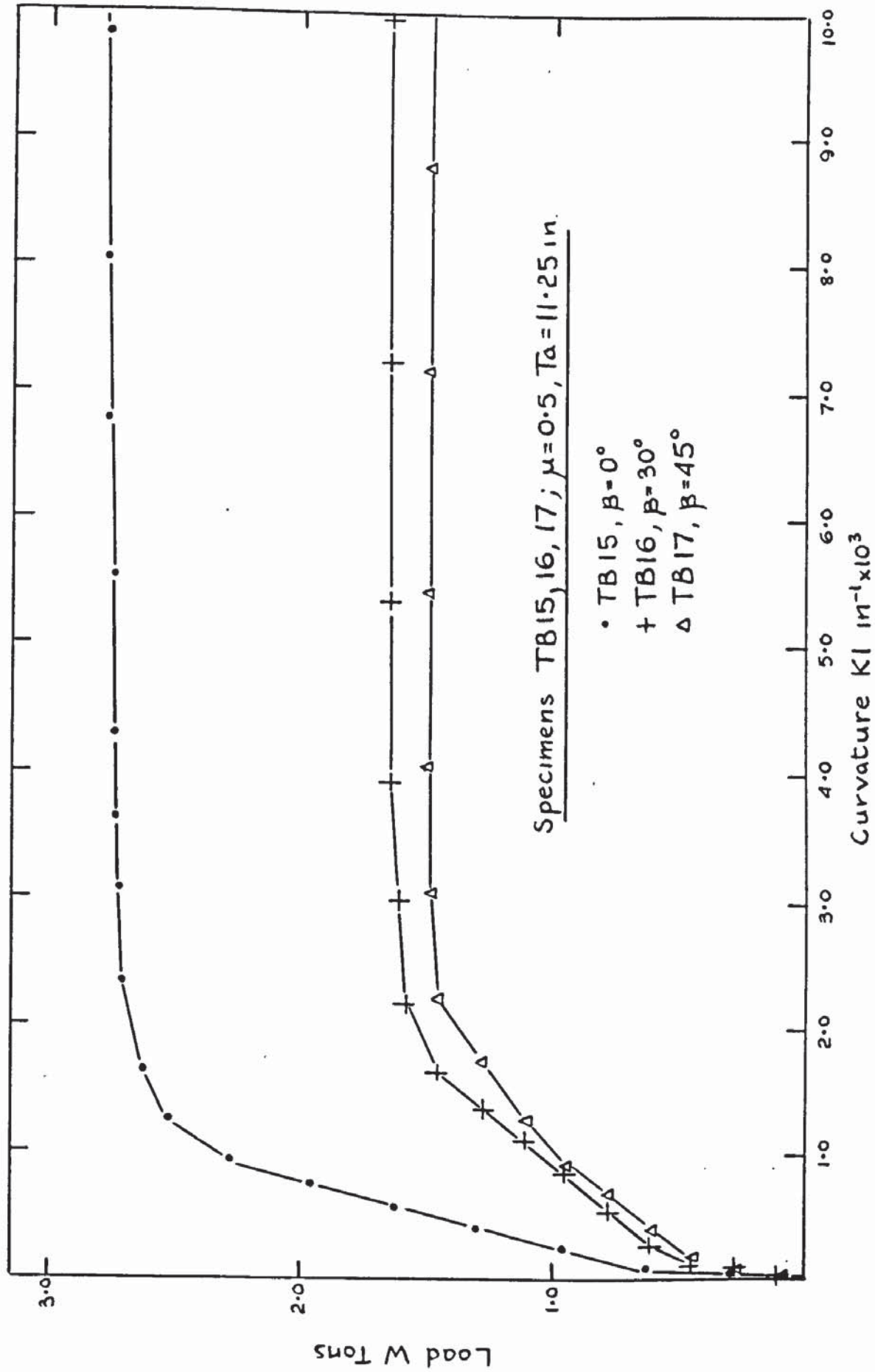


FIG 5-118 PLOT OF MAXIMUM PRINCIPAL CURVATURES-TB15,TB16,TB17.

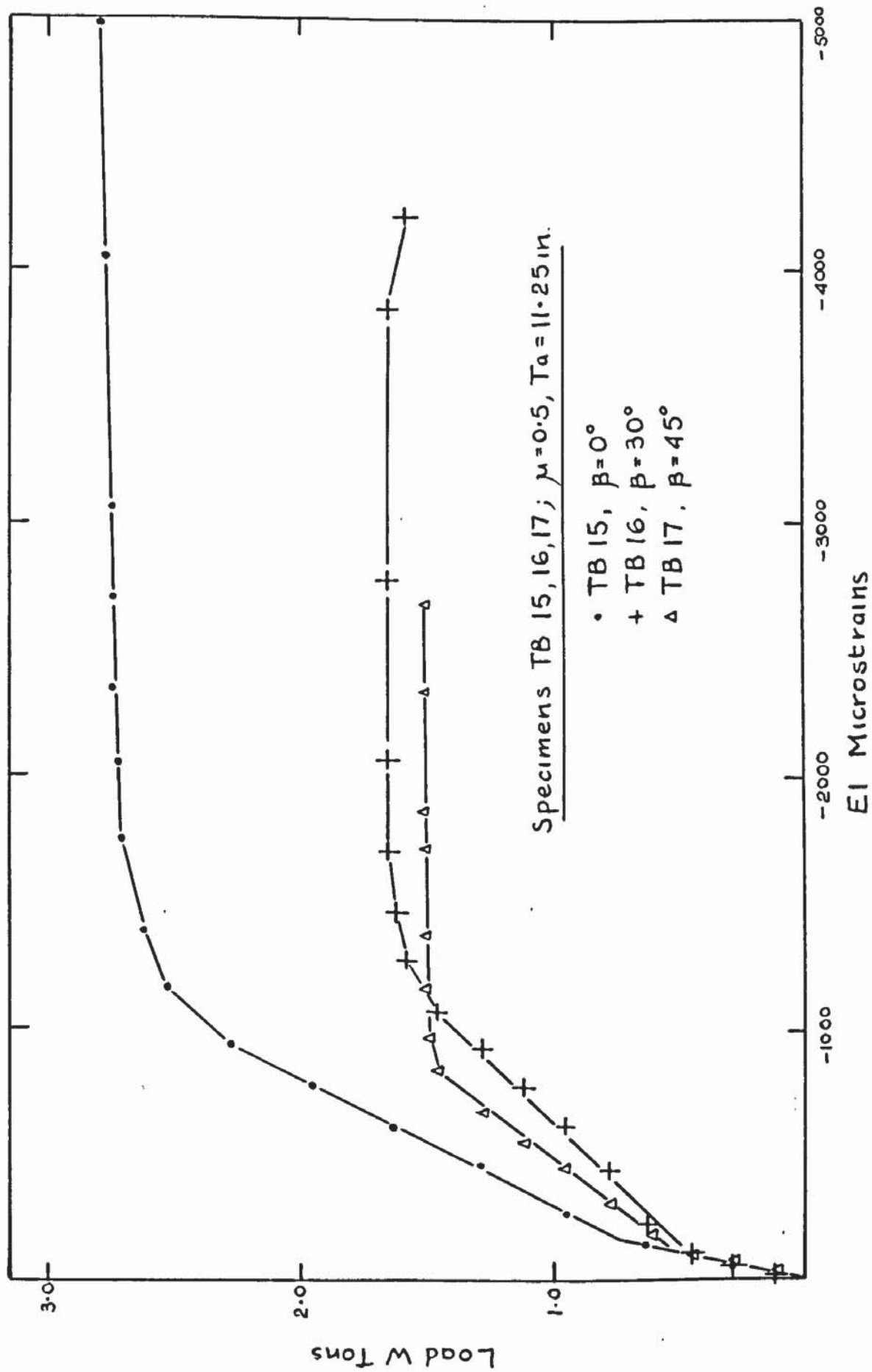


FIG 5-120 PLOT OF PRINCIPAL CONCRETE STRAINS EI-TB15,TB16,TB17.



LOAD W TONS	MIN. PRINC. CONC. STRAIN E2 μ STRAINS	MIN. PRINC. CURVATURE K2 in <sup>-1</sup> x10 <sup>3</sup>	STEEL STRAINS MICROSTRAINS										
			1	2	3	4	5	6	7	8			
0.00	0.00	0.00	0.0	0.0	0.0	0.0	0.0	0.0	0.0	0.0	0.0	0.0	0.0
0.12	2.47	.0064	0.0	14.0	4.7	-9.4	42.2	23.4	18.7	18.7	18.7	18.7	18.7
0.28	-6.94	-	-4.7	32.8	0.0	-37.5	117.4	155.0	65.7	65.7	65.7	65.7	65.7
0.45	-18.20	-.0036	0.0	84.5	46.9	-131.5	295.9	399.3	244.2	244.2	244.2	244.2	244.2
0.61	-38.00	-.0118	9.4	145.6	155.0	-46.9	559.0	681.1	488.5	488.5	488.5	488.5	488.5
0.70	-40.74	-.0167	42.2	169.1	216.0	37.5	681.1	826.7	601.3	601.3	601.3	601.3	601.3
0.78	-53.19	-.0768	46.9	178.5	244.2	56.3	775.1	887.8	699.9	699.9	699.9	699.9	699.9
0.95	-63.76	-.0446	93.9	206.7	300.6	103.3	1014.7	1141.5	948.9	948.9	948.9	948.9	948.9
1.07	-79.18	-.0489	206.7	253.6	347.6	140.9	1103.9	1216.7	1047.5	1047.5	1047.5	1047.5	1047.5
1.07	-67.93	-.0605	366.4	295.9	347.6	150.3	1132.1	1202.6	1042.8	1042.8	1042.8	1042.8	1042.8
1.07	-55.45	-.0749	591.9	418.0	328.8	150.3	4899.6	1752.2	1099.2	1099.2	1099.2	1099.2	1099.2
1.07	-80.83	-.1560	-	544.9	319.4	169.1	-	3875.5	-	-	-	-	-
1.07	-154.89	.0151	-	751.6	300.6	150.3	-	5228.5	-	-	-	-	-
1.07	-255.28	-.0200	-	845.5	272.4	159.7	-	4786.9	-	-	-	-	-
1.07	-299.58	-.0460	-	901.9	-	159.7	-	-	-	-	-	-	-
1.07	-321.91	.0079	-	911.3	-	169.1	-	-	-	-	-	-	-
1.03	-339.56	-.1373	-	930.1	-	187.9	-	-	-	-	-	-	-

Table 5.40 Minimum Principle Concrete Strains & Curvatures & Steel Strains TB.18

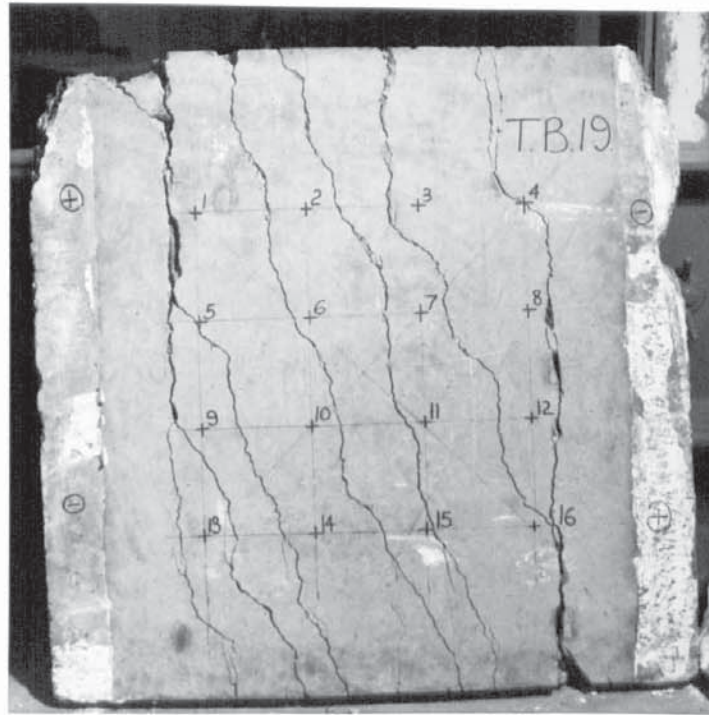


PLATE 5.47

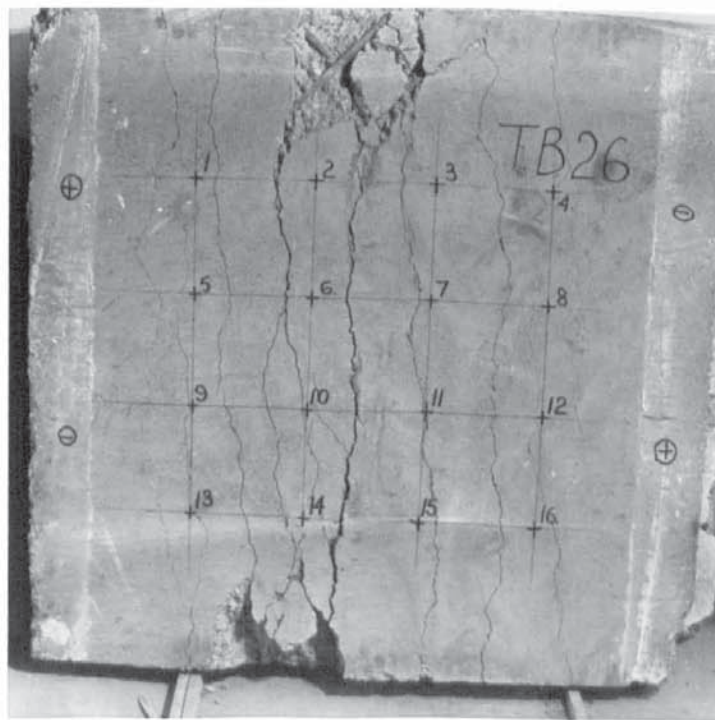


PLATE 5.48

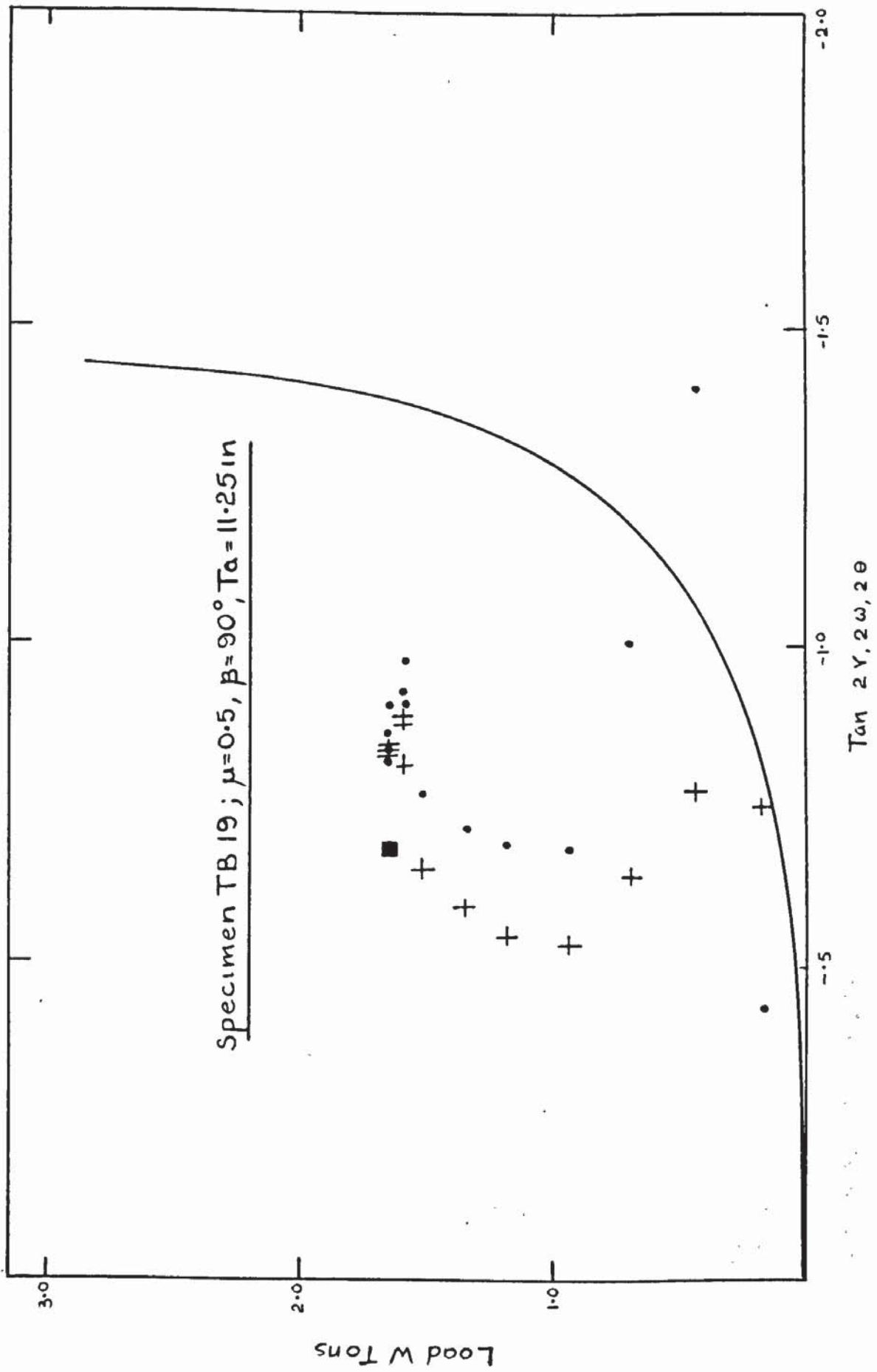
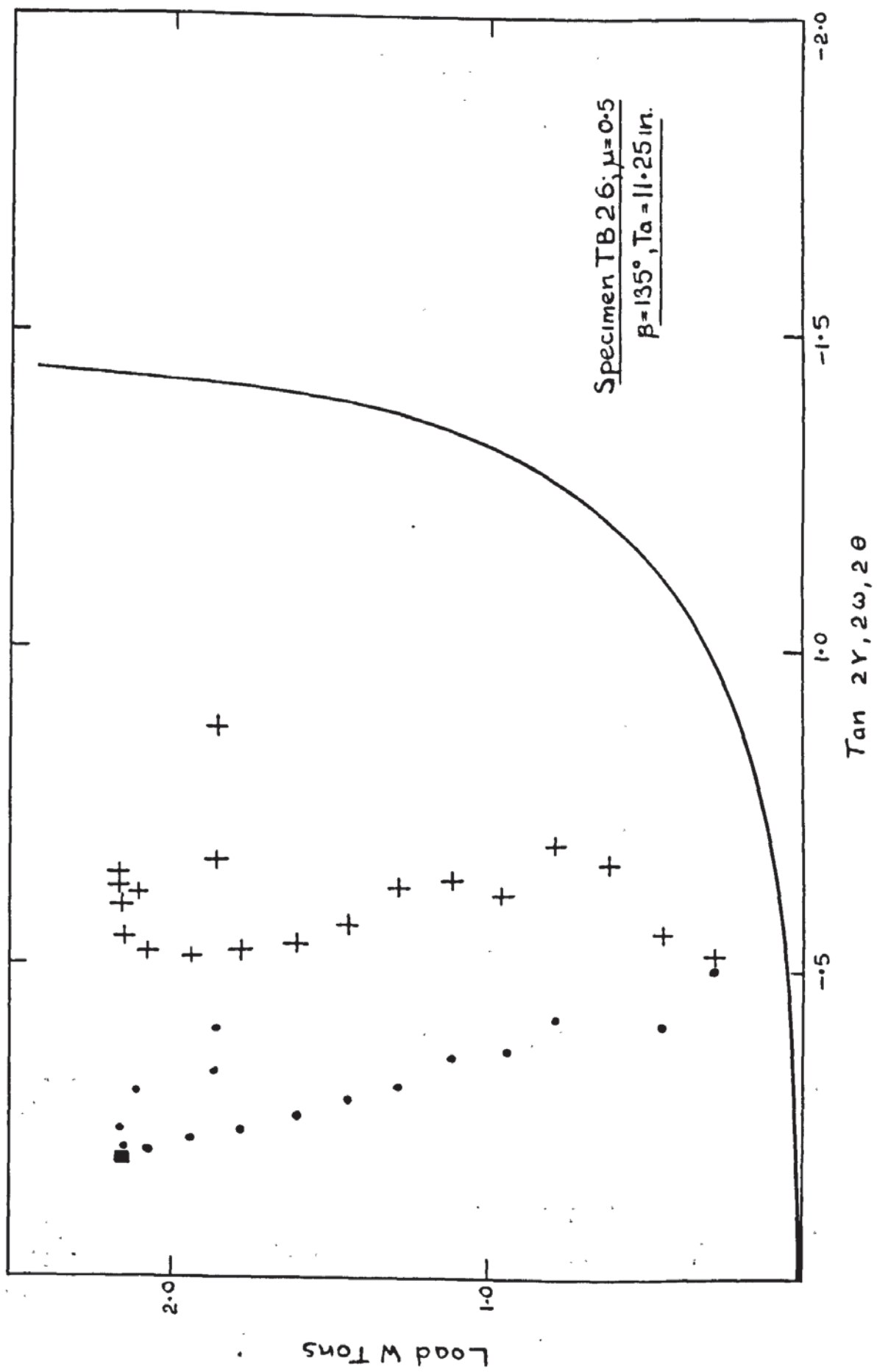


FIG 5.122 PLOT OF PRINCIPAL DIRECTIONS - TB19

LOAD W TONS	MIN.PRINC. CONC.STRAIN E2 μ STRAINS	MIN.PRINC. CURVATURE K2 in <sup>-1</sup> x10 <sup>3</sup>	STEEL STRAINS MICROSTRAINS										
			1	2	3	4	5	6	7	8			
0.00	0.00	0.00	0.0	0.0	0.0	0.0	0.0	0.0	0.0	0.0	0.0	0.0	0.0
0.18	-1.72	.0093	0.0	4.9	0.0	0.0	0.0	29.5	19.7	19.7	9.8	9.8	14.7
0.43	-12.75	.0223	9.8	14.7	9.8	9.8	9.8	137.9	59.1	59.1	49.2	49.2	44.3
0.68	-11.37	.0160	19.7	34.4	29.5	39.4	39.4	315.3	157.6	157.6	147.8	147.8	123.1
0.93	-14.82	.0089	29.5	93.6	88.6	88.6	88.6	522.2	374.4	374.4	404.0	404.0	423.7
1.18	-18.13	.0016	29.5	142.8	137.9	108.3	108.3	788.2	650.3	650.3	739.0	739.0	724.2
1.34	-19.57	-.0022	34.4	172.4	177.3	123.1	123.1	1014.9	847.4	847.4	965.6	965.6	921.3
1.51	-19.41	-.0058	59.1	211.8	216.7	137.9	137.9	1271.1	1024.7	1024.7	1182.4	1182.4	1152.8
1.59	-26.40	-.0330	108.3	290.6	246.3	167.5	167.5	1448.4	1103.6	1103.6	2010.1	2010.1	1256.3
1.59	-35.19	-.0661	266.0	320.2	275.9	177.3	177.3	1384.4	1083.9	1083.9	2453.5	2453.5	1276.0
1.59	-41.76	-.0837	335.0	339.9	344.8	206.9	206.9	1409.0	1074.0	1074.0	2591.5	2591.5	1285.9
1.64	-76.36	-.1128	404.0	369.5	492.6	305.4	305.4	1340.1	1054.3	1054.3	2956.1	2956.1	1295.7
1.64	-79.93	-.9353	492.6	793.2	512.3	305.4	305.4	1389.3	1074.0	1074.0	3636.0	3636.0	1285.9
1.64	-78.82	-.1666	620.7	1059.2	561.6	285.7	285.7	2276.2	1054.3	1054.3	6454.1	6454.1	1266.2
1.64	-88.29	-.2064	788.2	1295.7	670.0	285.7	285.7	2404.2	-	-	1.2x10 <sup>4</sup>	1.2x10 <sup>4</sup>	1276.0
1.64	-120.07	-.2261	837.5	1354.8	630.6	295.6	295.6	1872.2	-	-	-	-	-
1.64	-140.89	-.2554	847.4	1463.2	610.9	325.1	325.1	1867.2	-	-	-	-	-
1.65	-152.63	-.6006	-	1551.9	551.8	335.0	335.0	1744.1	-	-	-	-	-
1.65	-178.47	-.3158	-	1818.0	-	339.9	339.9	-	-	-	-	-	-
1.65	-201.28	-.2874	-	1980.5	-	325.1	325.1	-	-	-	-	-	-
1.67	-228.66	-.2322	-	2034.7	-	305.4	305.4	-	-	-	-	-	-

Table 5.41 Minimum Principle Concrete Strains & Curvatures & Steel Strains TB.19



LOAD W TONS	MIN.PRINC. CONC.STRAIN E2 μ STRAINS	MIN.PRINC. CURVATURE K2 in <sup>-1</sup> x10 <sup>3</sup>	STEEL STRAINS										
			1	2	3	4	5	6	7	8			
0.00	0.00	0.00	0.0	0.0	0.0	0.0	0.0	0.0	0.0	0.0	0.0	0.0	0.0
0.12	-9.60	-	9.4	9.4	9.4	4.7	4.7	9.4	9.4	9.4	9.4	9.4	9.4
0.28	-19.41	-.0017	18.7	18.7	18.7	9.4	9.4	18.7	18.7	18.7	18.7	18.7	18.7
0.45	-22.14	-.0027	28.1	28.1	28.1	18.7	18.7	28.1	28.1	28.1	28.1	28.1	28.1
0.61	-22.05	.0247	46.9	37.5	46.9	28.1	28.1	46.9	37.5	37.5	37.5	37.5	46.9
0.78	-29.57	.0046	89.2	75.1	103.3	93.9	93.9	103.3	93.9	93.9	93.9	93.9	84.5
0.95	-26.47	.0023	178.5	150.3	178.5	206.7	206.7	178.5	159.7	159.7	159.7	159.7	145.6
1.11	-38.24	.0046	300.6	281.8	300.6	338.2	338.2	300.6	338.2	338.2	338.2	338.2	239.5
1.28	-52.36	-.0040	404.0	413.4	375.8	441.5	441.5	375.8	479.1	479.1	479.1	479.1	328.8
1.44	-57.42	.0059	507.3	526.1	563.7	563.7	563.7	563.7	601.3	601.3	601.3	601.3	418.0
1.61	-61.40	-.0081	620.0	634.1	676.4	676.4	676.4	676.4	723.4	723.4	723.4	723.4	526.1
1.78	-82.07	.0067	732.8	798.6	789.2	789.2	789.2	789.2	836.1	836.1	836.1	836.1	648.2
1.94	-76.78	-.0115	845.5	920.7	901.9	1033.4	1033.4	901.9	977.1	977.1	977.1	977.1	779.8
2.08	-120.98	-.0261	1014.7	1155.6	1066.3	1362.3	1362.3	1066.3	1249.5	1249.5	1249.5	1249.5	1014.7
2.15	-149.62	-.0410	1056.9	1268.3	1127.4	1484.4	1484.4	1127.4	1428.0	1428.0	1428.0	1428.0	1240.1
2.16	-202.25	-.0810	1108.6	1296.5	1146.2	1550.2	1550.2	1146.2	3429.3	3429.3	3429.3	3429.3	1305.9
2.17	-264.73	-.1045	1174.4	1418.7	1212.0	1653.5	1653.5	1212.0	7713.5	7713.5	7713.5	7713.5	1484.4
2.17	-349.63	-.1628	-	2066.9	1235.4	1973.0	1973.0	1235.4	-	-	-	-	1935.4
2.11	-424.83	-.1931	-	-	1249.5	3955.4	3955.4	1249.5	-	-	-	-	2517.9
1.86	-499.47	-.2654	-	-	1465.6	-	-	1465.6	-	-	-	-	-
1.86	-900.13	-.3130	-	-	6680.0	-	-	6680.0	-	-	-	-	-

Table 5.42 Minimum Principle Concrete Strains & Curvatures & Steel Strains TB26

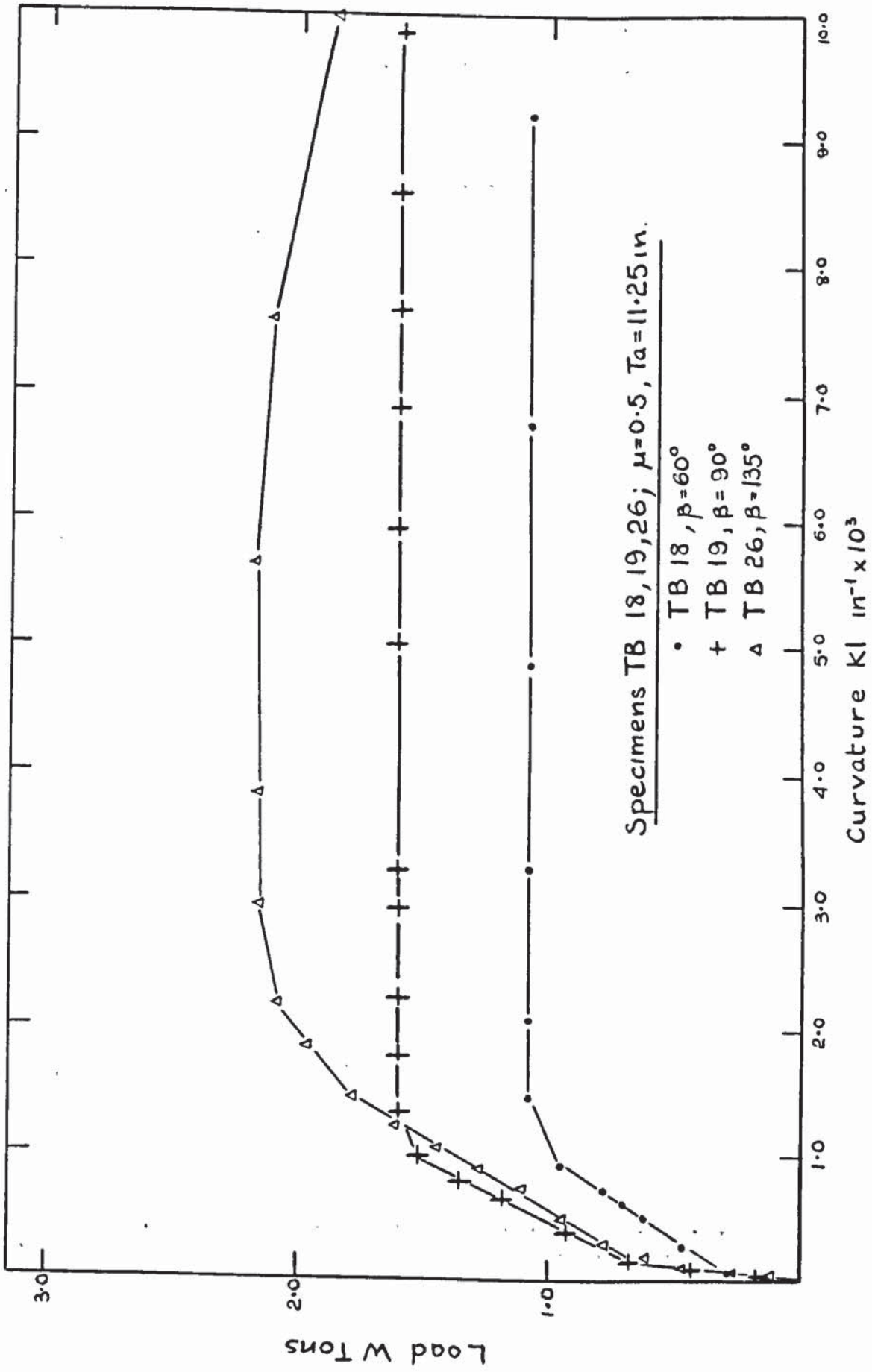
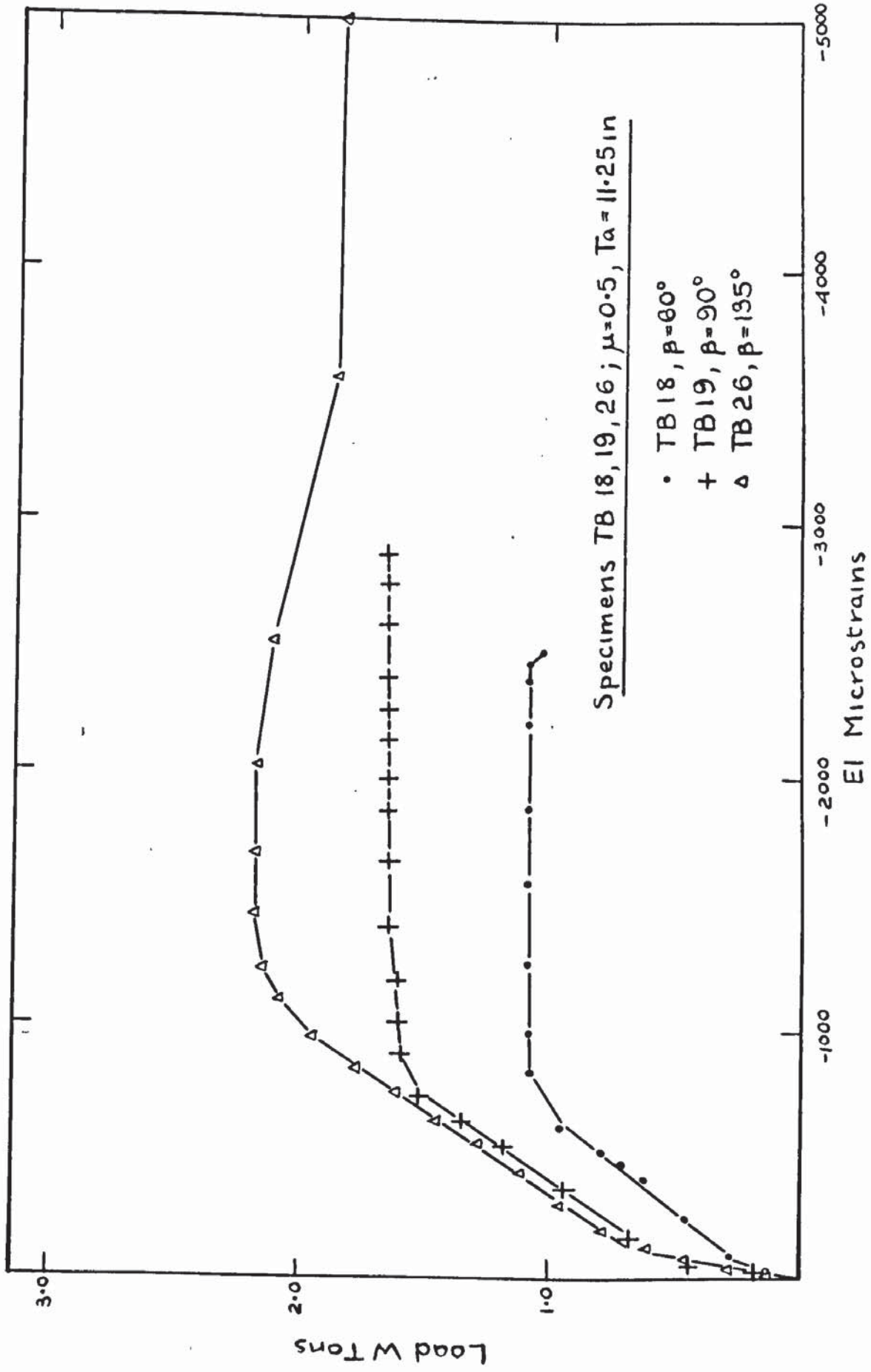


FIG 5-124 PLOT OF MAXIMUM PRINCIPAL CURVATURES - TB18, TB19, TB 26.



FIGS. 125 PLOT OF PRINCIPAL CONCRETE STRAINS EI-TB18, TB19, TB26.

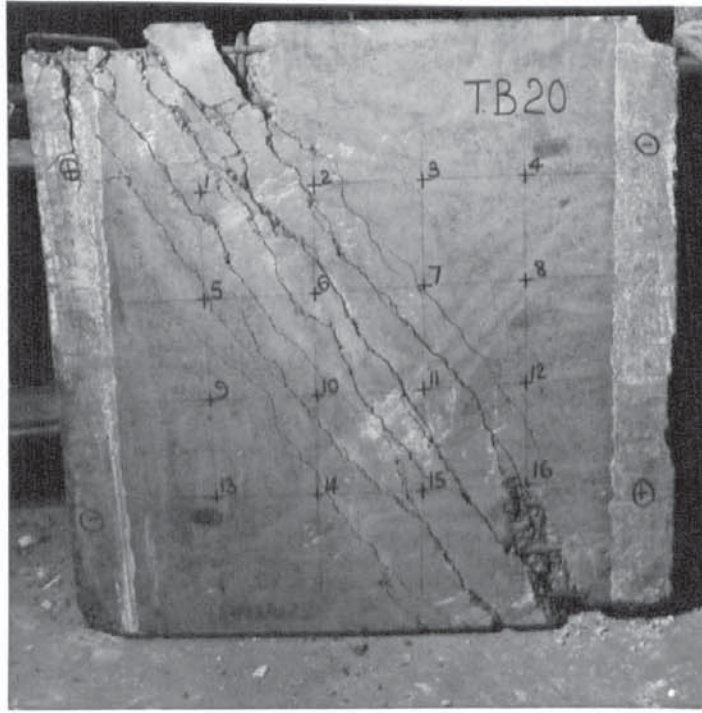


PLATE 5.49

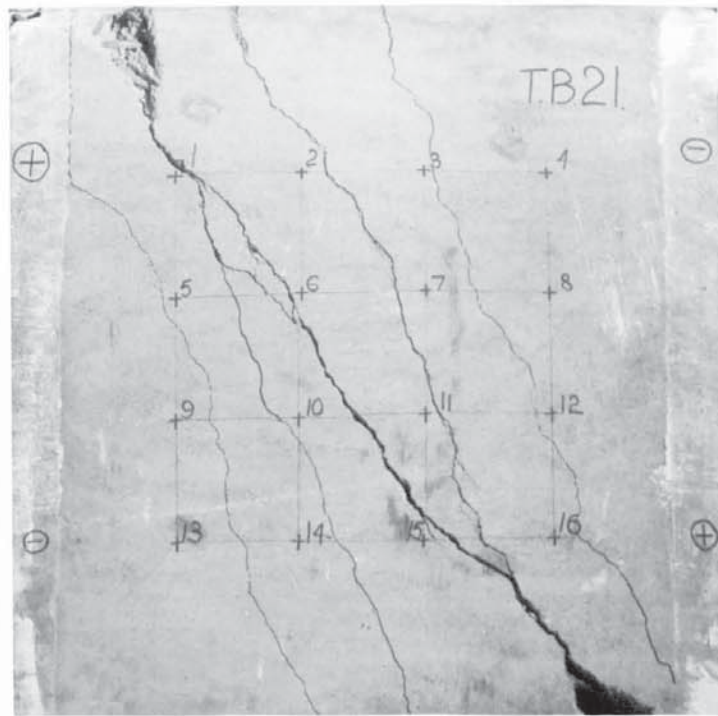
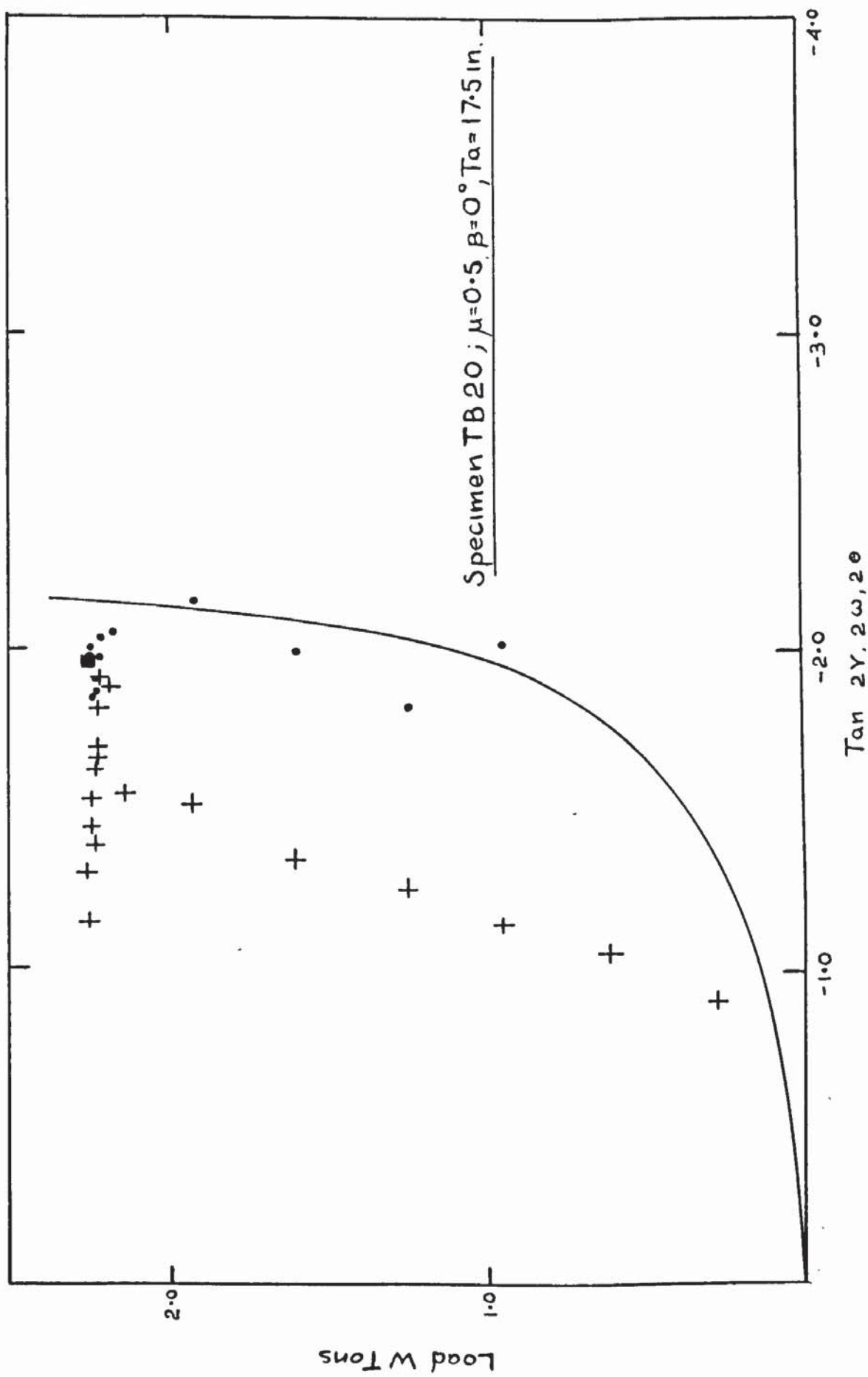


PLATE 5.50



FIGS. 126 PLOT OF PRINCIPAL DIRECTIONS - TB 20.

LOAD W TONS	M.N.PRINC. CONC.STRAIN E2 μ STRAINS	M.N.PRINC. CURVATURE K2 in <sup>-1</sup> x10 <sup>3</sup>	STEEL STRAINS										
			1	2	3	4	5	6	7	8			
0.00	0.00	0.00	0.0	0.0	0.0	0.0	0.0	0.0	0.0	0.0	0.0	0.0	0.0
0.28	-14.23	.0520	9.8	0.0	4.9	-29.5	-29.5	24.6	24.6	29.5	29.5	29.5	19.7
0.61	-44.64	.0433	39.4	19.7	34.4	-24.6	-24.6	93.6	93.6	113.3	113.3	98.5	78.8
0.95	-90.25	.0301	108.3	83.7	83.7	-19.7	-19.7	241.4	241.4	305.4	305.4	246.3	285.7
1.28	-149.87	.0080	236.4	202.0	182.2	49.27	49.27	458.2	458.2	571.5	571.5	517.3	561.6
1.61	-227.26	-.0323	394.1	354.7	280.8	128.1	128.1	674.9	674.9	808.0	808.0	758.7	798.1
1.94	-312.48	-.1223	630.6	591.2	507.4	241.4	241.4	1049.4	1049.4	1221.8	1221.8	1014.9	1014.9
2.15	-226.65	-.2231	1014.9	1261.2	1207.0	551.8	551.8	3098.9	3098.9	1517.4	1517.4	-88.6	1083.9
2.19	-568.48	-.2939	1251.4	2241.7	1532.2	709.4	709.4	4074.4	4074.4	1627.3	1627.3	-88.6	1157.8
2.22	-633.97	-.3762	1478.0	3616.2	2064.3	955.8	955.8	5000.7	5000.7	1694.8	1694.8	-236.4	1251.4
2.23	-637.72	-.3952	1813.0	4916.9	3000.4	1044.4	1044.4	6074.7	6074.7	2463.4	2463.4	-285.7	1231.7
2.23	-616.14	-.4694	2768.8	6636.4	3926.6	1113.4	1113.4	7148.8	7148.8	5793.9	5793.9	78.8	1251.4
2.23	-610.55	-.4781	3803.5	8198.2	4527.7	1005.0	1005.0	8163.7	8163.7	8907.7	8907.7	640.4	1369.6
2.24	-571.66	-.5258	5646.1	1.0x10 <sup>4</sup>	5399.8	926.2	926.2	-	-	-	-	1192.2	1704.6
2.24	-483.23	-.5779	7074.9	1.2x10 <sup>4</sup>	6429.5	1024.7	1024.7	-	-	-	-	1438.6	2315.6
2.25	-453.31	-.6587	8129.2	1.4x10 <sup>4</sup>	7779.4	1074.0	1074.0	-	-	-	-	1517.4	5025.3
2.26	-335.08	-.7158	8907.7	-	9296.9	1123.3	1123.3	-	-	-	-	1556.8	-
2.27	-95.71	-.8133	-	-	1.0x10 <sup>4</sup>	1024.7	1024.7	-	-	-	-	1655.4	-
2.27	-49.99	-.8638	-	-	1.2x10 <sup>4</sup>	1212.0	1212.0	-	-	-	-	1827.8	-
2.23	-82.80	-1.0271	-	-	-	1340.1	1340.1	-	-	-	-	2069.2	-

Table 5.43 Minimum Principle Concrete Strains & Curvatures & Steel Strains TB20

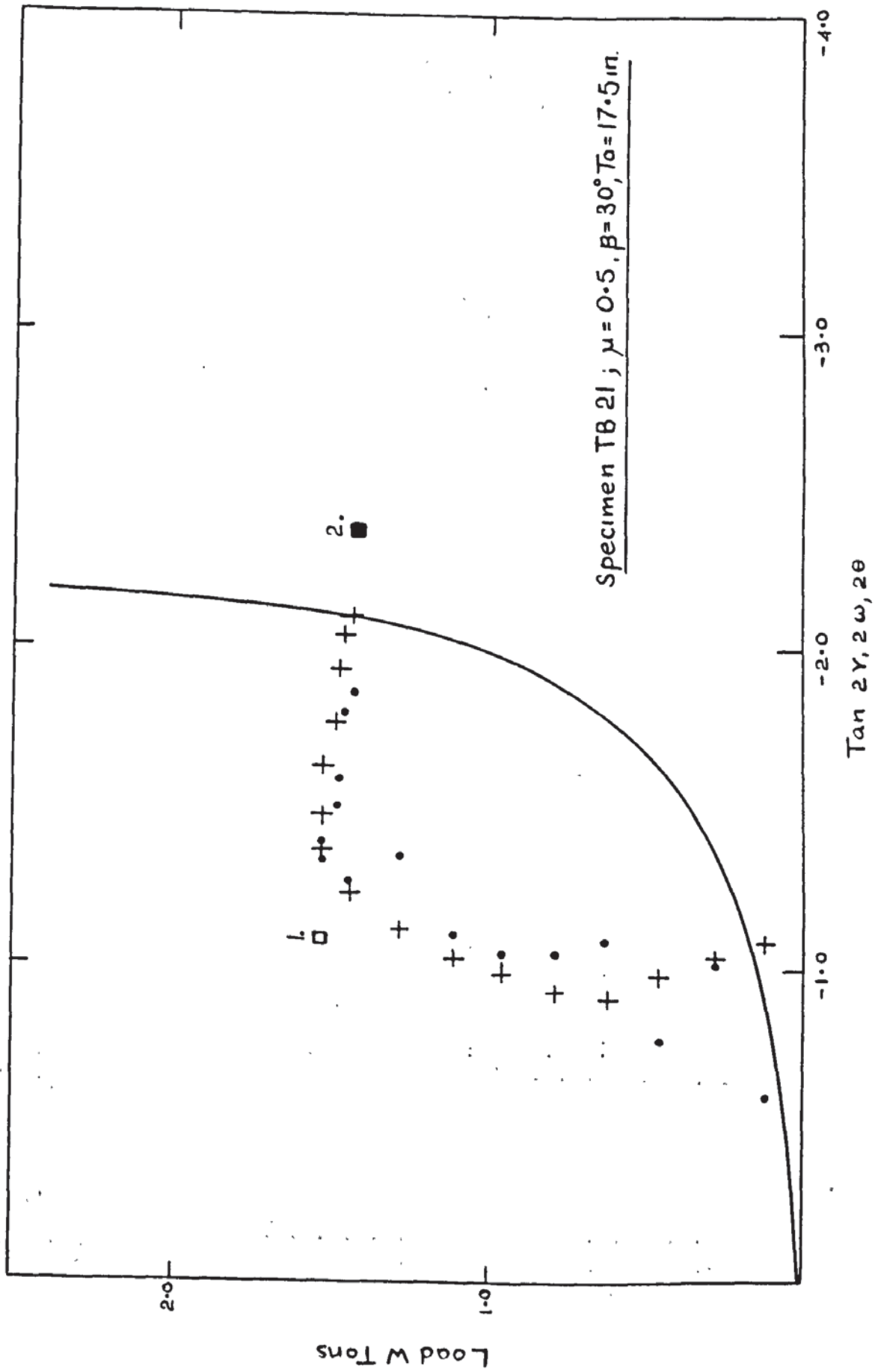


FIG 5.127 PLOT OF PRINCIPAL DIRECTIONS - TB 21.

LOAD W TONS	M.N.PRINC. CONC. STRAIN E2 μ STRAINS	M.N.PRINC. CURVATURE K2 in <sup>-1</sup> x10 <sup>3</sup>	STEEL STRAINS									
			1	2	3	4	5	6	7	8		
0.00	0.00	0.00	0.0	0.0	0.0	0.0	0.0	0.0	0.0	0.0	0.0	0.0
0.12	-9.86	-.0049	-	0.0	0.0	9.4	9.4	4.7	4.7	4.7	4.7	4.7
0.28	-14.57	-.0002	-	0.0	9.4	9.4	14.0	14.0	18.7	18.7	18.7	9.4
0.45	-20.92	-.0146	-	4.7	9.4	9.4	28.1	32.8	75.1	46.9	46.9	28.1
0.61	-22.53	-.0143	-	37.5	28.1	28.1	93.9	159.7	150.3	84.5	84.5	93.9
0.78	-35.21	-.0405	-	122.1	169.1	169.1	239.5	474.4	314.7	234.8	234.8	300.6
0.95	-54.67	-.0512	-	244.2	314.7	314.7	366.4	728.1	643.5	549.6	549.6	526.1
1.11	-67.90	-.1104	-	281.8	394.6	394.6	488.5	1028.7	948.9	854.9	854.9	779.8
1.28	-79.80	-.1014	-	450.9	488.5	488.5	544.9	1517.3	1277.7	1136.8	1136.8	981.8
1.44	-96.66	-.1586	-	563.7	601.3	601.3	685.8	-	1785.1	1761.63	1761.63	1174.4
1.53	-121.01	-.1894	-	742.2	704.6	704.6	1409.3	-	3297.7	3457.4	3457.4	1498.5
1.53	-162.45	-.2744	-	892.5	779.8	779.8	2076.3	-	6689.4	5275.4	5275.4	1822.7
1.53	-211.04	-.3357	-	1174.4	836.1	836.1	-	-	-	-	-	2940.7
1.49	-240.94	-.4194	-	1569.0	864.3	864.3	-	-	-	-	-	4256.0
1.48	-279.38	-.5960	-	9996.6	883.1	883.1	-	-	-	-	-	-
1.46	-350.45	-.8441	-	-	911.3	911.3	-	-	-	-	-	-
1.44	-411.93	-1.0002	-	-	-	-	-	-	-	-	-	-

Table 5.44 Minimum Principle Concrete Strains & Curvatures & Steel Strains TB.21

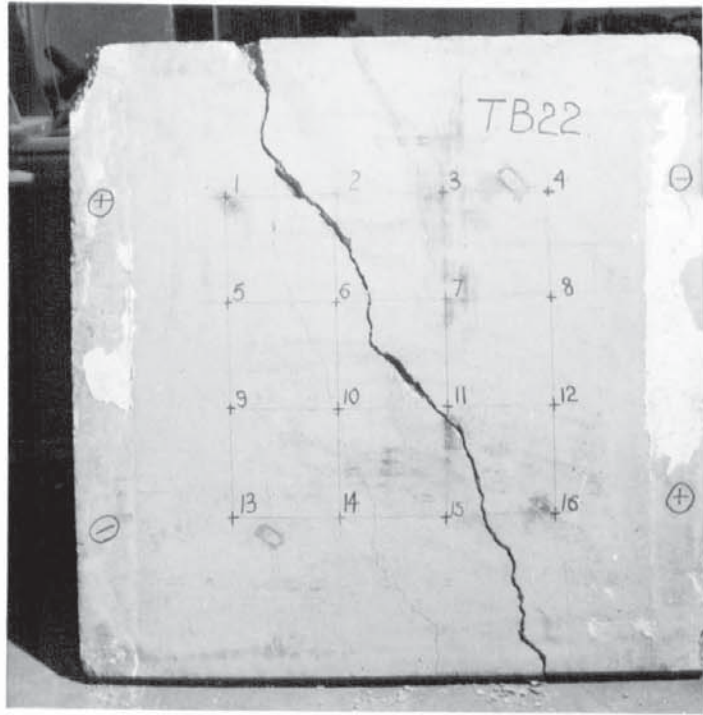


PLATE 5.51

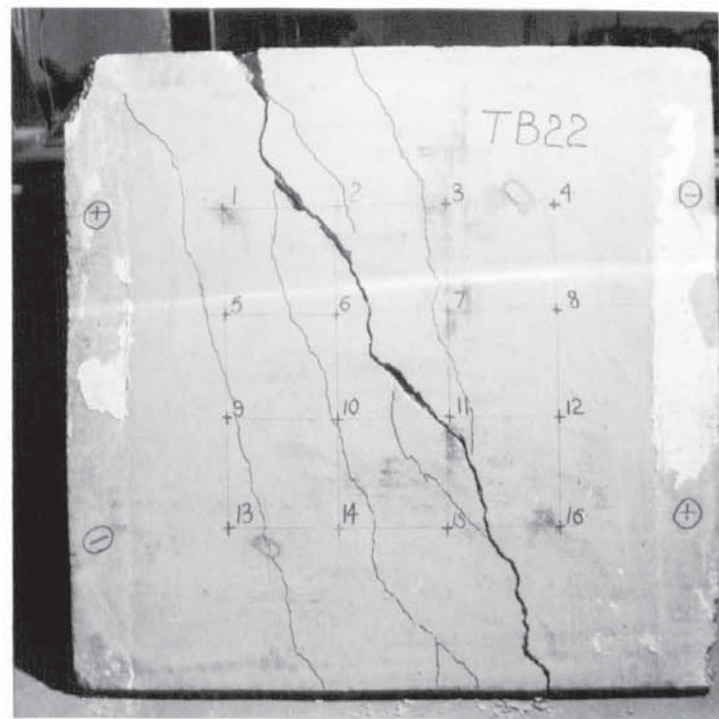


PLATE 5.52



LOAD W TONS	M.N.PRINC. CONC.STRAIN E2 $\mu$ STRAINS	M.N.PRINC. CURVATURE K2 $\text{in}^{-1} \times 10^3$	STEEL STRAINS										
			MI CROSTRAINS										
			1	2	3	4	5	6	7	8			
0.00	0.00	0.00	0.0	0.0	0.0	0.0	0.0	0.0	0.0	0.0	0.0	0.0	0.0
0.12	-8.44	-.0211	9.4	9.4	9.4	9.4	9.4	14.0	14.0	14.0	14.0	9.4	9.4
0.28	-17.02	-.0153	14.0	14.0	9.4	14.0	14.0	28.1	28.1	42.2	42.2	32.8	28.1
0.45	-20.86	-.0118	46.9	9.4	4.7	9.4	9.4	65.7	65.7	79.8	79.8	70.4	46.9
0.61	-27.77	.0018	84.5	14.0	9.4	18.7	18.7	183.2	183.2	183.2	183.2	197.3	93.9
0.78	-52.97	.0245	244.2	56.3	206.7	140.9	140.9	573.1	573.1	728.1	728.1	742.2	587.2
0.95	-85.52	-.0202	366.4	93.9	319.4	253.6	253.6	836.1	836.1	1061.6	1061.6	1113.3	1221.4
1.09	-95.73	.0137	488.5	253.6	404.0	394.6	394.6	1080.4	1080.4	2254.8	2254.8	1428.0	2395.8
1.14	-77.09	.0633	610.7	441.5	469.7	549.6	549.6	1146.2	1146.2	5735.8	5735.8	1662.9	4951.3
1.14	-55.43	.1181	695.2	591.9	497.9	695.2	695.2	1165.0	1165.0	8028.3	8028.3	1742.8	5280.1
1.14	-30.79	.1884	808.0	638.8	497.9	817.4	817.4	1216.7	1216.7	8986.6	8986.6	1794.5	6351.2
1.14	-23.68	.3187	883.1	662.3	488.5	864.3	864.3	3119.2	3119.2	9578.5	9578.5	1841.4	7046.5
1.13	-46.43	.3882	995.9	-	488.5	930.1	930.1	-	-	-	-	2189.1	-
1.13	-272.95	.5345	1042.8	-	483.8	939.5	939.5	-	-	-	-	-	-
1.05	-	.6359	1033.4	-	488.5	958.3	958.3	-	-	-	-	-	-

Table 5.45 Minimum Principle Concrete Strains & Curvatures & Steel Strains TB.22

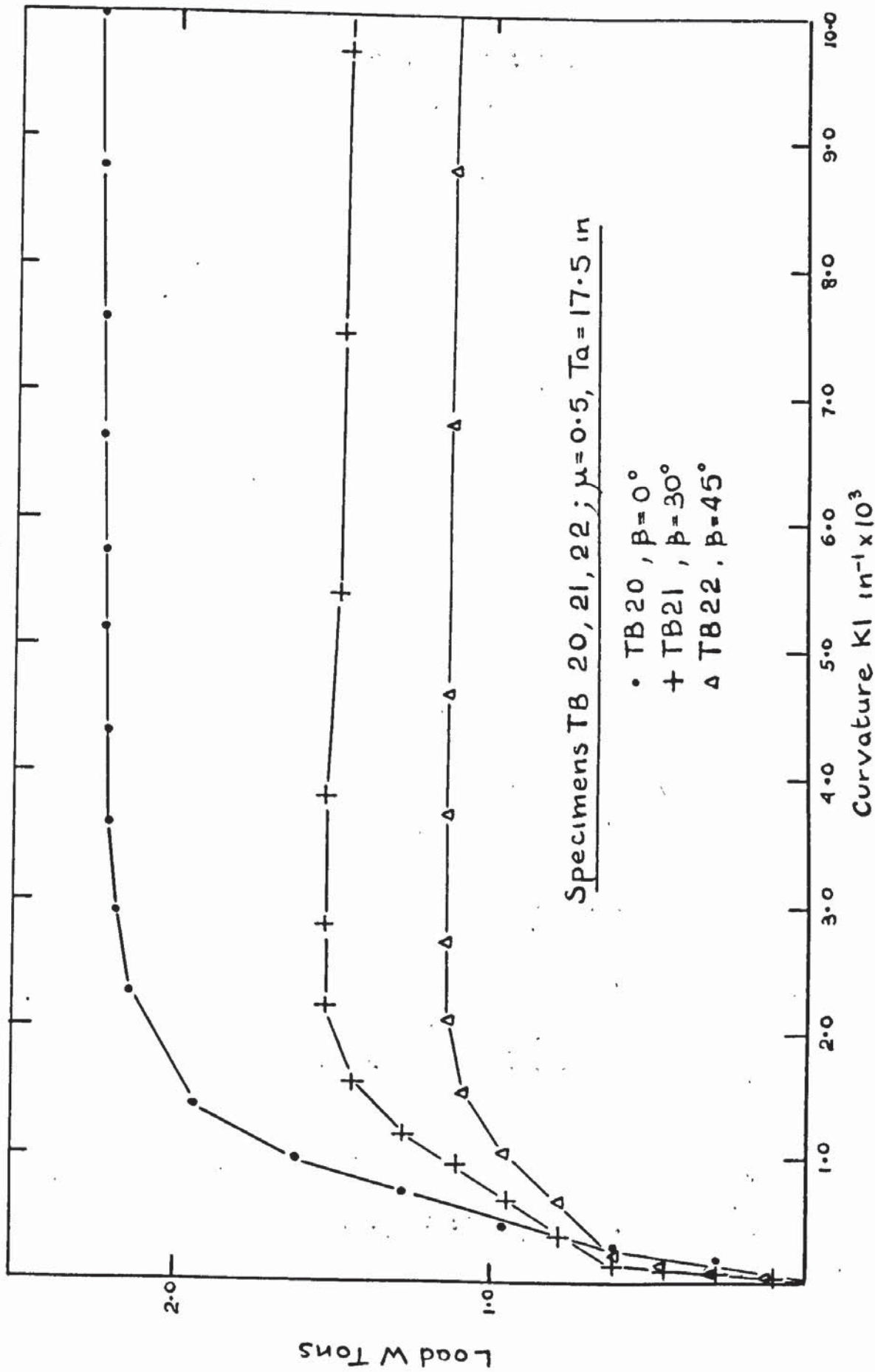


FIG 5.129. PLOT OF MAXIMUM PRINCIPAL CURVATURES -TB20,TB21,TB22.

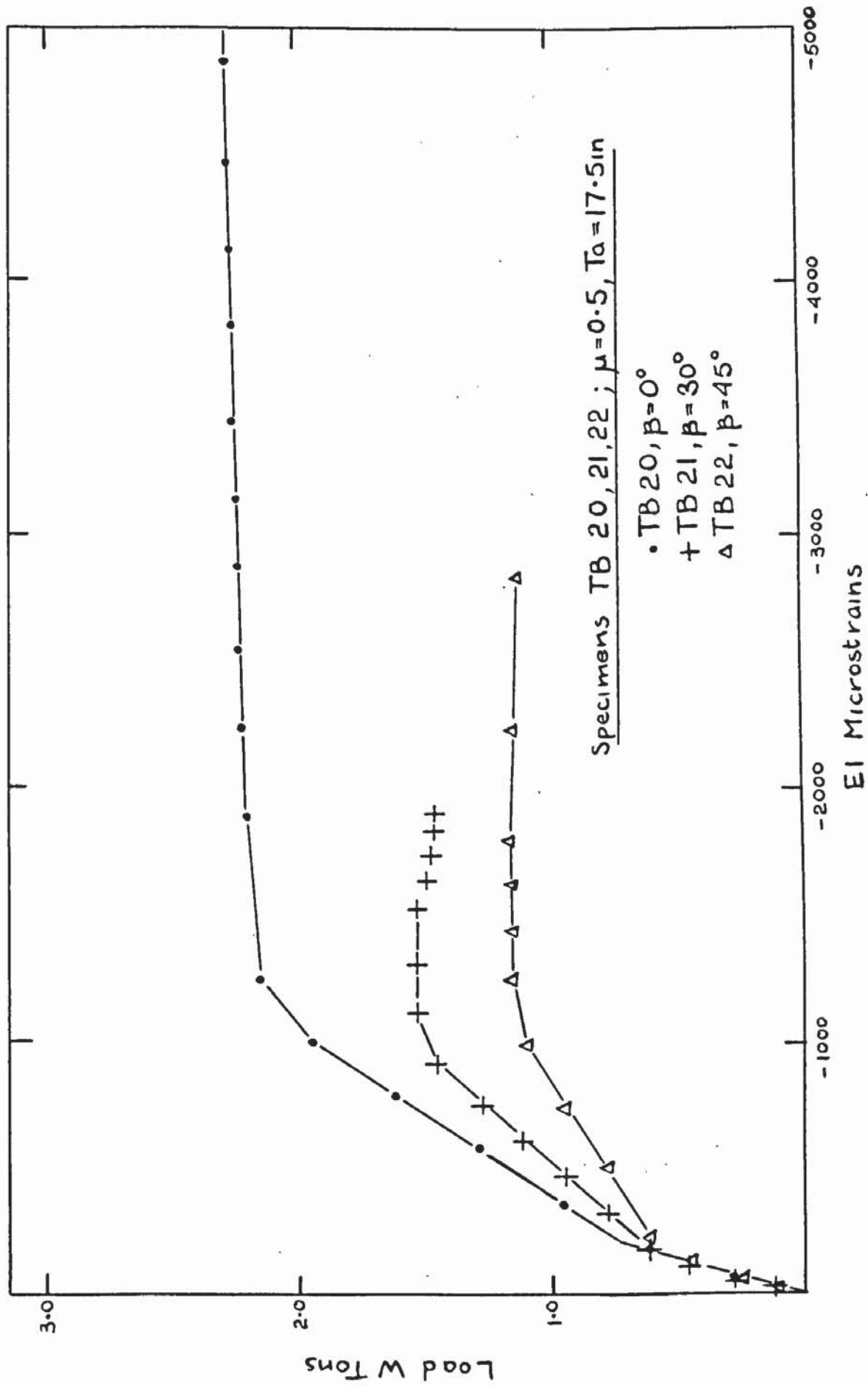


FIG 5.130 PLOT OF PRINCIPAL CONCRETE STRAINS EI - TB 20, TB 21, TB 22.

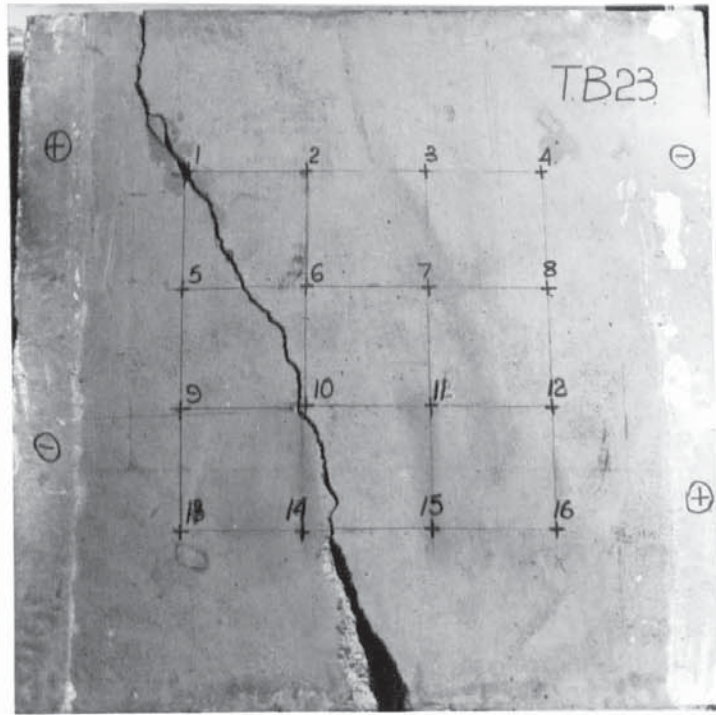


PLATE 5.53

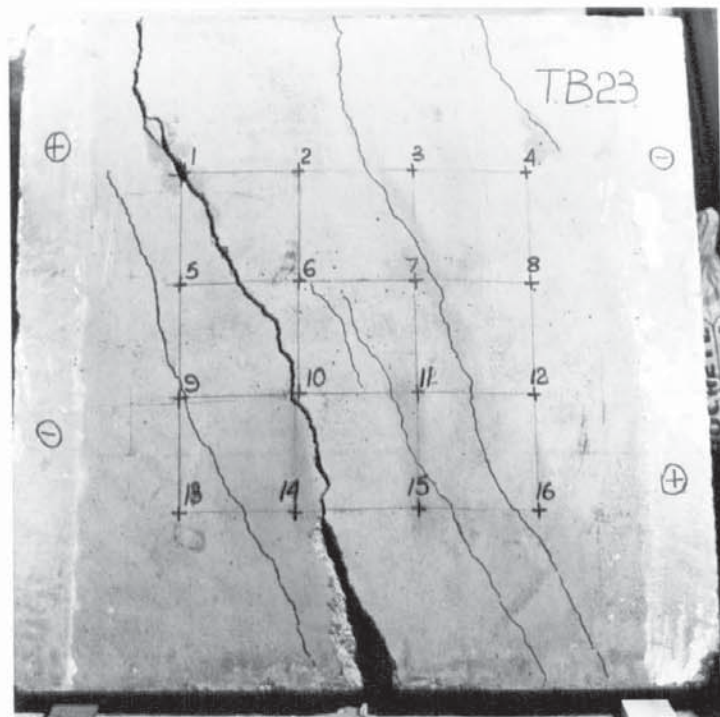


PLATE 5.54

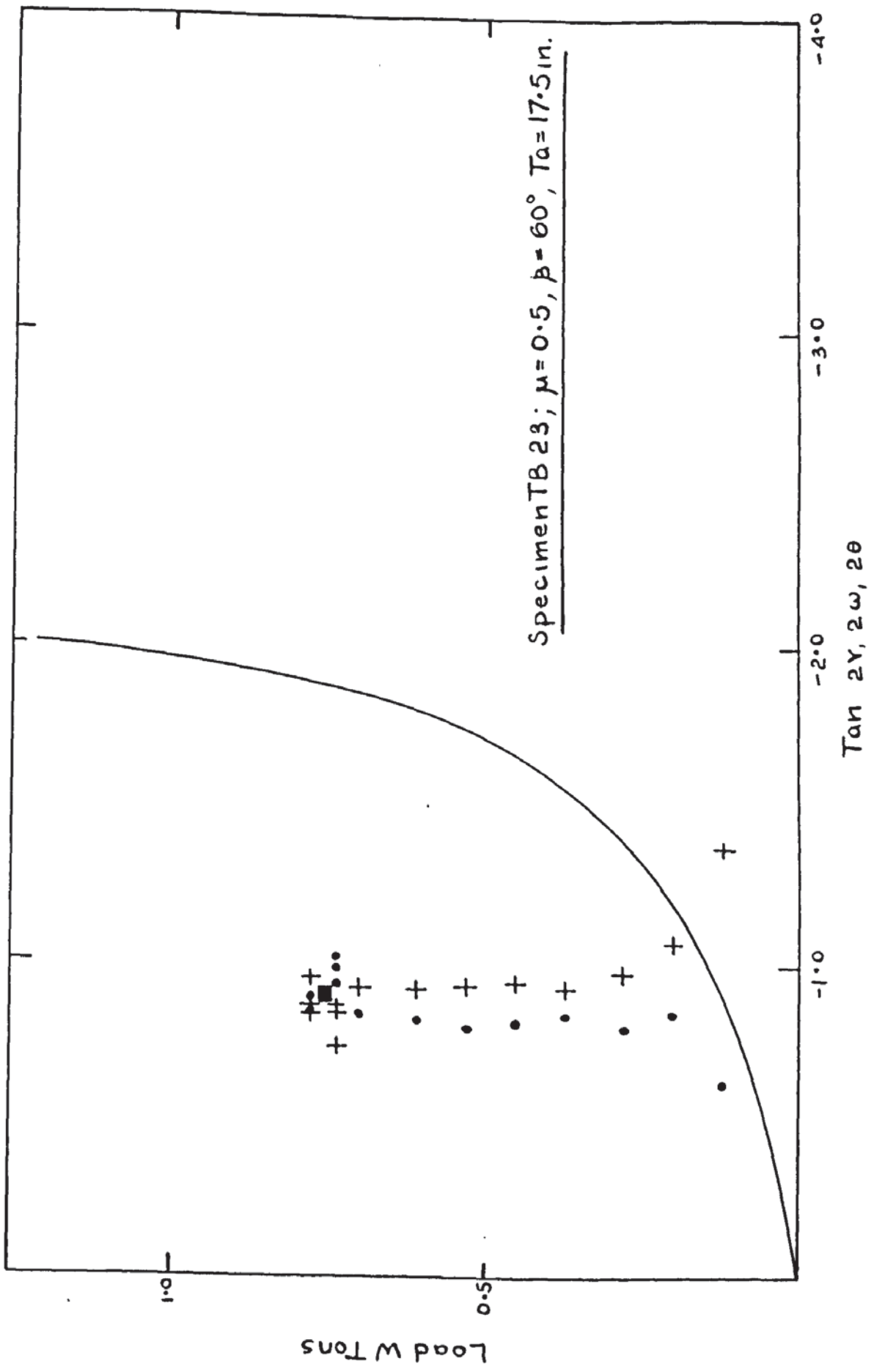


FIG 5-131 PLOT OF PRINCIPAL DIRECTIONS - TB 23.

LOAD W TONS	MIN. PRINC. CONC. STRAIN E2	MIN. PRINC. CURVATURE K2 in <sup>-1</sup> x10 <sup>3</sup>	STEEL STRAINS MICROSTRAINS																
			1	2	3	4	5	6	7	8									
0.00	0.00	0.00	0.0	0.0	0.0	0.0	0.0	0.0	0.0	0.0	0.0	0.0	0.0	0.0	0.0	0.0	0.0	0.0	0.0
0.12	-4.49	.0014	9.4	18.7	-28.1	-9.4	-9.4	37.5	28.1	37.5	28.1	37.5	28.1	37.5	28.1	37.5	28.1	37.5	28.1
0.20	-16.12	-.0077	9.4	28.1	-117.4	-4.7	-4.7	79.8	79.8	79.8	79.8	79.8	79.8	79.8	79.8	79.8	79.8	79.8	79.8
0.28	-15.34	-.0137	9.4	37.5	-61.0	-9.4	-9.4	319.4	319.4	319.4	319.4	319.4	319.4	319.4	319.4	319.4	319.4	319.4	319.4
0.37	-33.00	-.0214	9.4	37.5	-89.2	-9.4	-9.4	432.1	432.1	432.1	432.1	432.1	432.1	432.1	432.1	432.1	432.1	432.1	432.1
0.45	-45.06	-.0455	9.4	42.2	0.0	-14.0	-14.0	554.3	554.3	554.3	554.3	554.3	554.3	554.3	554.3	554.3	554.3	554.3	554.3
0.53	-53.86	-.0545	9.4	42.2	9.4	-14.0	-14.0	667.0	667.0	667.0	667.0	667.0	667.0	667.0	667.0	667.0	667.0	667.0	667.0
0.61	-66.46	-.0594	9.4	37.5	32.8	-14.0	-14.0	789.2	789.2	789.2	789.2	789.2	789.2	789.2	789.2	789.2	789.2	789.2	789.2
0.70	-59.64	-.0755	9.4	37.5	32.4	-14.0	-14.0	911.3	911.3	911.3	911.3	911.3	911.3	911.3	911.3	911.3	911.3	911.3	911.3
0.78	-70.23	-.0524	4.7	37.5	32.8	-9.4	-9.4	1080.4	1080.4	1080.4	1080.4	1080.4	1080.4	1080.4	1080.4	1080.4	1080.4	1080.4	1080.4
0.78	-47.89	-.0336	9.4	42.2	65.7	4.7	4.7	1174.4	1174.4	1174.4	1174.4	1174.4	1174.4	1174.4	1174.4	1174.4	1174.4	1174.4	1174.4
0.78	-36.44	-.0366	9.4	42.2	98.6	9.4	9.4	1179.1	1179.1	1179.1	1179.1	1179.1	1179.1	1179.1	1179.1	1179.1	1179.1	1179.1	1179.1
0.74	-38.05	-.0602	0.0	28.1	98.6	-	-	1188.5	1188.5	1188.5	1188.5	1188.5	1188.5	1188.5	1188.5	1188.5	1188.5	1188.5	1188.5
0.74	-21.86	-.1821	-9.4	18.7	89.2	-	-	1879.0	1879.0	1879.0	1879.0	1879.0	1879.0	1879.0	1879.0	1879.0	1879.0	1879.0	1879.0
0.74	-11.77	-.0189	-9.4	14.0	98.6	-	-	-	-	-	-	-	-	-	-	-	-	-	-

Table 5.46 Minimum Principle Concrete Strains & Curvatures & Steel Strains TB.23

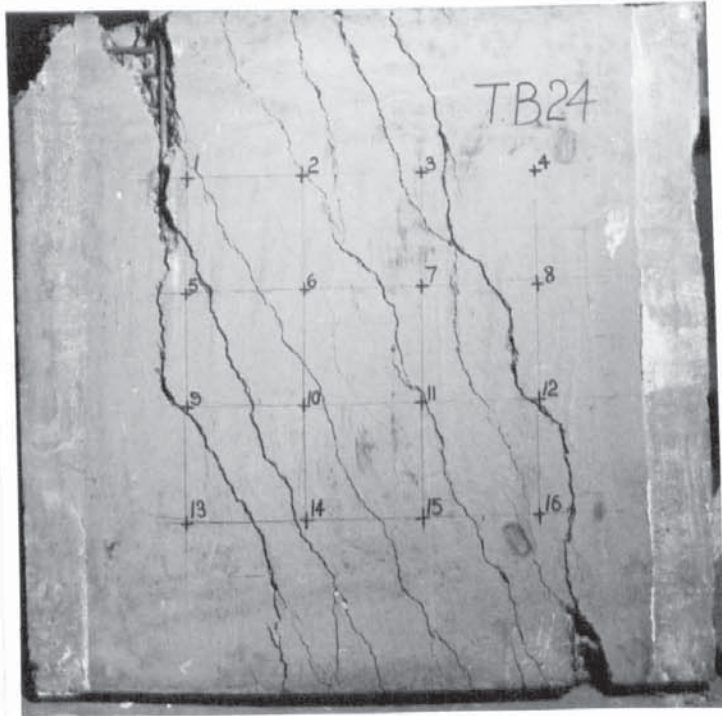


PLATE 5.55

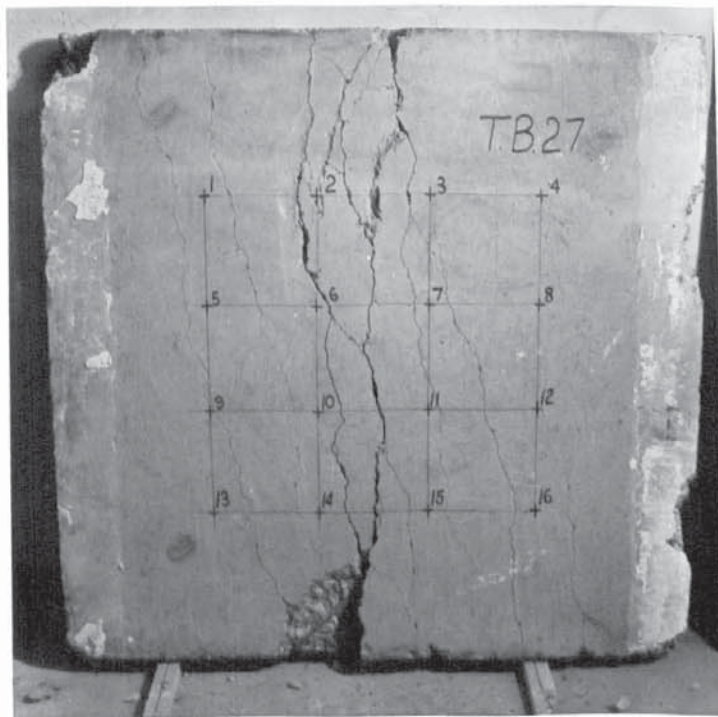


PLATE 5.56

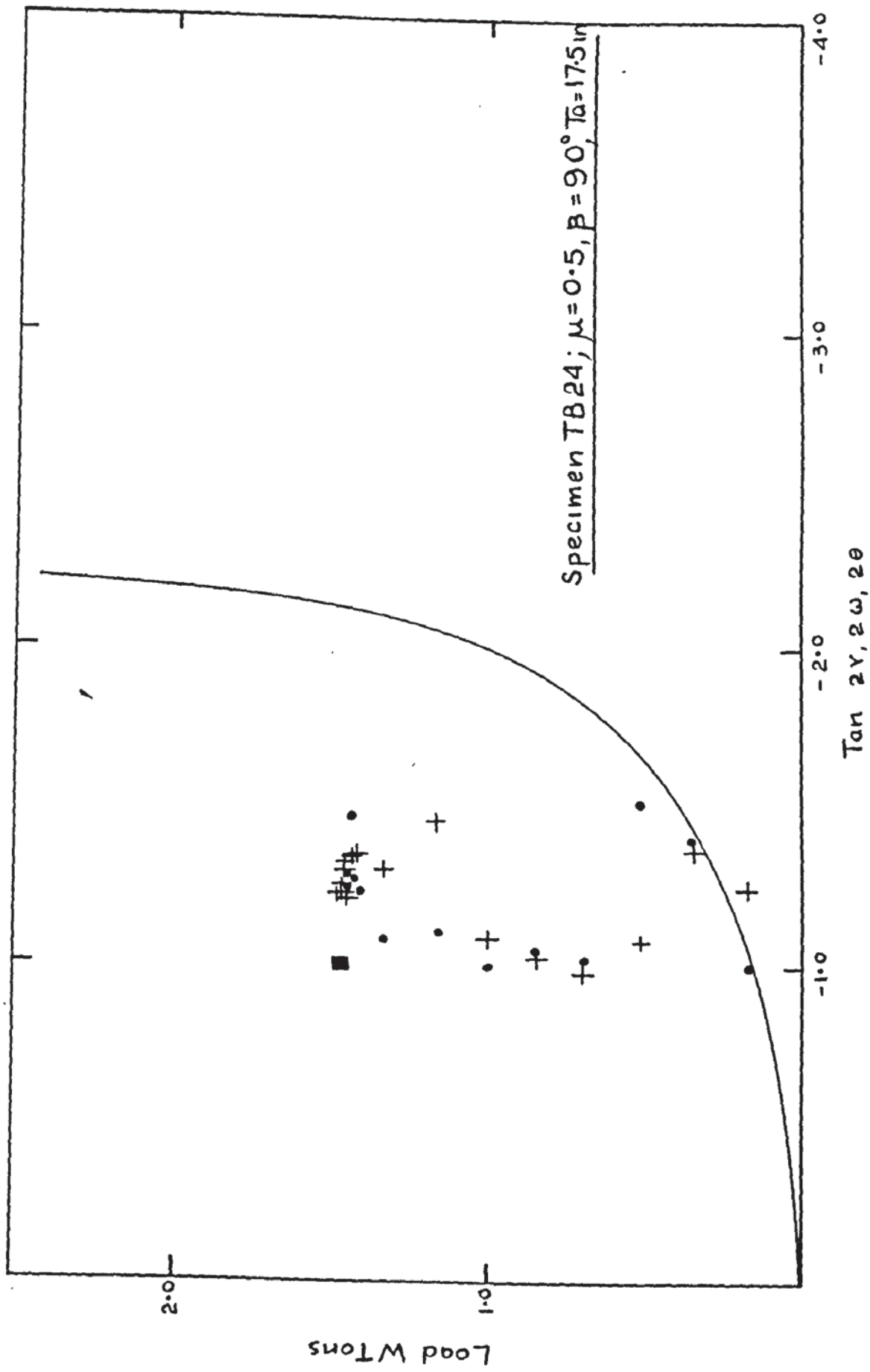


FIG 5.132 PLOT OF PRINCIPAL DIRECTIONS - TB 24.

LOAD W TONS	MIN. PRINC. CONC. STRAIN E2 μ STRAINS	MIN. PRINC. CURVATURE K2 in <sup>-1</sup> x10 <sup>3</sup>	STEEL STRAINS MICROSTRAINS										
			1	2	3	4	5	6	7	8			
0.00	0.00	0.00	0.0	0.0	0.0	0.0	0.0	0.0	0.0	0.0	0.0	0.0	0.0
0.17	-9.73	.0145	9.4	0.0	9.4	9.4	9.4	18.7	18.7	9.4	9.4	9.4	14.0
0.34	-38.49	.0067	28.1	-14.0	9.4	9.4	9.4	37.5	37.5	37.5	32.8	32.8	37.5
0.51	-29.75	-.0015	32.8	18.7	-14.0	18.7	18.7	84.5	84.5	75.1	75.1	75.1	112.7
0.67	-18.90	-.0066	28.1	56.3	18.7	18.7	32.8	225.4	225.4	206.7	206.7	206.7	234.8
0.84	-30.47	.0227	56.3	140.9	56.3	79.8	79.8	591.9	591.9	469.7	469.7	404.0	488.5
1.00	-38.29	.0415	84.5	202.0	103.3	145.6	145.6	840.8	840.8	751.6	751.6	667.0	723.4
1.17	-148.04	-.0712	178.5	253.6	169.1	216.0	216.0	1061.6	1061.6	1052.2	939.5	939.5	995.9
1.34	-180.72	.1128	281.8	300.6	225.4	300.6	300.6	1296.5	1296.5	1334.1	1174.4	1174.4	1761.6
1.42	-111.34	-.1471	404.0	380.5	347.6	394.6	394.6	1531.4	1531.4	1681.7	1212.0	1212.0	2564.9
1.44	-132.24	-.1661	422.7	394.6	460.3	460.3	460.3	1658.2	1658.2	1742.8	1193.2	1193.2	3034.7
1.46	-138.84	-.1982	465.0	300.6	554.3	563.7	563.7	1794.5	1794.5	1916.6	1188.5	1188.5	4397.0
1.46	-145.06	-.2191	544.9	216.0	606.0	761.0	761.0	1935.4	1935.4	-	1188.5	1188.5	6031.8
1.46	-150.46	-.2413	601.3	479.1	685.8	911.3	911.3	2273.6	2273.6	-	1197.9	1197.9	7967.2
1.47	-142.59	-.2724	709.3	671.7	742.2	1038.1	1038.1	3194.4	3194.4	-	1212.0	1212.0	1.1x10 <sup>4</sup>
1.47	-129.95	-.2853	-	761.0	808.0	1136.8	1136.8	4960.7	4960.7	-	1212.0	1212.0	-
1.48	-152.58	-.1764	-	779.8	883.1	1230.7	1230.7	-	-	-	1240.1	1240.1	-
1.47	-173.03	-.1672	-	836.1	930.1	1212.0	1212.0	-	-	-	1249.5	1249.5	-
1.47	-165.28	-.1248	-	986.5	986.5	1230.7	1230.7	-	-	-	1212.0	1212.0	-
1.45	-119.51	.3998	-	1385.8	1014.7	1155.6	1155.6	-	-	-	1108.6	1108.6	-

Table 5.47 Minimum Principle Concrete Strains & Curvatures & Steel Strains TB.24



PLATE 5.57

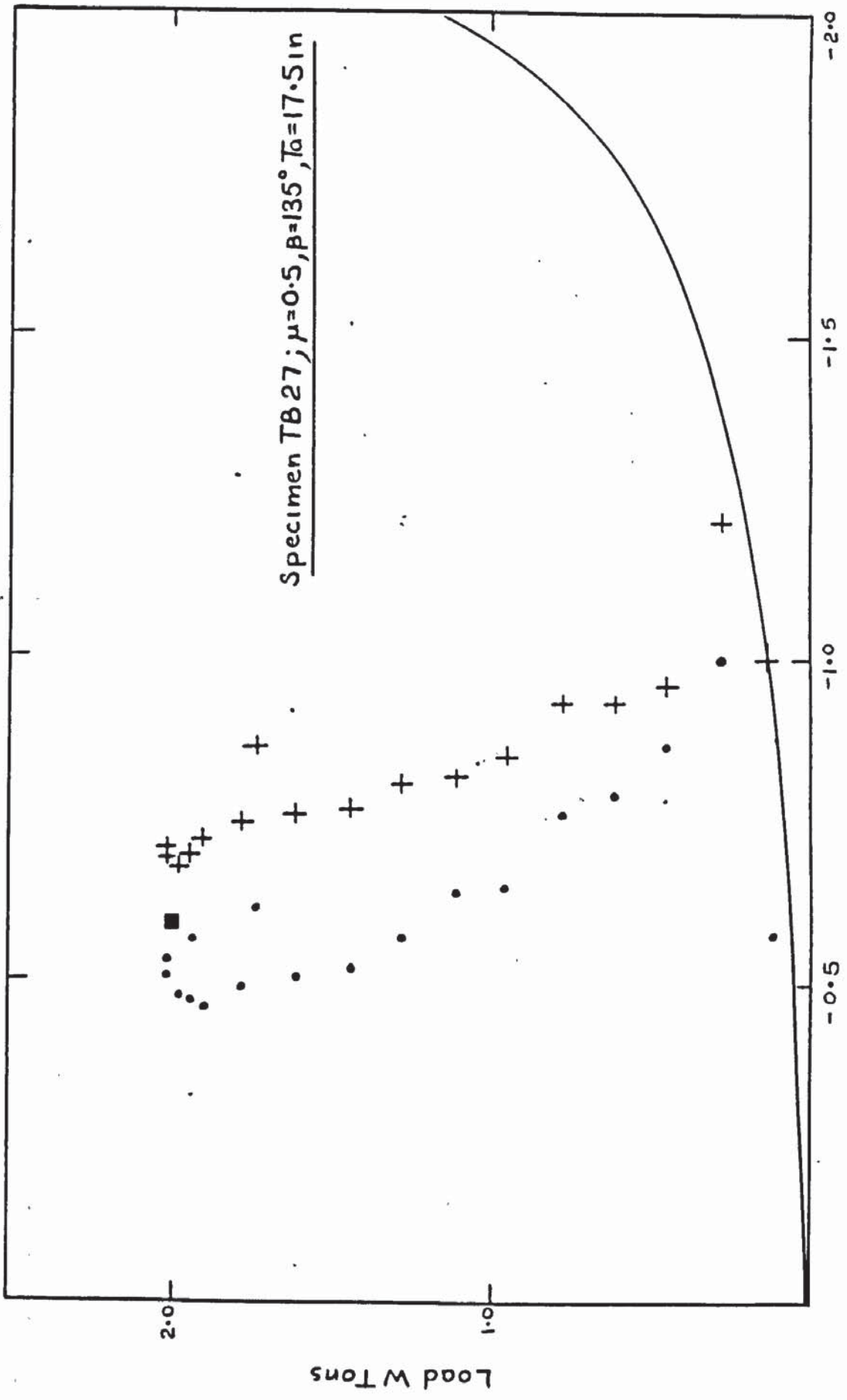


FIG 5-133 PLOT OF PRINCIPAL DIRECTIONS - TB 27

LOAD W TONS	MIN. PRINC. CONC. STRAIN E2 μ STRAINS	MIN. PRINC. CURVATURE K2 in <sup>-1</sup> x 10 <sup>3</sup>	STEEL STRAINS MICROSTRAINS										
			1	2	3	4	5	6	7	8			
0.00	0.00	0.00	0.0	0.0	0.0	0.0	0.0	0.0	0.0	0.0	0.0	0.0	0.0
0.12	-10.26	-.0175	9.4	9.4	4.7	4.7	0.0	0.0	4.7	4.7	4.7	4.7	9.4
0.28	-16.07	-.0241	18.7	28.1	23.4	23.4	0.0	0.0	9.4	4.7	4.7	4.7	9.4
0.45	-19.79	-.0126	37.5	56.3	56.3	56.3	0.0	0.0	9.4	14.0	14.0	14.0	9.4
0.61	-27.25	-.0256	89.2	93.9	126.8	126.8	150.3	28.1	28.1	23.4	32.8	32.8	28.1
0.78	-42.46	-.0414	187.9	206.7	230.1	230.1	328.8	79.8	79.8	42.2	65.7	65.7	70.4
0.95	-53.66	-.0452	319.4	319.4	352.3	352.3	375.8	126.8	126.8	84.5	108.0	108.0	112.7
1.11	-68.15	-.0498	469.7	460.3	474.4	474.4	450.9	291.2	291.2	140.9	169.1	169.1	178.5
1.28	-89.71	-.0627	620.0	591.9	606.0	606.0	582.5	291.2	291.2	192.6	239.5	239.5	239.5
1.44	-112.17	-.0864	770.4	723.4	728.1	728.1	732.8	394.6	394.6	258.3	333.5	333.5	310.0
1.61	-136.95	-.0832	911.3	845.5	869.0	869.0	901.9	488.5	488.5	314.7	427.4	427.4	375.8
1.78	-167.87	-.1287	1080.4	1033.4	1071.0	1071.0	1113.3	657.6	657.6	418.0	559.0	559.0	526.1
1.90	-198.53	-.1007	253.6	1305.9	1047.5	1047.5	1174.4	1005.3	1005.3	559.0	822.0	822.0	638.8
1.94	-205.34	.1530	1212.0	1381.1	1028.7	1028.7	1146.2	1230.7	1230.7	775.1	1010.0	1010.0	742.2
1.98	-217.03	-.1702	1258.9	1475.0	1047.5	1047.5	1183.8	1484.4	1484.4	925.4	1160.3	1160.3	836.1
2.01	-242.44	-.1748	1277.7	1559.6	1169.7	1169.7	1287.1	-	-	1066.3	1564.3	1564.3	1014.7
2.01	-283.28	-.1751	1343.5	1681.7	1348.2	1348.2	1399.9	-	-	1108.6	2175.0	2175.0	1099.2
1.93	-291.08	-.1880	-	-	-	-	-	-	-	1094.5	-	-	1155.6
1.73	-295.29	-.8165	-	-	-	-	-	-	-	-	-	-	-

Table 5.48 Minimum Principle Concrete Strains & Curvatures & Steel Strains TB.27

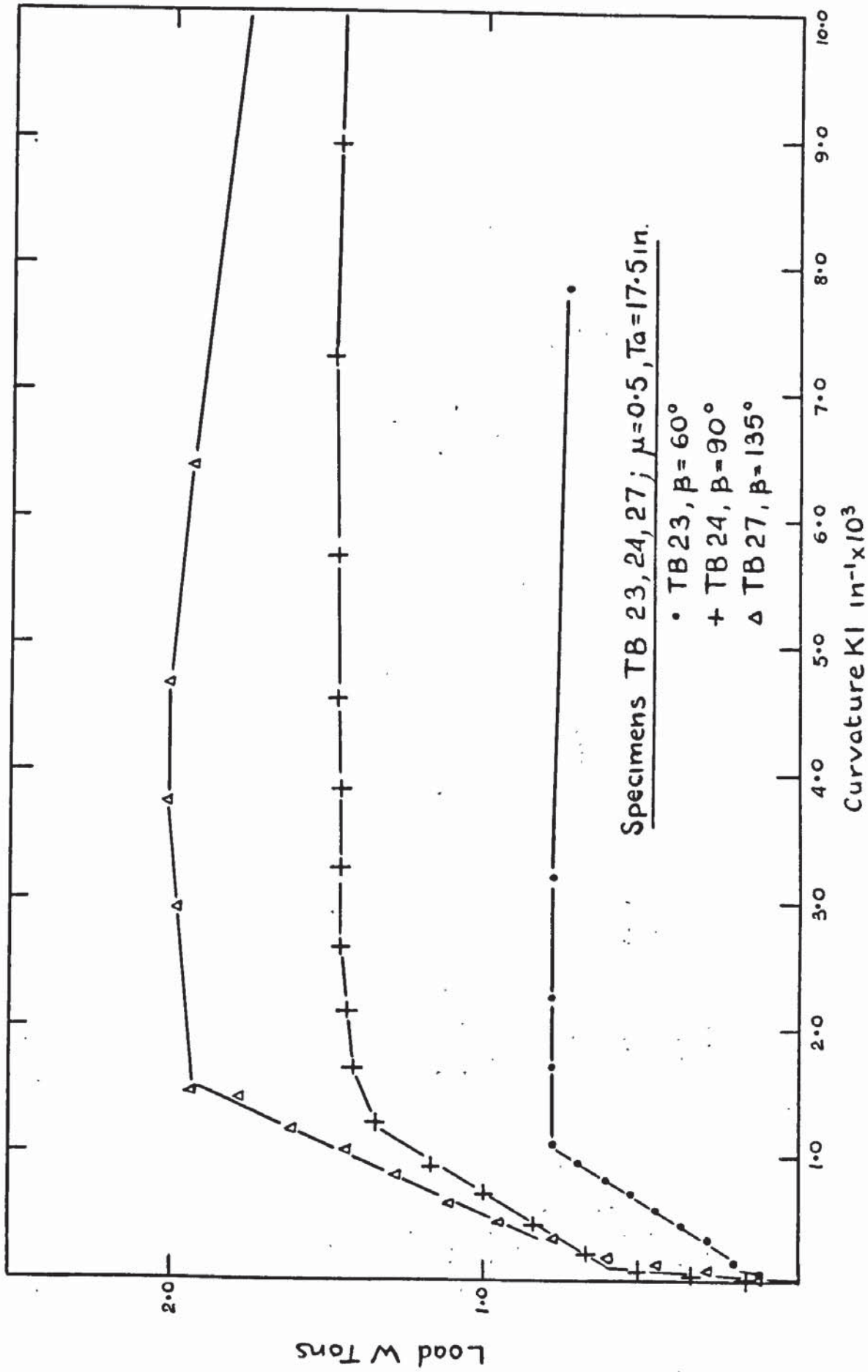


FIG 5.134 PLOT OF MAXIMUM PRINCIPAL CURVATURES - TB 23, TB 24, TB 27

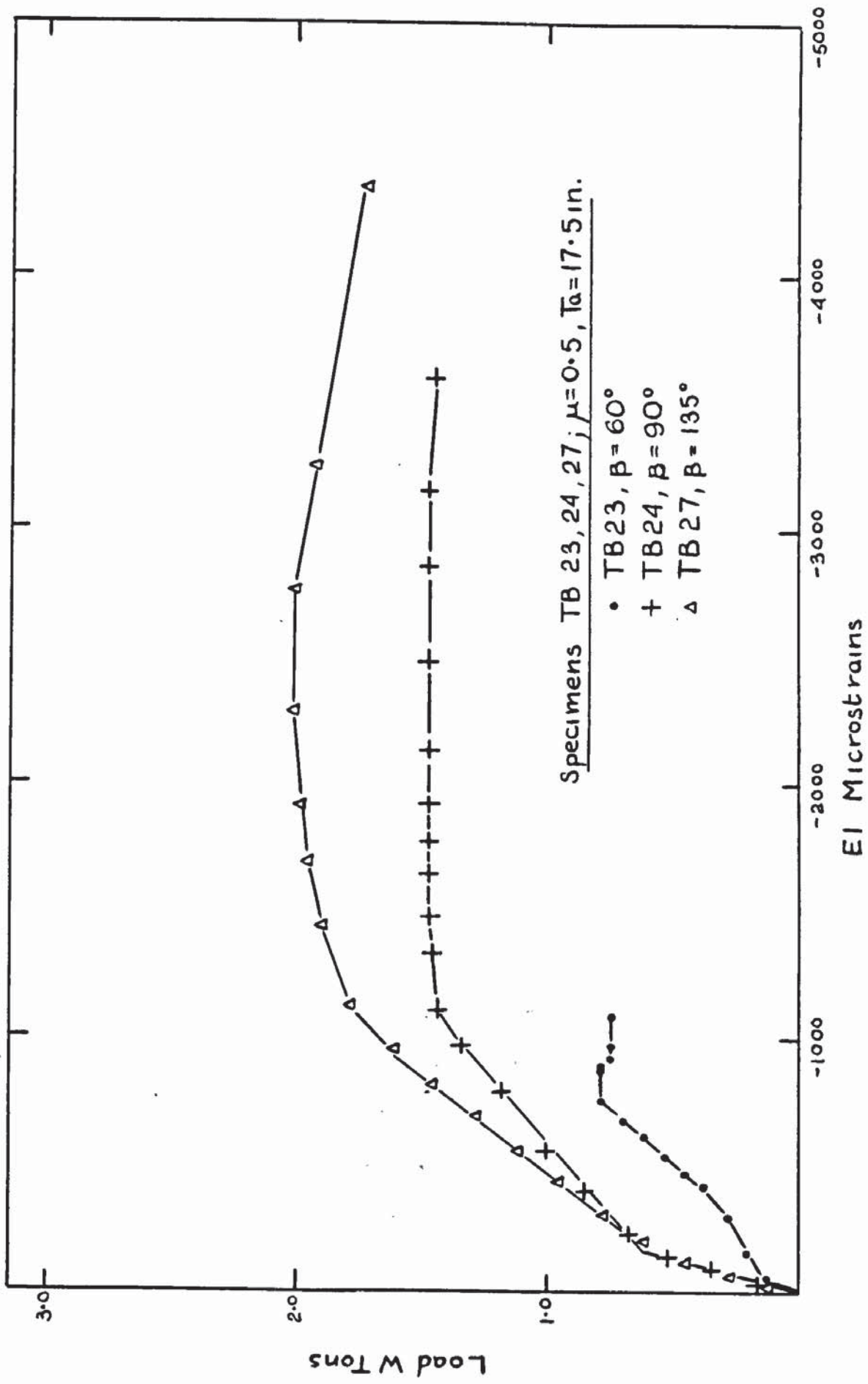


FIG 5.135 PLOT OF PRINCIPAL CONCRETE STRAINS EI - TB23, TB24, TB27

CHAPTER 6COMPARATIVE ANALYSIS OF RESULTS FROM THE PLANK TEST SERIES.6.1      Introduction

In the previous chapter the objective results of seventeen tests carried out on planks with various reinforcement arrangements and concrete strengths (see Chapter 4) have been presented. No attempt was made to directly compare these results with each other and it is therefore the object of this chapter to present the data in a more subjective manner. The behaviour of each slab is not only compared with that of other specimens but is related to the reference framework of existing theories in particular cases.

In most of the previous work carried out to obtain a yield criterion for reinforced concrete slabs under pure bending the normal ultimate moment on a yield line for varying mesh orientations has been taken as the over riding factor in establishing that criterion. In the case of 'isotropic' slabs, variations of 15% in the ultimate moment have been postulated and measured indirectly. This relatively small percentage is greatly affected by the arrangement of reinforcing bars within the slab and the necessity to formulate 'effective' slab widths has met with some criticism as described in Chapter 2. The importance of this 'effective' slab width in the analysis of the results will be indicated

in the following section, 6.3.

Standardization of slab properties such as concrete strength, which affects the ultimate moment, has been carried out and tabulated in section 6.2.

### 6.2. Standardization of section properties

It is normally assumed that the ultimate moment of a unit width of slab in which the reinforcement is layed parallel to the uniaxial moment acting on it can be evaluated from the expression: [10]

$$M_{ult} = \sigma_o A_s t d_1 \left( 1 - k \frac{\sigma_o A_s t}{u d l} \right) \quad (6.1)$$

where the constant  $k$  is a function of the shape of the compressive stress block at failure and the properties in bending of a particular concrete mix.  $\sigma_o$  is the yield stress of the steel,  $d_1$ , the effective depth of the reinforcement layer yielding;  $a$ , the cross sectional area of steel per unit width; and  $u$ , the compressive strength of the concrete measured by means of cube tests. Although this expression takes no account of the effect of the orthogonal steel layer and implies therefore that a slab reinforced and tested in the above manner acts simply as a series of parallel unit strips the approximation involved is of a small degree. Because the constant  $k$  is a function of the concrete properties made up in turn of the properties of the aggregates Morley [27] concluded that the same constant could be used for all orientations of mesh. Thus in both test

series, as the aggregates and hence the concrete mixes were alike nominally the same  $k$  value can be applied to specimens to forecast the ultimate moments of resistance in the bar directions and hence standardize results.

The ultimate moments of four slab elements were used to find the value of  $k$ . P1, P8, P13 and P17 all had reinforcement placed parallel to the span direction and by using the values of  $d_1$  and  $u$  measured, it was found that the average value of  $k$ , obtained by substituting these values into equation (6.1), was 0.475. This value is considerably less than the value obtained by Morley.

The major factor affecting the ultimate moment of resistance in the bar directions in each slab is the effective depth, as described in section 4.3.1 and 4.4.1. the slab thicknesses of each slab were measured and the cover to the reinforcement checked in random samples. These values of effective depth along with the values of cube strength and steel strength tabulated in chapter 4 were used to find the ultimate moments of resistance in the bar directions from equation (6.1) and are tabulated in Table 6.1. for the plank test series. Included with these values of  $m_a$  are values of  $\mu$  'the degree of orthotropy' which has been defined as the ratio  $\frac{m_b}{m_a}$  so that  $\mu < 1$ . It can be seen that due to the effect of variations in cube strength and thickness that although the 'isotropic' slabs have  $\mu$  values

Slab Slab $\alpha = \beta^{\circ}$	$m_a$ k.in/in	True $\mu$ value	Effective width $b_b$ in	$\frac{m_n}{m_n}$
P1 0	3.56	1.00	30	1.005
P2 30	3.44	0.99	25.69	1.054
P3 45	3.38	0.99	24.34	1.059
P4 0	3.48	0	30	0.877
P5 30	3.46	0	24.25	1.030
P6 45	3.45	0	16.97	1.282
P7 60	3.52	0	10.39	1.432
P8 90	3.44	.275	30	0.966
P9 30	3.40	.275	22.56	1.258
P10 45	3.42	.275	19.71	1.384
P11 60	3.36	.274	20.26	1.319
P12 90	3.47	.275	31.5	1.062
P13 0	3.29	.543	30	1.032
P14 30	3.40	.546	23.26	1.060
P15 45	3.25	.542	22.95	1.099
P16 60	3.49	.547	24.66	0.905
P17 90	3.41	.545	32.37	1.001

TABLE 6 . 1  
Ultimate moment values

close to unity the other nominal  $\mu$  values of 0.25 and 0.5 are closer to values of 0.275 and 0.55. These values of  $m$  and  $\mu$  are used in the presentation of comparative results later in the chapter.

### 6.3 The effect of bar arrangement on the 'effective' width of the slab

It is important that the effect of mesh orientation on the ultimate moment and general behaviour of a slab element is not masked by other phenomena. As mentioned several times in this thesis the maximum enhancement of normal moment across a yield line due to the orientation of an 'isotropic' reinforcement mesh predicted by various theories lies between 15 and 18% at a mesh angle of  $45^{\circ}$  to the uniaxial moment direction. This extra moment capacity can easily be hidden in tests by a combination of the following effects.

- a) Membrane action
- b) Bond failure at the edges
- c) Inherently weak sections due to the orientated mesh within a rectangular framework.

The effects of membrane action can be effectively prevented by the provision of strategic releases in the general test system. These releases, described in 4.3.2 have been made in the case of this test series.

The other two effects are more directly significant in most tests reported. Kwiecinski [22] reported bond failures at the edges thus reducing the number of bars actually resisting the applied moment. However no hooks were provided to enhance the bond and Lenschow and Sozen [29] who provided hooks at the ends of their reinforcement reported no bond failures. Contrary to this evidence however is that reported by Prince [37] in which although hooks were provided into the compression zone low values of ultimate moment were attributed to bond failure. In fact the reason for the ineffectuality of any bar, be it either from bond failure or from its geometrical position at the edge is not of critical importance. However its non-participation in the resisting of applied forces must be taken into account in the analysis of results.

Lenschow and Sozen [29] and Prince [37] use 'effective' widths of slab elements to convert total moments into moments per unit width. However although it is said to be the 'effective' width of the weakest section no detailed information is given concerning the method of evaluation of that width. In contrast Kwiecinski places particular importance on the evaluation of the 'effective' width of his slabs and it is on similar expressions that the effective widths of the slabs in this test series are based.

As described in Chapter 2 Johansens expression for the normal moment of resistance on a yield line was

derived from local equilibrium conditions on that yield line and therefore took the form

$$m_n = m \cos^2 \alpha + \mu m \sin^2 \alpha \quad (6.2)$$

This equilibrium equation considered a portion of yield line of length  $b$ , say and the moment values  $m_n$  and  $m$  refer to moments per unit width. Now a reinforcement mesh is made up of an integer number of bars whereas Johansens equations imply that non integer numbers of bars cross the portion of yield line considered. By simple geometry the number of bars crossing a given length of yield line  $b$  in. at an angle  $\alpha$  and spaced at  $s_1$  in. centres can be given as:

$$n_1 = \frac{b \cos \alpha}{s_1} \quad (6.2)$$

and for bars crossing the same yield line at an angle of  $90 - \alpha$  and spaced at  $s_2$  in centres can be expressed as

$$n_2 = \frac{b \sin \alpha}{s_2} \quad (6.4)$$

Thus from (6.3) and (6.4)

$$\begin{aligned} b \cos \alpha &= n_1 s_1 \\ b \sin \alpha &= n_2 s_2 \end{aligned} \quad (6.5)$$

Thus in a theoretical expression  $n_1$  and  $n_2$  need not be integer numbers. However in practice there is always a whole number of bars crossing the yield line.

Thus Johansens expression, equation (6.2) written before cancellation of terms in the form

$$m_n \times b = m b \cos \alpha \cos \alpha + \mu m b \sin \alpha \sin \alpha$$

can be expressed by using equation (6.5) as

$$m_n \times b = m (n_1 s_1) \cos \alpha + \mu m (n_2 s_2) \sin \alpha \quad (6.6)$$

where  $n_1 s_1$  and  $n_2 s_2$  are theoretical values. By using experimentally observed values of  $n_1 s_1$  and  $n_2 s_2$  the expression

$$m_n \times b^1 = m (n_1 s_1) \exp. \cos \alpha + \mu m (n_2 s_2) \exp. \sin \alpha \quad (6.7)$$

is obtained and by dividing equation (6.7) by equation (6.2)

$$b^1 = \frac{(n_1 s_1) \exp. \cos \alpha + \mu (n_2 s_2) \exp. \sin \alpha}{\cos^2 \alpha + \mu \sin^2 \alpha} \quad (6.8)$$

where  $b^1$  can be called the 'effective length' of yield line or in this test series the 'effective' width of the slab element. Thus by dividing the experimental bending moment by the effective width  $b^1$  the moment per unit width can be obtained.

The form of  $b^1$  presented in equation (6.8) gives experimental results as a direct comparison to Johansens equation. Kwiecinski<sup>22</sup> in formulating an expression for an 'effective' width of slab makes a direct comparison with his own theoretical expressions. It can be easily appreciated that a different value of 'effective' width will be obtained if an equation other than Johansens equilibrium equation is used. For instance if the expression for moment at failure on a yield line obeying the 'full kinking' criterion described in Chapter 2 was used to derive an expression for  $b^1$  the result would be

$$b^1 = \frac{(n_1 s_1) \exp + \mu (n_2 s_2)}{\cos \alpha + \mu \sin \alpha} \quad (6.9)$$

which will give different values of  $b^1$  for a given set of values of  $n_1, n_2$  etc. than will equation (6.8). It is therefore important when comparing theories and experimental results to ensure that all expressions plotted are relative to the same datum. Thus Kwiecinski, in plotting his results on a  $\frac{m}{n} v \propto$  set of axes, would have obtained different values of ultimate moment had the effective width been based on Johansens equation.

In order to compare experimental results of this type with several theories it can be seen that it is strictly necessary to plot the curves describing these various expressions as relative to whichever expression has been used in the determination of the 'effective' width  $b^1$ . In this chapter all experimental results of this type and all expressions describing other hypotheses have been plotted relative to Johansens expression, equation (6.2)

#### 6.4 Comparison of Results

This section is concerned with the presentation of representative results presented in Chapter 5 in a subjective form after allowance has been made for 'effective' width differences. The effects of mesh orientation and degree of orthotropy on

- a) The stiffness of the element up to yield
- b) The ultimate moment of the element.

are investigated separately.

In order to present the above effects in an easily

comparable form it was necessary to estimate the 'effective' slab widths using the techniques described in section 6.3. Criticism of Kwiecinski's estimates was made on the grounds that the need for personal experience in adjudging a bond failure could easily lead to incorrect conclusions and it is true that bond failures at the edges are difficult to judge visually. In this test series described, bond failures occurred on only one or two occasions and effective widths were influenced mainly by geometry. However when bond failures occurred they were accompanied by a drop in load and thus a good estimate could be made of the incidence of such failure.

Because the positions of the bars in the slabs were known it was possible by careful observation after testing to plot the main yield line positions onto a reference plan of the reinforcement mesh and consequently evaluate the number of bars acting at failure. Because little bond failure occurred at high loads it is possible to assume that the weak section was critical throughout the test and thus the 'effective' widths estimated at yield have been applied to results obtained in other load ranges. The 'effective' widths obtained from equation (6.8) are presented in Table 6.1 along with the ultimate moments values.

#### 6.4.1 The effect of mesh orientation on the stiffness of the element in the span direction before yielding

The stiffness of an element can be considered as the

ratio of moment to curvature in a given direction during any part of the loading history of the specimen. Thus the effective stiffness of the element changes at cracking again at first yield and finally becomes approximately zero when plastic flow occurs. Lenschow and Sozen [29] have stressed the importance of variations in stiffness in as much as it affects the rotational capacity of a yield line. In yield line theory, in present use, no check is made on the rotational capacities of individual yield lines. However, strictly, these rotations must be known so that failure of a yield line due to concrete crushing does not occur in a slab until the final yield line has formed thus rendering the slab a valid mechanism.

Both Morley [27] and Lenschow and Sozen [29] have shown that the stiffness is a function of both mesh orientation and degree of orthotropy. Both sets of results were obtained from tests on elements subjected to uniaxial moment and theoretical expressions were obtained assuming the bars to carry only axial stress in their original directions.

Thus Fig 6.1 - Fig 6.4 illustrate the behaviour of the specimens up to first yield. The effective widths listed in Table 6.1 have been used to convert the plots in Chapter 5 to subjective characteristics. The figures show moment per unit effective width plotted against curvature in the X - direction.

Fig 6.1 illustrates the effect on stiffness of the mesh orientation for 'isotropic' slab elements subjected to uniaxial moment. Although the stiffness before cracking appears to have been little affected by the mesh orientation it is evident that considerable difference occurred after cracking although cracking took place at the same moment and curvature value in all three slabs. Not only was the stiffness affected in this way but also, as would be expected, the curvatures at first yield became greater as the mesh orientation increased from  $0^{\circ}$  to  $45^{\circ}$ . Because of the symmetry of the isotropic elements only mesh orientations from  $0^{\circ}$  to  $45^{\circ}$  were needed to describe the behaviour at any orientation.

Fig 6.2 shows the same characteristics as the previous figure for  $\mu = 0$ . Again before cracking occurred the stiffnesses appeared to be similar although at cracking there was not the same immediate slope change indicated in Fig 6.1. P7, the specimen with a mesh orientation of  $60^{\circ}$  has not been plotted as the cracking moment of the concrete exceeded the resisting moment of the reinforcement.

Fig 6.3 shows the variation of stiffness for slabs with  $\mu = 0.25$ . Again the stiffness becomes less with greater mesh orientation upto a value near  $60^{\circ}$ . Although it is difficult to appreciate in Fig 6.3 the stiffness of P12,  $\beta = 90^{\circ}$  was slightly greater than P11,  $\beta = 60^{\circ}$ . In this series it is

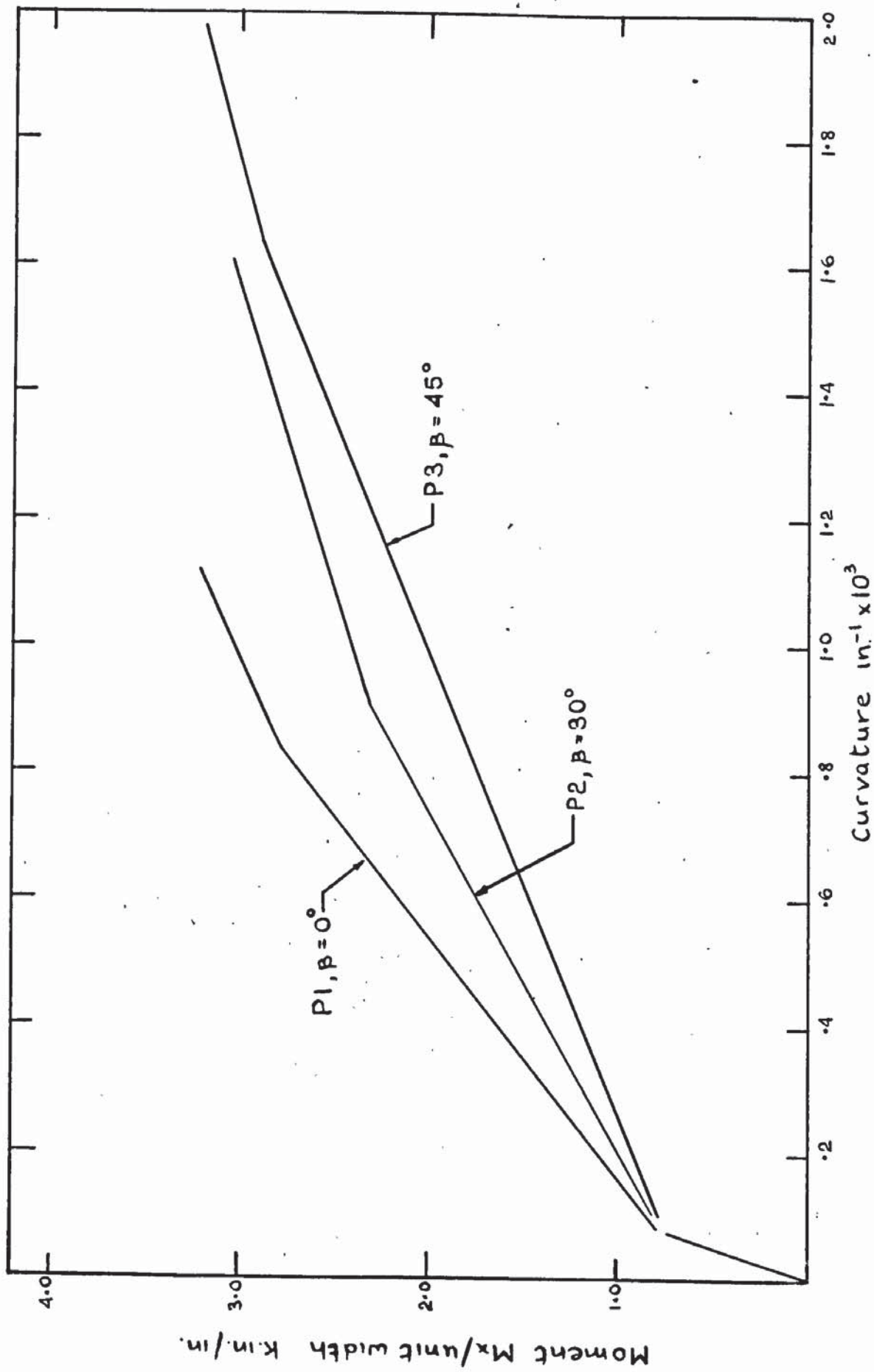


FIG 6.1 MOMENT - CURVATURE, PLANK SERIES,  $\mu = 1.0$

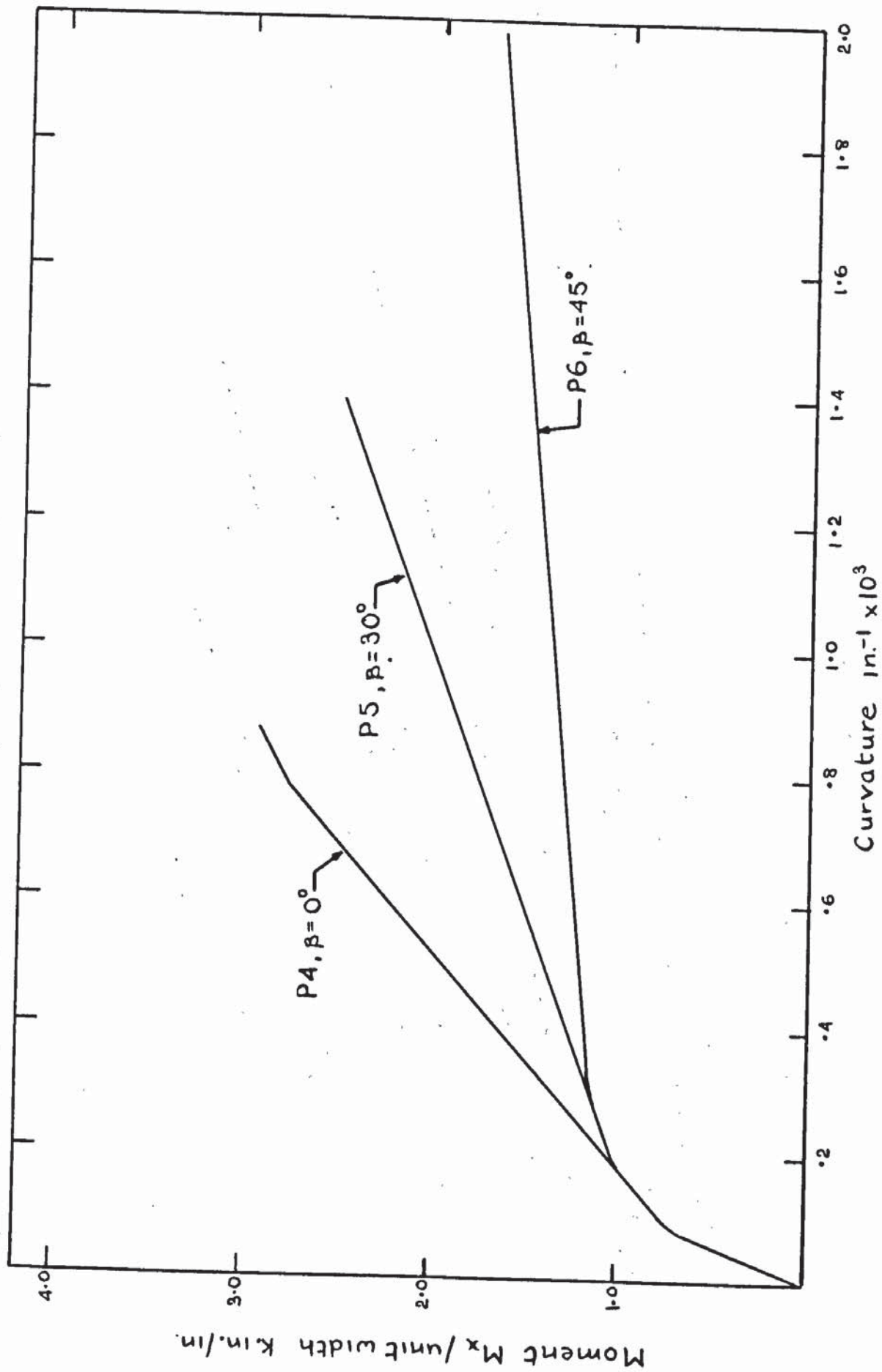


FIG. 6.2 MOMENT-CURVATURE, PLANK SERIES,  $\mu = 0$

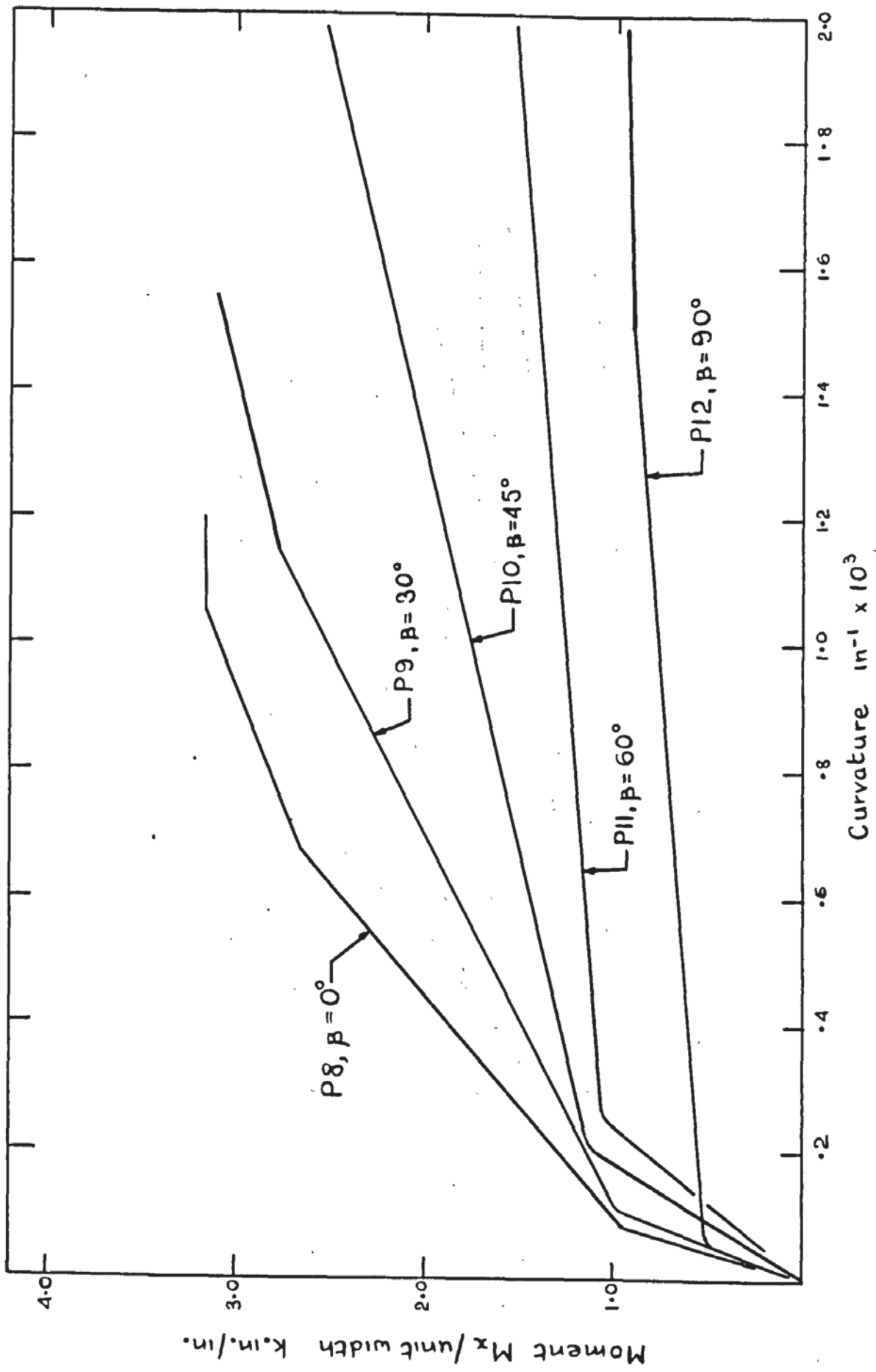


FIG. 6.3 MOMENT - CURVATURE, PLANK SERIES,  $\mu=0.25$

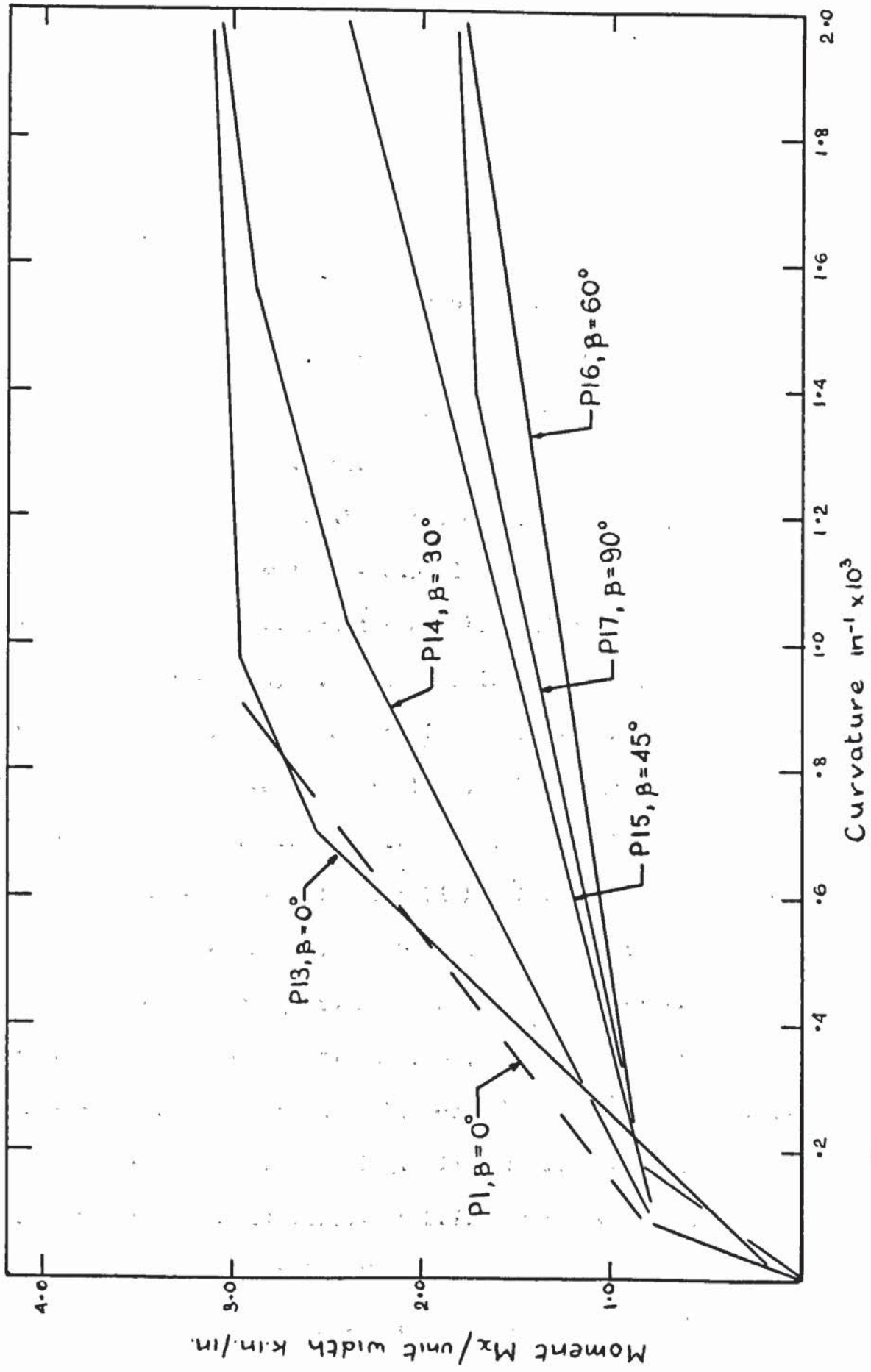


FIG 6.4 MOMENT - CURVATURE, PLANK SERIES,  $\mu = 0.5$

noticeable that the stiffness of the specimens varied before cracking as well as after and although the cracking moment was fairly constant the curvatures increased with mesh orientation. P12 however behaved somewhat differently than the other specimens plotted in Fig 6.3. It can be seen that although the stiffness before cracking was close to that of P9, cracking took place at a moment value of around half that reached by the other slabs.

In Fig 6.4, describing the elastic behaviour of specimens reinforced with  $\mu = 0.5$ , it can be seen that the moment curvature characteristic of P13 indicates no cracking. In Chapter 5 it was explained that this particular slab was badly vibrated resulting in bond losses in the centre of the slab before any load was applied. This lack of bond had the effect of precracking the specimen and leading to the plot shown. The plot for P1 has been superimposed on Fig 6.4 so that comparison can be made. Again it can be seen that there appeared to be no difference in stiffness before cracking for mesh orientations of  $0^\circ$ ,  $30^\circ$  and  $45^\circ$  although both P16 and P17 with mesh angles of  $60^\circ$  and  $90^\circ$  respectively were less stiff before cracking. In this figure it is noticeable that the stiffness of P17,  $\beta = 90^\circ$  was greater than that of P16,  $\beta = 60^\circ$  although at the same time less than P15,  $\beta = 45^\circ$ . The curvature at yield of the  $90^\circ$  reinforced slab was however lower than that of the  $45^\circ$

reinforced slab.

Lenschow and Sozen [29] have derived expressions describing the elastic behaviour of slab elements subjected to uniaxial moment. These expressions have been plotted in Fig 6.5 and are indicated by the dashed lines. The assumptions made in plotting these curves are the same as those used by Lenschow and Sozen. Thus the distance below the compressive face of the resultant steel force, denoted in their work by  $d_{nb}$ , has been taken as constant for both layers of reinforcement and made equal to 2.125 in. which in a 3in. deep slab is the distance to the interface between the layers. The area of steel per unit width in the main steel direction has been made equal to  $0.037 \text{ in}^2/\text{in}$ .  $E_s$ , the youngs modulus of the steel has been taken equal to  $29.5 \times 10^6 \text{ lb/in}^2$  and  $E_c$ , the concrete elastic modulus as  $4.2 \times 10^6 \text{ lb/in}^2$ . In their expressions Lenschow and Sozen have assumed that the stress in the steel at a crack is equal to the average stress in the steel between cracks. This assumption is not of course correct and hence their curves describe a material which does not have the discontinuity of slope at cracking associated with reinforced concrete beams and slabs. Thus it is evident that the values of stiffness obtained will be less than the element stiffness before cracking but greater than the element stiffness after cracking. The values of stiffness

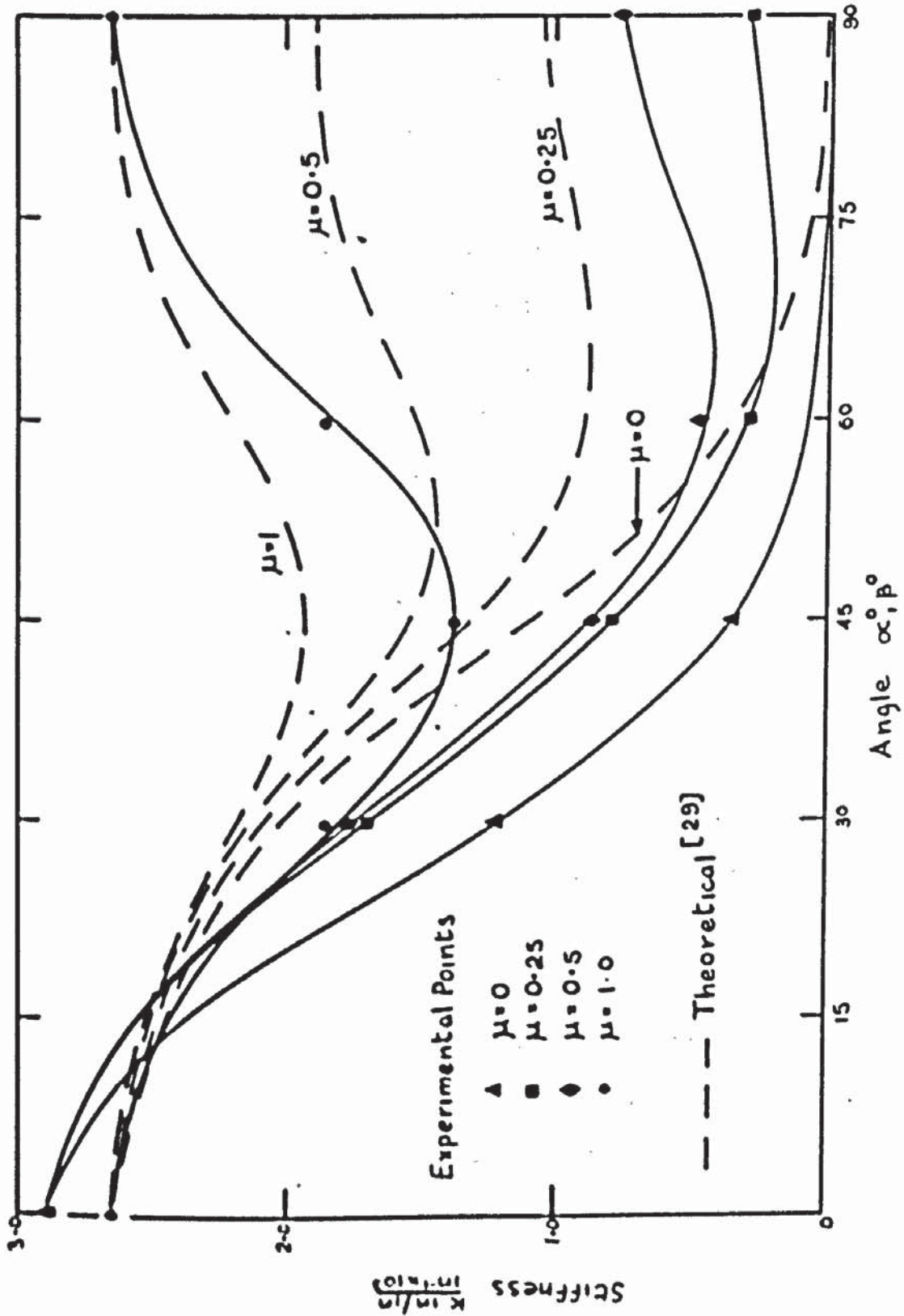


FIG 6-5 VARIATION OF STIFFNESS WITH MESH ORIENTATION - PLANKS

for all slabs after cracking and before yield are plotted in Fig 6.5 also. As expected the theoretical values are higher than those obtained from experiment. The values obtained from all the non-isotropically reinforced elements are considerably lower than those predicted. This is due in the most part to the different slopes considered by Lenschow and Sozen but may also be affected by the way the bar resists stress. As mentioned earlier the theoretical curves are based on an analysis in which the bars carry only axial stress whereas Prince [37] has suggested that shear stresses are also induced. As implied in Chapter 3 this effect of bar shear stiffness would alter the anisotropic properties of the element even in the elastic range. However it is felt that this effect would be small in this range.

These results relating to the pre-yield behaviour of reinforced concrete slab elements subjected to uniaxial moment have increased the information already presented by some other authors. They were obtained both as a check on previous work and for the purpose of making the whole test series complete. As past work has shown, the stiffness after cracking decreased with mesh orientation upto certain critical values and generally followed a curve of the type described by Lenschow and Sozen. However contrary to these authors results there was evidence of stiffness

differences before cracking. This was particularly apparent in the case of  $\mu = 0.25$  and  $\mu = 0.5$  as shown in Figs 6.4 and 6.5. There is no doubt that measurements of curvatures and load are more difficult to obtain accurately in this range and a special investigation may be required to clarify the behaviour. A particularly interesting point can be appreciated by inspection of the cracking moments and curvatures. Figs 6.1 - 6.4 show that except in one case the cracking moment for all specimens was fairly constant laying between 0.9 k.in/in and 1.0 k.in/in. However especially in Figs 6.2 - 6.4 it can be seen that the curvature at cracking varied. This implies that, contrary to the suggestion made in 3.3.1, the criterion at cracking is one based on stress conditions rather than strain conditions.

#### 6.4.2 The effect of mesh orientation on the ultimate moment of the element.

Most recent research has been concerned with the effect of mesh orientation relative to the principal moment directions on the ultimate moment of the slab as reviewed in Chapter 2. Several hypotheses have been put forward particularly for slabs subjected only to uniaxial moment. These fall approximately into two groups. The first suggests that Johansens original hypothesis (equation 6.2) is acceptable. This implies no moment enhancement with mesh orientation in isotropic slabs because bars remain straight and carry only axial stress. The second group of hypotheses suggest that

because of local effect at a crack such as partial kinking or bar shear stiffness the moment capacity is enhanced with mesh orientation. Of the most recent authors Kwiecinski [22], Prince [37] and Baus and Tolaccia [23] fall into the second category whilst Morley [27] and Lenschow and Sozen [29] fall into the first.

As described in section 6.3 the effective width of an element is greatly influenced by the orientation of the mesh. The 'effective' widths of the elements presented in Table 6.1 have been calculated with respect to Johansens normal moment criterion described by equation (6.1). Thus to present these experimental results in relation to other theoretical criteria it is strictly necessary to also present these expressions relative to Johansens expression. Fig 6.6 for instance shows the full kinking theory plotted in relation to Johansens criterion.  $m_n/m_{nj}$  is plotted against  $\alpha$  which in this case of uniaxial moment corresponds to  $\beta$  or the mesh orientation relative to the span.

$m_{nj}$  is the Johansen expression so that

$$m_{nj} = m \cos^2 \alpha + \mu m \sin^2 \alpha$$

which corresponds to equation (6.1)

The expression describing full kinking is written

$$m_n = m \cos \alpha + \mu m \sin \alpha$$

thus 
$$\frac{m_n}{m_{nj}} = \frac{\cos^2 \alpha + \mu \sin^2 \alpha}{\cos \alpha + \mu \sin \alpha}$$

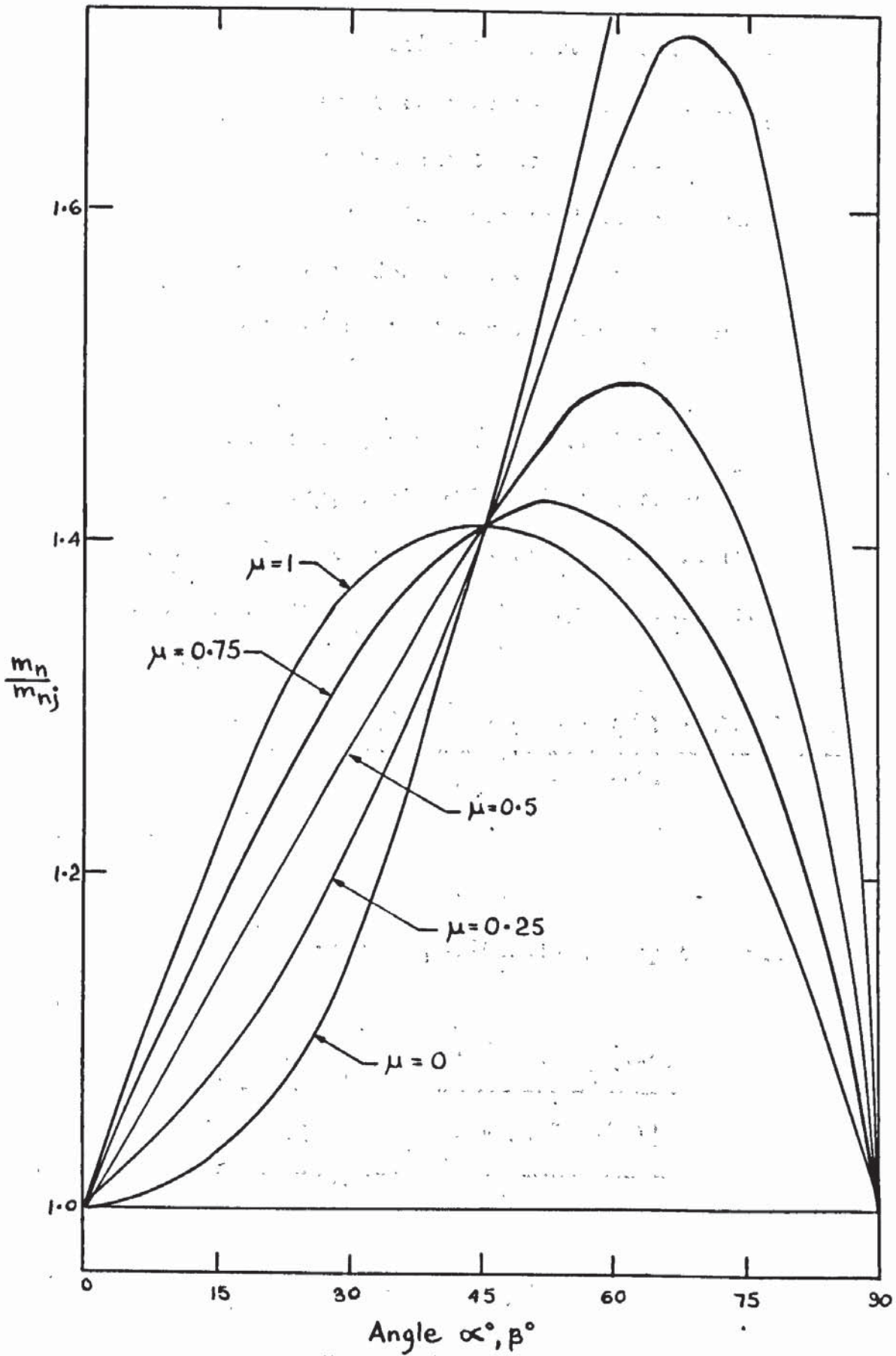


FIG 6.6  $\frac{m_n}{m_{nj}}$  v.  $\alpha^\circ$ , FULL KINKING.

It should be noted that by plotting the curves in this way the Johansen expression always reduces to a constant at  $m_n/m_{nj} = 1$  for all values of  $\mu$  and hence acts as a datum.

The ultimate moment values obtained experimentally and presented as relative to Johansens expression are presented in Table 6.1 and plotted for varying  $\mu$  values in Figs 6.7 - 6.10.

Fig 6.7 shows the test results in comparison to the full kinking theory, the partial kinking theory [22] and the strain compatibility theory [37] for  $\mu = 1$ . In the case of Kwiencki's partial kinking theory the curve in Fig 6.7 describes the expression

$$m_n/m_{nj} = \frac{(\sqrt{1 - A^2 \sin^2 \alpha}) \cos \alpha + (\sqrt{1 - A^2 \cos^2 \alpha}) \sin \alpha}{\cos^2 \alpha + \sin^2 \alpha}$$

where  $A = \sqrt{2 - \mu^2}$

and  $\mu = 1.188$

In the case of Princes strain compatibility theory the curve described the expression

$$m_n/m_{nj} = \frac{\frac{\cos^2 \alpha + K_1 \sin^2 \alpha}{(1 + 3K_1^2 \tan^2 \alpha)^{\frac{1}{2}}} + \mu \frac{\sin^2 \alpha + K_2 \cos^2 \alpha}{(1 + 3K_2^2 \cos^2 \alpha)^{\frac{1}{2}}}{\cos^2 \alpha + \mu \sin^2 \alpha}$$

$$\text{where } K_1 = \frac{3G}{3E + Gk^2 \sec^2 \alpha}$$

$$K_2 = \frac{3G}{3E + Gk^2 \sec^2 \alpha}$$

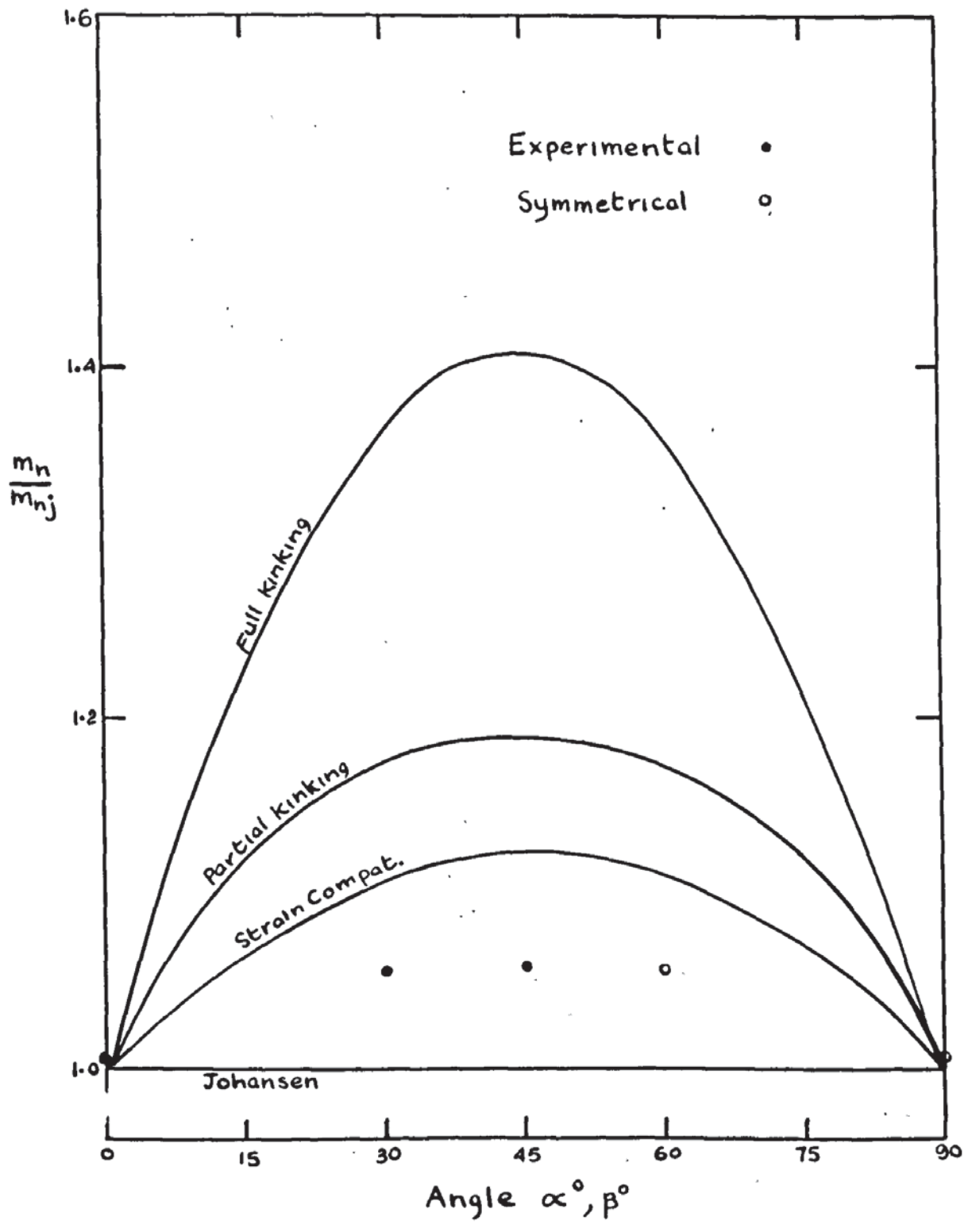


FIG 6.7  $m_n/m_{nj}$  v.  $\alpha$ , PLANKS  $-\mu=1$

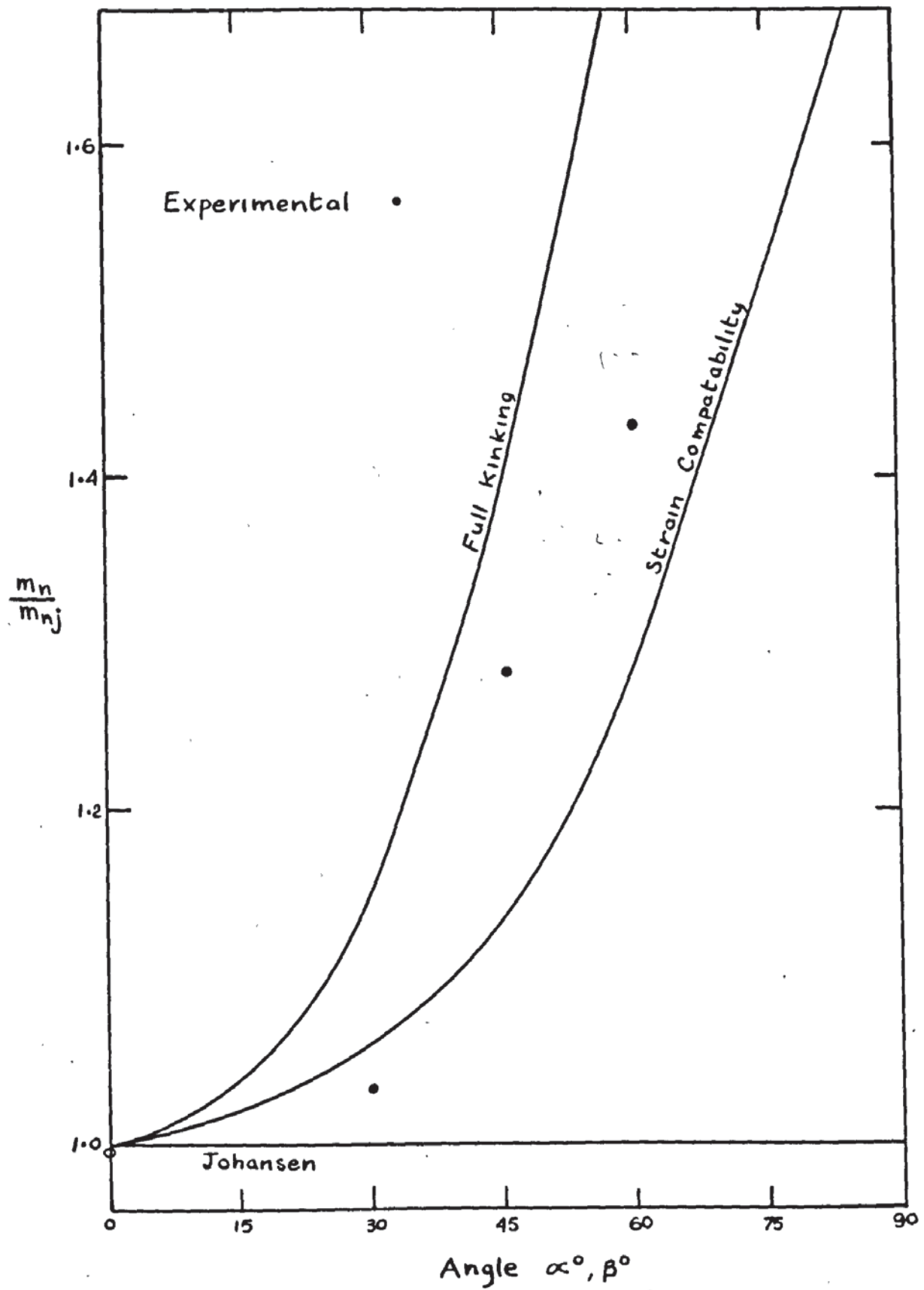


FIG 6.8  $\frac{m_n}{m_{nj}}$  v.  $\alpha$ , PLANKS -  $\mu=0$

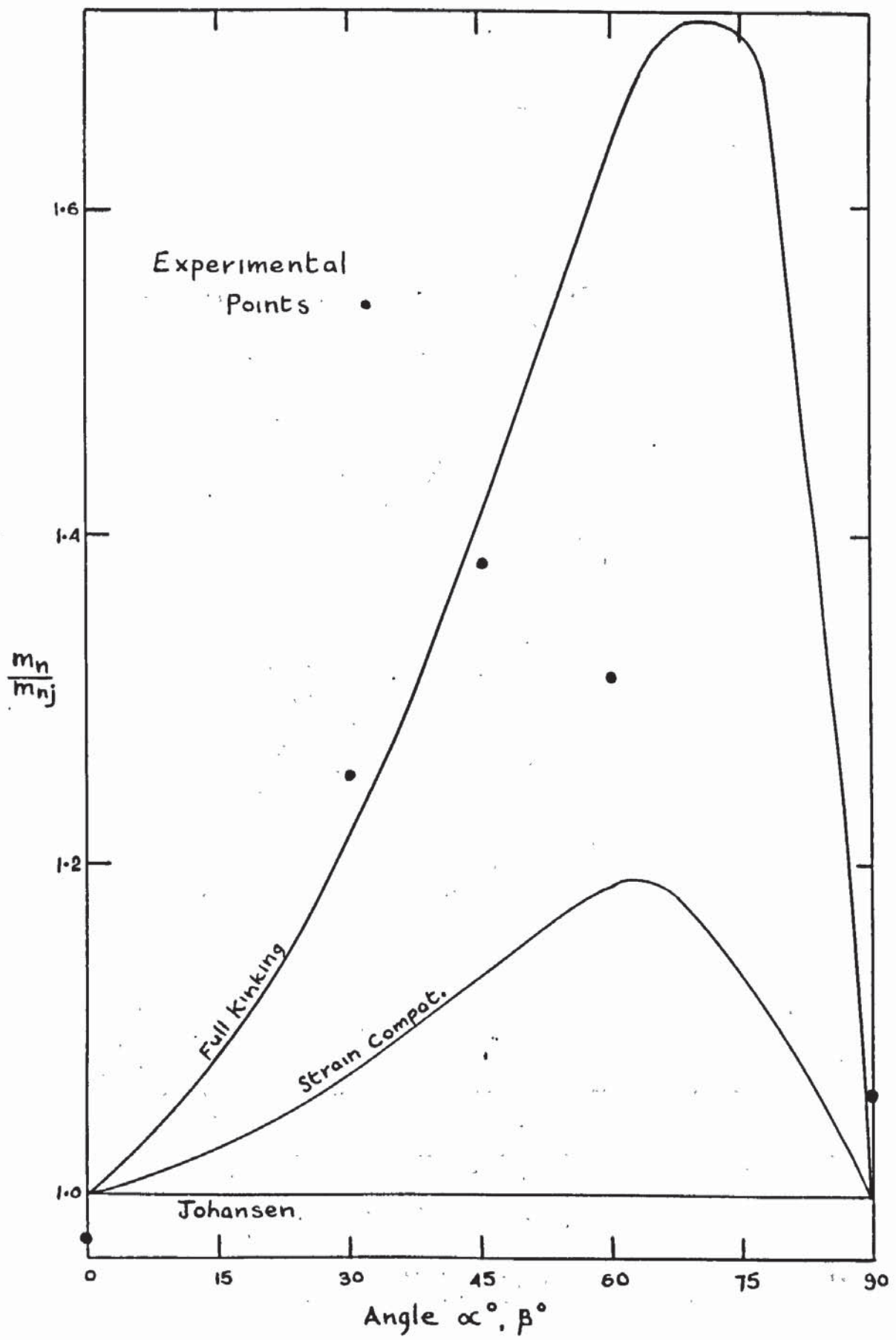


FIG 6.9  $m_n/m_{nj}$  v.  $\alpha^\circ$ , PLANKS -  $\mu=0.25$

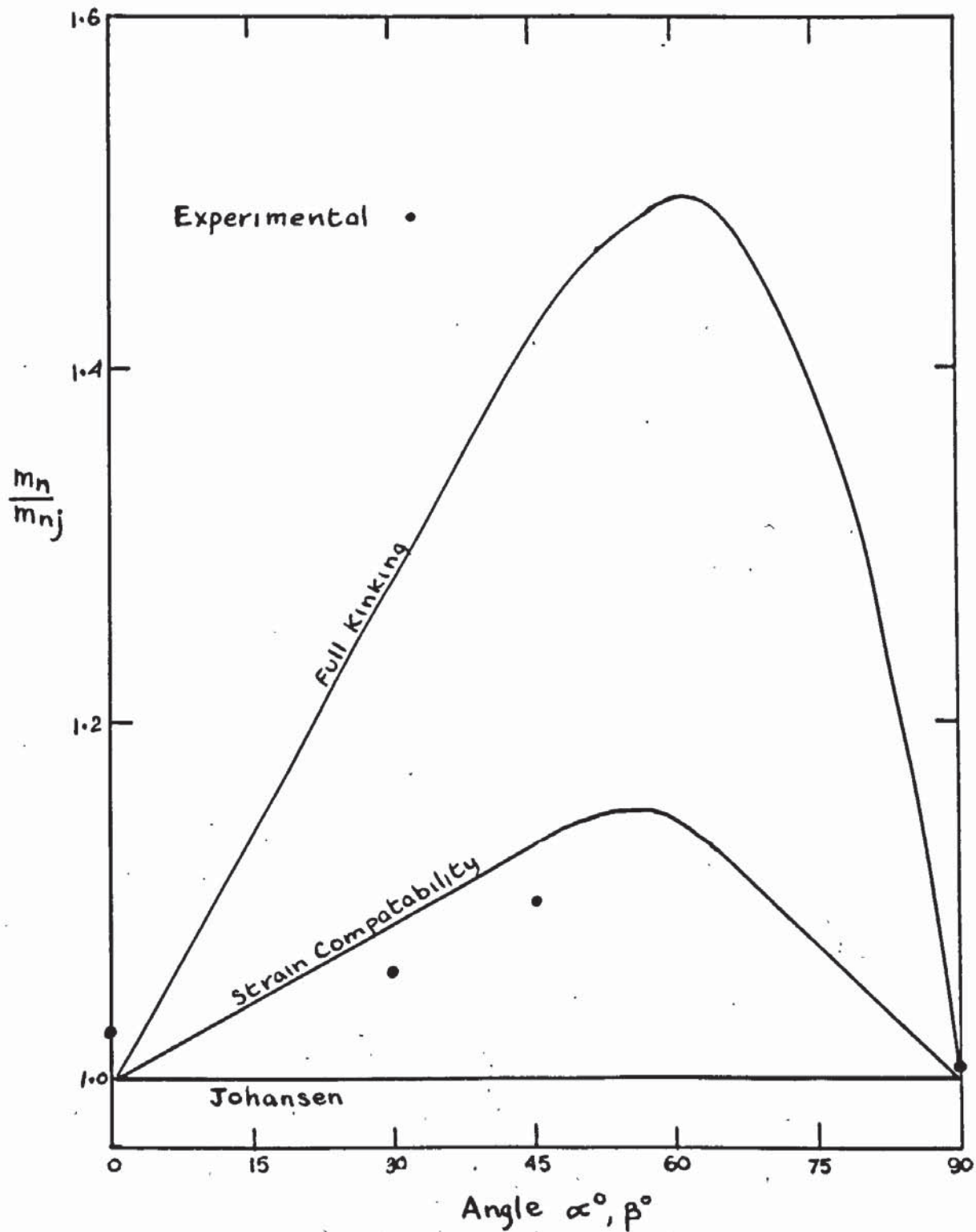


FIG 6.10  $m_n/m_{nj}$  v.  $\alpha$ , PLANKS- $\mu=0.5$

$$k = d/r = 2 = \frac{\text{crack width}}{\text{bar radius}}$$

$$E = 13 \times 10^3 \text{ Tons/in}^2 \quad G = 5.5 \times 10^3 \text{ tons/in}^2$$

$$\text{and } \mu = 1$$

In Figs 6.8 - 6.10  $\mu$  has been put equal to 0, 0.25, 0.5 respectively. It can be seen that there is a definite trend towards moment enhancement with mesh orientations up to  $45^\circ$ . This trend appears to take the same type of form as does Prince's curve although the maximum moment enhancement is of the order of 6% at  $45^\circ$  compared to about 13% from the strain compatibility curve.

Fig 6.8 illustrates the results obtained for slab elements P4 - P7 for which  $\mu = 0$ . In this case  $m_{ij} = 0$  at  $\alpha = 90^\circ$  and hence both fully kinking and strain compatibility curves approach infinity as  $\alpha \rightarrow 90^\circ$ . It was pointed out in Chapter 5 in the detailed description of tests that P4 had not reached concrete crushing and this is reflected by the low value indicated in Table 6.1. Again the trend of results is of the same type as the theoretical curves although in this case values in excess of those predicted by Prince occurred for  $\alpha = 45^\circ$  and  $60^\circ$ . As pointed out in Chapter 5 considerable twist occurred in these specimens resulting in the yield line forming at an angle of about  $20^\circ$  to the transverse direction. Consequently the results illustrated here must not be accepted as strictly correct.

Fig 6.9 shows the ultimate moment values for slabs

P8 - P12 for which  $\mu = 0.25$ . Again there is definite evidence that the trend of results has the same form as the theoretical expression, although the values for  $\alpha = 30^\circ$  and  $\alpha = 45^\circ$  appear to be very high. Both specimens were affected by possible bond failure and this may explain the high values attributed to them. However it is clear that moment enhancement was present.

Fig 6.10 shows the ultimate moment values for slabs P13 - P17 for which  $\mu = 0.5$ . P16 for which  $\beta = 60^\circ$  unfortunately did not reach concrete crushing as described in Chapter 5 and indicated in Table 6.1. Otherwise all the values of ultimate moment agree closely with the trend of the strain compatibility curve although as in Fig 6.7 the values are below that curve.

Figs 6.7 - 6.10 imply that there was moment enhancement with mesh orientation in all cases, For  $\mu = 0.5$  particularly the results indicate that an hypotheses based on Princes expressions would describe the actual behaviour of the elements at ultimate moment. It must be remembered that the curves representing the theoretical expressions are based on approximate material properties so that exact agreement could not be expected. However it is interesting to note the differences occurring in the trend of results in Fig 6.7 and 6.10 for  $\mu \neq 0$  and 0.25.

It was mentioned earlier that twisting was definitely noticed in slabs for which  $\mu = 0$  and although it was not apparent the anisotropy of the elements for which  $\mu = 0.25$  implies that some twisting may have occurred in these slabs giving unsatisfactory edge conditions which lead to high values of moment being deduced. Thus the higher the value of  $\mu$  the less tendency to twist on the supports and consequently the more exact the results presented.

#### 6.5 Concluding Remarks

These tests carried out under nominal conditions of uniaxial moment have shown that the stiffness values of the elements were markedly different after cracking for different values of mesh orientation. Before cracking occurred the difference in stiffness was not so apparent although for values of  $\mu$  of 0.25 and 0.5 there was definite evidence of variation.

Ultimate moment values indicate definite trends towards moment enhancement with mesh orientation. However in the case of 'isotropically' reinforced elements it is questionable as to whether the increased capacity of 6% at  $45^\circ$  is significant or not.

Both elastic and plastic characteristics show that anisotropic properties are present in all slabs, for even in the case of so called 'isotropic' slabs the load - deformation properties vary with mesh orientation.

Lifting from the supports in the case of  $\mu = 0$  inducing non-transverse yield lines to occur whilst the strain gauge rosettes on the isotropic concrete surface indicated that the principal strain direction was close to the span direction illustrate the way in which the truly isotropic compressive concrete layer and the anisotropic steel layer interact. As suggested in Chapter 3 the composite material formed by these layers must be subjected to a three dimensional analysis taking into account the compatibility of strains at the neutral surface.

CHAPTER 7COMPARISON OF RESULTS FROM THE GENERAL MOMENT TEST SERIES7.1 Introduction

In chapter 5, elastic characteristics and ultimate moment characteristics were compared for slab elements with varying mesh orientations and degrees of orthotropy in nominally uniaxial bending. In this chapter similar characteristics are investigated the case of slab elements subjected to combined bending and torsion. Firstly the elastic behaviour of both 'isotropic' and 'non isotropic' elements will be investigated by considering variations in stiffness with crack angle and mesh orientation and secondly the behaviour at failure for both types of slab element will be considered. The effects of element restraint are discussed in 7.2.

7.2 The elastic behaviour and variations in stiffness7.2.1 'Isotropically' reinforced elements

In the plank tests described in chapter 6 comparison was made between the stiffnesses in the span direction for varying values of mesh orientation under uniaxial bending. The effects of Poisson's ratio before yield was not significant as the graphs in chapter 5 indicate.

In the general moment test series curvature in the Y-direction must be assumed to have been effectively zero. In fact values were recorded, but were a small percentage of those measured in other directions. Lenschow and Sozen [29] have assumed

that the Poisson's ratio effect in cracked reinforced concrete slabs is insignificant. In a truly isotropic element this assumption would lead to the conclusion that no moment was induced in the Y-direction as a result of the restraint imposed. However in an anisotropic element this assumption may not lead to the same conclusion. Lekhnitskii [42] lists the equations at the generalized Hookes law as applied to a generally anisotropic body in the notation of Rabinovich. In the case of slabs in pore bending these equations reduce to:

$$\epsilon_x = \frac{1}{E_{xx}} (\sigma_x - \nu_{yx} \cdot \sigma_y + \eta_{xy,x} \cdot \tau_{xy}) \quad (7.1)$$

$$\epsilon_y = \frac{1}{E_{yy}} (-\nu_{xy} \cdot \sigma_x + \sigma_y + \eta_{xy,y} \cdot \tau_{xy}) \quad (7.2)$$

$$\gamma_{xy} = \frac{1}{G_{xy}} (\eta_{x,xy} \cdot \sigma_x + \eta_{y,xy} \cdot \sigma_y + \tau_{xy}) \quad (7.3)$$

where  $\nu_{xy}$  and  $\nu_{yx}$  are Poisson ratio values in the X and Y directions respectively,  $\eta_{xy,x}$  and  $\eta_{xy,y}$  are coefficients of mutual influence of the first kind and  $\eta_{x,xy}$  and  $\eta_{y,xy}$  are coefficients of mutual influence of the second kind. The Poisson ratios have the usual meaning assigned to them, the coefficient of mutual influence at the first kind characterize the stretching in the directions parallel to the axes induced by the tangential stresses and the coefficients of mutual influence of the second kind characterize shear strains in the planes parallel to the coordinate axes induced by the normal stresses. In orthogonally reinforced slabs such as those tested it is possible to say that for any given mesh

orientation  $\nu_{yx} = \nu_{xy}$ ,  $\eta_{xy,x} = \eta_{xy,y}$  and  $\eta_{x,xy} = \eta_{y,xy}$ . From these equations (7.1), (7.2) and (7.3) it can be seen that for  $\epsilon_y = 0$  not only has Poisson's ratio to be zero if  $\sigma_y$  is to be zero, but also the coefficients of mutual influence of the first kind.

It has already been shown that the moment-curvature relationships vary with mesh orientation in the plank tests, even for so called isotropic slabs, and although in normal plate theory only stresses and strains in the plane of the plate are considered an isotropic plate must still exhibit the same stress-strain characteristics in all directions. Thus, even 'isotropically' reinforced slabs behave anisotropically and must be analysed as such, particularly in the elastic range.

Figs. 7.1 - 7.4 show the moment-curvature relationships for slabs in which  $\mu = 1$ . Fig. 7.1 illustrates the way in which the stiffness of the element in the X-direction varies with the Torsion  $\text{orm}$ ,  $T_a$ , for slabs in which  $\beta = 0^\circ$ . Figs. 7.2 - 7.4 show similar relationships for which  $\beta = 30^\circ$ ,  $45^\circ$  and  $67.5^\circ$  respectively. It can be seen that for any given angle  $\beta$  before cracking the stiffness is constant for all values of  $T_a$ , allowing for the fact that measurement of the smaller quantities of curvature and load are subject to error. It can be concluded therefore that in a continuous anisotropic reinforced concrete plate, even if Poissons ratio were not equal to zero, as the variations in stiffness for any given value of  $\beta$  due to variations

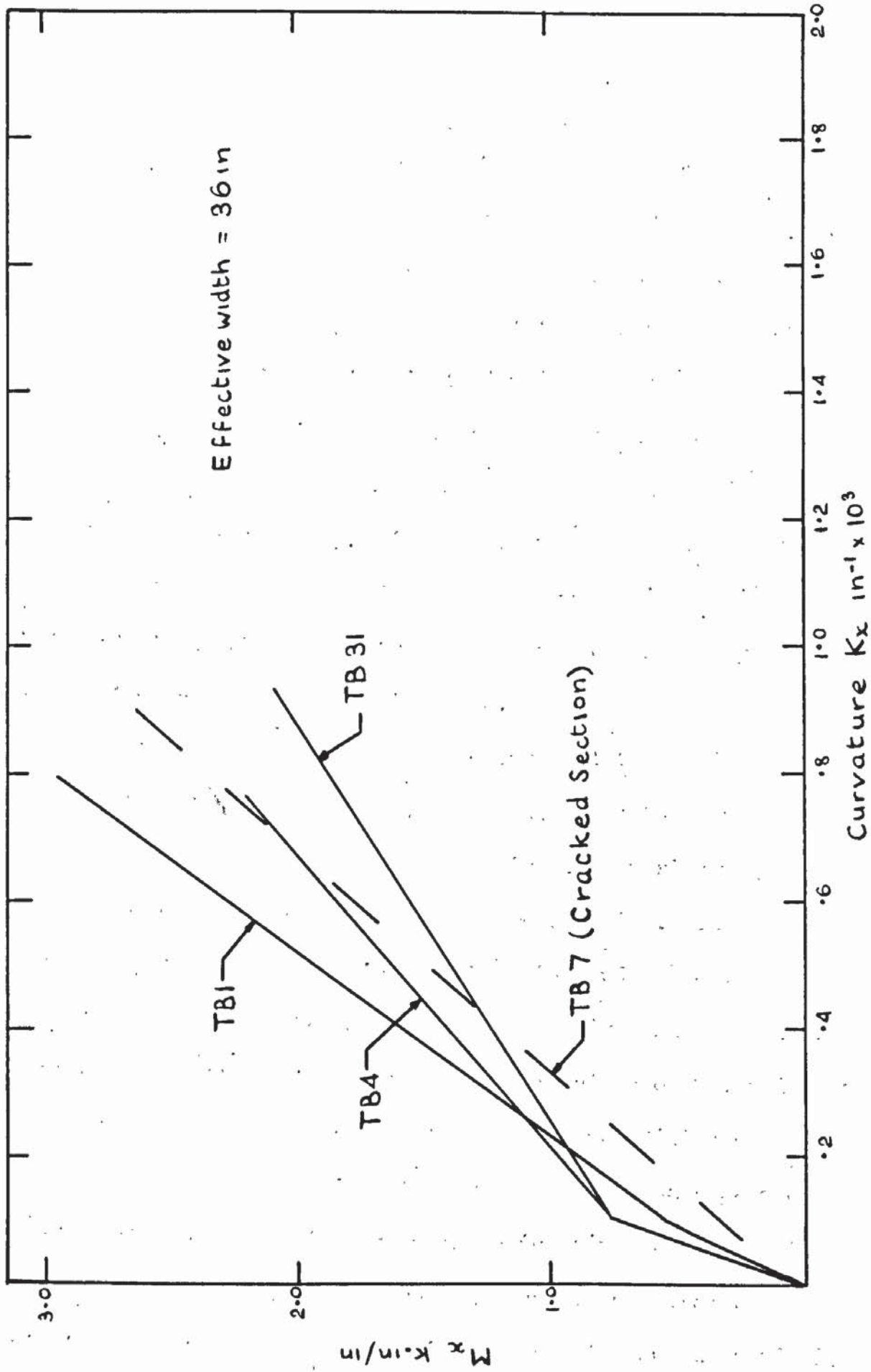


FIG 7.1 MOMENT-CURVATURE, GENERAL MOMENT -  $\beta=0^\circ$ ,  $\mu=1$

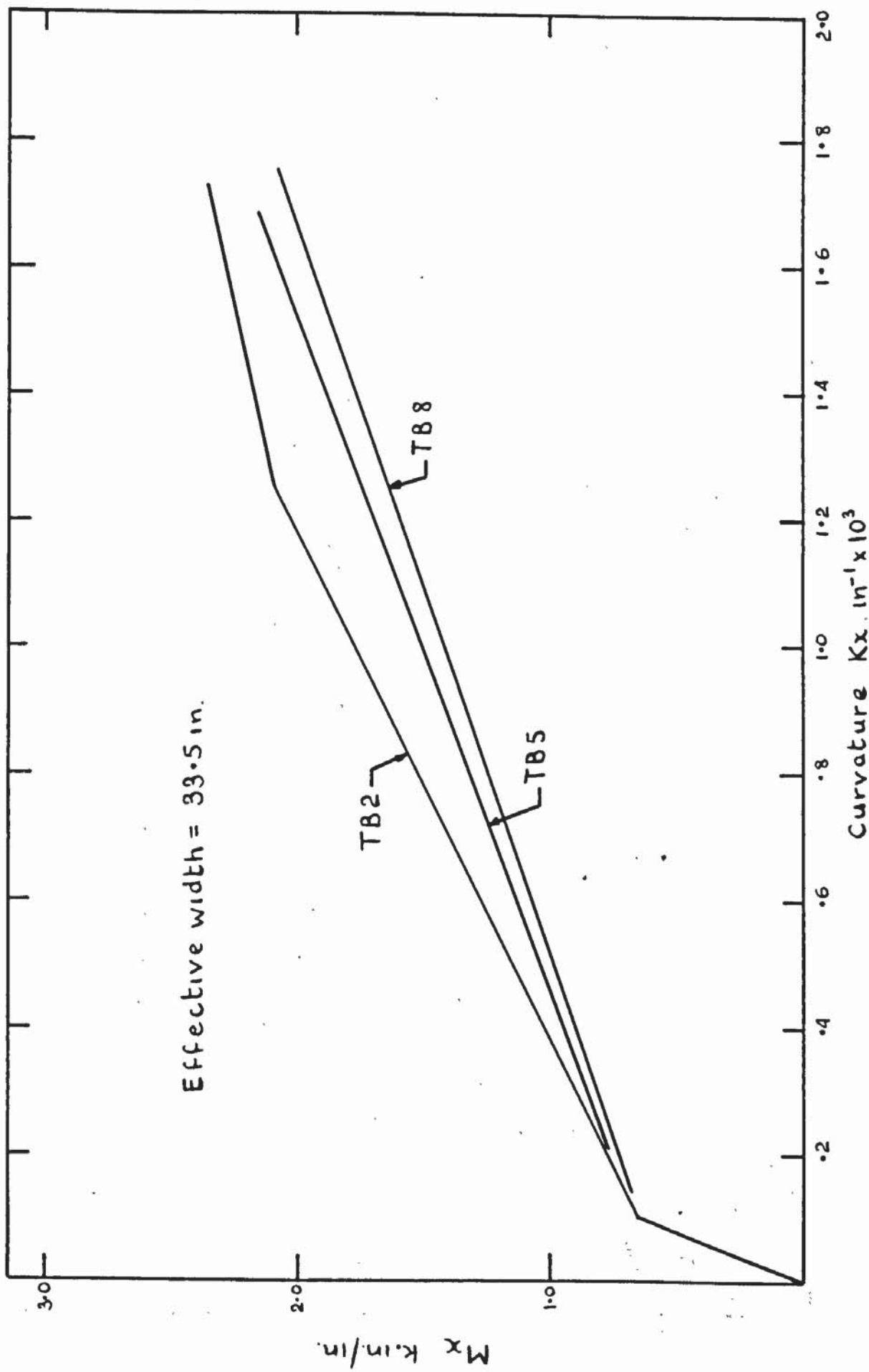
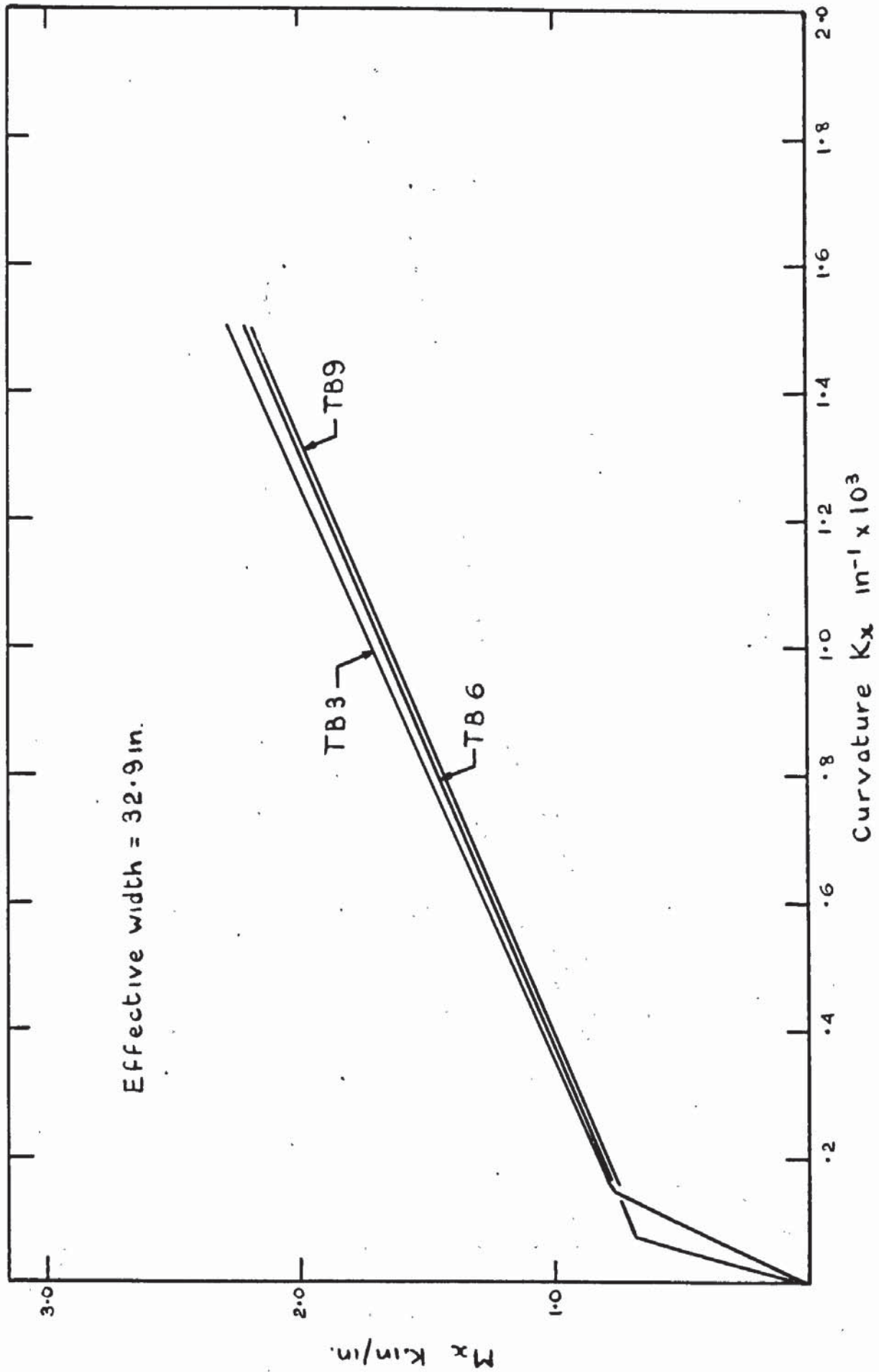


FIG 7.2 MOMENT - CURVATURE, GENERAL MOMENT -  $\beta = 30^\circ, \mu = 1$



**FIG 7.3 MOMENT - CURVATURE, GENERAL MOMENT -  $\beta = 45^\circ$ ,  $\mu = 1$**

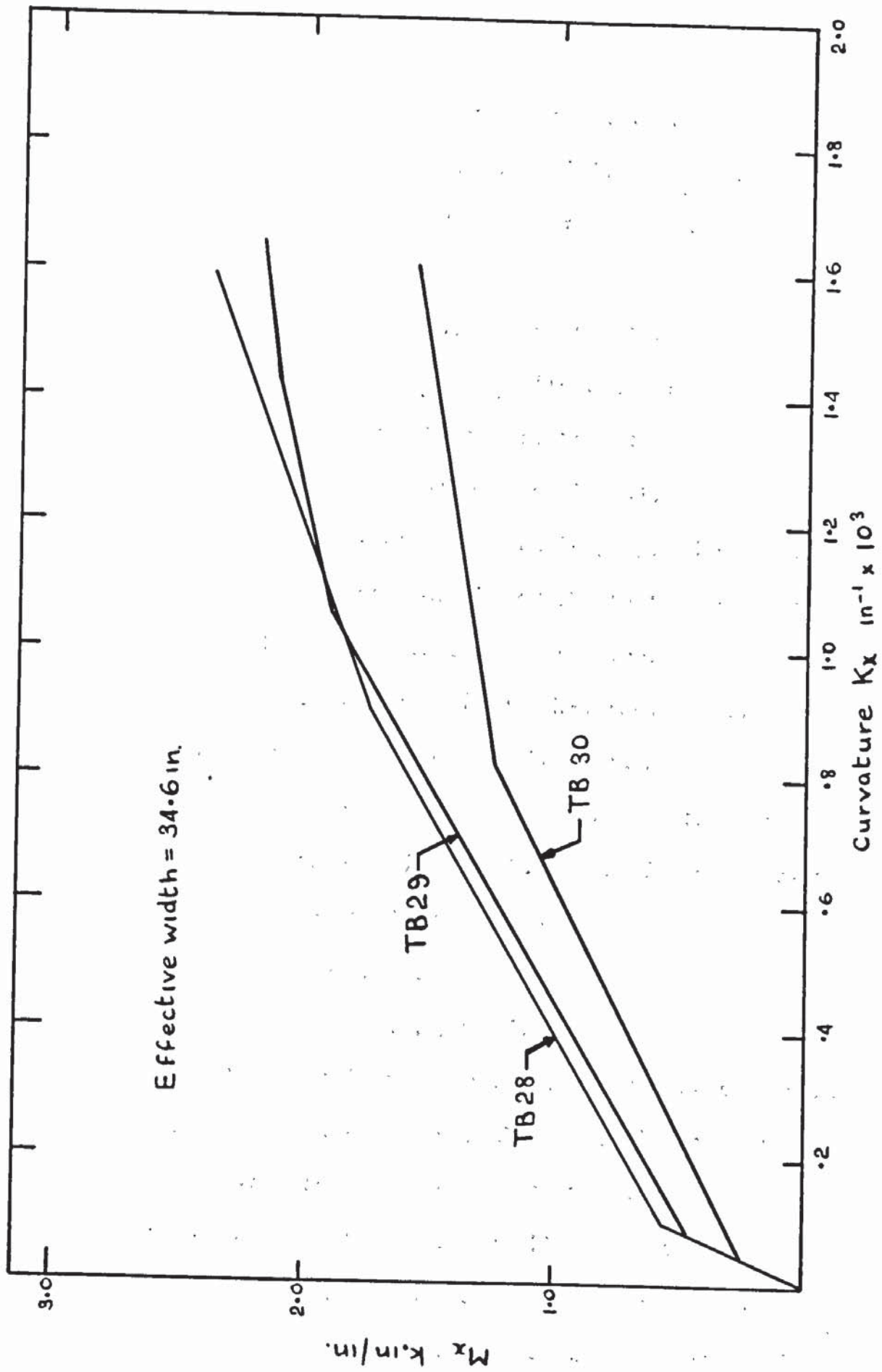


FIG 7.4 MOMENT - CURVATURE, GENERAL MOMENT -  $\beta = 67.5^\circ$ ,  $\mu = 1$

in  $T_a$ , would be due to the effects of the coefficients of mutual influence which for different values of  $\tau_{xy}$  effect  $\epsilon_x$  through the last two terms of equation (7.1), this constant has a value close to zero.

Assuming therefore that the Poisson ratio and coefficient of mutual influence effects are not significant, variations in stiffness will not be influenced by the restraint in the Y-direction. Thus the variations in stiffness after cracking illustrated in figs. 7.1 - 7.4, are due to another effect. It is proposed that this effect is due to the orientation of the cracks to the X-direction and the orientation of the mesh to the X-direction. Thus with reference to fig. 7.5 the stiffness in the X-direction will be a function of the angle between the crack direction and the main bar direction defined by  $\alpha = \psi - \beta$  and the orientation of the bar direction to the X-direction defined by  $\beta$ . Thus for given slab thickness and concrete and steel properties

$$S_x = f(\beta, \alpha) \quad (7.4)$$

$$\text{and } \alpha = g(\beta, \theta) \quad (7.5)$$

where  $S_x$  is the stiffness in the X-direction and  $\theta$  is the angle between the X-direction and the principal moment direction at cracking. In the plank tests the stiffness was a function of  $\beta$  only as the angle  $\psi$  was equal to zero in all calls of  $\mu = 1$ .

It was therefore necessary to examine the variation of  $\alpha$  with  $\beta$  and  $\theta$  as described in equation (7.5). The values of  $\psi$

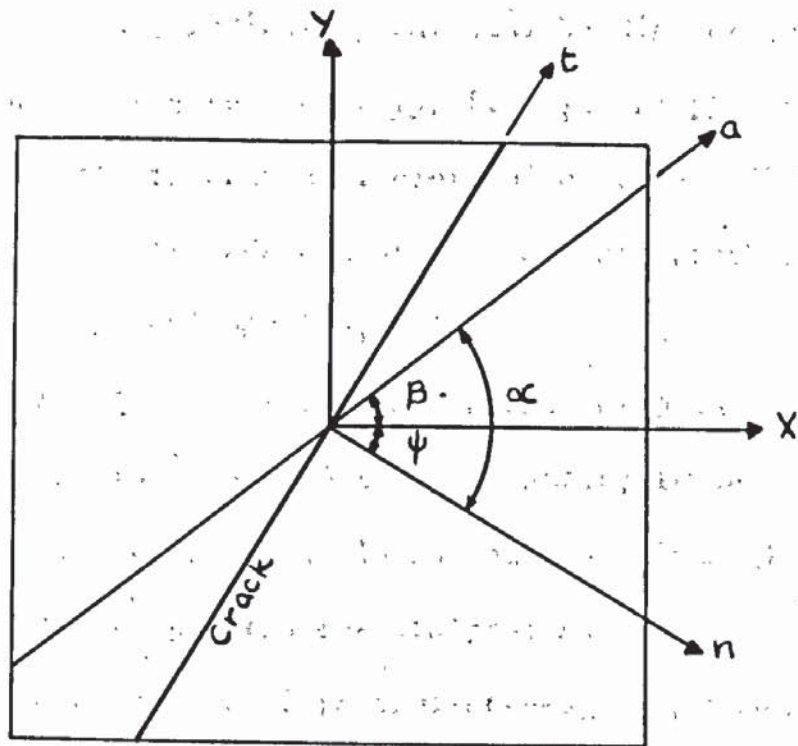


FIG 7.5 DEFINITION OF  $\alpha$

have been recorded in chapter 5, and are presented in tabular form in Table 7.1, as the average measured crack angle at failure and figure 7.6 shows the way in which  $\alpha$  varies with  $\beta$  for constant values of  $T_a$ , which was a measure of  $\theta$ . The dashed lines represent the extreme values of  $T_a$ , indicating uniaxial bending or pure torsion at  $T_a=0$  and  $T_a = \infty$  respectively, if  $\psi$  is independent of  $\beta$ . It can be seen that the experimental plots also run at  $45^\circ$  to the axes indicating that  $\psi$  was independent of  $\beta$  or that crack orientation was independent of mesh orientation.

The implications of this independence of  $\psi$  on  $\beta$  are important. Although in chapter 3 it was tentatively suggested that the criterion for cracking would be one of maximum strain in the concrete it appears from the results presented here that it is in fact closer to a criterion of maximum stress. Remembering that the stress-strain characteristics of a reinforced concrete slab vary with the mesh orientation it would be expected that the crack orientation would have been a function of the mesh orientation had a criterion of maximum strain been obeyed. However as this has been shown to be untrue it must be concluded that the criterion is one of maximum stress.

It must be pointed out that the point representing TB6 in fig. 7.6 appears to be too low. In fact, although the value of average crack orientation to the Y-direction,  $\psi$ , was measured as  $12.33^\circ$  the angle that the crushing line made with the Y-direction

TB	$\theta^{\circ}$	$\psi^{\circ}$ measure crack angle	$\mu$ actual	ma k.m/in	Ta.in
1	0	7.0	.99	3.41	3
2	30	5.8	.99	3.42	3
3	45	4.6	1.00	3.48	3
28	67.5	4.6	.97	3.18	3
4	0	20.3	1.00	3.51	11.25
5	30	19.5	.98	3.30	11.25
6	45	27.3	.99	3.41	11.25
29	67.5	27.1	.96	3.13	11.25
7	0	24.2	1.00	3.49	17.5
31	0	23.8	.99	3.40	17.5
8	30	27.5	.98	3.33	17.5
9	45	20.8	.99	3.40	17.5
30	67.5	22.3	.92	2.88	17.5
10	0	12.1	.55	3.42	3
11	30	18.6	.55	3.47	3
12	45	19.0	.55	3.42	3
13	60	11.7	.54	3.18	3
14	90	3.6	.54	3.29	3
25	135	-1.9	.54	3.17	3
15	0	26.8	.55	3.53	11.25
16	30	25.7	.55	3.33	11.25
17	45	25.1	.54	3.23	11.25
18	60	20.0	.55	3.41	11.25
19	90	16.8	.55	3.38	11.25
26	135	5.1	.54	3.15	11.25
20	0	32.2	.54	3.20	17.5
21	30	33.5	.55	3.42	17.5
22	45	30.5	.54	3.34	17.5
23	60	20.8	.54	3.22	17.5
24	90	22.4	.55	3.36	17.5
27	135	14.9	.54	3.24	17.5

TABLE 7 . 1

Ma values and  $\psi$  values - General moment series

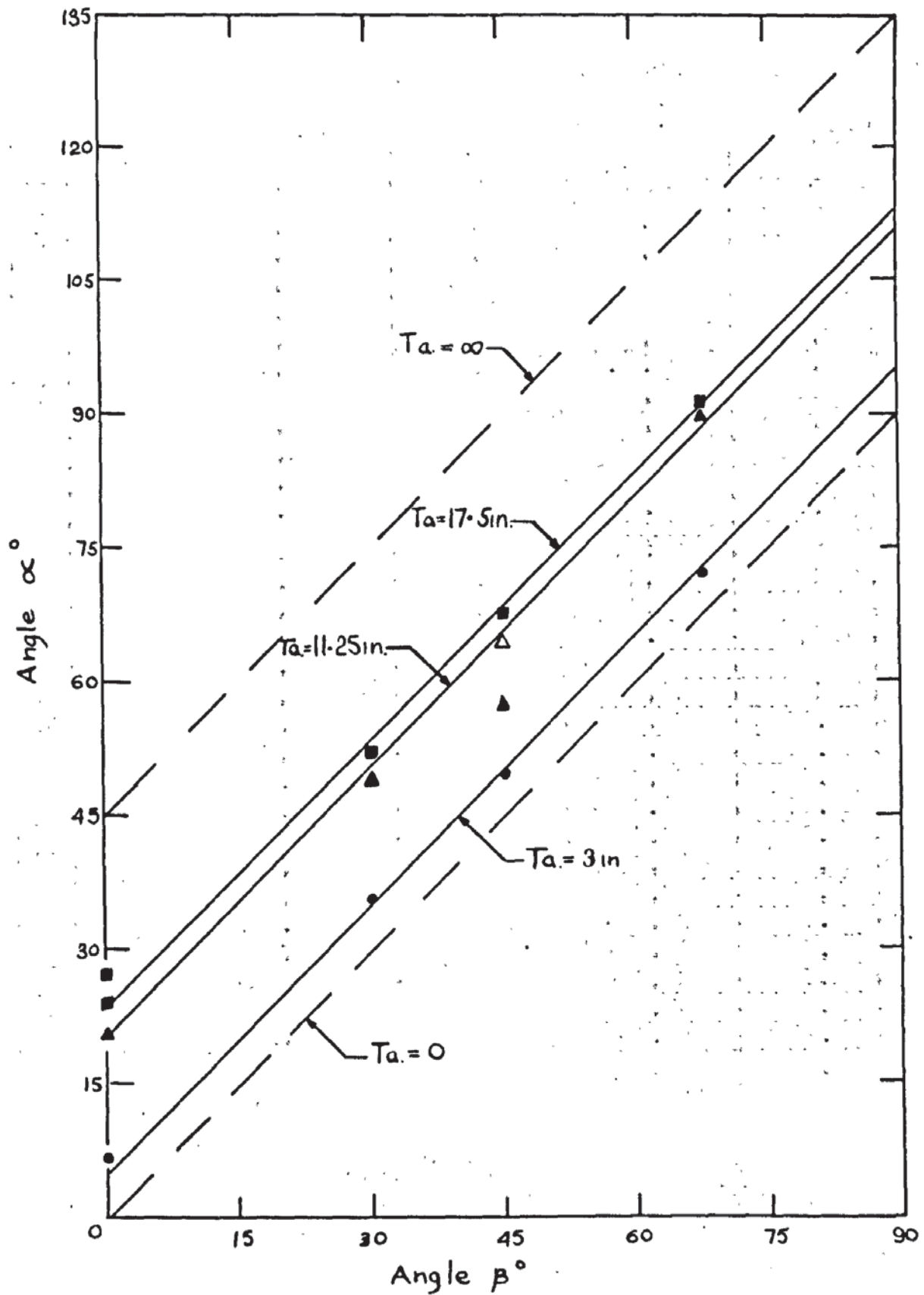


FIG 7.6 VARIATION OF  $\alpha$  WITH  $\beta$ ,  $\mu=1$ .

was  $19.5^\circ$ , a value which, if plotted in fig. 7.6, brings the value of  $\alpha$  for  $\beta = 45^\circ$ ,  $Ta = 11.25$  in, in accordance with the other points on the line. It can also be added that in the other slabs in which  $\mu = 1$  the difference in measured angle between the cracks and the crushing line was never more than  $2^\circ$ .

Fig. 7.7 shews the way in which the angle  $\alpha$  varies with  $Ta$  for given values of  $\beta$ . By extrapolation to  $Ta = 0$  it can be seen that the cracks would run in the Y-direction as expected. Other authors [29] have stated that cracks ran orthogonally to the maximum principal moment direction in all cases in which  $\mu = 1$ . As described in chapters 3 & 5 the moment field due to the self weight of the slab was superimposed automatically onto the moment field due to the applied moments. Thus instead of the principal moment direction being constant at all stages of testing it varied with applied load. However the curves drawn in broken lines in fig. 7.7 represent the directions of cracks relative to the a-direction if the self-weight moment effect is ignored and the crack direction is assumed to be normal to the principal moment direction. As  $Ta$  approaches infinity a state of pure torsion is simultaneously approached and the dashed curves in fig. 7.7 become asymptotic to  $\alpha = 45^\circ$ ,  $75^\circ$ ,  $90^\circ$  and  $112.5^\circ$  for  $\beta = 0^\circ$ ,  $30^\circ$ ,  $45^\circ$  and  $67.5^\circ$  respectively. The differences between the curves representing no self-weight moment field and the experimental results reflect the presence of a self-weight moment in the

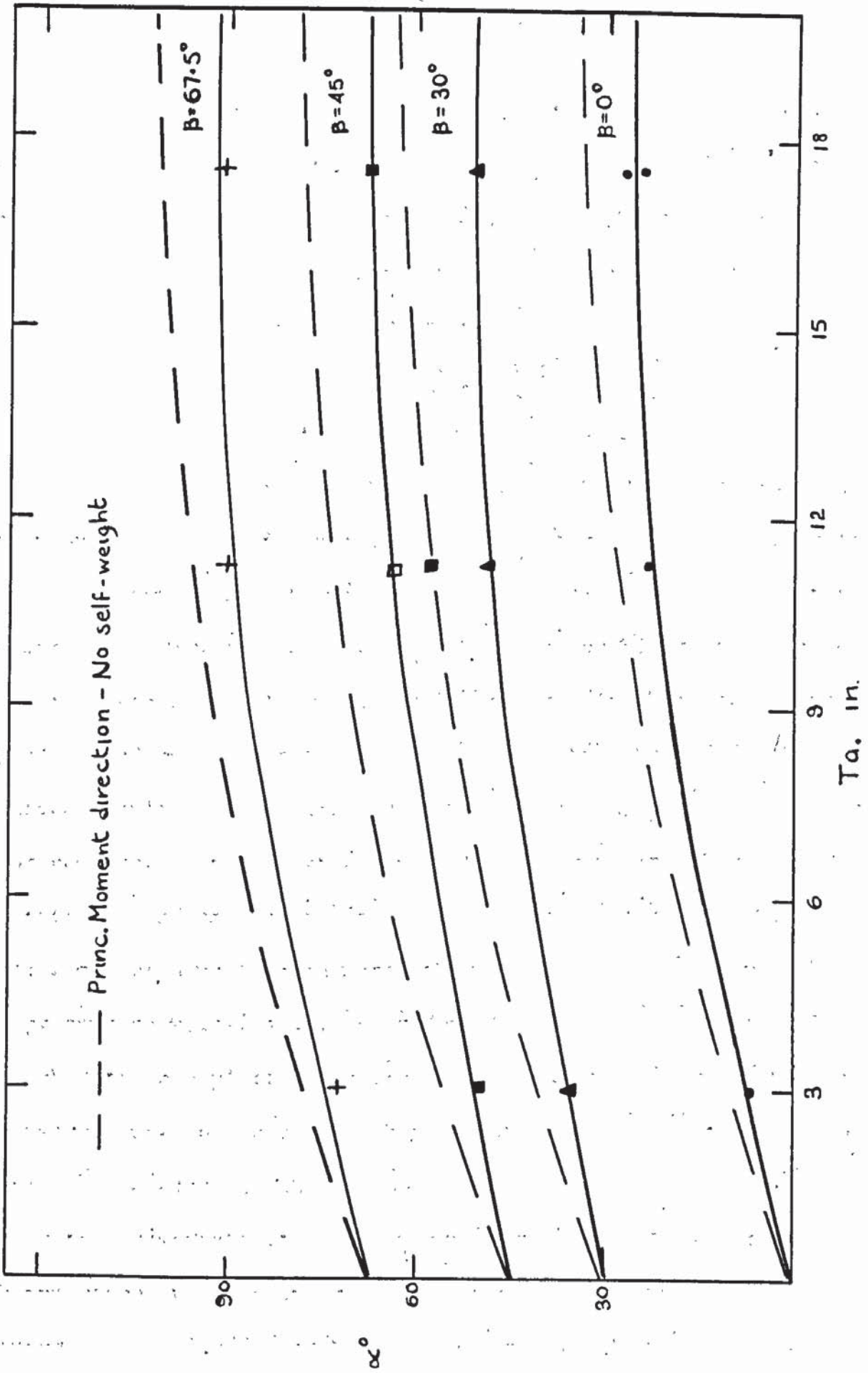


FIG 7.7 VARIATION OF  $\alpha$  WITH  $Ta.$ ,  $\beta$  CONSTANT -  $\mu=1$

X-direction. This difference in angle increases with the value of  $T_a$ , being zero at  $T_a = 0$  and reaching a value governed by the self weight moment field at  $T_a = \infty$  when both curves become asymptotic to a set angle  $\alpha$ . Both curves are functions of tangent curves, the dashed lines have the equation

$$\alpha = \tan^{-1} \frac{2 M_{xy}}{M_x} + \beta \quad (7.6)$$

It has been shown that the crack direction is independent of mesh orientation for  $\mu = 1$  and varies with the moment field as a tangent curve. The stiffness in any direction will as previously described vary with  $\alpha$  and  $\beta$ . Thus stiffness values after cracking obtained from figs. 7.1 -7.4 end relevant to the X-direction are plotted against  $\alpha$  in fig. 7.8. It can be seen that four overlapping curves result and by extrapolation the left hand end of each curve for constant  $\beta$  represents the stiffness in uniaxial bending and the right hand end the theoretical stiffness in pure torsion not allowing for a self weight moment field. The three points representing uniaxial stiffness for  $\beta = 0^\circ$ ,  $30^\circ$  and  $45^\circ$  from the plank tests are plotted and it can be seen that although there is a discrepancy in the case at  $\beta = 0^\circ$  the stiffness values for  $\beta = 30^\circ$  and  $45^\circ$  are close to the extrapolated values. As the curves overlap a given stiffness can be obtained by different mesh orientations under varying moment fields. The most noticeable trend in fig. 7.8 is the way in which the stiffness values for

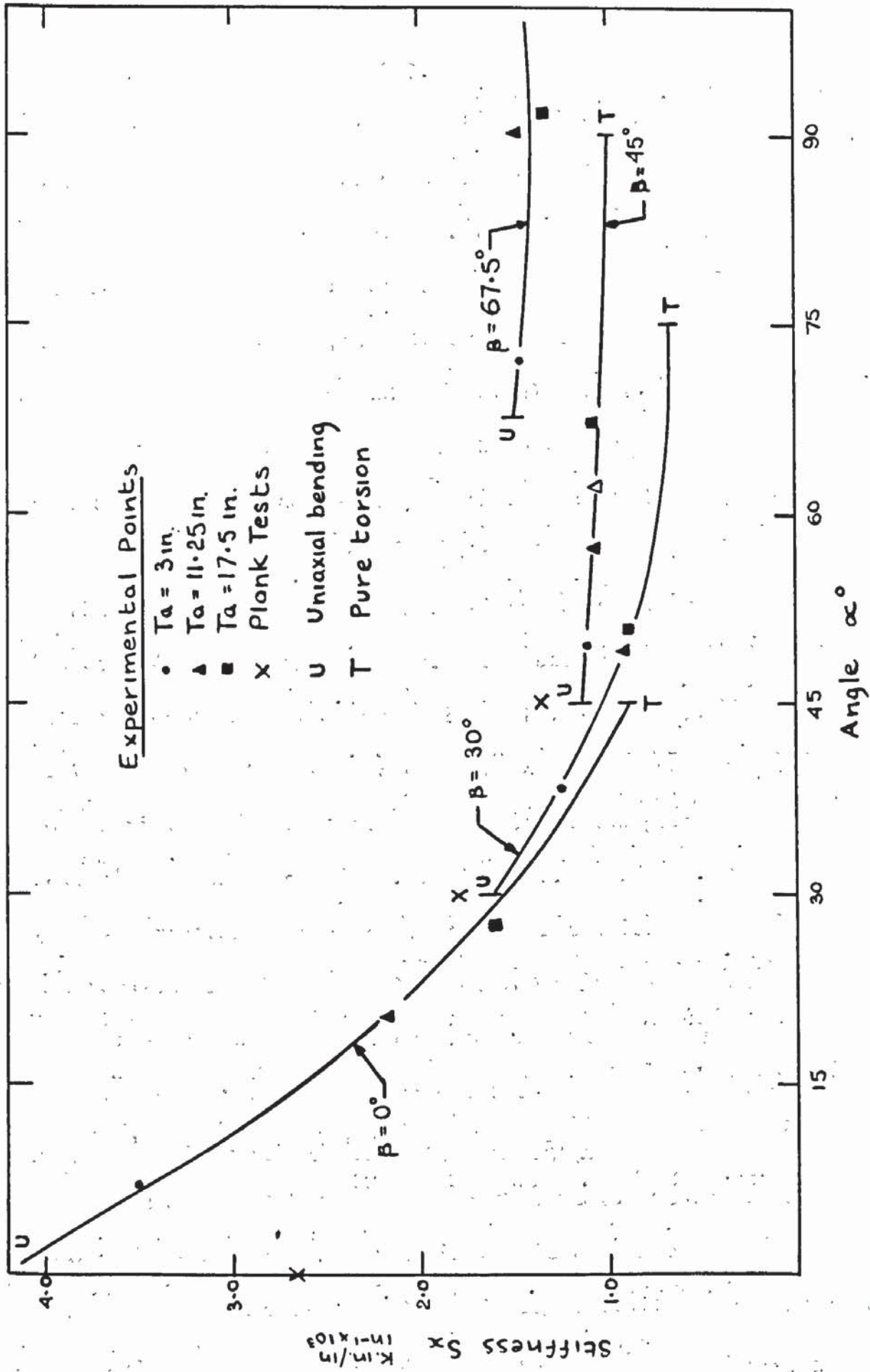


FIG 7.8 VARIATION OF  $S_x$  WITH  $\alpha$  -  $\mu = 1$

varying moment states vary differently for given values of  $\beta$ . For  $\beta = 0$  for example the stiffness was considerably less in torsion than it was in uniaxial bending whereas for  $\beta = 45^\circ$  the values of stiffness for all moment combinations were almost the same. It would be possible for practical purposes to draw an average line encompassing all angles of  $\beta$  between  $30^\circ$  and  $60^\circ$  for all moment combinations.

In conclusion it has been shown that the stiffness in any direction depends on the angle between the crack direction and bar direction and the angle of the bar direction relative to it. It was shown that  $\kappa$  was directly proportional to the mesh orientation and varied with  $Ta$  as a tangent curve. The stiffness in a given direction varied less with increasing  $\psi$  for a mesh orientation of  $45^\circ$  relative to that direction than for a mesh orientation of  $\beta = 0^\circ$  as fig. 7.8 indicates. The locis of the points representing uniaxial bending for all  $\beta$  values represents the stiffness variation in the X-direction for a uniaxial moment in that direction, similarly the loci of the points representing pure torsion and intermediate combined moment values represent the stiffness in the X-direction under those given moment fields.

### 7.2.2     'Non-isotropically' reinforced slab

Although it has been shown that it is incorrect to describe slabs in which  $\mu = 1$  as isotropic this section deals with the slabs tested in which  $\mu = 0.5$  and can generally be referred to as non-isotropic. The same general procedure has been used to

describe the elastic behaviour of these slab elements under varying conditions of applied moment and mech orientation. Figs 7.9 - 7.14 show the moment-curvature relationships in the X-direction for all slabs reinforced with  $\mu = 0.5$  under the three combined moment conditions for  $\beta = 0^\circ, 30^\circ, 45^\circ, 60^\circ, 90^\circ$  and  $135^\circ$  respectively. There appears to be more evidence of variations in stiffness before cracking than was noted in the case of slabs in which  $\mu = 1$  and considerable differences can be noted in relative stiffnesses when compared with the 'isotropically' reinforced slabs. It was shown in 7.2.1 that the stiffness was a function of  $\beta$  and  $\alpha$  and  $\alpha$  was a function of the moment field only. Thus for slabs in which  $\mu = 1$  cracking occurred in the direction of the principal moment at that time and was independent of  $\beta$  as others have postulated. The major difference between the conclusions made here and those made by other authors <sup>(29)</sup> has been the importance of the self weight moment field in the formation of cracks. In fact as the graphs in chapter 5 showing principal direction variations indicate there must have been twisting moments in the crack directions at failure. These questions will be discussed in section 7.3 which deals with ultimate moment behaviour.

In the case of slabs in which  $\mu \neq 0$  previous work [17, 29, 37] has shown that because the ultimate moment in any direction is now no longer constant, failure will take place in a direction other than the principal moment direction. Kemp [17] for example has

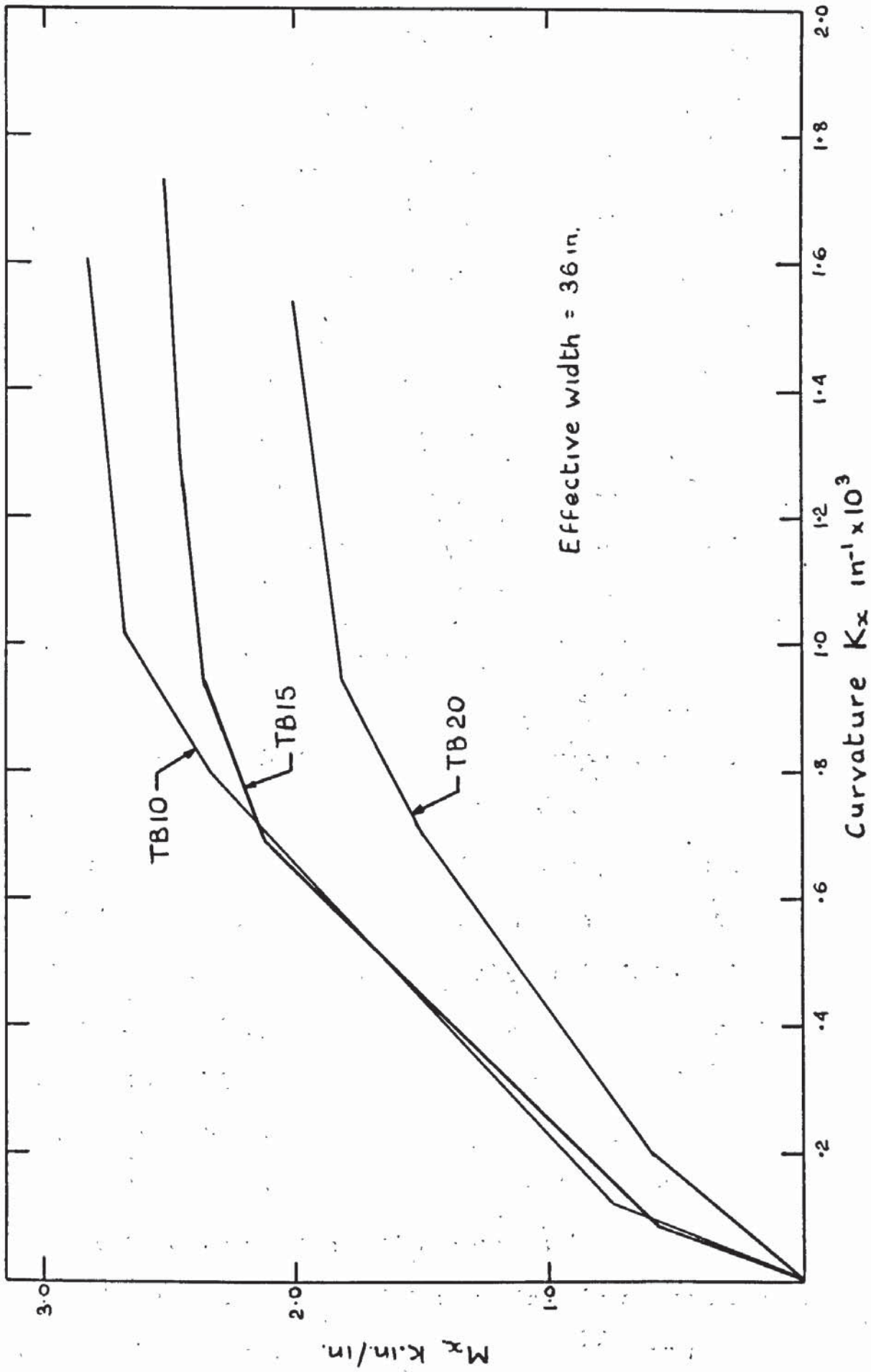


**FIG 7.9** MOMENT - CURVATURE PLOT -  $\beta = 0^\circ, \mu = 0.5$

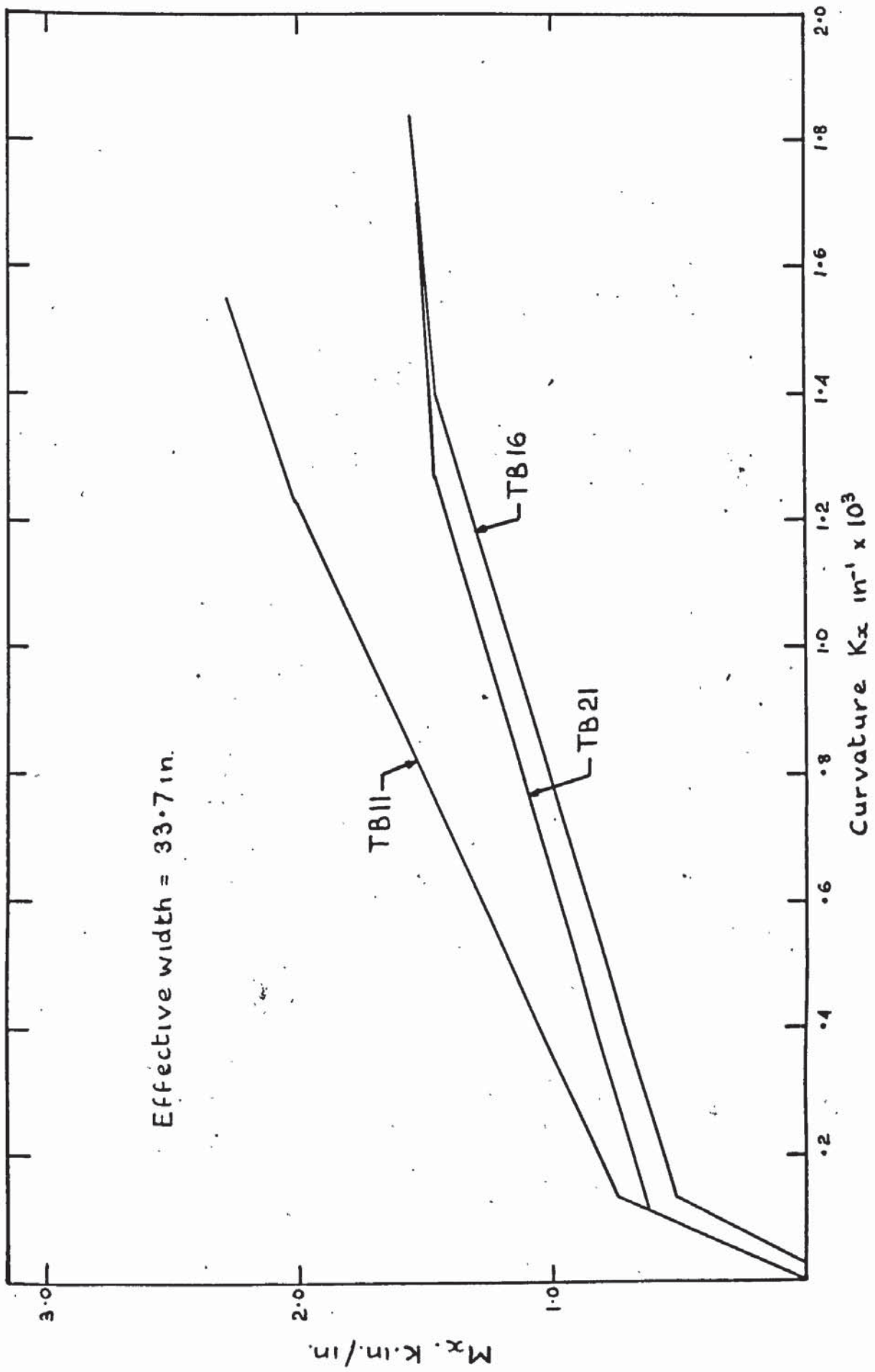


**FIG 7.10 MOMENT-CURVATURE PLOT -  $\beta = 30^\circ$ ,  $\mu = 0.5$**

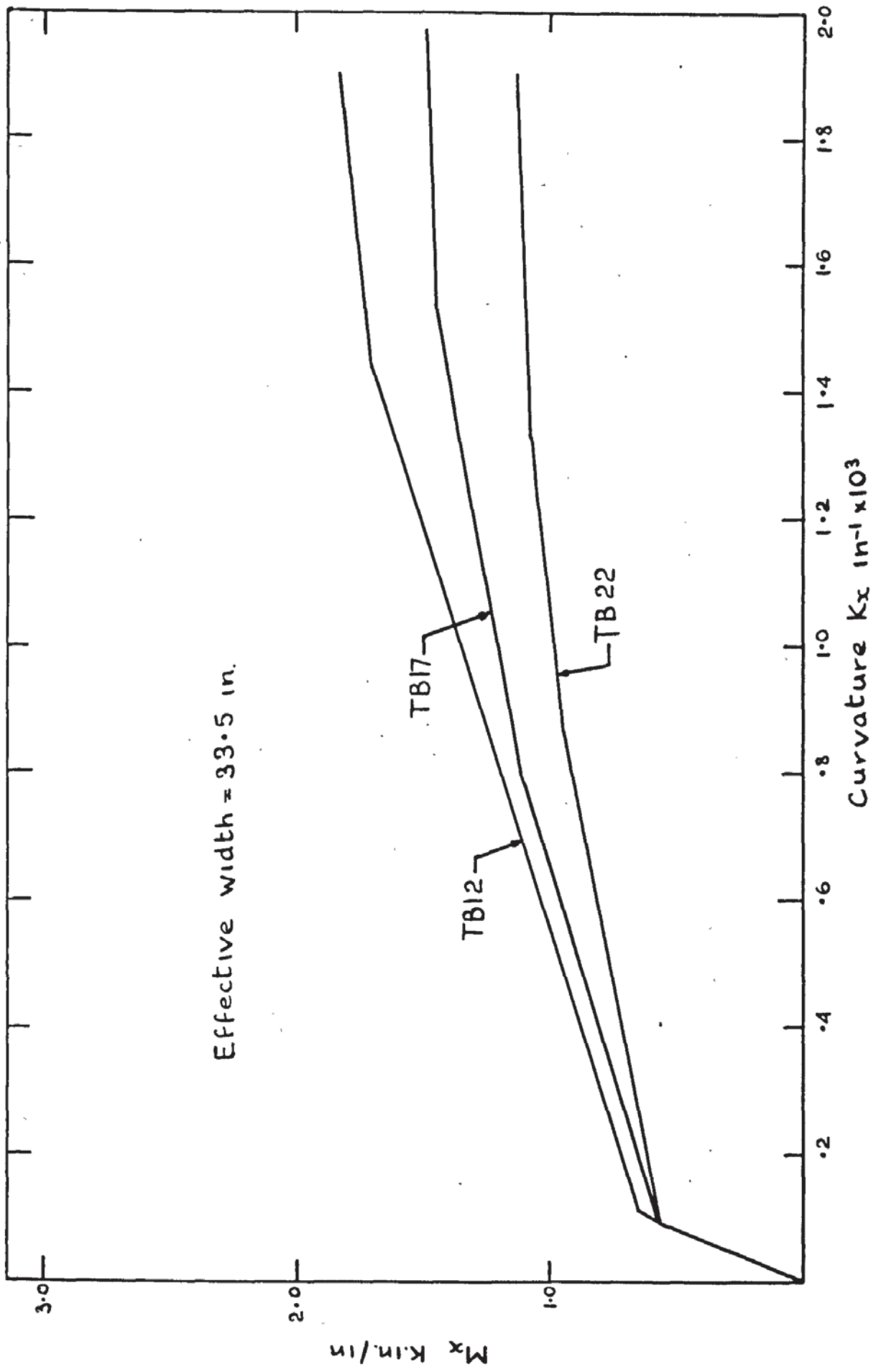


FIG. 7.11 MOMENT - CURVATURE PLOT -  $\beta = 45^\circ$ ,  $\mu = 0.5$

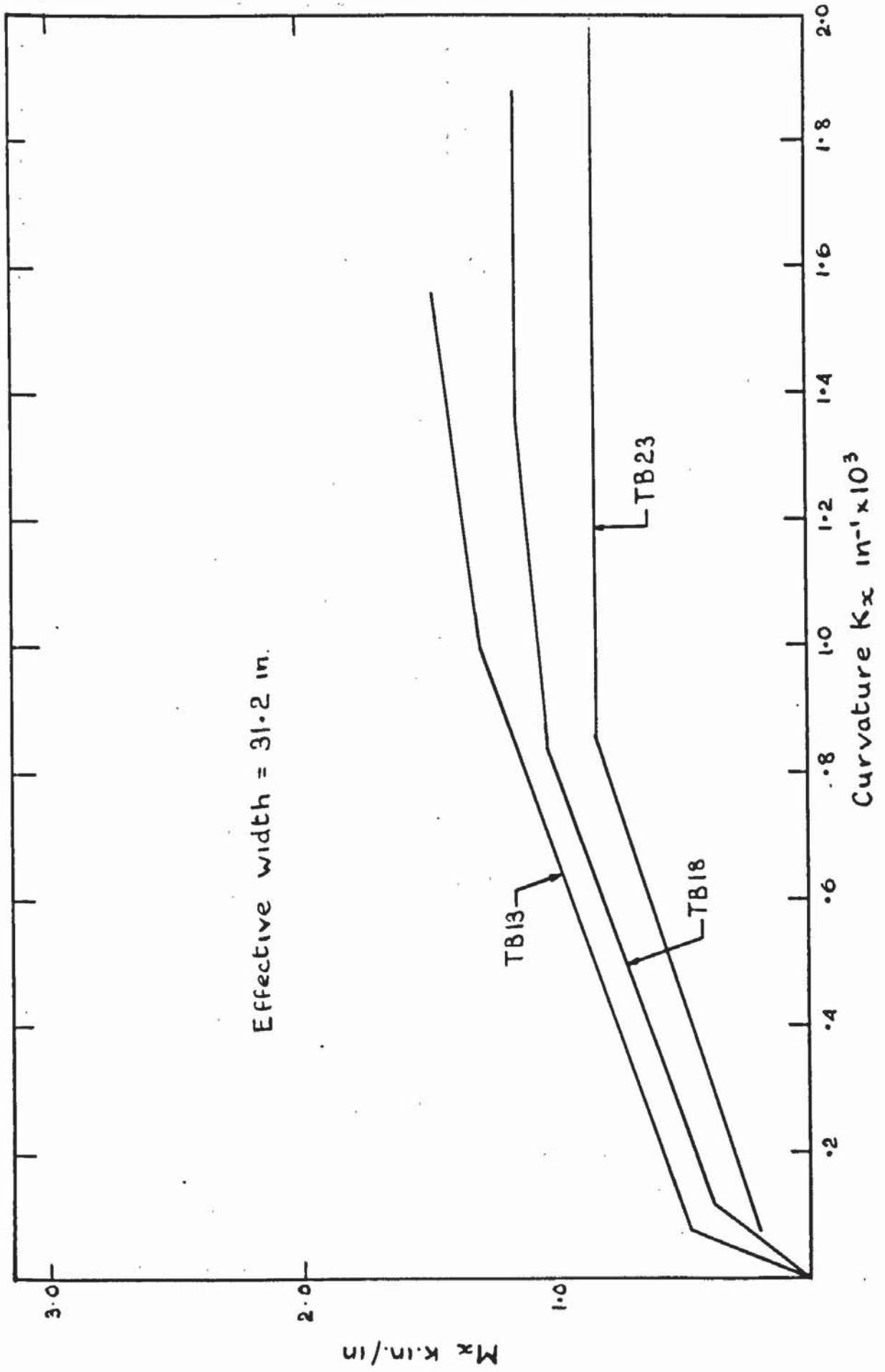


FIG.7.12 MOMENT-CURVATURE PLOT -  $\beta = 60^\circ$ ,  $\mu = 0.5$

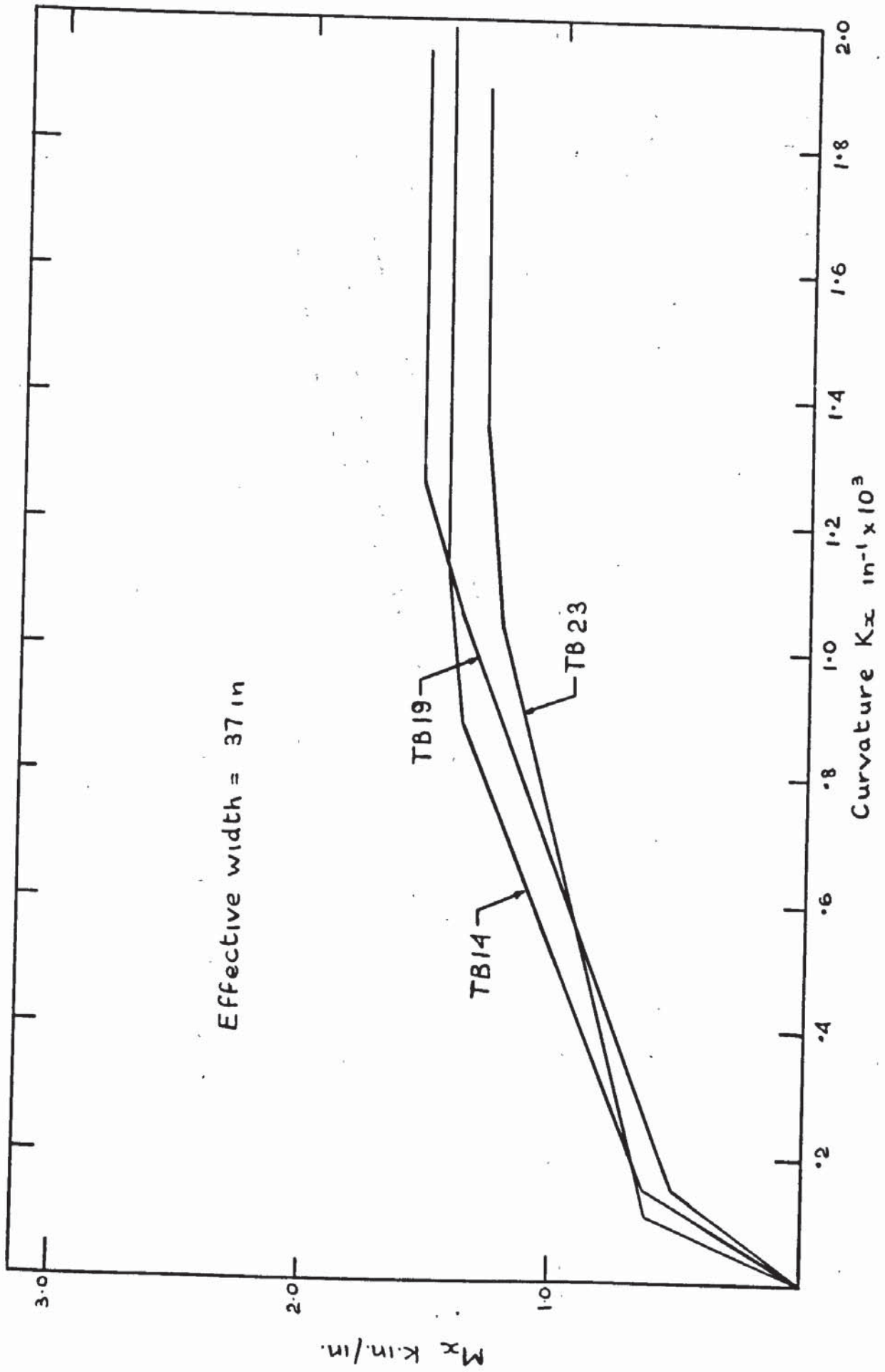


FIG 7.13 MOMENT-CURVATURE PLOT -  $\beta = 90^\circ$ ,  $\mu = 0.5$

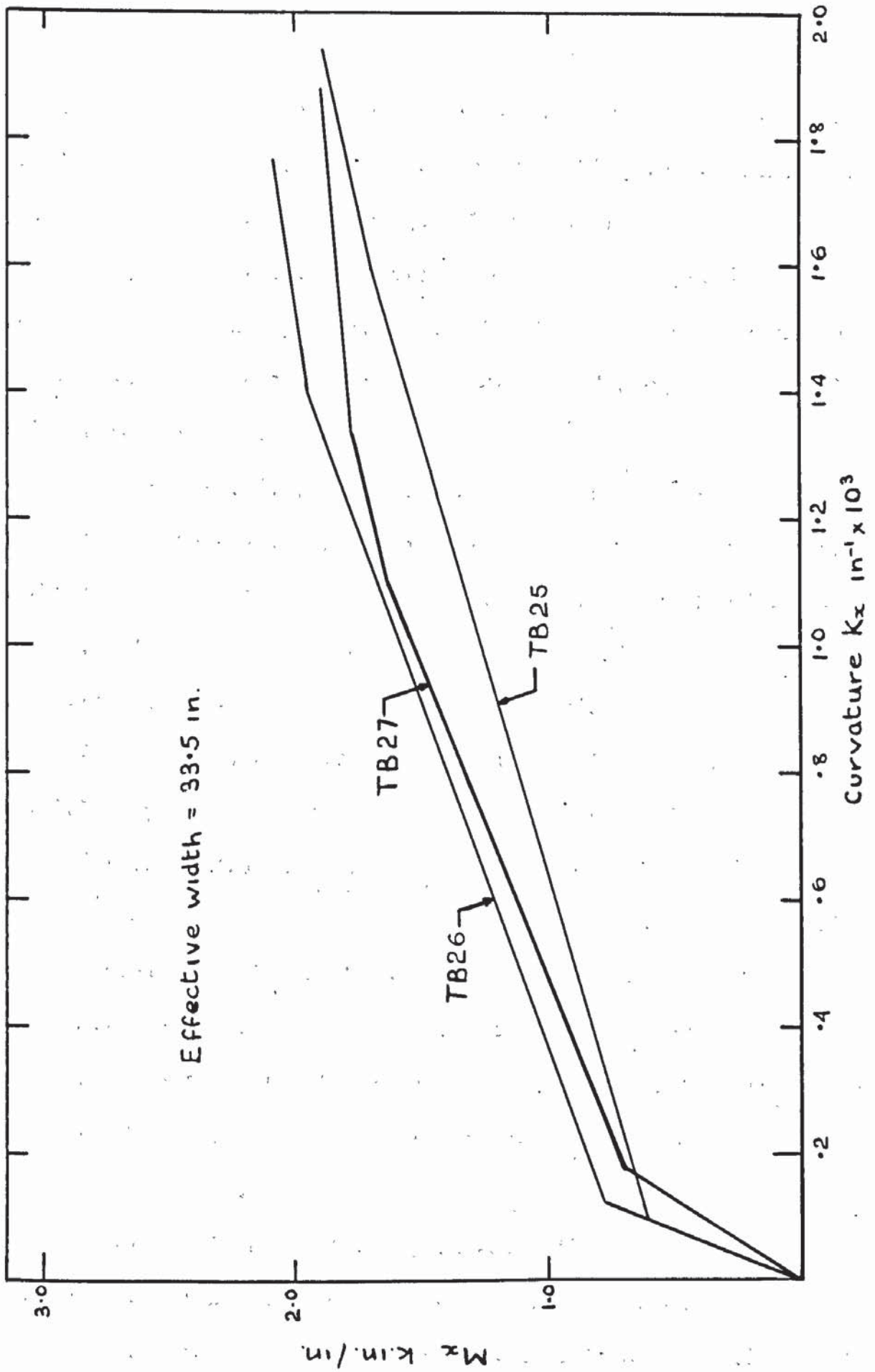


FIG. 7.14 MOMENT - CURVATURE PLOT -  $\beta = 135^\circ$ ,  $\mu = 0.5$

illustrated this concept, as shown in fig. 2.10, using Johansens normal moment criterion and the curve describing the variation in applied moment between  $M_1$  and  $M_2$ . Thus failure occurs in the direction in which the curves first touch as the applied moment field is proportionally increased. Lenshaw and Sozen [29] using the same basic concept have referred to this direction as the 'line of least resistance'.

Thus fig. 7.15 shows the way in which the crack orientation  $\psi$  to the Y-direction varies with mesh orientation  $\beta$ . In the case of TB 21 and TB 22, particularly, two points have been plotted. It can be seen in plate 5.50 and 5.52 that the main yield line crosses the original crack direction. The average value of slope at the yield lines causing failure represented in Fig. 7.15 appear to coincide closely to the trend of the other result for  $Ta = 17.5$  in. The dashed lines are those obtained from Lenschow and Sozens [29] equations (2.25) defining the yield line orientation. It can be seen that they exceed the values of  $\psi$  generally in all cases although the form of the curves are similar. The theoretical curves have been plotted neglecting the self weight moment and would therefore be expected to exceed the experimental values.

Fig. 7.16 shows the way in which the crack angle relative to the Y-direction varies with values of  $Ta$ . The dashed line in this case being the principal moment direction neglecting dead

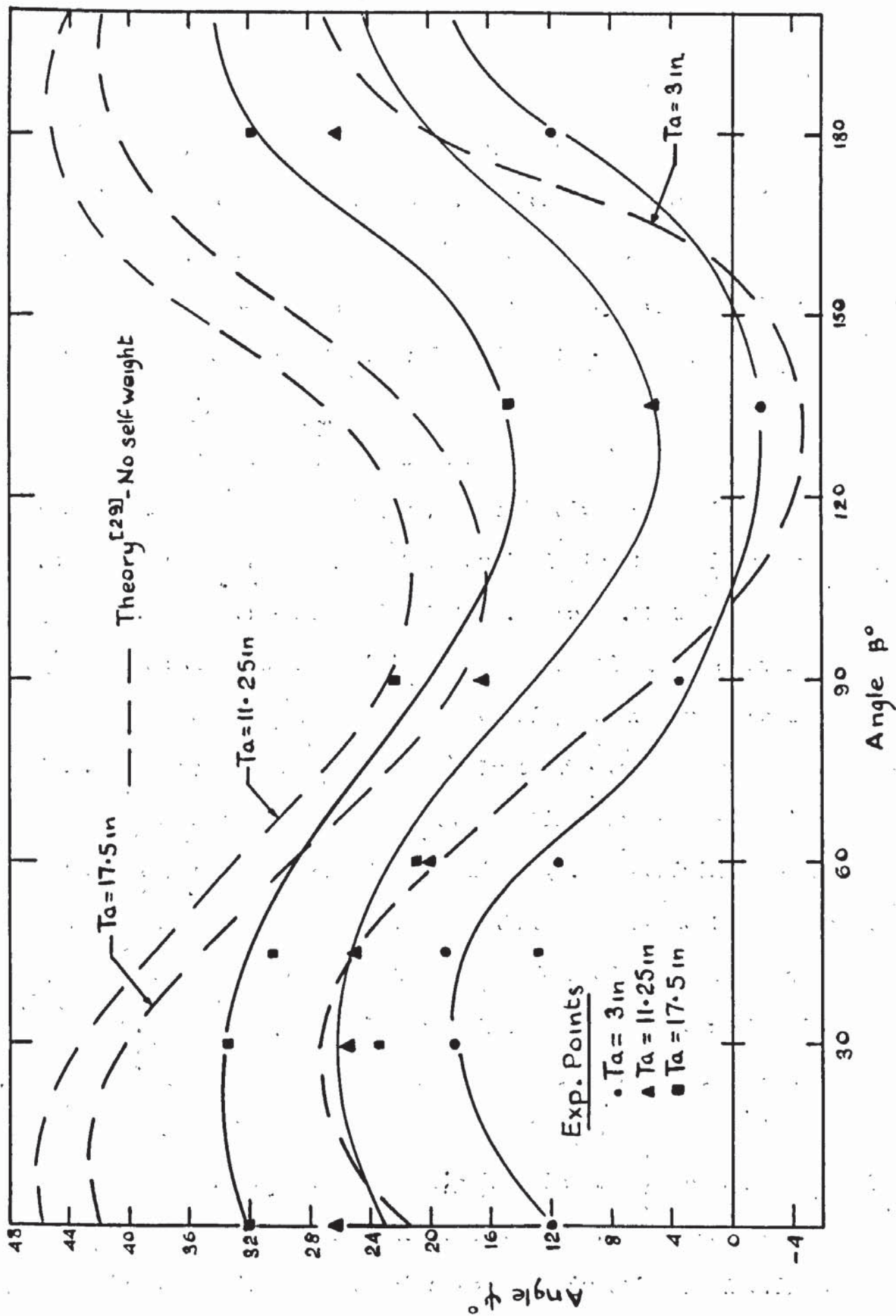


FIG. 7.15 VARIATION OF  $\psi$  WITH  $\beta$  —  $\mu = 0.5$

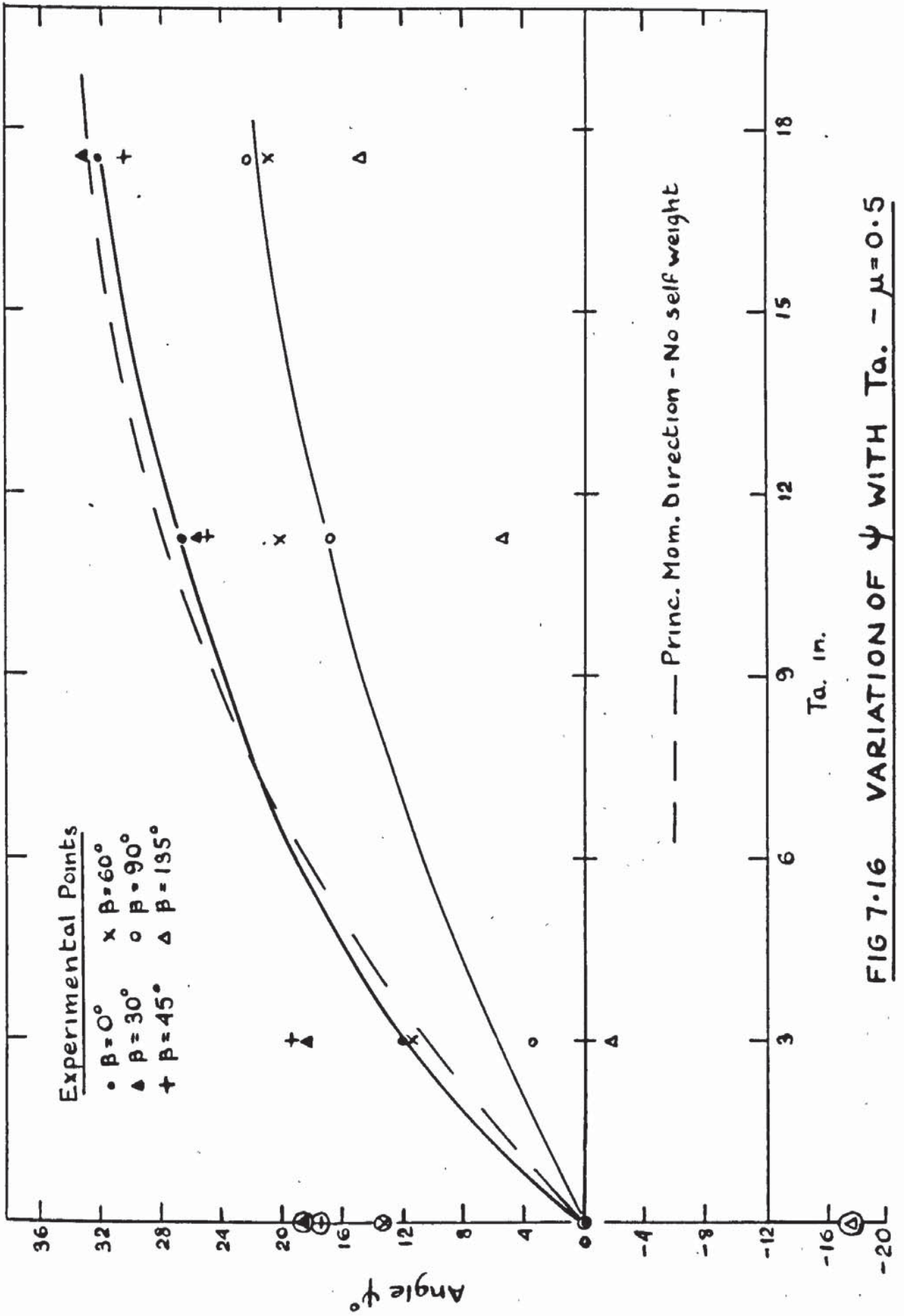


FIG 7-16 VARIATION OF  $\psi$  WITH  $Ta.$  -  $\mu=0.5$

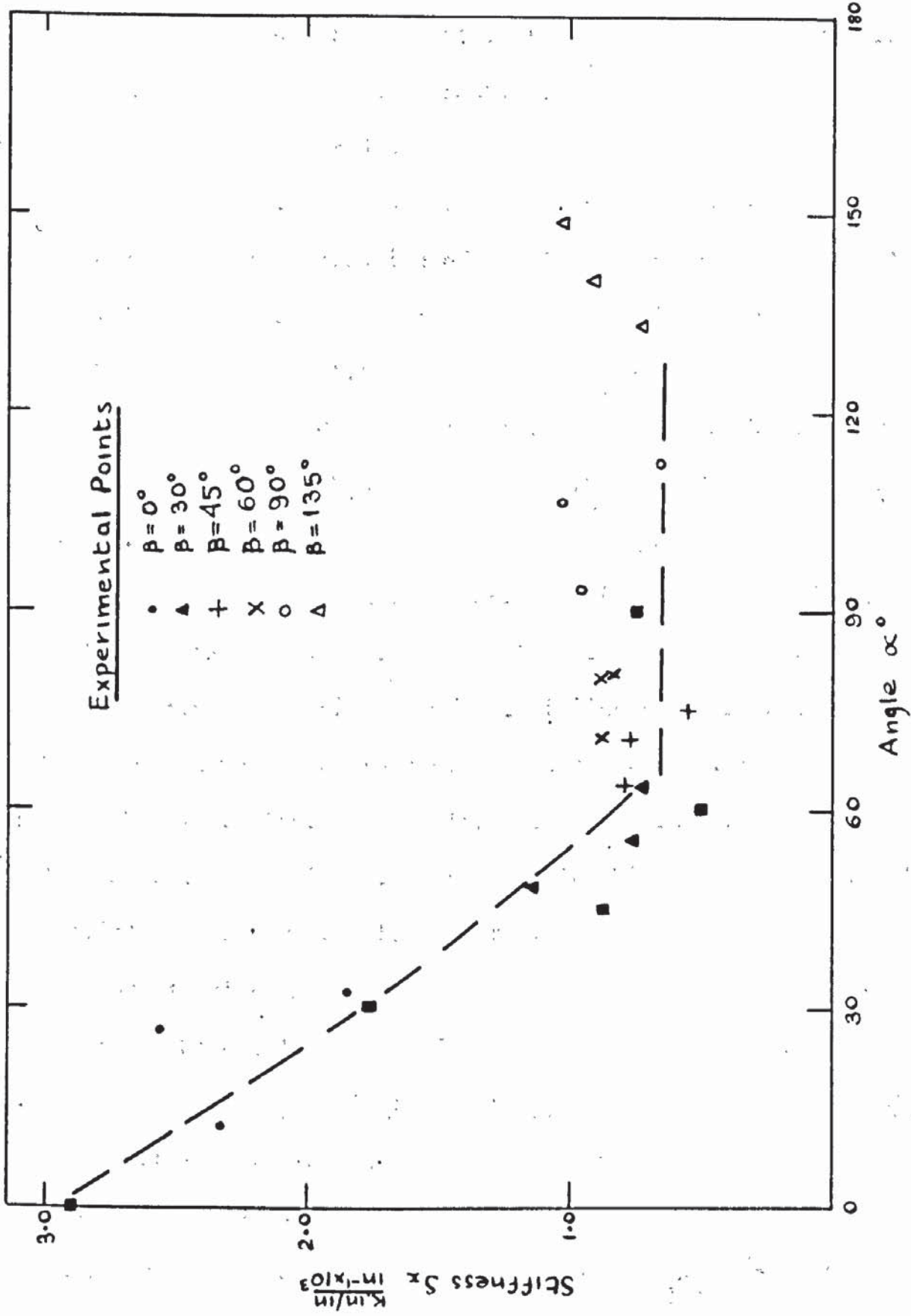


FIG 7.17 VARIATION OF  $S_x$  WITH  $\alpha$  -  $\mu = 0.5$

weight. It can be seen that the trends for  $\beta = 0^\circ$  and  $\beta = 90^\circ$  extrapolate to a value of  $\psi = 0$  at  $T_a = 0$  as would be expected for uniaxial moment in either bar direction. Lenschow and Sozens predicted values for  $T_a = 0$  are marked on this figure for the relevant values of  $\beta$ . Because of the fact that  $\psi$  is no longer independent of  $\beta$ , the variation of stiffness with  $\alpha$  is necessarily more complex than that of  $\mu = 1$ . However Fig 7.17 shows that again the variation in stiffness in the X-direction was small between  $\alpha = 60^\circ$  and  $\alpha = 130^\circ$  whatever the angle  $\beta$  or the torsional lever arm and the lower bound on these stiffness values is drawn in Fig. 7.17.

It has been shown for non-isotropic slabs, therefore, that although the crack angle was no longer independent of the mesh orientation the variation was of similar form to that predicted by Lenschow and Sozen but in general had a lower value of  $\psi$  for a given mesh orientation. The stiffness varied in a similar way to that described in fig. 7.8 for slabs in which  $\mu = 1$ . Although the variation was more complex due to the non-independence of  $\psi$  on  $\beta$ , a practical simplification could be made so that stiffness values could be easily predicted.

### 7.3 The yield behaviour of reinforced concrete slab elements

It is with the problem of yield and ultimate behaviour of reinforced concrete slabs that most of the past work reviewed in chapter 2 has been involved. It is one of the objects of this

work to experimentally verify or falsify the theories that have been put forward concerning the yield criterion of reinforced concrete slabs. As described in chapter 2 the most common theories concerning the yield behaviour have proposed that at yield the criterion at failure is purely one of normal moment on the yield line. Other moments acting on this yield line such as the tangential moment  $m_t$  and the twisting moment  $m_{ht}$  either have no effect on the normal moment strength or are not independent of it. In addition there is an increasing tendency to use the theorems of Limit Analysis described in chapter 2 with the proposed yield criteria. This involves strict conditions being satisfied, for example that yield obeys the plastic potential, the yield criterion is convex and plastic flow occurs in a constant direction after yielding has taken place. These conditions have been described more fully in chapter 2.

It is therefore necessary to check on the validity of the assumption that reinforced concrete slabs under pure bending constitute a material to which the yield criteria proposed and the conditions of Limit Analysis can be applied. The first observation that must be made is the meaning of the term yield line. This is usually described as a definite discontinuity in the concrete matrix normal to which plastic flow occurs. A study of the plots of principal directions presented for each specimen shows that in the majority of cases the direction of principal

curvature did not coincide with the final crack directions at least until failure. The plots show that on the whole the principal curvature direction approached the final crack orientation after yield whereas before yield the direction was nearly constant. In some specimens there was a definite tendency for the principal curvature direction to reduce in the elastic range until yield, whereupon the directions increased up to the final failure direction. Thus immediately it can be said that the condition of Limit Analysis demanding a constant direction of plastic flow after yield, was not obeyed in the tests. In most cases the principal curvature direction, which is a greater measure of plastic flow direction than any crack direction may be, varied between yield and ultimate failure. This fact throws considerable doubt on the assumptions of Prince<sup>[37]</sup> that the crack direction is at right angles to the principal strain direction during yield.

To investigate other aspects of the yield range it is necessary to compare the stress state on the yield line for each specimen. Thus the results presented in chapter 5 concerning the ultimate load were converted into principal moments by using figs. 5.70 and 5.71 and principal moment directions at failure from fig. 5.69. It was then possible to calculate the normal moment, the tangential moment and the

twisting moment in the final crack directions by making use of the effective crack length concept described in chapter 6. Although the final crack orientations have been presented in sections 7.1 and 7.2 it is necessary to investigate the variables likely to affect the yield criterion itself. These are  $m_n$  the normal moment on the yield line or more correctly the final crack direction,  $m_t$ , the tangential moment,  $m_{nt}$ , the twisting moment and  $\alpha$ , the angle between the main bar direction,  $a$ , and the  $n$  direction. In addition to the standardization of results due to effective width variations the values of moment were divided by the values of  $m_a$  presented in Table 7.1. Table 7.2 and 7.3 therefore show the values of moment and angle mentioned above for slabs in which  $\mu = 1$  and  $\mu = 0.5$  respectively. It can be seen from these tables that comparison of the four variables is made difficult by virtue of the fact that no particular variable is constant for varying values of the other three parameters. However to follow the procedure used in chapter 6 values of  $\frac{m_n}{m_t}$  have been plotted against  $\alpha$ . Fig. 7.18 shows the plot of failure moments for slabs in which  $\mu = 1$ . It can be seen that three distinct lines ensue.

The ratio of  $\frac{m_n}{m_t}$  varies but can be said to be equal approximately to -2.5, -4.0 and -40 for  $Ta$  values of 17.5 in,

TB	$M_n/m$	$m_t/m$	$m_{nt}/m$	$\mu$
1	1.07	-.030	-.0755	7.0
2	.95	-.021	-.0705	35.8
3	.985	-.021	-.0945	49.6
4	1.14	-.29	-.179	20.3
5	1.06	-.261	-.180	49.5
6	1.17	-.29	-.21	64.3
7	1.23	-.48	-.26	24.1
8	1.20	-.475	-.21	57.5
9	1.30	-.48	-.386	65.8
28	.96	-.015	-.110	72.1
29	1.1	-.282	-.108	90.2
30	1.15	-.43	-.292	89.7
31	1.22	-.478	-.274	23.7

TABLE 7 . 2

Moment Conditions on yield line at failure,  $\mu = 1$

TB	$\frac{m_n}{m}$	$\frac{m_t}{m}$	$\frac{m_{nt}}{m}$	$\alpha$
10	.945	-.030	+ .058	12.1
11	.800	-.007	+ .244	48.6
12	.660	-.005	+ .217	64.0
13	.626	-.017	+ .042	71.7
14	.554	-.008	- .127	93.5
25	.800	+.012	- .348	133.1
15	1.15	-.308	- .025	26.8
16	.835	-.212	- .038	55.7
17	.710	-.177	- .048	70.1
18	.650	-.148	- .167	80.00
19	.676	-.161	- .294	106.85
26	1.02	-.158	-1.13	140.1
20	1.28	-.52	- .025	32.2
21	.86	-.337	- .061	63.5
22	.76	-.288	- .044	75.5
23	.745	-.247	- .367	80.8
24	.854	-.314	- .415	112.4
27	1.26	-.431	-1.12	149.9

TABLE 7 . 3

Moment conditions on yield line at failure  $\mu = 0.5$

$\tau_a = 17.5$   
 $\tau_w = 11.24$

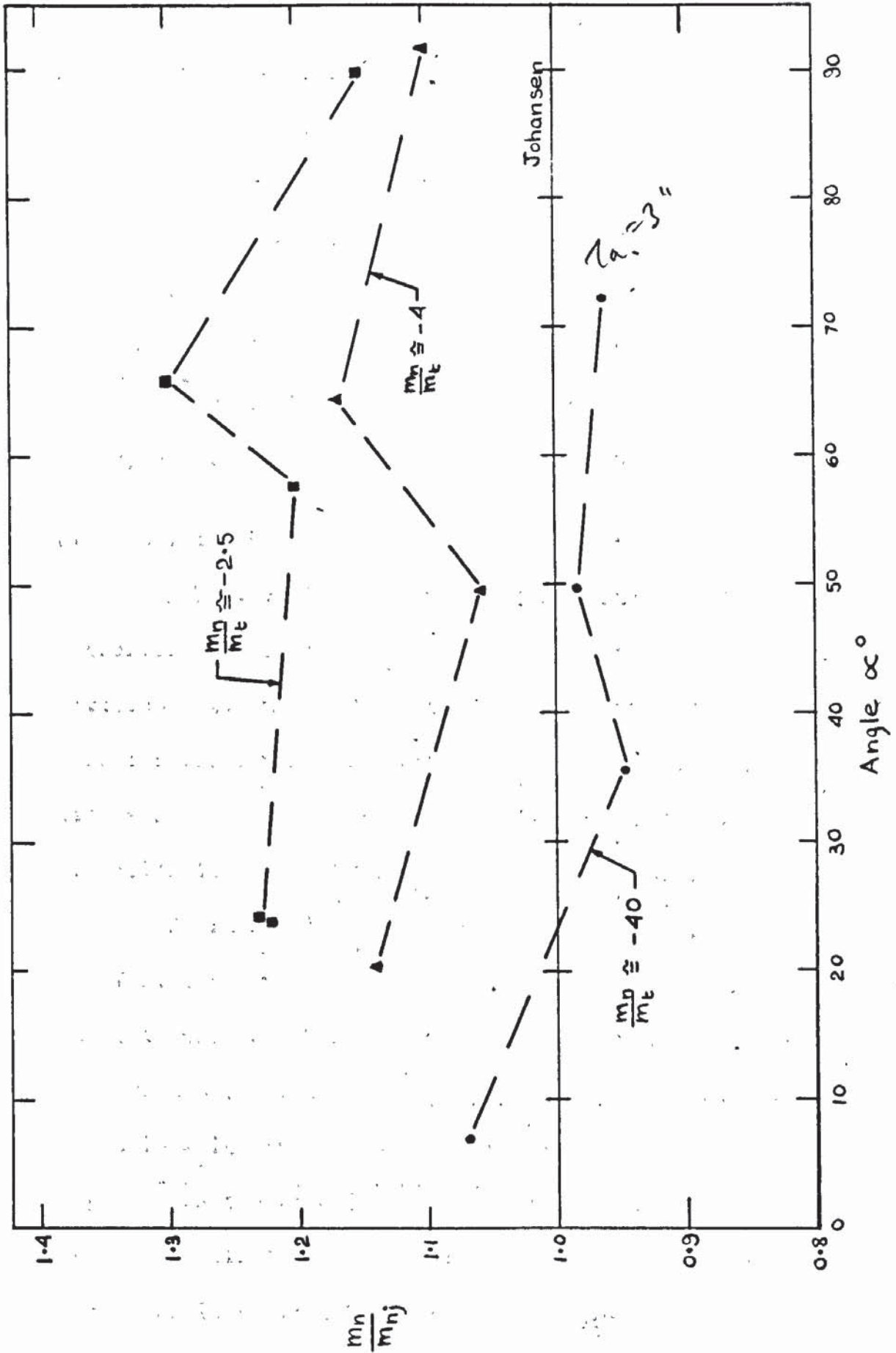


FIG 7.18  $\frac{m_n}{m_{nj}}$  v.  $\alpha$  -  $\mu=1$

11.25 in, and 3 in respectively. These three ratios of moment on the yield line can be seen to correspond to three distinct trend lines in fig. 7.18. Thus moment enhancement is not significantly affected by the value of  $\alpha$  but is very significantly influenced by the values of  $m_n/m_t$ . When  $m_n/m_t = -2.5$  there can be seen to be an increase in moment capacity of about 25%, when  $m_n/m_t = -4.0$  a moment increase of about 10% and when  $m_n/m_t = -40$  there appears to be a drop in moment capacity of a few percent if anything. From table 7.2 it can be seen that values of  $\frac{m_{nt}}{m_a}$  are generally nearly constant for the three ratios of  $m_n/m_t$ .

Fig. 7.19 shows the results of the slabs in which  $\mu = 0.5$  presented in the same way. There is an even more striking division between the three sets of points representing the three moment ratios. Again there appears to be little enhancement with  $\alpha$  but a very significant enhancement with moment ratio, amounting to about 45% in the case of  $T_a = 17.5$  in, 27% for  $T_a = 11.25$  in and 10% for  $T_a = 3$  in. These two figures, 7.18 and 7.19 show that very significant increases in normal moment capacity occurred when the ratio of normal to tangential moment was greatest. This conclusion can of course only be applied to slabs in which the normal and tangential moments were of opposite sign as was the case in these tests. These results agree on the whole with the results of Baus and Talaccia [23] in this range and if their other premises are correct, would lead to the

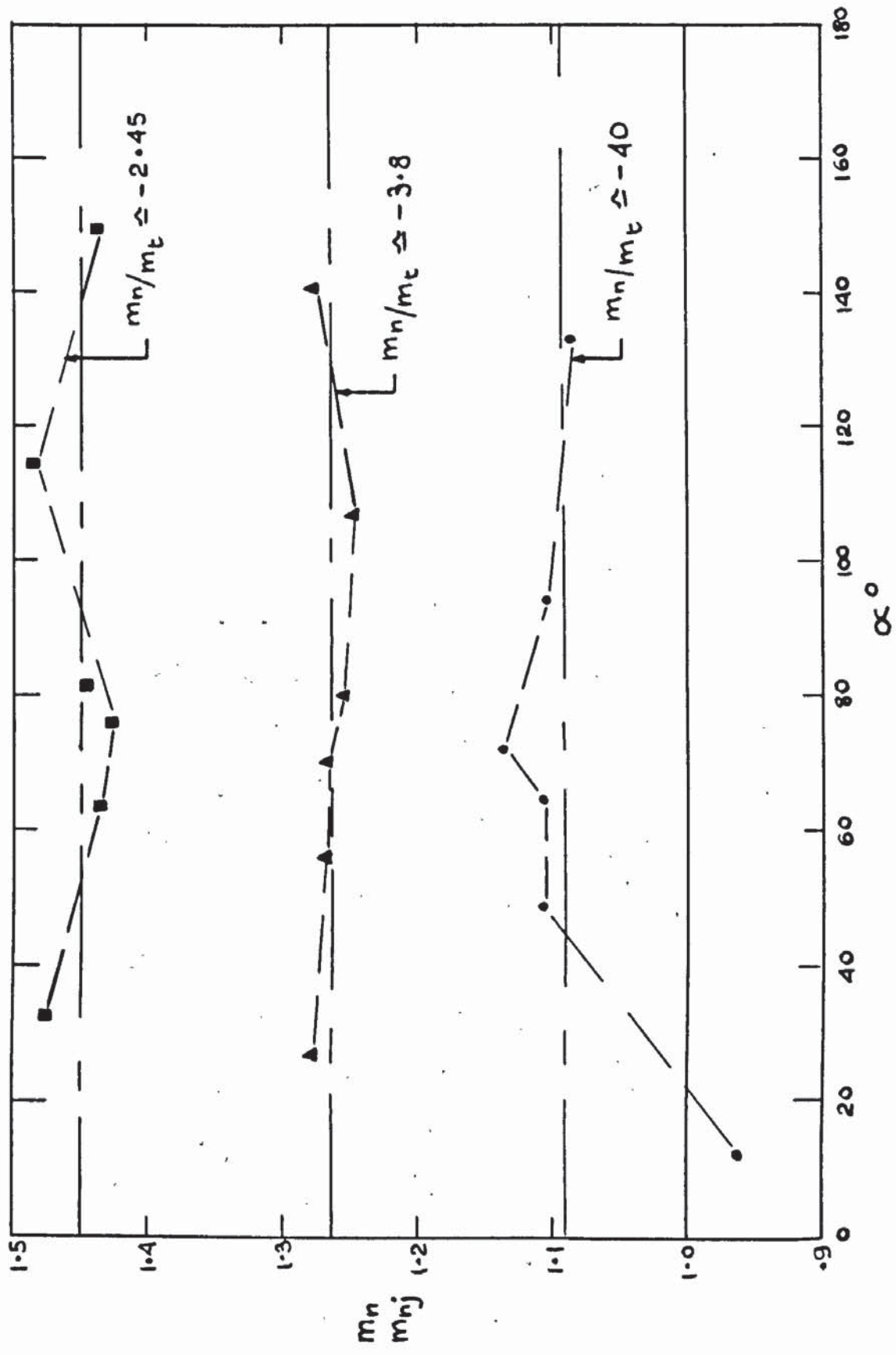


FIG 7.19  $m_n/m_{nj}$  v  $\alpha^\circ - \mu = 0.5$

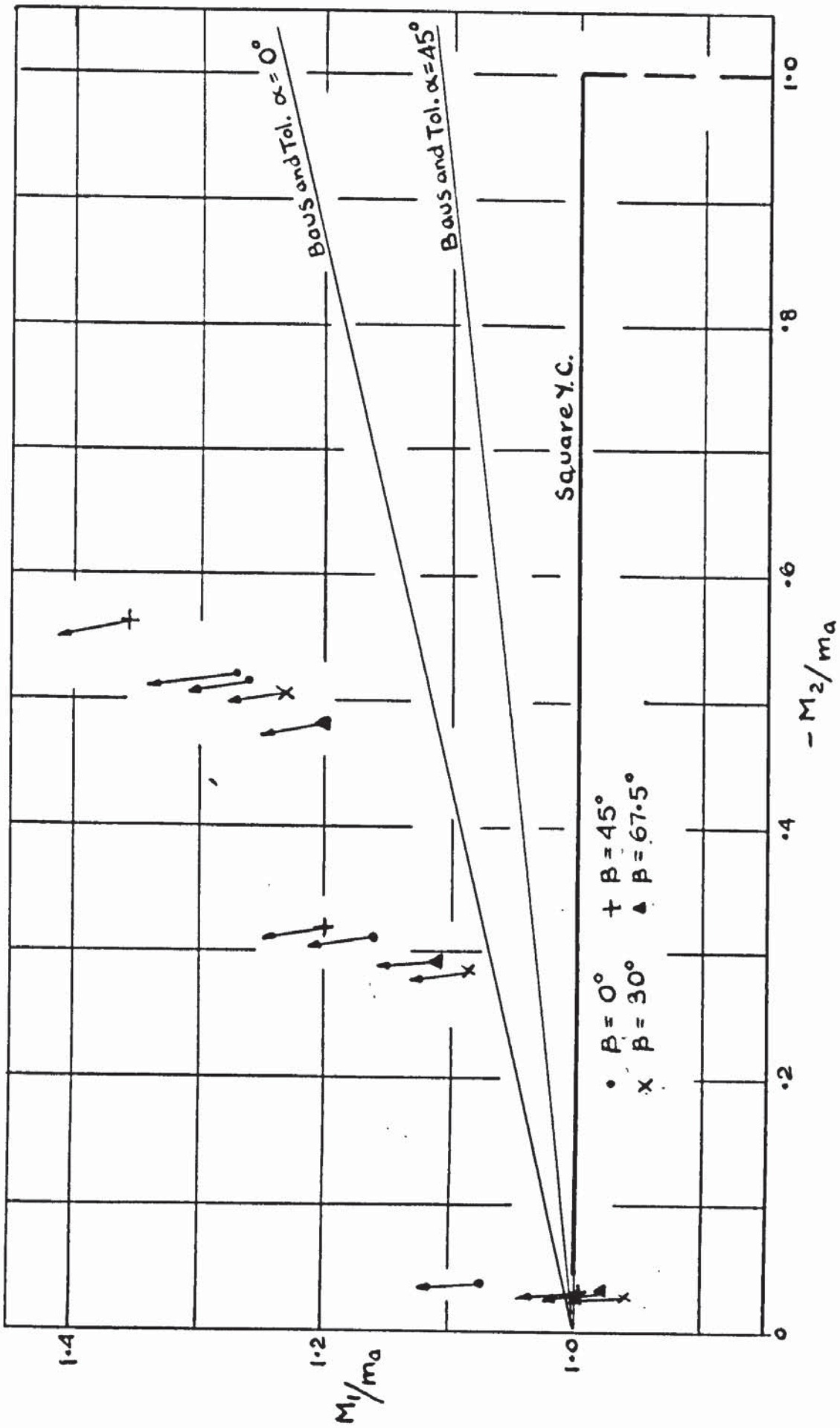


FIG 7.20 YIELD CONDITION -  $\mu=1$

fact that the yield locus was concave and hence inapplicable to the theorems at Limit Analysis.

It should be noted that because of the continually varying direction of principal moments, cracks appeared which were eventually yield lines and which had twisting moments acting on them even in the case of isotropic slabs as soon in chapter 5. These twisting moments must to a greater part have been resisted by the bars acting in shear.

To complete the presentation of failure moment results, the values obtained are plotted in principal moment space in the conventional manner in Figs 7.20 and 7.21 respectively. The arrows represent the final crack directions relative to the principal moment directions for each specimen. In Fig. 7.20 for  $\mu = 1$  slabs the angle of the yield lines to the principal moment direction increased with increasing negative  $M_2$  indicating a curved concave yield locus if plastic potential was obeyed. The plots in Fig. 7.21 are not however so clear although it should be noted that at very low values of  $M_1$  and  $M_2$  the direction of the yield lines is to the right of the principal moment direction whereas at higher values of moment it is to the left.

Other observations of particular interest during the experimental study were the formation of stepped yield lines. This phenomenon was particularly noticeable in specimens TB 13

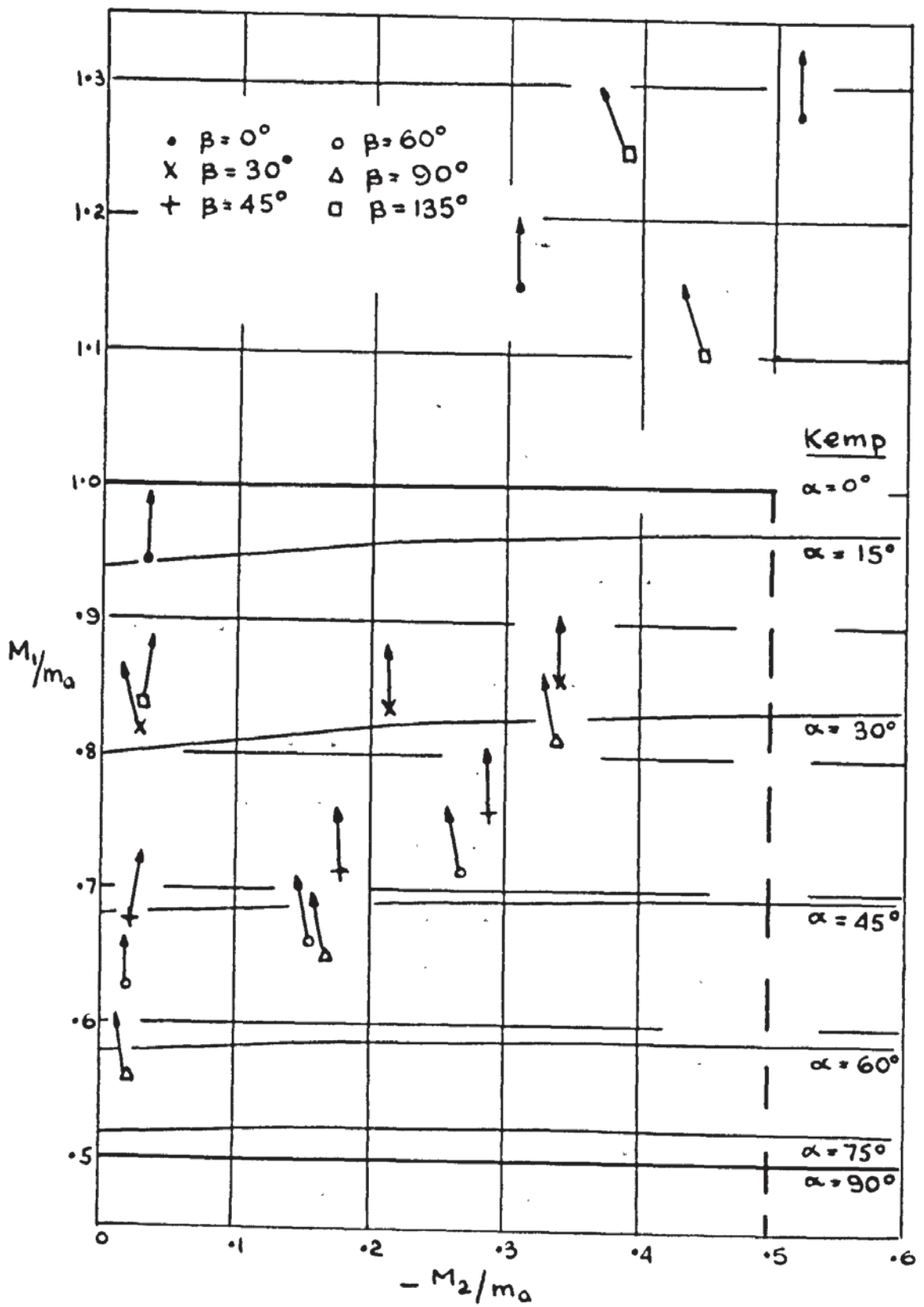


FIG 7.21 YIELD CONDITION -  $\mu = 0.5$

17, 18, 21, 22 and 23 and can be seen in plates 5.39, 5.45, 5.46, 5.50, 5.51 and 5.53. The principal moment directions were close to the bar directions in these cases and the yield lines ran along bars for a distance of about 4 in before jumping to the next bar and so on. This would imply a different stress state at different points on the stepped yield line. However, if the concept of dowel action and the possibility of slight reorientation of bars is taken into account it can be seen that the system could be kinematically admissible.

It can be concluded then from the results presented in this section that

- a) Principal curvature directions do not remain constant after yield.
- b) The yield locus would appear to be of a concave type unless the plastic potential is not obeyed. If either is true one of the conditions of Limit Analysis is violated.
- c) The yield criterion for reinforced concrete slabs does not depend only on the normal moment to the yield line but also to a very significant extent on the value of the tangential moment and possibly the twisting moment on the yield line, whereas the effect of mesh orientation appears small.

CHAPTER 8CONCLUSIONS8.1      General Behaviour

The general, overall object of this study was to carry out a predominantly experimental investigation into the behaviour of reinforced concrete slabs subjected to pure moment, with particular reference to the verification or otherwise of particular theories concerning the action of such slabs under load.

A total of forty eight slab elements have been tested under conditions of uniaxial moment and combined bending and torsion. Results have been presented appertaining to both the elastic and plastic behaviour of such slab elements. The principal variables have been the degree of orthotropy,  $\mu$ , and the combination of and direction of moments with respect to the orthogonal reinforcing mesh.

The way in which slabs were tested under combined bending and torsional moments resulted in a continuously varying direction of principal moment and it was suggested in chapter 3 that this would have a significant effect on the ultimate behaviour of the slab element as cracking would take place at a low load, forming the continuous composite into a discontinuous composite and thus changing its properties

significantly. This parameter would be of importance in all slab structures in which the self-weight moment field and the applied moment field did not coincide.

## 8.2      Elastic behaviour

With the new combined codes of practice concerning reinforced and prestressed concrete structures demanding checks on the Limit States of local cracking, deformations and ultimate load it is necessary to understand the elastic behaviour of the slab before and after cracking. It was shown that Lenschow and Sozen's theoretical analysis gives higher values of stiffness as an average over both ranges than the test results indicate for the cracked range. Although the form that these equations take are of similar form to the test results they are of fairly complex form and for practical purposes it may well be advisable to approximate linearly to the actual curves of stiffness against mesh orientation. The results presented show that there is a strong possibility that this idealization can be achieved as stiffness values under all moment combinations appear to be fairly constant within certain ranges of mesh orientation. For a slab of given steel and concrete properties and of given thickness it was shown that the stiffness in any direction is a function of the angles that the crack and the mesh make to that direction. For slabs in which  $\mu = 1$ , the original crack direction which formed when

when the principal moment reached a critical value remained constant up to failure and hence with a directionally varying moment field twisting moments are present on these yield lines from cracking until failure. It was shown that these crack directions were not a function of mesh orientation which implies for the anisotropic slab that the criterion of cracking is one of maximum principal stress rather than one of strain. The variation of stiffness with mesh orientation is positive proof that the slab has anisotropic elastic properties even for a slab in which  $\mu = 1$ . Elastic analysis must therefore be carried out with these varying elastic properties in mind and the concept of a material made up of an isotropic concrete compression layer and an anisotropic tensile layer both of which are in equilibrium and are compatible must lead logically to a three dimensional analysis being carried out as the principal strain directions will vary in and through either layer.

In slabs in which  $\mu \neq 1$  a more complex relationship exists between stiffness and mesh orientation as the crack direction is no longer independent of the mesh orientation under a given moment field. It was shown that the variation of the crack direction with the mesh orientation was of the same form as suggested by Lenschow and Sozen for different moment fields. However the equations of Lenschow and Sozen

do not take into account the change in slab properties at cracking and are based purely on a failure direction concept. The fact that directionally varying moment fields are not allowed for in Lenschow and Sozens analysis probably explains the difference between theoretical and experimental trends and generally it appears that the type of equation used in the prediction of failure directions is of the right form.

### 8.3 Post-yield behaviour

It is in this field that most work has been carried out and it was one of the major objects of this study to check on the assumptions and theories in use. At present all theoretical yield criteria are based on a normal moment criterion and the more advanced work in this field has shown that the laws of plastic potential are obeyed and hence the use of Limit Analysis endorsed. It was shown that certain basic requirements in general theories were not met in the yield behaviour of the specimens tested. They were

- 1) Plastic flow did not occur in the same direction after yield.

- 2) The crack direction was not necessarily normal to the principal curvature direction after yield but tended to coincide with it at failure.

- 3) The shape of the yield locus did not appear to be convex although conclusive proof of this was not obtained.

4) The yield criterion was a function of mesh orientation to the crack direction in the case of slabs tested under uniaxial moment, the concepts suggested by Prince appearing to be in closest agreement with the test results. Thus the shear stiffness of the reinforcing bar was a significant property in the slabs behaviour.

5) The yield criterion does not depend only on the normal moment to the yield line but is very significantly affected by the tangential and twisting moment acting on it. The effect of these parameters appearing to override or mask the effect of the mesh orientation on the moment capacity noticed in the uniaxial bending tests.

6) Failure could take place on 'stepped' yield lines for which different stress states occurred at different points on the crack thus enabling the entire mechanism to be kinematically possible.

From the above observations it may be directly concluded that the material does not strictly obey the requirements of Limit Analysis and that present yield criteria must be revised to take account of the tangential and twisting moments on the yield line or crack at failure. Although it is important that a criterion of failure must be of a simple form to allow mathematical solution it is important that the true behaviour of a reinforced concrete slab should be experimentally

verified before such simplification is possible.

#### 8.4      Suggestions for future research

Research is still needed into the experimental and theoretical aspects of the behaviour of reinforced concrete slabs.

A useful approach to the analytical study would be one in which the material is considered as an anisotropic, discontinuous, composite material in which the discontinuities have different properties to the continuous portions. A three dimensional analysis could be attempted taking into account the shearing stiffness of the reinforcing bar and allowances for initial crack directions could be made so that overall behaviour of the composites suggested in chapter 3 could be predicted up to failure.

At failure more experimental evidence is required at the relationships between normal, tangential and twisting moments on the cracks. Pre-cracked sections could be used and different ratios of the above variables applied to build up a complete picture of the significant variables and their relationship with each other. It is thought important that experimental studies are of greater priority than analytical work at present as there is the danger that highly sophisticated theoretical approaches will become mathematically unmanageable and outweigh the advantages of the simplicity of yield line theory at present in use.

REFERENCES

1. Prager, W., An Introduction to Plasticity, 1959, 148 pp., Addison - Wesley, Reading Mass.
2. Prager, W., and Hodge, P.G., The Theory of Perfectly Plastic Solids, 1951, J. Wiley and Sons.
3. Timoshenko, S., and Goodier, J.N., Theory of Elasticity, 1934, 506 pp., McGraw-Hill, New York.
4. Marin, J., 1935, Failure theories of materials subjected to combined stresses; Proc.Amer.Soc. Civ.Engrs., 61, 851 - 867.
5. Prager, W., Discontinuous fields of Plastic stress and flow; 1955, Proc. 2nd. U.S. Nat.Congress App.Mechs (Ann Arbor, Michigan, 1954), 21 - 32.
6. Hopkins, H.G., and Wang, A.J., 1954 Load-carrying capacities for circular plates of perfectly plastic material with arbitrary yield condition; J.Mech. Phys. Solids, 3, 117 - 129.
7. Hodge, P.G., "The theory of piecewise linear isotropic plasticity", in Grammel, R., Ed., On the deformation and flow of solids, 1956, Springer-Verlag, Berlin/Gottingen/Heidleberg, 147 - 170.
8. Hopkins, H.G., Some remarks concerning the dependence of the solution of plastic plate problems upon the yield condition; 1957, Proc. 9th Int.Congress App. Mechs. (Brussels, 1956), 6, 448 - 457.

9. Hill, R., The Mathematical Theory of Plasticity, 1950, 355 pp. Oxford, London.
10. Wood, R.H., and Jones, L.L., Yield-Line Analysis of slabs, 1967, 405 pp., Chatto- Windus and Thames and Hudson, London.
11. Timoshenko, S., and Woinowsky - Krieger, S., Theory of Plates and Shells, 1959, 580 pp., McGraw-Hill, New York.
12. Wood, R.H., Plastic and Elastic design of slabs and plates, 1961, 344 pp., Thames and Hudson, London.
13. Ingerslev, A., 1921, Om en elementar Beregningsmaade av Krydsarmerede, Ingeniøren, 27, 507 pp.  
The Strength of rectangular slabs, Paper read before Inst.Str.Engrs., London, December 1922.
14. Johansen, J., Pladeformler, 1949, Formelsamling Polytekisk Forenig; Copenhagen.  
Bludlinieteorier, 1952, Copenhagen.  
Yield Line Theory, 1962, 181 pp.  
Cement and Concrete Ass., London.
15. Kemp, K.O., Morley, C.T., Nielsen, M.P., Wood, R. H., and Jones, L.L., Recent Developments in Yield Line Theory, 1965, 74 pp., Mag.Conc.Res. Special Publication, Cement and Concrete Ass., London.
16. Wood, R.H., 1968, Some controversial and curious developments in the plastic theory of structures; symposium on Engineering Plasticity in honour of

- Sir John Baker, (Cambridge), 665 - 691.
17. Kemp, K.O., 1965, The yield criterion for orthotropically reinforced concrete slabs; Int.J.Mech. Sci., 7, 737 - 746.
  18. Save, M., 1967, A consistent Limit Analysis theory for reinforced concrete plates; Mag.Conc.Res., 19, No.58, 3 - 12.
  19. Houbolt, J.H., The effectiveness of various arrangements of reinforcement in Concrete slabs, 1942, 57 pp., M.Sc. Thesis, Dept. of Civ.Eng., University of Illinois.
  20. Silverj, D.G., Contriuto Teorico Sperimentale al Calcolo a Rottura Delte Piastre in Cemento Armato, 1965, 29 pp., Universita Degli Studi di Roma, Istituto di Scienza Delle Construzioni, Pubblicazione No.11 - 44.
  21. Peter, J., Zur Bewehrung Von Scheiben und Schalen für Hauptspannungen Shiefwinklig zur Bewehrungsrichtung, 1964, 181 pp., Dr. Ing. Thesis, Academy of Engineering, Copenhagen.
  22. Kwiecinski, M.W., Plastic behaviour of an orthogonally; reinforced slab, 1965, M.Sc. Thesis, University of Wales. Yield Criterion for isotropically reinforced slabs 1965, Mag.Conc.Res., 17 No.51, 97 - 100.  
Some tests on the yield criterion for a reinforced concrete slab; 1965, Mag.Conc.Res., 17 No.52, 135 - 138.

23. Baus, R., and Tolaccia, S., 1963, Calcul á la rupture des dalles en béton armé et étude expérimentale du critère de rupture en flexion pure; Annales de l'Institute Techniques du Bâtiment et des Travaux Publics, No 189, 869 - 894
24. Massonett, Ch., Louis, H., Baus, R., and Tolaccia, S., Étude expérimentale des critères de rupture par flexion dans les dalles en béton armé, 1963, Comité European du Béton, Bulletin d'information No.38
25. Nielsen, M.P., Limit Analysis of slabs, 1964, Acta Polytechnica Scandinavia, Civ.Eng., and Building Constr.Series, No.26.
26. Nielsen, M.P., Vridningsforsøg med Jernbetonplader, 1965, 157 pp., Academy of Engineering, Copenhagen.
27. Morley, C.T., The Ultimate bending strength of reinforced concrete slabs, 1965, Ph.D. Thesis, University of Cambridge.
28. Morley, C.T., 1966, On the yield criterion of orthogonally reinforced concrete slab elements, J.Mech. Phys.Solids., 14, 33 - 47
29. Lenschow, R.J., and Sozen, M.A., A yield criterion for reinforced concrete under biaxial moments and forces, 1966, 527 pp., Report on Ph.D. Thesis, Civ.Eng.Studies, Structural Research Series No 311 University of Illinois.

30. Mansfield, E., 1957, Studies in the collapse analysis of rigid-plastic plates with a square-yield diagram; Proc.Roy.Soc., A241, p.311.
31. Kemp, K.O., 1962, A lower bound solution to the collapse of an orthotropically reinforced slab on simple supports; 1962, Mag.Conc.Res., 14, No 41, 79 - 84.
32. Sawzuk, A., 1957., Grenztragfähigkeit der Platten; Banplanug Bautechnik, 11, No.7., 315 - 320; 11, No.8, 359 - 364.
33. Massonett, Ch., and Save, M., Calcul plastique des constructions. vol.2: 'Structures spatiales', 1963, 473 pp., Centre Belgo-Luxembourgeois d'Information de l'Acier.
34. Wolfensberger, R., Traglast und optimale Bemessung von Plattern, 1964, 119 pp., Wildeg, Technische Forshungs - und Beratungstelle der Schweizerischen Zement industrie.
35. Park, R., 1966; Membrane action at the ultimate load of laterally restrained concrete slabs, Comité European du Béton, Bulletin d'Information No.58.
36. Bach, C. and Graf, O., Deutscher Ausschuss fur Eisenbeton, 1915, 309 pp., 30.
37. Prince, M.R., The yield behaviour of unrestrained reinforced concrete slabs, 1967, Ph.D. Thesis,

University of London.

38. Jackson, P.W., and Cratchley, D., 1966, The effect of fibre orientation on the tensile strength of fibre reinforced metals; *J.Mech. Phys Solids*, 14, 49 - 64.
39. Cooper, G.A., 1966, Orientation effects in fibre reinforced metals; *J.Mech.Phys.Solids*, 14, 103-111.
40. Neville, A.M., *Properties of Concrete*, 1963, 532 pp., Pitman, London
41. Gesund, G., and Boston, L.A., 1964, Ultimate strength in combined bending and torsion of concrete beams containing only longitudinal reinforcement. *J.Am.Conc. Inst.Proc.*, V61, 11, 1453-1471.
42. Lekhnitskii, S.G., *Theory of elasticity of an anisotropic elastic body*, 1963, 404 pp., Translation from Russian by Fern, P., Holden-Day Inc., San Francisco.